ICOPMAS 2022

14th International Conference on Coasts, Ports and Marine Structures

9 & 10 May 2023, Tehran- IRAN

CONFERENCE PROCEEDINGS

14th International Conference on
Coasts, Ports and Marine Structures

9 & 10 May 2023 , Tehran-IRAN

ICOPMAS 2022

CONFERENCE PROCEEDINGS

Introduction

The Ports and Maritime Organization of Iran is going to hold the **14th International Conference on Coasts, Ports and Marine Structures (ICOPMAS 2022)** in cooperation with International Maritime Associations, domestic and foreign organizations, universities, contractors and consulting engineers in the Thirty-second anniversary of the conference. The conference emphasizes on technical and specialized cooperation among all countries, particularly between neighboring coastal countries.

In this respect, ICOPMAS secretariat recommends interested students, experts and scientists visit the website for more detailed information: http://icopmas.pmo.ir.

History of the Conference

On May 27, 1990 the first International Conference on Ports & Marine Structures took place at Tehran University, and the Thirteenth session of the conference (ICOPMAS 2018) was held on 26th-28th, NOV 2018 at Tehran Olympic Hotel with participation of more than 1300 related experts and scientists from 37 countries.

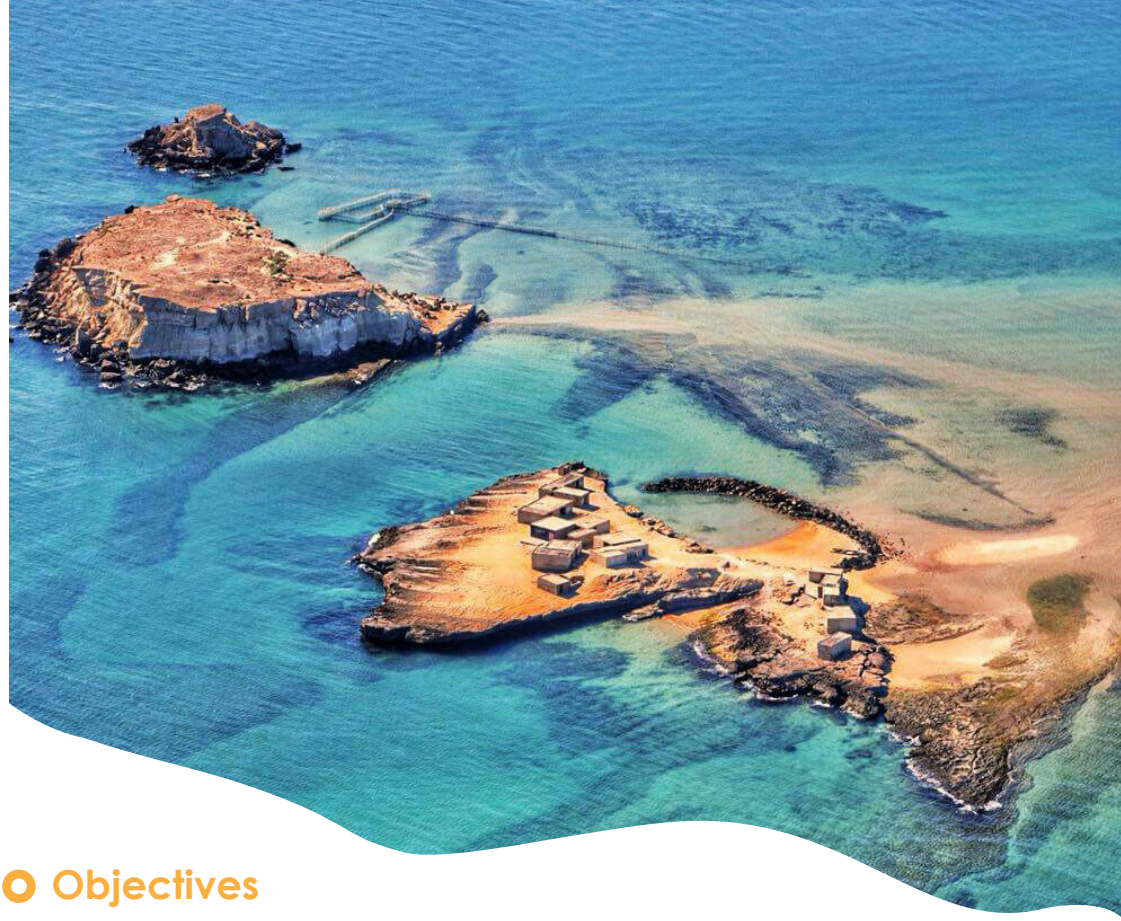

Objectives

As one of the most important technical and scientific events of Iran, ICOPMAS aims to provide an appropriate ground to exchange the latest scientific innovations and technical executive achievements. The conference affords a forum to promote coastal and marine engineering science and opens up new horizons for related experts to present their capabilities to the world. In addition, this conference leads to using new methods and modern devices in the marine industry to promote innovative management systems, strategic and economical technology and preparing the required ground for future cooperation among employers, investors and consultant engineers.

IMPORTANT DATES

Procedure	Deadline
Abstracts Submission Deadline	1st Jun. 2022
Authors Notification	1st Aug. 2022
Closure early bird registration	20th Oct. 2022
Conference Dates	9 & 10 May 2023

Language

The official language of the conference is English.

Organization

Aliakbar Safaei
President

Ali Fathi
Vice-President and Member of Planning Committee

Jalil Eslami
Member of Planning Committee

Hasan beik mohamadloo
Member of Planning Committee

Majid Ali nazi
Member of Planning Committee

Hamid Khalili Vavsari
Secretary

Hossein Khoshbakht
Chair of Executive Committee

Executive committee

No.	Executive	No.	Logistics
1	Vahid Komasi	1	Jamshid Abbasi Rad
2	Rasoul Ghanbari	2	Mohammad Hossein Allameh
3	Majid Fadaee	3	Shahla Esmaeilpour
4	Sepideh Atabakhshi	4	Saeed Khorsandi
5	Atefeh Afshoon	5	Loqman Parsi Nia
6	Mansour Mirzaei	6	Ayatallah Rezazadeh
7	Amirhamzeh Roudgoli	7	Khosrow Saraei
8	Mehrdad Aziminia		
9	Mahnaz Shamloo		
10	Abbas Mohammadsadeghi		
11	Ehsan Karami		
12	Reza Hatami		

ICOPMAS 2022

Board of Directors

No.	Organization
1	Navy of the Army of the Guardians of the Islamic Revolution
2	Strategic Navy of the Army of the Islamic Republic of Iran
3	Head of the National Geographical Organization of Iran
4	The President of The Iran Meteorological Organization
5	The President of Islamic Republic of Iran Meteorological Organization (IRIMO) and Vice Minister of Road and Urban Development
6	Vice President and Managing Director of Department of Environment
7	Acting Director General of National Cartographic Center of Iran
8	Commander of Khatam-ol Anbia Construction
9	Managing Director of Pars Special Economic Energy Zone
10	The Minister of Cultural Heritage, Tourism and Handicrafts of Iran
11	Deputy Minister of Mines and Mining Industries of Ministry of Industry, Mine and Trade
12	Managing Director of Kish Port and Airport Development and Management Company
13	Deputy Minister and Head of Renewable Energy and Energy Efficiency Organization
14	Managing Director of Iranian Offshore Engineering and Construction Company
15	Managing Director of Iranian Oil Terminals Company
16	Managing Director of Iranian Marine Industries Engineering Company
17	Managing Director of khazar exploration and production company
18	Managing Director of the Islamic Republic of Iran Shipping Line Group
19	Managing Director of Iranian Offshore Oil Company
20	Deputy Manager in the National Water and Wastewater Engineering Company of Iran (Abfa)
21	Advisor to the President and Secretary of the Supreme Council of Free Trade-Industrial and Special Economic Zones
22	President of the Sharif University of Technology
23	President of Islamic Azad University
24	President of Chabahar University of Maritime Sciences

No.	Organization
25	President of Malek Ashtar University of Technology
26	President of Khorramshahr University of Marine Science and Technology
27	President of Sahand University of Technology
28	President of the University of Tehran
29	President of Khajeh Nasir Toosi University of Technology
30	President of Tarbiat Modares University
31	President of Amirkabir University of Technology
32	President of Amirkabir University of Technology
33	President of Iran University of Science and Technology
34	President of Imam Khomeini Naval University of Noshahr
35	President of Isfahan University of Technology
36	Deputy Minister of Defense and Armed Forces Logistics
37	Deputy Minister of Jihad-e-Agriculture and Head of Forests, Range & Watershed Management Organization
38	Deputy minister of Urban Planning and Architecture
39	Deputy minister of engineering and passive defense of ministry of Defence and Armed Forces Logistics
40	Governor-General of Golestan Province of Iran
41	Governor-General of Guilan Province of Iran
42	Governor-General of Mazandaran Province of Iran
43	Governor-General of Khuzestan Province of Iran
44	Governor-General of Hormozgan Province of Iran
45	Governor-General of Sistan and Baluchistan Province of Iran
46	Governor-General of Bushehr Province of Iran

Scientific Committee

Mohsen Soltanpour

Chair of Scientific Committee
K. N. Toosi University of Technology

NO.	Name	Affiliation
1	Hamid Reza Abaei	Ports & Maritime Organization, Iran
2	Reza Ahmadian	Islamic Azad University, Iran
3	Ali Asghar Alesheikh	K.N. Toosi University of Technology, Iran
4	Abbas Ali Aliakbari Bidokhti	Institute of Geophysics, Iran
5	Behrouz Asgarian	K.N Toosi University of Technology, Iran
6	Peyman Badiei	University of Tehran, Iran
7	Mohammad Reza Bahari	University of Tehran, Iran
8	Babak Banijamali	Darya Bandar Consulting Engineers, Iran
9	Vahid Chegini	Islamic Azad University, Iran
10	Mohammad Daghigh	Pars Oil and Gas Company, Iran
11	Afshin Danehkar	University of Tehran, Iran
12	Ali Dastgheib	IHE Delft Institute for Water Education, The Netherlands
13	Mohammad Dibajnia	Baird Company, Canada
14	Amir Etemad-Shahidi	Griffith University, Australia
15	Sarmad Ghader	Institute of Geophysics, Iran
16	Ali Asghar Golshani	Islamic Azad University, Iran

NO.	Name	Affiliation
17	Naser Hajizadeh Zaker	University of Tehran, Iran
18	Habib Hakimzadeh	Sahand University of Technology, Iran
19	Kourosh Hejazi	K. N. Toosi University of Technology, Iran
20	Majid Jandaghi Alaee	Pouya Tarh Pars Consultant Engineers, Iran
21	Reza Kamalian	Qom University, Iran
22	Abdolreza Karbasi	University of Tehran, Iran
23	Alireza Kebriaee	Ports & Maritime Organization, Iran
24	Mohammad Javad Ketabdari	Amirkabir University of Technology, Iran
25	Abbas Khayyer	Kyoto University, Japan
26	Mohammad Reza Khedmati	Amirkabir University of Technology, Iran
27	Homayoun Khoshravan	Water Research Institute, Iran
28	Robert Kirby	Ravensrodd Consultants Ltd, England
29	Behzad Layeghi	Meteorological Organization, Iran
30	Han Ligteringen	Delft University of Technology, The Netherlands
31	Saeid Mazaheri	Beta International Associates, Australia
32	Majid Mohammadian	University of Ottawa, Canada
33	Masoud Montazeri Namin	University of Tehran, Iran

NO.	Name	Affiliation
34	Ahmad Reza Mostafa Gharabaghi	Sahand University of Technology, Iran
35	Ioan Nistor	University of Ottawa, Canada
36	Ali Pak	Sharif University of Technology, Iran
37	Iraj Rahmani	Building & Housing Research Center, Iran
38	Abdolkarim Razazan	Ministry of Industry, Mine and Trade, Iran
39	Michael Risk	McMaster University, Canada
40	Kabir Sadeghi	Near East University, Cyprus
41	Ali Akbar Safaei	Ports & Maritime Organization, Iran
42	Ahmad Sana	Sultan Qaboos University, Oman
43	Jun Sasaki	The University of Tokyo, Japan
44	Mehdi Shafieefar	Tarbiat Modares University, Iran
45	Siavosh Shayan	Tarbiat Modares University, Iran
46	Tomoya Shibayama	Waseda University, Japan
47	S. Mostafa Siadatmousavi	Iran University of Science and Technology, Iran
48	Mohsen Soltanpour	K. N. Toosi University of Technology, Iran
49	Marcel Stive	Delft University of Technology, The Netherlands
50	Andrea Sulis	University of Sassari, Italy
51	Hitoshi Tanaka	Tohoku University, Japan
52	Homayoun Zaker	Middle East Water and Environment Consultant Engineers, Iran

Venue

IRIB International Conference Center

IRIB International Conference Center, Jam Jam, Valiasr St., Tehran, Iran

ICOPMAS 2022

[xii]

Keynote Speakers

Prof. Mohammad Reza Bahari

University of Tehran, Iran

Topic: ˝Engineering and installation of offshore subsea pipeline in the Persian Gulf; past experience and future challenges˝

Prof. Ioan Nistor

University of Ottawa, Canada

Topic: ˝TSUNAMI-INDUCED Scour Around Infrastructure During Extreme Coastal Flooding: Field and Experimental Investigations˝

Prof. Balaji Ramakrishnan
Indian Institute of Technology Bombay, India

Topic: ˝Practical Challenges of Understanding the Hydro-Morpho-Dynamics from Coastal & Port Engineering Perspective˝

Prof. Jun Sasaki
The University of Tokyo, Japan

Topic: ˝Carbon Removal and Emission Processes and Promotion of Climate Change Mitigation in Tokyo Bay˝

Prof. Tomaya Shibayama
Waseda University, Japan

Topic: ˝Coastal Disaster Surveys and Assessment for Risk Mitigation˝

Topics

1. Hydrodynamics and Sediment
- Waves and Currents
- Tropical Storms and Tsunami
- Sediment Transport, Erosion and Geomorphology
- Metocean Measurements and Analysis
- Marine Renewable Energy

2. Port and Coastal Management
- Integrated Coastal Zone Management (ICZM)
- Crisis Management of Marine Hazards
- GIS and Remote Sensing
- Port Technologies and Management

3. Port Engineering and Coastal Structures
- Planning and Design of Ports
- Design and Construction of Coastal Structures
- Maintenance, Inspection and Repair of Coastal Structures
- New Equipment and Materials for Construction of Coastal Structures
- Hydrography and Dredging

4. Offshore and Pipeline Engineering
- Design and Construction of Offshore Structures
- Maintenance, Inspection and Repair of Offshore Structures
- Planning and Construction of Submarine Pipelines
- Marine Geotechnics

5. Marine Environment and Safety
- Ports and Maritime Safety Management
- International Convention, Regulations and Rules
- Pollution and Environmental Impacts of Structures and Marine Transportation
- Coastal and Marine Ecosystems


YORACO
PANAMA

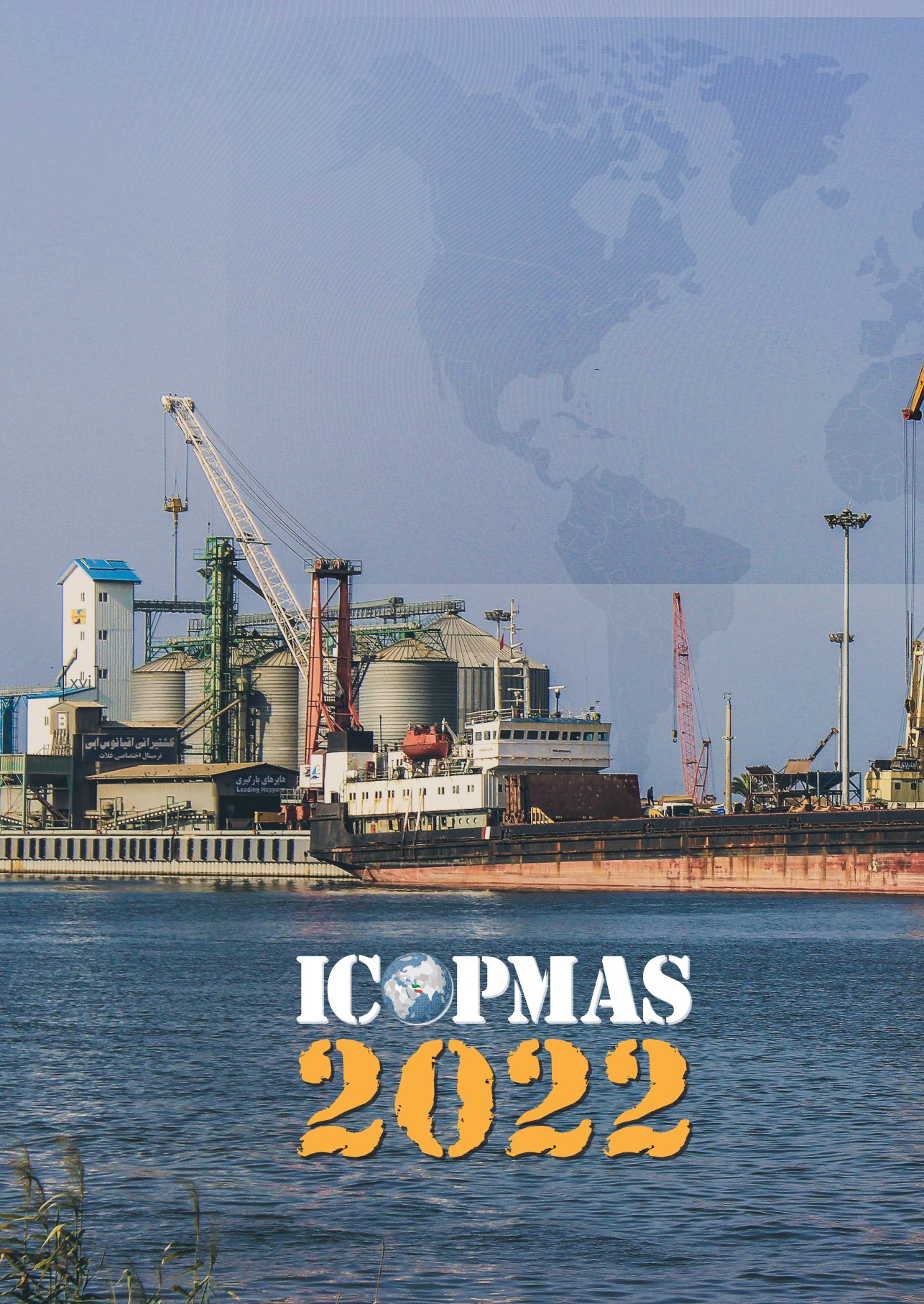
ICOPMAS
2022

14th International Conference on Coasts, Ports and Marine Structures

9 & 10 May 2023, Tehran-IRAN

چهاردهمین همایش بین‌المللی سواحل، بنادر و سازه‌های دریایی

Sponsors

The World Association for Waterborne Transport Infrastructure (PIANC)

International Hydrographic Organization (IHO)

International Harbour Masters Association (IHMA)

International Association of Marine Aids to Navigation and Lighthouse Authorities (IALA –AISM)

International Association for Hydro-Environment Engineering and Research (IAHR)

International Association of Ports and Harbors (IAPH)

Intergovernmental Oceanographic commission (UNESCO)

Coordinating Committee on Hydrometeorology & Pollution Monitoring of the Caspian Sea (CASPCOM)

Iranian National Commission (UNESCO)

Iranian Coastal & Marine Structural Engineering Association (ICOMSEA)

Iranian Hydraulic Association

Iranian National Institute for Oceanography and Atmospheric Science

Iranian Hydrographic Association

Iranian Association of Naval Architecture and Marine Engineering

Iranian Society of Marine Science and Technology

Iranian Shipowners Association

Iranian Association of Geomorphology

Shipping Association of Iran

Water Research Institute

Presidential Center for Progress and Development

Association of Sea Oriented Development

Islamic World Science Citation Center

9 & 10 May 2023 , Tehran-IRAN

ICOPMAS 2022

TABLE OF CONTENT

TABLE OF CONTENT

Keynote Lectures

HEDRODINAMIC AND SEDIMENT

PORT AND COASTAL MANAGMENT

PORT ENGINEERING AND COASTAL STRUCTUR

Offshore and pipline

MARINE ENVIROMENT

INDEX

9 & 10 May 2023 , Tehran-IRAN

ICOPMAS 2022

KEYNOTE LECTURES

ENGINEERING AND INSTALLATION OF SUBSEA EXPORT PIPELINES; PAST EXPERIENCE AND FUTURE CHALLENGES

Mohammad Reza Bahaari[1]

1) Professor, University Colleague of Engineering, School of Civil engineering, University of Tehran, Tehran, Iran, mbahari@ut.ac.ir

1. Introduction

Oil and gas construction projects are of great importance to support and facilitate the process of operation and production. However, these projects usually face chronic risks that lead to time overrun, cost overrun, and poor quality, affecting the projects' success. This is why very few projects complete within the expected costs and timetable.

2. World records circa 2017

2.1. Largest subsea pipeline networks [1]

Notable offshore production regions include the Gulf of Mexico (GoM), the North Sea, Brazil, West Africa, the Persian Gulf. Wherever there is a continental shelf and sedimentary basins, there exists the potential for commercial hydrocarbon deposits.

The US GoM has the greatest amount of offshore pipeline installed in the world because of its rich hydrocarbon basins, vintage, development strategies and licensing terms.

At the end of 2016, over 72,000 km of pipeline have been installed in federal waters since 1952 which would encircle the earth at the equator about two times. About 42,000 km of pipeline are active circa 2016 with the rest out-of-service or abandoned. The North Sea has the second largest pipeline network in the world with around 45,000 km installed pipeline since 1966. About 60% of the pipelines in both regions are export lines with the rest smaller diameter flow lines [2].

2.2. Deepwater pipelines

Deepwater production, defined as water depth greater than 300 m, is mostly cantered in the 'golden triangle' of the US GoM, West Africa and Brazil.

Pipelines in deepwater are subject to increased pressures, colder temperatures, stronger currents, possibly higher flow rates, greater lengths, challenging topography and difficult access for repair and monitoring.

3. Gas Export Pipeline Outstanding Concerns

Below enlisted are the main concerns regarding the offshore pipeline construction project that are classified subjectively:

- Technical Concerns
  - Transportation volume;
  - Route Selection: Data Acquisitions/ Comprehensive Survey
  - Gas Composition
- Integrated Management Scheme
  - Responsibility Matrix
  - Shares during construction and operation
- Financial Concerns
  - Finance Structure
  - Gas fee Structure/ Payments
- Long Lead Items Procurement
  - Line Pipe/ Compressor
- Legal Concerns
  - 3rd Party Interactions
  - National and International laws applicable to the transportation
  - Gas transportation contracts.

4. Transboundary offshore pipelines

4.1. Iran –Oman Pipeline Project

The pipeline route includes ab. 190 KM onshore section from Roudan to Kouh Mobarak Oil and Gas Terminal. The offshore section of the pipeline starts towards southern part of Oman.

The offshore pipeline route includes a landfall at Kouh Mobarak, runs through the Oman Sea to the Sohar area on the approximately 180 KM (Figure 1

Figure 1. Iran –Oman Gas Export Pipeline Route

As a minimum, a feasibility Study for this project contains below topics:

Gulf of Oman Characteristics; Results of Geohazard Study; Environmental Considerations; Third Party Interactions; Route Survey and Geohazard Design Requirements; Wall Thickness and Installation Feasibility

Evaluation of Route Options; Panel Discussion and Route Selection

4.2. Nord Stream

This is a Mega project that includes construction and subsequent operation of two 1,224-kilometre offshore natural gas pipelines [3] in Europe that runs under the Baltic Sea from Russia to Germany.

According to EIA report [4] on Potential National and Transboundary Impacts, with reference to the social environment the following assessment results needs to be documented for such projects:

· cultural heritage (in particular wrecks); fisheries
· marine traffic, tourism and recreation
· existing and planned installations (pipelines, cable, wind farms, etc.)
· existing and planned extraction sites
· military operations, dumping sites (dredged spoils, chemicals and munitions dumps)
· Long term monitoring stations

5. The main activities during the different phases of the lifetime of the pipeline Project include

- ✓ feasibility study and conceptual design
- ✓ engineering surveys and munitions screening
- ✓ detailed pipeline design
- ✓ environmental study, risk assessments
- ✓ permitting
- ✓ setting up infrastructure and logistics
- ✓ surveying of the pipeline installation corridor
- ✓ seabed intervention works prior pipe lay
- ✓ construction activities at the landfalls in both termination points
- ✓ preparation of crossings of existing offshore cables and pipelines
- ✓ offshore pipe lay and environmental monitoring
- ✓ pre-commissioning of the pipelines (flooding, cleaning, gauging, pressure-testing, dewatering, drying)
- ✓ hyperbaric tie-in of the different offshore pipeline sections
- ✓ commissioning (filling the pipelines with gas)
- ✓ operation, including inspection, maintenance, and repair
- ✓ decommissioning (abandonment) of the pipelines.

6. Conclusions & Recommendations

Export Pipelines may face immense technical, legal, political, economic, and social challenges and sometimes entail innovative solutions to mitigate environmental risk. For instance, lack of technology, expertise or facilities is one of the limitation. To overcome this challenge, indigenous infrastructure must be upgraded or borrowed. The shareholders, foreign investors or bank loans can finance project cost. An extensive and transparent communication strategy must be established to solve disagreement and political issues. Finally, the potential impact of the project must be evaluated to avoid possible negative effects on the environment.

Pipelines are the most economical and safest means for exporting gas. They are long term projects, hence require detailed planning. Benefits of parties, international regulations and neighboring countries' determinations govern settlements, so for making decision a collaborative approach must be adopted for these projects.

Export or import pipelines contribute to political security for countries, by pursuing compatible goals.

It is worth to allocate time, pay consideration and put efforts into these multidisciplinary projects due to their advantages and importance.

6. References

[1] Mark J. Kaiser, "The global offshore pipeline construction service market 2017 – Part I" Ships and Offshore Structures, DOI: 10.1080/17445302.2017.1342923, 2017

[2] Oil&GasUK. 2013.Decommissioning of pipelines in theNorth Sea region. London

[3] Nord Stream, "Logistics of the Pipeline", Brochure, August 2010.

[4] U.S. Energy Information Administration, 2017, "Natural gas imports and exports", https://www.eia.gov/energyexplained/index.php?page=natural_gas_imports, May 22, 2018.

TSUNAMI—INDUCED SCOUR AROUND INFRASTRUCTURE DURING EXTREME COASTAL FLOODING: FIELD AND EXPERIMENTAL INVESTIGATIONS

Ioan Nistor[1], Razieh Mehrzad[1], Colin Rennie[1]

1) Department of Civil Engineering, University of Ottawa, Canada, inistor@uottawa.ca

1. Introduction

Post-tsunami field survey evidence indicate that destructive tsunamis cause substantial coastal sediment mobilization. Measurements collected following several tsunami events, such as the 1992 Nicaragua Tsunami, the 2004 Indian Ocean Tsunami, and the 2011 Tohoku Tsunami provided substantial evidence of scour around damaged buildings and bridges. Tsunami-induced coastal inundation is characterized by high overland flow velocities, both during the inland flow phase as well as during the drawdown. These high flow velocities produce high bed shear stresses and large amounts of sediment movement over extensive areas, resulting in substantial beach erosion and significant scour around many of the structures located in the inundation zone.

A vast amount of research exists on scour depth in waves, currents and combinations of waves and currents. However, in the case of tsunami-induced scour, forensic engineering post-tsunami surveys are the primary source of scour data and the literature is limited. Numerous studies have pointed out scour around structures as the main failure factor for many coastal structures during the 2011 Tohoku tsunami (Jayaratne et al. 2016). Researchers such as Van et al. (2007), Mazumder and Ojha (2007), Zhao et al. (2010), Yeh (2010), Kato et al. (2006, 2012), Yeganeh-Bakhtiary et al. (2012), Arikawa et al. (2012), and Arya and Shingan (2012) performed experimental studies which investigated scour mechanisms around vertical cylinders and breakwaters. Yoshii et al. (2017) and Yoshii et al. (2018) investigated tsunami inundation and associated sediment transport and deposition in the coastal hinterland using two large wave flume studies. However, experimental work related to scour around structures attempting to simulate the local scour induced by tsunamis inundation are limited to a few studies.

2. Research Objectives and Novelty

This study will present results of several tsunami forensic engineering campaigns as well as results of a comprehensive new experimental program dealing with bore-induced local scour around structures. The hydrodynamic forcing conditions for the experimental program was due to a dam-break wave generated in a hydraulic flume located in the Hydraulics Laboratory at the University of Ottawa, Canada. This highly turbulent bore was generated by the rapid release of water impounded behind a rapidly-opening swing gate equipped with a lock and sudden release mechanism. A video system was used to record the evolution the of scour and vortex characteristics using video imaging obtained from inside of the structure model which was built from transparent PVC. Image processing allowed tracking the time and spatial evolution of the scour around the structure. Finally, new provisions for scour around structures stemming from this research which are now included in the ASCE7 Chapter 6 Tsunami Loads and Effects and which will be presented.

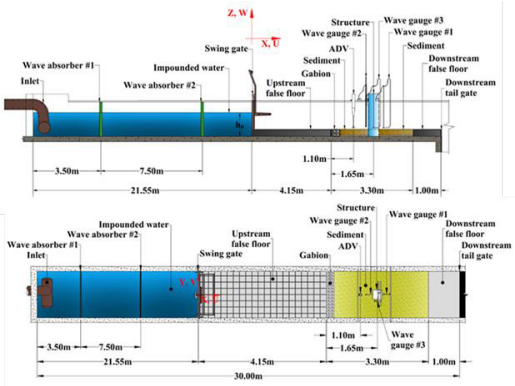

Figure 1 Experimental setting (not at scale)

The experimental setup was performed in the Dam-break Flume (30 m long, 1.5 m wide, and 0.8 m deep) at the University of Ottawa, Canada. The dam-break waves was were generated using a rapidly opening swing gate, which released an impounded volume of water generating a dam-break wave. Two false floors with a height of 0.20 m were installed in the downstream of the gate, before in front and after the sand bed section, to provide a section for the sediment bed. The latter which consisted of uniform sand with a mean sand diameter (D50) of 0.5 mm. Two sand beds with a horizontal slope and a positive slope of 5% were tested in this study as the bore front propagation over the false floor and the sandy section. The bore propagation over the bed s and the scour formation evolution were recorded with four video-cameras (GoPro Hero5). The dam-break waves were generated with four different

impoundment depths of 0.4 m, 0.35 m, 0.3 m, and 0.25 m and two still water depths of 0.1 m and 0.03 m were set in the sand section.

3. Results and discussion

Several parameters were measured and analyzed in this experimental program. Figure 2 (a), (b) and (c) show the evolution of the upstream scour hole geometry at different scour stages. The scour hole is characterized by a gradation of bed slope, an inner slope immediately adjacent to the structure and an outer slope, with a slope break in between them. The boundary between the two slopes within the front scour hole is shown with a dash line in Figure 2.

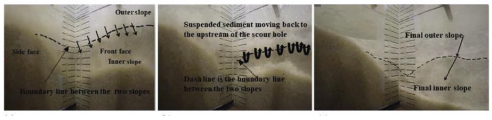

Figure 2 (a) Suspended sediment movement from outer slope to inner slope at t=6.41 s; (b) suspended sediment moving back to the upstream of scour hole and the oscillation of the boundary between two slopes at t =7.06 s; and (c) final scour hole geometry with outer and inner slopes at t=24 s, for Test 1 (hu=0.25 m).

First, suspended sediment entrained from the outer scour hole entered the inner hole due to slope failure of outer slope (slumping), as shown with arrows in Figure 2a. Additionally the boundary between the two slopes moved toward the downstream of the inner slope (the latter shown with the dash line in Figure 2b. Furthermore, the suspended particles moved back to the upstream of the inner scour hole while still remaining suspended, shown with arrows in Figure 2b. As a result, the boundary moved back to the upstream part of the scour hole. Subsequently, the suspended sediment was carried out transversely, along the structure, and moved into the inner scour hole all over again. The oscillation of the boundary between the inner and outer slopes demonstrates the oscillation of the horseshoe vortex in terms of its location and magnitude over time in stream-wise direction.

Figure 3 shows the measured results for the initial condition of hu = 0.25 m (Test1). Bore duration was approximately 120 seconds. The negative and positive values of the left axis represent scour and bore depth (m), respectively, whereas the right axis represents the stream-wise velocity (m/s). The black line represents the time-history of the horizontal flow velocity measured at X= 5.4 m from the longitudinal axis of the flume (40cm upstream of the structure). The red, light blue, and pink lines show the time-histories of the water surface elevation measured by the wave gauges located at the front, side and back face of the structure, respectively. Also, the red line with triangle pattern, light blue line with cross pattern and pink line with star pattern show the scour depth time-histories observed at the front, side and back of the structure, respectively. It can be seen that stream-wise velocities were captured after 2 s from the passage of the bore front as the ADV measurements were noisy for the first 2 seconds after the arrival of the advancing bore due to air bubble entrainment and cavitation formed around the head of the ADV.

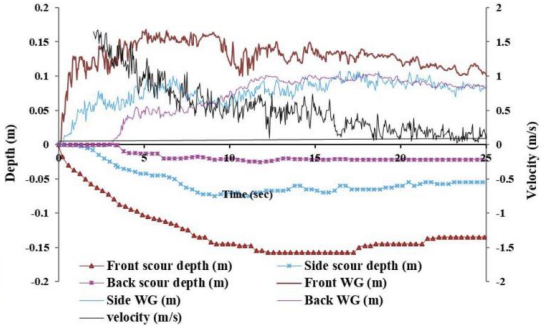

Figure 3 Time history of the water surface elevations measured by the wave gauges located at the front (red line), side (light blue) and back (pink line) face of the structure, and scour depth measured at the front (red line with triangle pattern), side (light blue line with cross pattern) and back (pink line with star pattern) face of the structure, and horizontal velocity (black line) measured 50 cm upstream of the structure for an impoundment depth, hu=0.25 m (Test 1).

The time-history of the bore depth at the front of the structure suddenly increased moments after initial impact and continued to increase beyond the first sudden rise until a maximum value of 0.166 m was reached, after which a decrease was observed. The initial bore front (recorded by the front WG) had an almost vertical front profile, and the maximum bore depth was attained within 5 seconds after initial bore impact. The bore depths measured by the wave gauges installed on the side and back of the column show smaller bore height values compared to the bore depth measured by the front wave gauge.

Figure 3 also illustrates that the maximum bore depth (runup) measured on the upstream face was approximately 1.6 times greater than that recorded by the side and back wave gauges. Scour at these three locations began shortly after the arrival of the bore at each face. Scour at the side of the structure started slightly later than the initiation of the scour at the front corner.

The critical velocity for the initiation of sediment motion was calculated using the Shields entrainment criterion. For the 1 mm grain size, the calculated critical velocity was 0.28 m/s. Figure 3 shows that the highest scour rate coincided with the largest flow velocities greater than the critical velocity Once the flow velocity decreased, the erosion rate slowed and the scour hole reached its maximum depth. As previously discussed, once the velocity decreased, slumping of the over-steep scour hole slopes towards the sediment's natural angle of repose was observed and filled the scour hole.

14th International Conference on Coasts, Ports and Marine Structures
9 & 10 May 2023 , Tehran-IRAN
ICOPMAS 2022

COASTAL DISASTER SURVEYS AND RISK MITIGATION

Tomoya Shibayama

Department of Civil and Environmental Engineering, Waseda University, Tokyo, Japan
Email: shibayama@waseda.jp

1. Introduction

Coastal disasters such as tsunamis, storm surges and high wind waves are natural disasters that can occur in any coastal area worldwide [1]. They occur when several natural conditions, such as earthquakes, typhoons, local topography, and social conditions, such as prior disaster experiences and preparedness, are combined as unfavourable circumstances for the coastal residents. They can occur at various time intervals, from tsunamis, which occur once every hundred or thousand years, to storm surges and high wind waves, which occur somewhere in the world every year due to typhoon strikes. They can be as extensive as the 2011 Tohoku earthquake tsunami or the 2004 Indian Ocean tsunami, which extended hundreds of kilometres along the coast, or as small-scale as the 2014 extratropical cyclone-induced storm surge in Nemuro, where the storm surge inundated land in a narrow area of a few kilometres.

2. Purpose of Field Surveys

The purpose of surveying coastal disasters worldwide is to analyse them and then recommend strategies for disaster mitigation from a local perspective, adapted to the actual conditions in each region. As Japan has historically experienced many coastal disasters over the years since the beginning of history, it is also essential to organise this experience and contribute to disaster reduction worldwide. In practice, the first step is to conduct post-disaster field surveys and organise the data numerically and descriptively. In order to incorporate new findings into disaster mitigation methods, hydraulic model experiments are used to observe phenomena in more detail and to understand the physical processes. The results are then incorporated into a numerical prediction model to reconstruct a more concrete image of the disaster. By sharing these results with the local residents, it will finally be possible to construct rational disaster prevention structures and create evacuation plans tailored to the actual conditions of the region.

3. Examples of Recent Coastal Disasters

Table 1 lists the significant tsunamis, storm surges and high wind waves that have caused damage in coastal areas in the last 20 years since the 2004 Indian Ocean tsunami. The author conducted post-disaster field surveys for all the disasters in this table. From the standpoint of coastal disaster research, from the 1970s onwards, for about 30 years, there were few significant coastal hazards. In coastal engineering, research interest was focused on coastal erosion and water quality in inner bays. However, since 2004, major coastal disasters have occurred every year, and for the first time in 30 years, research interest in coastal disasters has increased.

The author started studying coastal disaster management at the end of the 1970s, so we had vivid memories of the Ise Bay typhoon (1959) and the Chilean tsunami (1960). At that time, knowledge of coastal disaster prevention was still shared among limited experts but was not widespread among the general public. Later, after the Indian Ocean Tsunami (2004) and the Tohoku

Table 1. List of Major Coastal Disasters after 2004.

Year	Event	Locations	Dead (D) and Missing(M)
2004	Indian Ocean Tsunami	Sri Lanka, Indonesia,Thailand	220,000
2005	Storm Surge by Hurricane Katrina	USA (New Orleans)	1,200
2006	Java Tsunami	Indonesia	668
2007	Storm Surge by Cyclone Sidr	Bangladesh	5,100
2008	Storm Surge by Cyclone Nargis	Myanmar	138,000
2009	Tsunami in Samoa Islands	Samoa	183
2010	Chile Tsunami	Chile	500
2010	Tsunami in Mentawai islands	Indonesia	500
2011	Tohoku Tsunami	Japan	D15,782 M4,086
2012	Storm Surge by Hurricane Sandy	USA(New York City)	170 (USA: 80)
2013	Storm Surge by Typhoon Yolanda (Haien)	Phillipines	D4,011 M1,602
2014	Storm Surge in Nemuro	Japan (Hokkaido Island)	0
2018	Storm Surge by Typhoon Jebi	Japan (Kaisai Airport, OsakaBay)	D14
2018	Tsunami in Sulawesi Islands	Indonesia (Palu)	D2,081 M1,309
2018	Tsunami in Sunda Strait	Indonesia (Krakatoa Volcano)	D426 M29
2019	Storm Surge and High Waves by Typhoon Faxai	Japan(Tokyo Bay)	D9

Earthquake Tsunami (2011), knowledge of coastal disasters became widespread worldwide.

4. Recovery from 2011 Tohoku Tsunami: Japanese Choice of Reconstruction

In 2011, the great east Japan Earthquake tsunami (Tohoku tsunami) attacked the northern part of Japan. After the tsunami, there was a significant change in the engineering concept of protecting the coastal area from tsunamis based on field survey results and analysis. There are now two levels of protection. The "tsunami protection level" (level 1) is the level of the tsunami that can be handled by structures such as seawalls and is the height of the tsunami used in the design of coastal protection facilities. The tsunami protection level is for a tsunami that occurs once every 100 years. The "tsunami disaster mitigation level" (level 2) is above the protection level, which is the level of tsunami evacuation planning and is the maximum height necessary to save lives if a tsunami exceeds the protection level.

In the aftermath of the Tohoku tsunami, the recovery from the disaster was carried out through consensus building in each region, using a 32 trillion yen (300 billion USD) reconstruction budget based on public consensus. Different choices were made in each region based on local disaster experience and the history of the community. The following are some of the most common choices. These cases are instructive examples for the future choices of coastal communities.

1) To rebuild the community by building higher and stronger tsunami seawalls to prepare for the subsequent tsunami: In Taro District, the 10.0m tsunami embankment before the Tohoku Tsunami was breached by overflow, so a new 14.7m embankment was built closer to the coastline (Fig. 1).

(2) New artificial ground was constructed in the old urban area. A new urban area is constructed on the artificial ground: In Rikuzentakata, a new urban area was built on top of the old one, 10-12m above sea level. The surrounding hills (45 ha) and the new embankment (91 ha) were combined to create the new residential area (Fig. 2).

(3) The old low-lying area inundated by the tsunami is an open space without housing: In Onagawa, the old town is used as a railway station and shopping area. A new residential area was built on a natural hill, and the residents were relocated (Fig.3).

(4) Abolish the residential area and withdraw: The Arahama area in Sendai City was developed as a bedroom town of Sendai City before the tsunami. However, all the residents moved out and withdrew from this area following the heavy damage (Fig.4).

Figure 1. Case of Taro (High Embankment).

Figure 2. Case of Rikuzentakata (Artificial Hill).

Figure 3. Case of Onagawa (Open Space).

Figure 4. Case of Arahama (Withdrawal).

5. References

[1] Shibayama, T., Esteban, M. (Editors), "Coastal Disaster Surveys and Assessment for Risk Management", (Taylor & Francis、379p, 2022.

PRACTICAL CHALLENGES OF UNDERSTANDING THE HYDRO-MORPHO-DYNAMICS FROM COASTAL & PORT ENGINEERING PERSPECTIVE

Balaji Ramakrishnan

Professor, Department of Civil Engineering, Indian Institute of Technology Bombay, Mumbai, India, Email: rbalaji@iitb.ac.in, ramakrishnan.balaji@gmail.com

1. Introduction

Morphodynamics, driven by the hydrodynamic characteristics of the nearshore region, is a complex physical process, understanding of which is essential for engineers, especially for port and harbour, as siltation in navigational channel is undesirable for vessel movements. Dredging is an inevitable process, in order to keep the channels navigable, which cost significant expenditures to ports. On the other hand, sediment transport along coastline, influenced largely by wind waves, of great interest to coastal engineers for planning any suitable coastal management strategy. This paper presents our research efforts to understand the siltation behavior of navigational channels and nearshore region, through comprehensive analysis by using the powers of in-situ measurements, numerical modelling tools and remote-sensing techniques.

2. Siltation Dynamics in Ports

Siltation behaviour of navigational channels and basins of (i) Kandla, Gujarat (ii) Mumbai harbour (iii) Thane Creek using process based hydrodynamic and morphological model developed using Delft3D numerical scheme is discussed. The tidal levels and currents of the numerical model are validated with in-situ measurements at different location. We used input reduction technique [1] to estimate the annual siltation rates but with minimal computational efforts The modelling results revealed that siltation rates and morphological trends, which is useful for deriving the dredging management strategies. Site specific recommendation of sediment management system is also discussed.

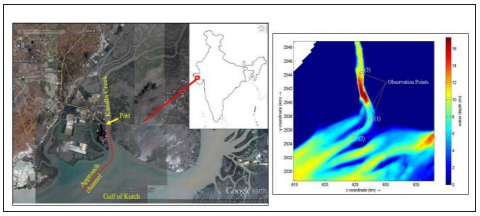

Figure 1. Location of Kandla creek

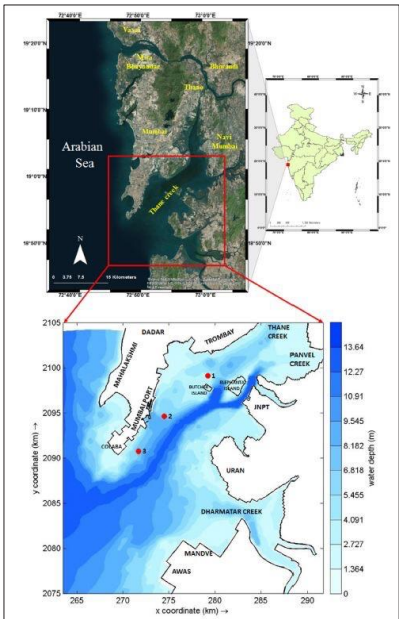

Figure 2. Location of Thane creek & Mumbai port

3. Morphological Changes along Beaches

Coastal zones are more susceptible to hazards as global ocean climate changes and utilization of coastal resources increases. Thus, coastal observation has to support the societal economy of the country by protecting coasts and the people. Our emphasis on the coastal observation and opportunities associated with it to understand the nearshore dynamics is established with several case studies. We have successfully adopted (a) Eulerian method of observation [2] (b) Lagrangian method of observation (c) Unmanned Aerial Vehicle (UAV) based coastal observation system and (d) Coastal monitoring programme for coastal protection works, as part of our field measurement campaigns. The various measurement types, sensors, and

moreover the recent advancement of data collection methods such as satellite imageries, lidar, and UAV etc. are discussed. These collected data are used for calibration and validation of ocean state forecast numerical model and satellite image processing.

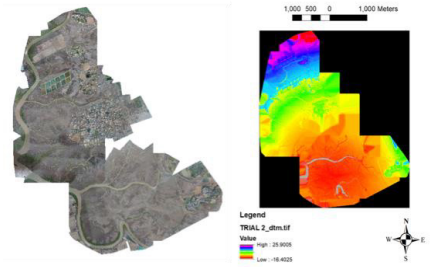

Krishnapur, Gujarat

Malgund beach, Ratnagiri, Maharashtra

Figure 3. Typical beach topographical data collected by UAV

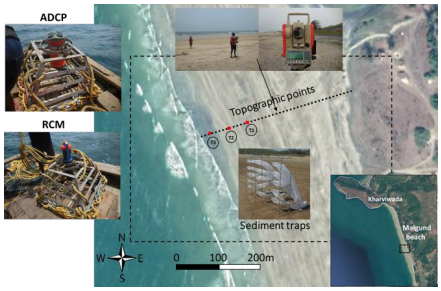

Figure 4. Typical in-situ measurement of hydro-morpho-dynamics

4. Summary

The talk highlights some of recent research and developments in the thematic domain of hydro- and sediment dynamics, pertaining to ports, waterways and nearshore environment, successfully accomplished by Ocean Engineering Division, Department of Civil Engineering, Indian Institute of Technology Bombay, Mumbai, in India.

5. References

[1] Balaji Ramakrishnan, Niraj Pratap Singh, Satheeshkumar Jeyraj, "Input reduction and acceleration techniques in a morphodynamic modeling: A case study of Mumbai harbour", Regional Studies in Marine Science 31 (2019) 100765.
[2] Satheeshkumar, J and Balaji, R., "Field Measurement and Modeling of Sediment Transport along a Sandy Pocket Beach, Central West Coast of India", ASCE Jrl. Of Waterway, Port, Coastal and Ocean Engineering, Vol. 147 (6), 2021, 05021014-1-13, DOI: 10.1061/(ASCE)WW.1943-5460.0000678.

9 & 10 May 2023 , Tehran-IRAN

ICOPMAS 2022

HEDRODINAMIC AND SEDIMENT

DETECTION OF INTERNAL WAVES IN THE GULF OF OMAN BY SATELLITE IMAGES IN 2020 AND 2021

Hamed Deldar [1], Hassan Yousefi[2], Akbar Rashidi Ebrahim Hesari[3]

1) Institute of Geophysics, University of Tehran, Tehran, Iran, h.deldar@inio.ac.ir
2) Department of Environmental Science, Tarbiat Modares University, Tehran, Iran, eng.hasanyou@gmail.com
3) Department of Marine Physics, Tarbiat Modares University, Tehran, Iran, akbar.rashidi@modares.ac.ir

1. Introduction

Internal waves are one of the most important marine phenomena due to their effect on how densities change in different layers. The internal waves formed and produced by the passage of tidal and ocean currents over the seabed's mounds. Internal waves appear as parallel ripple bands on the sea surface. So, for this reason, evaluating spatial and dynamic properties of internal waves, especially their propagation speed, is possible through satellite image processing. The detection of internal waves at the sea surface is done in satellite images with alternating traces almost similar to depressions and ridges at the sea surface [1, 2, 3, 4]. Internal waves consequently affect the ocean's sound and acoustic wave propagation [5]. Collecting images from an area with high temporal and spatial resolution using optical images and SAR radar images is an important application for studying internal waves [6]. Synthetic aperture radar (SAR), which is very sensitive to sea surface roughness, is a powerful tool for observing internal waves [7]. Using images from Sentinel-1 SAR-C band and Landsat-8 OLI Sensor satellites, it is possible to retrieve the spatial parameters of internal wave groups on the surface due to the high resolution of the data and repetitive imaging of an area [8]. The creation of internal waves is expected due to the bathymetry and characteristics of the water in this area. In this study, we examine the images to identify and detect these waves using satellite images and extract their parameters.

2. Materials and Methods

In this study, satellite images have been used in the Oman Sea region for the whole of 2020 and 2021 years. The Oman Sea is located in the southeast of Iran and the north of Oman and is in the eastern part of the Strait of Hormuz. Its coordinates are between 56.2 E and 59 E longitude and 23 N and 27 N latitude. In this study, 48 images per month of Landsat 8 ETM+[1], the panchromatic band (band 8) [9], and Sentinel 1, Band C, SAR sensor [10] were downloaded. The Landsat 8 satellite band 8 has a spatial accuracy of up to 15 meters, which is suitable for detecting minor features. After receiving these images, the initial radiometric and geometric corrections were first made on them by SNAP[2] and ENVI[3] Software. Internal waves were identified in two stages. First, visually, after adjusting the brightness and color of the image, these waves were detected in the area, and then, by the designed and developed edge-detection algorithm in MATLAB, these waves were detected. Areas containing wave packets were studied and measured to extract the parameters of wavelength, largest wavefront length, and calculation of propagation speed from the image. In this study, the temperature and salinity of the region were used according to the results of field measurements performed in previous studies in the Oman Sea, showing that we have a stronger thermocline and more stable stratification in the warmer seasons [11, 12].

3. Results

A Study of 48 images showed 15 internal wave packets, all identified between April and September. In other months of the year, no wave packet was observed, which could be the result of weaker stratification due to cold months and stronger stratification in warmer months (see Table 1).

Table 1. The Number of observed internal waves

Month	LANDSAT 8	SENTINEL1-SAR	Total
April	-	1	1
May	2	-	2
June	5	-	5
July	1	2	3
August	1	2	3
September	-	1	1

The Bathymetry changes in the region are very intense. The depth in the western part of the Oman Sea suddenly has decreased to about 1500 meters, which is one of the influential factors in creating internal waves in this area and making them visible on the surface (see Figure 1). This is consistent with the results of Small and Martin in 2002, who concluded that the position and curvature of the internal wavefronts observed in the Oman Sea indicate propagation from the edge of the continental shelf [13].

[1] Enhanced Thematic Mapper Plus

[2] Sentinel Application Platform

[3] Environment for Visualizing Images

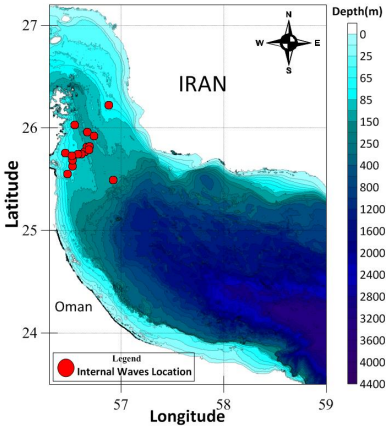

Figure 1. Bathymetry and Observed internal waves in the Oman Sea in 2020 and 2021. The red points are Internal Waves locations.

These waves are mainly seen in the western part of the Oman Sea, east of the Strait of Hormuz, and southeast of the Musandam Peninsula. In this study, a better-resolution image from each satellite was selected as a sample image to display the measured properties of the image. (see Figure 2-a) which is related to the Sentinel 1-SAR sensor, which shows about 3.6 km Wave-packet length. (see Figure 2-b) which is related to the Landsat 8 satellite, shows about 4 km Wave-packet length, and the length of the largest wavefront shown in blue is 21.3 km.

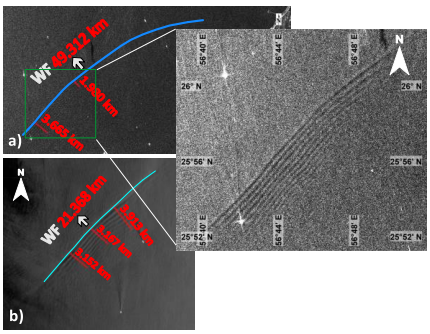

Figure 2. Internal waves in the Oman Sea, SAR image in 2020 (a), and LANDSAT8 image in 2021(b), the blue line is the wavefront, and the red lines are the packet length.

In the total of 15 observed wave packets, the average wavelength is about 465 meters, the biggest wavelength is about 726 meters, and the smallest wavelength is about to 86 meters. Also, the largest wavefront length is about 49.3 km, and the smallest is about 7.7 km. The average propagation speed is about 0.6 meters per second, and the average propagation angle is between 290 to 300 degrees in the northwest direction.

4. Conclusion

The results show that more internal waves occur in warm seasons near the area of intense depth changes in the western part of the Oman Sea near the Strait of Hormuz due to creating a stronger stratification in warmer seasons. The Landsat 8 and Sentinel1-SAR satellite images showed an excellent outcome for detecting internal waves. The wave Parameters such as wavelength, packet length, propagation speed, and angle of their propagation were extracted from the images. Also, due to consequently effect of internal waves on the sound and acoustic wave propagation in the ocean, identifying the occurrence locations can be applied in other fields as well.

5. References

[1] Rufenach, C., & Smith, C. (1985). Technical note Observation of internal waves in LANDSAT and SEASAT satellite imagery. International Journal of Remote Sensing, 6(7), 1201-1207.

[2] Lavrova, O. Y., Mityagina, M. I., & Sabinin, K. D. (2011, January). Study of internal wave generation and propagation features in non-tidal seas based on satellite synthetic aperture radar data. Doklady Earth Sciences (Vol. 436, No. 1, pp. 165-169). SP MAIK Nauka/Interperiodica.

[3] Deldar, H., & Bidokhti, A. A. A. A. (2020). Visualizations of density fluctuations before and after the passage of bluff body objects in a laboratory stratified tank. Ocean Engineering, 209, 107277.

[4] Lavrova O. Yu., Mityagina M. I., Sabinin K. D., Possible mechanisms for generating internal waves in the northeastern part of the Black Sea, Sovremennye problemy distantsionnogo zondirovaniya Zemli iz kosmosa, 2008, Vol. 2, Issue 5, pp. 128–136.

[5] Deldar, H. (2017). A laboratory study of the effect of internal waves on acoustic propagation. Journal of the Earth and Space Physics, 43(1), 181-192.

[6] Lavrova, O. Y. (2018). Internal Waves Observed in Satellite Images of the Northeastern Black Sea in July 2017. Sovremennye Problemy Distantsionnogo Zondirovaniya Zemli iz Kosmosa, 15(1), 309-315.

[7] Meng, J., & Zhang, J. (2002). Synergy ENVISAT ASAR, ERS-2 SAR, RADARSAT SAR, Landsat TM and MODIS Images to Research Propagation Features of Internal Solitary Waves in Northern of South China Sea.

[8] Jackson, C. (2007). Internal wave detection using the moderate resolution imaging spectroradiometer (MODIS). Journal of Geophysical Research: Oceans, 112(C11).

[9] Explorer, E. (2000). FS; 083-00. Geological Survey (US).

[10] ASF DAAC 2020 and 2021, contains modified Copernicus Sentinel data 2020 and 2021, processed by ESA.

[11] Ghazi, E., Bidokhti, A. A., Ezam, M., Azad, M. T., & Hassanzadeh, S. (2016). Physical properties of Persian Gulf outflow thermohaline intrusion in the Oman Sea. Open Journal of Marine Science, 7(1), 169-190.

[12] Rezai, H., Wilson, S., Claereboudt, M., & Riegl, B. (2004). Coral reef status in the ROPME sea area: Arabian/Persian Gulf, Gulf of Oman and Arabian Sea. Status of coral reefs of the world, 1, 155-170.

[13] Small, J., & Martin, J. (2002). The generation of non-linear internal waves in the Gulf of Oman. Continental shelf research, 22(8), 1153-1182.

INVESTIGATION OF INTERNAL WAVES GENERATED BY THE SEFIDRUD PLUMES IN THE SOUTHERN CASPIAN SEA

Hossein Farjami[1]

1) Iranian National Institute for Oceanography and Atmospheric Sciences, Tehran, Iran, hfarjami@gmail.com

1. Introduction

Horizontal river momentum in the stratified sea water generates waves which are known as internal or internal waves (IWs). Such waves form at the interface of two layers of the water column, which play an important role in ocean dynamics. IWs effect on ocean energy balance and coastal ecosystem processes. Therefore, detection of these waves can be used in various coastal and marine studies such as marine pollution transport, submarine navigation, and in ocean models to calculate converted kinetic energy[1].

Based on in-situ measurements and satellite imagery, the IWs are manifistated in the southwest of the Caspian Sea by Sefidrud plumes in Iran's Guilan province coasts. Then IWs characteristics are extracted using in-situ measurements, satellite imagery, and modeling.

2. Materials and Methods

In this study, IWs generated by Sefidrud plumes were investigated using field measurements, and Landsat 7 and 8 satellite, and Sentinel-2 images in the Guilan province coasts of IRAN [2].

The southern part of the Caspian Sea, which ends off the coast of Iran, has a maximum depth of 1025 meters. This section, which has an area of about 168,400 km^2, has an average depth of 350 meters [3]. The Sefidrud is a river with a length of about 670 km in the northwest of Iran that enters to the South Caspian Sea (Figure 1).

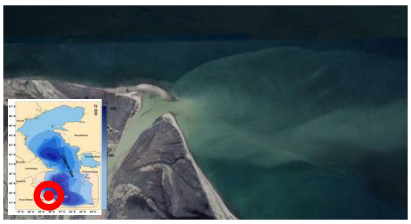

Figure 1. Entrance of Sefidrud in southwest of The Caspian Sea

The IWs effects on the sea surface are recognizable by satellite images [4]. Therefore, edge-finding algorithms were used to identify them. In order to achieve this aim, we collected Landsat 7, Landsat 8 and Sentinel-2 images in the Southern Caspian Sea. These images were then processed by SNAP, ArcMap and Matlab.

On the other hand, we used datasets from the southern Caspian Sea acquired by the Iranian National Institute for Oceanography and Atmospheric Science (INIOAS) an Ocean Seven 316 CTD. The essential condition for propagating IWs is the stratification of water columns. In-situ measurements show a rapidly changing density (Sigma-T) with depth. These data confirm the formation of pycnocline and thermocline in the study area, which are essential for forming IWs. The pressure and circulation of the water column can be changed by the large amplitude of IWs. The maximum vertical large-amplitude of an internal solitary wave can be estimated by the Dubreil-Jacotin-Long Equation Solver (DJLES) (equation 1) in the stratified fluid structures [5, 6].

$$\frac{\partial^2\eta(x,z)}{\partial x^2}+\frac{\partial^2\eta(x,z)}{\partial z^2}+\frac{N^2(z-\eta(x,z))\eta(x,z)}{c^2}=0 \qquad (1)$$

Here $\eta(x,z)$ is the height of the internal wave from the resting level, N^2 is the Brunt–Väisälä frequency, or buoyancy frequency, g is the acceleration of gravity, and c is the wave phase speed.

3. Results and Discussion

This study found concentrations of IWs activity on the continental shelf in the southwest of the SCS, near the coastal zone of Guilan province. An example of IWs identified is obviously shown in Figure 2, which were recorded by the mentioned satellites on May 30, May 2020 in the study area.

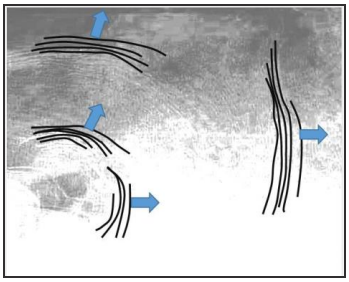

Figure 2. Example of detected IWs on entrance of Sefidrud in the South Caspian Sea

We can estimate the amplitude of IWs by numerical methods. Hence, in this study, we performed a numerical simulation based on equation 1 (see [7]) by using measurement data near the generation area on the continental shelf. Based on measurements taken on the continental shelf along the Sefidrud, the maximum amplitude of solitary IWs ranged from a few meters to about 20 m. Also, the maximum amplitude occurs at a depth of ~30 m and decreases with distance from that depth (Figure 3).

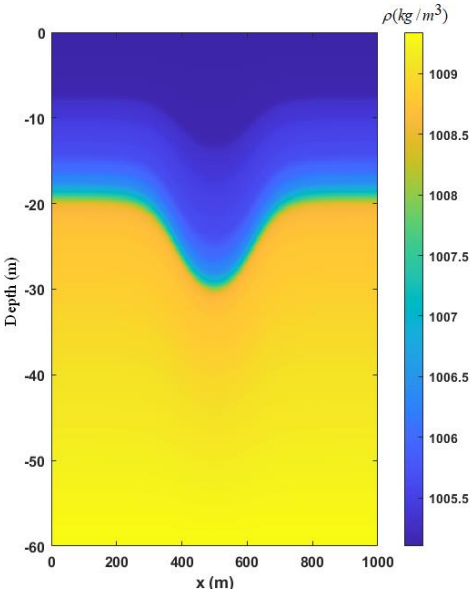

Figure 3. Vertical Amplitude of IWs in the south of Caspian Sea using in-situ data

The Caspian Sea, with complex geometry, inter-seasonal differences in surface temperature, complex sea surface wind, and dense flow through rivers, has a high potential for forming a variety of IWs. These waves can affect different marine pollution transports, such as microplastics in the study area.

As a result, the south Caspian Sea has a high potential for marine pollution because of the high population density in the coastal areas. IWs waves can capture, concentrate, and transport microplastic particles, floating plastic debris, larvae, contaminants, and toxic pollutants in this basin.

4. References

[1] V. Duchêne, "Asymptotic models for the generation of internal waves by a moving ship, and the dead-water phenomenon," *Nonlinearity,* vol. 24, no. 8, p. 2281, 2011.

[2] R. Mendes *et al.*, "On the generation of internal waves by river plumes in subcritical initial conditions," *Scientific reports,* vol. 11, no. 1, pp. 1-12, 2021.

[3] H. Farjami and A. R. E. Hesari, "Assessment of sea surface wind field pattern over the Caspian Sea using EOF analysis," *Regional Studies in Marine Science,* vol. 35, p. 101254, 2020.

[4] S. Andi, A. Rashidi Ebrahim Hesari, and H. Farjami, "Detection of internal waves in the Persian Gulf," *Remote Sensing Letters,* vol. 12, no. 2, pp. 190-198, 2021.

[5] K. R. Helfrich and B. L. White, "A model for large-amplitude internal solitary waves with trapped cores," *Nonlinear Processes in Geophysics,* vol. 17, no. 4, pp. 303-318, 2010.

[6] M. Stastna and K. G. Lamb, "Large fully nonlinear internal solitary waves: The effect of background current," *Physics of fluids,* vol. 14, no. 9, pp. 2987-2999, 2002.

[7] M. Dunphy, "DJLES: Dubreil-Jacotin-Long Equation Solver," 2019.

FORECASTING OF CYCLONE-INDUCED WAVES IN THE ARABIAN SEA

Mohammad Hossein Kazeminezhad[1]

1) Iranian National Institute for Oceanography and Atmospheric Science, Ocean Engineering and Technology Department, Tehran, Iran, mkazeminezhad@inio.ac.ir

1. Introduction

Availability of the forecasted wave data is of great importance for any marine activity. Today, not only the extreme waves are considered as a natural hazard but also lack of forecasted wave data in non-extreme conditions consider to be hazardous for many activities. Therefore, in the last decades, numerical wave models (e.g. WAVEWATCH III [1], SWAN [2]) forced with forecasted wind data have been implemented in operational mode to produce forecasted wave data. Forecasted wind data is the most important input data for operational wave forecasting models.

One of the areas that is affected by severe wind induced waves due to the pre-post monsoon tropical storms is the Northwest Indian Ocean, Arabian Sea. Performance evaluation of numerical model such as WAVEWATCH III model (hereafter WWIII) has been carried out in several studies [3-5]. However, in the previous studies analysis and reanalysis wind data have been used for model validation. In the present study, the WW III model is forced with the GFS (Global Forecast System) forecasted wind data in the period of tropical cyclone. Then the forecasted significant wave heights are compared with the buoy data as well as satellite observations.

2. Dataset

Operational wave forecasting has been carried out in the period of Nilofar Cyclone, i.e., from 25/10/2014 to 31/10/2014. The Nilofar Cyclone (the strongest cyclone in the Arabian Sea in 2014, Category 4 based on Saffir–Simpson hurricane scale classifications), originated from a low-pressure area in the Arabian Sea on October 25. As the system continued to track north-northeastwards (see Figure 1) it intensified into a cyclonic storm on October 26 and reached its peak intensity on October 28, with highest 3-minute sustained wind speed of 205 km/h.

GFS data provided by NCEP/NOAA has been utilized as a wind forcing of the WWIII model. The data includes wind speed components in 10 meters above the sea level with time resolution of 3 hours and spatial resolution of 0.5 degree for both geographic longitude and latitude.

The forecasted significant wave heights (Hs) were compared with remotely sensed data derived from GlobWave database as well as buoy data located at latitude and longitude of 15.062° and 68.878° with buoy ID of AD07 (see Figure 1).

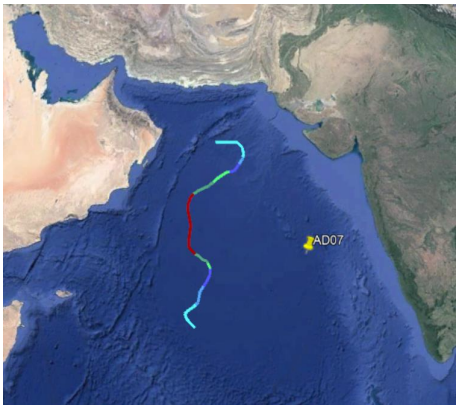

Figure 1. Study area, location of AD07 wave buoy and track of Nilofar cyclones.

3. Numerical Model

According to the previous studies (e.g. [6]), in this study Tolman and Chalikov's [7] (hereinafter TC) embedded in WWIII model ver. 4.18 is used for developing the wave forecasting system in the studied area. WWIII is a third-generation model based on the integration of wave spectral action balance equation, which states that the evolution of the wave field is controlled by a sum of source terms. More details about the numerical model can be found in [1].

4. Results

Figure 2 shows the comparison between measured Hs at AD07 buoy and forecasted ones using TC source term package. In this figure, as can be seen the time series of the forecasted data is well adapted to those of the measured ones for duration of Cyclone Nilofar. In order to better evaluate the WWIII capability over the entire computational domain, the forecasted Hs were compared with GlobWAVE satellite data during the Cyclone Nilofar in terms of the frequency scatter plot (see Figure 3). In scatter plot the colors indicate the number of data points in each pixel. The frequency scatter plot show that the TC source term package slightly overestimate the

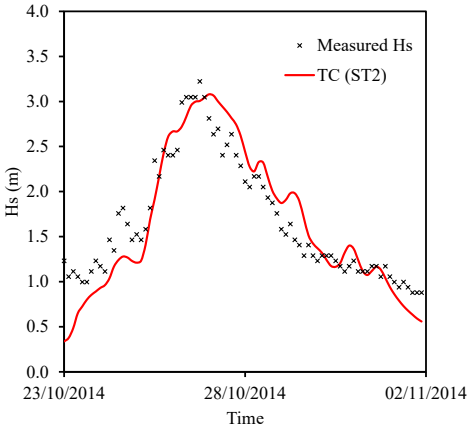

Figure 2. Comparisons of measured and forecasted Hs at AD07 station during tropical cyclones.

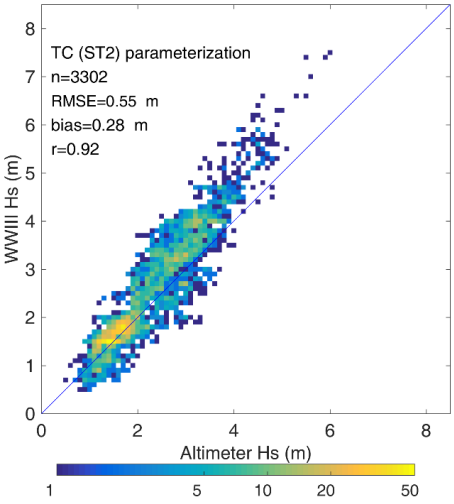

Figure 3. Frequency scatter plot of forecasted Hs versus altimeter Hs over the Arabian Sea during Nilofar cyclone

forecasted Hs, especially for the higher values of the Hs. Different statistical parameters are used to evaluate the forecasted Hs including normalized bias (NMB), scatter index (SI) and normalized root mean square error (HH). These parameters are calculated as follows:

$$\mathrm{NMB} = \frac{\sum(F_i - O_i)}{\sum O_i} \quad (1)$$

$$\mathrm{SI} = \frac{\sqrt{\frac{1}{N}\sum(F_i - O_i)^2}}{\bar{O}} \quad (2)$$

$$\mathrm{HH} = \sqrt{\frac{\sum(F_i - O_i)^2}{\sum(F_i O_i)}} \quad (3)$$

Table 1 shows that application of TC resulted in an average overestimation of 12% for Hs in the entire Arabian Sea. To further investigates the numerical results, the data has been divided into two parts i.e., higher wave highest data (Hs>3.0 m) and lower wave highest data (Hs<3.0 m). As can be seen, the TC parameterization overestimated the Hs in both lower and higher wave data cases.

Table 1. Error indicators of forecasted Hs for satellite data during Nilofar tropical cyclone.

SWH	Overall		
	NMB	HH	SI
Overall	0.12	0.21	0.24
SWH<3.0	0.11	0.23	0.25
SWH>3.0	0.15	0.19	0.21

5. Conclusion

In this study, WW III model has been used to forecast the cyclone induced waves in the Northwest Indian Ocean, Arabian Sea. GFS operational forecast wind data were used as the wave model forcing. Forecasted wave heights were compared with buoy data as well as remotely sensed data over the Arabian Sea. Results indicated that the GFS wind data can be used for operational forecasting of the cyclone induced waves and the use of GFS wind data with the TC parameterization leads to overestimation of the significant wave heights.

6. References

[1] Tolman, H.L., User manual and system documentation of WAVEWATCH III version 4.18. Technical report. 2014.
[2] Booij, N., et al., SWAN user manual SWAN cycle III version 40.41. 2004.
[3] Seemanth, M., et al., Sensitivity analysis of dissipation parameterizations in a third-generation spectral wave model, WAVEWATCH III for Indian Ocean. Ocean Engineering, 2016. 124: p. 252-273.
[4] Kalantzi, G.D., C. Gommenginger, and M. Srokosz, Assessing the Performance of the Dissipation Parameterizations in WAVEWATCH III Using Collocated Altimetry Data. Journal of Physical Oceanography, 2009. 39(11): p. 2800-2819.
[5] Amrutha, M.M., et al., Wave hindcast studies using SWAN nested in WAVEWATCH III - comparison with measured nearshore buoy data off Karwar, eastern Arabian Sea. Ocean Engineering, 2016. 119: p. 114-124.
[6] Kazeminezhad, M. H. Ghavanini, F.A., Numerical modelling of cyclone-induced waves using WAVEWATCH III™. 36th IAHR World Congress, 2015.
[7] Tolman, H.L. and D. Chalikov, Source Terms in a Third-Generation Wind Wave Model. Journal of Physical Oceanography, 1996. 26(11): p. 2497-2518.

14th International Conference on Coasts, Ports and Marine Structures
9 & 10 May 2023 , Tehran-IRAN
ICOPMAS 2022

ANALYSIS OF WATER WAVE INTERACTION WITH A SUBMERGED CIRCULAR MEMBRANE BREAKWATER

Elham Jafarzadeh [1], Abdorreza Kabiri-Samani[2] and Bijan Boroomand[3], Asghar Bohluly[4]

1) Department of Civil Engineering, Isfahan University of Technology, Iran, e.jafarzadeh@alumni.iut.ac.ir
2) Department of Civil Engineering, Isfahan University of Technology, Iran, akabiri@cc.iut.ac.ir
3) Department of Civil Engineering, Isfahan University of Technology, Iran, boromand@cc.iut.ac.ir
4) Institute of Geophysics, University of Tehran, Iran, bohluly@ut.ac.ir

1. Introduction

Modeling and testing inflatable membrane structures for rapidly deployable port infrastructures and their application as submerged breakwaters are essential for ensuring coastline stability. Exposure to waves, tides, winds, and human activities faces coastlines with the danger of change and destruction. In 1987, Ohyama et al. [1] introduced a "flexible mound" submerged breakwater as a thin membrane bag filled with water. The present submerged flexible mound breakwater consists of a multi-freedom system allowing the structure to move as a spring-damper system [2]. The analytical solution applies Hamilton's principle to evaluate the final equations obtained [3]. The space-time partial derivatives of Hamilton's principal function were identified as the energy-momentum tensor of the system. The effect of the structural displacement was investigated by implementing a rigid circular model in ANSYS 16.0 based on the obtained displacement to investigate the values of water free-surface perturbations caused by the structural displacements. This solution also used the superposition technique to investigate the wave's effects created by structure movements on the incident wave. Validation was performed using a laboratory model in which a movable circular model was played in the wave path. The wave height concerning the structure was recorded before and after the structure with the water level sensors. The present study focused on the structural movement and the wave interaction with a non-stretchable movable membrane to determine the effects of structural movements in different conditions using the laboratory data of waves generated by the movable submerged breakwaters.

2. Numerical Method

The observation systems mainly used a CMOS video camera with a frame rate of 60 frames per second. The scene of the interesting area was recorded using a sensor with a resolution of 1280×720 dpi. A rigid structure was then modeled in ANSYS and moved with the calculated displacement to evaluate the effect of the structure motion on the incident wave and the amount of wave generated. After obtaining the wave created by the motion of the movable structure, the interaction between the two radiation waves and the waves caused by the structure motion was investigated approximately based on the superposition technique. The wave heights obtained by the superposition were compared with the laboratory-obtained wave heights after colliding with the structure. ANSYS FLUENT (2016) was used for the numerical solution. To create geometry for the analysis, a two-dimensional model of the flume with a rigid circular structure was developed in ANSYS DesignModeler and discretized in ANSYS Meshing. The analytically-obtained structure displacement was numerically solved as the structure displacement velocity equation in ANSYS based on user-defined functions to specify flow-driven rigid-body motions. After solving a turbulent flow using a model developed based on the Reynolds averaged Navier-Stokes equations, which can be used to derive a turbulence model resembling the k-ε model, the results were compared with the laboratory findings. Movements of the rigid structure in the middle plane of the model made perturbations and waves. Therefore, the structure movement was modeled in FLUENT using a dynamic mesh to improve accuracy and reduce the computational burden locally. Since the moving object lay in the middle of the solution space, smoothing and remeshing were used in ANSYS FLUENT to improve element quality by transferring nodes concerning surrounding nodes and elements in a way that the mesh changed with the structure movement. The time step should be selected so that the current number lies in a proper range during the simulation. The adequately small time step of 0.0004 was therefore considered.

3. Experiment Setup

The schematic diagram of the submerged movable structure and the relevant study parameters are shown in Figure 1, where h represents the water depth, and D is the structure diameter equal to 0.14 m. A propagating wave traveled a distance of one wave length L (0.02-0.94 m) within a wave height H_i (0.6-1 m). The experiments were performed in a towing tank 14 m long, 0.4 m wide, and 0.6 m deep at the Hydraulic Laboratory of Isfahan University, Isfahan, Iran. The free-surface elevation was measured using parallel-wire resistance gauges at four different locations. The difference in wave height with and without

the structure was measured in the laboratory to determine the effect of structure movement on the wave.

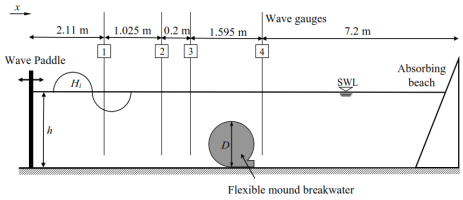

Figure 1. Schematic diagram of the experimental setup and test apparatus.

Throughout a test run, structure movements were continuously recorded within a predetermined section of 40×40 cm^2. Post-processing was performed by first converting video images to digital images, enhancing the digital images, and extracting the structure displacement from the digital data. Wave flume was measured in this part using a video camera.

4. Results and Discussion

As stated previously, the ANSYS model was used to investigate the effect of the structure motion on the incident wave heights. This model comprised a rigid structure with the same diameter as a movable structure. Changes in the height of the wave generated in a stationary fluid by the structure displacement were then investigated at an analytically-obtained speed. The experimental data were used to validate the results of the present analytical model. Wave height in the ANSYS model was compared with the wave height obtained from the experimental data in the presence and absence of the structure. Comparing the experimental data with the model simulation in ANSYS showed a power correlation between the results with a coefficient of determination of $R^2 = 0.94$. Figure 2 shows variations in the normalized height of the generated wave H/H_i, (where H is the height of the wave created by the structure disturbance in numerical and experimental models) versus wave steepness H_i/L. According to Figure 2, the numerical results compared well with the experimental data at a 0.19 m water depth.

Given that the ANSYS model uses the structure displacement obtained from the analytical model for wave generation, the structure appears capable of generating more waves at an average depth of 0.19 m, and the results at this depth are generally consistent with the laboratory data. The maximum water depth reduces the effect of the waves generated by the structure on the primary wave. At relatively-low wave heights, the difference between the results is more significant at the highest water depth than at higher waves. The difference is that the structure effect on these waves is not significant in the laboratory. However, ANSYS has created a greater wave height, given the higher movement of the structure. The associated numerical simulation showed an adequately-accurate prediction of the structural movement and the resultant wave height.

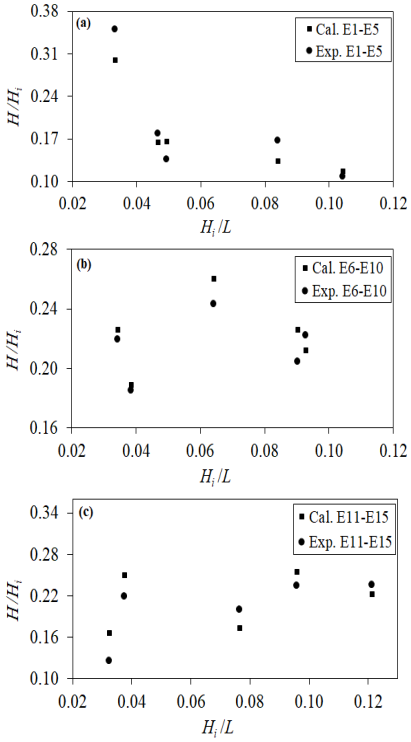

Figure 2. Calculated and measured H/Hi versus the wave steepness for (a) E1-E5 (h=0.29) (b) E6-E10 (h=0.19) (c) E11-E15 (h=0.15).

5. Conclusion

A rigid circular model was simulated in ANSYS 16.0 using the analytically-obtained displacement to investigate the perturbation caused by the structure displacement. Comparing the structure movement and the resultant wave height obtained by the numerical model and the experimental measurements suggested a consistency with minimum error values.

6. References

[1] Ohyama, T., Tanaka, M., Kiyokawa, T., et al. Wave deformation on a flexible submerged dike. In: *34th Japan conference on coastal engineering*, Tokyo, Japan, September 1987, pp.497–501. JSCE.

[2] Jafarzadeh, E., Kabiri-Samani, A., Mansourzadeh, S. and Bohluly, A., 2021. Experimental modeling of the interaction between waves and submerged flexible mound breakwaters. *Proceedings of the Institution of Mechanical Engineers, Part M: Journal of Engineering for the Maritime Environment,* 235(1), pp.127-141.

[3] Jafarzadeh, E., Kabiri-Samani, A., Boroomand, B., & Bohluly, A. 2022. Analytical modeling of flexible circular submerged mound motion in gravity waves. *Journal of Ocean Engineering and Marine Energy,* pp.1-10.

EVALUATION OF FLOW3D NUMERICAL MODEL TO STUDY THE SHOCK WAVE PROPAGATION ON THE SHORE WITH A GENTLE SLOPE

Ali Hafezi Bafti[1], Rasoul Memarzadeh[2], Majid Dehghani[3], Fatemeh boochani[4]

1) Department of Civil Engineering, Vali-e-Asr University of Rafsanjan, Kerman, Iran, ali.hafezi@stu.vru.ac.ir
2) Department of Civil Engineering, Vali-e-Asr University of Rafsanjan, Kerman, Iran, r.memarzadeh@vru.ac.ir
3) Department of Civil Engineering, Vali-e-Asr University of Rafsanjan, Kerman, Iran, m.dehghani@vru.ac.ir
4) Master's degree in water engineering and hydraulic structures, fatemeh.boochani1994@yahoo.com

1. Introduction

Coastal management emphasizing on sustainability, lower natural degradation, and improved environmental protection requires updated procedures for managing the impacts of waves on the coastline. One of the emerging approaches is the implementation of coastal vegetation along the coastline. Besides being efficient from an environmental perspective and having the potential to create a beautiful landscape, this approach has been empirically proved to be highly effective in reducing the adverse impacts of tsunami and shock wave [1]. Moreover, vegetation approaches are regarded as an appropriate substitute for artificial barriers from various economic, practical, and environmental standpoints. Therefore, study of this topic is highly significant in the coastal engineering field.

2. FLOW3D Numerical Model

One of the important tools to study hydraulic problems such as wave run-up on coasts is numerical models. In this study, numerical modeling using the FLOW3D numerical model, which is based on the Finite Volume Method (FVM), has been considered. The governing equations in FLOW3D software are the 3D Navier-Stokes equations. Accordingly, first, the FLOW3D numerical model was validated basis on experimental data without vegetation. Next, the model was verified to study the solitary shock wave movement on the coast in the presence of coastal vegetation.

3. Numerical Model Validation for Shock Wave Propagation on Shore without Vegetation

The experimental data of Fuchs and Hager [2] was used to validate the results of FLOW3D numerical model for the shore without vegetation. The modeled coast has a gentle slope of 1 to 2.5. The depth of water in the front of the coast was 0.2 m, and the height of the solitary wave was 0.14 m. The results of the free surface and its comparison with experimental data are shown in figure 1. The results of the numerical model and experimental data differed by approximately 4%. The results showed that the adjustment process of numerical model, including meshing, turbulence model, and determining boundary conditions was well done.

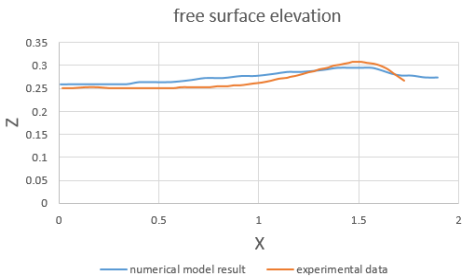

Figure1. Comparison of free surface between the numerical model and experimental data of Fuchs and Hager [1].

4. Numerical Model Validation for Shock Wave Run-up on Shore with Vegetation

At the next step, the movement of the solitary incident wave and its run-up on the shore with the presence of vegetation was modeled. The experimental data of Yao et al. [1] was used to evaluate the accuracy of model for the mentioned problem. The modeled coast has a slope of 1 to 8. The depth of water on the shore is 0.3 m and the height of the solitary wave is 0.06 m. Vegetation was simulated as vertical cylinders with a diameter of 1 cm and height of the 30 cm. The arrangement of simulated vegetation with experimental data is shown in figure 2.

As shown in figure 2, to compare the results of the numerical model with experimental data, the water level at station S4 (after the vegetation) is extracted from the numerical model. The comparison of free surface levels at this station between the results of the numerical model and experimental data was shown in figure 3. As can be seen from this figure, the FLOW3D numerical model was

successfully modeled the shock wave run-up on the gentle slope shore.

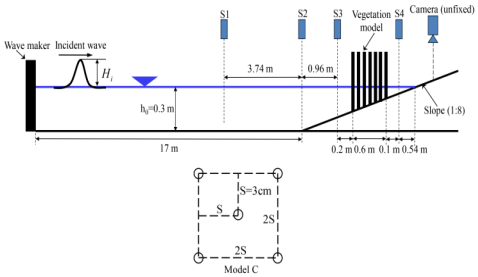

Figure 2. Experimental setup of shock wave run-up on shore with vegetation on the slope [2].

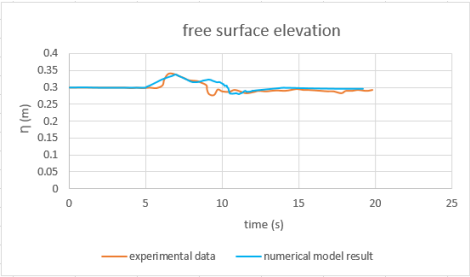

Figure3. Comparison of the free surface at S4 between the numerical model and experimental data of Yao et al. [2].

5. Conclusion

In the present study, one of the most important issues of coastal engineering, the movement of shock waves on the gently sloping shore, was studied numerically. The main purpose of this study was the evaluation of the accuracy of the FLOW3D numerical model for the simulation of the mentioned problem. Therefore, two laboratory tests, including coast without vegetation and with vegetation were selected. The results of this study showed that this model could be used to more accurately investigate the problem of shock wave propagation on vegetated beaches.

6. Acknowledgment

This research was supported by the Ports and Maritime Organization of I.R. of Iran.

7. References

[1] Yao, Y., Du, R., Jiang, C., Tang, Z., & Yuan, W. (2015). Experimental study of reduction of solitary wave run-up by emergent rigid vegetation on a beach. *Journal of Earthquake and Tsunami*, *9*(05), 1540003.

[2] Fuchs, H., & Hager, W. H. (2015). Solitary impulse wave transformation to overland flow. *Journal of Waterway, Port, Coastal, and Ocean Engineering*, *141*(5), 04015004.

NUMERICAL SIMULATION OF WIND AND WAVE IN THE STRAIT OF HORMUZ USING A COUPLED WRF-SWAN MODEL

Fatemeh Ameri [1], Sarmad Ghader [2] and S. Abbas Haghshenas [3]

1) Institute of Geophysics, University of Tehran, Tehran, Iran, Fatemeh.ameri@ut.ac.ir
2) Institute of Geophysics, University of Tehran, Tehran, Iran, sghader@ut.ac.ir
3) Institute of Geophysics, University of Tehran, Tehran, Iran, sahaghshenas@ut.ac.ir

1. Introduction

Reliable wave estimation in a complex body of water from a geographical point of view is a matter of high importance [1]. Main straits in the world, such as the Strait of Hormuz (SOH), are a major reference for this issue. Because of limited observations (in-situ, remote sensing, etc.) and measurement for such areas, employing wave simulations is a valuable option to understand wave climate variability.

Wave models strongly depend on the quality of wind field data. In the last two decades, many studies have been performed to analyze the accuracy of different wave and wind models and the sensitivity of wave predictions to wind fields in open ocean conditions [2] [3].

Interestingly, the conditions are different whenever the surface wind fields are affected by the presence of land use complexity. In such areas, the marine modeled surface wind speeds are often underestimated, with the bias depending on land-use complexity [1] .

The SOH is a particularly challenging region for atmospheric models. Because of the rugged mountain topography that lines both sides and closely borders the coast, climate conditions around the interesting area can vary spatially, and vary rapidly in time from the east to the west part of the strait, mainly when waves propagate into the central area of the strait. Some studies have been devoted to assessing the wind and wave climate in the SOH [4]. However, little attention has been given to wave growth under a developing wind field outflowing from a coast (land surface) and mountain. The mentioned studies are based on the ideal situation and do not consider orography complexity in the region.

This study investigates a wave simulation in the SOH using the wind data from the WRF (Weather Research and Forecasting) model for the SWAN (Simulating Wave Nearshore model) to generate a wave field. The result of the simulation for the wind speed, significant wave height, mean wave period, and mean wave direction are considered to compare against observations.

2. Methodology

The study focuses on investigating the variability and trends of wind speed (WS) and significant wave height (SWH) over the SOH.

WRF simulation with ERA-Interim as initial and boundary conditions (hereafter, WRFI) been used to simulate the wind field. Table 1 present the summery of physical parametrizations scheme used in this work and Figure 1 presents the computational domains of the WRF model covering PG and SOH.

Table 1. WRF model physics and dynamic options.

WRF model configurations		
Parameter	**Scheme**	**Reference**
Microphysic	**Lin**	**(Lin et al., 1983)**
PBL	**YSU**	**(Hong et al., 2006)**
Cumulus	**Kain Fritsch**	**(Kain, 2004)**
Short wave	**Goddard**	**(Chou & Suarez, 1994)**
Surface layer	**Revised MM5**	**(Jiménez et al., 2012)**
land Surface	**Noah**	**(Niu et al., 2011)**
Longwave radiation	**RRTM**	**(Mlawer et al., 1997)**

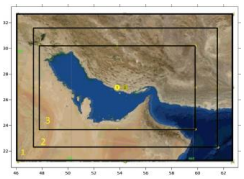

Figure 1. Configuration of the WRF parent domain (D01: resolution 0.25) and the two nested domains (D02: 0.1 resolution; D03: 0.03 resolution.

The SWAN cycle III version 41.31 employed for simulating wave. SWAN [5] which is based on an implicit propagation scheme and is suitable for simulating wave conditions in coastal and semi-enclosed environments.

The model was run in non-stationary mode with spherical coordinates and a time step of 2 min. The wave simulation period is from 19.01.2011 until 04.03.2011.

3. Result

Time series and the statistical parameters of simulated surface wind and Era5 data against the OSCAT for Jask station are given in Figures 2. The modeled surface wind speeds is underestimated as the bias is negative.

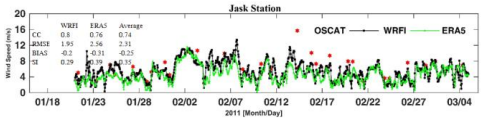

Figure 2. Comparison of the wind speed (m/s) from the scatterometer (OSCAT), WRFI and ERA5 wind data at Jask station.

Figure 3 and 4 show the time series of the modeled and measured wave for Jask and Larak stations. The comparisons show the model results using the WRF model winds are pretty good in estimating wave parameters compared to the ERA5 wind data at each stations. We find the Bias and RMSE (Root mean square), and SI (scatter index) are smaller for the Jask station in the eastern part. The CC (Correlation coefficient) is also better on the eastern side.

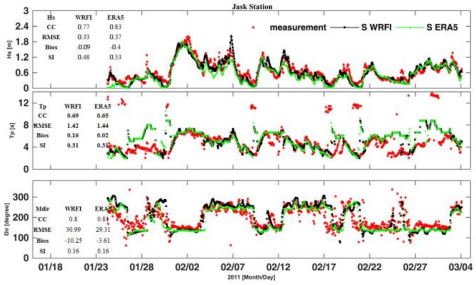

Figure 3. The significant wave height Hm_0 (upper panel), mean zero-crossing period Tm_{02} (middle panel) and mean direction (lower panel) obtained with S_WRFI (black square) and S_ERA5 (green diamond) Compare with observed (red star).

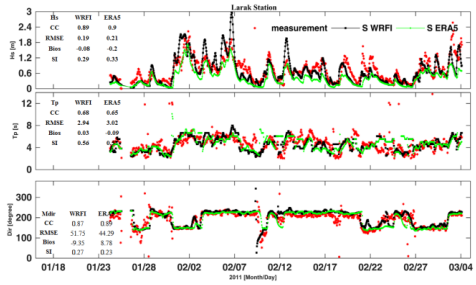

Figure 4. Evolution of the significant wave height Hm0 (upper panel), mean zero-crossing period Tm02 (middle panel) and mean direction (lower panel) obtained with S_WRFI (black sguare) and S_ERA5 (green diamond) Compare with observed (red star).

The scatter diagram of the distribution for Hs show that result of the hindcast model for Jask station (Figure 5) is reliable; large event wave (Hs >1.5) are accurately simulating apart from a slight underestimation of values between 1.5 and 2 m, and for Larak Station Wave S_WRFI show underestimation for the values less than 1 meter and overestimation for more than 1meter HS. For S_ERA5 there is underestimating in the whole simulating timeframe.

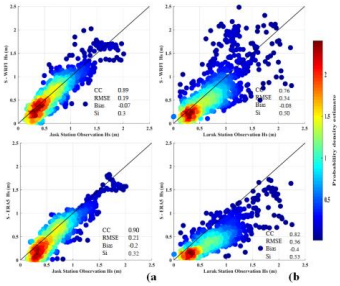

Figure 5. Wave height distribution versus the buoy measured data in left column for Jask station and right for Larak station. Darker marks include larger amounts of data. The result is shown from top to bottom for S_WRFI and S_ERA5.

4. Conclusions

The trend for wind speed compare with scatterometer observation shows a decrease in value of Bias moving to the east and west side with open areas. The Bias in stations near the coast and areas surrounded by orography (Larak station) were more significant than the one in the open sea (e.g. Jask station). The wind speed integrated from the atmospheric model in general is underestimated, and the Bias is negative both for ERA5 and WRF. Increasing the resolution (WRF) results in decreasing the Bias.

From our experience, the modeled wave and wind parameters for station in open sea (Jask) is in a better agreement with observations than the station with a fetch limit (Larak). At short fetches, the average Hs underestimate is 22% and the Bias decreases substantially moving southwesterly, wherein the open waters in front of the Oman Sea the value decreases to an average of 11%.

5. References

[1] Mariotti, G., et al., Biased wind measurements in estuarine waters. Journal of Geophysical Research: Oceans, 2018. **123**(5): p. 3577-3587.
[2] Bertotti, L., et al., Performance of global and regional nested meteorological models. Continental Shelf Research, 2014. **87**: p. 17-27.
[3]. Stopa, J.E. and K.F. Cheung, Intercomparison of wind and wave data from the ECMWF Reanalysis Interim and the NCEP Climate Forecast System Reanalysis. Ocean Modelling, 2014. **75**: p. 65-83.
[4] Haghshenas, S.A., et al., Iranian Seas Waters Forecast-Part I: An Improved Model for The Persian Gulf. Journal of Coastal Research, 2018(85 (10085)): p. 1216-1220.
[5] Booij, N., R.C. Ris, and L.H. Holthuijsen, A third-generation wave model for coastal regions: 1. Model description and validation. Journal of geophysical research: Oceans, 1999. 104(C4): p. 7649-7666.

STUDY OF WIND-WAVE CLIMATE CHANGES IN NORTH OF THE PERSIAN GULF USING MULTI-MODEL ENSEMBLE DATA OF CMIP5

Saeideh Baghanian [1], Mohsen Soltanpour [2]

1) Formerly, Civil Engineering Department, K.N. Toosi University of Technology, Tehran, Iran, baghanian@email.kntu.ac.ir
2) Civil Engineering Department, K.N. Toosi University of Technology, Tehran, Iran, soltanpour@kntu.ac.ir

1. Introduction

The sea state is the general condition of the ocean-free surface in a period between 0.5 hours to 6 hours, in which the energetic conditions are assumed to be uniform. Wave climate is the result of the long-term analysis of the sea state parameters such as the significant wave height, peak period, and mean wave direction at a specific location over a particular period. The spatial variability of the wave climate is in the order of 10 to 100 km in deep waters and about 100 m in near-shore areas of 10 to 30 m water depths. The wave climate is usually analyzed in annual periods, but it can also be examined monthly or seasonally [1].

The increase in the concentration of greenhouse gases and the consequent global warming is the driving force of climate change. The wind field, which is affected by the sea surface temperature, has a direct impact on wave characteristics [1]. Wave climate change can affect marine activities such as navigation and construction of coastal and offshore infrastructures [2]. It can also alter the shoreline and coastal flooding.

This study presents an analysis of wind and wave climate in the Persian Gulf (PG), using long-term CMIP5 multimodel ensemble results and CAWCR data collections, which derives global data for wave climate employing WAVEWATCH III [3]. The climate simulations are the outputs of global wind modeling under two future scenarios of greenhouse gas emission, i.e. RCP4.5 and RCP8.5, obtained from ensemble CMIP5 climate models.

2. Study Area

The PG is a shallow, semi-enclosed marginal sea, nearly 1000 km long water body located in the south of Iran with an average depth of about 36 m and a maximum depth of 170 m at its entrance, the Strait of Hormuz (Figure 1). The tide in the PG is very complicated, and the dominant pattern, i.e., primarily semidiurnal or diurnal, varies from one region to another [4].

The sea surface temperature of PG normally varies from 20 °C in February to 28 °C in November. The dominant wind over is Shamal wind which blows from the northwest with a speed up to 20 m/s. Shamal blows mainly during winters and summers. There are other winds such as seasonal southeasterly Kaus (Quas, Cowshee), which is most frequent between December and April. The Kuas wind is also called Sharki sometimes, especially more inland when it is turning dry and dusty. It is associated with the passage of winter depression and is often followed by a strong southwesterly wind, the Suahili.

Figure 1. Geography of the Persian Gulf.

3. Analysis of Wind and Wave Climate

The collected measurements, including winds at synoptic stations, Topex altimeter data of significant wave heights and buoy data at Bushehr and Asaluyeh stations are compared with winds/waves of ACCESS1.0 model subset of CMIP5 and CAWCR model outputs. CAWCR utilizes 3 hourly wind fields of global climate models and the linear interpolation of sea ice concentration on a monthly basis as data input for the WWIII wave model.

Figure *2* shows the spatial coverage of CAWCR data in the PG.

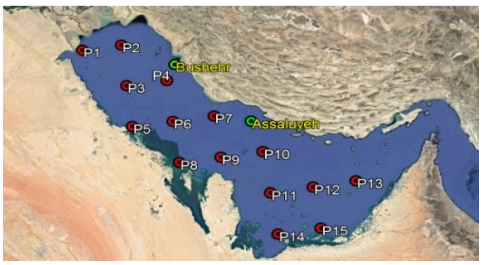

Figure 2. Spatial coverage of CAWCR data.

Figure 3 presents the comparison of global wind traits of ACCESS1.0 and 3-hour winds at Asaluyeh and Bushsher synoptic stations, using Cubic interpolation in climate Data Operation (CDO) to find the data at the desired locations. It is observed that the wind speedsof the climate model show lower values in both locations, in comparison to synoptic data. The study of model data in the mid-century (2026-2045) and end-century (2080-2099) shows that both significant wave height and peak wave period present lower values in the future, compared to the historical period (1980-2005).

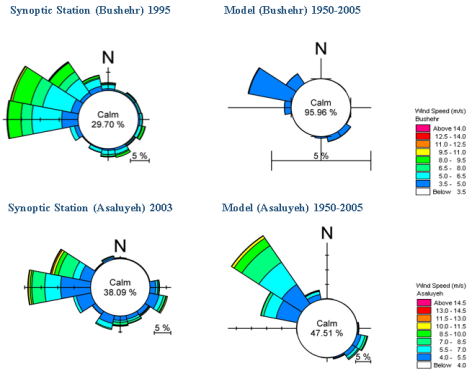

Figure 3. Comparisons of model wind roses and synoptic data at Asaluyeh and Bushsher (1950-2005).

The distance-weighted average remapping is employed to interpolate between CAWCR waves data, with 1°×1° spatial resolution, in the PG. Figure 4 shows the comparisons of model results and buoys data. Similar to wind outputs, the model is not able to simulate the dominant west direction at Asaluyeh. It is also observed that the modeled wave heights and wave periods are lower than the corresponding measured values. Moreover, three locations along five Topex tracks in the PG are selected for the comparison of model outputs with 6-hour satellite wave data. Figure 5 shows a sample comparison of time series at location (49.2, 28.9). It is seen that the model provides lower values than Topex measurements.

4. Summary and Conclusion

The present research aimed at the analysis of wind and wave data and climate change in the PG. Different comparisons revealed discrepancies between the model results and measurements. The poor agreement can be highly attributed to the low spatial resolution of model inputs, resulting in unreliable outputs. The downscaling of wind/wave outputs by developers does not provide accurate results without proper downscaling of model inputs. Unlike the large water bodies, winds in the enclosed PG are highly affected by surrounding lands and the mountains in the south part of Iran, which adds to the complexity of the wind field.

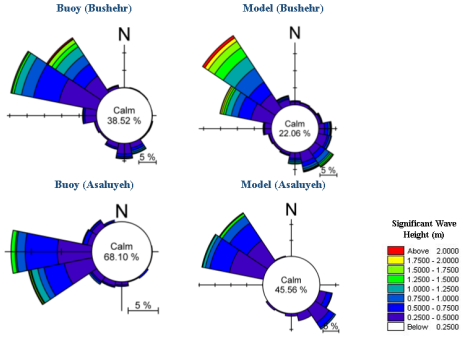

Figure 4. Comparisons of model wave roses (1980-2005) and buoy data at Asaluyeh (2003) and Bushsher (1995).

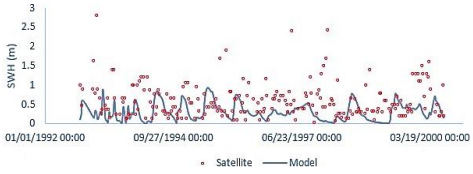

Figure 5. Time series comparisons between significant wave heights of Topex and model results.

5. References

[1] Méndez, F.J., & Rueda, A. (2020). *Wave climates: deep water to the shoaling zone.* Sandy Beach Morphodynamics, ch. 3.
[2] Lobeto, H., Menendez, M. & Losada, I.J. *Future behavior of wind wave extremes due to climate change*. Sci Rep 11, 7869 (2021). https://doi.org/10.1038/s41598-021-86524-4
[3] Hemer, Mark; Trenham, Claire; Durrant, Tom; Greenslade, Diana (2015): *CAWCR Global wind-wave 21st-century climate projections. v2. CSIRO. Service Collection*. https://doi.org/10.4225/08/55C991CC3F0E8
[4] Reynolds, R. M. *Physical oceanography of the Gulf, Strait of Hormuz, and the Gulf of Oman*. Marine Pollution Bulletin, 27(1993), 35–59.

14th International Conference on Coasts, Ports and Marine Structures
9 & 10 May 2023 , Tehran-IRAN
ICOPMAS 2022

NUMERICAL STUDY OF SOLITARY WAVE PROPAGATION ON SHORE WITH DIFFERENT SLOPES

Nematullah Zafarani[1], Rasoul Memarzadeh[2], Majid Dehghani[3]

1) Department of Civil Engineering, Vali-e-Asr University of Rafsanjan, Kerman, Iran, nemat.zafarani@stu.vru.ac.ir
2) Department of Civil Engineering, Vali-e-Asr University of Rafsanjan, Kerman, Iran, r.memarzadeh@vru.ac.ir
3) Department of Civil Engineering, Vali-e-Asr University of Rafsanjan, Kerman, Iran, m.dehghani@vru.ac.ir

1. Introduction

Flood management due to tsunami waves on the coasts is one of the most important issues in coastal management. A deep understanding of its effects will cause sustainable exploitation of the coast [1]. The tsunami wave behavior on the shore is influenced by many parameters, one of which is the shore slope. On the shore with a steep slope, the run-up occurs, while on the coast with a gentle slope, the tsunami wave breaks and propagates as the overland flow [2]. Therefore, solitary wave movement on the coasts has many details which understanding them requires widely numerical or experimental modeling.

2. Numerical Model

In the present simulations, the flow is considered an incompressible-viscose flow. The incompressible forms of 3D Navier-Stokes equations are applied to determine the flow parameters. In the present study, the powerful computational fluid dynamics (CFD) program Flow-3D is used. Flow3D solves the RANS equations using the finite volume formulation obtained from a rectangular finite difference grid.

3. Results

In this section, the propagation of the solitary wave, as a simplified tsunami wave, toward the coast and its interaction with it was modeled to study the efficiency and accuracy of the Flow3D model. The experimental data of Fuchs and Hager [3] was used to evaluate the accuracy of computations. In the study of Fuchs and Hager [3] different configurations were developed to study the effect of various parameters on solitary wave propagation on the shores. In the present study, among the experiments of Fuchs and Hager [3], three slopes for the shore were selected, including 11^0, 22^0, and 33^0. The depth of steel water was 0.2 m, and the height of solitary wave was 0.1 m. The schematic design of the models drawn in the FLOW3D software was shown in Figure 1.

The comparison between the computed free surface flows by the present numerical model and experimental data [1] for each of the models are shown in Figure 2 at time t = 5.7 s. It was seen that the flow patterns had prefect agreement with experimental data, and the FLOW3D numerical model has strong abilities for modeling of coastal engineering problems.

The quantified comparison of the essential features of the flow, including Maximum flow depth at the transition point (d_{max}) (i.e. the points which the overland flow has been formed) and the maximum propagation length on the shore (L_{max}) between experimental data and numerical results, was presented in Table 1. The comparisons demonstrated the ability of the present numerical model for the solitary wave flow model.

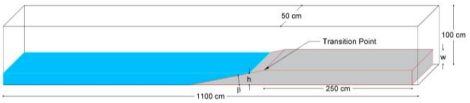

Figure 1. Schematic of geometry drawn in the FLOW3D numeric model.

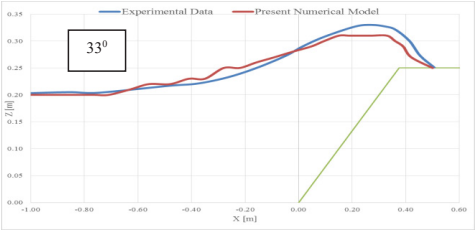

Figure 2 Comparison of free surface between the numerical model and experimental data of Fuchs and Hager [3] at t=5.7 s.

Table 1. Quantified comparison of hydraulic parameters between the numerical model and experimental data of Fuchs and Hager [3].

tanβ	h [m]	H [m]	L_{max} [m] Experimental	L_{max} [m] Numerical	Error	d_{max} [m] Experimental	d_{max} [m] Numerical	Error
11	0.2	0.1	0.314	0.330	5%	0.045	0.048	7%
22	0.2	0.1	0.310	0.301	3%	0.068	0.074	8%
33	0.2	0.1	0.270	0.283	5%	0.081	0.086	6%

4. Conclusion

In this paper, the FLOW3D numerical model was used to study the propagation of solitary waves as examples of tsunami waves on the coast. Using the numerical model on three different slopes, solitary wave motion was modeled on the coast. The modeling results show that on shores with a slower slope, the maximum propagation length of the wave on the horizontal shore will be longer. On the other hand, on shores with a steeper slope, the depth at the transition point will be greater. The results of the numerical model were in good agreement with the laboratory data.

5. References

[1] T. L. C. Vinodh and N. Tanaka, "A unified runup formula for solitary waves on a plane beach," Ocean Engineering, vol. 216. 2020, doi: 10.1016/j.oceaneng.2020.108038.
[2] Z. Zhai, Q. Hu, W. Ye, and H. Huang, "Analytical modelling of solitary wave diffraction from a V-shaped breakwater," Ocean Engineering, vol. 230. 2021, doi: 10.1016/j.oceaneng.2021.109014.
[3] Fuchs, H., & Hager, W. H. (2015). Solitary impulse wave transformation to overland flow. Journal of Waterway, Port, Coastal, and Ocean Engineering, 141(5), 04015004.

APPLICATION OF ERA5 WAVE AND WIND DATA IN THE ESTIMATION OF NEARSHORE CURRENTS AT NOWSHAHR PORT

Atena Amiri[1], Peyman Badiei[2], Gholam Reza Fazaee[3], Mohammad Hosein Nemati[4], Mohammad Bagheri[5]

1) Ph.D. Candidate, School of Civil Engineering, University of Tehran, Tehran, Iran, amiri.atena@ut.ac.ir
2) Associate Professor, School of Civil Engineering, University of Tehran, Tehran, Iran, pbadiei@ut.ac.ir
3) Khakbaft Consulting Engineers Company, Tehran, Iran, gh.fazaee.khakbaft@gmail.com
4) Ports and Maritime Organization, Coastal Engineering Department, mhn1982@gmail.com
5) Ports and Maritime Organization, Coastal Engineering Department, mbagheri@pmo.ir

1. Introduction

Estimation of nearshore currents in the vicinity of Nowshahr Port is an indispensable part of the study on the approach channel sedimentation of this Port which has become a major issue in recent years. Valuable hydrographic measurements have been carried out recently to obtain an insight into the sedimentation pattern in the channel and subsequent dredging endeavors to keep it navigable. The latest source of the available wave and wind estimates of this region goes back to the year 2013 when the Modelling and Monitoring studies of southern Caspian Sea coasts (MMCS) were implemented [1]. In the present study, more recent climatic data was required to be synchronized with available hydrographic measurements. ERA5 wind and wave data were applied and evaluated for the first time in this region [2]. The location of the focus of this study i.e. Nowshahr Port (Lat.: 36.65 degrees, Long.: 51.50 degrees) on the southern coasts of the Caspian Sea is illustrated in Figure 1.

Figure 1. Location of Nowshahr port

2. Wave Modelling Results

MIKE21 SW module was applied to obtain nearshore wave parameters taking ERA5 data as the offshore north boundary condition [2]. The computational domain and the applied mesh are shown in Figure 2. Modified wind data of the Nowshahr synoptic station was applied uniformly over the whole domain and the fully spectral nonstationary modeling approach was adopted.

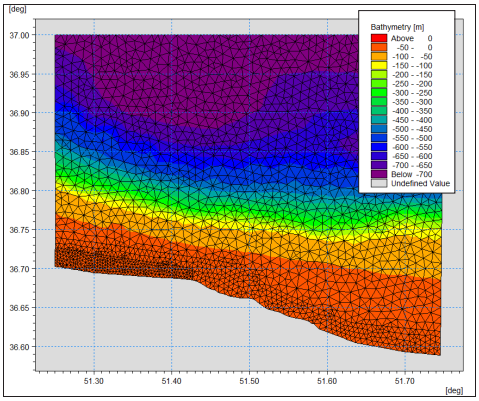

Figure 2. Grid and bathymetry in the wave model (includes 2109 nodes and 3998 elements)

As shown in Figure 3, a multiplication factor of 1.3 to ERA5 data was required to calibrate the modeling results with measured ADCP data at the site [1]. Nowshahr Synoptic data should also be corrected by an over-water to over-land wind factor. The ADCP wave measurements at the depth of 10 m near Nowshahr Port were acquired from MMCS measurements [1].

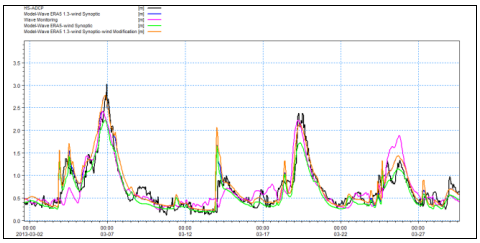

Figure 3. Comparison of modeling results of significant wave height in March (2013)

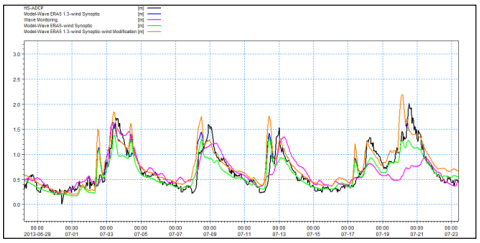

Figure 4. Comparison of modeling results of significant wave height in July (2013)

3. Flow Modelling Results

The numerical modeling of combined wave and wind-induced currents was carried out by the coupled Mike21-HD-FM package. An overview of the computational domain and mesh configuration is shown in Figure 5.

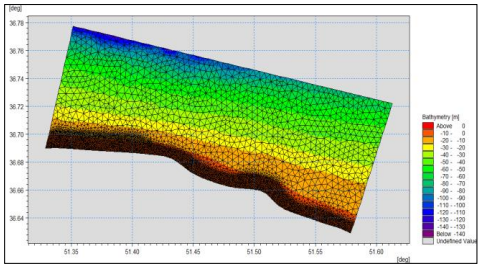

Figure 5. Grid and bathymetry in the flow model (includes 5890 nodes and 11319 elements)

Modeling results were calibrated against ADCP measurements at the depths of 5 and 10 meters close to the Port. These measurements were also performed through MMCS studies. For shallow coastal zone, up to a depth of 6 meters, Chezy bed roughness was taken as 40 $m^{1/2}/s$. In deeper water with a depth of more than 9 meters, this parameter was set as 65 $m^{1/2}/s$ Interpolated values were implemented for the depths in between. The wind friction coefficient was taken as 0.004.

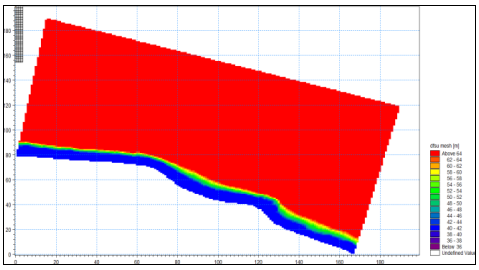

Figure 6. Chezy values- varying in domain

A comparison of modeling results of depth-averaged current speed with that of ADCP field measurements at two depths of 10m and 5m is illustrated in Figures 7 and 8.

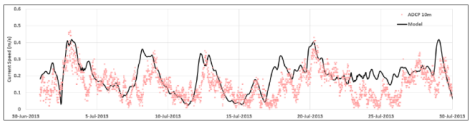

Figure 7. Comparison of modeling results of current speed with measured data (ADCP in depth=10m)

Figure 8. Comparison of modeling results of current speed with measured data (ADCP in depth=5m)

4. Conclusions

The present research aimed to investigate the applicability of large-scale ERA5 data to a site-specific study on nearshore hydrodynamics. It was concluded that:

- ERA5 data is a valuable source for such studies.
- Based on available field measurements, it is shown that the offshore wave heights of ERA5 need to be magnified by a factor of 1.3.
- A combination of onshore synoptic data and offshore ERA5 can considerably improve the performance of wind-generated wave modeling tasks.
- It is intuitively clear that the nearshore bed roughness is distinctly higher than the offshore one. This study made it quantitative so that a Chezy value of 40 $m^{1/2}/s$ was appropriate for shallow waters and a value of 65 $m^{1/2}/s$ for deeper zones.

5. References

[1] Monitoring and Modeling study of Northern coasts of Iran, Ports and Maritime Organization of Iran, 2015.
[2] https://cds.climate.copernicus.eu/cdsapp#!/dataset/reanalysis-era5-single-levels?tab=form-(ERA5 data)

INVESTIGATING THE EFFECT OF NAKHLE NAKHODA PIER (BANDAR ABBAS) CONSTRUCTION ON CURRENT PATTERN AND CHANGING TURBIDITY IN THE REGION AND PROCEDURE FOR TORBIDSHOOTING USING MODELING

Majid Zarezadeh[1]

1) Iranian National Standard Organization, Bandar Abbas, Iran, majid_zarezadeh_nu@yahoo.com

1. Introduction

The construction of coastal structures generally affects the natural process of sea-coast interaction and leads to changes in the hydrodynamics and morphology of the region. These changes in hydrodynamic arise from the imbalance between current factors and phenomena on the nature of the coastal region that has been formed over the years [1]. One of the structures that were made on the coast of Bandar Abbas over the past years is the Nakhle Nakhoda Pier. This Pier is located on the eastern side of the coast of Bandar Abbas in the position of latitude 27.1 degrees and longitude 56.3 degrees. Field visits, as well as sampling, show sedimentation around Nakhle Nakhoda Pier and swampy areas, on the other hand, the sedimentary beds of coastal areas are always affected by shear stresses caused by coastal currents. Also, due to the location of this area near the Strait of Hormuz, the current velocity in it is considerable. The purpose of this study is to investigate the effect of the construction of this Pier on the current in the region using the ROMS numerical model, evaluate the current conditions in the region.

2. Methodology

To measure the current velocity an ADCP device was installed on the south side of the Pier, at a distance of 500 meters from the jetty in the geographical position of 56.35 ° E and 27.16 ° N (Figure 1). It should be noted that after selecting the appropriate location, the ADCP was installed at a depth of 7 m and was measured for 30 days, taking into account the presence of two neap and spring in a period. Due to the depth of the area and changes in water level, an ADCP device with a frequency of 600 kHz was used [8]. To record the current in both x and y directions, the ADCP device settings were configured in 10-minute intervals in two layers with a thickness of 2 meters. Over a 30-day measurement period, more than 4300 current velocity data were obtained. The data required for the bathymetry of the region were obtained from the GEBCO (General Bathymetric Chart of the Ocean) database with a resolution of 2500 m by 2500 m, as well as the data of the National Cartographic Center of Iran, with a resolution of 500 m by 500 m. Other parameters, such as salinity, density, water turbidity, and temperature, were measured and monitored throughout CTD at 11 stations around Nakhle Nakhoda pier. ROMS numerical model was used to simulate the Pier and investigate the impact of its construction on the hydrodynamics of the region.

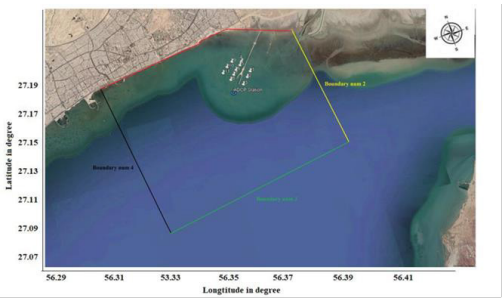

Figure 1. Location of ADCP installation station and monitoring location by CTD and simulation boundaries in ROMS model

To simulate the study area, a range of 5 km off the coast of Bandar Abbas was considered, and also a distance of 9 km perpendicular to the coast was considered, thus the model has a dry boundary on the coast of Bandar Abbas and three open maritime boundaries (Figure 1). Also, wet/dry capability was used for the ability to overlap near the land boundary and the place that is affected by tidal currents [10]. Tidal currents have different velocities and directions at various times. As expected, the maximum current velocity occurred at intervals of spring and the full moon. The flood current is to the north, the coast of Bandar Abbas, and the ebb current is to the southwest. CTD monitoring and sampling results show that the amount of turbidity in the east of Nakhle Nakhoda Pier is in the range of 9 to 12 NTU, while this amount has increased in the western part of the Pier and is in the range of 15 to 21 NTU.

3. Analysis of Simulation Results

To more accurately investigate the conditions in the area and how the construction of the Pier has affected the tidal current pattern and caused salinity and turbidity changes on both sides of the Pier as well as sedimentation in the area. The model was calibrated for 30 days with two scenarios, including Scenario (a) was implemented without

considering the Pier, and Scenario (b) was implemented with considering the Pier structure, the results of which are given in figure 2. After implementing the models and extracting the results with each other, it was observed that the general tidal current patterns before and after the construction of the Pier are completely different (Figure 2). The simulation output results for the average tidal current patterns are presented in Figure 2, which shows how the tidal current velocity is distributed on the coast of Bandar Abbas and around the Nakhle Nakhoda Pier.

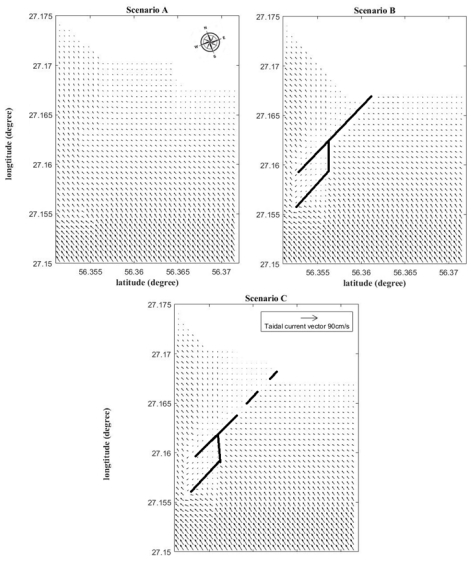

Figure 2. Average current pattern (A) without Nakhle Nakhoda Pier, and (B) with Pier, (C) with Nakhle Nakhoda Pier and canals

The simulation results show that the formation of a channel in the middle of the Pier has a good effect on changing the tidal current. This channel allows proper passage of seawater and thus reduces the number of suspended particles and sedimentation rate. According to the simulation (Figure 2.C), the creation of this channel increases 3×10^3 m^2 the amount of effective tidal surface and to some extent reduces the problem in creating this structure.

4. Conclusions

Field measurements showed that the turbidity in the western area of Nakhle Nakhoda Pier increases due to changes in magnitude and direction of tidal current, as this change leads to increased sediment mobility and suspended particles, resulting in increased turbidity in this region. The construction of the Pier and the change in the magnitude and direction of the tidal current in that area have increased the area of arid and inaccessible areas of the tidal current, and as the simulation time increases, this drying increases. A dramatic reduction in velocity in the Pier area and the horseshoe-shaped area, in addition to creating a suitable area for vessel traffic, will lead to a doubling of sedimentation in this area. A region in the western part of the Pier, salinity has decreased, which was not consistent due to the increase in turbidity and the direct relationship between turbidity and salinity. Because the tidal region is dominant, it seems that the construction of this structure and disturbing the nature of the current in that region has reduced the speed of the tidal current in the region and has been the main factor in increasing the coastline on the west side of the Pier. Comparison of the results of this research with similar articles shows that there is a good agreement between the work process and the output results.

5. References

[1] Bolanos R, Tornfeldt J V, Benetazzo A. Modeling Ocean currents in the northern Adriatic Sea. *Continental Shelf Research*. 2014;(87):54-72

[2] Hunter J.R, The physical oceanography of Persian Gulf, a review and theirical interpretation of previous observation, *First Gulf Conference on Enviroment and Pollution*. Kuwait 7-9 February 1982

[3] Azizpour Jafar, Siadatmousavi Seyed Mostafa, Chegini Vahid. Measurement of tidal and residual currents in the Strait of Hormuz. Estuarine, *Coastal and Shelf Science*. 2016;(178): 101-109

[4] Carpman N, Leilon M. MEASUREMENTS OF TIDAL CURRENT VELOCITIES IN THE FOLDA FJORD, NORWAY, WITH THE USE OF A VESSEL MOUNTED ADCP, *33rd International Conference on Ocean, Offshore and Arctic Engineering OMAE2014*, June 8-13, 2014, San Francisco, California, USA.

[5] Militello A, Hughes S A .Circulation Pattern at Tidal Inlets with Jetties. (2000), *US Army Corps of Engineers. 2000; ERDC/CHL CETN-IV-29*, September

[6] Masria A, Negm A, Iskander M, Saavedra O C. Numerical Investigation of the Impact of Jetties on Accretion Problem at Rosetta Promontory Egypt. *International Journal of Environmental Science and Development*, 2014; 5(6): 510-516

[7] Mueller D S, Wagner C R, Rehmel M S, Oberg K A, Rainville F. application of hydrodynamic, Measuring Discharge with Acoustic Doppler Current Profilers from a Moving Boat, 3 th ed, science *for changing word USGS*; 2013.p73-75

[8] Agoshkov.A.I, Ambrosi. D, Pennati.V, Quarteroni. A, Saleri. (1993), Mathematical and numerical modeling of shallow flow, *computational Mechanics* (1993) 11, 280-299

[9] Warner J C, Defne Z, Hass K, Arango H G. A wetting and drying sheme for ROMS. *Computer and Geosciences*, 2013;(58)54-61

[10] Togneri.A, Lewis.M, Neill.S, Masters.I. (2017), Comparison of ADCP observations and 3D model simulations of turbulence at a tidal energy site. *Renewable Energy*;(114) 273-282

RIP CURRENT MODELING AT SOUTHERN COAST OF THE CASPIAN SEA (CASE STUDY: WEST COAST OF BANDAR ANZALI)

Sajjad Gholami[1], Mohsen Soltanpour[2]

1) Civil Engineering, K. N. Toosi University of Technology, Tehran, Iran, sajjad.gholami@email.kntu.ac.ir
2) Civil Engineering, K. N. Toosi University of Technology, Tehran, Iran, soltanpour@kntu.ac.ir

1. Introduction

Rip currents, which are formed perpendicular to the shore, are among the important nearshore currents. They are effective in cross-shore sediment transport and can result in the change of seabeds and sand bars. However, these localized strong currents are particularly important for public safety as they flow away from the shoreline towards the sea and can be hazardous to swimmers.

2. Study Area

The Caspian Sea is the world's largest inland water, located in a semi-arid area between latitudes 36°-47°N and longitudes 47°-54°E. The basin is surrounded by five countries, i.e., Russia, Kazakhstan, Turkmenistan, Iran, and Azerbaijan (Figure 1). Three coastal provinces at its Iranian border are Gilan, Mazandaran and Golestan, from the west to the east.

Figure 1. Caspian Sea.

The green landscape of the south of the Caspian Sea is very popular among Iranian people as one of the main tourist destinations of the country for sightseeing and swimming. However, the recent data reveals that in average 46 people drown in the shores of Gilan province every year. The statistics show that 67% of the dead people in 2015 were trapped in rip currents, which reveals the necessity of definition and accurate modeling of rip currents. The rip currents at the west coast of Bandar Anzali in Gilan Province is studied in the present research, (Figure 2).

Figure 2. Study area at the west of Anzali Port in the southwest of the Caspian Sea.

3. Field Data

Shafiee Sabet and Barani (2011) measured the rip currents at the west coast of Anzali Port in 2008 and 2009 [1]. The gathered data includes bathymetry, wave characteristics and current velocities. Five GPS drifters were employed in a 700 (m) by 400 (m) area and a RCM9 flow meter was used to validate the current velocities. The submerged drifters moved far from the coast and then returned back to the shore, indicating the existence of rip current and a rotating cell in the area.

The wave characteristics was obtained from a buoy, installed 3 km offshore at 15 m water depth for the "Monitoring and Modeling studies of the southern Caspian Sea" project.

4. Numerical Modeling

The database of United States National Geophysical Data Center (NGDC) GEBCO is used for the general bathymetry of the global model [2]. This is combined with the data of hydrography survey for the modeling of nearshore areas of local model (Figure 3).

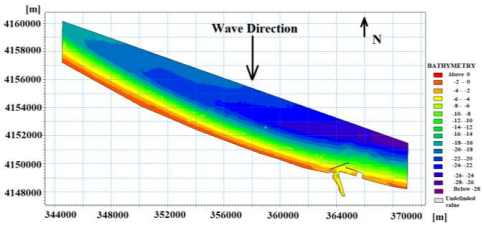

Figure 3. General bathymetry of the study area.

The wind field is extracted from reanalysis ERA-Interim data produced at the European Centre for Medium-Range Weather Forecasts (ECMWF) meteorological database.

MIKE 21 of Danish Hydraulic Institute (DHI, 2011) is selected for the hydrodynamic simulations of global and local models [3]. The unstructured mesh comprises 44490 nodes and 87410 elements with a grid cell size of 3000 m^2 that is decreased to 2000 m^2 and 1000 m^2 in intermediate and shallow areas, respectively (Figure 4). Modeling scenarios with different driving forces of wave and wind inputs are examined to investigate the formation and characteristics of rip currents in the study area.

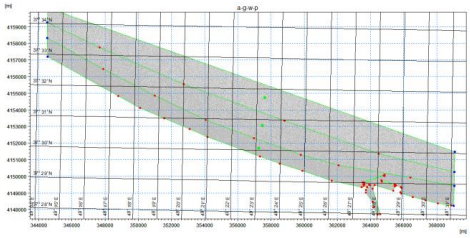

Figure 4. Computational grid.

Wave transformation is done by Spectral Waves (SW) model of MIKE 21. Table 1 presents the final input parameters for the calibration of SW model. The radiation stresses are introduced to the Flow module of MIKE 21 to simulate the nearshore currents. Table 2 offers the calibrated input variables to Flow model.

Table 1. The input parameters to SW model.

Bottom friction K_N	0.002
Wave breaking γ	0.8
White capping coefficient δ	0.8
White capping coefficient C_{dis}	2

Table 2. The input calibration parameters to Flow model.

Eddy viscosity	0.28
Bed resistance	38
Wind friction	0.0011

5. Results and Discussion

Figure 5 shows a time series of the favorable comparison between the modeled and measured longshore current velocities. Figure 6 shows the developed rip currents in the local model. Table 3 shows the overall comparison between the measured velocities and modeling results at different parts of the rip currents.

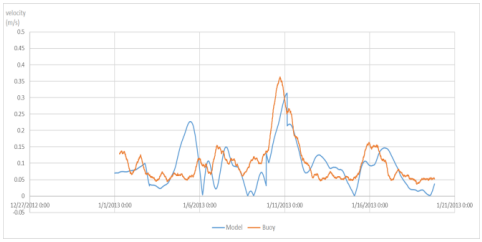

Figure 5. Comparison between the measured and modeled velocities of longshore current.

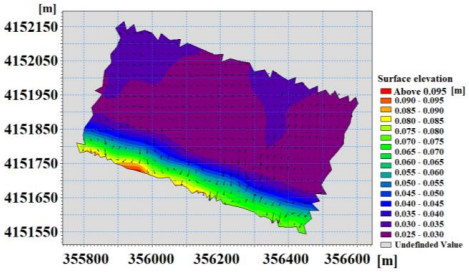

Figure 6. Water surface elevation and vectors of rip currents in local model.

Table 3. Measured and modeled velocities at different points of rip currents.

Velocity	Neck	Feeder	Head
Measured	0.30-0.72	0.12-0.35	0.12-0.35
Modeled	0.21-0.54	0.10-0.26	0.02-0.25

Comparisons of field measurements and modeling scenarios with different input driving forces, i.e., wind and wave, reveal that both wind-induced and wave-induced currents need to be carefully modeled for the successful modeling of rip currents at this area.

6. References

[1] Shafiei Sabet, B. and Barani, Gh. A., "*Field investigation of rip currents along the southern coast of the Caspian Sea", Journal of Scientia Iranica*, 18: 2011, pp. 878–884.
[2] Sandwell DT, Gille ST, Smith WHF (eds), "*Bathymetry from space: oceanography, geophysics, and climate", Geoscience Professional Services*, Bethesda, 2002, 24 p.
[3] Danish Hydraulic Institute (DHI) Water Environment, "*Mike 21 Spectral Wave, Mike 21 Flow model, Hydrodynamic Module User Guide*", 2012.

STUDY OF THE EFFECTS OF COASTAL STRUCTURES ON THE CURRENTS INSIDE THE BAY OF CHABAHAR USING COUPLED FLOW/WAVE MODELLING

Majid Samiee-Zenoozian[1], Mehrdad Shokatian-Beiragh[1], Masoud Banan-Dallalian[1], and Aliasghar Golshani[2]

1) Department of Water Resources Engineering, Faculty of Civil Engineering,, University of Tabriz, Tabriz, Iran, msamieezenoozian@gmail.com, m.shokatian.s@gmail.com, masoud.banan@hotmail.com
2) Faculty of Civil and Earth Resources Engineering, Islamic Azad University, Central Tehran Branch, Iran, ali.golshani@iauctb.ac.ir

1. Introduction

Urbanization requires an integrated strategy for land and environmental conservation, moving from maritime defense interventions focused primarily on protecting people and goods to coastal protection measures focused on the land [1]. Coastal protection structures such as groins, breakwaters, seawalls, and revetments have been constructed worldwide to limit the coastal erosion and to provide protection against hinterland flooding. In order to manage and control the effects of coastal structures constructed therein, a hydrodynamic study of the region is essential [2].

This study aims to characterize the complex nearshore process affected by coastal protection structures at Chabahar Bay using numerical modeling. Chabahar Bay is located in the southeast of Iran (Figure 1). Several coastal structures were constructed in Chabahar Bay during the last two decades. The change in mangrove forests (as an important ecosystem in this area) and the coastline there during this period highlight the effect of these man-made structures on the coastal process. In this study we address the complex current pattern changes due to the construction of the coastal protection structures after 2000.

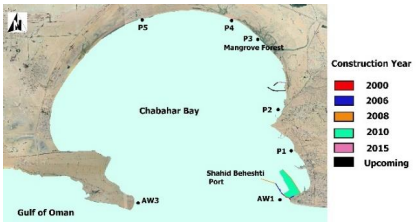

Figure 1. The study area location

2. Methodology

A methodological framework was established to evaluate the impact of man-made structures on current speed and direction in Chabahar Bay during last two decades. The framework focuses on boundary data preparation, coupling of wave and hydrodynamic models, and model calibration. To assess the impact of structures on the current (without affecting other factors), the model was run with same data of wave, wind, and hydrodynamic for each scenario of construction (data of Sept. 2006 used for simulation).

Hydrodynamic characteristics was simulated using a coupled MIKE 21 HD/SW (flow model/spectral waves) numerical model (the coupled model was used to consider wave-induced currents). The modeling system is based on the numerical solution of the two/three-dimensional incompressible Reynolds-averaged Navier-Stokes equations with Boussinesq and hydrostatic pressure as the underlying assumptions [3].

The numerical model extends 19 km offshore from the coastline, covering an area of approximately 200 km^2. The unstructured grid has 14,196 elements and 7366 nodes. The largest elements have a size of 0.4 km and they become finer towards the coast with the smallest approximately 3 m. The data collected from the instruments AW1 and AW3 (Figure 1) during September 1 to 30 (2006), were used as model boundary conditions (including current speed, current direction, water level, significant wave height, peak wave period, and mean wave direction). Meanwhile the model was forced by a 10 m wind field from ECMWF ERA5 dataset with a temporal resolution of one hour and a spatial resolution of 0.25°. In addition, the effects of eddy viscosity, bed resistance and Coriolis forcing on the flow field were considered.

3. Results and Discussion

Figure 2 shows the current patterns in Chabahar Bay based on the numerical models which were run in 2001, 2006, 2008, 2010, 2015 (years that man-made structures were constructed), and the eastern port development plan in the future. As shown in Figure 2, the construction of the coastal structures during the last two decades affects the current patterns in this area. Man-made structures were mostly built in the eastern part of this omega shape bay and so the eastern section of the bay has been more affected than the western part. The result of the current direction shows that the construction of coastal structures in the bay have changed the patterns of current direction all over Chabahar Bay, especially after 2010 (Shahid Behesti Port development- completion of phase 1).

Several optional points were chosen to study the hydrodynamic characteristics (Figure 1). Figure 3 depicts the time series of current speed in five selected nearshore locations in Chabahar Bay, as well as comparison of the maximum current speeds.

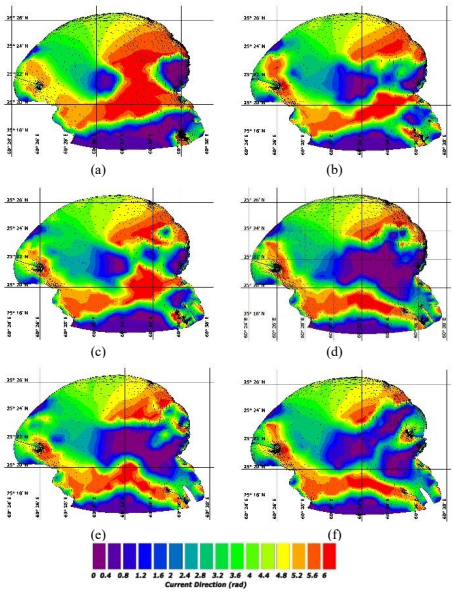

Figure 2. Current direction pattern in the Chabahar Bay. a) 2000, b) 2006, c) 2008, d)2010, e)2015, and f) future plan of the eastern port development

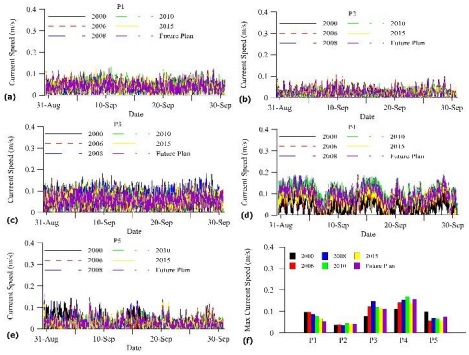

Figure 3. Time series of current speed in a) P1, b)P2, c) P3, d) P4, e) P5, and f) comparison of maximum current speed, during the last two decades

Based on Figure 3, after the construction of man-made structures in the bay, the maximum current speed has generally decreased over this time. The current speed at point P1 has decreased by 34% from 2000 to 2015 following development of the Shahid Beheshti Port and construction in the eastern part of the bay. Development of the Shahid Beheshti Port (phase 1) have reduced the maximum current speed at point P2. Despite that, due to the Shahid Behesti Port development (completion of phase 1 and phase 2), the current speed at this location has increased. However, the current maximum speed has not yet returned to 2000 levels. In contrast, the current speed trend at points P3 and P4 (in the bay's northeast) is distinct from that of the bay's eastern and southeastern parts. Due development of the Shahid Beheshti Port, the maximum current speed increased at these points. At the point P3, before the completion of Shahid Behesti Port development- phase 1 (2008), the current speed had increased by 83% on the 2000 value. However, as a result of the completion of Shahid Behesti Port development-phase 1 (post 2010), the maximum current speed has decreased, and by 2021 it had reached just 22% of its 2008 value. This is comparable to the trend in current speed at the point P4. The current speed at this point increased until 2010 and its value had risen by a factor of 1.43 since 2000. However, between 2010 and 2015, the maximum current speed has decreased by 9%. At point P5 (in the north of the bay), the current speed decreased by 23% from 2000 to 2015. The results of maximum current speed by consideration of the eastern port development plan in the future show that the current speed will be affected by this development. However, the maximum current speed will decrease at all optional points around the bay. The current speed in P1, P2, P3, P4, and P5 will reduced by 10%, 1%, 5%, 7%, and 1.5% compared to the 2015 scenario, respectively.

4.Conclusion

The hydrodynamics in Chabahar Bay has been affected by the construction of coastal structures over the last two decades. It seems that with the development of man-made structures since the year 2000, the current patterns have changed significantly. The results show that the maximum current speed in the southeast and north of Chabahar Bay has reduced over the last two decades, while the current speed in the east and northeast of Chabahar Bay increased between 2000 to 2010. This was due to the construction of the breakwater and the development of the port in the southeast of the bay. However, since 2010, by constructing the breakwater in the eastern part of the bay, the current speed has decreased in the eastern and north-eastern parts of the Chabahar Bay. The current speed will be affected by considering the eastern port development plan in the future so that the maximum current speed will decrease at nearshore around the Chabahar Bay.

5.References

[1] Banan-Dallalian M, Shokatian-Beiragh M, Golshani A, Mojtahedi A, Lotfollahi-Yaghin MA, Akib S. "Study of the Effect of an Environmentally Friendly Flood Risk Reduction Approach on the Oman Coastlines during the Gonu Tropical Cyclone (Case Study: The Coastline of Sur)." *Eng*, 2, 2, June 2021, pp. 141-55.

[2] Jäger, W. S., E. K. Christie, A. M. Hanea, C. den Heijer, and Thomas Spencer. "A Bayesian network approach for coastal risk analysis and decision making. "*Coastal Engineering,* 134, April 2018, pp. 48-61.

[3] Nigussie, T.A. and Altunkaynak, A. "Modeling the effect of urbanization on flood risk in Ayamama Watershed, Istanbul, Turkey, using the MIKE 21 FM model." *Natural Hazards*, 99, 2, November 2019, pp. 1031-1047.

EVALUATION OF THE EFFECTS OF WIND ON NEARSHORE CURRENTS AT NOWSHAHR PORT

Atena Amiri[1], Peyman Badiei[2]

1) Ph.D. student, School of Civil Engineering, Faculty of Engineering, University of Tehran, Tehran, Iran, amiri.atena@ut.ac.ir
2) Associate Professor, School of Civil Engineering, Faculty of Engineering, University of Tehran, Tehran, Iran, pbadiei@ut.ac.ir

1. Introduction

The present paper aims to evaluate the significance of wind-induced versus longshore waves generated due to the available current measurements carried out during the Modelling and Monitoring study of the southern coasts of the Caspian Sea (MMCS) [1], this research was performed in the vicinity of Nowshahr Port located at (Lat.: 36.65 degrees, Long.: 51.50 degrees), as shown in Figure 1. Delft3D open-source software was applied as a modeling tool for the present research.

Figure 1. Location of Nowshahr port in the Caspian Sea

2. Modelling Approach

The 2DH version of the Delft3D [2, 4] which solves the depth-integrated mass and momentum conservation equations on a curvilinear grid was applied. The coupled WAVE and FLOW modules are used to account for wave-induced currents [3]. This computational domain is composed of 89464 computational grids. Wave and wind data were obtained from MMCS studies [1]. The bathymetry of the computational and the grid configuration are shown in Figure 2.

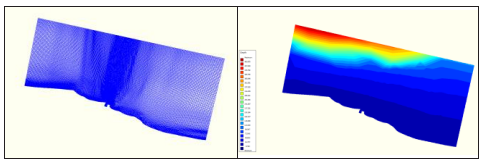

Figure 2. Computational grid and bathymetry

Based on the calibration of the simulated currents with field measurements, the Chezy coefficient of 40 was appropriate for the nearshore depths - up to 6 meters and a value of 65 for offshore depths – greater than 9 meters. A linearly interpolated value was applied for the depths, in between. Considering the above roughness values the simulated current speed versus the measured ones at two depths of 5 and 10 meters are shown in Figure 3.

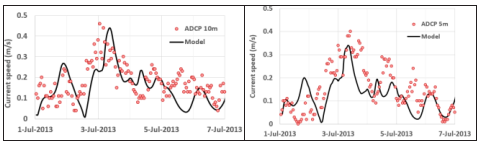

Figure 3. Comparing modeling results with measurement Data-Current speed (m/s)

Modeling results of waves at the same depths are compared with measured ones in Figure 4

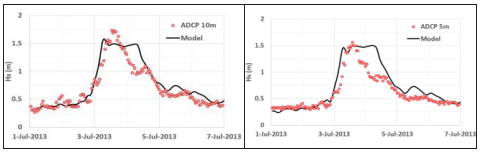

Figure 4. Comparing modeling results with measurement data- Hs (m)

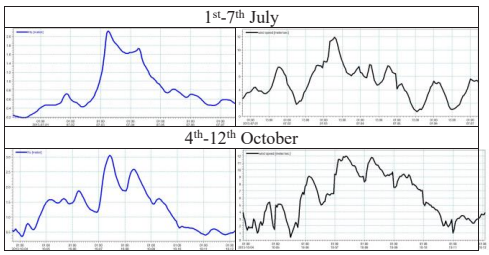

Figure 5. Significant wave height (m) and Wind speed (m/s) in models

Simulations were performed with the calibrated model for two storms at the intervals of 1st-7th July, and 4th-12th October 2013. Significant wave height at the offshore boundary of these simulations and wind speed are shown in Fig.5. For each of these time intervals, three modeling scenarios are considered as follows:

1) Only wave-induced current model
2) Only wind-induced current model
3) Combined wave and wind-induced current model

3. Results

Figure 6 shows the results of models at two depths of 5m and 10m located at the same points where previously mentioned measurements were performed. For the sake of illustrating the significance of wind-induced currents in this region, Figures 7 and 8 show the maximum values of current speed profiles during these storms along a line passing through the location of ADCP measurement stations for better understanding, Figures a. are zoomed in Figures b. For all the results shown below, the blue, black, and red lines represent; only wave, only wind, and combined wave and wind models, respectively.

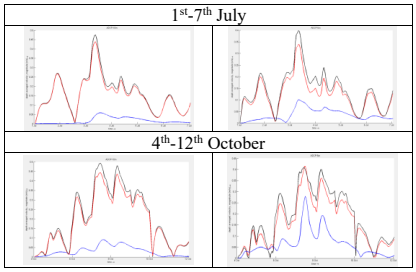

Figure 6. The results models-(ADCP-5m, ADCP-10m)

4. Conclusions

Figures 7 and 8 show the results of models in three different domains, in the surf zone (up to 5 meters), in the shallow zone (5-10 meters), and beyond 20 meters. Table 1 clearly shows the significance of wind-induced currents even inside the surf zone (more than 65%).

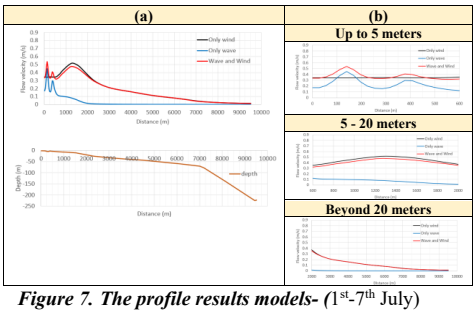

*Figure 7. The profile results models- (*1st-7th July)

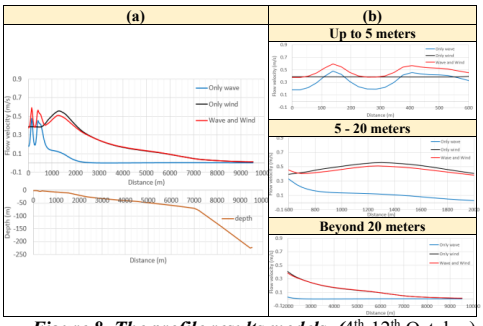

*Figure 8. The profile results models- (*4th-12th October)

Table 1. Percentage of the effects of wind and wave-induced currents

		1st-7th July	4th-12th October
Up to 5 m	Percentage of (V1/V3)	84 %	81 %
	Percentage of (V2/V3)	66 %	67 %
5 - 20 m	Percentage of (V1/V3)	26 %	64 %
	Percentage of (V2/V3)	109 %	109 %
Beyond 20 m	Percentage of (V1/V3)	4 %	7 %
	Percentage of (V2/V3)	105 %	106 %

V1= the maximum current speed in the only wave-induced current model
V2= the maximum current speed in the only wind-induced current model
V3= the maximum current speed in the combined wave and wind-induced current model

5. References

[1] Monitoring and Modeling study of Northern coasts of Iran, Ports and Maritime Organization of Iran, 2015.
[2] DELFT3D User Manual, Hydro- Morphodynamics, Deltares, October 1, 2017.
[3] DELFT3D User Manual, WAVE, Deltares, October 1, 2017.
[4] Lesser, G.R., Roelvink, J.A., Van Kester, J.A.T.M., Stelling, G.S., Development, validation of a three-dimensional model. Coast. Eng. 51, 2004, 883–915.

MULTI-OBJECTIVE SHAPE OPTIMIZATION OF MULTI-AXIS WAVE ENERGY CONVERTER

Alireza Shadmani[1], Mohammad Reza Nikoo[2], Amir H. Gandomi[3], Issa Al-Harthy[2] and Talal Etri[2]

1) Department of Maritime Engineering, Amirkabir University of Technology, Tehran, Iran, alireza.shadmani@aut.ac.ir
2) Department of Civil and Architectural Engineering, Sultan Qaboos University, Muscat, Oman, m.reza@squ.edu.om, aissa@squ.edu.om, t.etri1@squ.edu.om
3) Faculty of Engineering and Information Technology, University of Technology Sydney, Sydney, Australia, gandomi@uts.edu.au

1. Introduction

High energy potential is found in ocean waves. For this reason, many different types of wave energy converters (WECs) have been developed, with the purpose of designing devices with reduced costs and increased annual energy production (AEP). Design optimization offers the opportunity to explore more of the design space while avoiding expensive build and test iterations and it has been used to improve energy efficiency of a range of commercially developed systems.

From previous studies, it is known that one of the largest cost reduction potentials is associated with the WEC structure, i.e., hull. Apart from the high capital expenditure associated with the device hull, the geometry of the hull is crucial for the device hydrodynamic, and thus, for the AEP. A point absorber based on simple hull shapes using cylindrical geometries was studied by Gilloteaux et al. [1] to understand the effect of different control strategies on optimal device size.

The present work addresses this gap by finding a suitable and efficient optimization method for WEC geometry optimization. With this purpose, the geometry definition is studied. Different geometry definitions are compared; cylindrical, triangular, and octagonal shapes. In addition, two main objective functions, namely maximum power output and minimum construction cost are considered for a device oscillating in surge, heave, and pitch. A novel metaheuristic multi-objective optimization algorithm [2], i.e., multi-objective particle swarm optimization, is applied to discover optimal shape design in terms of radius, height, and draught.

2. Methodology

2.1. Multi-objective Particle Swarm Optimization

In 1995, Kennedy and Eberhart developed Particle swarm optimization (PSO), an algorithm inspired from swarm behavior such as exhibited in fish and bird schooling. To this end, one of the earlier attempts to solve multi-objective problems using PSO was made by Coello and Pulido using multi-objective Particle swarm optimization (MOPSO). The algorithms uses the concept of Pareto dominance to find solutions for multi-objective problems. It also employs a secondary population or external archive to store non-dominated solutions and guides the search of future generations. A special mutation operator is also implemented to improve the search procedure. MOPSO uses Pareto ranking scheme to handle multi-objective optimization problems. The algorithm store previously generated non-dominated solutions by recording the history of best solutions found by a particle.

2.2. Multi-axis WEC Shape Optimization

Obviously, most of the designed two-body point absorber (2B-PA) WECs generate energy from single mode of motion e.g., surge or heave. For this purpose, a design of multi-axis WEC could produce energy from multiple direction, like surge, heave, and pitch. In addition, different geometry of this 2B-PA was generated to compare its energy production and finding optimal design. The initial design of multi-axis WEC is illustrated in Figure 2.

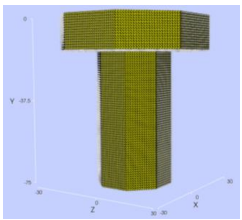

Figure 2. Design of multi-axis 2B-PA WEC

There are several design factors or characteristics that must be taken into account to determine the optimum geometry for any given WEC, including capturing highest wave energy from certain frequency range, wave direction effectiveness, and reducing extreme dynamic motion. For this reason, the objective function of geometry optimization was considered as maximum power output and minimum construction cost, which certainly focused on minimizing Levelized cost of energy (LCOE). A geometry database consist of cylindrical, triangular, and

octagonal shape has been created and employed in the MOPSO procedure. Additionally, the input of the optimization procedure was the wave energy spectrum based on the probability of occurrence of each sea state of a specified coastal region, which is depicted in Figure 3.

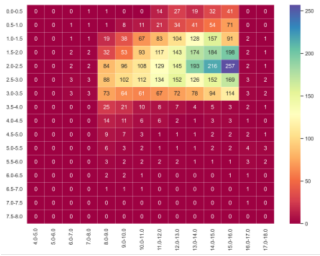

Figure 3. Probability of occurrence of sea state

3. Results

This study presents MOPSO to investigate the optimal design of a multi-axis two-body point absorber WEC. Different shape design, namely, cylindrical, triangular, and octagonal have been considered in this study to compare each shape annual energy production (AEP) in terms of volume surface. The dimension of radius varied between 1-35 m and height and draught was in the range of 1-18 m.

By solving dynamic equation of the floating body, the structural response of the device was obtained and the AEP and construction cost were calculated and compared.

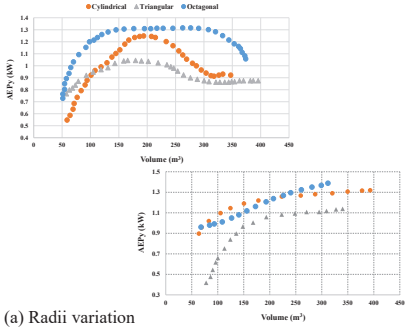

(a) Radii variation

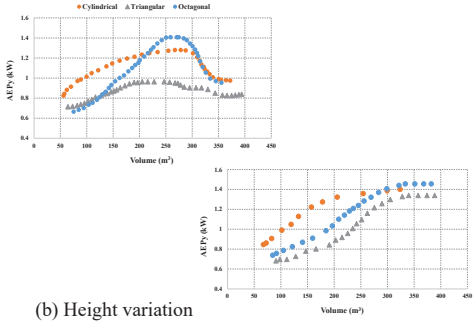

(b) Height variation

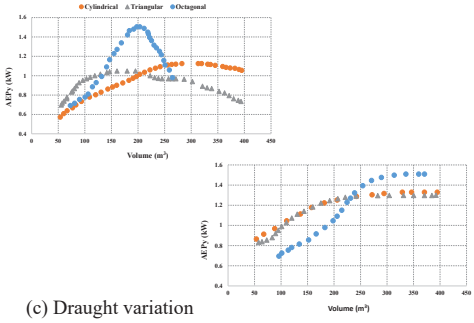

(c) Draught variation

Figure 4. AEP_y and Pareto front of cylindrical, triangular, and octagonal shapes

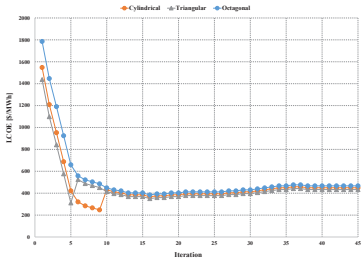

Figure 5. LCOE variation vs. iteration for cylindrical, triangular, and octagonal shapes

4. Conclusion

This research proposes multi-objective particle swarm optimization (MOPSO) framework for optimizing shape design of a multi-axis WEC considering different geometries. It has been shown that a novel model may be used to optimize wave power plants from a financial perspective, whereby minimizing the LCOE yields optimum solutions. The input used to determine the ideal geometry configuration was the annual wave energy spectrum. To this end, the optimal shape was the octagonal shape with radius of 29 m, height of 13.6 m, and draught of 16.3 m, respectively.

References

[1] J.-C. Gilloteaux and J. Ringwood, "Control-informed geometric optimisation of wave energy converters," *IFAC Proceedings Volumes*, vol. 43, no. 20, pp. 366–371, 2010.

[2] A. Shadmani, M. R. Nikoo, R. I. Al-Raoush, N. Alamdari, and A. H. Gandomi, "The Optimal Configuration of Wave Energy Conversions Respective to the Nearshore Wave Energy Potential," *Energies (Basel)*, vol. 15, no. 20, 2022.

WATER CIRCULATION OF CHABAHAR BAY

Alireza Bahmanzadegan Jahromi[1], Mojtaba Ezam[2], Hesam Taghi Abadi[1], Darush Askari[1] and Ahmad Dordizadeh[1]

1) Port and Maritime Authority of Hormozgan Province, Bandar Abbas, Iran, ar.bahmanzadegan@gmail.com
2) Marine Science Department, Faculty of Natural Resources and Environment, Science and Research Branch, Islamic Azad University, Tehran, Iran, ezam@srbiau.ac.ir

1. Introduction

Chabahar Bay (CB) is a semi-enclosed and shallow omega-shaped bay, located on the south-eastern coasts of Iran. Despite, some oceanographic expeditions in the CB, it seems necessary to have a reliable numerical simulation in order to better understand the water circulation of the Bay. Most of the previous studies conducted in the Chabahar region are about the hydrodynamic conditions, wind and storm effects on the region [1-4] and there is little knowledge about the physical properties and water masses formation in the Bay [5, 6]. In addition, a comprehensive spatial-temporal measurement is not available, most of the studies have a limited time frame and are limited to specific points and do not provide a three-dimensional and complete view of the circulation of the Bay. Few studies have been conducted on modeling the circulation of water in CB. For example, Soltanpour and Dibajnia (2015) examined tidal currents and water circulation in the Bay using the MISED model; they indicate that the tidal currents mostly enter the Bay at the eastern headland and exit at the western part. Hassannezhad, Soltanpour, and Haghighi (2011) [7] also investigated tidal currents in the Bay using the MIKE 21 model. They found that hydrodynamics of CB is complicated and dominated by tidal and wind driven current.

2. Material and Methods

The FVCOM model was employed to conduct the numerical experiments in CB. The computational domain of the numerical model covers the entire CB and part of the Oman Sea (25.00–25.45°N, 60.00–61.00°E). The computational domain consists of 3,397 nodes, 6,290 triangles (elements) and 10 uniform σ-layers. The horizontal grid resolution is between 5 km in the deep ocean to 500 meters in the interior of CB. The vertical resolution changes between less than 1 meter in shallow water to more than 50 meters in deep ocean. Results from the 1/12-degree global HYCOM model with 6-hour time steps were interpolated and used to determine the open boundary temperature and salinity at the 10 σ-layers. In addition, the 6-hourly NCEP Reanalysis_2 datasets were used for the calculations of the atmospheric fluxes at the surface of the model. The forcing data consist of u and v wind speed components (m/s), sea level pressure (Pascal), the rate of evaporation_ precipitation (m/s), heat fluxes (W/m^2) and air temperature (°K). The NCEP data have a spatial resolution of 2.5×2.5°. The Tidal Model Driver [8] was used to extract the water level at the open boundary. ETOPO1 bathymetry data with 1 arc-minute spatial resolution [9] was used for entire of the model domain, and field data with 100 meters' resolution from the Port and Maritime Organization was used for interior part of CB. The model domain and its bathymetry are shown in Figure 1. The FVCOM model was run for a twelve-year period from 2006 to 2017 in hydrostatic baroclinic mode.

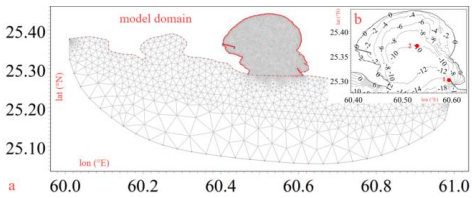

Figure 1. A) Model domain and b) Hydrography of CB versus (1) Tide Gauge Station and (2) ADCP Station.

The modelling results of the surface water level were compared with the measurement data from the Chabahar tide gauge (Station 1) for November 2016 (Figure 2 (a)). In order to validate the current velocity of the model, the model results were compared with ADCP (Acoustic Doppler Current Profilers) data for May 2007 (Figure 2 (b)). The tide gauge and ADCP data are provided by the Ports and Maritime Organization of Iran. The correlation coefficients between modeled results and measurements data for surface water level and current velocity are 0.99 and 0.84, respectively.

3. Results and Discussion

The average monthly of current velocity at the surface and bottom versus sigma-t values, related to February and August are shown in Figures 3. Also, a schematic of water circulation in CB is presented in Figure 4.

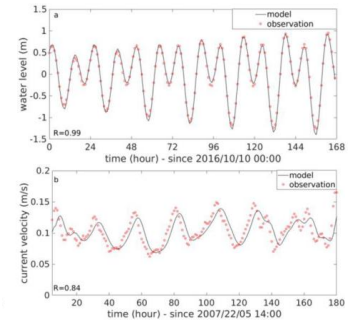

Figure 2. Comparison of model outputs (black lines) versus observed data (red circles) for a) water level and b) current velocity. R is correlation coefficient.

By comparing the monthly mean values of the current velocity at the surface and the bottom, two main patterns for water circulation can be distinguished (Figure 4). Almost at every month, the denser water of the Oman Sea from the bottom enters the Bay. In winter monsoon only one surface anticyclonic system is seen at the surface (Figure 4 (a)). In this season, the bottom inflows almost penetrate to the northern and western parts. In these parts, waters come to the surface and due to the existence of north-eastern winds in this season, southern and southwestern surface currents are created. Blowing the wind from the northeast at the winter monsoon creates a mixed layer in shallow waters of the north. In summer monsoon, due to the high north-south gradient of temperature, the bottom incoming waters, just penetrate to the middle parts of the Bay and there is a dominant anticyclonic system at the western parts and a weaker cyclonic system at the eastern parts (Figure 4 (b)). The southwestern winds at the summer monsoon cause upwelling in western regions and a mixed layer at shallow water of the north and east. The order of bottom inflow and surface outflow current related to the density gradient, are 2 cm/s and 4 cm/s, respectively.

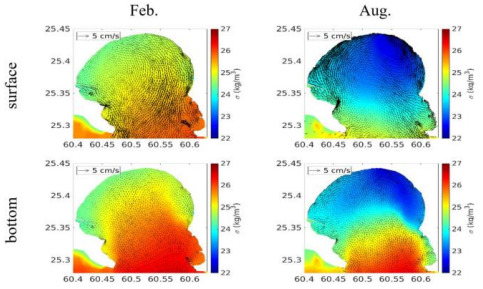

Figure 3. The mean monthly average of current velocity (cm/s) versus sigma-t (kg/m3) at surface (up) and bottom (down) for February (left) and August (right).

4. Conclusion

The most of the previous hydrodynamic studies of the CB have mainly considered the currents induced by tide and wind using barotropic models. Our finding of short time tidal circulation is consisting with their results. It is worth to note that the barotropic models cannot provide information about residual current induced by the density gradient, and the stratification effects of the water column. The 3D FVCOM model in baroclinic setup, with more accurate data as boundary conditions, may predicts current velocities in the interior of the Bay better than results of 2D MIKE 21 model and the 3D MISED model.

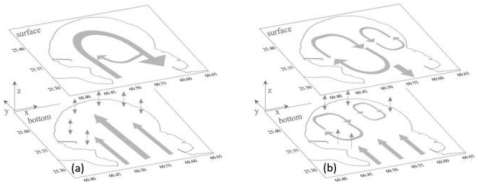

Figure 4. Schematic of CB circulation at the surface and the bottom, during: a) winter monsoon and b) summer monsoon.

5. References

[1] Soltanpour, M., and M. Dibajnia. 2015. Field measurements and 3D numerical modeling of hydrodynamics in CB, Iran. International Journal of Maritime Technology 3 (winter & spring):49–60.

[2] Payande, A. R., M. H. Niksokhan, and H. Naserian. 2015. Tsunami hazard assessment of CB related to megathrust seismogenic potential of the Makran subduction zone. Natural Hazards 76 (1):161–76.

[3] Saket, A., A. Etemad-Shahidi, and M. H. Moeini. 2013. Evaluation of ECMWF wind data for wave hindcast in Chabahar zone. Journal of Coastal Research 65:380–5.

[4] Akbarifard, S., H. Zarei, and E. Zalaghi. 2018. Hourly and daily prediction of sea wave height In the Chabahar area. Iranian Journal of Eco Hydrology 4 (4):1129–40.

[5] Komijani, F., V. Chegini, V. Banazadeh, and M. S. Sanjani. 2011. Study of changes physical parameters in Chahbahar Bay water in winter monsoon (2006–2007). Journal of the Earth and Space Physics 37 (4):195–216.

[6] Azizpour, J., V. Chegini, M. Khosravi, and A. Einali. 2014. Study of the physical oceanographic properties of the Persian Gulf, strait of Hormuz and Gulf of Oman Based on PG-GOOS CTD Measurements. Journal of the Persian Gulf 5 (18):37–48.

[7] Hassannezhad, M., M. Soltanpour, and S. Haghighi. 2011. 2D Hydrodynamic modeling and measurements of CB. Journal of Coastal Research 64nos. :1043–7.

[8] Padman, L. 2005. Tide Model Driver (TMD) Manual.

[9] Amante, C., and B. W. Eakins. 2009. ETOPO1 1 Arc-Minute Global Relief Model: Procedures, data sources and analysis. NOAA Technical Memorandum NESDIS NGDC 24.

14th International Conference on Coasts, Ports and Marine Structures
9 & 10 May 2023 , Tehran-IRAN
ICOPMAS 2022

EXPERIMENTAL STUDY OF REEF BALL UNITS PERFORMANCE IN SUBMERGED BREAKWATERS

Mohammad Hosein Golchin[1], Peyman Badiei[2], and Soroush Aliasgary[3]

1) School of Civil Engineering, College of Engineering, University of Tehran, m.hossein.golchin@ut.ac.ir
2) School of Civil Engineering, College of Engineering, University of Tehran, pbadiei@ut.ac.ir
3) School of Civil Engineering, College of Engineering, University of Tehran, Soroush.asgary@ut.ac.ir

1. Introduction

In recent years, the Reef Balls (RB) have been used worldwide to enhance the habitat quality of marine environment, as their shape, texture, and material are very attractive to marine life [1]. In the last two decades, in addition to using these units to enhance the marine environment, they have been used as submerged breakwaters in several projects to control coastal erosion. In this study, the performance of this type of submerged breakwater in wave energy dissipation and transmission coefficient has been studied through physical modeling. Considering the limited number of similar laboratory studies, new configurations have been designed, and physical tests were performed in the Hydraulic Laboratory of the School of Civil Engineering, University of Tehran. New configurations were designed to optimize the performance of these units as a submerged breakwater in terms of wave attenuation and transmission. In wide domains, data related to dimensionless variables based on structure width, water depth, wave height, and wave period were defined to fill the information gaps of previous experiments. With such a more comprehensive data set, a more reliable prediction of the performance of submerged breakwater made of RBs is achievable.

2. Previous Studies

Despite using RB units in various projects to protect beaches, there is still weakness in predicting their performance against wave action. Two studies have been reviewed to estimate the wave transmission coefficient of this type of breakwater in the past. The first study was conducted by Armono, H. D., and Hall, K. R. 2003. In this study, RB units were used with 1, 2, and 3 layers, which in some cases, they were placed on a base [2]. Another study was conducted to protect part of the beaches of Miami, Florida, USA, in which all the layouts had only one layer. These two groups of experiments were analyzed by Buccino et al. 2014, and predictive relationships were proposed [3]. Based on the results of the two previous groups of experiments, it was attempted to select the best arrangement of units in terms of application and performance against the wave action. Accordingly, new set of data have been added to the already available ones to complete the data set and enable achieving more comprehensive prediction equations.

3. Description of New Experiments

The experiments were performed in a wave flume with total length of 25.3 meters, width of 1 m, and height of 1.2 m. The distance between the wave paddle and the end of the flume was 24 m. The sides of the flume are made of glass. The bed was covered with a layer of impermeable concrete. As shown in Figure 1, the units were placed on top of a platform with a 0.41 height above the bottom connected to it with a 1:10 slope. The placement of the units and wave gauges are illustrated in the same Figure. Crushed stones were used as wave absorber at the end of the flume. To separate the incident waves from the reflected ones, six sensors were used in the experiments. Determination of distances and analysis of their results were performed according to the Mansard method.

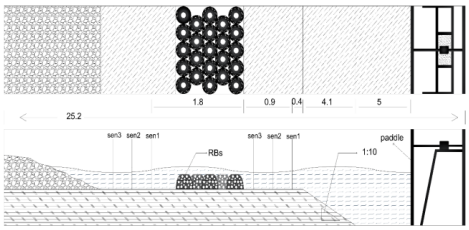

Figure 1. A view of experiments specifications

Since Goliath ball units in the RB category have suitable dimensions for use as submerged breakwaters and were also in the second group of experiments, this type of unit was used, in the present experiments with a scale of 1:10. The units had a dimension of 15 cm in height and 20 cm in diameter with 38 holes with diameters of 23 and 28 mm on their lateral surface. The weight of the units varied between 2.6 to 3 kg. The appearance of the units is shown in Figure 2.

Figure 2. A view of units made of RB type

In order to obtain sufficient information to examine the effect of structure width, 5 values, and to evaluate the effect of the ratio of structure height to water depth, 4 values for depth were examined. At each depth 3 values of significant wave heights and 9 values of peak wave period were considered. As a result, a total of 180 experiments were performed. Table 1 shows the experiments specifications including water depth, wave height and wave period for each width arrangements of units. It should be noted that the actual values of the wave heights and periods in these tests were slightly different from the target values mentioned in this Table.

Table 1. Specifications of tests in each arrangement of RBs

Structure width (m)	h (m)	T (s)	H_{si} (m)	d (m)
0.55-1.25	0.15	1 - 2.2	0.045-0.075	0.15
0.55-1.25	0.15	1 - 2.2	0.055-0.09	0.175
0.55-1.25	0.15	1 - 2.2	0.06-0.1	0.2
0.55-1.25	0.15	1.1 - 2.2	0.07-.011	0.225

4. Analysis and Conclusion

Four dimensionless parameters based on the results of these experiments were drawn as follows:

$$\frac{H_{st}}{H_{si}}; \frac{h}{d}; \frac{h}{B}; \frac{H_{si}}{gT^2}$$

where *Hst* and *Hsi* are respectively the transmitted and incident significant wave heights, h is the unit height, *d* is the water depth, *B* is the width of embedded units and *Tp* is the peak wave period. The variation of transmission coefficient, *Kt* (first parameter) was investigated against the other three while keeping two of them as constants.

Two samples of the results are illustrated in Figures 3 and 4. As expected, by comparing these two Figures, it is seen that the wave transmission coefficient increases by decreasing the relative height (*h/d*) of RB units. It is observed that at higher relative heights, the effect of the width change is more significant. It can thus be concluded that by decreasing the relative height of the units, the effects of the width become negligible.

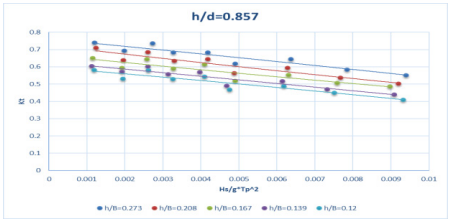

Figure 3. Test results based on different h/B at h/d=0.857

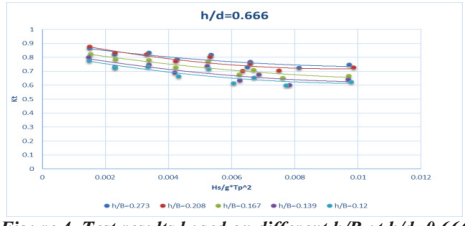

Figure 4. Test results based on different h/B at h/d=0.666

Armono, H. D., and Hall, K. R. 2003, came to the same conclusion and points out that if the height of the structure is less than 70% of the water depth, the effect of changing the width of the structure will be negligible [2]. It is also noted that by increasing the wave steepness (H_s/gT_p^2), the transmission coefficient decreases. This decrease is almost linear for higher relative heights. With the same water depth and relatively equal wave period, it is observed that increasing the wave height will reduce the transmission coefficient. Also, increasing the wave period increases the transmission coefficient at the same water depth and wave height. Carefully in Figure 4, contrary to expectations, it can be seen that in all layouts, the endpoint shows a higher transmission coefficient compared to their previous point. While the wave height is almost constant, and the wave period is smaller than its previous point. To justify this phenomenon, we can say that the amplitude of wave elliptical currents depends on the wave period. As a result, reducing the wave period at high immersion depths does not always reduce the wave transmission coefficient, and from somewhere, it increases the wave transmission coefficient.

5. References

[1] Reef Ball Foundation. 2008. "A step-by-step guide for grassroots efforts to reef rehabilitation" www.reefball.org.

[2] Armono, H. D., and Hall, K. R. 2003. "Wave transmission on submerged breakwaters made of hollow hemispherical shape artificial reefs." Proc., 1st Coastal, Estuary and Offshore Engineering Speciality Conf. of the Canadian Society for Civil Engineering, Canadian Society for Civil Engineering

[3] Buccino, M. Vita, I. D. and Calabrese, M. 2014. "Engineering Modeling of Wave Transmission of Reef Balls" Journal of Waterway, Port, Coastal and Ocean Engineering· July 2014. DOI:10.1061/(ASCE)WW.1943-5460.0000237

14th International Conference on Coasts, Ports and Marine Structures
9 & 10 May 2023 , Tehran-IRAN
ICOPMAS 2022

INVESTIGATING the EFFECT of BLADES HELICITY ON THE DARRIEUS TIDAL TURBINE EFFICIENCY

Soroush Sakhaei[1], Madjid Abbaspour[2]

1) Mechanical Engineering Department, Sharif University of Technology, Tehran, Iran, soroush.sakhaei@mech.sharif.edu
2) Mechanical Engineering Department, Sharif University of Technology, Tehran, Iran, abbpor@sharif.edu

1. Introduction

One of the prominent turbines for extracting energy from tidal currents is the Darrieus turbine. The geometric format of turbine blades plays an important role in the efficiency of these turbines. Darrieus turbines generally have straight blades. Another common format is the helical blade. For the first time in 1998, Gorlov made a Darrieus turbine with a helical blade and claimed that the efficiency of this turbine is higher than the Darrieus turbines with straight blades. [1] But by conducting experimental tests, Shiono et al. (2002) showed that the efficiency of the helical turbine is lower than the efficiency of the straight blades Darrieus turbine. [2]

Since there is no consensus on the effect of blade helicization on the efficiency of the Darrieus turbines, this research intends to investigate the effect of the helicization of blades on turbine efficiency with the help of computational fluid dynamics simulation. Two turbines with the same dimensions have been designed, one of which has three straight blades and the other has three helical blades. To create equal conditions for the two turbines under research, the distribution of the blades in the turbine area is done in such a way that the surface area in front of the flow is the same for both turbines. This area has a direct relationship with the input power to the turbine.

2. Methodology

In this research, the computational fluid dynamics method is used to obtain the characteristics of the flow around the turbines. The main equations governing the flow regime are the two equations of conservation of mass and conservation of momentum. To solve the governing equations, the Finite Volume Method has been used. For this purpose, OpenFOAM is used which is an open source CFD software. Since the purpose of the research is to compare a straight blade Darrieus turbine with a helical one, to reduce the size of the grid, a 1:10 scale of the turbines has been used. To model the turbulence, the k-ε model has been used, which is a subset of the RANS model. The value of parameter y^+ is set equal to 300. Based on this, five layers are considered around the turbine geometry, and the thickness of the first layer is equal to 0.00025. The grid contains one million cells. The dimension of the simulation domain and the external view of the grid are shown in Figure 1 and Figure 2, respectively.

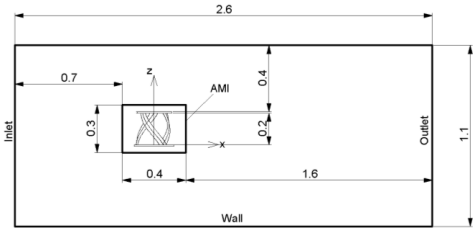

Figure 1. Dimension of the domain (Units:m)

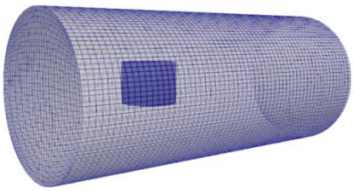

Figure 2. Grid external view

2.1 Simulation Strategy

To simulate the behavior of the turbine, two strategies are followed. In the first strategy, the turbine inside the water flow rotates around its central axis at a fixed speed given as the input of the domain. The second strategy is that the turbine is stationary at the first moment and the forces acting on the turbine from the water cause it to rotate. This strategy is called flow-induced rotation. In this research, the flow-induced rotation strategy is used. This strategy is close to the physics of a tidal turbine and can be used to obtain changes in angular velocity over time.

3. Results

For validation, laboratory data from a 2008 Darrieus turbine study by Hill et al. has been used. [3] The angular velocity diagram obtained from the simulation with the model used in this research and the angular velocity diagram obtained in the experimental research of Hill et al. are presented in Figure 3.

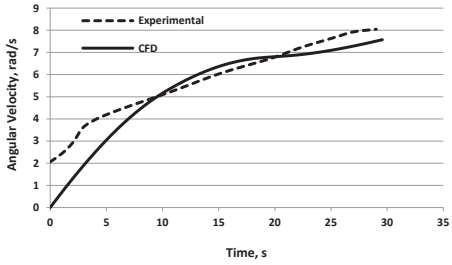

Figure 3. Simulated angular Vel. Vs. experimental tests

As it is clear from the diagram in Figure 3, the results of the simulation with the help of the model used in this research are in good agreement with the data obtained from the experimental tests. The average error obtained is 18%.

Equation (1) is used to estimate turbine efficiency. P_i is the input power and P_t is the output power from the turbine.

$$\mu = \frac{P_t}{P_i} \quad (1)$$

The input power is obtained from Equation (2) and the output power is obtained from Equation (3).

$$P_i = \frac{1}{2}\rho A V^3 \quad (2)$$

$$P_t = \omega T \quad (3)$$

In Equation (2), ρ is the density of water, A is the cross-sectional area of the turbine in front of the water flow and V is the velocity of the flow upstream. In Equation (3), ω is the angular velocity and T is the torque on the turbine.

The average diagram of the hydrodynamic efficiency of two Darrieus and helical turbines in terms of the tip speed ratio is shown in Figure 4.

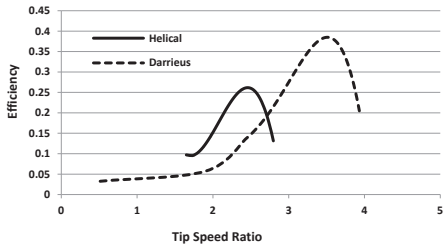

Figure 4. Efficiency of Darrieus Vs. Helical turbine

As shown in Figure 4, the maximum hydrodynamic efficiency of the Darrieus turbine is greater than that of the helical turbine. This data confirms the results obtained by Shiono et al.

In Table 1, the maximum hydrodynamic efficiency of the turbines is presented.

Table 1. T.S.R. per Max. efficiency

Turbine	Optimal T.S.R.[1]	Max. Efficiency
Helical	2.5	%26.2
Darrieus	3.5	%38.5

As it showed in Table 1, in the straight blade Darrieus turbine, the high-efficiency operation occurs at a larger tip speed ratio than the helical turbine. This is considered an advantage for this turbine. Because generators that convert mechanical energy into electrical energy generally need a high rotation speed, and the optimal performance of the turbine at a higher tip speed ratio requires a gearbox with a lower conversion factor. [4]

4. Conclusion

According to the results of this research, helicizing the Darrieus turbine blades does not increase its efficiency. Therefore, this research cannot confirm Gorlov's claim that the efficiency of the helical turbine is higher than that of the Darrieus turbine. So, the Shiono et al. research results are confirmed.

5. References

[1] A. M. Gorlov, "Helical turbines for the gulf stream: Conceptual approach to design of a large-scale floating power farm," *Mar. Technol. SNAME News*, vol. 35, no. 3, pp. 175–182, 1998, doi: 10.5957/mt1.1998.35.3.175.
[2] M. Shiono, K. Suzuki, and S. Kiho, "Output Characteristics of Darrieus Water Turbine with Helical Blades for Tidal Current Generations," in *Proceedings of the International Offshore and Polar Engineering Conference*, 2002, vol. 12, pp. 859–864, doi: ISOPE-I-02-133.
[3] N. Hill, R. Dominy, G. Ingram, and J. Dominy, "Darrieus turbines: The physics of self-starting," *Proc. Inst. Mech. Eng. Part A J. Power Energy*, vol. 223, no. 1, pp. 21–29, 2009, doi: 10.1243/09576509JPE615.
[4] A. L. Niblick, "Experimental and Analytical Study of Helical Cross-Flow Turbines for a Tidal Micropower Generation System," University of Washington, 2012.

[1] Tip Speed Ratio

PROJECTIONS OF SEA LEVEL HEIGHT THROUGHOUT TWENTY-FIRST CENTURY IN THE GULF OF OMAN USING A CMIP5 MODEL

Amirmahdi Gohari [1], Nasser Hadjizadeh Zaker [2]

1) School of Environment, College of Engineering, University of Tehran, Tehran, Iran, mahdi_gohari@ut.ac.ir
2) School of Environment, College of Engineering, University of Tehran, Tehran, Iran, nhzaker@ut.ac.ir

1. Introduction

Although there is natural variability in climate when measured over millions or billions of years, the speed of climate change has accelerated as a result of human activity [1]. These changes typically persist for an extended period, typically decades or longer [2]. One of the most serious and certain consequences of climate change is the increase in sea level height. Major concern is expressed for coastal regions of the planet where much of the world's population is found, because of the disastrous flooding that would follow from rapid melting or collapse of a major polar ice sheet [5, 8]. Using a combination of satellite altimeter data with the more traditional measurement of tide gauges, scientists have concluded that the sea level is rising globally, and that the rate of sea-level rise is likely to increase [7]. They have documented a direct relationship between climate change and sea-level rise through its two major contributors, which are the mechanisms of the expansion of water volume associated with ocean warming, and the absorption of more solar energy that accompanies the melting of glaciers and ice sheets [6, 8].

2. Material and Method

Assessment of sea level height variations due to climate change was carried out in 10 grid points alongside the Gulf of Oman (Figure 1). The Gulf of Oman is located in the north of the Indian Ocean and is connected to the Persian Gulf through the Strait of Hormuz. It borders Iran and Pakistan in the north, Oman on in south, and the United Arab Emirates in the west. Study of sea level rise on the Gulf of Oman is very necessary because of its inevitable association with flood risk, coastline changes and resulting threats to coastal cities and habitats.

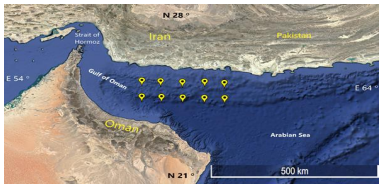

Figure 1. Location of Gulf of Oman in southern part of Iran between Persian Gulf and Arabian Sea

In this study a CMIP5 model, BCC-CSM1.1 (Beijing Climate Center) model with monthly temporal and 1° × 0.74° spatial resolution is selected for future projections. As the reference, the Global Ocean Gridded L4 satellite datasets from the Copernicus Marine Environment Monitoring Service (CMEMS) project covering all the globe with monthly temporal and 0.25° × 0.25° spatial resolution is selected. In order to perform comparisons, model and satellite datasets were interpolated onto the same grid as 1° × 0.5° using Climate Data Operator (CDO).

3. Results and Discussion

According to the satellite observation data presented in the Figure 2, the yearly mean sea surface height during the historical period for the satellite observation data is 61.92 cm. The highest sea surface height according to satellite dataset is 67.24 cm in year of 2015 and the lowest height is 57.57 cm in year of 2001. Within this period, the estimated rate of rise is 0.45 cm/year.

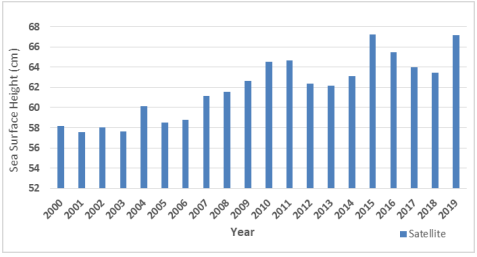

Figure 2. The satellite dataset for yearly mean sea surface height during the historical period

The projections of sea surface height during the first future period (2050-2070) under the RCP8.5 scenarios are depicted in Figure 3. In this period, the highest sea surface level is predicted for the year of 2052 with the 75.53 cm and the lowest height belongs to the year of 2062 with 64.64 cm. The average sea level height for the first future period is predicted 71.93 cm and compared to the historical period with 61.92 cm, it shows a rise of 10.01 cm. Within this period, the estimated rate of rise is 0.14 cm/year.

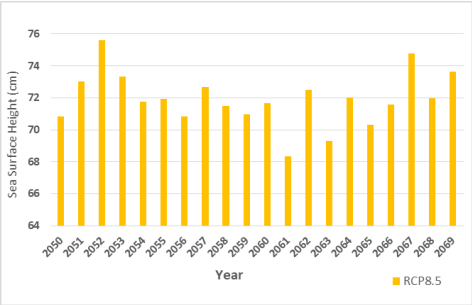

Figure 3. Projections of sea surface height during the first future period

The projection of sea surface height during the second future period (2080-2100) under the RCP8.5 scenarios are represented in Figure 4. In this period, the highest sea surface level is projected for the year of 2096 with the 82.64 cm and the lowest height is belonging to the year of 2082 with 73.51 cm. The average sea level height for the first future period is predicted 78.43 cm and compared to the historical period with 61.92 cm, it shows a rise of 16.51 cm. Within this period, the estimated rate of rise is 0.21 cm/year.

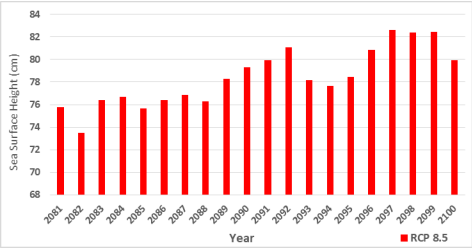

Figure 4. Projection of sea surface height during the second future period

Summary of the different period's analysis is in the Table1.

Table 1. Summary of sea surface height during different periods (cm)

Period	Time Slice	Average Height	Max	Min	Rise rate within the period (cm/year)
Historical	2000-2020	61.92	67.24	57.57	0.45
First Future	2050-2070	71.93	75.53	64.64	0.14
Second Future	2080-2100	78.43	82.64	73.51	0.21

4. Summary and Conclusions

In this study, using a CMIP5 model, Sea Level Height were projected for two 20-year future periods over the Gulf of Oman under RCP8.5, the highest emission scenario and the results were compared to the historical satellite observation datasets of the 2000-2020-time period. In the historical period, the average sea surface height was estimated 61.92 cm and the highest value is shown in the year 0f 2015 with 67.24 cm and the lowest one is for the year 2001 with 57.57cm. Within this period, the estimated rate of rise is 0.45 cm/year. In the first future period (2050-2070), the height of sea was estimated averagely 71.93 cm. Therefore, compared to the historical period, in the first future period an increase of 10.01 cm is predicted. The rise rate of sea height is expected to be 0.14 cm/year. In the second future period (2080-2100) the average height of sea is anticipated 78.43 cm. Thus, the sea surface rise is forecasted 16.51 cm and the average rise rate within this period is calculated 0.21 cm/year.

5. References

[1] R. Palm and T. Bolsen, "The Science of Climate Change and Sea-Level Rise," in Coastal Research Library, 2020.
[2] IPCC, "Part A: Global and Sectoral Aspects. (Contribution of Working Group II to the Fifth Assessment Report of the Intergovernmental Panel on Climate Change)," Clim. Chang. 2014 Impacts, Adapt. Vulnerability. 2014.
[3] I. IPCC Working Group 1 et al., "IPCC, 2013: Climate Change 2013: The Physical Science Basis. Contribution of Working Group I to the Fifth Assessment Report of the Intergovernmental Panel on Climate Change," IPCC, vol. AR5, 2013.
[4] C. B. Field et al., Climate change 2014 impacts, adaptation and vulnerability: Part A: Global and sectoral aspects: Working group II contribution to the fifth assessment report of the intergovernmental panel on climate change. 2014.
[5] V. Prescott, "Sea Level Rise: History and Consequences (Bruce C. Douglas et al. (eds.))," Int. J. Mar. Coast. Law, 2001, doi: 10.1163/15718080120493173.
[6] M. F. Meier *et al.*, "Glaciers dominate eustatic sea-level rise in the 21st century," *Science (80-.).* 2007, doi: 10.1126/science.1143906.
[7] D. R. Cayan *et al.*, "Climate change scenarios and sea level rise estimates for the California 2008 climate change scenarios assessment," *Calif. Clim. Chang. Cent.*, 2009.
[8] E. P. Maurer and H. G. Hidalgo, "Utility of daily vs. monthly large-scale climate data: An intercomparison of two statistical downscaling methods," *Hydrol. Earth Syst. Sci.*, 2008, doi: 10.5194/hess-12-551-2008.

INVESTIGATION OF TIDAL INTRUSION IN BAHMANSHIR AND ZOHREH ESTUARY

Mohammad Hadi Moeini[1], Ebrahim Jafari[2] and Majid Jandaghi Alaee[3]

1) PhD in Coastal Eng., Pouya Tarh Pars Cons. Eng. Company, Tehran, Iran, mhmoeini@gmail.com
2) PhD in Hydraulic Eng., Water and Wastewater Co., Tehran, Iran, jafari.hydrostructure@gmail.com
3) PhD in Coastal Eng., Pouya Tarh Pars Cons. Eng. Company, Tehran, Iran, m.j.alaee@ptpco.com

1. Introduction

An estuary is a partially enclosed coastal body of brackish water with one or more rivers or streams flowing into it, and with a free connection to the open sea [1]. Estuaries form a transition zone between river environments and maritime environments and are an example of an ecotone. Estuaries are subjected both to marine influences such as tides, waves, and the influx of saline water, and to fluvial influences such as flows of freshwater and sediment. Therefore, estuaries are among the most productive natural habitats in the world [2].

The estuaries are the dominant geographical landforms in the coastal zones of Khuzestan province of Iran. Two of the most important ones of them are Bahmanshir and Zohreh estuaries. Bahmanshir estuary was actually one of the branches of Karun River. The Karun River is split into two branches in Khorramshahr city: one leads to Arvand River through the Hafar channel and the other flows in Bahmanshir. Bahmanshir flows nearly parallel to the Arvand River towards the Persian Gulf, passing through the cities of Abadan and Choebdeh. The Bahmanshir River is about 90 km long and its width varies from 60 m in upstream to 450 m in the mouth. In the past, Bahmanshir was connected directly to Arvand River through the Hafar Canal, while nowadays that entrance is physically blocked and the water enters from Karun River by pumping through the Mared canal.

The Zohreh estuary is the other important estuary in the region. It collects the waters of a vast areas of Ardakan, Noorabad Fars, southern Doganbadan, Behbahan and Handijan and then flows into the Persian Gulf. Fishing and aquaculture is considered as one of the main jobs of the residents along the riverside. Therefore, there are several traditional fishery landing sites and small ports along the river. The length of the estuary from the Persian Gulf to the upstream of its main branches is more than 400 km, but only the first 60 km is navigable for commercial and fishery ships due to the limitation in the river depth.

The hydrodynamic condition of these estuaries is important due to the important ports that located in them and also commercial and fishery exploitations of these water bodies. The Choebdeh and Qofas ports in Bahmanshir estuary and Sajaafi commercial and fishery ports in the Zohreh are among the most important active ports in this region. The studies of tidal hydrodynamics in these rivers, not only provides essential data for the operation of existing coastal structures and ports, but also helps to proper recognition of natural state of the river and provide basic information for other studies.

Figure 1. The location of Bahmanshir (up) and Zohreh (down) in the coasts of Khuzestan province of Iran.

The Iranian Port and Maritime Organization (PMO) initiated a project, led by Pouya Tarh Pars Consulting Engineers to study the hydrodynamics of these estuaries. Limited previous studies have been performed to study these water bodies, however in this study, the tidal hydrodynamics of them are investigated by numerical simulations applying new accurate hydrography and also water level measurements (which also performed in this project).

2. Study Area and Employed Data

The study area for the Bahmanshir estuary includes the total length of it from Mared canal to the end of the estuary at Persian Gulf. For the Zohreh estuary on the other hand, the navigable part of the estuary (from the Persian Gulf to about 50 km upstream) is considered for the simulation.

The coast line was extracted from satellite images, considering the pictures that taken at the time of highest tidal level. For the river depth data, hydrography with a scale of 1: 10,000 has been performed in the present project. It should be noted that more accurate hydrographic data with a scale of 1:1000 was also available and used for certain areas such as Sajaafi port.

The water level data were used for the calibration and verification of numerical model results. Observations have been performed as a part of this study in different locations of both Bahmanshir and Zohreh estuaries which has shown in Figure 1. The measurements have been performed using tide gauges for about one month in 2017.

3. Simulation and Results

In this study, 2D simulations of tidal flow in the estuaries were performed using MIKE21 flow model. A combination of triangular and quadrangular mesh was used for the simulation, in which the river mouth and some irregular curve areas of the river spatially discretized using triangular meshes while for the main river body quadrangular mesh was used.The boundary condition for the downstream of the estuaries was defined as the predicted water level using tidal constituents extracted from measurements. For the upstream, the discharge of 60 m^3/s and 85 m^3/s has been used based on the previous measurements for Bahmanshir and Zohreh, respectively.

As mentioned, the model was calibrated and verified by comparing the results with water level observations. Figure 2 and Figure 3 show the comparison of the model water level results with the observations in different stations at Bahmanshir and Zohreh, respectively. It can be seen that the performance of the model for the simulation of water level is quite accurate. The average of correlation coefficient for the results in various stations is 0.96.

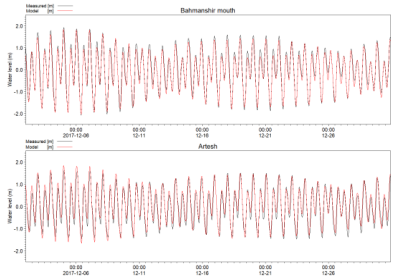

Figure 2. Comparison of the model water level results with the measurements of tide gauges (observed in this study) in Bahmanshir estuary.

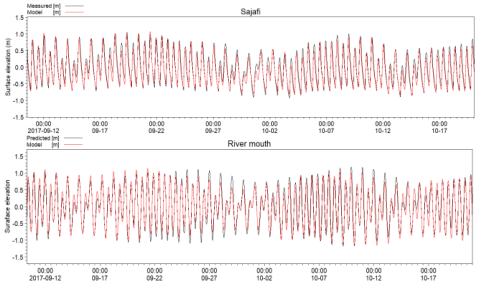

Figure 3. Comparison of the model water level results with the measurements of tide gauges (observed in this study) in Zohreh estuary.

The streamwise profiles of the minimum, average and maximum water level along the estuaries from the mouth to the upstream are shown in Figure 4. These profiles are extracted based on a one-year simulation. According to the figures, the water intrudes from the Persian Gulf into the whole of the river length for Bahmanshir and the whole of study area in Zohreh and the tidal variation of the water level can be seen in the upstream of the both estuaries. By moving from the mouth to the upstream, the difference between the minimum level and the maximum level decreases. It should be noted that this difference does not necessarily mean the tidal range of the region, because the maximum water level may occur on a different day than the minimum water level.

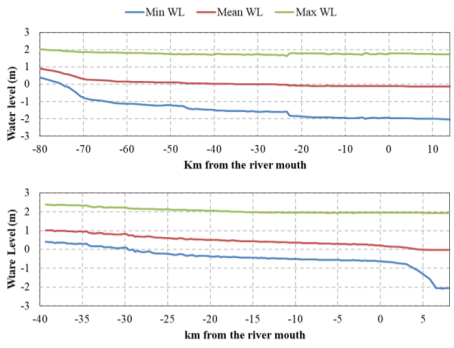

Figure 4. The streamwise profiles of the min, mean and max water level along the estuaries from the mouth to the upstream (up: Bahmanshir, down: Zohreh).

4. References

[1] Pritchard, D.W. “What is an estuary: physical viewpoint.” American Association for the Advancement of Science Publication, Vol. 83. Washington, DC., 1967, pp. 3–5.

[2] McLusky DS, Elliott M. “The estuarine ecosystem: ecology, threats and management”. Oxford University Press; 2004 Apr 29.

PREDICTION OF SHORT-TERM CASPIAN SEA LEVEL USING ARTIFICIAL NEURAL NETWORK

Nikta Iravani[1], Peyman Badiei[2], Mohammad Hosein Nemati[3] and Mohammad Bagheri[3]

1) Khakbaft Consulting Engineers, Tehran, Iran, nikta.iravani@ut.ac.ir
2) School of Civil Engineering, College of Engineering, Tehran, Iran, pbadiei@ut.ac.ir
3) Ports and Maritime Organization, Coastal Engineering Department

1. Introduction

Sea level is a key factor in port planning, coastal protection and dredging projects. Caspian Sea, being the largest lake in the world, has experienced considerable fluctuations during the last two decades, exceeding 3 m. The overall trend is decreasing. Global warming leading to decrease in rainfall and river discharges, and increase in evaporation is one of the main factors of declining closed lake levels. Excess water use due to agricultural and industrial growth is another important reason for falling of the Caspian Sea level.

There are several ports around the Caspian Sea which play an important role in transportation and economic trade. Having a reliable estimate of the sea level in the coming years is essential for the operation and development of these ports. Researches have been carried out to estimate long-term and short-term fluctuations of the Caspian Sea ([1] - [4]). In the current paper, Artificial Neural Network (ANN) is used to predict the Caspian Sea level for the next 10 years based on the available time-history of the sea level. This research was done as part of the project undertaken by Khakbaft Consulting Engineers for the Ports and Maritime Organization.

2. Method

The longest record of the Caspian Sea level is available at the Baku station in Azerbaijan starting at 1837. This data has been used as the basis of the current analysis. It should be noted that the sea level at Baku station is measured with respect to the Baltic Sea, i.e., -28 m. The time series of the Caspian Sea level during 1837-2021 is shown in Figure 1.

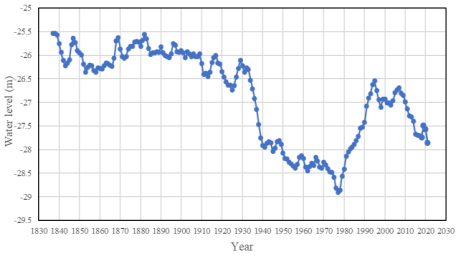

Figure 1. Caspian Sea level measured at Baku station

Two abrupt changes can be identified in the time series which, based on the literature, may be related to human interventions. To be able to predict the natural trend, these sharp changes need to be taken out of the time series. To detect the change points, Pruned Exact Linear Time (PELT) and Binary Segmentation methods have been used. Based on the results, the sea level corresponding to 1934-1941 and 1978-1988 have been omitted (see Figure 2).

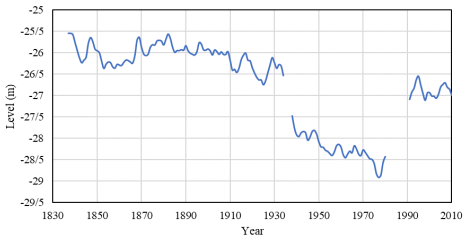

Figure 2. Sea levels corresponding to 934-1941 and 1978-1988 are omitted by detecting change points.

The next step is to fill the missing data and move the sea level corespondig to 1941-1978 to correspond to the filled data. In order to do so, ANN is used. First the time series is detrended using the differencing method. A neural network with different number of lagged data (P) is used. To predict the missing data in 1934-1942, the data for the previous 20 years has been used to train the network.

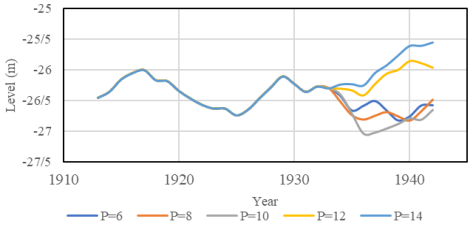

Figure 3. Predicting the sea level during 1934-1942

As seen in Figure 3, the value of P has a sginificant influence on the result. To choose the right value for P, the nueral network is further used to reconstruct the sea level during 1943-1977. Then the results are compared with the available measured data to see which network leads to the closest results. The results corresponding to P = 8 shows the most consistency with the measured data (Figure 4). Having the data in 1933-1942 and the sea level differences in 1943-1977, the time series is reconstructed and used to predict the sea level for 1978-1988. The same method is used. The reconstructed time series is shown in Figure 5.

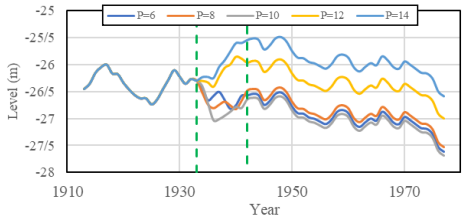

Figure 4. ANN results for different number of lagged data

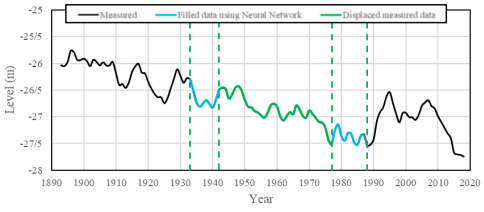

Figure 5. Reconstructed time series

3. Results

The reconstructed time series is ready to be used for prediction. To choose the most apporpriate value for P and also, the proper numebr of data to train the network, a further analysis is carried out. The neural network is used to predict the sea level during 2000-2010 and 2010-2020. 20 years and 30 years data have been used and P=6, 8, 10, 12 and 14 has been considered. The results show that if using 30 years data to train the network, it's better to set the number of lagged data to 6 or 8. On the other hand, when using 20 years data for training, P= 6, 10 and 14 lead to better results.

Using the above mentioned configurations, different networks are used to predict the sea level during 2021-2031 (Figure 6). The maximum, minimum and average values of the results are calculated and shown in Figure 7 and Table 1.

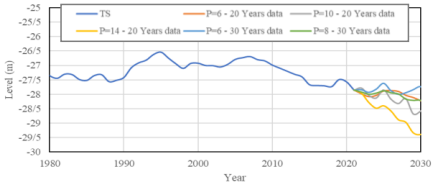

Figure 6. Prediction of the Caspian sea level during 2021-2030

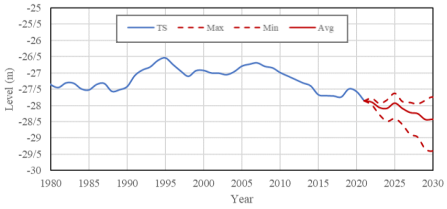

Figure 7. Maximum, minimum and average of the predicted values during 2021-2030

Table 1. Predicted Caspian Sea levels at Baku station (2021-2030)

	Max	Min	Avg
2021	-27.86	-27.86	-27.86
2022	-27.78	-27.99	-27.90
2023	-27.94	-28.29	-28.07
2024	-27.83	-28.48	-28.09
2025	-27.62	-28.40	-27.93
2026	-27.88	-28.58	-28.09
2027	-27.91	-28.88	-28.22
2028	-27.95	-28.97	-28.26
2029	-27.84	-29.33	-28.44
2030	-27.74	-29.39	-28.43
2031	-27.98	-29.22	-28.45

4. Conclusion

An ANN method was used to predict Caspian Sea level for the next 10 years. To remove the direct effect of the industrial developments, the abrupt changes in the data were omitted and later reconstructed using a neural network. The method was verified by using the model to predict the data in the intervals which measured data was available. The prediction shows that in the next 10 years, the average sea level can decrease up to 60 cm.

5. References

[1] Hoseini & Soltanpour, "Long-term prediction of Caspian Sea level under CMIP6 scenarios using artificial neural networks", *Coastal Engineering proceedings*, 2020

[2] Caspian Sea, state of the environment, *CaspEco Project*, 2010

[3] Nandini-Weiss et al., "Past and future impact of the winter North Atlantic Oscillation in the Caspian Sea catchment area", *International Journal of Climatology*, July 2018.

[4] Sergei N. Rodionov, "Global and regional climate interaction: The Caspian Sea experience", *Kulwer Academic Publishers*, 1994

COMPARATIVE ANALYSIS of SEA SURFACE TEMPERATURE PATTERN IN THE PERSIAN GULF USING SATELLITE DATA

Shirin Farkhani [1], Nasser Hadjizadeh Zaker [2]

1) Graduate Faculty of Environment, University of Tehran, Tehran, Iran, s_farkhani @ut.ac.ir
2) Graduate Faculty of Environment, University of Tehran, Tehran, Iran, nhzaker @ut.ac.ir

1. Introduction

The sea surface temperature (SST) is one of the most important oceanic variables [1]. It is a vital property of the marine ecosystems which controls the physical, biological, and chemical characteristics of the environment [2] and modulates the exchange of heat between the ocean and the atmosphere [3]. Climate change refers to any long-term significant change in the weather pattern of a specific area or the whole earth, due to natural or human-caused variability. Excessive use of fossil fuels by human activities which increases the concentration of greenhouse gases and causes the global temperature to rise has been identified as the primary reason for ongoing climate change [4]. This phenomenon has altered the Earth's energy balance, resulting in the accumulation of thermal energy in the climate system [5]. Over the past fifty years, more than 80% of this extra energy has been absorbed into the oceans with a primary consequence of raising SSTs [6]. These temporal and spatial changes of SST impact the atmospheric system, aquatic life, marine currents, and other characteristics of seas.

The Persian Gulf is one of the most valuable aquatic ecosystems in the world. The high temperature and salinity of water in the Persian Gulf cause the creatures of the Persian Gulf region to be in a state of extreme salinity and temperature. Hence, a slight increase in water temperature will have a great impact on the ecosystem of this region. Therefore, it seems necessary to evaluate the effects of climate change on the temperature of this water body.

In this paper, SST satellite data are used to study the effects of climate change on the water temperature in the Persian Gulf. In this regard, monthly and seasonal average AVHRR SST data for the years 1980 and 2015 are compared.

2. Materials and Methods

2.1. Study Area

The Persian Gulf (24–30°N; 48–57°E) is a semi-enclosed, shallow water body, with an average water depth of 36 m (Figure 1). It is spread over an area of 239×10^3 km^2 and is 990 km in length. It is connected to the Gulf of Oman through the 56 km wide Strait of Hormuz. Because the region is located in a hyper-arid region [7], mean annual evaporation exceeds both mean annual precipitation and freshwater run-off, which results in more saline and denser waters of the gulf. In the Persian Gulf, the seasonal differences of insolation, along with cold winds from the nearby highlands, result in extreme temperature (ranging from 16°C to 35°C) [8] and salinity (ranging from 36 to 43 parts per thousand) conditions [9]. The Persian Gulf is not just strategically important because of its rich sources of oil and natural gas but is also the hot spot of marine biodiversity, which are so sensitive to thermal changes in water.

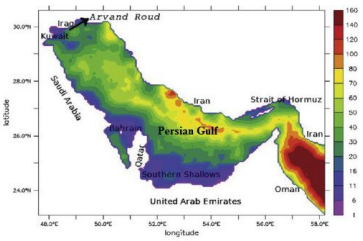

Figure 1. Study area location and bathymetry

2.2. Data Sources

A new high-resolution sea surface temperature (SST) analysis product has been developed by NOAA National Centers for Environmental Information (NCEI) using optimum interpolation (OI) of Advanced Very High-Resolution Radiometer (AVHRR) infrared satellite SST data. The analyses have a spatial grid resolution of 0.25 degrees and a temporal resolution of 1 day, which is available from January 1980 [10]. In this study the daily NOAA AVHRR dataset at 0.25-degree resolution was obtained from NOAA National Centers for Environmental Information (https://www.ncei.noaa.gov/), for the years 1980 and 2015, to evaluate the impacts of climate change on the SST of the Persian Gulf.

3. Results

The mean monthly SST of the Persian Gulf for the years 1980 and 2015 are shown in Figure 2. As can be seen, the minimum and maximum thresholds both increased in 2015. *Figure 3* shows the comparative diagram of the monthly climatological mean SST in the region for the

mentioned years. The results demonstrate that the surface temperature was increased in all months. The highest and lowest increment belonged to March with a value of 2.31°C and January with a value of 0.5°C, respectively. We can see a distinct uni-modal SST curve in the Persian Gulf. The graph shows that the minimum SST for this water body was in February and the maximum SST was in August, in both years.

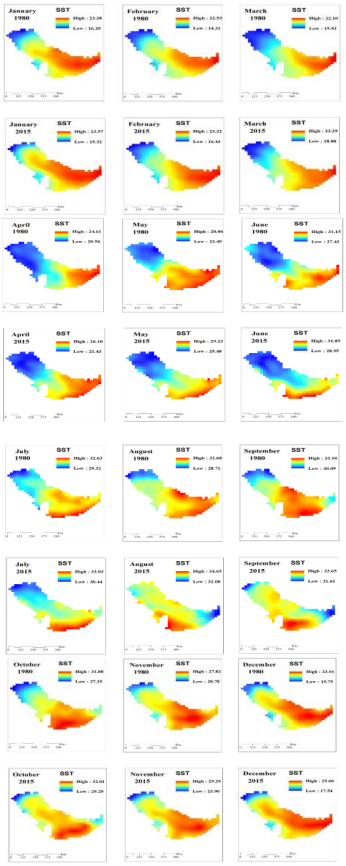

Figure 2. AVHRR Monthly mean SST of the Persian Gulf for the years 1980 (Upper panels) and 2015 (lower panels)

The seasonal mean SST comparison for the years 1980 and 2015, over the Persian Gulf, is shown in Figure 4. According to this figure, in comparison to the year 1980, spring had the highest (1.61°C) and winter had the lowest (1.1°C) SST increment in the year 2015. Summer and autumn had a 1.26°C and 1.24°C rise in SST. However, the general trends of the two years seem to be similar.

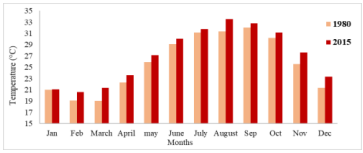

Figure 3. Monthly mean SST comparison for the years 1980 and 2015

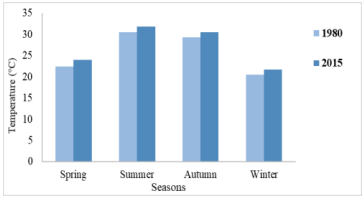

Figure 4. Seasonal mean SST comparison for the years 1980 and 2015

4. References

[1] Park, K.-A., Lee, E.-Y., Li, X., Chung, S.-R., Sohn, E.-H. & Hong, S. 2015. Noaa/Avhrr Sea Surface Temperature Accuracy In The East/Japan Sea. International Journal Of Digital Earth, 8, 784-804.

[2] Brewin, R. J., Smale, D. A., Moore, P. J., Dall'olmo, G., Miller, P. I., Taylor, B. H., Smyth, T. J., Fishwick, J. R. & Yang, M. 2018. Evaluating Operational Avhrr Sea Surface Temperature Data At The Coastline Using Benthic Temperature Loggers. Remote Sensing, 10, 925.

[3] Pisano, A., Marullo, S., Artale, V., Falcini, F., Yang, C., Leonelli, F. E., Santoleri, R. & Buongiorno Nardelli, B. 2020. New Evidence Of Mediterranean Climate Change And Variability From Sea Surface Temperature Observations. Remote Sensing, 12, 132.

[4] Bernstein, L., Bosch, P., Canziani, O., Chen, Z., Christ, R. & Riahi, K. 2008. IPCC, 2007: Climate Change 2007: Synthesis Report. IPCC.

[5] Trenberth, K. & Jt, F. 2014. Balmaseda Ma. Earth's Energy Imbalance. J. Clim, 27, 3129-3144.

[6] A., Clarke, L., Dahe, Q. & Dasgupta, P. 2014. Climate Change 2014: Synthesis Report. Contribution Of Working Groups I, Ii And Iii To The Fifth Assessment Report Of The Intergovernmental Panel On Climate Change, IPCC.

[7] Sheppard, C., Al-Husiani, M., Al-Jamali, F., Al-Yamani, F., Baldwin, R., Bishop, J., Benzoni, F., Dutrieux, E., Dulvy, N. K. & Durvasula, S. R. V. 2010. The Gulf: A Young Sea In Decline. Marine Pollution Bulletin, 60, 13-38.

[8] Chao, S. Y., Kao, T. W. & Al-Hajri, K. R. 1992. A Numerical Investigation Of Circulation In The Arabian Gulf. Journal Of Geophysical Research: Oceans, 97, 11219-11236.

[9] Reynolds, R. M. 1993. Physical Oceanography Of The Gulf, Strait Of Hormuz, And The Gulf Of Oman—Results From The Mt Mitchell Expedition. Marine Pollution Bulletin, 27, 35-59.

[10] Turton, J. V., Mölg, T. & Collier, E. 2020. High-Resolution (1 Km) Polar Wrf Output For 79 N Glacier And The Northeast Of Greenland From 2014 To 2018. Earth System Science Data, 12, 1191-1202.

APPLICATION OF MULTI-LAYER PERCEPTERON-NEURAL NETWORK FOR THE DECADAL CASPIAN SEA LEVEL PREDICTION

Faezeh Zalpoor[1], S. Abbas Haghshenas [2], Asghar Bohluly[3], Shadan Nasseri Doust[4]

1) Institute of Geophysics, University of Tehran, Tehran, Iran, faezeh.zalpoor@ut.ac.ir
2) Institute of Geophysics, University of Tehran, Tehran, Iran, SAHaghshenas@ut.ac.ir
3) Institute of Geophysics, University of Tehran, Tehran, Iran, bohluly@ut.ac.ir
4) Institute of Geophysics, University of Tehran, Tehran, Iran, Shadan.nasseri.d@ut.ac.ir

1. Introduction

The Caspian Sea is the most extensive inland body of water in the world, with a surface size of around 371,000 km2 (excluding the Kara-Bogaz-Gol Bay) and a length of 1200 km. Five nations border the Caspian Sea, which is situated in an endorheic (no outflow) basin between Europe and Asia: Russia, Kazakhstan, Turkmenistan, Iran, and Azerbaijan [1]. The dynamics of water displacement and sea-level monitoring have long been the attention of several studies due to their significance in managing water resources and addressing environmental concerns [2, 3, 4, 5, 6, 7, 8]

The Caspian Sea is a closed basin, fluctuations in water level changes both in the past and in the future have a significant effect on its progress and regression on coasts and environmental impact, as well as on the destruction of coastal areas and wetlands and the loss of economic resources and maritime industry. In this study, the aim is to predict future balance changes for the year 2020-2030, considering the changes in the observed observational balance in the past and the trend of its changes. Therefore, climatic data such as effective parameters such as precipitation, temperature and evaporation and their effect on changes in the Caspian Sea Level (CSL) in the neural network were used. The procedure uses the available climatic data as input and observation data as output in the neural network, then run 20 times and finally calculates the average compared with existing data. This trend has also been used to predict the future, showing that balance changes will increase by about 40 cm in the next 10 years, with a 68.2% chance of occurring from -20 to 80 cm per year. Although the balance between river intake and precipitation and outflow from surface evaporation essentially accounts for CSL variation, a thorough understanding of massive, decadal CSL oscillations is still missing.

The main motivation of the present study is to develop an understanding of past changes through a comprehensive analysis of hindcast data [9, 10], river discharge (R), and climate model estimates of precipitation (P) and evaporation (E) fluxes. The goal is to reconstruct past long-term CSL variations using integrated P, E, and R fluxes and to lay the groundwork for predictions of future CSL trends.

2. Materials and Methods

ANNs are data processing methods consisting of input, output, one or more hidden layers and fundamental processing components. The perceptron is a binary classifier and the most fundamental type of artificial neural network. A Multi-Layer Perceptron (MLP) is a fully connected class of feedforward Artificial Neural Network (ANN). MLP networks learn to simulate the behavior of a complex and nonlinear system through learning algorithms and training data. Learning algorithms, such as back-propagation [11], delta-bar-delta [12], conjugate gradient [13], and Levenberg–Marquardt (LM) [14], are commonly used to find an optimal set of parameters of MLP models. Three different training algorithms, LM, conjugate gradient and gradient descent with adaptive learning rate, were employed before [15] for the ANN models, from which LM performed better than the others. Therefore, the MLP model was used with the LM learning algorithm. One to 10 neurons were used in the hidden layer to assess the effect of network structure on its performance in simulating the CSL and the data set were divided into training (75%), testing (20%) and validation (5%).

Table1: Characteristics of Artificial Neural Network

Training set	**75%**
Validation	**5%**
Test set	**20%**
Training algorithm	**Levenberg-Marqardt**
No.of neurons in hidden layer	**10%**
No.of network layers	**2%**

3. Results and Discussions

In this study, CSL climatological parameters were used as input variables. Precipitation, rainfall, evaporation, surface runoff and sea level changes were used as hindcast data. As a result, the diagram of precipitation and CSL vs the predictions is presented in Figure1-3 which show the changes in precipitation, evaporation, surface runoff and sea level change in the Caspian Sea between 2020 to 2030, with a probability of 68.2%. As a result, we have a 40 cm increase per year. Moreover, the evaporation will be between 110 to 120 cm per year, and the precipitation will

be between -40 to 33 cm per year. The surface runoff also would change between -60 to 40 cm per year.

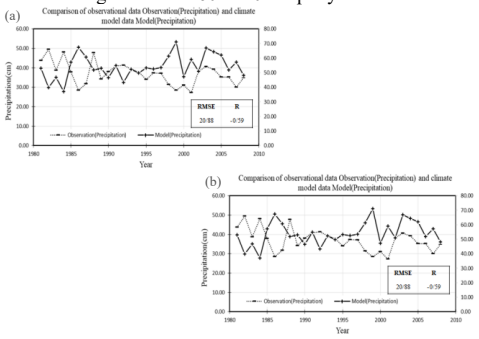

Figure 1. Prediction of the precipitation parameter using the climate model (a); reproduction of the precipitation using the climatic precipitation parameter as the result of the neural network (b).

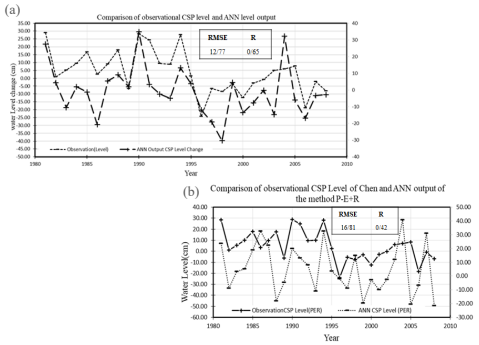

Figure 2. Recovery of water level changes using neural network (a); reproduction of observed level changes and neural network output using the relationship P-E+R (b)

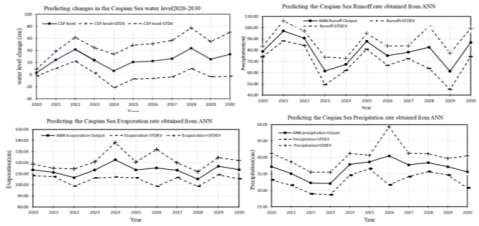

Figure 3. The Prediction of changes in water level, runoff, evaporation and precipitation of the Caspian Sea using neural network

The model runs 20 times while using the climatological model results. The uncertainty of any single data is always Δx, the uncertainty in the mean Δx_{avg} becomes smaller (by a factor of 1/ N); Therefore, the predicted data averaged through 20 times of various runs. Utilizing the distribution function, the results would be as follows:

Table2: The range of changes in water level, runoff, rainfall and evaporation for the years 2020-2030

Evaporation	Precipitation	Run off	CSL
+110-120	-33+40	-60+40	+40

4. References

[1]. Chen, J. L., Pekker, T., Wilson, C. R., Tapley, B. D., Kostianoy, A. G., Cretaux, J.-F., & Safarov, E. S. (2017). Long-term Caspian Sea level change. Geophysical Research Letters, 44(13), 6993–7001. doi:10.1002/2017gl073958

[2]. Kosarev, A. N., and E. A. Yablonskaya (1994), The Caspian Sea, p. 259, Academic, The Hague

[3]. Kosarev, A. N., and A. G. Kostianoy (2005), Kara-Bogaz-Gol Bay, in The Caspian Sea Environment, edited by A. G. Kostianoy and A. N. Kosarev, pp. 211–221, Springer, Berlin

[4]. Kosarev, A. N., A. G. Kostianoy, and I. S. Zonn (2009), Kara-Bogaz-Gol Bay: Physical and chemical evolution, in Aquatic Geochemistry, Special Issue: Saline Lakes and Global Change, vol. 15, N 1-2, pp. 223–236, Springer Science+Business Media, Berlin, Germany, doi:10.1007/s10498-008-9054-z.

[5]. Panin, G. N. (2007), Caspian Sea level fluctuations as a consequence of regional climatic change, in Global Change: Enough Water for All, edited by J. L. Lozán, et al., pp. 216–219, Wissenschaftliche Auswertungen, Hamburg.

[6]. Panin, G. N., I. V. Solomonova, and T. Yu. Vyruchalkina (2014), Regime of water balance components of the Caspian Sea, Water Resour., 41(5), 505511, doi:10.1134/S0097807814050078.

[7]. Chen, J. L., Pekker, T., Wilson, C. R., Tapley, B. D., Kostianoy, A. G., Cretaux, J.-F., & Safarov, E. S. (2017). Long-term Caspian Sea level change. Geophysical Research Letters, 44(13), 6993–7001. doi:10.1002/2017gl073958

[8]. Memarian Sorkhabi, O., Asgari, J., & Amiri-Simkooei, A. (2021). Monitoring of Caspian Sea-level changes using deep learning-based 3D reconstruction of GRACE signal. Measurement, 174, 109004. doi: 10.1016/j.measurement.2021.10

[9]. Lebedev, S. A., & Kostianoy, A. G. (2008). Integrated Use of Satellite Altimetry in the Investigation of the Meteorological, Hydrological, and Hydrodynamic Regime of the Caspian Sea. Terrestrial, Atmospheric and Oceanic Sciences, 19(1-2), 71. doi:10.3319/tao.2008.19.1-2.71(sa)

[10]. Chen, J. L., Wilson, C. R., Tapley, B. D., Save, H., & Cretaux, J.-F. (2017). Long-term and seasonal Caspian Sea level change from satellite gravity and altimeter measurements. Journal of Geophysical Research: Solid Earth. doi:10.1002/2016jb013595

[11]. Rumelhart, D.E., Hinton, G.E., Williams, R.J., et al. (1988) Learning Representations by Back-Propagating Errors. Cognitive Modeling, 5, 1.

[12]. Jacobs, R. A. (1988). Increased rates of convergence through learning rate adaptation. Neural Networks, 1(4), 295–307. doi:10.1016/0893-6080(88)90003-2

[13]. Charalambous, C. (1992). Conjugate gradient algorithm for efficient training of artificial neural networks. IEE Proceedings G Circuits, Devices and Systems, 139(3), 301. doi:10.1049/ip-g-2.1992.0050

[14]. Hagan, M. T., & Menhaj, M. B. (1994). Training feedforward networks with the Marquardt algorithm. IEEE Transactions on Neural Networks, 5(6), 989–993. doi:10.1109/72.329697

[15]. Karimi, S., Kisi, O., Shiri, J., & Makarynskyy, O. (2013). Neuro-fuzzy and neural network techniques for forecasting sea level in Darwin Harbor, Australia. Computers & Geosciences, 52, 50–59. doi: 10.1016/j.cageo.2012.09.015

14th International Conference on Coasts, Ports and Marine Structures
9 & 10 May 2023 , Tehran-IRAN
ICOPMAS 2022

DIURNAL OSCILLATIONS RESPONSE TO THE SEA BREEZE ON THE INNER SHELF OFF THE SOUTHERN CASPIAN SEA

Mina Masoud[1], Rich Pawlowicz[2]

1) Dept. of Earth, Ocean and Atmospheric Sciences, University of British Columbia, 2207 Main Mall, Vancouver, B.C. Canada V6T 1Z4, mina.masoud30@gmail.com
2) Dept. of Earth, Ocean and Atmospheric Sciences, University of British Columbia, 2207 Main Mall, Vancouver, B.C. Canada V6T 1Z4

1. Introduction

The Southern Caspian Sea has a persistent sea-breeze pattern, present through most of the year [5]. Here, we investigate the nature of a geophysical water column response on a shelf to periodic sea-breeze forcing in the lack of confounding tidal effects [6] using measured current records at 5 well-separated locations along the southern Caspian shelf obtained between late 2012 and late 2013. Analytical solutions to a coupled two-layer rotating wind-driven shallow-water model are compared with observations and show good agreement.

2. Material and Methods

The details of wind and current meter datasets used here can be found in [4, 5]. In brief, we use WRF wind data [2] and current measurements at five locations a few kilometers offshore in depths of about 10m over the southern Caspian shelf from 2013 to 2014. In order to concentrate our attention on the sea breeze forcing and response and ignoring the low-frequency variability discussed in [4], we use a Butterworth 4th-order band-pass filter to remove periods less than 6 hours and more than 30 hours.

3. Results

The average diurnal water response has a similar pattern at all locations along the South CS in general. Therefore, here we only show an "average" day only at Roodsar. The detailed analysis of diurnal water response at all stations were fully described in [4, 5].

3.1. The Mean Diurnal Cycle

In the morning, there is an offshore flow in the surface layer, apparently matching the offshore wind stress, and onshore flow at the bottom layer. An opposite response with an onshore flow in the surface layer (and an onshore wind stress) and offshore flow at the bottom layer can be observed during afternoon. (Figure1)

In the alongshore response, a noticeable barotropic flow can be seen, in addition to a baroclinic response. Current maximums and minimums of O(0.01m/s) near the bottom lag those at the surface by about 1/4 wave period, so that they reach a maximum while surface values approach zero (and vice versa). In the diurnal alongshore current pattern, there is a positive (leftward) flow in the morning and negative (rightward) flow in the afternoon. The cross-shore response is almost entirely baroclinic, with a node at a height above bottom of around 6 to 7.7m (Fig.1).

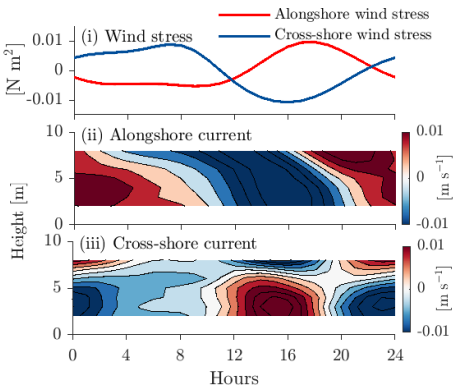

Figure 1. The 24h averaged daily cycle of (i) wind stress, (ii) alongshore and (iii) cross-shore current at Roodsar statin.

3.2. Theoretical Water Response to the Sea Breeze

To understand the linkages between the diurnal surface wind stress and the diurnal currents, we now attempt to model the dynamics. Instead of following the depth-dependent "oscillating Ekman-layer" approach of [1] which has been used by many authors, we restrict ourselves to a mathematically simpler coupled two-layer system, as suggested by our observations, for which analytical solutions are more straightforward to obtain. The details of our analytical model described in [5].

Fitting sinusoids with a period of one day to the daily wind stress time series to estimate T_0^y and T_0^x is straightforward (Figure2), as these time series are clearly dominated by the daily variations. Next, we estimate the barotropic response by averaging observed current velocities at equal distances above and below the

apparent layer interface, and the baroclinic response by subtracting current velocity at these depths (Figure2). For comparison with the observations, the analytical solution is computed with decay offshore scale of α^{-1} as 40km, the friction of $5\times10^{-4}s^{-1}$ at all stations, and zero interfacial friction (Figure2). The predicted responses are reasonably close to our observations in both amplitude and phase. Particularly, the predicted amplitude and phase of barotropic alongshore and cross-shore current are in a reasonable agreement with the observations.

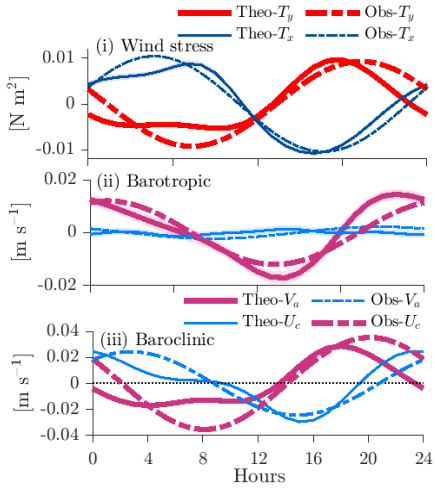

Figure 2. The 24h averaged daily cycle of theoretical and observational (i) wind stress, (ii) alongshore and (iii) cross-shore current at Roodsar station.

4. Conclusion

The daily-frequency current variations of 0.02m/s are clearly consistent with the water column response to the local sea breeze forcing all along the southern Caspian coast (Figure1). In both the along-shore and cross-shore directions, the daily response is large and baroclinic; there is also an along-shore barotropic component which is about half as large, and an even smaller cross-shelf barotropic component linked to coastal water level changes. In comparison, lower-frequency coastally-trapped waves in the same area, generated by lower frequency wind variations, are associated with barotropic current variations over the shelf, of O(0.1m/s), mostly in the along-shelf direction, and surface height changes of O(0.1m) [4]. Thus, the water column response to the sea breeze does not dominate time series of currents, although it is clearly an important factor in short-term coastal water level changes [5], resulting in a small "tide-like" daily cycle.

In the cross-shore direction, currents are baroclinic with a zero crossing near the middle of the water column (Figs.1 and 2). The sea breeze forces onshore surface flow and offshore bottom flow in starting in the late morning, which reverses sometime before midnight. A diurnal current response to diurnal wind stress with a combined barotropic/baroclinic response in the alongshore direction and two-layer baroclinic structure in the cross-shore direction exist in our case which has been observed in other case studies around the world's ocean.

Our observations clearly suggest a two-layer response, without along-shore propagation of long waves, which is superimposed on lower-frequency variations arising from coastally-trapped waves [4], and so we have developed a linear two-layer model [5], including interfacial and bottom friction but without along-shore variations, to investigate the sea breeze response and the important factors governing this response in a more general way. Analytical solutions for this forced system greatly simplify the identification of important factors in the response, without making prior judgments about their importance. Generation of the baroclinic flow was driven mostly by the local effects of wind stress on the surface layer, with coupling to an oppositely directed flow in the lower layer through the coastal boundary condition.

Finally, the sea breeze response in the southern Caspian accounts for nearly half of high-frequency variance and may be the dominant mechanism driving baroclinicity, and thus, in turn, may be the major source energy driving vertical mixing in this area. This is an area which requires further investigation.

5. References

[1] Craig PD. A model of diurnally forced vertical current structure near 30 latitudes. Continental Shelf Research. 1989 Nov 1;9(11):965-80.

[2] Ghader S, Montazeri-Namin M, Chegini F, Bohluly A. Hindcast of surface wind field over the Caspian Sea using WRF model. InProceedings of the 11th International Conference on Coasts, Ports and Marine Structures ICOPMAS 2014 Nov (pp. 24-26).

[3] Hyder P, Simpson JH, Christopoulos S. Sea-breeze forced diurnal surface currents in the Thermaikos Gulf, North-west Aegean. Continental Shelf Research. 2002 Mar 1;22(4):585-601.

[4] Masoud M, Pawlowicz R, Namin MM. Low frequency variations in currents on the southern continental shelf of the Caspian Sea. Dynamics of Atmospheres and Oceans. 2019 Sep 1; 87:101095.

[5] Masoud M, Pawlowicz R. Currents generated by the sea breeze in the southern Caspian Sea. Ocean Science. 2022 May 13;18(3):675-92.

[6] Medvedev IP, Kulikov EA, Fine IV. Numerical modelling of the Caspian Sea tides. Ocean Science. 2020 Feb 5;16(1):209-19.

14th International Conference on Coasts, Ports and Marine Structures
9 & 10 May 2023 , Tehran-IRAN
ICOPMAS 2022

SKILL ASSESSMENT OF THE WRF MODEL FOR SIMULATING THE SURFACE WINDS; APPLICATION TO THE FARSI ISLAND

Morteza Keshtgar[1], Seyed Mostafa Siadatousavi[2] and Javad Karami[3]

1) School of Civil Engineering, Iran University of Science and Technology, Tehran, IRAN, m_keshtgar@civileng.iust.ac.ir
2) School of Civil Engineering, Iran University of Science & and Technology, Tehran, IRAN, siadatmousavi@iust.ac.ir
3) Atmospheric Science and Meteorological Research Center (ASMERC), Tehran, IRAN, karamij@yahoo.com

1. Introduction

Determining surface parameters on ocean environments has many applications, especially in the field of wind-wave prediction as well as ocean modeling. Using numerical meteorological models is one of the common methods to fulfill this purpose. One of the most challenging issues in determining the surface parameters such as wind and surface temperature is the use of mesoscale numerical models in microscale atmospheric modeling, which imposes high computational costs. The WRF numerical model has the ability to simulate small scale domains (with a resolution of less than 1 km), but it requires the use of heavy hardware resources. The aim of this study is to provide a reasonable simulation of wind speed near a small island with optimal use of hardware resources and high-resolution bandwidth.

The Farsi Island is one of the islands of the Bushehr province in Iran located in the Persian Gulf. This island is the border between Iran and Saudi Arabia and it is the last Iranian island in terms of location around which oil facilities are still active.

In this study, mesoscale modeling with a range of 15 km and 5 km was used; hence, the geographic data (topography and land cover) used have a 30-second resolution, which is fine-enough for mesoscale numerical modeling. Due to the small size of the Persian Gulf, this type of modeling faces challenges regarding the lack of high-resolution model set-ups (resolution less than 1 km) and consequently, the lack of higher resolution land data.

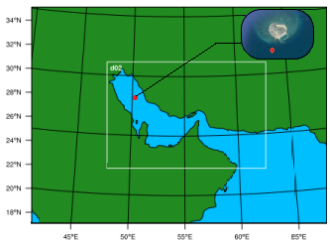

Figure 1. The domain used for simulations – Farsi Island location and observation buoy were also shown

2. Methodology

Observed data were provided by an offshore buoy shown in Figure 1.

The WRF Model [1], version 4.3, developed by NCAR was employed for modeling mesoscale wind in the Persian Gulf region. Two-way nested WRF simulations were performed with two grids as shown in Figure 2. The outer domain uses a 15-km grid resolution and the inner domain has a 5-km resolution. To find the best configurations, 21 physical schemes presented in Table 1, were evaluated to find out whether or not a small island can be well simulated in this large resolution using WRF physical ensembles. [2-5]

Table 1. Different parametrizations used for simulations.

NO	MP	CU	LW	SW	PBL	SFC	SFS
1	WSM3	BMJ	CAM	CAM	YSU	R MM5	N-MP
2	WSM5	BMJ	CAM	CAM	YSU	R MM5	N-MP
3	WDM5	BMJ	CAM	CAM	YSU	R MM5	N-MP
4	WDM5	KF	RTM	Dudhia	MYJ	Eta	N-MP
5	WSM3	BMJ	RTMG	RTMG	MYJ	Eta	N-MP
6	WSM5	BMJ	RTMG	RTMG	MYJ	Eta	N-MP
7	WDM5	BMJ	RTM	Dudhia	MYJ	Eta	N-MP
8	WDM5	BMJ	RTMG	RTMG	MYJ	Eta	N-MP
9	WSM6	KF	RTM	Dudhia	MYNN	Eta	U Noah
10	WDM7	KF	RTM	Dudhia	MYJ	Eta	U Noah
11	WSM6	GF	RTM	Dudhia	QNS	QNS	N-MP
12	WDM7	GF	RTM	Dudhia	MYJ	Eta	N-MP
13	WSM6	GF	RTM	Dudhia	TMF	TMF	N-MP
14	P Lin	KF	RTM	Godard	ACM2	PI–Xiu	N-MP
15	P Lin	KF	RTM	Godard	MRF	R MM5	N-MP
16	P Lin	KF	RTM	Godard	YSU	R MM5	N-MP
17	WSM3	KF	RTM	Dudhia	MRF	MM5 S	N-MP
18	WSM6	KF	RTM	Dudhia	YSU	MM5 S	5–layer
19	WSM6	GF	RTM	Dudhia	MYJ	Eta	N-MP
20	WSM6	GF	RTM	Dudhia	QNSE	QNSE	N-MP
21	WSM6	GF	RTM	Dudhia	TEMF	TEMF	N-MP

The initial and boundary conditions were obtained from ERA5. The simulations were carried out for a 10-day period starting from 1st September 2013.

3. Model Evaluation

The ensembles ability to simulate the meteorological conditions of the two case study periods were assessed using methods that quantify bias in magnitude and measures similarity in temporal and spatial variability. The model performance was evaluated using the mean bias and Root Mean Square Error (RMSE):

$$Bias = \frac{1}{N}\sum_{i=1}^{N}|M_i - O_i| \quad (1)$$

$$RMSE = \sqrt{\frac{1}{N}\sum_{i=1}^{N}M_i - O_i} \quad (2)$$

$$IOA = 1 - \left[\frac{IJ.RMSE^2}{\sum_{j=1}^{J}\sum_{i=1}^{I}|P_j^i - M_O| - |O_j^i - M_O|}\right] \quad (3)$$

where M_0 is the average of the observed values.

4. Results

Although the modeling resolution is not suitable for micro-scale atmospheric modeling, the sensitivity of WRF wind data to physical schemes is considerable. The area of Farsi Island is only 7.5 km^2; hence, in order to numerically model the wind over this island optimally, the working resolution should be less than 1 km. But in this study the configuration of the model was larger; however, the wind speed on this island was well modeled with a special physical configuration. This configuration can be generalized to other small islands in the Persian Gulf.

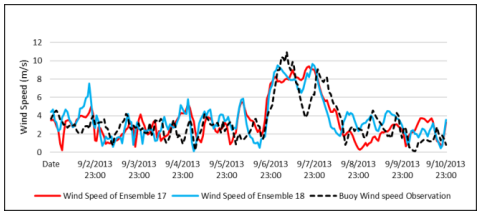

Figure 2. Time-series comparison of WRF wind speed ensembles 17 and 18 with in situ observations.

The results of numerical modeling presented in Table 2 showed that ensemble 17 and 18 performed well in this situation. The use of the mentioned configurations increased the accuracy in wind modeling by the WRF model with meso-scale resolution, and it is recommended to be used close to the small islands. In Figure 2, the time series of the results of these two ensembles were compared with the Buoy observational data.

Table 2. Results of statistical evaluation

NO	IOA	R	RMSE	MBIAS
1	0.585	0.419	2.17	-0.04
2	0.571	0.412	2.141	-0.08
3	-0.18	-0.09	2.701	-0.02
4	0.209	0.125	2.634	0.571
5	-0.09	-0.05	2.904	0.714
6	-0.05	-0.03	2.947	0.551
7	0.11	0.061	2.835	0.577
8	-0.02	-0.01	3.065	0.833
9	0.653	0.495	2.003	0.001
10	0.669	0.534	2.033	0.597
11	0.054	0.029	2.776	0.416
12	0.056	0.031	2.826	0.583
13	0.521	0.367	2.203	-0.21
14	0.465	0.321	2.221	0.118
15	0.447	0.302	2.269	-0.006
16	0.009	0.005	2.633	0.09
17	0.825	0.703	1.692	0.11
18	0.809	0.688	1.739	0.349
19	0.106	0.06	2.7	0.497
20	0.087	0.047	2.742	0.386
21	0.51	0.364	2.166	0.047

5. Conclusion

Based on the results, it was determined that ensemble No. 17 with mp-physic WSM3, CU physic KF and short and longwave radiation RRTM/Dudhia as well as PBL MRF and surface and surface layer physics of MM5 and Noah-mp, provided more accurate results both statistically and in terms of peak detection. Secondly, ensemble 18, with some modifications to ensemble 17, such as WSM6 microphysics instead of WSM3, YSU pbl instead of MRF, and 5-layer thermal diffusion model instead of Noah-mp, provided good results in estimating speed and wind direction near the Farsi islands in the Persian Gulf.

6. References

[1] Skamarock, W.C., et al., *A description of the advanced research WRF model version 4.* National Center for Atmospheric Research: Boulder, CO, USA, 2019. **145**: p. 145.

[2] Coniglio, M.C., et al., *Verification of convection-allowing WRF model forecasts of the planetary boundary layer using sounding observations.* Weather and Forecasting, 2013. **28**(3): p. 842-862.

[3] Done, J., C.A. Davis, and M. Weisman, *The next generation of NWP: Explicit forecasts of convection using the Weather Research and Forecasting (WRF) model.* Atmospheric Science Letters, 2004. **5**(6): p. 110-117.

[4] Donelan, M.A., et al., *On the dependence of sea surface roughness on wave development.* Journal of physical Oceanography, 1993. **23**(9): p. 2143-2149.

[5] Floors, R., et al., *The wind profile in the coastal boundary layer: Wind lidar measurements and numerical modelling.* Boundary-layer meteorology, 2013. **147**(3): p. 469-491.

ESTIMATION OF MIXED LAYER DEEPENING INDUCED BY THE TROPICAL CYCLONE SHAHEEN (2021) IN THE GULF OF OMAN AND NORTHERN ARABIAN SEA: APPLICATION OF SATELLITE SST DATA AND ANALYTICAL MODELS

Mohammad Nabi Allahdadi[1], Kamran Koohestani[2], and Nazanin Chaichitehrani[1]

1) Department of Marine, Earth, and Atmospheric Sciences, North Carolina State University, Raleigh- NC, USA, mallahd@ncsu.edu, nchaich@ncsu.edu
2) Department of Civil Engineering, Iran University of Science and Technology, Tehran, Iran, kamrankoohestani@alumni.iust.ac.ir

1. Introduction

Catastrophic atmospheric events like hurricanes and tropical cyclones can significantly mix the upper ocean and increase the mixing depth from days to weeks [1]. The severe upper ocean mixing can substantially enhance the physical and biogeochemical process in the upper ocean, including water column re-oxygenation and phytoplankton bloom [2]. Due to an apparent increase in the frequency of occurrence of the tropical cyclones entering the northern Arabian Sea and the Gulf of Oman during the last two decades, it is imperative to study the mixing properties of such events in the region. In this study, two approaches based on analytical models and also application of satellite sea surface temperature (SST) data are employed to study the mixing induced by the Tropical Cyclone Shaheen (2021) and estimation of the mixed layer depth (MLD) in these regions.

2. Tropical Cyclone Shaheen

Cyclone Shaheen was formed on 30 September 2021 in the northeast of the Arabian Sea from the remnant of Cyclone Gulab that had been formed on 24 September in the Bay of Bengal and had been dissipated to a tropical depression after traveling across India. At this time, the predominant wind field in the region was the southwesterly summer monsoon of the northern Indian Ocean [3]. The reorganized cyclone in the Arabian sea moved in the general direction west and gradually strengthened as entering the Gulf of Oman. With an approximate west-to-northwest direction, the storm upgraded to a category 1-equivalent tropical cyclone on 2 October at 6:00 UTC while its eye was approximately off the Gavater Bay, Iran (Figure 1). After reaching its closest distance from the Iranian coast offshore of Chabahar Bay on the same day, the cyclone changed its direction to the southwest until it finally made landfall along the northern coast of Oman in the Gulf of Oman on 3 October at 20:00 UTC.

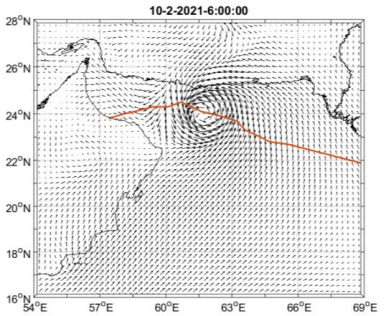

Figure 1. ERA5 wind vectors at the time that Shaheen upgraded to a category one storm. The solid red line shows the track of Shaheen.

3. Using Satellite SST for MLD Estimation

The first approach for estimating the cyclone-induced mixed layer in this paper is based on simplifying the heat budget equation across the mixed layer and using satellite SST data as the mixed layer temperature [4]. This results in the following equation for the mixed layer depth:

$$T = \frac{1}{D}\int_{-D}^{0} T_0(z)dz \qquad (1)$$

In this equation, T is SST, D is the mixed-layer depth (MLD), $T_0(z)$ is the initial temperature profile, and z is the vertical coordinate within the water column. SST data are provided from the operationally-interpolated product (OI), providing 9-km spatial resolution maps of SST based on measurements in near-infrared and microwave bands (Figure 2). The pre-storm (initial) temperature profile is obtained from the climatology data of WOA.

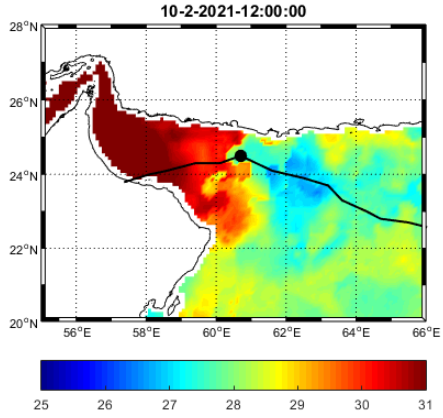

Figure 2. Satellite-measured SST(ºC)at 6 hours after Shaheen upgraded to a category one storm. The solid black line shows the track of Shaheen.

This approach was successfully implemented by Koohestani et al. [5] to estimate MLD for the regions affected by Cyclone Gonu(2007) in the Gulf of Oman and Northern Arabian Sea with an RMSE=5 m for estimated MLD. Equation (1) results in logarithmic relationships between the MLD and SST. It should be noted that this equation is only valid for the regions that are affected by the severe cyclone winds. Figure 3 shows an example of the estimated maps of MLD from SST data for the radius of 200 km around the cyclone's eye at the time, similar to Figure 2. Available ARGO data is used for the evaluation of the estimated MLDs.

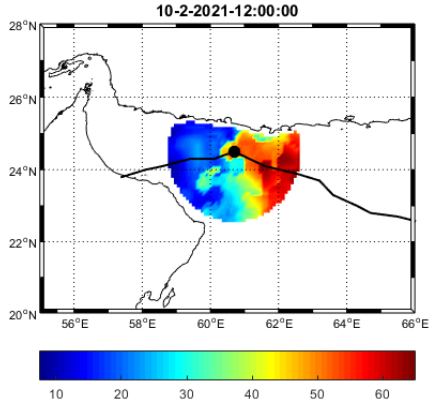

Figure3. Estimated MLD (m) s using satellite SST within 200km of the cyclone's eye at 6 hours after Shaheen upgraded to a category one storm

4. Application of analytical models

During the last several decades, some analytical models have been developed to estimate wind-induced mixed layer depths. The main approach is solving the mixed layer heat budget equation by including the wind stress as the surface boundary condition. In this paper, two approaches presented by Cushman-Roisin [6] and Ushijima and Yoshikawa [7] are used. The first approach simplifies the governing equation to a turbulent erosion model, while the second approach considers the effect of Coriolis force on inhibiting the wind-induced shear. Based on Ushijima and Yoshikawa [7], the MLD is proportional to:

$$MLD \propto {U_*}/{\sqrt{Nf}} \quad (2)$$

For which U_* is the wind friction velocity, N is the initial buoyancy (calculated using WOA climatological profiles), and f is the Coriolis force. The scaling factor for this equation was estimated as 1.6-1.7. Results from this section are compared to the estimated MLDs from satellite SST and ARGO measurements.

5. Conclusions

The results from this study provide a quick and low-cost estimation of the MLD during tropical storms with good accuracies. In the absence of expensive 3D baroclinic models, this estimation can be used as first-hand metrics for different met-ocean and biogeochemical studies in the region.

6. References

[1] Allahdadi, M., 2014. Numerical Experiments of Hurricane Impact on Vertical Mixing and De-Stratification of the Louisiana Shelf Waters. LSU Doctoral Dissertations.

[2] McGee, L., He, R., 2018. Mesoscale and submesoscale mechanisms behind asymmetric cooling and phytoplankton blooms induced by hurricanes: a comparison between an open ocean case and a continental shelf sea case. Ocean Dynamics 68, 1443–1456. https://doi.org/10.1007/s10236-018-1203-3

[3] Chaichitehrani, N., Allahdadi, M.N., 2018. Overview of Wind Climatology for the Gulf of Oman and the Northern Arabian Sea. American Journal of Fluid Dynamics 8, 1–9.

[4] Pan, J., Sun, Y., 2013. Estimate of Ocean Mixed Layer Deepening after a Typhoon Passage over the South China Sea by Using Satellite Data. Journal of Physical Oceanography 43, 498–506. https://doi.org/10.1175/JPO-D-12-01.1

[5] Koohestani, K., Allahdadi, M.N., Chaichitehrani, N., 2021. Oceanic Response to Tropical Cyclone Gonu (2007) in the Gulf of Oman and the Northern Arabian Sea: Estimating Depth of the Mixed Layer Using Satellite SST and Climatological Data. Journal of Marine Science and Engineering 9, 1244. https://doi.org/10.3390/jmse9111244

[6] Cushman-Roisin, B., 1981. Deepening of the wind-mixed layer: A model of the vertical structure. Tellus 33, 564–582. https://doi.org/10.1111/j.2153-3490.1981.tb01782.x

[7] Ushijima, Y., Yoshikawa, Y., 2020. Mixed layer deepening due to wind-induced shear-driven turbulence and scaling of the deepening rate in the stratified ocean. Ocean Dynamics 70, 505–512. https://doi.org/10.1007/s10236-020-01344-w

EFFECTS OF COLUMN GEOMETRY ON TSUNAMI-INDUCED SCOUR USING FLOW-3D

Reza Arefi[1], Ioan Nistor[2] and Majid Mohammadian[3]

1) Department of Civil Engineering, University of Ottawa, Ottawa, Canada, reza.arefi@uottawa.ca
2) Department of Civil Engineering, University of Ottawa, Ottawa, Canada, inistor@uottawa.ca
3) Department of Civil Engineering, University of Ottawa, Ottawa, Canada, majid.mohammadian@uottawa.ca

1. Introduction

In recent decades, tsunamis induced considerable destructive effects on coastlines and nearshore infrastructure and have caused the death of many people around the world [1]. The structural damages related to this phenomenon can be due to direct hydrostatic and hydrodynamic loading from inundation, impact forces from water-borne debris, fire spread by floating debris and combustible liquids, and associated scour and slope/foundation failure.

Scour can be defined as erosion caused by the action of the flowing stream or flood flows and can be classified as *general scour*, in which the sediment particles are transported by flow without the presence of structures, and *local scour* which occurs due to the interaction of flow with structures. Local scouring depth can reach one order of magnitude greater than general scour, a fact that emphasizes the importance of this type of localized scouring.

2. Methodology

The FLOW-3D software was used to investigate the effects of the column's shape on scouring caused by tsunami inundation. In this regard, this numerical model was first calibrated against the experimental results. By using the calibrated numerical model, three different shapes of the column were considered to conduct numerical modeling of the scouring due to tsunami inundation.

3. Numerical Model

In this study, the FLOW-3D software was used to study the scouring around the column. FLOW-3D solves the Navier-Stokes mass and momentum equations, allowing a fully non-hydrostatic solution methodology for the flow. Two nested cubic grids whose sizes were different at regions far and near the column location were considered (3 cm and 1.5 cm).

4. Calibration

To calibrate the numerical model, the experimental results of Mehrzad et al. (2016) [2] which were carried out in the Dambreak Flume at the University of Ottawa, were considered. To study the spatiotemporal evolution of scouring around a square column generated by a dam-break wave, they used a flume with the length, width, and height of 30 m, 1.5 m, and 0.5 m, respectively (Figure 1).

In the sediment transport model, the entrainment coefficient was selected as a calibration parameter [3], and the value of 1.5 was selected which resulted in the highest agreement with the experimental outputs. A comparison between the final bed level changes in the experimental and calibrated numerical model is depicted in Figure 2 for two cross sections.

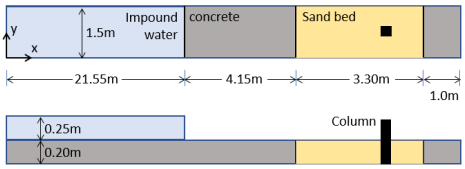

Figure 1: Experimental setup from Mehrzad et al. (2016) (not at scale).

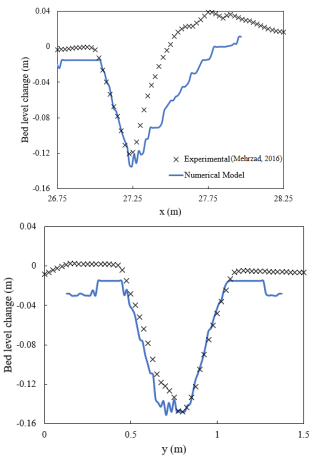

Figure 2: Comparison between experimental and numerical results along x-x and y-y sections.

5. Results and Discussion

To study the effects of column geometry on scouring features, three different geometries with equal transversal areas (0.04 m^2) were considered for the column section. The main difference between these shapes is the performance of the column on flow blockage and how the flow crosses the column. Figure 3 shows the flow field (upper part) as well as the final scour depth (downer part) for different column geometries.

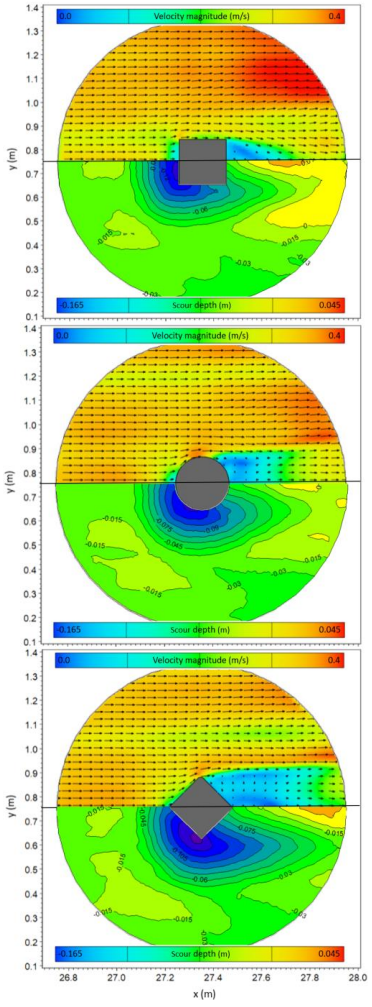

Figure 3: Flow pattern and final scour depth for different column geometries.

As can be seen, the maximum scour depth did not occur at the same locations for different column geometries, and the maximum scour depth for square, circle, and diamond cross shapes was 15, 14, and 16 cm, respectively.

Due to the interaction of flow with the diamond column, a greater downstream extension of scouring was observed for this geometry compared to the other two. It seems that this phenomenon is due to the stronger velocity gradient in the x-z direction. On the other hand, scouring in front of the circular column, and deposition behind it, is less than the other column shapes.

The downstream current speed, just behind the column, decreased because of the formation of a shadow zone behind the column. This shadow zone affects the sedimentation pattern behind the structures, where the current velocity in the x-direction decreased or sometimes its direction changed toward the upstream (in negative x-direction). The scale of the shadow zone has a direct relationship with the surface area of the structures which faces the tsunami inundation. Given the same cross-sectional area for different column geometries, the width of the surface facing the current for the square, circle, and diamond column geometries was 0.2, 0.23, and 0.28 cm, respectively. The shadow zone behind the diamond column was observed to be greater than the others.

The shape of the circle column without sharp edges causes the flow pass by the column with less flow disturbance compared to the other geometries investigated. Less disturbance leads to less turbulence and velocity gradient around the column, and this is the main reason why the maximum scour depth around the circular column is less than that observed in the case of the other two investigated geometries. Of course, the circle shape is not necessarily the optimum shape to minimize the scouring around columns, but among these three simple geometries, the circular one caused minimum interaction between the flow, column, and the bed material.

6. References

[1] Nistor, I. and Palermo, D., 2015. Chapter 20: Post-tsunami engineering forensics: Tsunami impact on infrastructure—Lessons from 2004 Indian Ocean, 2010 Chile, and 2011 Tohoku Japan tsunami field surveys. In: Esteban, M.; Takagi, H., and Shibayama, T. (eds.), Handbook of Coastal Disaster Mitigation for Engineers and Planners. Amsterdam, The Netherlands: Elsevier, pp. 417–435. doi:10.1016/B978-0-12-801060-0.00020-4

[2] Mehrzad, S.; Nistor, I., and Rennie, C.D., 2016. Experimental modeling of supercritical flows induced erosion around structures. Proceedings of CoastLab16: The 6th International Conference on the Application of Physical Modelling in Coastal and Port Engineering and Science (NRC, Ottawa, Canada), 10p

[3] Le Quere, P. A., Nistor, I., & Mohammadian, A. (2020). Numerical Modeling of Tsunami-Induced Scouring around a Square Column: Performance Assessment of FLOW-3D and Delft3D. Journal of Coastal Research, 36(6), 1278–1291. https://doi.org/10.2112/JCOASTRES-D-19-00181.1

HYDRODYNAMIC ANALYSIS OF PELAMIS P2 UNDER THE EFFECT OF MULTI_PEAK WAVE SPECTRA ON THE EASTERN COASTS OF THE MAKRAN

Ebrahim Shabani [1], Mohammad Adibzade [2]

1) Faculty of Engineering, Ahvaz Azad University, Ahvaz, Iran, m.e.shabani@gmail.com
2) Department of Civil and Environmental Engineering, Tarbiat Modares University, Tehran, Iran, mohammad.adibzade@modares.ac.ir

1. Introduction

Wave energy is one of the cleanest energy sources available to humankind; prominently renewable energy that is both periodical and predictable. Wave energy has been an interesting topic in the last few decades, hence many devices such as surface attenuators, oscillating water columns, water overtopping devices, and so on are being developed to harvest energy in ocean waves efficiently. One of the most known wave energy converters (WEC), Pelamis P2, is a semi-submerged, articulated structure formed of cylindrical sections linked by hinged joints. Motion from the waves is resisted by hydraulic rams, which pump high-pressure oil through a system of hydraulic motors via smoothing accumulators to generate electricity. The device is moored to a fixed location but can change its direction to face incoming waves for maximum power generation. The joints used to connect each tubular section are configured to induce wave power from small sea states. They can be actively controlled to use the phenomenon of resonance, allowing power generation to be maximized in small seas. As both the geographic location and ocean climate influence WEC's performance, design cannot be developed on a global and generic basis. The design must be based on the characteristics of the local deployment site and estimated sea state to maximize the power outputs. Complex sea states, including a wind-sea component combined with one or more swell components, are generated far from the area and reach the area. These swells superimpose on wind-sea waves and produce complex seas that result in bimodal or even multi-peaked spectra. Consequently, for an accurate description of WEC performance in a realistic sea state, it is imperative to clarify the peak periods of various wave components and the spreading status of energy [1].

2. Wave Data and Method

Adibzade et al, (2021) provided a parametric description of the main patterns of the wave climate at a 210-km-long area in the Makran region using measured wave data in 2016 by the Iranian Ports & Maritime Organization. Accordingly, multi-peak spectra in Roodik and Pasabandar (Stations 6 and 7 in Figure 1) are selected based on the region-driven dominant climatology of the monsoon seasons. We used ANSYS AQWA software as a core tool for computation, and we carefully considered the existing software restrictions and our study objectives. The hydrodynamic parameters come with AQWA software based on the boundary element method and linear potential wave theory. Therefore, it is suitable for modeling floating WECs [3].

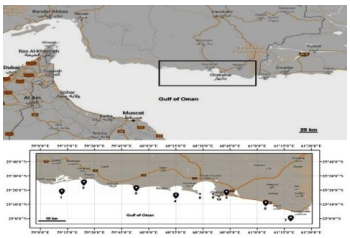

Figure 1. Location of wave measurement stations in the Gulf of Oman [2]

3. Model Validation

Two series of simulations were performed to validate the model by estimating the horizontal F_x and the vertical forces F_y acting on a horizontal cylinder with a radius of 0.05 m and a height of 0.295 m. In the first series, incident waves have different amplitudes with a frequency of 1 Hz and a wavelength of 1.539 m. In the second series, waves have different frequencies and wavelengths, but this time with a fixed wave amplitude of 0.02 m. It should be noted that the theory used to model waves is Stokes's second-order. The modeling results in AQWA (BEM), along with the experimental data as well as the results of a simulation by the Finite Volume Method (FVM) [4], are shown in Figure 2.

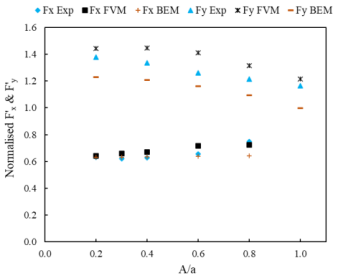

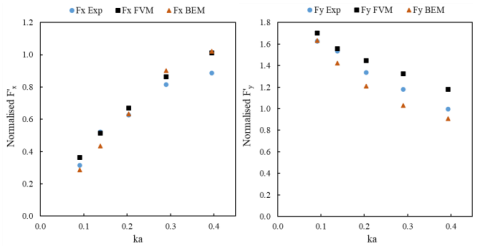

Figure 2. Comparison of normalized values of F_x and F_y results with laboratory data

4. Result and Discussion

This section presents the hydrodynamic response of Pelamis P2 in the governing sea states of the eastern coasts of Makran. For this simulation, a depth of 60 m and water density of 1025 kg/m3 were considered. The device consists of 5 parts, parts 1 to 5, connected through 4 connection points, joint 1 (connects part 1 to part 2) to joint 4 (the connection between part 4 to part 5). The joints are of the hinged type. The mass of each segment was defined centrally at its COG. Four spectra measured during monsoon seasons were selected and exerted to WEC. Spectra and their Specifications are shown in Figure 3 and Table 1. Also, a single peak JONSWAP spectrum was used with a H_{m0} of 3.2 m, gamma of 1, and a peak frequency of 0.09 Hz. The total simulation time is 500 Sec. The time response of the joint 1 force is presented in Figure 4. In order to compare force values created at all joints, their dimensionless values are calculated and given in Table 2.

Table 1. Specifications of the used multi-peak spectra

Case	Station	Date		H_{m0} (m)
1	Pasabandar	2016/07/10	9:00	3.21
2	Pasabandar	2016/07/19	5:00	3.24
3	Pasabandar	2016/06/01	11:00	2.00
4	Roodik	2016/03/17	12:00	1.27

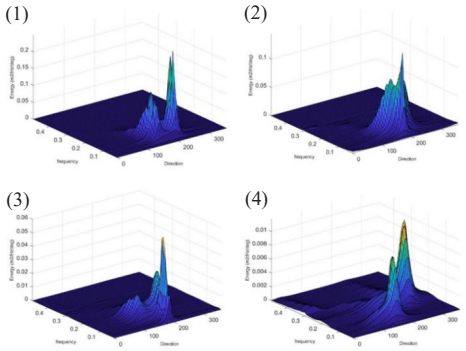

Figure 3. Measured multi-peak spectra in frequency-direction domain

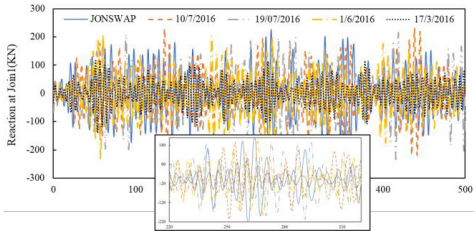

Figure 4. Time series of forces created in the joint 1

According to the dimensionless values (suppressing H_{m0}), the forces created in the joints in cases 3 and 4 of the sea conditions, where there are at least two distinct peaks in the frequency domain, are higher. While cases 1 and 2 are multi-peak, there is no significant difference compared to the JONSWAP single-peak spectrum because their peak values are approximately the same in the frequency domain. The performance of the other joints aligns well with joint 1 and shows higher values in cases 3 and 4.

Table 2. Dimensionless values of forces created in joints in different sea states

Joint	JONSWAP	Case 1	Case 2	Case 3	Case 4
1	3.37	3.34	3.33	4.93	4.72
2	3.65	3.62	3.56	5.2	4.25
3	3.44	3.43	3.38	4.85	3.79
4	2.79	2.8	2.76	3.9	3.13

5. Conclusion

In this research, using the ANSYS AQWA software, the Pelamis P2 WEC is simulated in the sea condition governing monsoon seasons on the southeastern coast of our country (east of Makran). Several simultaneous wave components can be seen in the spectra measured at the Eastern stations (Pasabandar and Roodik) in monsoon seasons. In such spectra, the swell components, which often propagate from the Indian Ocean and reach this area, have a lower frequency than the wind waves are usually from the west. According to the results in Table 2, the presence of these components with different peak frequencies creates more forces in the joints, which will result in increased energy converter efficiency.

6. References

[1] Wang Y. Predicting absorbed power of a wave energy converter in a nonlinear mixed sea. Renewable Energy. 2020 Jun 1; 153:362-74.
[2] Adibzade M, Shafieefar M, Akbari H, Panahi R. Multi-peaked directional wave spectra based on extensive field measurement data in the Gulf of Oman. Ocean Engineering. 2021 Jun 15; 230:109057.
[3] M Ji X, Al Shami E, Monty J, Wang X. Modelling of linear and non-linear two-body wave energy converters under regular and irregular wave conditions. Renewable Energy. 2020 Mar 1; 147:487-501.
[4] Loh TT, Pizer D, Simmonds D, Kyte A, Greaves D. Simulation and analysis of wave-structure interactions for a semi-immersed horizontal cylinder. Ocean Engineering. 2018 Jan 1; 147:676-89.

RESEARCH PRIORITIES GIVEN THE MRE CONVERTERS: A CASE STUDY IN WALES

Ali Pourzangbar[1], Alireza Vakili[2]

1) Dipartimento di Ingegneria, Civile, Edile e di Architettura, Università Politecnica delle Marche, Ancona, Italy, A.pourzangbar@staff.sut.ac
2) Department of Engineering, University College of Nabi Akram, Tabriz, Iran Vakili.meceng@yahoo.com

1. Introduction

Marine wave energy is being increasingly regarded in many countries as a major and promising renewable resource [1]. It can be divided into offshore wind, tides (tidal stream and tidal ranges), ocean currents, waves, ocean thermal energy, salinity gradients, and biomass. Wave energy has the potential to provide at least 15% of the UK's annual electricity and help the country meet its Net Zero greenhouse gas emissions target by 2050 [2]. Climate change is already happening in the UK - the ten hottest years on record have all been since 1990. In response to international concern surrounding the impacts of climate change, the UK government has committed to ambitious carbon emission reduction targets of at least 80% by 2050. To achieve these targets, it is estimated that a key portion of the UK electricity will need to be generated from renewable sources [3]. The marine renewable energy industry is expanding globally in response to increased energy demands and the desire to curtail greenhouse gas emissions.

2. MRE Converters in Wales

2.1. Minesto

Minesto are developing their Deep Green project off the coast of Anglesey with a 10MW array. Deep Green is a unique technology that can operate cost effectively in low velocities. They have also established a manufacturing and assembly hall in Holyhead, from which they plan to export devices globally.

Increased performance, reduced costs, and scalable for commercial installations**:** Using extensive CFD modelling, ocean scale model testing and operational data, Minesto's technology development team has been able to improve the energy conversion and at the same time refine the power plant by reducing the number of power plant subsystems and components. In addition, it simplifies handling during installation and maintenance, which is crucial when Minesto now scales up the technology to megawatt-sized power plants for commercial installations.

Tailored to customer needs and operating conditions: The Dragon Class design scale effectively and will thus be available in different sizes tailored for maximum yield depending on site conditions like water flow rate and depth.

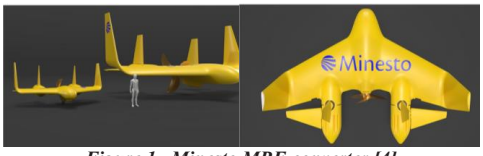

Figure 1. Minesto MRE converter [4]

2.2. Nova Innovation

Nova is developing a 1MW array, building on the success of deploying the world's first commercial tidal array in Shetland in 2016. Rapid deployment: our plug and play system enables our turbines to be containerized, transported, and installed anywhere in the world using locally available infrastructure.

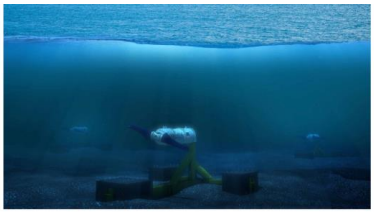

Figure 2. Minesto MRE converter [5]

2.3. BOMBORA Wave Power:

Bombora is an Australian wave energy developer (Figure 3) that has developed an innovative and patented wave energy converter called the mWave. Bombora has developed a patented membrane-style wave energy converter, mWave™. mWave™ is unique among wave energy converters as it simultaneously addresses the cost of energy and ocean wave survivability challenges.

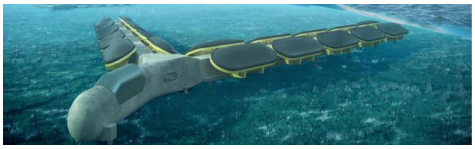

Figure 3. Bombora wave converter [6]

2.4. Marine power systems limited (see Figure 4):

Marine Power Systems (MPS) Ltd. have developed and tested the *WaveSub Wave Energy Converter (WEC)* which has undergone sea trials in FaBTest. They are now constructing a full-scale prototype which will also function as a floating offshore wind foundation.

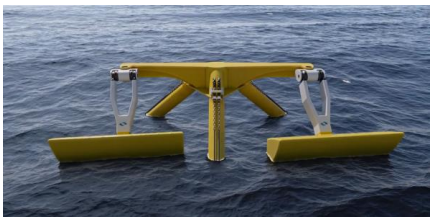

Figure 4. MPS wave converter [3]

3. Research Priorities

There is room for improvement of energy extracting devices in the different phases' ranging from design, test, fabrication to implementation into the real environment. The research priorities can be classified into four categories including:

3.1. Data Collection and Analysis, Wave Simulation Tools and Installation Point

To design energy converters, we need to analyze the wave, tide, and wind data using statistical approaches. Although these methods will provide us with valuable information, they are not adequate for an efficient and robust design. There are two issues given the data: (1) data collection, and (2) data analysis

There are various methods such as in-situ measurements, remote sensing such as satellite observations, or mathematical models. There are some services that provide various data sources for a wide range of regions. For instance, Copernicus can provide data given the 6 core services including marine data.

To design the converters, we need local data, but usually the data at hand are collected a few km away from the construction site. For instance, the wave data collected in deep waters must be manipulated using wave transformation equations such as shoaling, refraction, diffraction, among others, to be accurate for local use. To determine the local wave parameters from the collected data, we have to use wave simulation tool such as Swan or Delft3D Wave module. The results of the wave simulation tool will highlight the positions prone to the high levels of wave energy.

The collected data are not so accurate in some cases, they contain many missing values and have several outliers. All these limitations compel us to exploit Data mining approaches to hindcast/forecast/predict the data of different resources such as wind, wave and even tides. Data mining approaches can help us to have high quality predictions which can be used for robust and stable designs during the life span of the converters. I am an expert in this field.

3.2. Environmental Effects of Energy Converters

When the energy converter locates in the water, it changes the hydrodynamics and morphodynamics of the nearshore zone. For instance, the structures locate on seabed onshore such as tidal lagoons or mWave converter designed by Bombora wave power, the interaction of the flow (wave)-seabed-structure will change the flow pattern regarding its capability in sediment transport, turbulence, vortex generation, among others. Furthermore, their existence may cause the waves break far from the coastline (breaking zone) and consequently some sand bars will generate in their vicinity which pose a threat to their stability and functionality.

One of the possible consequences will be the scour at the converters which threaten their stability and may cease their functionality.

3.3. Design Optimization

Recently, data-driven and optimization approaches such as Genetic Programming (GP) and Particle Swarm Optimization (PSO) [7] are integrated into the design process of marine structures to achieve the optimal configuration. Accordingly, the converter design must not be static. In other words, depending on the environmental condition, some components can be added/removed automatically. To do this, we can embed the design procedure to an optimization process and determine the most optimal configuration based on the selected design wave/wind/tide conditions. However, we can consider some moving components whose implementations can improve the quality of design under different conditions. For instance, under storm conditions, we can predict the storm using data mining and then active the special components considered for this condition. Nowadays, integrated systems like Multiple Wave Energy Converters Placed on a Floating Platform are increasing since they can provide different types of energy using one converter. Being successful in their design and fabrication may enhance the performance of energy converters in comparison to conventional ones.

4. References

[1] Falcao, A.F.O., “Wave energy utilization: A review of the technologies”, *Renewable and Sustainable Energy Reviews*, 14, 2010, pp. 899-918.

[2] Roche, R.C., Walker-Springett, K., Robins, P.E., et al., “Research priorities for assessing potential impacts of emerging marine renewable energy technologies: Insights from developments in Wales (UK)”, *Renewable Energy*, 99, 2016, pp. 1327e1341.

[3] www.marineenergywales.co.uk

[4] Skopljak, N., " Minesto unveils new range of power plants", September 20, 2021

[5] Marine Energy Wales, “Welsh government invests in the world’s first blue energy island”, November 2020.

[6] Bombora, “Wales on Route to a Clean Marine Energy Future,” Bombora, July 2020.

[7] Pourzangbar, A., Vaezi, M., Mousavi, S.M., Saber, A., 2020. “Effects of brace-viscous damper system on the dynamic response of steel frames”. *Int. J. Eng*. 33, 720–731.

14th International Conference on Coasts, Ports and Marine Structures
9 & 10 May 2023 , Tehran-IRAN
ICOPMAS 2022

MARINE FOULING EFFECTS ON THE RENEWABLE ENERGY HARVESTING FROM VORTEX-INDUCED VIBRATION OF CIRCULAR OSCILLATORS

Mohammadreza Rashki[1], Mostafa Zeinoddini[1], and Mohammadmahdi Aalami Harandi[1]

1) Faculty of Civil Engineering, K.N. Toosi University of Technology, Tehran, Iran,
m.r.rashki@email.kntu.ac.ir, zeinoddini@kntu.ac.ir, Mahdi.aalami@ut.ac.ir

1. Introduction

Vortex-Induced Vibration Aquatic Clean Energy (VIVACE) harvesting has been an attractive marine engineering research topic in recent years. It was first proposed by Bernitsas and Raghavan [1] at the University of Michigan. Many aspects of VIVACE harvesting have been examined [2-5]. What has not received previous attention is that immediately after a structure is placed in the seawater, marine fouling begins to inhabit its submerged surfaces. Marine fouling includes various species of different sizes and textures. They change the flow regime around the body by increasing its dimensions and surface roughness. In the case of VIVACE, marine fouling affects the amplitude of the Vortex-Induced Vibrations (VIVs), thus the magnitude and quality of the energy harvested from an oscillator. Jadidi and Zeinoddini [6] studied hard marine growth's effect on renewable energy harvesting from a single degree of freedom circular oscillator. They showed that hard marine growth negatively affects VIVACE harvesting. This paper presents the first study on the effects of soft marine growth on renewable energy harvesting from a single degree of freedom circular oscillator.

2. Laboratory Equipment and Modelling

The in-water VIVs towing tank experiments are performed on a vertical circular cylinder. The one degree of freedom mass-spring system used in this research is similar to that in the Jadidi and Zeinoddini [6], Assi et al. [7], and Zeinoddini et al. [8] experiments. The system consists of a rigid aluminum cylinder, a two-directional loadcell, and two leaf springs, which are placed between two horizontal stiff aluminum slabs. The upper aluminum slab is fixed underneath the carriage of the towing tank (Figure 1(top)). Based on the Terry and Picken study [9], hydroids have the highest frequency among soft marine growths observed on marine structures. Polishing fabrics are used in the present study to model the hydroid-type soft marine fouling. Three coverage ratios of 33, 67, and 100% are examined. Figure 1 (mid) illustrates a test cylinder with artificial soft marine fouling. Figure 1 (bottom) provides a picture of a natural community of hydroids [10].

3. Validation of the Experimental Set-up

Figure 2 depicts the non-dimensional amplitude of transverse oscillations ($A^*=A/D$) versus the reduced velocity ($U^*=U/f_nD$) from present VIVs tests conducted on a clean and smooth cylinder. Here, A is the amplitude of the oscillations, D is the cylinder diameter, f_n is the system's natural frequency, and U is the flow velocity. Figure 2 also provides the results of Kiu et al. [11] and Jadidi et al. [12] experiments on similar clean circular cylinders. The figure shows that the amplitude responses for the smooth cylinder from the current study are satisfactorily comparable with those from the two other studies.

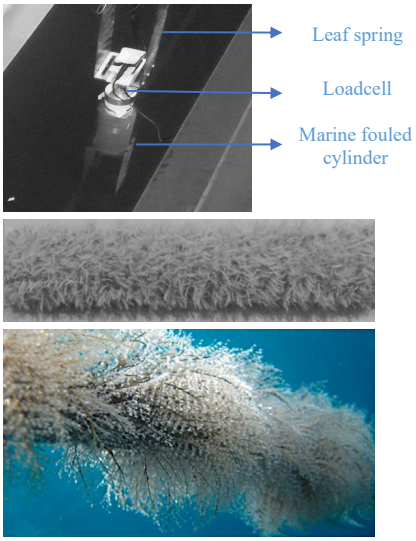

Figure 1. Towing tank VIVs testing of a marine-fouled cylinder (top), a test cylinder with artificial soft marine fouling (mid), and a natural community of hydroids [10] (bottom).

4. Renewable energy equations

The equation of motion of a cylinder in the cross-flow direction can be expressed as follows:

$$M_{osc}\ddot{y} + C\dot{y} + Ky = F_{\text{fluid}} \quad (1)$$

where M_{osc} is the mass of the system (sum of the oscillating masses and the added mass), C is the system's damping, K is the system stiffness, y, $\dot{y}$, $\ddot{y}$, are the

oscillator's displacement, velocity, and acceleration, respectively, and F_{fluid} is the viscous lift force applied to the oscillator. The mechanical power (P_{Mech}), the fluid power (P_w), and the energy ratio (η) can be derived from the VIVs test results as follows:

$$P_{Mech} = \frac{1}{T}\int_0^T C\dot{y}^2 dt \quad (2)$$

$$P_w = \frac{1}{2}\rho U^3 (D + 2A_{max})L \quad (3)$$

$$\eta = \frac{P_{Mech}}{C_{Betz} \times P_W} \quad (4)$$

where T is the time period, L is the length of the cylinder, C_{Betz} is 0.59, ρ is the water density.

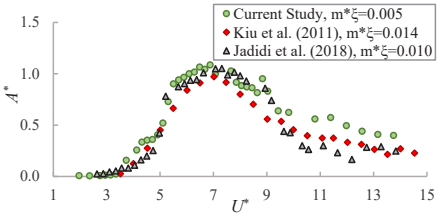

Figure 2. The VIVs response amplitude of a clean circular cylinder in different experiments.

5. Marine Fouling Effect

Figure 3 (top) compares the amplitude response of the clean and marine fouled cylinders with three different coverage ratios. It shows that the soft marine fouling reduces the oscillations' amplitudes (A^*) noticeably compared to A^* in the clean cylinder. The reduction becomes more pronounced by increasing the fouling coverage ratio. Figure 3 (bottom) shows that the energy harvesting ratio also markedly reduces in the presence of marine fouling. In general, the higher the coverage percentage, the more significant the decrease in the energy harvesting ratio.

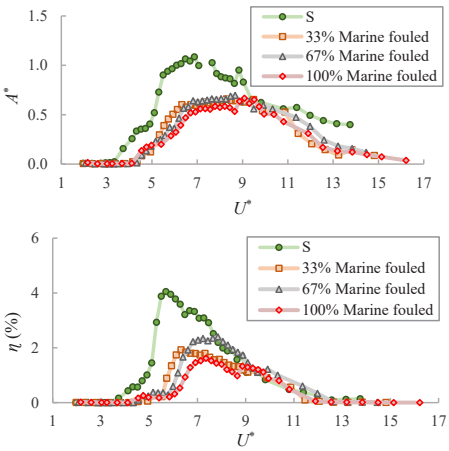

Figure 3. Effects of soft marine fouling on the VIVs response amplitude (top) and energy harvesting ratio (bottom).

6. Conclusions

This experimental study deals with renewable energy harvesting from VIVs and, in particular, the effects of soft marine fouling on the mechanical energy output from a circular oscillator. The results show that soft marine fouling noticeably affects energy harvesting. The fouling may halve the maximum energy harvesting ratio. The reduction in the energy harvesting ratio becomes more pronounced by increasing the marine fouling coverage ratio.

7. References

[1] M.M. Bernitsas, K. Raghavan, Converter of Current/tide/wave Energy, Provisional Patent Application, US Patent and Trademark Office Serial (60/628,252), 2004.
[2] J. Zhang, F. Liu, J. Lian, X. Yan, Q. Ren, Flow Induced Vibration and Energy Extraction of an Equilateral Triangle Prism at Different System Damping Ratios, Energies, Volume 9, Issue 1996-1073, 2016.
[3] H. Sun, M. M. Bernitsas, Bio-Inspired adaptive damping in hydrokinetic energy harnessing using flow-induced oscillations, Energy, Volume 176,2019, Pages 940-960.
[4] H. Sun, M. M. Bernitsas, M. Turkol, Adaptive harnessing damping in hydrokinetic energy conversion by two rough tandem-cylinders using flow-induced vibrations, Renewable Energy, Volume 149,2020, Pages 828-860.
[5] V. Tamimi, M. S. Seif, S. Shahvaghar-Asl, and S.T.O. Naeeni, and M. Zeinoddini, FIV Energy Harvesting from Sharp Edge Square and Diamond Oscillators, International Journal of Maritime Technology, Volume 12(0), 2019.
[6] P. Jadidi, M. Zeinoddini, Influence of hard marine fouling on energy harvesting from Vortex-Induced Vibrations of a single-cylinder, Renewable Energy, Volume 152,2020, Pages 516-528.
[7] G.R.S. Assi, J.R. Meneghini, J.A.P. Aranha, P.W. Bearman, E. Casaprima, Experimental investigation of flow-induced vibration interference between two circular cylinders, Journal of Fluids and Structures, Volume 22, 2006, Pages 819-827.
[8] M. Zeinoddini, V. Tamimi, Sh Maleki, S. Shahvaghar-Asl, A. Bakhtiari, Experimental study of viv of single tapered circular cylinders, Taper,2013
[9] L.A. Terry and G.B. Picken, Chapter 13 Algal Fouling in the North Sea, in Studies in Environmental Science, L.V. Evans and K.D. Hoagland, Editors. 1986, Elsevier. Pages 179-192.
[10] M. Bosch-Belmar, A. Escurriola, G. Milisenda, VL. Fuentes, S. Piraino. Harmful fouling communities on fish farms in the SW Mediterranean Sea: composition, growth and reproductive periods. Journal of Marine Science and Engineering. Volume 7(9) ,2019. Pages 288.
[11] K.Y. Kiu, B. Stappenbelt, K.P. Thiagarajan, Effects of uniform surface roughness on vortex-induced vibration of towed vertical cylinders. Journal of Sound and Vibration, 2011, Pages 4753-4763.
[12] P. Jadidi, M. Zeinoddini, M. Soltanpour, A.P. Zandi, M.S. Seif. Towards an understanding of marine fouling effects on VIV of circular cylinders: Aggregation effects. Ocean Engineering, 2018; 147: 227-242.

FEASIBILITY of OSCILLATING WATER COLUMN WAVE CONVERTOR IN PERSIAN GULF

Mohammad Reza Mirahmad[1] and Mohammad Hossein Jahangir[2]

1) College of Agriculture & Natural Resources, University of Tehran, Tehran, Iran, mirahmad.mreza@ut.ac.ir
2) Faculty of New Sciences and Technologies, University of Tehran, Tehran, Iran, mh.jahangir@ut.ac.ir

1. Introduction

The growing energy demand, along with the environmental problems caused by the consumption of fossil fuels, has led to an increasing desire for renewable energy. Among renewable energies, wave energy has always been considered because of its availability on most days of the year and its high potential. Ocean waves are an important source of renewable energy; If extensively used, they can significantly contribute to the power supply of coastal zone countries. Wave energy is not economically competitive at present, but thanks to the high power of the sea waves and its potential utilization, it is still attracting engineers. Efforts to capture the power of the ocean and understand its behavior have become a major challenge that increased the demand for investment in innovation and technology, as well as the growth promotion and competition in the maritime economy of many strategic regions around the world. The development of maritime activities requires robust and more reliable systems. An oscillating water column converter is one of the converters which converts sea wave energy into electrical energy. Because of the fluctuation of the water level at the outlet to the sea in this converter, the trapped air inside the chamber is removed and re-entered to move the turbine located at the other outlet (Figure1).

Figure 1. OWC structure

2. Literature Review

In a study, Bouali and Larbi by performing simulations in CFX software showed that the chamber size, the depth of immersion of the front wall of the device, and its orientation toward the flow direction have a very important effect on the performance of the device [1]. Hashemi et al. extracted the governing relationships of the OWC converter with the shape of a cylindrical chamber [2]. Rodriguez et al. showed that with increasing the thickness of the front wall, bandwidth on efficiency curves decreases [3]. Luo and Cooper observed that in completely nonlinear waves, increasing the wave height will significantly decrease the hydrodynamic absorption efficiency of the OWC, which indicates a significant deviation from the linear wave state [4].

3. Methodology

In this study, daily data of Persian Gulf waves for one year (2018) were received from the National Institute for Oceanography and Atmospheric Sciences (INCOD). These characteristics include wave height, wavelength and, wave period with an interval of one hour per day. Then, with the help of coding using Python language, the latitude and longitude of the points inside the sea border of Iran were extracted. Since this type of converter is located on the rocky shore wall, among the extracted points, those that are closer to the shoreline were isolated. Then the potential of the Persian Gulf region limited to the interior of the Iranian border for using this type of converter has been measured.

4. Results

The results show that some of the studied areas have the acceptable potential for using this type of converter. For instance, the waves in the Parsian region of Hormozgan province in Iran have a good potential to use this converter. The wavelengths of the mentioned area are longer than other points; therefore, it has a great effect on the power of the waves and ultimately the converter power (Table 1).

Table 1. Stations and their efficiencies

Station number	latitude	Longitude	η %
1	30.125	50	2.8
2	28.75	51	3.1
3	27.75	52	4
4	27.125	53	15
5	26.75	54	1
6	26.625	55	1
7	27	56	0.5

After analyzing the data in this particular area, the dimensions of the converter were changed to improve its efficiency. In the best possible case and using a converter with an efficiency of about 15%, it is possible to produce an average power of about 79 kW.

5. References

[1] B. Bouali and S. Larbi, "Contribution to the Geometry Optimization of an Oscillating Water Column Wave Energy Converter," Energy Procedia, vol. 36, pp. 565–573, Jan. 2013, doi: 10.1016/J.EGYPRO.2013.07.065.
[2] M. J. Hashemi, M. J. Khanjani, M. R. Baradaran and V. Kalantari, "Hydrodynamic investigation of a water oscillating column (owc) inside a floating cylinder," International conference on styling and earthquake, 2010, coi: ICLWCE01_092, [In Persian]
[3] A. A. M. Rodríguez, J. M. B. Ilzarbe, R. S. Casarín, and U. I. Ereño, "The Influence of the Chamber Configuration on the Hydrodynamic Efficiency of Oscillating Water Column Devices," Journal of Marine Science and Engineering 2020, Vol. 8, Page 751, vol. 8, no. 10, p. 751, Sep. 2020, doi: 10.3390/JMSE8100751.
[4] Y. Luo, J. R. Nader, P. Cooper, and S. P. Zhu, "Nonlinear 2D analysis of the efficiency of fixed Oscillating Water Column wave energy converters," Renewable Energy, vol. 64, pp. 255–265, Apr. 2014, doi: 10.1016/J.RENENE.2013.11.007.

WAVE ENERGY VARIATION IN THE PERSIAN GULF UNDER SSPs CLIMATE SCENARIOS

Saeideh Baghanian[1], Mohammad Javad Alizadeh[2]

1) Formerly, Civil Engineering Department, K. N. Toosi University of Technology, Tehran, Iran, baghanian@email.kntu.ac.ir
2) Caspian Sea National Research Center, Water Research Institute, Tehran, Iran, mjalizadeh@mail.kntu.ac.ir

1. Introduction

The energy generation from fossil fuels is considered to be related to environmental pollution, and also to produce CO_2, which is currently recognized for its adverse effect on climate change.

These resources are limited, and due to the increasing rate of population growth and the overwhelming demands for energy consumption, which depends a lot on hydrocarbon deposits, alternative methods like utilizing renewable energy sources should take place [1]. They are clean, and almost all regions can facilitate their nation depending on their environmental features, using different types of renewable energy like wind and wave energy.

2. Study Area and Data Description

The study location of this research is the Persian Gulf which is a shallow, semi-enclosed marginal sea, with an average depth of 35 m in the south of Iran [2]. This region produces almost one-third of the world's oil and has reserved a significant portion of the world's natural gas.

The dominant wind over the Persian Gulf is the Shamal wind, which blows from the northwest and may have a speed of up to 20 m/s. There are also some monsoons, such as Kaus which blow from the southwest, and play a remarkable role in creating the cold and warm circulation of the ocean.

In this study, the hourly wind data obtained from some global climate models' projections in the CMIP6, is calibrated by ERA5 reanalysis data, downscaled by a Weibull method [3], and applied as the primary input data in the SWAN wave model and obtain the wave model that best represents the study area.

The bathymetric data was extracted from GEBCO (General Bathymetric Chart of the Oceans) using a 30 arc-second interval grid. Northward and eastward wind speeds at 10 m were obtained from the 10 CMIP6 GCMs and subsequently bias-corrected according to the reference data (ERA5). The modified wind fields for various climate change scenarios have been used to force the numerical wave model (SWAN).

To analyze the performance of the wave model outputs, data observations for significant wave height were used at two buoy stations, Asaluyeh and Bushehr. Besides statistical analysis has been performed, and based on the values of correlation variance obtained from each model and being closer to 1, as well as considering the mean relative error, among the climate models, the model ACCESS 1.0 has been designated as the most appropriate one for the Persian Gulf, and the wave climate analysis in this study is made based on it.

Figure 1 illustrates the wave roses for the historical period and SSP5-8.5. The dominant mean wave direction is preserved in the direction of the Shamal wind. In the northern part of the gulf, the waves incline to the west (P1, and P2). In the deeper water and the middle of the gulf, there are stronger wave incidences, and the direction is mostly in the northwest. Since the wave model simulates more powerful waves in points P3 to P5, the study of wave energy is based on the P4 results as a representative point.

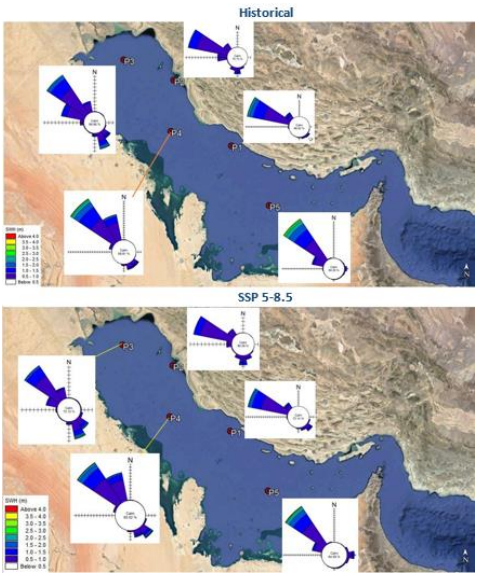

Figure 1. The wave roses in the Persian Gulf in Historical Time Spans, and Future Projection

As illustrated in Figure 1, wave direction variability under a high emission scenario (SSP5-8.5) from CMIP6 is marginal. Moreover, the rose plot reveals a partial decrease in high waves (the green petals).

3. Modeling Process

The wave energy is calculated using Equation 1. In each sea state, i.e., every 6 hours in the total time spans for historical data (1981-2000) and the future projections (2081-2100) under SSP1-2.6, SSP-.4.5, and SSP5-8.5 scenarios.

$$E = \frac{\rho g H^2 L}{8} \quad (1)$$

Where ρ is water density, g is the acceleration of gravity, H is the significant wave height, and L is the wavelength that is assumed $1.56T_p^2$ in deep water.

4. Results and Discussion

The mean of wind speed, wave energy, and significant wave height for the historical period and the future projection under the three forcing scenarios are illustrated in Figure 2. All mean values show a descending trend. For wind speed, the result of SSP 5-8.5 which is considered the most severe climate forcing scenario, has a 40% relative difference from the corresponding historical results.

Wave Energy is dependent on the wave height and the waves are generated by surface winds. Therefore, any changes in the wind characteristics result in wave climate change.

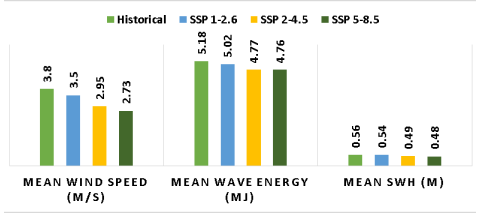

Figure 2.The Comparison of Wind Speed, Wave Height, and Wave Energy under different Climate Scenarios

The variation of wave energy relative to the wind speed is presented in Figure 3. In wind speeds below 10 m/s, there is no significant difference between historical and future wave energy. However, in the wind speed above 12, there is a noteworthy difference between wave energies. As is illustrated in the speed of 14 m/s, the wave energy is around 70 MJ for the historical period, while the corresponding wave energy for SSP5-8.5 is about 140 MJ. However, the Persian Gulf and Oman Sea are considered as the areas with wave energy potential less than 5 Kw/m [1], which is not applicable for energy conversion, and the possibility of the occurrence of 14m/s wind speed in the Persian Gulf is very low, and it may only come about in some extreme conditions, which are also very improbable.

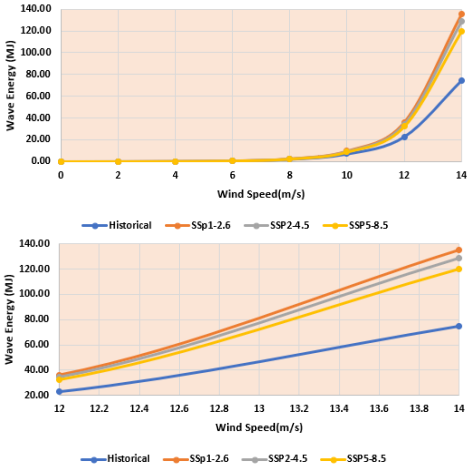

Figure 3. Wave Energy is based on Wind Speed under different Climate Scenarios

5. References

[1] Pecher, A.; Kofoed, J.P. Erratum: Handbook of ocean wave energy. In Ocean Engineering & Oceanography; Springer: Cham, Switzerland, 2017; p. E1.

[2] "The Persian Gulf Pilot", The United Kingdom Hydrographic Office, United Kingdom, 2005.

[3] Alizadeh, Mohamad Javad, Mohamad Reza Kavianpour, Bahareh Kamranzad, and Amir Etemad-Shahidi. "A Weibull distribution-based technique for downscaling of the climatic wind field." Asia-Pacific Journal of Atmospheric Sciences 55, no. 4 (2019): 685-700.

FLUORESCENT SAND-TRACER EXPERIMENT IN AMIRABAD PORT COASTAL ZONE IN THE CASPIAN SEA

Nasser Hadjizadeh Zaker[1], Pendar Hadinezhad [2]

1) Associate Professor, University of Tehran, College of engineering, Faculty of environment, Tehran, Iran, nhzaker@ut.ac.ir
2) University of Tehran, College of engineering, Faculty of environment, Tehran, Iran, Pendar.hadinezhad@ut.ac.ir

1. Introduction

Construction of coastal structures significantly affects the natural sediment transport and could cause deposition on the up-drift side and erosion on the down-drift side of the structure. The former could result in major problems for navigation and the latter may result in certain environmental damages. Therefore, clear understanding of the dynamics of coastal sediment transport is of great importance for the design of coastal structures including breakwaters, jetties and groins as well as finding solution for sedimentation problems of the constructed ones.

However, the dynamics of coastal sediment transport is very complex and its understanding faces major difficulties, especially in coastal areas with extensive development of coastal structures.

One of the best methods available to provide reliable field data for coastal sediment transport study is fluorescent sand tracing. In this method, the marked sands with fluorescent inks are injected in the coastal area, and their movement are traced (Silva et al. 2007; Badr and Lotfy 1999; Ciavola et al., 1998; Duane et al. 1980; Fields and Weishar 1987; Madsen 1987; Muñoz-Perez et al. 1999; Sherman et al. 1990; Silva et al. 2007; Vila-Concejo et al. 2004)

Amirabad Port in the southern coast of the Caspian Sea. faces major sedimentation problems and requires considerable dredging in its access channel and inside its breakwater and certain actions for reducing the port sedimentation is needed. However, knowledge about sediment transportation dynamics in the coastal area of Amirabad Port is mainly based on numerical modeling studies.

This paper provides information about the use of sand tracer method in the coastal area of the Amirabad Port.

2. Materials and Methods

Before the field experiment, a comprehensive set of tests of the marking process carried out in the laboratory of Iranian Institute for Color Science and Technology including the test of different inks, components proportions and marking processes. From the results of these tests, four inks were selected and used for marking sand traces (Figure 1).

Fig. 1: Marking sand traces with four inks of yellow, orange, red and green, using sands from Amirabad Port coastal area

Four different color tracers (yellow, orange, red and green) were injected at four depths of 2m, 5m, 8m and 10m along a cross-shore line in Amirabad coastal area in September 2019 (Figure 2).

Fig. 2: Injection of colored traces into coastal waters of Amirabad Port.

Sediment samples were collected over a wide part of the Amirabad coastal area during two field experiments conducted 30 and 60 days after tracer injection. The samples were examined for the detection of sand tracers by use of UV radiation (Figure 3).

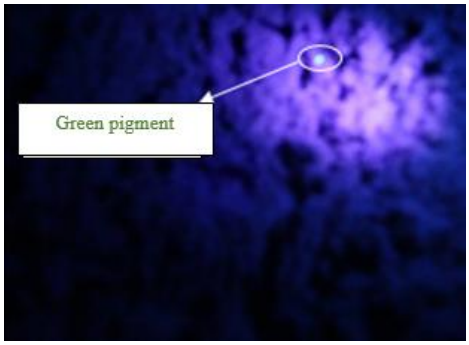

Fig. 3: Detection of sand traces using UV radiation.

3. Results

Among 83 sediment samples that were collected in two field experiments 30 and 60 days after tracer injection, in 41 of samples sand tracers were detected. The results showed successful performance of the experiment and provided data for the study of sediment transport in the study area. The results also provided information, knowledge and experience for conducting similar experiments in other coastal areas of Iran.

4. References

[1] Badr, A. and Lotfy, M., Tracing Beach Sand Movement Using Fluorescent Quartz Along the Nile Delta Promontories, Egypt. Journal of Coastal Resseach, 1999, Vol. 15, No.1, 1999, 261-265
[2] CIAVOLA, P.; DIAS, N.; FEREIRA, O´.; TABORDA, R., and DIAS, J.M.A.,1998. Fluorescent sands for measurements of longshore transport rates: a case study from Praia de Faro in southern Portugal. Geo-Marine Letters, 18, 49–57.
[3] Duane, D.V., James, W.R., 1980. Littoral transport in the surf zone elucidated by an eulerian sediment tracer experiment. J. Sediment. Petrol. 50 (3), 929–942.
[4] Fields, M.L., Weishar, L.L., 1987. Distribution of sediment tracers seaward of the breaker zone-Duck85. Proc. Coastal Sediments. ASCE, New York, pp. 848–864.
[5] Madsen, O.S., 1987. Use of tracers in sediment transport studies. Proc. Coastal Sediments. ASCE, New York, pp. 424–435.
[6] Muñoz-Perez, J.J., Gutierrez-Mas, J.M., Parrado, J.M., Moreno, L.,1999. Sediment transport velocity by tracer experiment at Regla Beach (Spain). J.Waterw., Port Coast., Ocean. Eng. 125, 332–335.
[7] Sherman, D.J., Bauer, B.O., Nordstrom, K.F., Allen, J.R., 1990. A tracer study of sediment transport in the vicinity of a groin: New York, U.S.A. J. Coast. Res. 6 (2), 427–438.
[8] Silva, A., et al., Longshore drift estimation using fluorescent tracers: New insights from an experiment at Comporta Beach, Portugal. Marine Geology, 2007. 240(1-4): p. 137-150.
[9] Vila-Concejo, A., Ferreira, Ó., Ciavola, P., Matias, A., Dias, J.M.A., 2004. Tracer studies on the updrift margino of a complex inlet system. Mar. Geol. 208, 43–72.
[10] Silva et al. 2007; Badr and Lotfy 1999; Ciavola et al., 1998; Duane et al. 1980; Fields and Weishar 1987; Madsen 1987; Muñoz-Perez et al. 1999; Sherman et al. 1990; Silva et al. 2007; Vila-Concejo et al. 2004

14th International Conference on Coasts, Ports and Marine Structures
9 & 10 May 2023 , Tehran-IRAN
ICOPMAS 2022

ONLINE MONITORING OF DREDGING OPERATION AND MEASURING SEDIMENT CONCENTRATION PASSING THROUGH DREDGER PIPE

Nazilla Tarabi[1], Hossein Mousazadeh[2], Ali Jafari[3] and Jalil Taghizadeh-Tameh[4]

1) Mechanical Engineering of Biosystems, University of Tehran, Iran, tarabi99@ut.ac.ir
2) Mechanical Engineering of Biosystems, University of Tehran, Iran, hmousazade@ut.ac.ir
3) Mechanical Engineering of Biosystems, University of Tehran, Iran, jafarya@ut.ac.ir
4) Mechanical Engineering of Biosystems, University of Tehran, Iran, taghizadeh68@ut.ac.ir

1. Introduction

Dredging is a routine necessity in waterways because sedimentation gradually fills channels and harbors. In comparison with other sediment transportation in pipelines, the control of dredged materials faces the following challenges; Firstly, the dredged slurry differs from a homogeneous material, such as mineral slurry [1], oil [2], and may include coarse particles of hard rocks that vary in size [3]. Secondly, the dredger ship is usually located several kilometers away from the final disposal area, and the dredged slurry must be transported to the area with a high concentration [4]. Moreover, the distribution of solid particles along the pipeline is uneven, and the particles tend to accumulate at the bottom of the pipeline because of gravity. Thus, if the flow rate is too slow, the solid particles of slurry will be deposited on the bottom of the pipeline, causing blockage accidents. Therefore, the method of measuring the concentration of these sediments should be a non-intrusive method and cover the entire section of the pipe. Conventional sensing techniques of dredging sediments concentration, are based on nuclear mass flow meters. Due to use of a radioactive source in the nuclear mass flow meter, while its environmental and economic impact, insurance, transport, supervision, certification training and disposal, caused many researches to concentrate for using an alternative method. Also, online measuring of the sediment concentrations and showing a dredging map will increase dredging efficiency, dredger life, reduce costs, and increase user satisfaction. Therefore, in the present study, a special electrical impedance tomography (EIT) system is designed and constructed to monitor performance of the dredging process. EIT system is online imaging systems that in contrast to most non-tomography sensing techniques, which can provide only a single-point measurement value, EIT sensing technique can provide a cross-sectional image of a measurement object or process and represent further information. Also, the EIT system does not have the limitations of conventional tomography such as MRI and CT scan. The objectives of this system are to determine online the concentration of passing sediments, velocity and efficiency of dredging, filling of the hopper in hopper suction dredger, prevention of pipes blockage in cutter suction dredger and the determination of the dredged locations with the amount of extracting in each point.

2. Materials and Methods

A high-speed EIT-based instrument abbreviated as BDSS (Basir Dredge Support System), designed and developed in the mechatronics Lab. of University of Tehran. This system was actually developed to measure the concentration of sediment passing through large dredger pipes. The system was installed and its performance investigated on the Khazar dredger ship, a Suction Hopper Dredger (SHD) with hopper capacity and pipe inner diameter of 650 m^2 and 610 mm respectively. According to Figure 1, 16 sensors are embedded at equal distances in perimeter of a vertical pipe with outer diameter about 700 mm. The diameter of each sensor is 60 mm. Liquid phase in the phantom under test was saline water with ratio of 12.5 $gr.lit^{-1}$ of NaCl (equivalent to conductivity of 18 $ms.cm^{-1}$ in temperature of 25 oC).

Figure 1. Suction Hopper Dredger of Khazar and Basir Dredge Support System

A graphical user interface (GUI) was designed that shows online dredging operation for user at the bridge (Figure 2). The GUI has two main screens. On the first page (Figure 3), a map of dredged sediments is drawn and shows the intensity of sediment extracting using colors.

The second page (Figure 4) shows the tomogram drawn by the EIT system as well as other fluid characteristics such as concentration, velocity, mass flow rate and efficiency.

Figure 2. Display unit of EIT system at bridge of Khazar ship

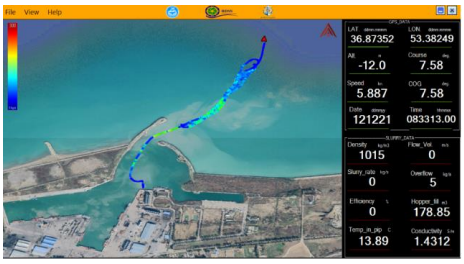

Figure 3. Map of dredged sediments that is designed by graphical user interface

3. Results and Discussion

Figure 4 illustrates the reconstructed image from the cross section of pipe in the different solid volumetric concentrations and velocity for the dynamic experiments. Effect of main variable parameters, such as variation of temperature and salinity of liquid phase (seawater) on performance of the BDSS was evaluated.

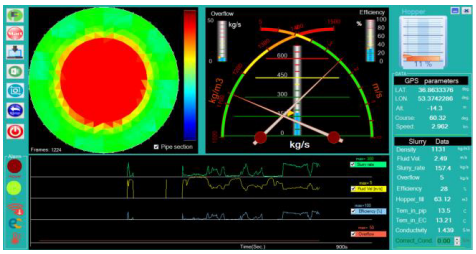

Figure 4. Reconstructed images from the cross section of pipe and changes of velocity with sediment concentration

The results show a linear trend and acceptable correlation between the data obtained from tomography and the measured data by the sampling method. The coefficient of determination is almost 0.98 to 0.99 for each curve in different levels of temperature and salinity. So, according to these curves accuracy of BDSS is in acceptable range and change in temperature and salinity could be compensated by the algorithm in a right manner.

Results of the evaluation of system on the dredger showed that the system is able to measure the maximum mass flow (330 kg/s) of materials that passing through the dredging pipe. The results of this study also showed that with increasing the concentration of load passing through the pipe, the velocity of sediment passage through the pipe decreases. So that the maximum velocity for seawater through the pipe is 5 m/s and the minimum velocity for high concentrations is 1.5 m/s.

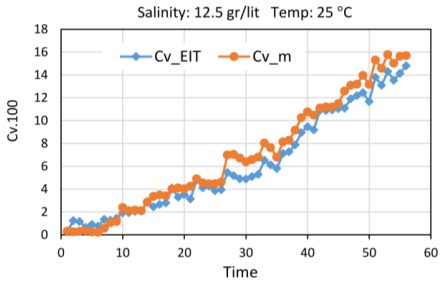

Figure 4. Volumetric concentration of BDSS and manual sampling

4. Conclusion

This manuscript presents a slurry concentration monitoring system in dredger pipeline with the ability to measure mass concentration of up to 650 gr/lit and mass flow rate of 330 kg/s. An electrical impedance tomography system was developed and evaluated for online monitoring of solid-liquid two-phase fluid (dredging sediments) passing through a 610 mm diameter pipe. The results showed that due to the fast response of the system and its resolution, tomography technique can be used to measure the concentration of load passing through dredged pipes and is an appropriate alternative to nuclear density meters.

5. Acknowledgment

Authors would like to acknowledge the Ports and Maritime Organization for funding the project by grant No. 3528/S20, 2018-2020.

6. References

[1] Singh, M.K., Kumar, S., Ratha, D., Kaur, H., 2017. Design of slurry transportation pipeline for the flow of muti-particulate coal ash suspension. Int. J. Hydrogen Energy 42 (30), 19135–19138

[2] Priyanka, E., Maheswari, C., Thangavel, S., 2018. Online monitoring and control of flow rate in oil pipelines transportation system by using plc based fuzzy-pid controller. Flow Meas. Instrum. 62, 144–151.

[3] Ting, X., Xinzhuo, Z., Miedema, S.A., Xiuhan, C., 2019. Study of the characteristics of the flow regimes and dynamics of coarse particles in pipeline transportation.

[4] Bai, S., Li, M., Kong, R., Han, S., Li, H., Qin, L., 2019. Data mining approach to construction productivity prediction for cutter suction dredgers.

14th International Conference on Coasts, Ports and Marine Structures
9 & 10 May 2023 , Tehran-IRAN
ICOPMAS 2022

LABORATORY STUDY OF THE OF CARBONATE SEDIMENT TRANSPORT IN STEADY UNIFORM FLOW

Erfan Amiri[1], Mohsen Soltanpour[2]

1) Formerly, Civil Engineering Dept., K. N. Toosi University of Technology, Tehran, Iran, erfanamiri1374@gmail.com
2) Civil Engineering Dept., K. N. Toosi University of Technology, Tehran, Iran, Tehran, Iran, soltanpour@kntu.ac.ir

1. Introduction

Sediment transport is an important ingredient of coastal and river engineering as it highly affects sediment accumulation in channels, erosion around structures, nearshore morphological change, etc. Terrigenous sediments, derived from weathering and erosion of continental rocks, are predominant along the continental margins in mid-to high latitude. The terrigenous sediment in origin are replaced by carbonate sediments, i.e. carbonate sands and fine-grained carbonate muds, along arid coastlines and other areas, where the supply of terrigenous sediment is limited or absent [1]. Coral reefs are the great engines of carbonate sediment production [2].

Most of solid material is carried within the water flow as suspended sediment but some is rolled or bounced along the bed as bed-load. Many researchers have proposed equations for bed-load transport rate (e.g., Shields (1936) [3], Meyer-Peter and Müller (1948) [4], Engelund and Fredsoe (1976) [5]).

In the present study, a series of laboratory tests is designed in a circulating rectangular flume to study the bed-load transport of carbonate sediments. Following Roseberry et al. (2012) [6], open-source ImageJ software is employed for particle tracking, i.e. to measure the particle velocities for the calculation of bed-load [7]. Dimensional analysis is used to define the important dimensionless variables, e.g. Shields number, for data analysis [8]. Finally, Lab Fit is employed for multiple regression to derive the bed-load transport formula of carbonate sands.

2. Laboratory Setup

The tests are performed in a rectangular flume of 12 m in length, 30 cm in width, and 45 cm in height at Hydraulic Models Lab. of K. N. Toosi University of technology (Figure 1). Two samples of natural carbonate sediments were taken from the coasts of the Persian Gulf with median sizes of D_{50}=0.4mm and D_{50}=0.42mm and the density of sediments of ρ_s=2830 kg/m^3 and ρ_s=2620 kg/m^3, respectively. A part of sediment particles is fixed to the flume bed to provide similar roughness of natural environments.

A high-speed camera of 30 frames per second (fps) is fixed to top of the flume to monitor the particle motions above the water surface (Figure 1). The water depth and flow rate are measured at some stations along the flume to ensure the steady uniform flow. Feeding 0.5 gr of sediment from the top at each laboratory test case, 31 test runs are performed with different flow rates. Table 1 shows the sediment characteristics and hydraulic parameters of laboratory tests.

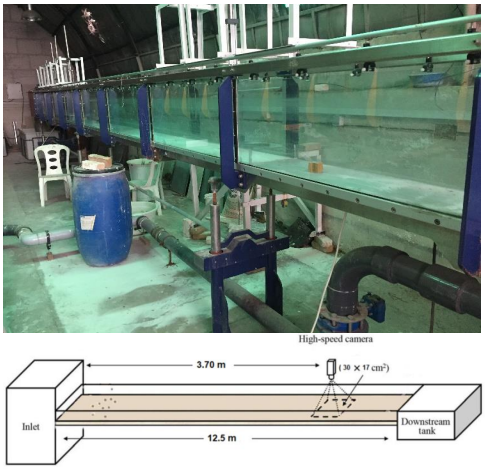

Figure 1. Side view of flume (top) and laboratory setup (bottom, not to scale).

3. Dimensional Analysis

Considering the important parameters, the rate of the bed-load transport can be generally expressed as:

$$q = f\left(u_*, H, g, \rho, \rho_s, D_{50}, \nu, S\right) \quad (1)$$

where u_* is shear velocity, H is flow depth, g is gravity acceleration, ρ is flow density, ρ_s is sediment density, D_{50} is median sediment diameter, ν is the kinematic viscosity of

Table 1. Hydraulic parameters and sediment characteristics.

	1st sediment sample	2nd sediment sample
D_{50} (m)	0.0004	0.00042
Q (m^3s^{-1})	0.004-0.016	0.007-0.01
S	0.0016	0.0016
H (m)	0.044-0.095	0.058-0.073
V (ms^{-1})	0.3-0.56	0.4-0.45
τ_* (Nm^{-2})	0.084-0.145	0.11-0.13
u_* (ms^{-1})	0.025-0.032	0.027-0.03
ρ_s (kgm^{-3})	2830	2620

water and S is bed slope. By Buckingham π theorem, Eq. (1) is reduced to 6 non-dimensional parameters:

$$q_* = g\left(R, Re_s, \tau_*, \frac{D}{H}, S\right) \quad (2)$$

where

$$\pi_1 = \frac{\rho_s - \rho}{\rho} = R,$$

$$\pi_2 = \frac{\sqrt{RgD^3}}{\upsilon} = Re_s,$$

$$\pi_3 = \frac{u_*^2}{RgD} = \tau_*,$$

$$\pi_4 = \frac{D}{H},$$

$$\pi_5 = S, \text{ and}$$

$$\pi_6 = \frac{q}{\sqrt{RgD^3}} = q_*$$

Multiple Regression Method by LabFit results in the following formula for non-dimensional bed:

$$q* = 3.628 \times (R^{1.754} \times \frac{D}{H}^{1.026} \times Re_s^{1.532} \times \tau*^{3.114}) \quad (3)$$

where R is relative density, Re_s is settling Reynolds number, and τ_* is Shields number.

4. Discussion and Conclusion

Statistical parameters of Root Mean Square Error (RMSE) and Mean Absolute Error (MAE) can be used to evaluate the overall differences of model results and measurements:

$$\text{RMSE} = \sqrt{\frac{1}{N}\sum_{i=1}^{N}\left\{g_{bM}(i) - g_{bC}(i)\right\}^2} \quad (4)$$

$$\text{MAE} = \frac{1}{N}\sum_{i=1}^{N}\left|g_{bM}(i) - g_{bC}(i)\right| \quad (5)$$

where N is number of test cases, g_{bM} is the measured bed load by image processing, and g_{bC} is the calculated bed load by empirical formulas [9].

Table 2 shows the prediction errors of Eq. (3) and different bed load formulas. It is observed that Duboys, Meyer-Peter and Rottner formulas show better agreement with the conducted laboratory tests. The derived Eq. (3) can be used for the estimation of bed-load transport rate but its good performance needs to be further evaluated with more samples of carbonate sediments from different coasts.

Table 2. Prediction errors of Eq. (3) and existing bed load transport formulas.

	RMSE($kgm^{-1}s^{-1}$)	MAE($kgm^{-1}s^{-1}$)
Parker	0.0156	0.1142
Fernandez	0.0164	0.1227
Engelund	0.0685	0.2473
Ashida	0.0237	0.1426
Duboys	0.0004	0.0188
Meyer-Peter	0.0004	0.0189
Rottner	0.0004	0.0189
Wong1	0.0041	0.0600
Wong2	0.0040	0.0591
Shields	0.0004	0.0189
Present study	0.0000	0.0000

5. References

[1] The Open University, 1999. Waves, Tides and Shallow Water Processes, 2nd edition. Butterworth-Heinemann, Oxford, 227 p.

[2] Sami, S., M. Soltanpour, and R. Lak., "Sedimentology of the west coastlines of nayband bay and the impact of carbonate sediment on the sedimentation in asaluyeh fishery port". *Journal of Marine Engineering*, 2010. **6**(11): pp. 45-57.

[3] Shields, A., "Anwendung der Ähnlichkeitsmechanik und der Turbulenzforschung auf die Geschiebebewegung Mitteilungen der Preußischen Versuchsanstalt für Wasserbau und Schiffbau". Heft, 1936. **26**: pp. 1-36.

[4] Meyer-Peter, E. and R. Müller. "Formulas for bed-load transport". *in IAHSR 2nd meeting, Stockholm, appendix 2*. 1948. IAHR.

[5] Engelund, F. and J. Fredsøe, "A sediment transport model for straight alluvial channels". *Hydrology Research*, 1976. **7**(5): pp. 293-306.

[6] Roseberry, J.C., M.W. Schmeeckle, and D.J. Furbish, "A probabilistic description of the bed load sediment flux: 2. Particle activity and motions". *Journal of Geophysical Research: Earth Surface*, 2012. **117**(F3).

[7] Shim, J. and J.G. Duan, "Experimental study of bed-load transport using particle motion tracking". *International Journal of Sediment Research*, 2017. **32**(1): pp. 73-81.

[8] Lajeunesse, E., L. Malverti, and F. Charru, "Bed load transport in turbulent flow at the grain scale: Experiments and modeling". *Journal of Geophysical Research: Earth Surface*, 2010. **115** (F4).

[9] Gouml, et al., "Experimental investigation of sediment transport in steady flows". *Scientific research and essays*, 2010. **5**(6): pp. 582-591.

14th International Conference on Coasts, Ports and Marine Structures
9 & 10 May 2023 , Tehran-IRAN
ICOPMAS 2022

AN IMPROVEMENT IN SURF ZONE SEDIMENT TRANSPORT PREDICTION IN COASTAL ENVIRONMENT UNDER ASYMMETRY WAVES

Mohammad Nabavianpour[1], Ahamad Shanesazzadeh[2]

1) University of Isfahan, Department of Civil Engineering, Isfahan, Iran, nabavianpour@gmail.com
2) University of Isfahan, Department of Civil Engineering, Isfahan, Iran, a.shanehsazzadeh@eng.ui.ac.ir

1. Introduction

The sediment transport models still heavily rely on physical data obtained in laboratory and field studies [1]. The objective of this study is to introduce a reliable, robust and rather simple formula for predicting total load transport subject to asymmetric waves in coastal environment.

General bed load formulas are considered in this study as the basis for calibration and verification of total sediment transport in the surf zone under asymmetric waves. The time-dependent transport was treated in a quasi-steady manner using the instantaneous Shields parameter for the two consecutive half-periods of the wave to implement in the 8 well known bed load formulas. The bed load formulas are calibrated using data from experimental measurement for a wide range of flows and sediment conditions.[2] The predictions are well improved by application of different threshold shear stress for onshore and offshore half-periods.

2. Background

The bed load transport is often represented by the following non-dimensional parameter:

$$\Phi = \frac{Q_B}{d\sqrt{(s-1)gd}} \quad (1)$$

Several relationships for bed load transport under a steady current have been proposed where the rate is related to the dimensionless bottom shear stress or Shields parameter, as follows:

$$\Phi \propto (\theta - \theta_c)\sqrt{\theta} \quad (2)$$

Where Shields parameters (θ)are defined as follows:

$$\theta = = \frac{\tau_0}{g\rho(s-1)d} \quad (3)$$

θ_c is the critical Shields parameter. In this study, a number of well-known general bed load relationships are applied for prediction of the total load in the surf zone under asymmetric waves.

3. Materials and Methods

Among the bed load relationships, 8 formulas including Meyer-Peter (1948), Bagnold (1966), Van Rijn (2007), Yalin (1963), Wilson (1966), Ashida and Michiue (1972), Madsen (1991) and Nielsen (1992) are considered as the main bed load formulas in order to apply in asymmetric waves [3-10]. The quasi-steady approach of Soulsby is applied to calculate the sediment transport in a wave orbit. The instantaneous velocity and bed shear stress is applied to calculate the instantaneous sediment transport, where the instantaneous sediment transport rate (q) is positive in the onshore direction and it is negative when velocity is in the opposite direction. The instantaneous rate is then integrated over the entire wave cycle [11].

The results are compared with the laboratory measurements. Different threshold velocities are applied for offshore direction to calibrate the formulas.

4. Result

The comparison between the results of the models and the measured values (40 different experimental data in total) are presented in Fig. 1, where comparatively more accurate prediction of Bagnold model is evident.

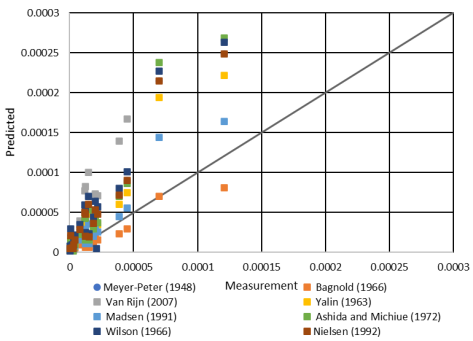

Figure 1. The comparison between the results of the models and the measurement

The comparison between the results of the models and measurements is presented in Table 1 in terms of root-mean-square error (RMSE) and percentage of correct estimate of direction. The threshold in offshore is generally considered less than onshore for better results both in terms of the amount and the direction of the sediment movement. According to Table 1, the root-mean-square error of Bagnold's method is about 1.2, which is much lower than

other methods. Also, by this method in 69%, the direction of sediment transport is correctly predicted by the model. Therefore, Bagnold's relationship with the following formula is considered as the best formula for predicting the total load in surf zone.

$$\emptyset = F_B \theta^{0/5} (\theta - \theta_{cr}) \quad (4)$$

$$F_B = \frac{0/1}{C_D^{1/2} (\tan \emptyset_i + tan\beta)} \quad (5)$$

Where, the angle of inclination Øi and the bed slope β are positive during onshore and negative during offshore direction of the half waves.

Table 1. The root mean square (RMSE) and the percentage of the correct direction of predicted sediment rates using measured data

	RMSE	Correct direction estimate of sediment transport (%)
Meyer-Peter (1948)	**1.9**	**69.0**
Bagnold (1966)	**1.2**	**69.0**
Van Rijn (2007)	**3.0**	**71.4**
Yalin (1963)	**4.3**	**42.9**
Madsen (1991)	**2.3**	**69.0**
Ashida (1972)	**1.7**	**71.4**
Wilson (1966)	**2.3**	**64.3**
Nielsen (1992)	**3.3**	**69.0**

5. Conclusion

The application and modification of the bed load transport formulas for non-cohesive sediment, based on the quasi steady bed-shear concept is introduced for predicting total sediment transport under asymmetric waves at coastal zone. The results indicate that Bagnold is the best in predicting the sediment rate of asymmetric waves in compare to the other well-known bed load based formulas More accurate prediction in terms of direction and value are achieved when threshold in offshore is considered less than in onshore direction.

Among the advantages of this study is introducing a rather simple method for the first hand estimate of sediment rate in the surf and swash zone, which can be applied in engineering practices.

6. References

[1]. Camenen, B., Larson, M. (2008): A general formula for noncohesive suspended sediment transport, Journal of Coastal Research, 615-627.
[2].Camenen, B., Larson, M. (2005): A bedload sediment transport formula for the nearshore, Estuarine, Coastal and Shelf Science, 63(1-2), 249-260.
[3]. Meyer-Peter, E. and Müller, R., 1948. Formulas for bed-load transport. In IAHSR 2nd meeting, Stockholm, appendix 2. IAHR.
[4]. Bagnold, R. A. (1966), An approach to the sediment transport problem from general physics, U.S. Geol. Surv. Prof. Pap., 422-I, 1–42.
[5].Van Rijn, L.C., 2007c. Unified view of sediment transport by currents and waves. III: graded beds. Journal of Hydraulic Engineering 133 (7), 761–775.
[6].Yalin, M.S., 1963. An expression for bed-load transportation. Journal of the Hydraulics Division, 89(3), pp.221-250.
[7].Wilson, K.C., 1966. Bed-load transport at high shear stress. Journal of the hydraulics division, 92(6), pp.49-59.
[8].Ashida, K. and Michiue, M., 1972, October. Study on hydraulic resistance and bed-load transport rate in alluvial streams. In Proceedings of the Japan society of civil engineers (Vol. 1972, No. 206, pp. 59-69). Japan Society of Civil Engineers.
[9].Madsen, O.S., 1991, July. Mechanics of cohesionless sediment transport in coastal waters. In Coastal sediments (pp. 15-27). ASCE.
[10].Nielsen, P., 1992. Three simple models of wave sediment transport. Coastal Engineering 12, 43–62.
[11]. Soulsby, R., 1997. Dynamics of Marine Sands, A Manual for Practical Applications. Thomas Telford, H.R. Wallingford, England, ISBN 0-7277-2584X.

MODELLING OF SEDIMENTATION AT BABOLSAR FISHERY PORT, IRAN

Hani Ghasemi[1], Mohsen Soltanpour[2], Ali Dastgheib[3] and Aref Farhangmehr[4]

1) Dept. of Civil Engineering, K. N. Toosi University of Technology, Tehran, Iran, hanighasemi@email.kntu.ac.ir
2) Dept. of Civil Engineering, K. N. Toosi University of Technology, Tehran, Iran, soltanpour@kntu.ac.ir
3) Dept. Coastal Engineering, Institute for Water Education, Delft, Netherlands, a.dastgheib@un-ihe.org
4) Institute of Geophysics, University of Tehran, Tehran, Iran, aref.farhangmehr@ut.ac.ir

1. Introduction

Port development in estuaries can have a considerable impact on estuary dynamics, resulting in hydrodynamic changes that alter sediment transport patterns. Understanding these consequences is critical because of socioeconomic importance and high sensitivity of the complex natural systems of estuaries [1].

Babolsar Fishery Port is located at the mouth of the Babolrood River in the southern part of the Caspian Sea (Figure 1). The lengths of the main and secondary rubble-mound breakwaters are 1100 m and 150 m, respectively. After the completion of the breakwaters in 1995, large sedimentation was observed. The water depth at the harbor decreased from 3 m to 1 m, based on the hydrography surveys of 1996 and 1999. In order to maintain the navigation depth along the river, the first remedy solution was to build a short guide-wall by steel sheet piles in 1999. However, the next hydrography surveys in 2000 and 2002 showed that this method is not capable to effectively reduce the infiltration of river sediments into the harbor and continuous dredging at the port entrance and along the river is still needed. In 2011, it was finally decided to construct a new rubble-mound breakwater, extending the guide-wall towards the port entrance (Figure 1) [2,3].

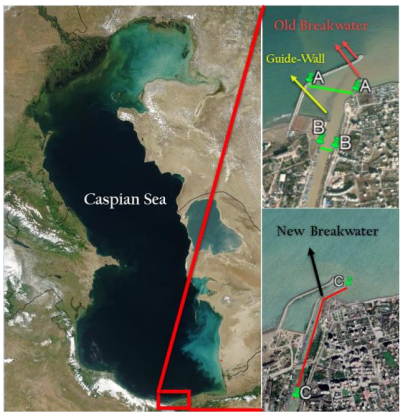

Figure 1. Babolsar Fishery Port

The purpose of this paper is to study the sedimentation problem at Babolsar Fishery Port and the morphological changes of Babolrood River as well as the effectiveness of remedy solutions.

2. Hydrography Surveys

Figure 2 presents four sets of conducted hydrography surveys at the site from 2000 to 2014. Bathymetry data at the river mouth in 1993, i.e., before the construction of the port, and after the construction of the guide-wall in 1999 are also available. The high fluctuations of the Caspian Sea water level should also be considered in the morphological analysis of these hydrographic surveys (Figure 3). It is observed that the water level is falling down since 1995.

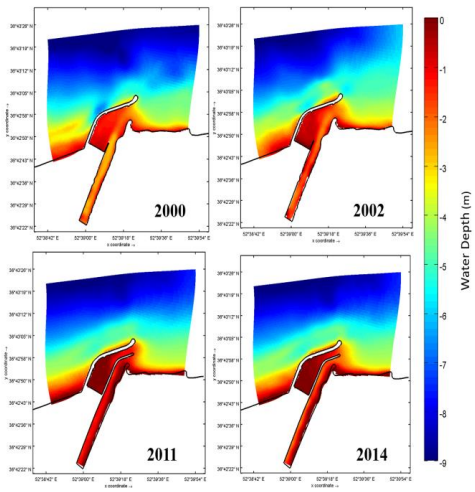

Figure 2. Bathymetry changes before and after constructing the new breakwater (2000-2014).

3. Numerical Modelling

The process-based morphological model of Delft3D, which simulates currents, waves, sediment transport, and bed level change, is selected in this study. The model

incorporates density gradients, wave generation and propagation, and sediment transport of cohesive and non-cohesive fractions [4].

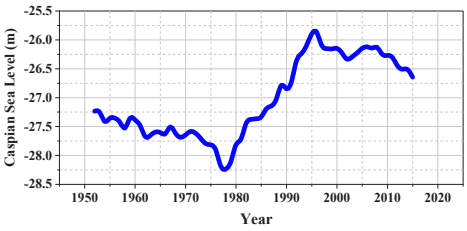

Figure 3. History of Caspian Sea water level (1941-2021).

The model is run from 2000 to 2002 in the 1st case, where the guide-wall is also included. The second modeling is after the final extension starting from 2011 to 2014. Boundary conditions include time-series of the total discharge and sediment concentration on river boundaries, water levels along the offshore boundary, and Neumann boundaries prescribed on the eastern and western sides. The model is calibrated and verified using data from river flow velocities and periodic hydrography surveys.

4. Discussion and Conclusion

Figure 4 shows the amount of erosion and sediment in the model between 2000 and 2002. The increase of sedimentation in the harbor and slight erosion along the river can be justified by comparing the hydrographic surveys of 2000 and 2002 (See Figure 2).

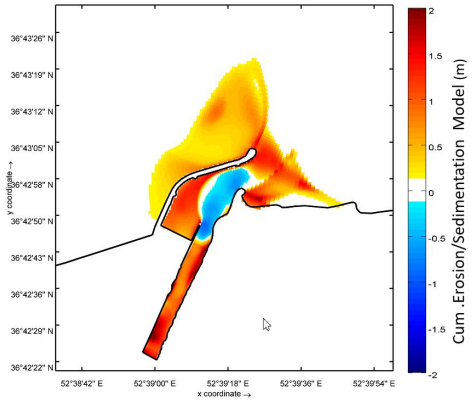

Figure 4. Modeling results of erosion/sedimentation between 2000-2002.

Figure 5 presents the comparison of the modeled bathymetry and hydrography data along three sections, A-A, B-B, and C-C of Figure 1. In spite of existing discrepancies, it is observed that the process-based Delft3D model can simulate the sedimentation rates and the complex bathymetry of river and harbor, both before and after the 2011 extension.

The study showed that the extension of the guide-wall is successful in protecting the harbor from river sediments. However, the sedimentation along the river still affects the navigation of fishing boats towards the old pier.

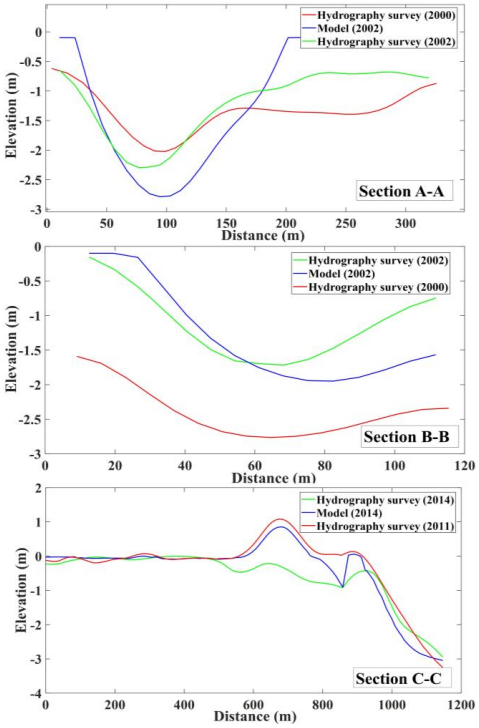

Figure 5. Morphology changes before and after new breakwater, 2000-2014.

5. References

[1] Prumm M, Iglesias G. Impacts of port development on estuarine morphodynamics: Ribadeo (Spain). Ocean \& Coast Manag. 2016; 130:58–72.
[2] Soltanpour M. Sedimentation in Fishery Ports of Iran, 8th Int Conf Coasts, Ports Mar Struct. 2004;1–3.
[3] Zaker N, Etemad-Shahidi A. Sedimentation in Babolsar and Pozm Fishery Ports in Iran. J Coast Res. 2006;2004(39):424–7.
[4] Deltares. Delft3D-Flow. User Man. 2014;712.

14th International Conference on Coasts, Ports and Marine Structures
9 & 10 May 2023 , Tehran-IRAN
ICOPMAS 2022

THE EFFICIENCY OF SYNTHETIC SPONGE TO CONTROL THE SEDIMENTATION IN THE HARBOUR ACCESS CHANNELS

Masoumeh Hashempour[1], Morteza Kolahdoozan[2]

1) Department of Civil and Environmental Engineering, Amirkabir University of Technology, Tehran, Iran, m.hashempour@aut.ac.ir
2) Department of Civil and Environmental Engineering, Amirkabir University of Technology, Tehran, Iran, mklhdzan@aut.ac.ir

1. Introduction

Navigation channels are prone to sedimentation. They behave like a sediment trap and their capacity reduces annually by sedimentation. Thus high annual costs have to be spent on dredging operations. Three main strategies can minimize harbor sedimentation: keep sediment out, keep sediment moving, and keep sediment navigable [1]. It is essential to use a method that has cost effective and low environmental impacts. *Tubular marine sponges* are the main coral reefs elements. They are immobile and have a perforated-cylindrical shape. They can clean their residence and receive nutrition by suction/pumping mechanism [2]. Therefore they can be a good choice for inspiring and finding a solution to cure the sedimentation problems. In the current study by inspiring the cylindrical sponge's physical shape and suction/pumping mechanism, its effects on flow hydrodynamics and momentum exchange were investigated. The RANS numerical model and image processing technique were deployed to investigate the sponge-flow interactions (i.e., Von-Karman street, and Counter Rotating Vortex Pair (CRVP)) behind the sponge.

2. Computational Method and Details of Validation

Modeling the effects of sponge (which will be called synthetic sponge from now on), was carried out by the interFoam solver of OpenFOAM V.1812. For validating step, an experimental program by Palau-salvador et. al (2009) was considered [3]. The experiment was carried out in a rectangular channel with 152×56×30 cm (L×W×H). The current flow has a depth of 30 cm and an initial velocity of 0.54 m/s. A rigid finite height cylinder with body diameter (D) and height (h) of 8 and 20 cm respectively, was placed at 32 cm from the upstream boundary. For numerical modeling, a block mesh was designed with 0.065 h cm × 0.044 h × 0.04 h dimensions (Figure 1). The no-slip boundary condition was chosen for both cylinder and channel wall boundaries. For inlet and outlet of the channel fixedValue and zeroGradient were chosen respectively. The K-Omega shear stress transport (K-OmegaSST) was used as a turbulence closure model. The validation results of the mean horizontal velocity confirmed that the numerical modeling has reliable accuracy for modeling the flow hydrodynamics around the cylinder with a correlation coefficient of $R^2 > 0.90$ (Figure 2).

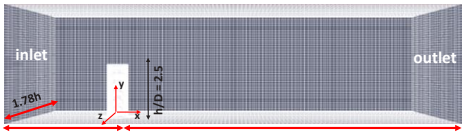

Figure 1. Computational domain

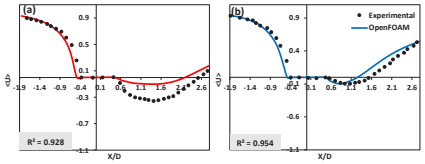

Figure 2. Results of mean longitudinal velocity validation for (a)Z/h = 0.2 and (b)Z/h=0.6

3. Model Setup

Suction/pumping mechanism was simulated by introducing an appropriate boundary condition on the cylinder body perforation and top outlet as shown in Figure 3. The CATIA and SnappyHexMesh also were utilized for the design and mesh generation of the sponge body (Figure 3).

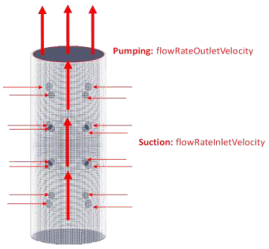

Figure 3. Sponge boundary conditions and mesh generation

Three different scenarios were considered to study the suction/pumping discharges effects on the vortical flow behind the sponge, as shown in Table 1.

Table 1. Modeling scenarios.

Scenario	Perforation diameter (cm)	Suction/pumping discharge (lit/hr)
M1	0	0
M2	1	150
M3	1	600

4. Results

4.1. Von-Karman Street

For rigid-finite height cylinders which have h/D ≤ 2.5, the Von-Karman street (VK-S) is laminar (Von-Karman Type I) and the momentum exchange through the width of the channel does not occur. Changing the h/D ratio and replacing longer cylinders will turn the laminar street into a nearly turbulent (shedding) street [4]. Figure 4 illustrates that the suction/pumping mechanism acts the same as changing the h/D ratio. This means that by changing the suction/pumping discharge, the Von-Karman street type I turns into the Von-Karman streets type II and III. The suction function causes the shrinkage of the re-circulation bubble (R-B) close to the cylinder wall. The pumping flow increases the Re number behind the sponge, and the widening occurs by flapping the shear layer. Thus increasing the suction/pumping function can enhance the momentum transfer through the width of the channel. It is worth to point out that the widening of the Von-Karman is a rare phenomenon that can not easily be observed behind the rigid finite-height cylinders.

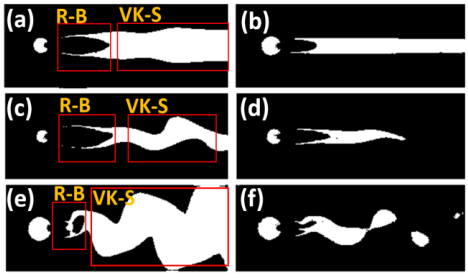

Figure 4. Von-Karman street visualization at Z/h = 0.2 (left panels) and Z/h = 0.6 (right panels) for (a,b) M1, (c,d) M2, and (e,f) M3

4.2. Counter Rotating Vortex Pairs (CRVP)

The outflow jet generally produces two vortex pairs on the water column. They are also proof of the vertical momentum exchange [5]. When the perforated cylinder with the suction/pumping phenomenon exists, the partial of tip-vortex on the leading edge will be carried by CRVP. In this regard combination of bubble and spiral will be generated. It can be called a sharp-edge delta wing vortex [6].

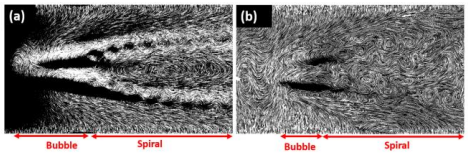

Figure 5. CRVP visualization on the free surface by image processing technique for (a) M2 and (b) M3

This type of vortex can weaken the downward flow by enhancing the uplift force. Consequently, in turbidity flow, the probability of particle deposition reduces, and sediment transport enhances.

5. Conclusion

In the current study, a synthetic sponge was designed to enhance the momentum transfer through the navigation channels. The synthetic sponge by suction/pumping mechanism and its special physical shape, can increase the momentum transfer laterally and vertically. The lateral momentum transfer emerged by shedding and rare widening vortex street. The vertical momentum exchange was also triggered due to the sharp-edge delta wing formation. In this vortex, the combination of tip-vortex and CRVP leads to the increase of the buoyancy force and diminishes the strength of the downward flow. In this regard, the possibility of sedimentation reduces. Overall, the idea of the synthetic sponge can be practical where the Access channels suffer from loss of capacity by sedimentation and the high cost of dredging. So, the synthetic sponge can enhance sediment transport by changing the flow hydrodynamics.

6. Acknowledgment

This paper is part of Masoumeh Hashempour Ph.D. thesis which is granted by the Iran National Science Foundation (INSF) with No. 99018691.

7. References

[1] Deltares, "Sedimentation in channels and ports", Report.
[2] Goldstein, J., Riisgård, HU. and Larsen, PS., "Exhalant jet speed of single-osculum explants of the demosponge Halichondria panicea and basic properties of the sponge-pump", *Journal of Experimental Marine Biology and Ecology*, 511, 2019, pp. 82-90.
[3] Palau-Salvador, G., Stoesser, T., Fröhlich, J., Kappler,M. and Rodi, W., "Large Eddy Simulations and Experiments of Flow Around Finite-Height Cylinders". *Flow, Turbulence and Combustion*, 84 (2), 2009.
[4] Shi, X., Alam, M. and Bai, H "Wakes of elliptical cylinders at low Reynolds number", *International Journal of Heat and Fluid Flow*, 82, 2020.
[5] Luckring, JM, "The discovery and prediction of the vortex flow aerodynamics", *The Aerodynamics Journal*, 123, 2019.

A STUDY ON THE MAIN PROCESSES INFLUENCING THE HYDRODYNAMIC CHARACTERISTICS OF THE ANZALI WETLAND - PORT SYSTEM

Hasan Heidarnejad[1], Peyman Badiei[2], Mehdi Sanayei[3], Mohammad Hosein Nemati[4], Mohammad Bagheri[5]

1) Khakbaft Consulting Engineers Company, Tehran, Iran, heidarnejad94@gmail.com
2) University of Tehran, College of Engineering, School of Civil Engineering, Tehran, Iran, pbadiei@ut.ac.ir
3) Khakbaft Consulting Engineers Company, Tehran, Iran, mehdi.sna@gmail.com
4) Ports and Maritime Organization, Coastal Engineering Department, Tehran, Iran, mhn1982@gmail.com
5) Ports and Maritime Organization, Coastal Engineering Department, Tehran, Iran, mbagheri@pmo.ir

1. Introduction

The focus of the present paper is to obtain an insight into the hydrodynamic behavior of the Anzali Port – Wetland complex and quantify the effects of the main influencing processes. There are several sensitive and challenging issues in the domain of this study, shown in Figure 1, that have led to a severe environmental degradation and the present study can be considered as a first step towards addressing these issues. This study was carried out as a part of "Anzali Port Sedimentation Study" by Khakbaft Consulting Engineers for Ports and Maritime Organization of the Islamic Republic of Iran [1].

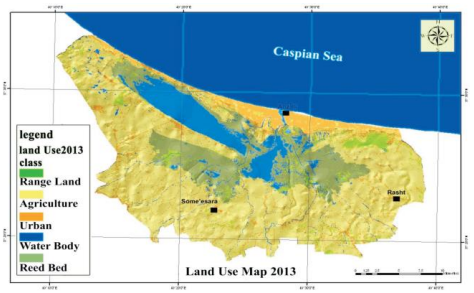

Figure 1. Location of Anzali Port and Wetland

2. Modelling Approach

The open source 2DH curvilinear Delft3D-FLOW module [2] was applied as the computational tool. River inflow and precipitation data at stations delineated in Figure 2 were obtained from hydrometric and synoptic stations respectively in the region [3].

Hydrography and topography of the region were obtained by combining the data from bathymetric survey [4] and satellite imagery digital elevation model (DEM) [5]. Mesh configuration and bathymetry of the computational domain are shown in Figure 3. Valuable data acquired from current velocity measurements [6] carried out at the location shown in Figure 4, was used for calibration and verification of numerical simulations.

Figure 2. Location of hydrometric stations as model boundary

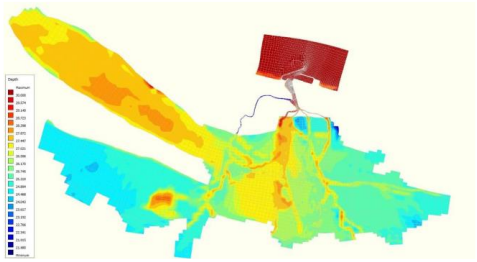

Figure 3. Model Domain and Bathymetry

Figure 4. Velocity measurement station

3. Simulation Results

Hydrodynamic simulations were carried out for 40 days of flooding during the fall of 2019. In Figure 5 current velocity magnitudes are shown over the whole computational domain (top) and in the Port zone (bottom). During a flood event, as shown in the top of Figure 5, in addition to the Abkenar reservoir (red zone), two distinct zones can be identified; the main channels and the flood plains (green zones).

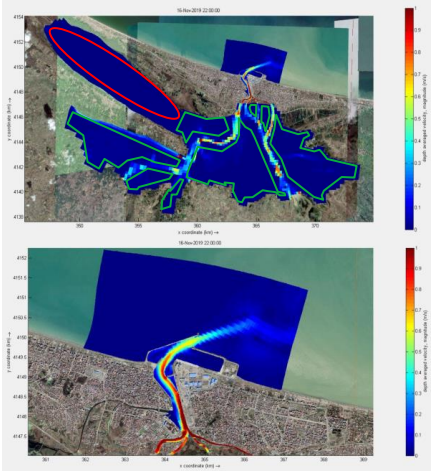

Figure 5. Flow pattern at the Anzali wetland and port

Two main factors that are considered to have significant effects on the results of simulations i.e., the effects of vegetation, in flood plain zones, and precipitation are investigated. The effect of vegetation is taken into account through bed roughness. Simulated depth averaged velocities are compared with the measured one for two cases where a constant Manning roughness coefficient of 0.02 is assumed over the whole domain, and a second case where this is taken as 0.02 for main water ways and 0.5 for flood plains and vegetated zones. These results are illustrated in Figure 6.

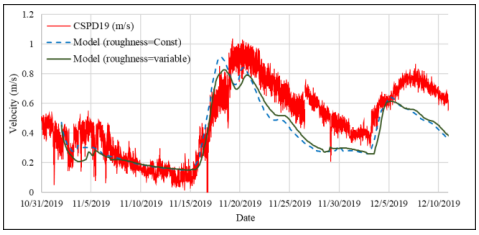

Figure 6. Flow velocity at the observation point in the preliminary model and measurements

The effect of precipitation over the computational domain downstream of hydrometric stations was taken into account. This zone has an area of 200 million square meters and precipitation data used in the calculations is shown in Figure 7.

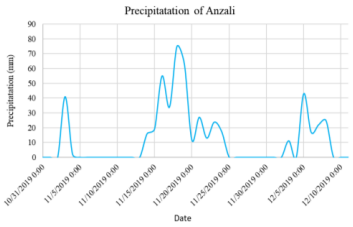

Figure 7. Timeseries of precipitation in the model area

The effect of accounting for precipitation is shown in Figure 8. It is obvious that constant roughness yields a higher peak than observed values.

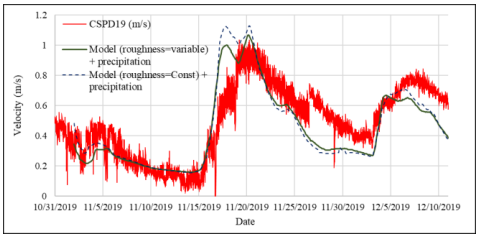

Figure 8. Flow velocity at the observation point in the adjusted model and measurements

4. Conclusions

The complex system of Anzali Wetland was numerically simulated using Delft3D-FLOW open-source software. The effects of flood plain vegetation and precipitation over the wetland were investigated. It was shown that:

1- Accounting for precipitation brings the simulated peak of the flow through the harbor area, closer to the observed one.
2- Accounting for higher roughness caused by vegetated flood plains yield more realistic results

5. References

[1] Mathematical Modeling of Anzali Port, Khakbaft Consulting Engineers.

[2] Delft3D. Hydro-Morphodynamics User Manual, Deltares

[3] Hydrological Study of Anzali Port, Khakbaft Consulting Engineers.

[4] Deputy Directorate for Maritime Affairs, Ports and Marine Administration of Guilan Province.

[5] https://asf.alaska.edu/

[6] Coastal and Ports Engineering Department, Ports and Marine Administration of Guilan Province.

DEVELOPMENT AND EVALUATION OF AN ONLINE NON-NUCLEAR SLURRY DENSITY-METER IN DREDGING SCALE BASED ON APPLIED CURRENT MAGNETIC INDUCTION TOMOGRAPHY (AC-MIT)

Jalil Taghizadeh-Tameh[1], Hossein Mousazadeh[1], Shahin Rafiee[1], Nazilla Tarabi[1]

1) Mechanical Engineering of Biosystems, University of Tehran, Tehran, Iran,
Taghizadeh68@ut.ac.ir, hmousazade@ut.ac.ir, shahinrafiee@ut.ac.ir, Tarabi99@ut.ac.ir

1. Introduction

Slurries are two-phase flows in which insoluble solid particles are dispersed in a liquid carrier and are an importance part of many industrial processes such as petroleum, food processing, pharmaceutical, nuclear, mineral, chemical and dredging industries. Dredging is an essential environmental and economic action in coastal and riverine systems around the world, and may be carried out with the aims of land reclamation, contamination remediation [1], deepen and maintain navigation channels and harbor entrances [2] (Figure 1).

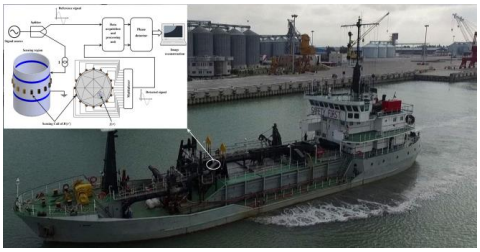

Figure 1. Dredger ship, Density-meter installation position.

Online measurement of fluid density during dredging operations plays an important role in increasing efficiency of dredging operations, reduction energy consumption, reduction costs, etc. Many different methods and techniques have been studied and developed for measuring slurry density in pipelines which can be divided into two methods: invasive method and non-invasive method. Techniques such as Coriolis tube [3] and fork density measurement are the invasive method for measuring the density of multiphase flow in pipelines. The non-invasive methods for measuring slurry density included ultrasonic attenuation, γ-ray method, optical method, differential pressure, electromagnetic waves and electrical tomography which each of these methods is used based on the characteristics of slurry flow. Tomography is imaging by sectioning, through the use of a penetrating wave or field, in other words, it is a technology to get target features, such as concentration and distribution by a non-contact or non-invasive means. Compared with the conventional measurement methods, which can only provide a single point measurement value, tomographic measurement techniques can provide accurate information from total cross section of slurry in pipelines.

Due to characteristics such as nondestructive, non-invasive, non-nuclear and contactless technique, Magnetic Induction Tomography (MIT) technique has gained increasing research interest for the visualization of a conducting phase in multiphase flow [4]. MIT has many potential applications spanning a diverse range of problems and industrial challenges, from biomedical imaging through to non-destructive testing and conductive flow imaging [5]. For a typical MIT system, coils are used as transmitter and receiver sensors [6], but for large diameter of imaging region (Usually 50 cm or more), the magnetic flux cannot pass through the region optimally. For such cases, the transmitter coils would be substituted by a pair of electrodes while the receivers are still coil. This system was titled as Applied Current Magnetic Induction Tomography (AC-MIT). Therefore, in order to monitor multiphase flow in pipelines with large diameters, AC-MIT system would be a favorable candidate.

In the present study, a special AC-MIT system is designed and constructed for measuring slurry density in dredger ship pipeline. Also, effect of salinity and temperature on performance of AC-MIT system was evaluated.

2. Materials and Methods

In this study, according to the need of the Ports and Maritime Organization (PMO) of Iran to measure the density of multiphase fluid inside dredger ships, the studied fluid was selected as seawater with a mixture of sand and soil.

The AC-MIT system works based on electromagnetic induction law. The main parts of this system include transmitter and receiver sensors, data acquisition system and image reconstruction algorithm. In the AC-MIT system, innovative transmitter sensors were used, which include two annular electrodes and mounted on the wall of the media. Receiver sensors include sixteen coils that are installed around the media (Figure 2). In AC-MIT system, constant current, I, is applied into conductive object Ω through a pair of annular electrodes that mounted to object's boundary. By changing the electrical properties of the media, the amplitude and phase of the induced voltage in the receiver sensors change.

For solving the governing equation, forward problem computes the current density within an electrically conducting domain, magnetic flux density surrounding the object and phase difference between reference signal and detected signal from the known conductivity distribution according to the boundary value problem and Biot-Savart law (Equation 1). Inverse problem involves estimating the object conductivity distribution from the measured mutual inductances between the receiver coils and annular electrodes, which is an ill-posed problem. In this research, Iterative Gauss-Newton algorithm with Tikhonov regularization was used to solve the inverse problem.

$$\vec{B}(r') = \frac{\mu_0}{4\pi}\int_{\Omega}\vec{J}(r)\times\frac{\vec{r'}-\vec{r}}{\left|\vec{r'}-\vec{r}\right|^3}\,dv \qquad (1)$$

In order to evaluate the performance of AC-MIT system in the laboratory, saline water was used as the carrier phase and soil-sand mixture was used as the solid phase. The effect of temperature and salinity was investigated using the response surface method and analysis of variance of mass concentrations.

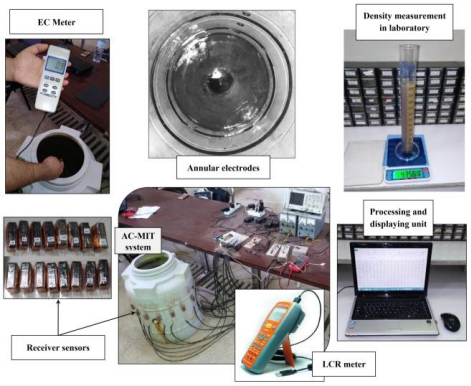

Figure 2. Evaluation of developed AC-MIT system in lab.

3. Results and Discussion

The results of evaluation of AC-MIT system showed that there is a linear relationship between the solid mass concentrations measured in both manual and measured by the AC-MIT system with an acceptable correlation coefficient. The correlation coefficient of each curve for different salinity and temperature levels is approximately in the range of 0.98 to 0.99 (Figure 3). The results of statistical analysis showed that temperature and salinity levels of the carrier phase did not have a significant effect on system performance. Also, the interaction of temperature and salinity had no significant effect on the performance of AC-MIT system.

The results of evaluations showed that the error of the AC-MIT system is in the range of 1% to 11%. At low fluid concentrations, the measurement error of AC-MIT system was about 10% and with increasing fluid concentration, the measurement error decreases (about 1%).

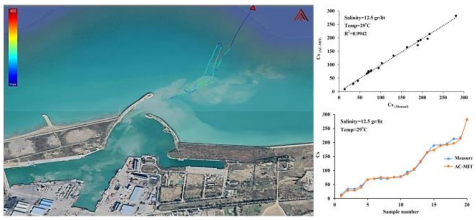

Figure 3. Online display of volume and position of removed sediment by dredger ship (a); Solid mass concentration Measured by AC-MIT system and manual measurement (b).

Maučec and Denijs measured the concentration of sediment-like materials using a gamma-ray densitometer. Their results showed that the error of gamma ray densitometer in measuring the concentration of sediment-like material with water is 10% and with increasing sediment concentration, the measurement error increases.

4. Conclusion

In this study, design, construction and evaluation of a special AC-MIT system for measuring the density of multiphase fluid were investigated. The results showed that there is a linear relationship between the mass concentrations measured in two modes with an acceptable coefficient of determination. Also, the error of AC-MIT system in measuring density of high concentration fluids is less than 5%. By using AC-MIT system with GPS system on dredger ships, the density of dredging fluid can be measured online and volume and position of removed sediment can be shown on map. This will prevent re-dredging of dredged positions.

5. Acknowledgment

The authors would like to acknowledge Ports and Maritime Organization for funding the project by grant No. 3528/S20, 2018-2020.

6. References

[1] Trevisan, C. L., Vicente, M. C., Rocha, B. C. S., and Wasserman, J. C., "Development of a Dredging Sensitivity Index, applied to an industrialized coastal environment in Brazil", *Science of the Total Environment*, 748, 2020, pp. 141294.

[2] Erftemeijer, P. L., and Lewis III, R. R. R., "Environmental impacts of dredging on seagrasses: a review", *Marine pollution bulletin*, *52*(12), 2006, pp.1553-1572.

[3] Wang, L., Yan, Y., Wang, X., Wang, T., Duan, Q., and Zhang, W., "Mass flow measurement of gas-liquid two-phase CO2 in CCS transportation pipelines using Coriolis flowmeters", *International Journal of Greenhouse Gas Control*, *68*, 2018, pp.269-275.

[4] Ma, L., McCann, D., and Hunt, A., "Combining magnetic induction tomography and electromagnetic velocity tomography for water continuous multiphase flows", *IEEE Sensors Journal*, *17*(24), 2017, pp. 8271-8281.

[5] Ma, L., and Soleimani, M., "Magnetic induction tomography methods and applications: A review", *Measurement Science and Technology*, *28*(7), 2017, pp.072001.

[6] Wei, H. Y., and Wilkinson, A. J. "Design of sensor coil and measurement electronics for magnetic induction tomography", *IEEE transactions on instrumentation and measurement*, *60*(12), 2011, pp. 3853-3859.

14th International Conference on Coasts, Ports and Marine Structures
9 & 10 May 2023 , Tehran-IRAN
ICOPMAS 2022

NUMERICAL MODELING OF WAVE-INDUCED SCOUR UNDER PIPLINE

Mohammadreza Torabbeigi[1], Javad Souri[2] and Mehrdad Tokalloo[3]

1) Civil and Environmental Engineering, Tarbiat Modares University, Tehran, Iran, m_torabbeig@modares.ac.ir
2) Civil and Environmental Engineering, Tarbiat Modares University, Tehran, Iran, j.soori@modares.ac.ir
3) School of Civil Engineering, Iran University of Science and Technology, Tehran, Iran, me_tokaloo@cmps2.iust.ac.ir

1. Introduction

Submarine pipelines are mostly used for transporting oil, gas, or water at low cost. In a shallow water environment, a pipeline is subjected to waves and currents. Below the pipeline, there is a bowl-shaped depression caused by the scour hole. A scour can cause the pipeline to become curved, resulting in lateral instability and breakage. As a result, pipeline scour remains a crucial topic for extending the relevant knowledge and numerical scour modeling capabilities.

In order to study pipeline scour using numerical models, various numerical investigations have been conducted. By solving the incompressible Reynolds-Averaged Navier-Stokes (RANS) equations with the k turbulence model and morphological solver, Brørs [1] analyzed pipeline scour under a steady current. Using a rigid lid to represent the free surface of a pipeline, the free surface was modelled as steady flow. Fuhrman et al [2] studied pipeline scour under waves with a RANS-based numerical model and found that the backfilling process includes an initial re-distribution phase that reorganizes sediments close to the pipeline. They analyzed wave motion as an oscillatory flow, but did not resolve the free surface. Ahmad et al [3] developed a numerical model of pipeline scour under the combined action of waves and current, including the prediction of the unsteady free surface. The numerical modelling is performed with the open-source CFD model REEF3D. In this model, Reynolds Averaged Navier-Stokes (RANS) equations and the k-ω turbulence model are combined with a sediment transport algorithm. The model is rigorously validated for the hydrodynamics of co-directional waves and currents to ensure its accuracy. In this paper, we evaluate Ahmad et al's [3] method for simulating the interaction between free surface dynamics, represented here by wave motion, and sediment dynamics. Experimental measurements are compared with model results to determine the model performance quantitatively. Simulation and validation are based on test number (3) of Sumer and Fredsoe's experimental data and setup.

2. Governing Equations

The hydrodynamics flow field is calculated by solving the incompressible Reynolds-Averaged Navier-Stokes (RANS) and the continuity equations as given Equation (1) and (2), respectively.

$$\frac{\partial u_i}{\partial x_i} = 0 \tag{1}$$

$$\frac{\partial u_i}{\partial t} + u_j \frac{\partial u_i}{\partial x_j} = -\frac{1}{\rho}\frac{\partial p}{\partial x_i} + \frac{\partial}{\partial x_j}\left[(v + v_t)\left(\frac{\partial u_i}{\partial x_j} + \frac{\partial u_j}{\partial x_i}\right)\right] + g \tag{2}$$

u_i p

Where is the fluid velocity, is the pressure, ρ is the fluid density, v_t is the eddy-viscosity, and g is the gravitational acceleration. The *k-ω* model is used as closure for the RANS equation to calculate the eddy-viscosity [4]. The convection terms of the RANS equations are discretized with the fifth-order accurate conservative Weighted Essential Non-Oscillatory (WENO) scheme [5]. The time step for the transient flow is determined using the adaptive time stepping method. In this method, the time step is controlled with the Courant-Freiderichs-Lewy (CFL) number [6]. Further details of the governing equations can be found in Bihs et al [3]. A basic assumption of the scouring process is that when the acting bed shear stress τ is higher than the critical bed shear stress τ_c, sediment particles undergo initial motion. A morphological model calculates the shear stress, the load, the suspended load, and the elevation change of the bed. Details of the morphological model are described in Ahmad et al [3].

3. Numerical Setup

As shown in Figure 1, the numerical domain in this case is 2DV. The initial sediment bed thickness is 2D = 0.1 m and the free surface is 0.40 meter above the bed. The pipeline is located in the center of the domain and the domain extends in each direction by 70D. Simulations were carried out using variable mesh sizes from 5 mm at the free surface to 1 mm at the bed interface. The time step was variable, but was constrained to a maximum s and a maximum Courant number of 1.0. The experiment was conducted in a piston wave flume of width equal to 0.6 m and mean water depth equal to 0.40 m.

The experiment was carried out in a piston type wave flume with a width of 0.6 m and a mean depth of 0.40 m. A hydraulic smooth pipe of diameter D = 0.05 m was placed in contact with a packed sand bed. This experiment used

sand with a median particle diameter of 0.58 mm and a density of 2700 kg/m3. The carrier fluid is water of density ρ_w=1000 kg/m^3 and viscosity. In Sumer and Fredsoe [7], although the wave height was not explicitly reported, a wave height of H w= 0.15 m was found to correspond to U_m = 0.228 m/s, which resulted in KC = 7.0 with a wave of T_w = 1.43 s.

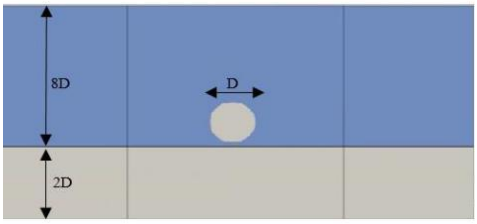

Figure 1. The computational domain of the pipeline scour experiment setup

4. Result and Discussion

According to Sumer and Fredsoe [7] the lee-wake of the pipeline is the main action that governs the scour below a pipeline in waves. In order to model this process adequately, *k-ω* model was used for turbulence modeling in this case. Figure 2 illustrates the interaction between the wave, the pipeline and sediment bed.

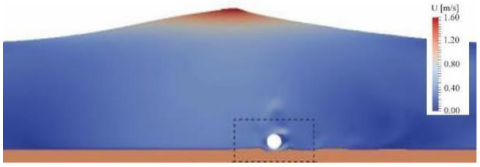

Figure 2. Velocity of wave profile over the submerged pipeline

The temporal evolution of the bed scour profile is shown at time t=12 s (0.2 min) and t=300 s (5 min) from the start of the simulation. Those figures show a qualitative similarity between the scour profile reported in Sumer and Fredsoe [7] and numerical model that utilized in this study. The fluid velocity extension of the scour hole is also consistent with experimental values. In contrast to the experiment, both the upstream and downstream sand dunes were completely washed away by the vortex shedding in the numerical model at this time. This is believed to be primarily due to the k- model's overestimation of eddy viscosity in the wake of the pipeline, which is known to overestimate turbulent kinetic energy and eddy viscosity in the separated flow.

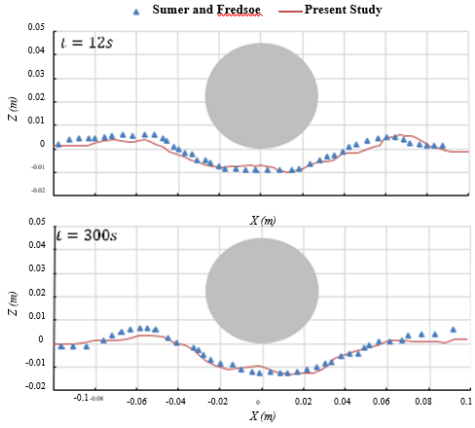

Figure 3. Comparison of scour profile with experimental results of Sumer and Fredsoe [7]

5. Conclusion

In this study, by solving the RANS equations with the k- turbulence model and a sediment transport model, the open-source CFD model REEF3D is used to simulate the flow hydrodynamics. The validated model is used to investigate pipeline scour under combined waves and current while resolving the dynamic free surface emotion. Compared to Sumer and Fredsoe [7] experimental data, the numerical model predicts pipeline scour under the combined waves and current satisfactorily

6. References

[1] B. Brørs, "Numerical modeling of flow and scour at pipelines," *J. Hydraul. Eng.*, vol. 125, no. 5, pp. 511–523, 1999.
[2] D. R. Fuhrman, C. Baykal, B. M. Sumer, N. G.Jacobsen, and J. Fredsøe, "Numerical simulation of wave-induced scour and backfilling processes beneath submarine pipelines," *Coast. Eng.*, vol. 94, pp. 10–22, 2014.
[3] N. Ahmad, H. Bihs, D. Myrhaug, A. Kamath, and Ø. A. Arntsen, "Numerical modelling of pipeline scour under the combined action of waves and current with free-surface capturing," *Coast. Eng.*, vol. 148, pp. 19–35, 2019.
[4] D. C. Wilcox and others, *Turbulence modeling for CFD*, vol. 2. DCW industries La Canada, CA, 1998.
[5] G.-S. Jiang and C.-W. Shu, "Efficient implementation of weighted ENO schemes," *J. Comput. Phys.*, vol. 126, no. 1, pp. 202–228, 1996.
[6] T. Gerstner and M. Griebel, "Numerical integration using sparse grids," *Numer. algorithms*, vol. 18, no. 3, pp. 209–232, 1998.
[7] B. M. Sumer and J. Fredsøe, "Scour around pipelines in combined waves and current," 1996

14th International Conference on Coasts, Ports and Marine Structures
9 & 10 May 2023 , Tehran-IRAN
ICOPMAS 2022

NUMERICAL SIMULATION of SCOURING BENEATH SUBMARINE PIPELINE USING MODIFIED LOW-REYNOLDS K-EPSILON TURBULENCE MODEL WITH SEDFOAM

Javad Souri[1], Hossein OmidvarMohammadi[2], Mohammadreza Torabbeigi[3]

1) Civil and Environmental Engineering, Tarbiat Modares University, Tehran, Iran, Email; j.soori@modares.ac.ir
2) Civil and Environmental Engineering, Tarbiat Modares University, Tehran, Iran, Email; h.omidvar@modares.ac.ir
3) Civil and Environmental Engineering, Tarbiat Modares University, Tehran, Iran, Email; m_torabbeigi@modares.ac.ir

1. Introduction

The mismatch between sediment transport models and experimental data lies at the basis of the research efforts of the authors. Despite all the efforts since Rouse [1], at present it is still impossible to reproduce all the details (especially near the bed) of measured sediment concentration profiles in steady uniform flume experiments for non-dilute conditions.

The data of Cellino [2] shows that non-dilute conditions prevail in the lowest 2-3 cm in his experiments, characterized by turbulence which is no longer fully-developed and therefore a low-Reynolds modelling approach is require. A New Turbulence Model (NTM) [3] with damping function which are applied on the standard k - ε model is introduced, which implies that the model is applicable over the entire cross-stream dimension including the low Reynolds number region (viscous sublayer).

The present study carries out two-dimensional numerical simulations of scouring beneath a single submarine pipeline subjected to a current flow condition using SedFOAM (an open-source, multidimensional Eulerian two-phase solver for sediment transport based on OpenFOAM). The turbulence model is modified Low-Reynolds k - ε. The particle-particle interactions and the particle stresses are modeled using the dense granular flow rheology.

2. Governing Equations and General Setup

In the low-Reynolds k-ε model, where the damping functions f_μ, f_1 and f_2 are introduced to correct the original k-ε equations. Various forms have been proposed in the literature, most of which contain correction factors which are a function of the distance from the wall [4]:

$$\frac{\partial_k}{\partial_t}+u\frac{\partial_k}{\partial_x}+w\frac{\partial_k}{\partial_z}=\frac{\partial}{\partial_x}\left\{\left(\upsilon+\frac{\upsilon_t}{\sigma_K}\right)\frac{\partial_k}{\partial_z}\right\}+ \upsilon_t\left(\frac{\partial_u}{\partial_z}\right)^2-\varepsilon-B_k \quad (1)$$

$$\frac{\partial_\varepsilon}{\partial_t}+u\frac{\partial_\varepsilon}{\partial_x}+w\frac{\partial_\varepsilon}{\partial_z}=\frac{\partial}{\partial_x}\left\{\left(\upsilon+\frac{\upsilon_t}{\sigma_\varepsilon}\right)\frac{\partial_\varepsilon}{\partial_z}\right\}+ C_{1\varepsilon}f_1\frac{\varepsilon}{k}\upsilon_t\left(\frac{\partial u}{\partial z}\right)^2-C_{2\varepsilon}f_2\frac{\varepsilon^2}{k}-\frac{\varepsilon}{k}C_{3\varepsilon}B_k \quad (2)$$

Here k is the turbulent kinetic energy, ε is the dissipation rate, $\nu_t = c_\mu f_\mu k^2/\varepsilon$ is the eddy viscosity, c_μ = 0.09 is a coefficient, f_μ is a coefficient as listed below, σ_k and σ_ε are turbulent Prandtl-Schmidt numbers for k and ε, respectively; B_k is the buoyancy flux and $c_{3\varepsilon}$ is coefficient, which are related to stratification effects.

$$f_\mu=\left(1+4.1/R_t^{0.75}\right)\left(1-exp\left(-z^*/15.75\right)\right)^2 \quad (3)$$

$$f_2=\left(1-0.3exp\left(-\left(R_{t/6.5}\right)^2\right)\right)\times\left(1-exp\left(-z^*/3.64\right)\right)^2 \quad (4)$$

$$R_t=k^2/(\varepsilon\upsilon) \quad (5)$$

$$z^*=(\varepsilon\upsilon)^{1/4}z/\upsilon \quad (6)$$

The various coefficients in the standard k - ε model and NTM model are summarized in Table 1.

Table 1. Coefficients in the standard k − ε and NTM turbulence model.

	c_μ	F_μ	$c_{1\varepsilon}$	$c_{2\varepsilon}$	σ_k	σ_ε	f_1	f_2
Standard	**0.09**	**1.0**	**1.44**	**1.92**	**1.0**	**1.3**	**1.0**	**1.0**
NTM	**0.09**	f_μ	**1.45**	**1.90**	**Var.**	**Var.**	**1.0**	f_2

The numerical domain dimensions are presented in Figure 1. The inlet was decomposed into two parts. From the bottom to y = 1.5D, a wall-type boundary condition was applied. From y = 1.5D to the top, a log law velocity profile was used following the expression:

$$u_f^+ = (y) = \frac{u_*}{k} ln\left(\frac{30y}{k_s}\right) \quad (7)$$

where κ = 0.41 is the von Karman constant, u_*=0.04318m/s is the bottom friction velocity, and k=2.5d is the Nikuradse roughness length. The physical property of the particles (diameter and density) and of the fluid (density and kinematic viscosity) have been set to the values given in Mao, (1986) [5].

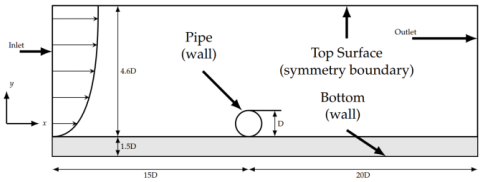

Figure 1. Sketch of the geometry and the boundary conditions used for the computational domain [5]**.**

3. Results and Discussion

Figures 2 and 3 illustrates the time evolution of the maximum scour depth and the shape of the sediment bed.

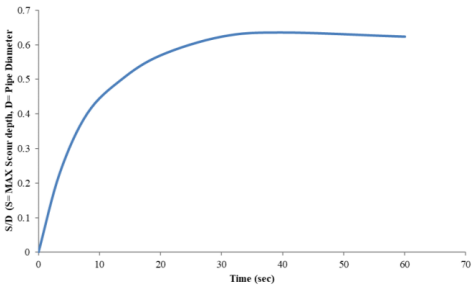

Figure 2. Time evolution of the maximum scour depth

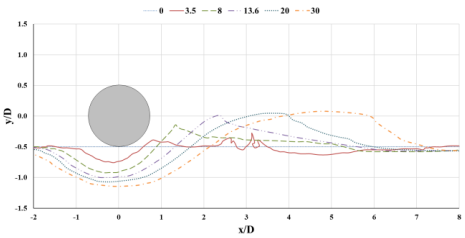

Figure 3. Time evolution of the sediment bed's shape.

Figure 4 shows the ability of the current numerical model to capture the role of vortex shedding in the scour process. Moreover, the presence of the pipeline caused an increase in the near-bed wave-induced velocities in the gap between the bed and the pipeline. This gives rise to the so-called "tunnel erosion" below the pipeline which is one of the crucial aspects that control the pipeline scour especially in the initial stages [6], [7]. The snapshot provided in Figure 4 confirms that the erosion was caused by the vortices in the wake of the cylinder. A strong sediment flux was associated with a vortex reaching the sand dune downstream of the pipeline.

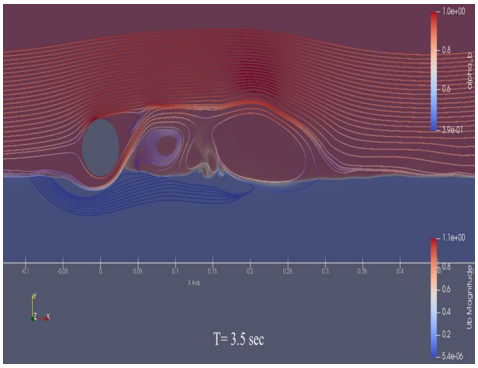

Figure 4. Vortex shedding in the wake of pipeline.

4. Conclusion

The consistent modelling of turbulent flows with non-dilute conditions, using k- ε turbulence model, requires several modifications to the standard implementation. Modifications include adding some damping functions to the model. This study, successfully implemented modified Low-Reynolds k- ε turbulence model in simulating scouring beneath submarine pipeline using SedFOAM.

5. References

[1] H. Rouse, "Modern conceptions of the mechanics of fluid turbulence," *Trans. Am. Soc. Civ. Eng.*, vol. 102, no. 1, pp. 463–505, 1937.
[2] M. Cellino, "Experimental study of suspension flow in open channels," EPFL, 1998.
[3] A. Sana, A. R. Ghumman, and H. Tanaka, "Modification of the damping function in the k–ε model to analyse oscillatory boundary layers," *Ocean Eng.*, vol. 34, no. 2, pp. 320–326, 2007.
[4] L. Zuo, D. Roelvink, Y. Lu, and H. Wang, "Modelling and analysis on high sediment concentration layer of fine sediments under wave-dominated conditions," *Coast. Eng.*, vol. 140, pp. 205–231, 2018.
[5] Y. Mao, "The interaction between a pipeline and an erodible bed. Series paper 39." Ph. D. thesis. Tech. Univ. of Denmark, 1986.
[6] B. E. Larsen, D. R. Fuhrman, and B. M. Sumer, "Simulation of wave-plus-current scour beneath submarine pipelines," *J. Waterw. Port, Coastal, Ocean Eng.*, vol. 142, no. 5, p. 4016003, 2016.
[7] M. Ouda, "Multiphase Modelling of Sediment Transport and Bed Erosion for the Study of Coastal Morphodynamics," 2019.

ESTIMATION OF THE IMPACT AREA OF THE ZOHREH RIVER SEDIMENTARY PLUME IN THE PERSIAN GULF USING SATELLITE IMAGES

Ebrahim Jafari[1], Mohammad Hadi Moeini[2], Majid Jandaghi Alaee[3], and Mahmood Pourali[4]

1) PhD in Hydraulic Eng., Water and Wastewater Co., Tehran, Iran, jafari.hydrostructure@gmail.com
2) PhD in Coastal Eng., Pouya Tarh Pars Cons. Eng. Company, Tehran, Iran, mhmoeini@gmail.com
3) PhD in Coastal Eng., Pouya Tarh Pars Cons. Eng. Company, Tehran, Iran, m.j.alaee@ptpco.com
4) PhD candidate in Hydraulic Eng., Pouya Tarh Pars Cons. Eng. Company, Tehran, Iran, mahmoud.pourali@gmail.com

1. Introduction

The Zohreh River is one of the main rivers in Khuzestan province that flows into the Persian Gulf. It collects the waters of a vast areas in the Fars and Khuzestan province. The length of the river from the Persian Gulf to the upstream of its main branches is more than 400 km, and it brings a large number of sediments into the Persian Gulf during floods. Due to the rising commercial and fishery activities in the estuary of the river, investigation of its sediment plume has a great importance for the engineers.

The suspended sediment concentration in the sea water at the river outlets is commonly evaluated by taking field samples in scattered places at the time of flooding. Although these measuring are quite accurate, it cannot be done in regular intervals due to high financial and time costs. On the other hand, it is not possible to take a water sample in large areas or multiple points. Therefore, it would not be possible to track the sediment plume area in intensification and weakening of the storm and flooding. One of the new and suitable tools for conducting such studies is to monitor the satellite images. In the areas where the type of sediments is fine-grained and sea water becomes muddy under the effect of the high flow of the rivers during floods, satellite images can determine the extent of the sediment plume in the river outlet at the sea. Using the available satellite images, it is possible to study the spread of sediments plumes from the rivers into the sea.

The Iranian Port and Maritime Organization (PMO) initiated a project, led by Pouya Tarh Pars Consulting Engineers to study the hydrodynamics of estuaries and outlets located on the Khuzestan province. Limited previous studies have been performed to study these water bodies. According to the drainage basin of the rivers located on the coasts of Khuzestan province and based on the available evidence, the Zohreh River brings the largest sediment load to the Persian Gulf compared to other ones such as Bahmanshir and Arvand [1]. Therefore, in this study, the sediment plume area of the Zohreh River is evaluated using satellite images, and the correlation of sediment plume area with the precipitation on the drainage basin is also investigated.

2. The Extent of the River Plume

In this study, the extent of the Zohreh River plume was evaluated using satellite images for different days. The landsat8 images with the 30m resolution [2] were used to track the plume area. For example, Figure 1 shows a sample of sediment plume and its estimated area in the Zohreh River outlet at March 2, 2020.

The analysis of satellite images on different dates showed that in general, the number of days that the Zohreh River enters the suspended sediment load into the Persian Gulf is much more than the number of days that the plume of suspended sediments is observed in the mouth of other rivers such as Arvand. Therefore, although the discharge and the width of the Arvand estuary may be greater than that of the Zohreh, the Zohreh River brings more sediment load to the Persian Gulf.

Figure 1. A sample of sediment plume and its estimated area in the Zohreh River outlet at March 2, 2020.

Table 1 presents the extracted sediment plume extent of the Zohreh River at its outlet area in the Persian Gulf, estimated based on the satellite images of different dates. Based on the obtained values, the extent of the sediment plume is variable in different times according to the amount of rainfall and flood discharge.

Table 1. The extracted sediment plume extent of the Zohreh River based on the satellite images.

Date	Plume Area (km^2)	Date	Plume Area (km^2)	Date	Plume Area (km^2)
4/28/2020	167	12/6/2019	66	9/1/2019	19
4/19/2020	25	11/27/2019	105	8/16/2019	49
4/12/2020	215	11/20/2019	90	8/7/2019	89
3/11/2020	130	11/11/2019	10	7/31/2019	65
3/2/2020	223	10/19/2019	35	7/22/2019	130
1/30/2020	273	10/10/2019	50	7/15/2019	235
1/23/2020	260	10/3/2019	160	7/6/2019	210
1/7/2020	60	9/24/2019	39	6/29/2019	81
12/29/2019	335	9/17/2019	36	6/20/2019	182
12/22/2019	115	9/8/2019	114	6/13/2019	167

3. The Correlation between Sediment Plume Extent and the Precipitation

Normally, after the rain falls on the drainage basin of river, the resulting runoff carries the bed material of the basin into the downstream of the river. Therefore, it is expected that there is a direct relationship between the size of the sediment plume extent in the river outlet and the amount of rainfall at the upstream of the basin. Of course, the rainfall on the basin needs to travel a distance to become surface runoff and reach the mouth of the river in the sea, and therefore the peak of sediment plume would be with a delay compared to the peak of rainfall. As an example, Figure 2 shows the variation of the extent of the sediment plume and cumulative precipitation in the Zohreh River outlet for the March of 2017. As seen, the increase in the size of the sediment plume extent occurs with a delay compared to the rainfall.

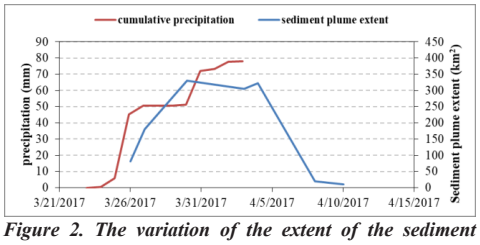

Figure 2. The variation of the extent of the sediment plume and cumulative precipitation in the Zohreh River estuary for the March of 2017.

Figure 3 is obtained by extracting the amount of cumulative precipitation and the maximum extent of the sediment plume for different independent storms. Investigations showed that the variation of type and intensity of rainfall in the region is low. Therefore, the use of cumulative rainfall as an input has somehow considers the effect of intensity and duration of rainfall and for this reason, there is a good correlation between the data of the sediment plume extent and the cumulative rainfall. The Figure 3 graph and the resulting equation can be used to estimate the maximum extent of the sediment plume in the mouth of river after a specific rainfall.

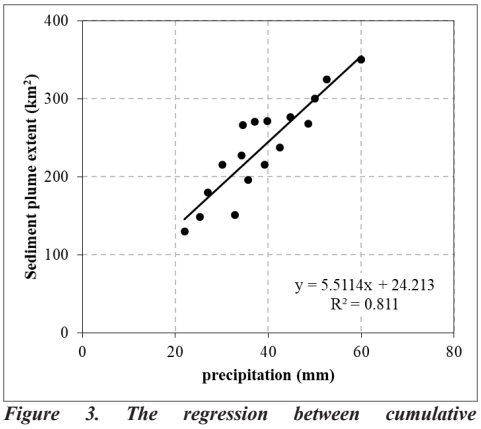

Figure 3. The regression between cumulative precipitation and the maximum extent of the sediment plume in the Zohreh River estuary for different independent storms.

4. References

[1] Gharibreza M, Habibi A, Imamjomeh SR, Ashraf MA. "Coastal processes and sedimentary facies in the Zohreh River Delta (northern Persian Gulf)." Catena. 2014 Nov 1; 122:150-8.

[2] Roy DP, Wulder MA, Loveland TR, Woodcock CE, Allen RG, Anderson MC, Helder D, Irons JR, Johnson DM, Kennedy R, Scambos TA. "Landsat-8: Science and product vision for terrestrial global change research." Remote sensing of Environment. 2014 Apr 5; 145:154-72.

9 & 10 May 2023 , Tehran-IRAN

ICOPMAS 2022

PORT AND COASTAL MANAGMENT

CONCEPTUAL MODELS FOR DEVELOPING OF SHORELINE MANAGEMENT PLAN OF BUSHEHR PROVINCE

Mohammadreza Gharibreza[1]

1) Department of River and Coastal Engineering, Soil Conservation and Watershed Management Research Institute, Agricultural Research, Education and Extension Organization (AREEO), Tehran, Iran, gharibreza4@yahoo.com

1. Introduction

Shoreline Management Plan (SMP) is an integral part of the Integrated Coastal Zone Management (ICZM) studies in Bushehr province, through which a significant section of the "Sea-oriented" perspective forms in the planning and realization of its intended goals. The SMP development for Bushehr Province [1] stepwise in 4 following procedures:

- Updating spatial distribution of the SMP zone planning and determining specific boundaries.
- Identifying and evaluating functional and induced problems and issues in the coastal zone.
- Developing the thematic and spatial action plan to deal with and reduce the adverse effects of existing issues and problems.
- Developing the thematic and spatial action plan to balance and modify issues and problems raised by existing land uses and planned land uses.

2. Material and Methods

Accordingly, considering the strategic programming behind the SMP studies to develop conceptual models (Figures 1 and 2). Therefore, the SMP objectives are designed based on specified definitions [2]. An updated explanation for the ICZM is the "problem-oriented" but "goal-directed" program for the protection of natural resources (biological, non-biological, and human), natural and artificial hazard management, and sustainable coastal development through a balanced use of land and natural resources.

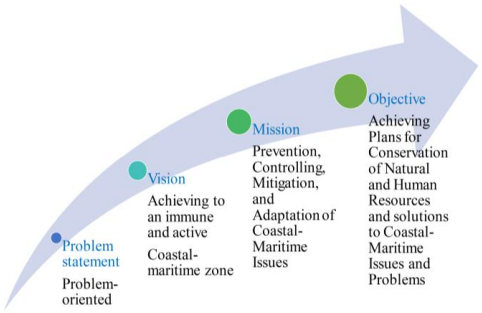

Figure 1. The overall trend to obtain the conservation plan of the SMP of Bushehr Province

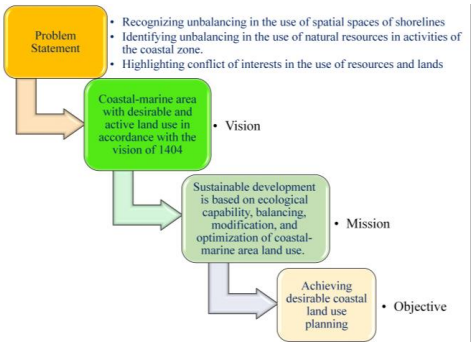

Figure 2. The overall trend to obtain the desirable land use planning of the SMP of Bushehr Province

The SMP conceptual models of the Bushehr Province obtained regarding the ICZM concept have conservation, development, and integration approaches. Conservation is one of the main approaches that emphasize three levels of conservation, protection, and preservation of natural resources (biological, non-biological, and human health) and their sustainable activities. Sustainable development was another approach that the SMP plan introduced for decision-makers to deal with the issues and problems in both thematic and spatial places along the shorelines. Identification, statement, strategies, and measures of the plan analyses using the DPSIR framework [3]. Accordingly, driving forces (D) for causing problems, pressures (P) induced from issues on environment and stakeholders, the state (S) established through existing problems on the coastal zone and users, impacts (I) of specific issues raised on environment and stakeholders, and responses (R) or actions regarding each mentioned terms specified. The concept behind the DPSIR framework and its strategies were applied to provide conservation and development action plans. Besides the DPSIR framework, the SWOT model is used to evaluate issues and problems of the Bushehr Province ports and to present relevant

3. Results

The conservation, development, and integrated approach in the mission and action plans for stockholders formed the conceptual models for the SMP of Bushehr Province. The Checking of the resultant models and data performed by the advisory and technical committee of the Port and Maritime Organization in terms of applicability and thematic duties of the shoreline management plan. For instance, the conceptual model for identification and providing an action plan of SMP to deal with issues and problems of shorelines of Bushehr Province is illustrated in Figure 3. Reviewing literature [4-6] indicates that the conceptual models of the SMP of Bushehr Province open a new window to manage existing issues and implement specific measures for the conservation of natural resources and sustainable development in a highly challenging area of the coastal zone of Iran in terms of development projects.

4. Results

The conservation, development, and integrated approach in the mission and action plans for stockholders formed the conceptual models for the SMP of Bushehr Province. The Checking of the resultant models and data performed by the advisory and technical committee of the Port and Maritime Organization in terms of applicability and thematic duties of the shoreline management plan. For instance, the conceptual model for identification and providing an action plan of SMP to deal with issues and problems of shorelines of Bushehr Province is illustrated in Figure 3. Reviewing literature [4-6] indicates that the conceptual models of the SMP of Bushehr Province open a new window to manage existing issues and implement specific measures for the conservation of natural resources and sustainable development in a highly challenging area of the coastal zone of Iran in terms of development projects.

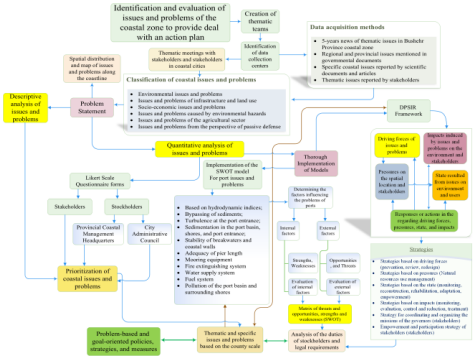

Figure 3. Conceptual model of the action plan for dealing with the issues and problems, the SMP of Bushehr Province

5. References

[1] Gharibreza, M., *Conceptual models and Methods*, in *Integrated Coastal Zone Management of Bushehr Province, phase 1*, F. Vafaei, Editor. 2018, Nanodishan Fan & Trade Engineering & Trading Company: Tehran. p. 187.

[2] Gharibreza, M., *Integrated Coastal Zone Management of Bushehr Province (Synthesis report of Bushehr)*, in *Integrated Coastal Zone Management of Bushehr Province*, F. Vafaei, Editor. 2021, Nanodishan Fan & Trade Engineering & Trading Company: Tehran. p. 403.

[3] Bradley, P. and S. Yee, *Using the DPSIR Framework to Develop a Conceptual Model*, in *Technical Support Document*, A.E. Division, Editor. 2015, US Environmental Protection Agency: Office of Research and Development: Narragansett. p. 82.

[4] Mangor, K., et al., *Shoreline Management Guideline*, in *COADAPT*, B. Edill and L.S. Madsen, Editors. 2017, Danish Hydraulic Institute, DHI: Horsholm, Denmark. p. 449.

[5] MPOB., *Rapid Assessment Report* in *The program of projecting the territory of Bushehr province* 2017, Maab Consultant Engineers Company: Boushehr. p. 258.

[6] PMO., *Report on Integrate Coastal Zone Mangement Conclusions*. 2010, High Council for Urbanism and Architecture of Iran, Maab Consultant Engineers Company: Tehran. p. 261.

SPATIAL ANALYSIS OF HAZARDS ASSOCIATED WITH URBAN AND RURAL SETTLEMENTS OF COASTAL AREA IN SISTAN AND BALUCHESTAN PROVINCE

Maryam Yaghoubzadeh[1], Rasoul Ghanbari Moman[2], Fatemeh Kordi[3]

1) Environmental expert, Sazeh Pardazi Iran Consulting Engineers, Tehran, Iran, yaghobzadehmaryam@yahoo.com
2) Port & Maritime Organization, Tehran, Iran, rghanbari@pmo.ir
3) RS and GIS expert, Sazeh Pardazi Iran Consulting Engineers, Tehran, Iran, fateme.kordi92@gmail.com

1. Introduction

Coastal communities have increasingly exposed to various types of hazards [1]. Natural hazards are naturally occurring events that might have negative effects on people or the environment [2]. In this regard, a "coastal hazard" defines as a phenomenon, which has the potential of causing damage to natural ecosystems, buildings, and infrastructure in the coastal area [3]. The main coastal hazards include Tropical storms and hurricanes, Storm surges, Tsunamis, Flooding, Landslides, Volcanic eruptions, Earthquakes, etc. The Coastal Zone is a region where interaction of the sea and land processes occurs in a very complex and dynamic way [4]. Since an ever-increasing population inhabits this zone, it subjected to a number of natural coastal hazards [5]. Environmental hazards in the coastal zone are among the influential factors in regional planning process and establishment of human communities and facilities. Failure to pay attention to natural coastal hazards and their detrimental effects in the coastal region leads to loss of capital and destruction of natural and human resources. For this reason, attention to environmental hazards is very important in the studies of integrated coastal zone management (ICZM)[1].

2. Material and Methods

2.1. Study Area

The study area is the coastal zone of Sistan and Baluchestan province including the area affects the coastal zone [6] (Figure 1). The surface area of the coastal zone in this province is 12341.74 km^2.

2.2. Methodology

Coastal areas expose to damages caused by various natural hazards, so planning is necessary to provide appropriate measures to prevent or reduce the effects of these hazards. The aim of this study is the identification of natural hazards to urban and rural settlements in coastal areas of Sistan and Baluchestan province and introducing them to management sections and local authorities in order to reduce the risk and managing the risk factors. The initial list of hazards, with 14 identified threats, provided by reviewing internal and external references. Based on the identified threats, a questionnaire was prepared and its results examined both qualitatively and quantitatively. The final list of threats was determined using Delphi method (five hazards were identified) (Table1). After finalizing the main threats, the Hazards map was prepared by using ArcGIS software, and the number of possible hazards for each of the urban and rural settlement in the coastal zone depicted on the map [7, 8].

Figure 1. Study area.

Table 1.List of Hazards

Hazards	Rural settlements	Urban settlements
Landslide	*	*
liquefaction	*	*
Activity of sand dunes	*	*
Risk of meteorological drought	-	-
The intensity of stormy winds	-	-
The intensity of wind erosion	-	-
Soil salinization potential	-	-
Possibility of changing soil texture	-	-
Severity of flood risk	*	*
Danger of encountering high waves	-	-
The flooded area caused by the tsunami event	*	*
Average maximum flow speed	-	-

*natural hazards affecting urban and rural settlements

[1] This article is part of a comprehensive study regarding natural hazards in the Integrated Coastal Zone Management Plan of Sistan and Baluchestan Province, which examines the hazards associated with urban and rural settlements.

3. Results

The results indicated that most of the hazards for urban settlements occur in the coastal zone and the number of hazards reduces by moving from the shoreline towards the inland (affecting area). A large part of the coastal zone subjected to the undesirable effects of at least one or two hazards (see Figure 2). Areas with three or four hazards were located in the western part of the coastal area of Sistan and Baluchestan province, especially behind the Gordim port and the Gulf of Pozm. In these areas, there exist risks of tsunamis, liquefaction and flood. It is noteworthy that the most extensive hazard for urban settlements found to be inundation caused by the tsunami, which means that part of the coastal area may inundated by seawater.

Similar studies conducted for rural settlements. The results revealed that most of the rural settlements subjected to one or two hazards and the number of hazards increased to three or four in the western part of the coastal area adjacent to Hormozgan province (Figure 3). The studies showed that, in addition to the risk of liquefaction and tsunami, the activity of sand dunes also threatens the rural settlements of these areas.

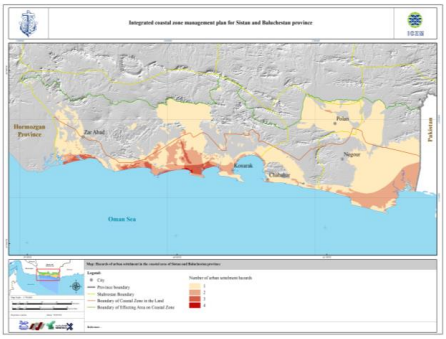

Figure 2. Hazards of urban settlements in the coastal area of Sistan and Baluchestan province

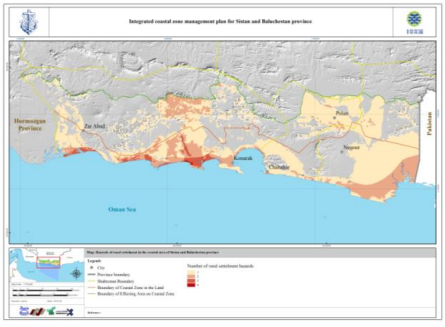

Figure 3. Hazards of Rural settlements in the coastal area of Sistan and Baluchestan province

4. Acknowledgement

The authors acknowledge the support of Port and Maritime Organization (PMO). In addition, we express sincere thanks to all the experts who participated in this study.

5. References

[1] Bukvic, A. and Harrald, J. “Rural versus urban perspective on coastal flooding: The insights from the US Mid-Atlantic communities”. *Climate Risk Management, 23, 2019, pp.7-18.*

[2] Marone, E., R. De Camargo, and J. S. Castro. "Coastal hazards, risks, and marine extreme events: what are we doing about it, " *Physical Sciences, Natural Hazard Science, Hydrology, Atmospheric Sciences, Geophysics,* 2017.

[3] Cambers, G. "Professional development programme: Coastal infrastructure design, Construction and Maintenance; Coastal Hazards and Vulnerability". *Antigua, the University of the West Indies, June 18-22, 2001, pp. 1-21.*

[4] Zhang, K., Douglas, B. C., and Leatherman, S. P. "Global Warming and Coastal Erosion". *Climatic Change 64, 2004, pp. 41–58.*

[5] Kaiser, G. "Risk and vulnerability analysis to coastal hazards-an approach to integrated assessment". *PhD thesis, Christian Albrecht University, Kiel, Germany*, 2006, 253p.

[6] Port and Maritime Organization (PMO). "Boundaries of the coastal area report (Scrutinizing the ICZM plan for Sistan and Baluchestan province) ". 2021, 131p.

[7] Yaghoubzadeh, M., Salmanmahiny, A., Mikaeili Tabrizi, A, R., Danehkar, A., and Moslehi. M "Prioritizing Environmental Hazards of Mangrove Forests in Hormozgan Province." *Journal of Natural Environmental Hazards 10, no. 30, 2022, pp.62-82.*

[8] Yaghoubzadeh, M., Danehkar, A., Haghighat, M., Mashhadi Rafiee, M., and Lotfikhah, S. "Coastal Zoning of Sistan and Baluchestan Base on Environmental Sensitivity." *Journal of Natural Environment, 2022, pp. 49-63.*

EROSION AND SEDIMENTATION STATUS ALONG THE BUSHEHR PROVINCE SHORELINE, KEY INFORMATION FOR SHORELINE MANAGEMENT PLAN

Mohammadreza Gharibreza[1]

1) Department of River and Coastal Engineering, Soil Conservation and Watershed Management Research Institute, Agricultural Research, Education and Extension Organization (AREEO), Tehran, Iran, gharibreza4@yahoo.com

1. Introduction

Shoreline Management Plan (SMP) is one of the fundamental parts of the Integrated Coastal Zone Management (ICZM) studies in Bushehr Province, through which a significant part of the "Sea-oriented" perspective organizes the planning and realization of its intended goals. [1]. The study of changes in the position of coastlines in a specific period is the basis for determining the status of erosion and sedimentation in the coastal area. Shorelines are the water borders of land with open seas representing different geographical, geological, and hydrodynamic features at varying elevations and forms. This critical boundary undergoes short- and long-term changes. Such changes result in relocating the position of shorelines and the sedimentary regimes of the coasts that are progressive and regressive regarding the sea. [2-4]. Balancing between land and sea driving forces causes the stable location of shorelines. An imbalance in these forces and processes will cause the shoreline to be higher and lower than before. Therefore, the present study aimed to measure coastal changes and erosional and depositional regimes along the Bushehr Province.

2. Material and Methods

Studying coastal change and its spatial zoning in relation to erosion and sedimentation is an important part of geological, geomorphological, technical, and management studies. [5-8]. Therefore, a variety of criteria, indices, and methods have been introduced to identify and sketch shorelines related to conventional elevation codes (MSL[1] or CD[2]). According to previous works and experiences [5-8], recognition and sketching of shorelines based on berm crest is the most reliable reference for coastal changes in complex coastal sedimentary environments such as the coastal area of Bushehr Province. High uncertainty and recording of water lines instead of shorelines are common mistakes in some new remote sensing studies. Therefore, interpretation of shoreline, especially the line of the berm crest along sandy coasts and permanent shoreline of estuaries and tide-dominated areas, which is an index of the Mean Sea Level (MSL), was detected and sketched using the on-screen digitizing method in two-time series of satellite images. The research material included the IRS and Sentinel-2A (panchromatic band) with 6 and 10 m spatial resolution, respectively. Besides, orthophotos of the coastal zone of Bushehr Province with a scale of 1:2000 scale (2007) was obtained from Pars Especial Economical Zone to increase the accuracy of sketched shoreline. Several control points with accurate coordinates are considered to improve the georeferencing accuracy and the overlapping of shorelines.

3. Results

Results showed that from the north of Bushehr Province till the headland of Bushehr, an area of 974 hectares experienced coastal erosion, land transgression or sedimentation has occurred about 1360 hectares, artificial land development into the sea was 1115 hectares, and coastal structures and ports have occupied 68 hectares from the sea. The urban area of Bushehr and Negin, and Sadra islands have 921 hectares distributions experienced the maximum coastal changes. As a result, a depositional regime dominated in the north of Bushehr Province until the port of Genaveh. Results showed that from the Genaveh to the southern area erosion process of the shoreline increased against sedimentation. The rate of erosion, especially erosion of sand spits is three times sediment accumulation in Abbassak Bay. Coastal change investigation revealed that from the Bushehr headland to the Nayland headland about 876 hectares of shorelines are subject to erosion, and 430 hectares are under sediment accumulation. Besides, about 811 hectares are land extracted from the sea, and finally, 164 hectares of coastal structures and new breakwaters have been constructed. A severe erosional regime was observed along the Bushehr headland to Halileh port and from Mohammad-Ameri port to Lavar port. Such a condition also was obtained with 4.5 times the intensity of erosion against sedimentation from Methanol to Assaluyeh port. Sediment input from Mond and Gavbandi rivers has decreased locally the relation of erosion rate against sedimentation to 1.4 and 2.5 times, respectively. The long-term drought resulted in a decrease in sediment discharge from the watershed, and the construction of several breakwaters or jetties has caused an erosional regime along most of the shorelines of Bushehr Province.

[1] Mean Sea Level
[2] Chart Datum

Figure 1. Severe coastal erosion of rocky shorelines of Genaveh city

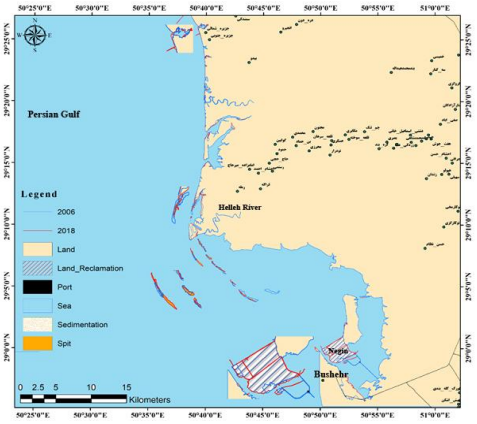

Figure 2. High rate of coastal change through land erosion and reclamation from the sea along Bushehr shorelines

4. References

[1] Gharibreza, M., *Conceptual models and Methods*, in *Integrated Coastal Zone Management of Bushehr Province, phase 1*, F. Vafaei, Editor. 2018, Nanodishan Fan & Trade Engineering & Trading Company: Tehran. p. 187.

[2] Anfuso, G., Pranzini, E., Vitale, G., *An integrated approach to coastal erosion problems in northern Tuscany (Italy): Littoral morphological evolution and cell distribution.* Geomorphology, 2011. **129** p. 204-214.

[3] Davis, R.A., *Coastal Sedimentary Environments*. 1985, New York: Springer-Verlag 378.

[4] Gharibreza, M., *Recognize and evaluate the issues and problems in the coastal zone of Bushehr Province with respect to management units*, in *Integrated Coastal Zone Management of Bushehr Province, phase 2*, F. Vafaei, Editor. 2019, Nanodishan Fan & Trade Engineering & Trading Company: Tehran. p. 468.

[5] Anders, F.J. and M.R. Byrnes, *Accuracy of Shoreline Change Rates as Determined from Maps and Aerial Photographs* Shore and Beach, 1991. **59**(1): p. 17-26.

[6] Demir, N., M. Kaynarca, and S. Oy, *Extraction of Coastlines With Fuzzy Approach Using Sentinel-1 SAR Image.* The International Archives of the Photogrammetry, Remote Sensing and Spatial Information Sciences, 2016. **XLI-B7**: p. 747-751.

[7] Gharibreza, M., *Iran's Coastal Changes*. 2002, Department of River and Coastal Engineering, Soil Conservation and Watershed Management Research Institute: Tehran. p. 163.

[8] Pardo-Pascual, J.E., et al., *Assessing the Accuracy of Automatically Extracted Shorelines on Microtidal Beaches from Landsat 7, Landsat 8 and Sentinel-2 Imagery.* Remote Sensing, 2018. **10**(2): p. 326.

14th International Conference on Coasts, Ports and Marine Structures
9 & 10 May 2023 , Tehran-IRAN
ICOPMAS 2022

ANALYSIS OF FACTORS AFFECTING THE DEVELOPMENT OF COASTAL TOURISM WITH A SUSTAINABLE DEVELOPMENT APPROAC (CASE OF STUDY: ARVAND FREE ZONE)

Asad Ziaee Mehr[1], Leila Andervazh[2]

1) Master Of International Business Management, Expert In Port Standards And Conventions Of Khorramshahr Port, Iran, asad.ziaeemehr@yahoo.com
2) Assistant Professor, Department Of Business Management,Khorramshahr International Branch,Khorramshahr,Iran, leila.andervazh@gmail.com

1. Introduction

The purpose of this research is to analyze the factors affecting the development of coastal tourism with a sustainable development approach. In terms of the purpose of this research, it is a development that was carried out using a combined method in two stages, including the identification of indicators by the method of thematic analysis and its testing by the method of structural equation modeling. The statistical population of the research was formed from 2 quantitative sections where 384 tourists were selected from the free areas of Arvand and the qualitative section was composed of 15 coastal tourism experts using the snowball method. The statistical sample size of 384 people was randomly selected and analyzed.

The conceptual model of the research was designed based on the research and a questionnaire was prepared and the desired data was collected. The validity of the questionnaire was confirmed using content validity and the reliability of the research was confirmed using Cronbach's alpha method. Finally, by using structural equation modeling and through AMOS software, research hypotheses were investigated and it was determined that cultural and social factors, individual factors, economic factors, political factors, and infrastructure factors affect the formation of factors affecting the development of coastal tourism with a sustainable development approach. Are effective.

2. Area of study

Arvand commercial-industrial free zone is located in the northwest of the Persian Gulf and the southwest of Khuzestan province in Abadan and Khorramshahr cities with an area of more than 173 square kilometers at the confluence of Arvand river and Karun and has a common border with the countries of Iraq and Kuwait. This geographical area has always been important as one of the tourist destinations in the province and the country due to its special weather conditions in different seasons and its strategic location. The presence of various air, road, rail, and sea communication routes is one of the characteristic features of this region, which, due to this variety, has provided the possibility for tourists to choose their desired route. In general, it can be said that Arvand free zone has a variety of tourist attractions, including; it is natural and rural, cultural, historical, religious, holy defense, industrial, urban, commercial and recreational, sports, etc. Therefore, the existence of all kinds of actual and potential tourist attractions in the Arvand free zone, along with sea tourism, promises the growth and development of coastal tourism.

3. Methodology

The statistical population of the research in the quantitative phase included all the tourists of the Arvand Free Zone. Due to the large size of the statistical population, the available random sampling method was used. The sample size was determined using Cochran's formula of unlimited societies to the number of 384 people and the research questionnaires were prepared and distributed. After returning, the questionnaires were collected and adjusted using Amos and spss22 software and using the structural equation modeling technique. Analysis was done.

To answer the main question of the research and according to the research method, interviews were conducted with 15 professors, managers, and tourism experts. The interviews were conducted with experts for data analysis and to measure the reliability of the results were examined and analyzed separately by the research team (researcher and two colleagues) the absence of differences in the results obtained by each of the researchers indicates the reliability of the results. Had been obtained to measure the validity of the method, in addition to the comprehensive, organizing, and basic themes that were selected and confirmed based on the theoretical foundations and background of the research, opinions, and views of a group of experts were also used.

Figure 1 is a visualization of the factors affecting the development of sustainable tourism from the point of view of tourists, which is drawn based on the data obtained from interviews and their analysis using the thematic analysis method.

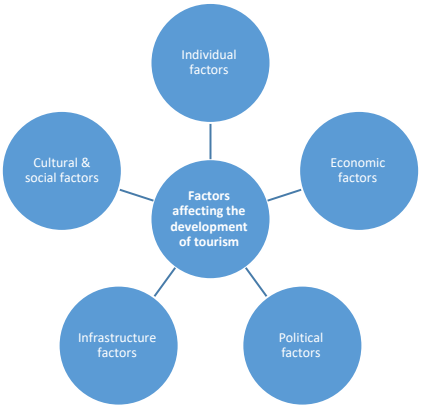

Figure 1. Structural factors affecting the development of sustainable tourism (made by a researcher)

4. Results and Discussion

Tourism, as one of the service sectors, has a significant contribution to increasing growth and development, especially in less developed countries. Due to its connection with other economic sectors and also its impact on macroeconomic variables, especially incomes and employment, this industry causes an increase in the income of different strata, a decrease in unemployment, economic prosperity, and as a result, an improvement in the quality of life of the people and an increase in social well-being. This research has identified the factors affecting the development of coastal tourism with a sustainable development approach to provide the necessary foundations for the formation of sustainable coastal tourism in the Arvand Free Zone and ultimately to improve the tourism situation in the country. In this study, factors affecting the development of coastal tourism with a sustainable development approach were identified in the form of 13 indicators and five dimensions as follows. It was determined that cultural and social factors, individual factors, economic factors, political factors, and infrastructure factors are effective in the formation of factors affecting the development of coastal tourism with a sustainable development approach.

5. References

[1] Bramwell, B., & Lane, B. (2010). Priorities in sustainable tourism research. Journal of Sustainable Tourism,16 (1) ,1-4.
[2] Fazenda, N. and Da silva, F.N. and Costa, C. (2010). Douro Valley Tourism Plan; The plan as part of a sustainable tourist destination development. process,Journal of World Hospitality and tourism, vol.2, No.4, pp: 428-440.
[3] Gharazhloo, M ,Ramenzanzade ,M&Galinsharifi. (2015). Environmental Impact of Tourism on Coastal Ramsar, Journal of Human Geography, 1(3): 28-37.

[4] Hall, C.M. (2017). Trends in ocean and coastal tourism: the end of the last frontier?, Ocean & Coastal Management, 1(4): 1-19.

[5] Izadi, M., Saadat, S. H., Ayoubian, A., Dehaghi, Z. H., Karbasi, M. R., & Jalali, A. R. (2014). "Health tourism in Iran; identifying obstacles for development of this industry.", International Journal of Travel Medicine and Global Health, 1(2).
[6] Jaafar, M., Ismail, S. and Rasoolimanesh, S.M. (2015). Perceived social effects of tourism development: a case study of kinabalu national park, Theoretical and Empirical Researches in Urban Management, vol. 11, no. 2: 5- 21.
[6] Liu, Z. (2013). Sustainable tourism development: A critique. Journal of Sustainable Tourism, 11 (6) ,459-475.
[7] Reihanian, A. & Beinti Mahmood, N.Z. & Kahrom, E. & Wan Hin, T. (2012). Sustainable tourismdevelopment strategy by SWOT analysis: Boujagh National Park, Iran. Tourism
[8] Management Perspectives 4: 223- 228. anese tour guides, African Journal of Business Management, vol.5, No.4, pp: 1325-1333.
[9] Shabiri, S.M., Meibodi, H., & Hajihoseini, A. (2016). The environmental consequences of tourists on coastal areas of the Mazandaran Sea from the point of view of the people and authorities, Journal of Tourism Planning and Development, 2(5): 129-145.
[10] Tsai, Wen-Hsien. (2013). an integrated approach for selecting corporate social responsibility programs and costs evaluation in the international tourist hotel, International Journal of Hospitality Management. 29, 385–39.
[11] Asghari, fisherman; Taghilou, Ali Akbar and Asghari, Saleh (2017). Analysis and evaluation of the potential environmental effects of the implementation of the tourism project in the Safaiyah section of Khoi city, Scientific-Research Quarterly of Tourism and Development, 7th year, 1st issue, 118-134.
[12] Bidakhti, Ali Akbar and Sharifi, Navid (1391). Investigating the relationship between tourism boom and social capital in the coastal areas of the Caspian Sea, scientific-research quarterly of tourism management studies, 7th year, number 17, 121-149.
[13] Zardan, Maitham and Mansour Bahmani, Muslim (2014). Rural tourism and principles of sustainable tourism development, National Civil and Architecture Conference with an approach to sustainable development, 1-15.
[14] Shatrian, Mohsen; Gholami, Yunus and Mirmohammadi, Mohammad (2016). Evaluation of sustainable urban tourism development indicators of a case study (Kashan city), Applied Research Journal of Geographical Sciences, 17th year, No. 46, 214-195.
[15] Mohseni, Reza Ali (1388). Sustainable tourism in Iran: functions, challenges and solutions, Journal of Geographical Space, ninth year, number 28, 149-171.
[16] Nasrallahi, Zahra; Jahanbazi, Neda and Naseri, Tahereh (2014). Ranking of the country's provinces according to tourism attractions, scientific-research quarterly of tourism management studies, 9th year, number 28, 17-37.

14th International Conference on Coasts, Ports and Marine Structures
9 & 10 May 2023 , Tehran-IRAN
ICOPMAS 2022

ESTIMATION OF SEA LEVEL EXCEEDANCE PROBABILITIES USING STATIONARY AND NON-STATIONARY EXTREME VALUE METHODS IN THE CASPIAN SEA

Mohammad Hadi Bahmanpour[1], Babak Banijamali[2], Hamid Khalili[3], Rasool Ghanbari[4], Ali Azimi[5], Mahya Hoseini[6], Shahin Mohebkhodaee[7], Mojtaba Hoseini Chavoshi[8]

1) Darya-Bandar Consulting Engineers, Tehran, Iran, m.h.bahmanpour@daryabandar.com
2) Darya-Bandar Consulting Engineers, Tehran, Iran, banijamali.babak@gmail.com
3) General Directorate of Coastal and Port Engineering, Ports and Maritime Organization, Tehran, Iran, hkhalili@pmo.ir
4) General Directorate of Coastal and Port Engineering, Ports and Maritime Organization, Tehran, Iran, rghanbari@pmo.ir
5) General Directorate of Coastal and Port Engineering, Ports and Maritime Organization, Tehran, Iran, aazimi@pmo.ir
6) Darya-Bandar Consulting Engineers, Tehran, Iran, sm.hoseini@mail.kntu.ac.ir
7) Darya-Bandar Consulting Engineers, Tehran, Iran, shahinmohebkhodaee13@gmail.com
8) Darya-Bandar Consulting Engineers, Tehran, Iran, mojchavooshi92@gmail.com

1. Introduction

Fluctuations of the Caspian Sea (CS) water level are mainly controlled by this land-locked basin's balance of hydrological variables (mainly river run-off and precipitation minus evaporation). As a result, predictive capabilities are restricted by the ability to forecast hydrological components, which are too complex to model and/or measure. Moreover, uncertainties in predicting future trends in part due to climate change make the study of CS water levels even more challenging [1- 2]. At present, CS water level stood at dangerously low levels of around -27.5 m relative to open seas mean sea level, with the possible further downfall in future years due to climate factors. Globally, extreme value analysis (EVA) is used as a statistical tool to predict a parameter's maxima and/or minima. Numerous applications of this technique on sea level parameters have been reported in the literature [e.g., 3]. To the best of our knowledge, EVA theory has not been applied to CS level forecasts so far. In this paper, exceedance probabilities (i.e., return periods associated with return values) will be calculated and assigned to various predicted water levels for CS. Results from this study can inform the decision-making process for future planning of a wide range of activities (i.e., shipping, navigation, construction, recreation, conservation, management, etc.).

2. Data and Methods

In the present study, EVA theory was applied to existing monthly sea level measurements (1941-2021) from Anzali port to predict sea level exceedance probabilities within the next 20 years. Furthermore, frequency domain analysis including wavelet and spectral analysis was also performed. For EVA analysis, two classes of methods were adopted: (1) stationary analysis using MIKE ZERO EVA module and (2) non-stationary analysis using NEVA (non-stationary Extreme value analysis) in MATLAB [4]. The basics of both techniques have been covered in many publications [e.g., 5]. Unlike stationary methods that assume no underlying change in the basic probability distribution from which data is withdrawn, in non-stationary methods change of probability distribution with a covariate (usually time) is taken into account. This ensures a more meaningful result in the case where a significant trend exists in input data (CS water level shows dramatic changes in the form of increasing or decreasing trend (see below figure)).

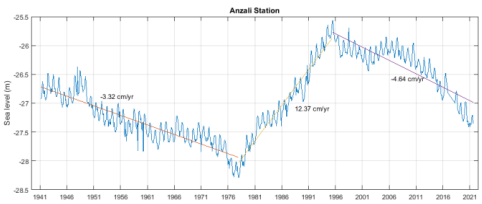

Figure 1. Monthly-averaged sea level measurements from Anzali station. Regressed lines indicate a linear trend

3. Results

3.1. Spectral Analysis

Under results obtained from power spectral density analysis, various significant (in statistical terms) peaks were found in raw data (i.e., 3 and 6-monthly peaks plus two peaks at 1 and 4 years) (Figure 2). The yearly signal is due to changes in CS water level due to variation of hydrological input (i.e., river run-off). Also, based on wavelet analysis, the time variation of the above-mentioned peaks was investigated. It was found that the yearly signal showed little variation with time (see Figure 3) while other peaks (particularly 4-yearly or 10-yearly) indicated much stronger change with time). This has perhaps to do with the difference in forcing of each spectral peak.

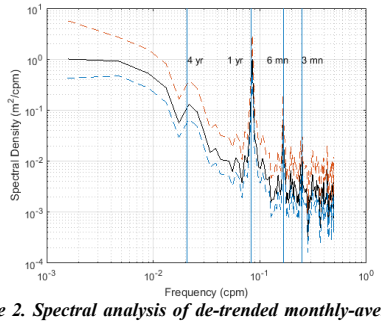

Figure 2. Spectral analysis of de-trended monthly-averaged CS water levels. The dashed lines indicate the 95% confidence interval. Significant peaks were marked with an upright blue line.

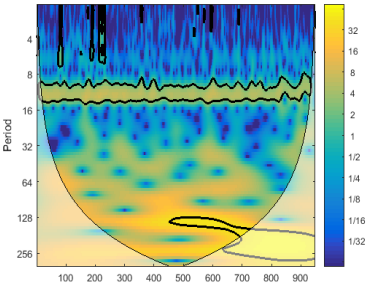

Figure 3. WAVELET analysis of monthly-averaged CS water level. The narrow black line indicates the Cone of influence. The vertical axis's unit is a month and the horizontal axis is a function of time.

3.2. Stationary Analysis of Long-Term Fluctuations

Stationary analysis was performed using the entire length of the monthly-averaged record (Tables 1 and 2). Using the annual maximum method yielded 80 records for analysis. Two assumptions were made: (1) a scenario where sea level will rise in the future (analysis using negative values) and (2) a scenario where sea level will fall in the future (analysis using positive values).

Table 1. Return periods associated with CS water level in a sea level rise scenario. This analysis was performed using raw (no change of sign) input data for CS water level (which is recorded as negative values)

Return Period	5	10	20	50	100
Water Level	-25.9	-25.7	-25.7	-25.6	-25.5

Table 2. Same as Table 1 for the sea level downfall scenario

Return Period	5	10	20	50	100
Water Level	-27.8	-28.0	-28.2	-28.4	-28.6

3.3. Non-Stationary Analysis of Long-term Fluctuations

Non-stationary analysis, as its name suggests, needs to take into account significant trends in input data. As a result, it was not possible to perform the analysis throughout the recorded period. Non-stationary analysis was performed for the recent period during which a downfall in CS water level has been recorded (beginning in 1995). As a result, various return levels (2, 10, 25, 50, and 100 years) were calculated (Figure 4). It is evident from the investigation of results depicted in Figure 4, that CS water level return periods change as a function of time, due to the existence of an underlying trend in raw input data. Another analysis was performed using the same segment of input data with a sea level rise scenario (not shown).

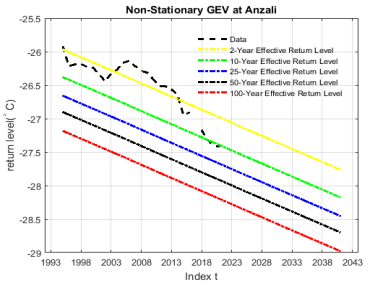

Figure 4. Non-stationary return levels of CS as a function of time.

4. Conclusions

A wide range of statistical methods both in frequency and time domain were employed to predict CS water level exceedance probabilities. In addition to using the conventional stationary EVA method, a more robust method with the assumption of non-stationary water level was taken into account. Table 3 presents the main findings of the present study, including results for both the stationary and non-stationary assumptions.

Table 3- Return levels for the year 2042 (with omitted negative sign) associated with CS water levels.

	Applied EVA technique					
	Non-stationary			Stationary		
R.P.	10	25	100	10	25	100
Rise scenario	27.6	27.5	27.5	25.7	25.7	25.5
Downfall scenario	28.2	28.4	29	28	28.2	28.6

5. References

[1] Elguindi, N. and Giorgi, F., 2006, Projected changes in the Caspian Sea level for the 21st century based on the latest AOGCM simulations, Geophysical research letters, 33(8).
[2] Prange, M. Wilke, T. and Wesselingh, F.P. 2020, The other side of sea level change, *Commun. Earth Environ.,* 1, 69.
[3] Wahl, T. Haigh, I.D. Nicholls, R.J. Arns., Dangendorf. S, Hinkel, J. Slangen, ABA., 2017, Understanding extreme sea levels for broad-scale coastal impact and adaptation analysis, Nature communications, 33.
[4] Cheng, L., AghaKouchak, A., Gilleland, E., and Katz, W.R., 2014, Non-Stationary extreme value analysis in a changing climate, *Climatic Change,* 353-369.
[5] Coles, S., 2001, an introduction to statistical modeling of extreme values, Springer.

14th International Conference on Coasts, Ports and Marine Structures
9 & 10 May 2023 , Tehran-IRAN
ICOPMAS 2022

A ZONATION STUDY FOR RISK OF OCCURRENCE OF RIP CURRENTS ALONG SOUTHERN COASTS OF CASPIAN SEA USING HYDRODYNAMIC AND GEOMORPHOLOGICAL CONTROLS

Mohammad Hadi Bahmanpour[1], Babak Banijamali[2], Hamid Khalili[3], Rasool Ghanbari[4], Ali Azimi[5], Shahin Mohebkhodaee[6], Mojtaba Hoseini Chavoshi[7], Mahya Hoseini[8]

1) Darya-Bandar Consulting Engineers, Tehran, Iran, m.h.bahmanpour@daryabandar.com
2) Darya-Bandar Consulting Engineers, Tehran, Iran, banijamali.babak@gmail.com
3) General Directorate of Coastal and Port Engineering, Ports and Maritime Organization, Tehran, Iran, hkhalili@pmo.ir
4) General Directorate of Coastal and Port Engineering, Ports and Maritime Organization, Tehran, Iran, rghanbari@pmo.ir
5) General Directorate of Coastal and Port Engineering, Ports and Maritime Organization, Tehran, Iran, aazimi@pmo.ir
6) Darya-Bandar Consulting Engineers, Tehran, Iran, shahinmohebkhodaee13@gmail.com
7) Darya-Bandar Consulting Engineers, Tehran, Iran, mojchavooshi92@gmail.com
8) Darya-Bandar Consulting Engineers, Tehran, Iran, sm.hoseini@mail.kntu.ac.ir

1. Introduction

Globally, a large number of drowning incidents take place each year in the coastal ocean [1]. The majority of these incidents were blamed for a ubiquitous feature of surf zone circulation known as rip current: a strong (0.3- 2 ms^{-1}) offshore-directing surface flow formed as a response to near-shore mass and momentum balance due to asymmetric wave breaking. Along the Caspian Sea (CS) in northern Iran, at least more than a hundred fatalities due to drowning (Iranian part only) occur per year. Details of rip current dynamics and its formation mechanism were covered in many past studies [e.g., 2-3]. Rip currents could be broadly categorized as being formed due to either hydrodynamic controls (transient rips) or morphological controls (rip channels) with morphologically-driven currents usually being stronger. Near-shore bathymetry usually consists of transverse bars and rips under skewed or normal waves which facilitate rip current formation.

Analytic models, along with experimental studies, were developed to study rip currents [4-5]. In recent years, a wide range of novel approaches including usage of numerical modeling, Doppler velocity measurements, drifter or dye tracking, etc., were used to study rip currents with various degrees of success [e.g., 2, 6]. These methods are often limited in scope (both spatial and temporal) and fail at providing a comprehensive mapping of rip current hazard levels. Another approach is to determine "beach profile shape" through well-defined criteria and to relate that to rip current hazard level. This will enable a zonation of rip current hazards all along the entire coastline using this simple approach. In the present study, this methodology has been applied for the zonation of hazard levels.

2. Data and Methods

"beach shape profile" could be classified with the following two formulas [7-8]:

$$\Omega = \frac{H_b}{\omega T} \quad (1)$$

$$\mathrm{RTR} = \frac{\mathrm{TR}}{H_b} \quad (2)$$

Table 1- "Beach profile shape" classification [9]

Criteria range	Description
$RTR < 3$ & $\Omega \sim 2-5$	Barred beaches (B)
$RTR \sim 3-7$ & $\Omega \sim 2-5$	Low Tide Bar/Rip beaches (LTBR)
$RTR \sim 3-7$ & $\Omega < 2$	Low Tide Terrace beaches with Rip currents (LTTR)
$RTR < 3$ & $\Omega > 5$	Barred Dissipative (BD)
$RTR > 3$ & $\Omega > 5$	Non-Barred Dissipative Beaches (NBD)
$RTR < 3$& $\Omega < 2$	Completely Reflective Beaches (R)
$RTR > 7$ & $\Omega > 2$	Ultra-Dissipative beaches (UD)

Where H_b is the breaking wave height (m), ω is the sediment settling velocity (ms^{-1}) (see [10]), T is the wave period, and TR is the tidal range (m). It has been reported that the first two types of beach profile shapes listed in Table 1 possess the highest risk of rip current formation (B and LTBR beach profiles). LTTR and BD beach profiles possess a medium risk of the rip current formation while the remaining beach profile shapes possess the lowest risk of rip current formation (NBD, R, and UD). In this paper, equations 1-2 along with beach profile shape classification as presented in Table 1 will be used for rip current hazard classification. A similar approach for rip current hazard classification was adopted in previous studies [e.g., 11].

To obtain wave parameters in the surf zone, a spectral wave transformation model (MIKE21-SW) was employed. The model was run for the entire simulation year of 2013 to obtain near-shore wave characteristics for one year. Offshore wave data was provided by a wave hindcast product provided by the ports and maritime organization of Iran. An algorithm was used in MATLAB to find breaking

wave height based on calculated radiation stresses (at each time step and each location along the coastline).

3. Results

In Figure 1, the zonation of CS based on rip current hazard level has been presented (for June). In Table 1, the number of areas identified as having high hazard levels for rip currents was presented. It follows that area "C-1", from Kelachay to eastern parts of Chalus has the highest number of areas with high hazard levels.

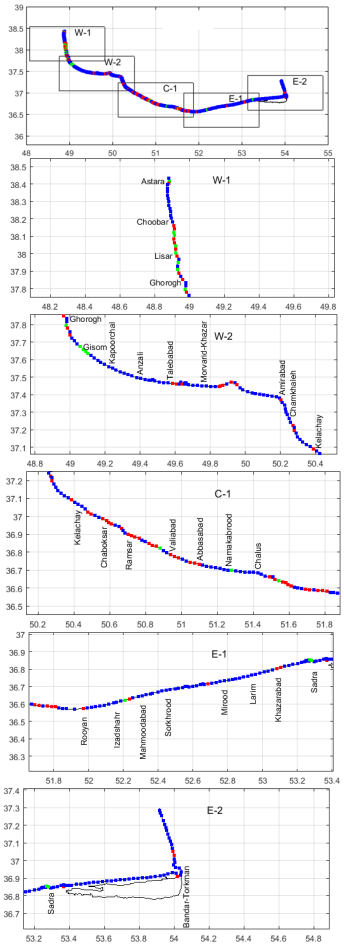

Figure 1. Rip current hazard levels in June (red: high, blue: medium, and green: low). Zoomed-in sections (C-1 – E-2) were also presented.

Table 2- Number of areas identified as high risk in zoomed-in sections of Figure 1 per month

	W-1	W-2	C-1	E-1	E-2
Jan	12	8	8	4	5
Feb	5	20	32	11	4
Mar	7	8	19	10	6
Apr	6	21	34	19	6
May	5	35	37	22	6
June	10	16	35	11	4
Jul	9	10	33	11	2
Aug	6	15	35	12	3
Sep	7	10	31	12	4
Oct	6	3	16	8	5
Nov	11	14	35	12	5
Dec	9	3	16	8	6

4. Conclusions

CS drowning data from various data sources were also evaluated. It was found that coastal areas of Rasht and Anzali in Gilan province and Babolsar and Mahmoodabad in Mazandaran province possess the highest rate of drowning incidents. The largest proportion of zones falls into the "medium risk" category with the highest rates of drowning belonging to the same category. This indicates the necessity of taking into account other factors (e.g., coastal accessibility, population density, etc.) for a holistic approach to risk analysis of rip currents in CS.

5. References

[1] Trimble, S. M, 2017, Addressing the International Rip Current Health Hazard, Doctoral dissertation, Texas A & M University.

[2] Dalrymple. R, et al., 2011, Rip Currents, Annual Reviews of Fluid Mechanics, 43, 551-581.

[3] Castelle. B, et al., 2016, Rip Current Types, Circulation and Hazard. Earth Science, 163, 1-21.

[4] Dalrymple. RA, 1978, Rip currents and their causes, 16th conference of Coastal engineering, 1414-1427.

[5] Haller. MC, Dalrymple. RA, Svendsen. IA, 2002, Experimental studies of nearshore dynamics on a barred beach with rip channels, Journal of Geophysics, 107, 3061.

[6] Shafiei Sabet. B, Barani. G. A, 2011, Field investigation of rip currents along the southern coast of the Caspian Sea, Scientia Iranica, 18, 878-884.

[7] Wright. LD, Short. AD, Morphodynamic variability of surf zones and beaches: A synthesis, 1984, Marine Geology, 93-118.

[8] Masselink. G, Short. A.D, 1993, The effect of tide range on beach morphodynamics, a conceptual model, Journal of Coastal Research, 9, 785-800.

[9] Li. Z, Zhu. Sh, 2018, Why there are so many drowning accidents happened at Dadonghai beach, Hainan, China: Morphodynamic analysis, Journal of Coastal Research, V: 81, 741-745.

[10] Ferguson. R.I, Church. M., 2004, A simple universal equation for grain settling velocity. Journal of Sedimentary Geology, V: 74, 933-937.

[11] Ferrari. M, et al., 2019, A geomorphological and hydrodynamic approach for beach safety and sea bathing risk estimation, Science of the total environment, 671, 1214-1226.

14th International Conference on Coasts, Ports and Marine Structures
9 & 10 May 2023 , Tehran-IRAN
ICOPMAS 2022

RISK ASSESSMENT OF THE OUT-OF-SERVICE OF DREDGING EQUIPMENT IN IRANIAN PORTS AND WATERWAYS USING THE BOWTIE METHOD

Romina Yazdanmadad [1], Ashkan Babazadeh[2], Abbas Alishahi[3]

1) Department of Maritime Engineering, Amirkabir University of Technology, Tehran, Iran, rominay@aut.ac.ir
2) Department of Maritime Engineering, Amirkabir University of Technology, Tehran, Iran, ashkanbabazadeh@aut.ac.ir
3) Port and Maritime Organization, Tehran, Iran, a.alishahi@pmo.ir

1. Introduction

Risk is an inseparable part of marine operations; therefore, to predict possible risks and prevent their consequences, risk management and its assessment in marine projects are of special importance. Risk assessment in projects requires the selection of appropriate and accurate methods so that by using these methods it is possible to reduce risks and their consequences before they occur. Not allocating enough time to carry out the necessary checks to identify and assess risks in projects and not having enough expertise in choosing and applying the proper method of risk assessment increase the possibility of faults, failures and occurrence of catastrophic events in projects.

In order to increase the safety of marine operations, including navigational safety, protection of life, marine environment and marine infrastructure and the safety of offshore projects, structured and systematic standards have been prepared by classification societies and various international organizations as a guidance for selection and application of risk assessment techniques.

Dredging often is focused on maintaining or increasing the depth of navigation channels, anchorages, or berthing areas to ensure the safe passage of boats and ships. Vessels require a certain amount of water in order to float and not touch bottom. Water depth in mentioned areas decreases over time due to deposition of sediments and thus making problem for safe passage of ships. Since massive ships carry the bulk of the goods imported into the country, dredging plays a vital role in the country's economy [1].

In Iran ports in any region have their own dredging vessels which are handed over to subcontractors via certain contract for a certain time. Subcontractors must keep the waterways and ports safe for the passage of ships by providing required water depth. Therefore, the first and primary responsibility of the subcontractor is to keep the dredgers in operable condition.

Ports and waterways are strategic infrastructure of countries and must be kept open continuously. Therefore, threats, consequences of this vital issue must be investigated and barriers to avoid them must be determined through a proper risk assessment analysis. In this study risk assessment of the out-of-service of dredging equipment in Iranian ports and waterways using the qualitative bowtie method is carried out based on guidance notes of ABS classification society on risk assessment applications for the marine and offshore industries.

2. Bowtie Analysis

Based on ABS's guidance notes on risk assessment, bowties are a visual method of describing, documenting, and dictating the link between initial threats (i.e., causes) to any process or situation, the resulting consequences of these threats if they were to trigger an undesired event, and the barriers and measures put in place to prevent this chain of events being acted out in fullness.

Bowties are useful tools for risk assessment (e.g., identification of causes and consequences) and barrier management. Bowties are often used to highlight and facilitate the management of barriers that are in place to prevent accidents [2].

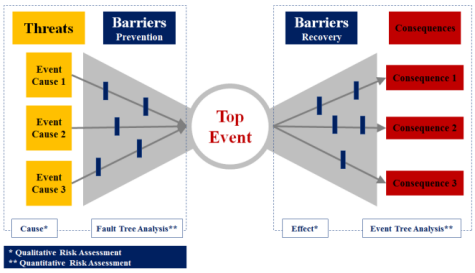

Figure 1. Generic example of a bowtie

3. The Out-of-Service of Dredging Equipment

The out-of-service condition for dredging equipment is defined as any conditions under which the equipment cannot fulfill their primary objective – maintaining required water depth of the ports and waterways through dredging. This can be either due to technical or managerial issues. Technical issues are obviously those that may make the vessel inoperable such as failure of main and auxiliary machinery, navigational equipment, dredging equipment, etc. On the other hand, detention of the ship, failure in

insurance or any obligatory certification renewal, prolongation of docking and machinery overhaul, etc. may also cause the vessel not to be able to fulfill its objective properly.

4. Risk Assessment of the Out-of-Service of Dredging Equipment

Here the top event is out-of-service condition for dredging equipment. Here qualitative bowtie which uses simpler cause–effect scenarios with barriers to communicate the risk to an audience is used. Bowties are barrier-orientated and focus on the preventative barriers between the causes and the top event and the recovery barriers between the top event and the consequences. Threats to the operability of the vessel and their consequence are determined based on previous experiences of dredging operations in various ports of Iran and are tabulated in Table 1 and Table 2. Preventative barriers and recovery barriers are derived based on the opinion of a panel of experts as shown in Table 3.

Table 1. Events (Causes)

Event Level	Event Symbol	Event Description
E	E1	Financial and contractual disputes
	E2	Poor vessel management
	E3	Failure to comply with the rules
	E4	Poor project management
F	F1	Failure in certification renewal
	F2	Failure in insurance renewal
	F3	Machinery failure
	F4	Prolongation of docking
	F5	Prolongation of machinery overhaul
	F6	Using the equipment in another port or other projects

Table 2. Consequences (Effects)

Consequence Symbol	Consequence Description
C1	Endangering safety of waterway (e.g., Grounding)
C2	Increased accumulated dredging
C3	Damage to the equipment and crew
C4	Damage to other vessels and port facilities
C5	Damage to the environment
C6	Decreasing port income (capacity)

5. Conclusion

The Bowtie methodology facilitates the understanding of the interactions between risk management and barrier performance as well as the integration between the barriers and operations as a whole. Bowtie diagram for the out-of-service condition of dredging equipment is shown in Figure 2. This study can be used as a basis for a quantitative bowtie risk assessment using fault tree together with an event tree and barriers escalation factors to calculate risk more precisely.

Table 3. Preventative barriers and recovery barriers

Barrier Type	Barrier Symbol	Barrier Description
P	P1	Monitoring and inspection
	P2	ISM Compliance Obligation
	P3	Considering Penalty
	P4	Training of crew
	P5	Handover checklist
R	R1	MOM for substitution of the equipment
	R2	Considering equipment capacity tolerance
	R3	Set the minimum required dredging volume in contract

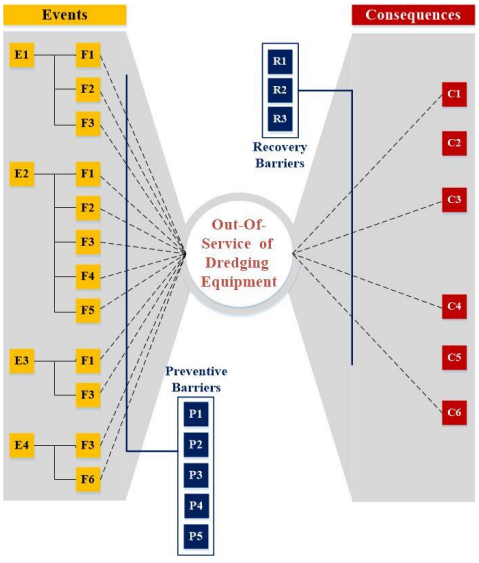

Figure 2. Bowtie diagram for the out-of-service condition of dredging equipment

6. References

[1] "Guidance notes on risk assessment applications for the marine and offshore industries", *American Bureau of Shipping*, Texas, USA, May 2020.
[2] https://oceanservice.noaa.gov/facts/dredging.html

OFFENSIVE RISK MANAGEMENT OF THE CASPIAN COASTAL ZONE FROM A PASSIVE DEFENSE PERSPECTIVE

Omidreza Safiyari[1], Fatemeh Ektafaei[2], Reza Ahmadian[3] and Rasoul Ghanbari Maman[4]

1) Director of Passive Defense Studies and Crisis Management, Sodreh Sazeh Pars Engineering Consultant, Tehran, Iran, safiyari@ut.ac.ir
2) Master of Passive Defense Projects, Sodereh Sazeh Pars Engineering Consultant, Tehran, Iran, shimaektefaei@yahoo.com
3) Project manager of the Caspian Sea Integrated Coastal Zone Management Studies, Tehran, Iran, rahmadian2001@gmail.com
4) Head of Coastal Management Office, General Directorate of Coastal and Port Engineering, Ports and Maritime Organization, Tehran, Iran, rghanbari@pmo.ir

1. Introduction

The Caspian coastal zone contains a wide range of resources and functions, considered national assets and capital. In addition to the risk of extinction and natural destruction, these resources also face unnatural biological threats. Therefore, identifying and protecting these resources against a wide range of threats is necessary and inevitable.

Population density, the concentration of various urban, industrial, and tourism areas and marine facilities in the coastal zone, accessibility and communication network, commerce role, military forces distribution, and the surrounding strategic space are among the issues that govern the coastal area from a security point of view.

In these studies, it has been tried to plan the risk management of coastal areas from the point of view of passive defense, relying on the identification of possible offensive threats in coastal areas and investigating the probability of occurrence of these threats, identifying the weak points and vulnerabilities of defense, and following the results of the offensive risks assessment and possible consequences, appropriate and optimal strategies for facing security risks in the Caspian coastal zone have been explained.

2. Methodology

Security risks in the coastal zone are evaluated according to the nature and characteristics of these areas (containing various activities, uses, and ecosystems) based on the FEMA method. The Caspian coastal zone is not an exception to this rule and the security risk assessment in this region is based on the FEMA method.

The risk assessment method used in this study has been done according to the following steps:

- Assets identification
- Asset value assessment
- Threat identification
- Threat assessment
- Vulnerability assessment
- Risk assessment

Figure 1. Offensive Risk Assessment Steps

3. Risk Management

Risk management is based on strategic planning and analysis. In this regard, after assessing the security risks in the Caspian coastal zone and categorizing the quantitative and qualitative results of the risk, the appropriate strategy has been determined. Usually, for those risks that have many consequences and the probability of their occurrence is also high, you can use the "Risk Acceptance" strategy, for those risks that have many consequences but the probability of their occurrence is low, you can use the "Risk Transfer" strategy, for those risks that have low consequences and the probability of their occurrence is high, the "Risk Treatment" strategy can be used, and for those risks that have low consequences and the probability of occurrence is low, the "Risk Reduction" strategy can be used.

4. Conclusion

Offensive risk management in integrated Caspian coastal management studies will lead to forming a resilient zone, while protecting key infrastructure, saving people (residents, clients, and tourists), and providing essential needs to facilitate emergencies. Accordingly, passive defense strategies have been explained aimed at resolving fundamental challenges and vulnerabilities, managing security risks, and controlling and mitigating the consequences of offensive hazards in the Caspian coastal zone following the passive defense topics: physical, cyber, chemical, biological, radiation, urban, and people-oriented.

To achieve this, the passive defense programs in the Caspian coastal zone are proposed as follows:

- Determine the safety, security, and defense sub-zones and governing rules related to each of the hazardous facilities located in the Caspian coastal zone, prepare a master security plan for special economic and energy zones, and prepare an Emergency Response Plan (ERP) in the coastal zone in proportion to the possible consequences,
- Prepare a passive defense plan and a public emergency evacuation plan for urban areas located in high-risk regions,
- Locate safe and secure zones for temporary residence in urban areas proximity (within the legal boundaries),
- Apply passive defense considerations in (future) development plans of port areas and complexes, obligation to consider passive defense studies in all tourism projects in the Caspian coastal zone,
- Develop and equip the communication network of the Caspian coastal zone to provide alternative routes and facilitate emergency management,
- Equip medical centers with special and modern devices to improve the quality of services in emergencies and offensive crises (especially for CBRNE scenarios) and also prepare a cooperation plan to create parallel medical networks with neighboring provinces to meet the medical requirements,
- Perform training courses and exercises to make people and personnel ready as well as improve preparedness in the face of emergencies and crises.

Considering the different roles and position of each coastline, strategic location and peripheral communications, challenges, and unique issues of each region resulting from the main functions, and characteristics, besides key resources, key assets, and critical infrastructures in each coastal zone, it is rational that the current applied methodology of security risk management in the Caspian coastal zone, could be proposed to implement in other coastal zones of the country.

A PSO-ANN MODEL TO PREDICT LIQUEFACTION POTENTIAL OF SANDY SOILS IN CASPIAN SEA

Mohamad Javad Alizadeh[1], Amin Eslami[2] and Ali Ghorbani[3]

1) Caspian Sea National Research Center, Water Research Institute, Tehran, Iran, mjalizadeh@mail.kntu.ac.ir
2) Geotechnical Engineering, University of Guilan, Rasht, Iran, amin_eslami@phd.guilan.ac.ir
3) Civil Engineering, University of Guilan, Rasht, Iran, ghorbani@guilan.ac.ir

1. Introduction

Liquefaction disaster is defined as loss of strength of granular and cohesionless saturated or partially saturated soil in response to earthquake shaking. Liquefaction potential analysis in coastal areas is of paramount importance for coastal management and disaster mitigation. In coastal regions of Caspian Sea, about 11 million people live where main urban centers are near the western and southern coasts. In this regard, suitable prediction of liquefaction potential in these areas can provide useful information for coastal vulnerability assessment. However, it is a complicated process due to its nonlinear behavior and also its dependency on various soil properties [1]. Furthermore, sandy soils may be mixed with fine contents which affects its potential for liquefaction. There are a large number of research studies exploring effect of fine contents on the soil resistance against liquefaction [2-3].

Energy-based models are a common approach to assess liquefaction potential. It is usually quantified in terms of capacity energy which is defined as accumulation of maximum stored energy per unit volume until the onset of liquefaction [3]. Thus, different techniques can be employed to find the relationship between the capacity energy and soil properties and also the other influencing factors such as loading frequency. [1] developed a numerical model based on genetic programming to estimate capacity energy of sandy soils using different parameters including relative density (D_r), mean grain size (D_{50}), percentage of fine content (FC), coefficient of uniformity (C_u) and soil initial effective mean confining pressure ($Sigma_{max}$).

The main purpose of this study is to develop a prediction model for capacity energy of sandy soil of Anzali located in the southern coast of Caspian Sea. An artificial neural network (ANN) model combined with a metaheuristic training algorithm called particle swarm optimization (PSO) is used to estimate capacity energy based on a limited number of input parameters. An attempt is made to choose the input variables which can be easily measured mainly dependent on the soil gradation. It is noteworthy that the model is solely based on the results of laboratory tests conducted for Anzali soil.

2. Methodology

2.1. Data

The dataset used in this study obtained from the experimental data presented by [3]. The data consist of 63 experimental tests conducted for Anzali soil. The capacity energy (liquefaction potential) was determined from shaking table test. Apart from availability of the results of experiment for various parameters for these 63 samples, this study considers a limited number of them as tentative input variables for the model development. In other words, percentage of fine content (FC), mean grain size (D_{50}), curvature coefficient (C_c), uniformity coefficient (C_u), and plasticity index (PI) are used as the potential input variables. These parameters can be determined from the soil gradation (sieve analysis) and PI can be obtained from Atterberg's limits as:

$$PI=LL-PL \quad (1)$$

$$C_u=D_{60}/D_{10} \quad (2)$$

$$C_c=D_{30}^2/D_{10}*D60 \quad (3)$$

where LL and PL are liquid and plastic limits, respectively.

Correlation matrix displaying linear dependence of different variables can be used as a helpful tool to find effective parameters in prediction models. However, this approach may be misleading for variables with nonlinear behavior and necessitates further investigation. Figure 1 illustrates correlation between different variables considered for this study.

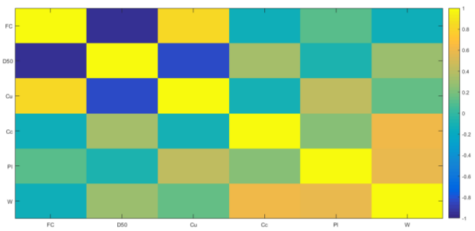

Figure 1. Correlation between the variables

Regarding Figure 1, the highest correlation of the input variables with the target is obtained for C_c and PI. Mean grain size (D_{50}), FC (negative correlation) and C_u are ranked latter.

2.2. Modelling Procedures

The modelling procedures can be divided into: data manipulation, training the ANN model, model performance evaluation, and the results analysis. The datasets cover clean, silty and clayey sands with fine contents in a range of 0 to 45%. ANN models have been frequently used to capture nonlinear relationship between input and output variables. A usual ANN is formed from three distinguished layers including input, output and hidden layer. Neurons of each layer are connected with neurons in the next layer. Strength of the connections is determined by a term called weight. The training procedure is viewed as a process to find the optimum weights and biases [4]. In this study, a metaheuristic optimization algorithm (PSO) is used to train the ANN model. Different combinations of the variables are taken under consideration to find the best model performance. 80% of the data are used for the model training and 20% left for testing purpose. Evaluation of the model efficiency are carried out using mean squared error (MSE) and coefficient of determination (R^2). Finally, the trained model is used to predict capacity energy.

3. Results and Discussion

Initially, the PSO-model gained all the candidate variables for predicting the capacity energy. Afterwards, several models have been developed excluding a specific parameter to examine importance of the variable individually. Table 1 gives the inputs variables and performance of the models for the testing dataset.

Table 1. Performance of the PSO-ANN models

No.	Inputs	R^2	MSE(J/m^3)
1	FC, D_{50}, C_u, C_c, PI	0.86	0.0106
2	D_{50}, C_u, C_c, PI	0.93	0.0074
3	FC, C_u, C_c, PI	0.87	0.0089
4	FC, D_{50}, C_c, PI	0.89	0.0087
5	FC, D_{50}, C_u, PI	0.93	0.0063
6	FC, D_{50}, C_u, C_c	0.87	0.0106
7	D_{50}, C_u, PI	0.84	0.0086

According to Table 1, the model including all the variables does not necessarily yield the best predictions for the capacity energy. The best model performance is achieved when curvature coefficient is not among the input variables (model No. 5). The model excluding PI or D_{50} gives the least accurate predictions demonstrating that the target variable is mostly dependent on these variables. Juxtaposition of Figure 1 and Table 1 reveals that the variable with the highest correlation (C_c) does not necessarily contribute to the best model performance. Moreover, it can be found that C_u has the lowest correlation with capacity energy while its excluding from the input structures deteriorates the model performance remarkably. The main reason for this issue is initiated from the nonlinear behavior and relationship of the input (e.g., C) and the output variables. On the other hand, in case of C_c, its effect may be indirectly reflected in D_{50} and FC since it is strongly correlated with them. Figure 2 displays the measured capacity energy against predicted values.

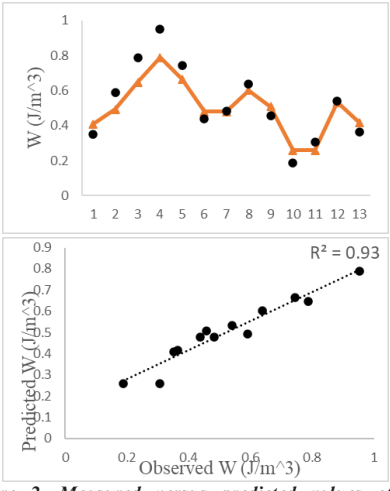

Figure 2. Measured versus predicted values of the capacity energy

Generally, Figure 2 shows a good agreement between the observed and predicted values of capacity energy. The proposed model has the potential to predict the target variable for a wide range of variation from 0.2 to 1 J/m^3 accordingly. Results of this study are promising to gain capability of the model to predict liquefaction potential using only a limited number of input variables which are easily measured from laboratory tests. Our future study will focus on the preparation of hazard map for liquefaction potential across the southern coasts of the Caspian Sea by including data samples from other locations throughout the coasts.

4. References

[1] Alavi, A.H., and Gandomi, A.H. "Energy-based numerical models for assessment of soil liquefaction", Geoscience Frontiers, 3(4), 2012, pp.541-555.
[2] Polito, C.P., and Martin II, J.R. "Effects of nonplastic fines on the liquefaction resistance of sands", Journal of geotechnical and geoenvironmental engineering, 127(5), 2001, pp.408-415.
[3] Ghorbani, A., and Eslami, A. "Energy-based model for predicting liquefaction potential of sandy soils using evolutionary polynomial regression method", Computers and Geotechnics, 129, 2021, p.103867.
[4] Alizadeh, M.J., Shabani, A., and Kavianpour, M.R. "Predicting longitudinal dispersion coefficient using ANN with metaheuristic training algorithms", International journal of environmental science and technology, 14(11), 2017, pp.2399-2410.

TOWER NAVIGATIONAL WATCH ALARM SYSTEM (TNWAS}

Mohsen.Maygoli [1], Mehdi.Ahmadnia [2]

1) BPMO Technical department member, Bushehr, Iran, info_rmb@yahoo.com
2) BPMO Technical department member, Bushehr, Iran, ahmadnia@yahoo.com

1. Introduction

The Port traffic control tower and MRCC are equipped with many communication devices to keep sailing safe for the seamen around the world. If MRCC operators do not perform their duties, even if control tower equipped correctly, what will happen? This is a human error and it can create major hazard. Administrators must have plans to service marine requirement 99.98% up on IALA regulation [1].

2. Description

In this paper we consider a device called TNWAS as a tower navigational watch alarm system. The idea of the work is similar to that of BNWAS, which instead of the command bridge of the ships is obtained for the telecommunications of the port control towers which have a much heavier duty [2]. The registered proposal of this work dates back more than a decade [3]. Operator in this situation must acknowledge every 45 minutes by pushing key used for TNWAS to do it as a daily job. After a while if operator forgets or becomes ill or by any other reason such as high traffic day, etc. doesn't not give feedback, TNWAS sends alarm to the boss. Boss can be more than one person and becomes aware and take their part one after another. The level of safety for more information will accumulated in data base of system and can be monitored from long distance via network. In addition, it can create a history through time for making new programing monthly and yearly. TNWAS implementation schedule varies with ships [4]. The Purpose was construction of a warning device for the standby status of operators in order to improve the operation of telecommunication control towers.

3. Work Process

See TNWAS laboratory diagram in Figure 1. In this laboratory design, the central controller of the Smart Logo 230RCE model, which was a locally produced PLC, was used. For this purpose, the relevant software (LOGO) was prepared and installed on the laptop. Mushroom stop was also used for the required keys. Also, a normal lamp was used as a visual warning and a common sounder of fire alarm equipment was used for the sound warning system. The laboratory device was designed in such a way that after 20 seconds, if the first key is not reset, the sounder will ring. Will ringing. 5 seconds later, that is, in the 25th second, while maintaining the alarm status at the operator's location, this alarm is visually transmitted to the supervisor's location. Then this warning will be doubled with an audio warning for 5 seconds later (i.e. on the 35th). In the third step, this work will transfer the alarm to the supervisor. At each stage when the next domain is activated (for example, activation of the supervisor domain), that domain itself and the previous domain (the operator domain) can reset the system counter by pressing the corresponding keys. This scenario helps the supervisor to ensure that the operator is ready to respond in the telecommunication control towers. Telecommunication control towers are equipped with a lot of expenses in order to carry out governance duties in waterways and ensure their health and readiness. This is an important point.

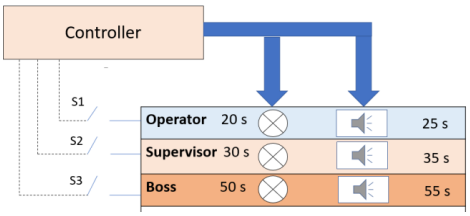

Figure 1. Diagram of TNWAS

4. Additional Report

The software used in this PLC was the popular LOGO Soft Comfort program (figure2). One of the capabilities of this controller was the networking capability, which can be created jointly by adding this equipment to a network (for example, 11 telecommunications stations of the General Administration of Ports and Maritime Affairs of Bushehr Province in Bushehr Port). The simulation done on circuit has shown in figure3. Below the software window, there are warning lights and control keys available to the tester, which can reset the controller counter to zero and repeat the process by pressing the key. Figure 4,5 shows the dimensions of the device. As you can see, one of the advantages of the device is the use of PLC, which enables its operation in an industrial environment [5].

5. Limitations

This equipment is designed in a laboratory and can be optimized with the following specifications:

1- Setting up the SMS sending module.
2- Launching the classic dialer with pre-recorded voice.
3- Adding a key with fingerprint recognition.
4- Adding a module for reporting the status of the device.

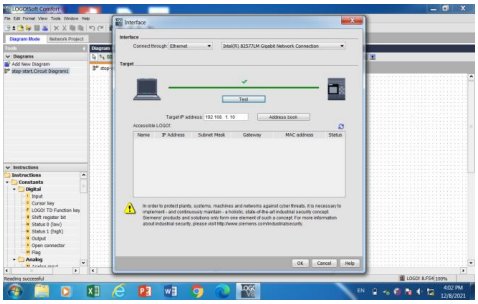

Figure 2. Software Environment.

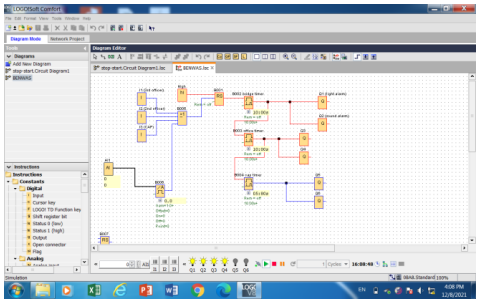

Figure 3. Circuit Diagram.

Figure 4. Device Picture & Size.

Figure 5. User Friendly Tools.

6. Conclusion

This device was made in the summer of 2021 by colleagues in the research and development group of administrative equipment of the General Administration of Ports and Maritime Affairs of Bushehr province, and the results were acceptable [5].

7. References

[1]. IALA Recommendation V-128، On ،Operational and Technical،Performance for،VTS Equipment, rue Schnapper, 78100 Saint-Germain-en-Laye, France. Edition 3.0، June 2007.
[2]. IMO resolution MSC.128 (75) Recommendation on performance standard for a bridge navigational watch alarm system (BNWAS).
[3]. The proposal registered in the proposal system of the General Administration of Ports and Shipping of Bushehr Province by Mohsen and Ismail Maygoli to equip the control towers of the Ports and Maritime Organization in 2010.
[4]. Hapcon (yang Zhou) Automation Technology Co.L.td. Certificate No. NJ13P00602_33, May.7.2013.
[5]. Technical department of Bushehr port maritime organization, M.Maygoli et al. 2021 report.

14th International Conference on Coasts, Ports and Marine Structures
9 & 10 May 2023 , Tehran-IRAN
ICOPMAS 2022

THE CASPIAN COASTAL ZONE STRATEGIC MANAGEMENT IN INTERACTION WITH IOC INDICATORS FROM A PASSIVE DEFENSE PERSPECTIVE

Fatemeh Ektafaei[1], Omidreza Safiyari[2] and Reza Ahmadian[3] and Hamid khalili[4]

1) Master of Passive Defense Projects, Sodereh Sazeh Pars Engineering Consultant, Tehran, Iran, shimaektefaei@yahoo.com
2) Director of Passive Defense Studies and Crisis Management, Sodreh Sazeh Pars Engineering Consultant, Tehran, Iran, safiyari@ut.ac.ir
3) Project manager of the Caspian Sea Integrated Coastal Zone Management Studies, Tehran, Iran, rahmadian2001@gmail.com
4) Head of General Directorate of Coastal and Port Engineering, Ports and Maritime Organization, Tehran, Iran, hkhalili@pmo.ir

1. Introduction

The world coastal zones problems, including population concentration, indiscriminate construction, rising seawater, coastal erosion, and other environmental hazards, environmental pollution, biodiversity reduction, natural resources loss, inconsistency, and conflict between different executive organizations have led to a new global approach, which is called "Integrated Management of Coastal Zones". The study of the Integrated Management of Coastal zone started in the late 70s in Iran and detailed investigations were carried out regarding the explanation of the situation of the coasts of Iran in terms of problems and limitations. Based on this, the scope of the coastal zone and its borders were determined on the south and north coasts of the country. The coastal zone of the Caspian Sea corresponds to the Golestan, Gilan, and Mazandaran provinces, which are more than 7600 square kilometers, and the coastline length is calculated to be about 890 kilometers.

2. Methodology

This article is based on the strategic planning approach. Main issues and challenges have been identified in the Caspian coastal zone based on the objectives of passive defense in interaction with the IOC indicators. After recognizing and evaluating the Caspian coastal zone, main policies and strategies have been explained to reduce the vulnerabilities against probable and possible man-made hazards in the Caspian coastal zone, from the point of view of passive defense. Finally, main plans and considerations of passive defense have been set to reduce the vulnerabilities and respond to possible offensive threats in the Caspian coastal zone.

The evaluation of the integrated management process of coastal areas has been explained based on environmental, economic-social, and governance indicators. In this article, the relationship between these indicators in interaction with the basic concepts of passive defense has been investigated to create an alignment between the key indicators of IOC and macro indicators of passive defense to an improved model in the integrated coastal areas management context. In this way, the concepts of passive defense have penetrated the essence of these studies, and considering passive defense perspective with engineering tools and knowledge approach within the scope of the studies is possible and operational. In this regard, the concepts of promotion, sustainability (biological, economic, and socio-cultural), education and participation, and considerations and requirements of passive defense have been compiled in the form of an optimized table of passive defense strategies in interaction with IOC indicators.

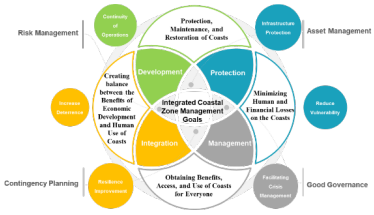

Figure 1. Communication diagram of ICZM goals in interaction with the macro goals of Passive Defense

3. Conclusion

The strategic management of the Caspian coastal zone from the perspective of passive defense is based on the main goals of passive defense in interaction with the goals of integrated coastal zone management; In connection with the "governance" indicator, one of the main indicators in evaluating the coastal zones performance, to establish coordination at different levels, facilitating emergency management and crises, management of key resources, assets and infrastructure in coastal zones and reduce or control probable consequences caused by offensive hazards, the concept of "management" is included alongside the three major approaches of ICZM, including protection, development, and integration. The presented model could apply to implementation in other coastal zones according to their nature, functionality, and location. Hence, the main policies and strategies of passive defense are explained as a result of internal and external factors analysis in the Caspian coastal region to achieve key goals of passive defense in interaction with governance (management), socio-economic and environmental indicators in such a way that, it also includes physical, cyber, chemical, biological, radiation, and people-oriented fields in addition to the above three indicators.

The passive defense main strategies for the strategic management of the Caspian coastal zone are presented as follows:

- Prepare passive defense and master security plans for key assets and infrastructures in the Caspian coastal zone,
- Efficient land planning to prevent unauthorized land use changing (thus preventing incompatible allocation from a passive defense point of view) as well as preventing illegal construction permits in the Caspian coastal zone and getting necessary approvals for locating activities in the Caspian coastal zone,
- Establish a centralized command and crisis management center on the north coast of the country to monitor threats and the passive defense alarm system,
- Identify emergency accommodation centers in the Caspian coastal zone and provide necessary services for population areas in emergencies,
- Plan to meet the basic and essential requirements of people in emergencies, during short, medium, and long periods,
- Organizing, developing, and upgrading the particular capacity of relevant organizations and agencies for emergencies in the Caspian coastal zone,
- Improve the security of coastal and maritime border areas through developing defensive infrastructure and capabilities,
- Develop environmental detection and monitoring systems, supplementing alarm systems, to assess chemical threats in the Caspian coastal zone,
- Expand the particular operational capacities for limiting or eliminating pollution, controlling loss and chemical waste management in the Caspian coastal region,
- Upgrade the defensive capabilities and protection apparatus of the infrastructures that are located in port areas,
- Make up sustainable living opportunities for the population in the Caspian coastal zone,
- Establish an appropriate structure and procedure for surveying and the risk assessment, make-up population, and tourism areas in the Caspian coastal safe zone.

14th International Conference on Coasts, Ports and Marine Structures
9 & 10 May 2023 , Tehran-IRAN
ICOPMAS 2022

MODELING LAND USE CHANGE USING MARKOV CHAIN AND LCM MODELS, CASE STUDY: COASTAL AREA OF SISTAN AND BALUCHESTAN PROVINCE

Fatemeh Kordi[1], Hamid Khalili Vavsari[2], Maryam Yaghoub Zadeh[3] and Majid Mashhadi Rafiee[4]

1) Sazeh Pardazi Iran Consulting Eng.co, Tehran, Iran, Fateme.kordi92@gmail.com
2) Port & Maritime Organization, Tehran, Iran, hkhalili@pmo.ir
3) Sazeh Pardazi Iran Consulting Eng.co, Tehran, Iran, yaghobzadehmaryam@yahoo.com
4) Sazeh Pardazi Iran Consulting Eng.co, Tehran, Iran, majidrafiee@gmail.com

1. Introduction

Land refers to all natural conditions of a place such as climate, topography, hydrology, etc. Land-use change and land cover are the result of complex interactions among geophysical, ecological and social processes. Detection of changes of land-use and its trend is required to take care of the ecosystem, especially in areas with rapid and often unplanned change that is common in developing countries. Detection of land-use changes using remote sensing data and modeling its future changes provide a good understanding of how the land-use has changed and provides appropriate solutions for its management in the future. By predicting land-use changes, the amount of exploitation of resources and possible destruction of the environment can be determined and the changes can have directed towards right directions.

Cellular automata (CA) is a cell-based method that can model spatial phenomena. Modeling based on CA method is suitable for studying the temporal and spatial distribution of any phenomenon. Examples of this method are Land Change Model (LCM) and Markov Chain Analysis. Using these models for examining the trend of time-dependent changes is appropriate. Land-use models are tools for analyzing the causes and consequences of land use change by which one can identify future land-use and land cover changes according to different scenarios[1].

2. Methodology

In order to extract the land-use maps of the studied area over the planning time to predict the future land-use changes, the following steps are performed (Figure 1). This method has used for analyzing the changes of land-use of the coastal area of Sistan and Baluchestan province.

3. Data

In this study, the satellite images of 2001, 2010 and 2020 as well as other basic data such as 1:50.000 digital topographic maps of the Geographical Organization of the Armed Forces, 1:25.000 topographic maps of the Iran surveying organization and digital elevation model (DEM) of the area were used. In this study, ENVI5.1, TERRSET2020 and Arc GIS 10.7 software used for data processing, highlighting, modeling and acquiring the output. The capabilities of Google Earth and SAS Planet software have also used to review and control the results.

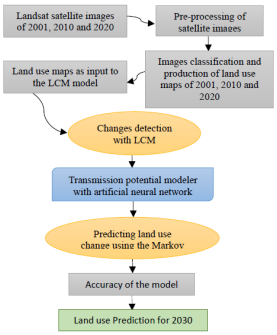

Figure 1- Graph of Methodology

4. Production of Land-use / Land-cover Maps

After performing atmospheric, geometric and radiometric corrections on the raw input data, which were satellite images of ETM + and OLI Landsat 7 and 8 sensors for all three years, the final processing was performed. According to the studies, 12 land-use classes identified and delineated in the study periods, which presented in the land-use maps of the studied periods. Various classes of uses that identified in the study zone are the following:

- Man-made installations and facilities;
- Agricultural lands;
- Rangelands;
- Mixed vegetation lands (groves and mangrove forests);
- Coastal Landforms (sand dunes, sandy beaches, rocky outcrops, swamps and marshes;
- Water resources and fishponds.

Land-use maps for 2001, 2010 and 2020 were prepared by combining classification methods and using the results of hybrid bands such as NDVI in the GIS environment with the help of images from Google Earth software.

[1] This article is part of a comprehensive study regarding population forecasting in Integrated Coastal Zone Management (ICZM) Plan of Sistan & Baluchestan Province.

5. Detection of Changes, And Modeling of Land-Use Changes using LCM

Detection of land use change is an essential tool for environmental analysis, area planning and watershed management. This process determines the status of changes based on images obtained at different times. The modeling carried out in four steps:

- Review and analysis of changes
- Transmission force modeling
- Modeling land-use change
- Assess modeling accuracy

Land-use maps produced in 2001 and 2010 were selected as the input for the LCM to analyze the existing regional changes and predict the land cover and land use changes for a long time period in the future until 2020. Auxiliary variables such as digital elevation model (DEM), slope, direction of slope, distance from constructions and residential areas (dynamically) and probability map of evidence prepared from the extracted uses, were selected and entered into the model. Transfer potential modeling expresses the tendency of each image cell to receive a change from one type of use to another with respect to auxiliary variables (such as height, distance from residential areas, etc.) over a certain period. The change from one use to another estimated in the form of sub-models called transfer sub-models.

In order to simulate land-use changes for future, the LCM model in TerrSet software is used. This model combines an artificial neural network for image classification and CA Markov for future prediction.

6. Discussion and Conclusion

The results of the modeling process according to the below table and chart show that in the study period over 7500 hectares of the coastal area of Sistan and Baluchestan province have been construction/ residential areas. Around 7500 hectares of agricultural area increased. On the other hand, during this period, about 16,000 hectares of rangeland reduced.

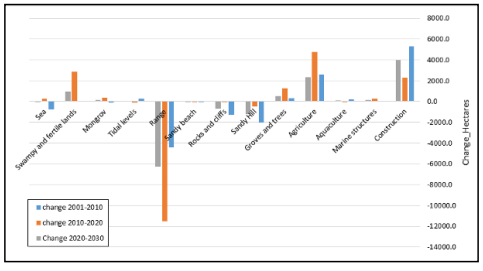

Figure 2- Graph of land use area changes in time periods

Table 1- Land use area in in the study area

Class	Area (ha)				change		
	2001	2010	2020	2030*	2001-2010	2010-2020	2020-2030
Construction	18568	23859	26160	30133	5291	2301	3972
Marine structures	92.9	108	383	540	15	275	156
Aquaculture	4378	4562	4561	4645	184	-1	84
Agriculture	4985	7575	12333	14676	2589	4758	2342
Groves and trees	3401	3697	4971	5475	296	1273	504
Sandy Hill	104943	102905	102432	101199	-2037	-473	-1232
Rocks and cliff	478756	477489	477484	476815	-1266	-5	-668
Sandy beach	1067	995	992	986	-71	-3	-6
Range	607109	602704	591168	584883	-4404	-11536	-6285
Tidal levels	8126	8377	8268	8342	251	-108	73
Mangrove	469	358	725	872	-110	367	147
Swampy & fertile	1782	1793	4662	5592	11	2868	930
Sea	2837	2090	2373	2355	-747	284	-18

Most of the forecasting models are based on the constant inter-relationships between changes and their causes over time, however, the processes of land-use change are dynamic, and thus modeling should be performed for short periods. According to the presented chart of land use and land cover changes during different periods (based on the matrix of probability of land use transfer), if the current trend of land use change will continue in the future, there will be a substantial decrease in rangelands and a considerable increase in construction areas. The land-use map simulated in this study can be a good guide for managers and planners of natural resources and other sectors. In addition, the Predicted land use maps can use as a warning about the consequences and future impacts of unplanned land-use changes in the region.

7. References

[1] Guan, D.; Li, H.; Inohae, T.; Su, W.; Nagaie, T. & Hokao, K. 2011.Modeling urban land use change by the integration of cellular automaton and Markovmodel.Ecological Modelling. 222 (20–22): 3761-3772.

[2] Junfeng, L., Zhibao, D., Guangyin, H., Changzhen, Y., Zhenhai, W. and Xiang, S. (2011). Land use and land cover change and its driving forces in the source region of the Yangtze River during 1990–2005. In Water Resource and Environmental Protection (ISWREP), 4, 2571-2574

[3] Lee, Y. & Chang, H. 2011. The Simulation of Land Use Change by Using CA-Markov Model: A Case Study of Tainan City, Taiwan. 19th international conference on geoinformatics, 24-26 June. China.

[4] Samat, N.; Hasni, R. & Eltayeb Elhadary, Y. A. 2011.Modelling Land Use Changes at the Peri-Urban Areas

[5] Sang, L.; Zhang, C.; Yang, J.; Zhu, D. & Yun, W. 2011.Simulation of land use spatial pattern of towns and villages based on CA–Markov model. Mathematical and Computer Modelling. 54(3–4): 938-943.

[6] Singh, S. and Rai, P.K. (2016). Application of Earth Observation Data for Estimation of Changes in Land.

14th International Conference on Coasts, Ports and Marine Structures
9 & 10 May 2023 , Tehran-IRAN
ICOPMAS 2022

INVESTIGATION OF CHANGING TREND OF LAND USE IN COASTAL ZONE OF SISTAN AND BALUCHESTAN PROVINCE

Majid Mashhadi Rafiee[1], Monir Haghighat[2], Fatemeh Kordi[3] and Maryam Yaghoubzadeh[4]

1) RS and GIS expert, Sazeh Pardazi Iran Consulting Engineers, Tehran, Iran, majidrafiee@gmail.com
2) Port & Maritime Organization, Tehran, Iran, mhaghighat@pmo.ir
3) RS and GIS expert, Sazeh Pardazi Iran Consulting Engineers, Tehran, Iran, fateme.kordi92@gmail.com
4) Environmental expert, Sazeh Pardazi Iran Consulting Engineers, Tehran, Iran, yaghobzadehmaryam@yahoo.com

1. Introduction

Land use changes (LUC) considered as an important factor for monitoring the global environmental change and sustainable development [1]. Examining the processes and trends of LUC via quantitative analysis is a prerequisite to gain a deep understanding of LUC and help the policy makers to set improvement targets in specific areas and adopt appropriate practices while maintaining other fields of sustainability [2].

Since the beginning of the 21st century, alongside the continuous global extension of human activities from land to sea [3], more than 40% of the world population has concentrated in a 100 km stripe along the coastline [4]. In addition, coastal lands developed very fast through establishments of residential, industrial and commercial centers. The analysis of land use changes over time can lead to better understanding in exploring suitable growth pattern for future development [5].

This study is conducted with the aim of investigating land use changes (LUC) in the coastal areas in order to obtain an insight understanding of changing trend and evaluating the sustainability of the future development[1].

2. Materials and Methods

2.1. Study Area

The study area is located in the southern part of Sistan and Baluchestan province, this region is part of the coastal zone including coastal area and effecting area [6].

2.2. Data Collection and Processing

The Landsat images for the years 2001 and 2020 used for image classification to identify land use patterns and create LUC maps. Landsat-7 satellite images obtained for 2001. Similarly, Landsat-8 satellite images acquired for 2020. The Landsat images had the spatial resolution of 30 m. Only images with uniform weather conditions throughout the study period and cloud cover of less than 5% selected to maintain quality. The Landsat images acquired from USGS through their earth explorer web portal. The satellite images were analyzed and processed (geo-referencing, mosaic, and extraction) to correct its geospatial imagery. Satellite images processed using the ENVI 5.3 software package. ANN classifier, a supervised classification approach in ENVI 5.3, used in this study. The theory behind supervised classification is that a user may pick sample pixels in an image that are indicative of certain classes and then instruct the image processing software to utilize these training samples as references for the categorization of all other pixels in the image. In this work, uniformly dispersed Regions of Interest (ROI) in the study area for all class types identified using visual interpretation of Landsat images to train the classification. True and false composites employed to improve the feature visualization so that LUC classes can easily distinguished in the image. The digital elevation model (DEM), and public map datasets used as references when collecting the training samples and for validating the classified maps.

The adopted LUC classification scheme for this study consisted of 12 classes, namely: Aquaculture, Groves and forests, Sandy Hill, Mangroves, Tidal flats, Agriculture, Sandy beach, Construction, Marine structures, Range, Rocks and cliffs, and Sea.

An accuracy assessment of maps created from any remotely sensed product is a universal requirement in image classification since it allows for self-evaluation, offers a quantitative comparison of various approaches, algorithms, and analysts, and assures higher dependability of the resultant maps [7]. In this study, an assessment of the accuracy of the classification carried out using derived measures generated from the error matrix. The error matrix is the most common way to represent the classification accuracy of remotely sensed data [8].

3. Result

Land use change (LUC) maps obtained from the image classification shown in Figure 1 and Figure 2. The overall accuracy of the classifications for years 2001 and 2020 is 93%, and 92% with Kappa values of 0.94 and 0.92, respectively. The result of individual land-change classes shown in Table 1.

[1] This article is part of a comprehensive study regarding landuse investigation in the Integrated Coastal Zone Management (ICZM) Plan of Sistan and Baluchestan Province.

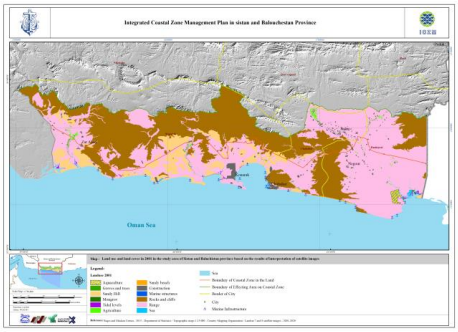

Figure 1. LUC maps of the study area for 2001

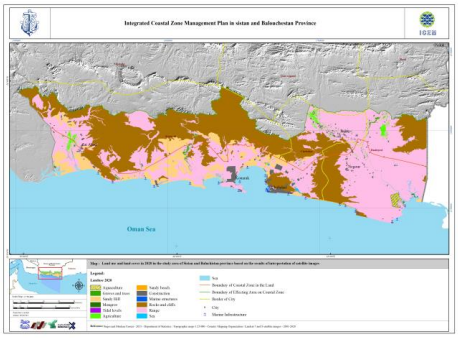

Figure 2. LUC maps of the study area for 2020

Table 1. LUC classes between 2001 and 2020.

LUC classes	Area (hectare)	
	2001	2020
Aquaculture	4364.75	4549.12
Groves and trees	3367.40	4965.71
Sandy Hill	105051.72	102345.39
Mangroves	470.57	735.33
Tidal flats	3237.75	5816.37
Agriculture	5028.21	12304.05
Sandy beach	1066.38	991.27
Construction	18669.06	26160.31
Range	606929.72	591878.58
Rocks and cliffs	477662.25	476691.07
Marine structures	94.33	119.52
Sea	8232.18	7617.49

4. Conclusions

Monitoring the trend of changes of the land use over a certain time is a valuable tool for governors and regional planners to study the level of success of the development plans and its sustainability in the region. This study used Landsat7 ETM+ and Landsat8 OLI image data, which downloaded and classified to detect the LUC changes in Coastal Zone of Sistan and Baluchestan province of Iran. ANN supervised classification used to produce accurate LUC maps for 2001 and 2020, which used in detecting the land use changes over a 20-year period. The overall accuracy and kappa coefficient values met the classification criteria. The results of the study revealed that there had been a significant change in LUC during the 19-year study period in the area.

The obtained results showed that there was a decrease (from the initial area) in the area of Sandy Hill, Range, and Rock and cliffs, while the area of Aquaculture, Groves and trees, Mangroves, Tidal level, Agriculture, Sandy beach, Construction and Marine Structure increased between 2001 and 2020. The highest decrease was in the class of Range during the study period. The rate of decline of Rangeland was 66.2%, and most of the land in this class converted to agricultural land (27.33%) and marine structures (18.07%) between 2001 and 2020. Several factors identified as contributing to the LUC in the study area, including population increase, social-economic growth, climate change, poor planning, and poor plan implementation. Therefore, LUC change is essential for both the land administration and land use planning activities in the coastal zone of Sistan and Baluchestan province.

5. Acknowledgement

The authors acknowledge the support of Port and Maritime Organization (PMO).

6. References

[1] Hu, Y. & Dong, Y. & Batunacun. An automatic approach for land-change detection and land updates based on integrated NDVI timing analysis and the CVAPS method with GEE support. ISPRS Journal of Photogrammetry and Remote Sensing 146, 347–359 (2018).

[2] Akram, M., Qian, Z. & Wenjun, L. Policy Analysis in Grassland Management of Xilingol Prefecture, Inner Mongolia. In The Future of Drylands (eds Lee, C. & Schaaf, T.) (Springer Netherlands, 2009).

[3] Liu, Yansui, Fang Fang, and Yuheng Li. "Key issues of land use in China and implications for policy making." Land Use Policy 40 (2014): 6-12.

[4] Bao, Junlin, Shu Gao, and Jianxiong Ge. "Dynamic land use and its policy in response to environmental and social-economic changes in China: A case study of the Jiangsu coast (1750–2015)." Land Use Policy 82 (2019): 169-180.

[5] Pourebrahim, Sharareh, Mehrdad Hadipour, and Mazlin Bin Mokhtar. "Impact assessment of rapid development on land use changes in coastal areas; case of Kuala Langat district, Malaysia." Environment, development and sustainability 17, no. 5 (2015): 1003-1016.

[6] Port and Maritime Organization (PMO). "Boundaries of the coastal area report (Scrutinizing the ICZM plan for Sistan and Baluchestan province) ". 2021, 131p.

[7] A. Anand, “Accuracy Assessment,” in Processing and Classification of Remotely Sensed Images, IGNOU, New Delhi, India, pp. 59–77, 2017.

[8] R. G. Congalton, “A review of assessing the accuracy of classifications of remotely sensed data,” Remote Sensing of Environment, vol. 37, no. 1, pp. 35–46, 1991.

14th International Conference on Coasts, Ports and Marine Structures
9 & 10 May 2023 , Tehran-IRAN
ICOPMAS 2022

EVALUATION OF DIFFERENT METHODS OF EXTRACTING SHORELINE FROM SATELLITE IMAGES (CASE STUDY: AMIRABAD PORT)

Mohammad Reza Hoseinkhani[1], Seyed Peyman Badiei[2], Wanko Ahmadi[3], Ali Ghadiri[4], Mohammad Hosein Nemati[5] and Mohammad Bagheri[6]

1) Iran University of Science and Technology, Tehran,Iran, hoseinkhani9611@yahoo.com
2) University of Tehran, College of Engineering, School of Civil Engineering,Tehran,Iran, pbadiei@ut.ac.ir
3) Khakbaft Consulting Engineers Company,Tehran,Iran, vaankoahmadi@modares.ac.ir
4) Khakbaft Consulting Engineers Company,Tehran,Iran, ghadiri1979@gmail.com
5) Ports and Maritime Organization, Coastal Engineering Department,Tehran,Iran, mhn1982@gmail.com
6) Ports and Maritime Organization, Coastal Engineering Department,Tehran,Iran, mbagheri@pmo.ir

1. Introduction

Determining, drawing, quantifying, and monitoring shoreline changes play an important role in coastal planning, management, and engineering, and are key to calibrating numerical models with the ability to predict shoreline changes in the future. Remote sensing data and satellite images in different periods are considered as one of the most reliable and relatively accurate sources for studying and interpreting changes and quantitative measurements. Here, five shoreline extraction methods for the coasts around Amirabad port are investigated.

2. Materials and Methods

In order to extract the shoreline numerous indices have been developed and refined, including the Normalized Difference Water Index (NDWI), Normalized Difference Vegetation Index (NDVI), Modified Normalized Difference Water Index (MNDWI), Coastal Water Index (CWI), Tasseled Cap Wetness (TCW), Coal Mine Index (CMI), and Automated Water Extraction Index (AWEI). The main purpose of these indices is to increase the contrast between the water and the land pixels in the image. In this study, the NDWI, MNDWI, CWI and AWEI indices are used, the definition of which is presented in Table 1. CWI and AWEI indexes were developed specifically for bands in Landsat images, which limits their applications, but the NDWI index can be applied to any satellite with near-RGB and near-infrared (NIR) bands, and therefore Which is more widely used.[1]

The performance of these indices is also compared with the CoastSat tool. CoastSat uses Google Earth Engine capabilities to effectively retrieve Landsat and Sentinel-2 images cropped in any area of interest to the user. This new shoreline detection technique combines a supervised image classifier and a subpixel border delimiter to map the shoreline position to an accuracy of 10 meters. [3]

The study area is the northern coast of Iran in the east and west of Amirabad port (Figure 1). In order to extract the coastline of Surface Reflection images of Landsat 9 satellites and Sentinel 2 has been prepared for 19 April, 2022 by Google Earth Engine. (https://earthengine.google.com/)

Considering the better spatial resolution of Centile 2 (10 meters), we chose the shoreline extracted from this image as a basis for evaluation, and because other indices use SWIR Badns with a spatial resolution of 20 meters, we used the NDWI index to extract the shoreline from that.

Table 1: Different water indices

Definition of index	Applicable Satellites	Reference
$NDWI = \frac{G - NIR}{NIR + G}$	Landsat, Sentinel, Planet scope, RapidEye	[4]
$MNDWI = \frac{G - SWIR1}{G + SWIR1}$	Landsat, Sentinel	[4]
$CWI = \frac{Max\,(SWIR\,2) * B}{Max\,(B) * SWIR\,2}$	Landsat	[5]
$AWEI_{nsh} = 4(\rho 2 - \rho 5) - (0.25\rho 4 + 2.75\rho 7)$	Landsat	[6]

Figure 1. Study area for shoreline extraction

3. Results and Discussion

The results of applying different coastline extraction indices in Figure 2 to 5 and result of CoasSat tool in Figure 6 are shown. Figure 7 also shows a view of the extracted shore lines. In order to quantitatively evaluate the obtained results, the Root Mean Square Error (RMSE) index on transects perpendicular to the shoreline has been used. The distance of transects is 200 meters.

Figure 2. Land and sea separation with NDWI index

Figure 3. Land and sea separation with MNDWI index

Figure 4. Land and sea separation with CWI index

Figure 5. Land and sea separation with AWEI index

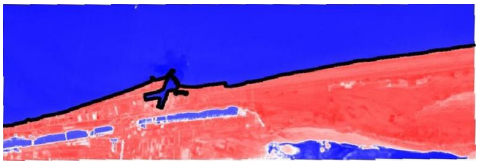

Figure 6. Land and sea separation with CoasSat

The RMSE values for the different methods in Table 2 show that the CoasSat tool has a good ability to extract the shoreline.

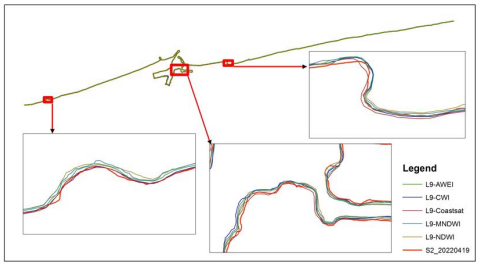

Figure 7. Extracted coastlines with different indicators (L means Landsat and S means sentinel)

Table 2: RMSE statistical index values for different shoreline extraction methods

Method	RMSE
NDWI	9.44
MNDWI	9.65
CWI	8.05
AWEI	6.53
CoastSat	5.58

4. Conclusions

In this study, the ability of four coastline extraction indices (NDWI, MNDWI, CWI and AWEI), along with CoasSat tool for the Amirabad port area was tested. For this purpose, two simultaneous images of Landsat 9 and Sentinel 2 satellites were used. After applying different methods and comparing RMSE values, it was observed that the CoasSat tool has a good ability to extract the shoreline, which can be due to downscaling and pansharpening processes. After that, the AWEI index had a better performance than other indices.

5. References

[1] Abdelhady, H. U., Troy, C. D., Habib, A., & Manish, R. (2022). A simple, fully automated shoreline detection algorithm for high-resolution multi-spectral imagery. Remote Sensing, 14(3), 557.

[2] Bishop-Taylor, R., Sagar, S., Lymburner, L., Alam, I., & Sixsmith, J.(2019). Sub-pixel waterline extraction: Characterising accuracy and sensitivity to indices and spectra. Remote Sensing, 11(24), 2984.

[3] Vos, K., Splinter, K. D., Harley, M. D., Simmons, J. A., & Turner, I. L. (2019). CoastSat: A Google Earth Engine-enabled Python toolkit to extract shorelines from publicly available satellite imagery. Environmental Modelling & Software, 122, 104528.

[4] Ouma, Y.O.; Tateishi, R. A water index for rapid mapping of shoreline changes of five East African Rift Valley lakes: An empirical analysis using Landsat TM and ETM+ data. *Int. J. Remote Sens.* 2007, *27*, 3153–3181.

[5] Ghorai, D.; Mahapatra, M. Extracting Shoreline from Satellite Imagery for GIS Analysis. *Remote Sens. Earth Syst. Sci.* 2020,*3*, 13–22.

[6] Feyisa, G.L.; Meilby, H.; Fensholt, R.; Proud, S.R. Automated Water Extraction Index: A new technique for surface water mapping using Landsat imagery. *Remote Sens. Environ.* 2014, *140*, 23–35.

PRESENTING A PRACTICAL SOLUTION FOR USING DREDGED SOIL STABILIZED WITH CEMENT AND A NEW MINERAL POLYMER MATERIAL

Masoud Sadeghpour-Monfared [1], Iraj Rahmani[2] and Ata Aghaei Araei[3]

1) Building & House Research Center (BHRC), Road, Housing & Urban Development Research Center, Tehran, Iran. E-mail: m.sadeghpour@bhrc.ac.ir
2) Corresponding author. Assistant Professor, Soil and Foundation, Road, Housing and Urban Development Research Center, Tehran, Iran. E-mail: i.rahmani@bhrc.ac.ir
3) Associate Professor, Soil and Foundation, Road, Housing and Urban Development Research Center, Tehran, Iran. E-mail: aghaeiaraei@bhrc.ac.ir

1. Introduction

This paper studies the using possibility of the Persian Gulf Dredged soil (PGD) (obtained from the construction of Shahid Rajaei Port in Iran) modified with cement (C) and mineral polymer additive (N) as the base or subbase layer of road pavement. To this end, unconfined compressive strength (UCS) tests were performed with different curing times (7, 28, and 56 days) and results showed that dredged soil stabilized with a 1% combination of a new mineral polymer plus 8% cement (C8N1) had the better-unconfined strength than dredged soil stabilized with 9% cement (C9). Considering the superior properties of C8N1 we propose that the dredged soil will be used as a borrow source to construct access roads in the port. In addition to UCS, an Indirect Tensile Strength Test was performed. Therefore, ITS results have shown a better performance of C8N1. At last, an economic comparison between three different options (conventional, C8N1, and C9 as base or subbase layer) has been made.

2. Materials

Dredged materials are those dredged or capable of dredging [1]. Marine dredged sands/sediments can be successfully used as new materials for pavement layers [2], construction, agriculture, and environmental issues [3, 4], but since they have poor geotechnical properties, they are often stabilized for use [5]. Dubios et al. (2009) [4] have confirmed the use of stabilized marine sediments as the pavement's base-layer materials. Many studies (e.g. [6-9]) have used cement for stabilization. In a comprehensive study, Sadeghpour-Monfared et al. (2021) [10] reviewed various methods of stabilizing dredged and carbonated soils. In some soil types, traditional stabilizers are not only ineffective but also have negative effects ([11]). In [12], the authors have shown some polymer types are useful in stabilizing silty sands and poorly graded sand soils.

As Shahid Rajaei Special Economic Zone, Bandar Abbas, Iran (Fig. 1) needs infrastructures (roads, docks, etc.), the area lacks suitable borrow sources, and PGD soil can solve the problem. Based on the gradation of the ASTM D 6913-04 Standard, this dredged soil lacks plasticity properties and is classified based on the SP-SM unified method (AASHTO A-3). The optimum moisture of the PGD soil is 13.6% and its maximum specific gravity = 17.50 kN/m3 based on the ASTM D 1557-12 modified density test. Chemical test results of the PGD soil show that it is a "calcareous silica" type based on the classification of reference [13].

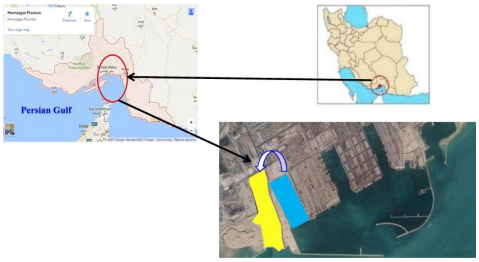

Figure 1. Location of dredging in Shahid Rajaei port.

This research has stabilized the PGD soil with Type 2 Portland cement (C) and a new mineral polymer material (N) as an additive the merits of which are reduced environmental pollution, execution time and cost and high durability, cold resistance, and very low permeability. The color of this material is gray, its density is 8-12 kN/m3 and its moisture content is more than 2% with a maximum of 1% grains larger than 0.315 mm. As this new mineral polymer material is non-toxic, non-carcinogenic, and inflammable, it is not dangerous and useable in cold areas. It has a hydrophobic, Portland cement-compatible composition and increases the stabilized-soil strength by forming microcrystals and creating a resistant texture.

3. Test Results

PGD soil is not very resistant in the unmodified state because it lacks cohesion, but adding cement or a combination of new mineral polymer and the cement will cause particles to adhere and create a homogeneous structure leading to an increase in the strength of the stabilized compound. Table 1 lists the maximum UCS of the stabilized PGD soil specimens.

Table 1. Results of UCS test of cylindrical specimens with a diameter of 100 mm

Curing Period	C9	C8N1
7Days	10.70	43.51
28Days	19.20	37.82
56Days	14.90	52.43

Table 2 compares the Indirect Tensile Strength and UCS of C9 and C8N1 specimens.

Table 2. Comparison of ITS and UCS test results of cylindrical specimens with a diameter of 100 mm

	ITS (Kg/cm^2)	UCS (Kg/cm^2)	ITS to UCS Ratio (%)
C9	4.63	19.20	24.11
C8N1	6.92	37.82	18.30

The tensile strength ratio of stabilized specimens is more than Portland cement concrete (10%). Results show that C8N1 has better specifications than C9.

4. Technical and Economic Comparison of Different Materials for Use as Base or Subbase Layer of Pavement

Table 3 compares the cost of base or subbase layer construction with different materials/methods.

Table 3. Economic comparison of different construction methods

	Cost of $1m^3$ Road Construction (IR Rial)	Road Length (cm)	Cost of 1km Road Construction (IR Rial)
Conventional	706,436	78	905,687,719
C8N1	1,027,559	110	934,144,596
C9	513,780	92	558,456,008

Based on table 3 results, the cheapest method of constructing the base/subbase layer is to use C9. Due to the inappropriate strength of this compound, it is not possible to use it for base and subbase layers. Therefore, this combination has an economical but not technical advantage. Despite not considering the costs related to the entry and exit of aggregate materials to Shahid Rajaei port, the total price for the two traditional methods and the superior combination (C8N1) are not much different from others.

The main advantage of constructing the base/subbase layer from C8N1 is the simplicity of making the mix on site, as well as the availability of PGD soil and therefore the small volume of input materials (cement and new mineral polymer material) compared to the traditional and common road construction method. In addition to the mentioned items; we can mention the speed of execution, the use of deposited dredged soil, and the reduction of environmental pollution due to less fuel consumption.

5. References

[1] Druijf, B. (2016), “The use of additives to stabilise dredged material”, M.Sc. Thesis, Delft University of Technology, the Wrocław University of Science and Technology, and the University of Miskolc.
[2] Siham, K., Fabrice, B., Vincent, D. and Nor Edine, A. (2005), “Beneficial use of marine dredged sand and sediments in road construction”, Conference of Waste Engineering, Albi, France, May 2005.
[3] Pak, A.; Rahmani, I.; Moghaddam, M. and Derakhshan Nik, P. (2011), "Dredging - Volume II: Guide to Environmental Impact Assessment", Transportation Research Institute, Department of Transportation and Marine Technology, Tehran, 2011 (in Persian).
[4] Dubois, V., Abriak, N.E., Zentar, R. and Ballivy, G. (2009), “The use of marine sediments as a pavement base material”, Waste Management 29 (2), pp. 774–782. doi: 10.1016/j.wasman.2008.05.004
[5] Chan, C.M. and Shahri, Z. (2016), “Geo-characterisation of dredged marine soils for potential reuse assessment in civil engineering”, ARPN Journal of Engineering and Applied Sciences, Vol. 11, No. 11, June 2016, pp. 7193- 7197.
[6] Kang, G., Tsuchida, T. and Kim, Y. (2017), “Strength and stiffness of cement-treated marine dredged clay at various curing stages”, Construction and Building Materials, Vol. 132, Feb. 2017, pp. 71–84. doi: https://doi.org/10.1016/j.conbuildmat.2016.11.124
[7] Kang, G., Tsuchida, T., Tang, T.X. and Kalim, T.P. (2017), “Consistency measurement of cement-treated marine clay using fall cone test and Casagrande liquid limit test”, Soils and Foundations, Vol. 57 (5), Oct. 2017, pp. 802-814. doi: https://doi.org/10.1016/j.sandf.2017.08.010
[8] Shinsha, H. and Kumagai, T. (2018), “Material properties of solidified soil grains produced from dredged marine clay”, Soils and Foundations, Vol. 58 (3), June 2018, pp. 678-688. doi: https://doi.org/10.1016/j.sandf.2018.03.003
[9] Zhang, W.L., Zhao, L.Y., McCabe, B.A., Chen, Y.H. and Morrison, L. (2020), “Dredged marine sediments stabilized/solidified with cement and GGBS: Factors affecting mechanical behaviour and leachability”, Science of The Total Environment, Vol. 733, Sep. 2020, 138551, pp. 1-16. doi: https://doi.org/10.1016/j.scitotenv.2020.138551
[10] Sadeghpour-Monfared, M., Rahmani, I. And Aghaei Araei, A. (2021), "Various methods of stabilizing dredged and carbonated soils", Road, Year 19, No. 106, Vol. 1, Spring 2021, pp. 11-42. doi: 10.22034 / ROAD.2021.123064 (in Persian)
[11] Rezaeimalek, S., Huang, J. and Bin-Shafique, S. (2017), “Evaluation of curing method and mix design of a moisture activated polymer for sand stabilization”, Construction and Building Materials, Vol. 146, Aug. 2017, pp.210–220. doi: https://doi.org/10.1016/j.conbuildmat.2017.04.093
[12] Muhunthan, B. and Sariosseiri, F. (2008), “Interpretation of Geotechnical Properties of Cement Treated Soils”, The Federal Highway Administration U.S. Department of Transportation, July 2008, Research Report, FHWA Contract DTFH61-05-C-00008, Compaction Control of Marginal Soils in Fills.
[13] Poulos, H., G., "Marine Geotechnics", 1st ed., London, Unwin Hyman, 1988.

14th International Conference on Coasts, Ports and Marine Structures
9 & 10 May 2023 , Tehran-IRAN
ICOPMAS 2022

MULTIPURPOSE SMALL BREAKWATERS: ACHIEVEMENTS, OPPORTUNITIES AND CHALLENGES

Mohammad Hadi Moeini[1]

1) PhD in Coastal Eng., Pouya Tarh Pars Cons. Eng. Company, Tehran, Iran, mhmoeini@gmail.com

1. Introduction

A project started in 2009 by the Iranian Ports and Maritime Organization, in which it was planned to design and construct a number of small ports (about 50) along the Southern Iranian coastlines, the Persian Gulf and Gulf of Oman. The background of this project is related to the 90s decade aiming to development of the Southern Iranian coastlines by providing small ports for small coastal communities. So far, only the breakwaters of the most of the above mentioned ports have been constructed, hence the project is known as Small Breakwaters. In this paper, the benefits and challenges of the constructed breakwaters along the coastlines of Khuzestan, Bushehr and Hormozgan provinces are discussed, which can be used for similar breakwaters, particularly for those in Sistan province.

At the beginning of the project, 39 sites were selected for construction of the breakwaters along the coastlines of the three mentioned provinces. Table 1 shows the names and Figure 1 depicts the location of sites. Three of these sites are located on the tidal inlets of Khuzestan province, namely Gooban, Govarian and Khour-e-Semayeli and the others are located on the open coasts. The three inlet sites are sheltered, thus they do not need breakwaters. Therefore, berthing facilities were designed and constructed, instead.

Figure 1. Location of the small breakwaters on the southern coastlines

Until now, the breakwaters of the 36 sites located on the open coast and the piers have been completed based on the primary program. Seven sites out of the 36 are located along the Iranian islands. According to the project, about 38000 m of rubble mound breakwaters were constructed in total and about 310 Hectares basins have been obtained from the open coast sites.

Table 1. List of the small breakwaters

1	Gooban*	14	Bonood	27	Abumusa+
2	Govarian*	15	Teben	28	Berkeh Soflein
3	Khour-e-Semayeli*	16	Ziarat Parsian	29	Kandaloo+
4	Ghamar	17	Shiyo	30	Shibderaz+
5	Emam Hasan	18	Mogham	31	Messen+
6	Bolkheir	19	Kalat	32	Rigoo+
7	Khour Shahab	20	Gorzah	33	Zakeri+
8	Karri	21	Tahooneh	34	Khour Karpan
9	Chapahn	22	Moghuyeh	35	Ziarat Sirik
10	Ouli	23	Divan	36	Berizak
11	Dayyer	24	Faroor+	37	Bonji
12	Parak	25	Shenas	38	Yekboni
13	Haleh	26	Hameiran	39	Bahal
* located in tidal inlet +located in Islands					

2. Achievements and Opportunities

The population along the southern Iranian coastline is much lower than the other coastal areas in the world. In 1995, nearly 40 percent of the world population were living in the coastal margins. Most of the large cities in the world are located in the coastal areas, such as Shanghai, New York, Hong Kong, Sydney, Cape Town, Buenos Aires and Rio de Janeiro. Iran has the rank of 106 in population density in coastal areas among 123 coastal countries in the world [1-4].

In Japan, with about 30000 km coastline, as a developed country, there are nearly 3000 fishing ports [5]. It means that there is just a fishing port in every 10 km in Japan, while there will be a fishery port in every 50 km on the southern coastline of Iran if we have 100 ports (by taking the small breakwaters into account). The small breakwaters can also be used for other purposes such as marine tourism. Thus, the construction of the small breakwaters was a step towards creating the necessary infrastructures for the development of the southern coastlines. Some of the other achievements and opportunities of these facilities are presented in the following.

The achievements and opportunities of the small breakwaters project can be discussed from social, economic and technical viewpoints. As mentioned before, one of the significant achievements of the construction of these breakwaters is creating necessary infrastructures for development and improvement of the population centers.

These facilities can improve employment in different issues. One of these issues is marine tourism, which is one of the most important ways for improving the economic condition of Iran. Some examples of the improvement of marine tourism have been observed in Rigoo, Shibderaz and Kandaloo, the small breakwaters in Qeshm Island (Figure 2).

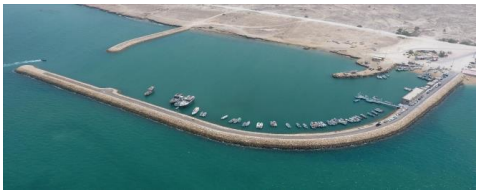

Figure 2. Kandaloo small breakwater

Another case of using these small breakwaters for job creation and development of population centers is fishing activities such as fish farming cages (fish breeding in cages in the sea). The constructed small breakwaters are an appropriate infrastructure for supporting these activities. Some of the small ports are now used for this purpose, but the potential capacity is much more. The constructed small basins can be used in other economic activities such as local export bases and industrial activities. The noticeable point is that the cost of construction of these small breakwaters was so far insignificant compared to the cost of constructing large ports. Thus, it seems that the cost of creating job opportunities by using these facilities is lower than that of larger ports and industries.

Generally, the constructed small breakwaters can act as the bases of job opportunities in different areas and prevent the migration of people living in southern coastal regions. The development and demographic prosperity in the southern coastal areas is an important step towards passive defense and enhancing the security of these areas.

Another achievement of the small breakwaters project is technical achievement. Design and construction of the small breakwaters led to preparation of a complete data bank of rock materials for breakwater construction on the southern coastlines. Executive experiences of construction of these breakwaters can also increase the knowledge of breakwater construction. Analyzing the behavior of different kinds of breakwaters against the environmental forces and improvement of the design methodology of static and berm breakwaters are another technical opportunities of the small breakwaters project.

3. Challenges

In this section, the consequent challenges of construction of small breakwaters are described. One of the challenges is to oversee the ongoing activities in these sites and to prevent illegal issues such as smuggling. Another challenge is related to technical issues. The small breakwaters are facing more challenges about sedimentation due to their smaller basin and less extension to the sea than the larger ports. The necessary programs should be made by the owners for monitoring of the sedimentation around these breakwaters. Environmental issues are the other challenges of this project. Such as all of the human made structures, these breakwaters can also be a source of environmental pollution. This issue should be controlled by appropriate planning and training of the users.

Another in fronting issue is completing the infrastructures of these ports to reach to a standard level for operation. In most of the selected points, the breakwaters have just been constructed and the necessary plans should be made for creating other facilities such as piers, water supplies, electricity, fuel systems etc.

4. Conclusions

Construction of the small breakwaters has led to the creation of valuable infrastructures along the southern Iranian coastlines. The important issue in this stage is the continuation of the work in both the optimal planning section and the completion and development section. Making appropriate plans for optimal operation of each basin based on the territorial condition is very important. Entering the private sector for doing the remaining works and facilitating the devolving of port affairs to this sector will also reduce the works of the public sector and accelerate the development of these ports.

5. References

[1] Percentage of total population living in coastal areas, Center for International Earth Science Information Network (CIESIN) of Columbia University. 2006. CSD Coastal Population Indicator: Data and Methodology Page, http://sedac.ciesin.columbia.edu/es/csdcoastal.html.
[2] IOC/UNESCO, IMO, FAO, UNDP. (2011). A Blueprint for Ocean and Coastal Sustainability. Paris: IOC/UNESCO
[3] Cohen, J.E., C. Small, A. Mellinger, J. Gallup, and J. Sachs. 1997. Estimates of coastal populations. Science 278 (5341): 1211-1212.
[4] Dao, Hy. 1998. Calculated for Earthwatch by Hy DAO, Department of Geography, University of Geneva, using ArcWorld (1: 3,000,000) with horizontal distances corrected for latitude.
[5] http://factsanddetails.com/japan/cat24/sub159/item937.html.

COMPARISON OF THE INTENSITY OF COASTLINE CHANGES AND EROSION OF THE MAIN PORTS ON THE CASPIAN SEA COAST

Homayoun Khoshravan[1], Parisa Poursafari Yekrang[2]

1) Water research institute& Ministry of Energy, Tehran, Iran, h.khoshravan@wri.ac.ir
2) Water engineering Department, Guilan University, Rasht, Iran, Parisa.Poursafari@ut.ac.ir

1. Introduction

The sort and quantity of deformation of coastlines, the rate of retreat and increase of Caspian Sea water in coastal lands, and the severity of abrasion of the coasts of the primary ports inside the north of Iran are the principal questions in this take look at the decrease of the Caspian Sea water level commenced in 1930 and by way of 1978 the sea level reduced about 3 m.

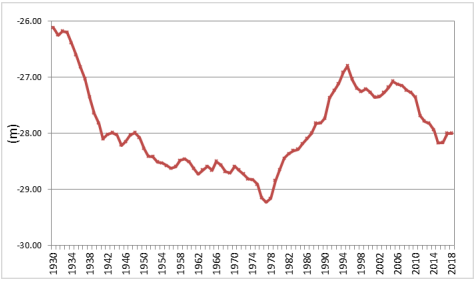

Figure 1. Water level fluctuations of the Caspian Sea from 1930 to 2019

The results of studies on the shoreline of the Sefidrud Delta have shown that coastal landforms have gone through significant changes over the years due to fluctuations in the water level of the Caspian Sea. The Changes in coastlines around the main ports in the north of Iran during the period (2005-2012) were studied by the Ports and Maritime Organization (2008) using Landsat satellite images and it turned into determined that the coastline replacement is a function of fluctuations within the Caspian Sea water degree and processes. Due to the lack of comprehensive statistical studies on the impact of coastlines on the main ports of northern Iran from fluctuations in the Caspian Sea water level changing during the decreasing phase from 1995-2019, which became observed through a 1.5-meter decrease in sea level, this study has been done to determining and comparing the amount of shoreline replacement in the main ports of the southern shores of the Caspian Sea and assessing the severity of their erosion. To determine the number of shoreline changes and the level of sedimentation and erosion of the coasts of the main ports of the north of Iran, Landsat multi-Temporal satellite images (1995-2021) in the GIS environment and the Digital Shoreline Analysis System (DSAS) software had been used.

2. Research Method

This research has been done by documentary study method and software analysis. At first, the necessary acquaintance with the characteristics of natural geography and morphology of the study area became accomplished by reviewing scientific documents, including specialized reports, research articles, and thematic maps. Then, by initial processing of existing satellite images through Google Earth software (Google Earth Pro, 2020), the morphological appearance of the coast in the main ports of northern Iran was examined and erosion and sedimentation of coastal areas had been identified. 100 m distance in the software of digital line analysis system of coastlines (DSAS) and Landsat multi-time satellite images (TM and LOI sensors) with a spatial resolution of 30 m in the environment of GIS with the help of software (Arc-Map) ESRI version 10.6.1 turned into analyzed alongside the coastlines overlooking the selected ports from 1995 to 2019. Also, by analyzing the digital data in the GIS environment, the level of retreat and advancement of the coast during the above period was analyzed. To calculate the shoreline displacement in the GIS software environment, multi-temporal images of Landsat satellite sensors were processed and based on the data in the band (5), which belongs to the near-infrared (NIR) spectrum. The border between the dry coast and the shallow part of the sea Separation and coastlines were drawn. Then the amount of shoreline replacement in the mentioned period (MSN) and its annual average (EPR) compared to the baseline in the software of digital coastline analysis (DSAS) and with the help of a transect module at distances of 100 m, was drawn and calculated. All numerical data were processed in the form of data tables in the Microsoft Excel software environment and graphs related to the shoreline displacement and the level of erosion and sedimentation along the coasts of the main ports of northern Iran have been generated.

3. Discussion

In this study, for the first time, the coastlines of the main ports of Iran were evaluated in a period corresponding to the decreasing phase of the Caspian Sea water level from 1995 to 2019. A few results in this study have shown, that the amount of shoreline replacement in the main ports in the north of Iran does not have a uniform and similar trend. Sometimes the joint impact of two or more port structures increases the shoreline displacement and the development of erosion and sedimentation processes. As the slope of the Caspian Sea bed increases in coastal areas, the shoreline replacement decreases. Therefore, two very important criteria for controlling the shoreline displacement include: the direction of currents parallel to the shore, which is an important factor for sedimentation, and the morphological and geometric structure of the shore

4. Results

Maximum and minimum shoreline replacement during the study period in the western part of Amirabad port (432 meter, - 132 m) within the western part of Fereydoonkanaar port (270 m, -25 m), in the eastern part of Nowshahr port (304m,44m) respectively and the eastern and western part of the coastline of Anzali port (226 m, 113 m) and within the northern and southern part of the coastline of Astara port (858 m, -350 m). Average shoreline displacement, sedimentation level, and erosion level in Amirabad port 171 m, 3600000, m^2 and 300000 m^2, in Fereydunkenar port 50 m, 820000 m^2, and 49000 m^2, in Nowshahr port 155 m with sedimentation area of 600000 m^2, In the coastline of Anzali port, 150 m with a sedimentation area of 410,000 m^2 and in the coastline of Astara port, 150 m with a sedimentation area of 120,000 m^2 and the area of the eroded beach is 140,000 m^2. Fluctuations in the water level of the Caspian Sea are taken into consideration as a serious threat to the social and economic infrastructure concentrated in the coastal areas.

The results have shown that the behavior of the coastlines of the main ports in the north of Iran on the subject of the reduction of the Caspian Sea water level has been very distinctive and varied in terms of quantity and quality. Geographical location and length of coastlines, location of sediment supply sources such as rivers, and coastal morphological status are essential criteria for the behavioral response of coastlines of major ports to fluctuations in the Caspian Sea water level. The studied ports are divided into three main groups in terms of coastline displacement (severe positive and negative displacement, moderate positive and negative displacement, and non-negative displacement). They are also classified into types (high, medium, and low) in terms of the extent of erosion and sedimentary surfaces.

Figure 2. Curve of shoreline displacement in the area of Amirabad port.

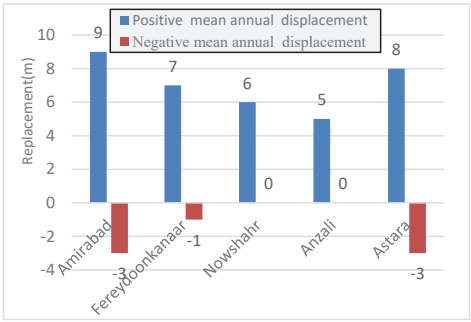

Figure 3. Comparison of the average annual displacement (positive and negative) of the coastline of the main ports of northern Iran

5. References

[1] Alemi Safaval, P, Kheirkhah Zarkesh, M, Neshaei, SA & Ejlali, F 2018, "Morphological changes in the southern coasts of the Caspian Sea using remote sensing and GIS". Caspian Journal of Environmental Sciences,2018, 16: 271-85

[2] Del Río, L., Gracia, F. J., &Benavente, J. "Shoreline change patterns in sandy coasts. A case study in SW Spain". Geomorphology, (2013). 196, 252–266

[3] Hapke, C. J., Kratzmann, M. G., &Himmelstoss, E. A. (2013). "Geomorphic and human influence on large-scale coastal change". Geomorphology, 199, 160–170

[4] Khoshravan, H., "Beach sediments, Morphodynamics and risk assessment Caspian Sea coast", Quaternary international journal, Iran,2007, 167-168, 35-39

14th International Conference on Coasts, Ports and Marine Structures
9 & 10 May 2023 , Tehran-IRAN
ICOPMAS 2022

SHIP WASTE MANAGEMENT: CHALLENGES AND OPPORTUNITIES FOR PORTS

Maryam Rasouli[1]

1) Marine Pollution Expert, Ports and Maritime Organization, Rasouli.maryam@gmail.com

1. Introduction

Waste management is the collection, transport, processing or disposal, management, and monitoring of waste materials. The term usually relates to materials produced by human activity, and the process is generally undertaken to reduce their effect on health, and the environment. The most considerable purpose of waste management plans and reception facilities is to reduce and eliminate dumping wastes illegally into the sea environment. Many examples have already demonstrated that unsatisfactory waste handling and even illegal dumping take place in many ports around the world due to inefficient waste management operations, lack of control, recovery systems, and inefficient information flow.

MARPOL Annex V requires governments to ensure that adequate port reception facilities are in place at ports and terminals and the Ships can use them as needed without causing undue delays to ships. Meanwhile, a Port Reception Facility Database) PRFD) has been established in the IMOs Global Integrated Shipping Information System (GISIS) to provide relevant data on port reception facilities. This basis, Iran has all imposed requirements on port reception facilities, requiring ports and terminals to provide port reception facilities in good condition without delaying the ships. We also require ports, terminals, loading and unloading stations, and units engaged in ship repair and building to be equipped with corresponding Pollutant monitoring facilities to reduce the illegal discharge of ship waste.

Special area refers to a sea area that requires the adoption of a different compulsory measure from in other sea areas because of its special marine ecological environment or transportation conditions to prevent ship-caused pollution. Designating a special area is an effective measure to control ship waste pollution and protect the marine environment. Due to the special water environment in special areas, the applicable ship waste management regulations should be more stringent. For this reason, targeted treaties and laws specific special areas are often applied. For some special areas, MARPOL Annex V requires the adoption of special mandatory methods to prevent ship waste pollution to the sea For the Persian gulf.

The Government of the Islamic Republic of Iran ratified Annexes I, II, and V in the year 2002, and Annexes III, IV and VI in 2009. Under these provisions, the ports of the country need to be equipped with adequate facilities to receive wastes from ships, including petrochemical materials and oily wastes, used oil, sludge, bilge water, and garbage.

2. International, Regional and National Requirements for Port Reception Facility

All ships that go to and from Iranian ports must comply with the following national, regional, and international requirement. International Marpol Convention requirements that include:

- Article 11(1) (d)
- Reg.38 of Annex I
- Reg.18 of Annex II
- Reg.12 (1) (2) of Annex IV
- Reg.7 (1) (2) of Annex V
- Reg.17 (2) of Annex VI
- The Basel Convention on the Control of Transboundary Movements of Hazardous Wastes and Their Disposal, usually known as the Basel Convention.1380
- Kuwait Regional Convention for Co-Operation of the Marine Environment from Pollution.1357
- The Law on the Protection of the Sea and Navigable Rivers against Pollution by oil substances approved 1389 .act 89
- Waste management law approved 1383
- Wastewater discharge standards was approved 1373
- The law on how to prevent air pollution approved in 1374

3. Prevention and Reduction of Marine Plastic

A global project called Glolitter with the cooperation of IMO and Norway has started working with a budget of 3.5 million dollars. The main plans of the project include:

- Investigating the existence of suitable and adequate facilities for receiving waste in ports.
- Raising the awareness of the shipping and fisheries sectors, especially sailors and Fishermen, regarding the problem of plastic waste in the sea.
- Encouraging operators to mark fishing equipment to make it possible to trace their owners
- Developing guides and training materials to help implement related regulations, such as the fifth annex of the MARPOL Convention
- Emphasis on the implementation and application of the London Convention and Protocol, Including evaluation of wastes before issuing a permit for their disposal

- Attracting the participation of the private sector, through industries, and also encouraging the cooperation of Fishermen and fishing companies.
- The statistics of receiving waste materials from ships in the year 1400

inspection (item)	Bilge (m^3)	Oily residues (sludge)	Garbage	Sewage
7754	7216.279	5031.795	4407	221.7

4. Challenges and Solutions Related to Waste Reception Facilities in Iranian ports and Terminals

Not all solid wastes were segregated and the amount of recyclable/reusable wastes was not estimated. Total solid waste amounts for any waste type were remarkable in comparison to the overall waste generated from the municipality. There should be adequate monitoring and tracking of ship-generated wastes and residues.

It will be beneficial to know how many ships are equipped with an onboard incinerator in which both sludge and household waste can be burned or if they have a compressor for diminishing the volume of solid waste.

Furthermore, communities should be motivated to participate fully in the public awareness campaign on importing proper waste management for health and wellbeing.

The authorized companies providing the reception facilities services Waste within the area will have an approved emergency response plan (CONTINGENCY PLAN) in place in the event of emergency pollution caused during the receipt of liquid, solid, or hazardous residues or due to an accident, damage or damage to its means.

Establish laws and deterrent offenses in dealing legally with the personnel of faulty vessels that pollute the marine environment.

Adjusting and updating the tariff for receiving, processing, and disposing of waste from ships based on the average tariff of the country's maritime regions by conducting comparative studies of other foreign ports.

The Proper information to applicants for waste collection facilities and the possibility of surveys and suggestions to improve the provision of services through the Internet.

Preparation of training program for personnel of non-conventional vessels in the field of facilities for receiving and processing waste from ships and the need to deliver waste to facility centers to spread the environmental culture

Currently, due to the enforcement of the IMO 2020: Consistent Implementation of MARPOL Annex VI on fuel consumed by ships, it has been changed to low-sulfur fuel and diesel fuel, and this has caused the fuel waste received from ships to be minimized, and mainly water, which is mostly caused by washing the engine room, has been received. Received contaminated water does not have financial value for the contractors of facilities for receiving waste materials, and only for its processing; a heavy cost must be done in order to dispose it correctly and with environmental approval. Solving this problem requires a review of the investment plans due to the changes made in the materials received from the ships and the decrease in fuel in the waste of the ships.

To ensure the strict implementation of international regulations and requirements by the countries, the International Maritime Organization (IMO) has approved an audit framework. There are facilities for port reception facilities. Also, one of the tools of IMO to conduct an audit of countries and monitor them regarding facilities for receiving waste materials, entering information related to facilities for receiving waste materials and entering information by countries about companies active in the field of facilities for receiving waste materials, contact information and details related to their activities. It is inside the site that should be updated inside the site. The year of conducting this audit for Iran is 2024. According to the fifth article of the law on the protection of navigable seas and rivers against oil pollution. Act 89, the Ports and Maritime Organization must provide adequate facilities in ports, wharves, and oil terminals to receive ballast water and oil sludge from oil tankers, ships, and vessels. Fees for using these facilities are received from the ships based on the approved regulations.

Following the rules related to the collection of waste, ensuring the possibility of timely delivery of all waste from incoming ships to the ports and monitoring the work, reducing the production and recycling of waste as much as possible and raising the awareness of relevant industries will lead to proper management of waste in ports.

5. References

[1] SATIR, Tanzler, ALKAN, G.,"Port Reception Facilities, using multi -criteria Decision Making, 2007
[2] Shin-young, H., Sung - Gigue, "Improving the port reception - facility system ", Journal of Navigating and port research, *Dece*mber 2020, pp. 488-493.
[3]A. Gabriela, |"Environmentally sound management of ship wastes: challenges and opportunities for European ports", Journal of shipping and trade, 2020, pp5-12.
[4] A. Carpenter, S. M. Magical., "The EU Directive on port reception Facilities For Ship-Generated Waste and cargo residues", Marine Pollution Bulletin, 2005, pp. 1541-1547.
[5] MEPC.1/Circ.671,Guide to Good Practice For Port Reception Provider and User
[6] -Revised Consolidated Format for Reporting Alleged Inadequacies of Port Reception Facilities (MEPC.1/Circ.469/Rev
[7] MEPC69/11, Inadequacy of reception facilities, updated version of the Manual on port reception Facilities-How to do it

14th International Conference on Coasts, Ports and Marine Structures
9 & 10 May 2023 , Tehran-IRAN
ICOPMAS 2022

5-YEARS FIELD EXPOSURE STUDY: THE DETERIORATION MECHANISMs FOR IMPROVING THE SULFATE RESISTANCE, PORE STRUCTUREs, AND CHEMICAL COMPOUNDs OF SWSSC IN TIDAL CONDITIONs

Mohammad Jahani[1], Saeed Moradi[1,2], Shore Shahnoori[3] and Moslem Zebardast[4]

1) Department of Civil Engineering, University of Hormozgan, Bandar Abbas, Iran. Jahani.m.edu@gmail.com
2) Road, Housing &Urban Development Research Center, Bandar Abbas, Iran. Saeed.moradi69@yahoo.com
3) Department of the Built Environment, Eindhoven University of Technology (TU Eindhoven), Eindhoven, The Netherlands. s.shahnoori@tue.nl
4) Shipbuilding Industry Expert, Bandar Abbas, Iran. Moslem.zebardast@gmail.com

1. Introduction

The durability and service life of concrete structures exposed to the marine environment require long-term field exposure studies. In the marine condition, the service life of concrete relates explicitly to its durability, the interaction of its chemical compounds' reaction mechanisms and physical characteristics [1-3]. The vulnerability of concrete subjected to the marine circumstance in terms of physical and chemical degradation depends on various factors. For instance, the chemical effects of SW (See-Water) as mixing water or curing water on hydration processes and products of cement form micro-cracks due to crystallization pressure of existing salt if the concrete is affected by consecutive wet/dry cycles (tidal condition).

Over one billion tones of freshwater (FW) annually are consumed as mixing water in concrete. Providing FW incorporates significant difficulties; similar is the situation for the mine aggregates on islands and marine environments [1]. Therefore, using SW, with its vast scale resources, rather than FW, in concrete marine construction would be a beneficial option in terms of environmental and economic viewpoint [2]. Therefore, this research focuses on suppressing the degradation mechanism of Sea-Water Sea-Sand Concrete (SWSSC) exposed to a tidal zone of the Persian gulf for 5-years.

Marine construction sites might encounter an inevitable crisis of FW shortage and aggregate extraction, consequently increasing environmental impacts and unpredicted costs in the near future. The essential issue for concrete in tidal conditions is the ions attack, such as chlorides and sulfates. This condition is susceptible to concrete, which is constantly subjected to alternating cycles of wetting and drying, which can accelerate the impressions on concrete composites. The reduced w/c ratio of SW-paste and using supplementary cementitious materials (SCMs) significantly improved the durability test results of SWSSC in 5 years. In particular, the sustainability of SWSSC was highly improved by using 10% Silica Fume (SF).

Meanwhile, a previous study showed that using SW in concrete does not affect the air content in fresh concrete or the water permeability. At the same time, the needle-shaped texture of C-S-H and expansive products such as ettringite and gypsum was observed [4]. Hence, another research examining the pore microstructure (MIP) reported that using SW reduces the diameter of larger pores and refines pore structures. Generally, the size of the pores is smaller than that of FW, and the volume of pores smaller than 10 nm, considerably increases while using SW compared to that of control concrete.

Figure 1. Placing the samples in tidal conditions to investigate SF's effectiveness on the characteristics of SWSSC after curing

2. Experimental Program

The experimental program is categorized into three main phases. First is the design and programming of the mixes, in addition to the required tests on the raw materials. The second phase relates to the specimens preparations (mixing, casting, curing etc.). The final stage is the microstructural and compositional analysis of the samples. The latter is due to the sulfate and chloride attacks in the marine environment and the primary ions source in SW and DMS. The samples were prepared with water-to-cement (w/c) ratios: of 0.35 and a certain percentage of supplementary cementitious materials (SCMs) replacement for the cement (ratio 400

kg/m^3) and DMS replacement for the fine aggregates (#4). The samples were cured for 7 and 28 days in laboratory conditions. Then, they were transferred to the tidal zones on the coast of the Persian Gulf (Close to Shahid Rajaee Port) for 5 years. Afterwards, they were subjected to several destructive and non-destructive tests related to chemical compounds, sulfate, and chloride resistance, including RCPT, SEM, MIP, XRD and EDX.

3. Outcomes of the Laboratory Tests

Despite an early-age improvement due to porosity refinement, SWSSC was not resistant to recurring wet/dry cycles, carbonation, gradual crystallization, pore structure deterioration, and the sulfate attacks caused by the marine circumstance, neither did control concrete. Adding SF to SWSSC, by suppressing chloride penetration, crystallization and sulfate ions attack (specifically $MgSO_4$), has developed and enhanced pore structure, chemical composites of SWSSC with elapse of exposing time [5]. In this research, SF densified the C-S-H gel in Sw-paste minimized $Ca(OH)_2$ and ettringite volume, while in control concrete, more $Ca(OH)_2$ was observed. Using SW as the mixing water has changed C-S-H to a needle-shaped structure with a deep pore.

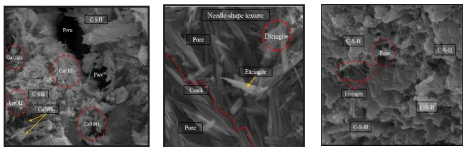

reference concrete *SWSSC* *SWSSC + SF*

Figure 2. SEM images for Comparing the effects of SW and FW on morphology and hydration of ITZ.

SF's properties led to a faster reaction with the crystallized $Ca(OH)_2$ and SW. In particular, the durability and, thus, sustainability of SWSSC are highly improved by using 10% SF. As seen in SEM images, XRD analysis also shows expansive product formation such as Ettringite in all mixtures with only slight differences in their peak intensity. The presence of a higher amount of calcite (C) in the XRD analysis was due to higher carbonation and reaction between CO_2 with C-S-H. Higher portlandite (P) in ordinary concrete and SWSSC has been formed, cement's most vulnerable hydration product. Calcite peak (C) indicates the carbonation process, which was higher in ordinary concrete and SWSSC, even more than quartz (Q). These compounds were all improved by using 10 % SF.

Table 1. Pore structure analysis results of 5 years exposed to tidal zone samples using mercury intrusion porosimetry (MIP).

Mixtures	Total porosity (%)	Average pore diameter (nm)
Control	10.4	10
SWSSC	12.9	18.7
SWSSC+SF	7.4	10.1

4. Discussion and Conclusion

concrete structures in the marine environment are invaded by destructive ion attacks and chemical compounds such as CO_2, Mg^{2+}, Cl^-, SO_4^{2-}, even by microorganisms, oysters, and seashells. Then, erosions begin through external surface layers. SWSSC and ordinary concrete did not resist long-term exposure to tidal conditions. Due to sulfate attacks and the formation of harmful expansive products such as ettringite and portlandite, micro cracks and porous microstructures develop accordingly. Using SF by optimizing pore structure and cement matrix formed more quartz, which could be related to a high amount of SiO_2 in its chemical compounds, consequently suppressing sulfate attack by filling capillary pores.

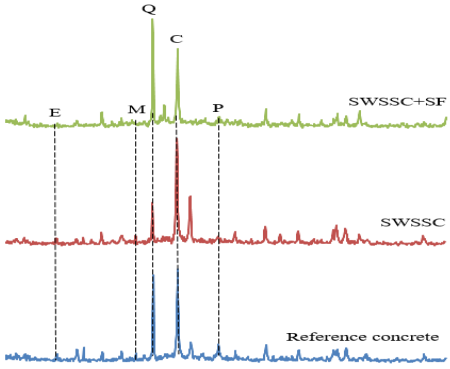

Figure 3. XRD (X-ray diffraction) analysis, 5-years exposed to tidal conditions samples; Q: Quartz, C: Calcite, E: Ettringite, M: Magnesium sulfate, P: portlandite.

5. References

[1] Jahani, M., Shahnoori, S., Moradi, S., & Ershadi, C. (2022). Cleaner Production Towards a Green Concrete: Multi-scale Experimental Study on Long-term Performance of a Sustainable Modified-SWSSC. American Journal of Construction and Building Materials, 6(1), 43-59.

[2] Jahani, M, Shahnoori, S., & Moradi, S. (2022). Long Term observations in an Experimental study on durability of a Sustainable Concrete Made with Sea-water and Sea-sand in Tidal Conditions. 182. 2th International conference of circular systems for the built environment, Advanced Technological and Social Solutions for Transitions ICSBE2.

[3] S. Moradi and S. Shahnoori, "Eco-friendly mix for Roller-Compacted Concrete: Effects of Persian-Gulf-Dredged marine sand on durability and resistance parameters of concrete," Constr. Build. Mater., vol. 281, p. 122555, 2021.

[4]. J. Wang, E. Liu, and L. Li, "Multiscale investigations on hydration mechanisms in sea-water OPC paste," *Constr. Build. Mater.*, vol. 191, pp. 891–903, 2018.

[5] Q. Li, H. Geng, Z. Shui, and Y. Huang, "Effect of metakaolin addition and sea-water mixing on the properties and hydration of concrete," *Appl. Clay Sci.*, vol. 115, 2015, DOI: 10.1016/j.clay.2015.06.043.

9 & 10 May 2023 , Tehran-IRAN

ICOPMAS 2022

PORT ENGINEERING AND COASTAL STRUCTUR

14th International Conference on Coasts, Ports and Marine Structures
9 & 10 May 2023 , Tehran-IRAN
ICOPMAS 2022

CHAMKHALE MARINA, AN ENGINEERING SOLUTION TO MINIMIZE LONG SHORE TRANSPORT EFFECTS

Majid Jandaghi Alaee[1], Mohammad Hadi Moeeni[2] and Mahdi Kamyab Roudsari[3]

1) Head of Technical Department, Pouya Tarh Pars Consultant Engineers (PTP), Tehran, Iran, mja@ptpco.com
2) Head of coastal group, Pouya Tarh Pars Consultant Engineers (PTP), Tehran, Iran,
3) Executive manager for recreational ports, Ports and Maritime Organization, Tehran, Iran, mkamyab@pmo.ir

1. Introduction

Chamkhaleh, one of the small towns along the Iranian coasts of the Caspian Sea, is among the most beautiful parts of Gilan province. As it is seen in Figure 1, Chamkhaleh area, to its southern end, meets the conjunction of two rivers i.e., Langrood River and Shalmanrood. Sandy beaches together with very green and calm area create a wonderful opportunity for Chamkhaleh to become a successful recreational region with potential advantages for future investments such as in marinas, marine sports, sea routes for passenger vessels.

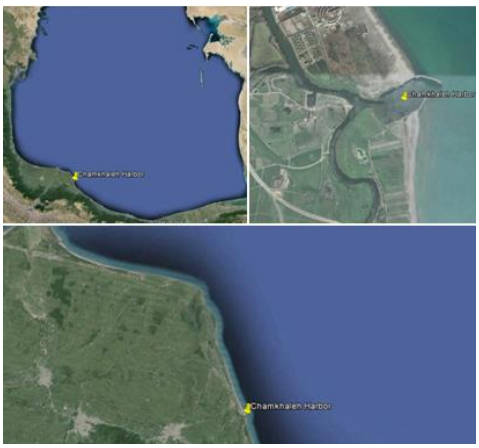

Figure 1. Location of the Chamkhaleh, Gilan province.

In 2000, two rubble mound breakwaters were constructed to protect the river mouth basin against waves and sedimentation. However, the basin suffered from both siltation during the river floods and sedimentation from the sea. Satellite imagery depicts the evolution of the coastline in the neighborhood of the basin. Figure 2 clearly shows that the dominant left to right longshore sediment transport (LST), (in reality, north-south LST due to alignment of the coastline), resulted in a considerable growth of the left beach, considerably. However, we should remember that during the period of 2003-2015 the Caspian Sea level decreased by 0.5 m. Hence, for the comparison between the coastlines, necessary corrections must be applied (done for the likely presentation).

Future plans for having a modern marina for Chamkhaleh required a full investigation on the ongoing sediment transport in the area, and propose creative ideas to avoid any unfavorable morphology change. This paper describes an engineering solution to have a frog leap from the surf zone and prevent any collision between the longshore current and marina structures.

Figure 2. Evolution the coastlines around Chamkhaleh river-mouth basin (Green 2003, Red 2015), Rotated 90 degree counterclockwise

2. Methodology

Reliable wind, wave, current data and bathymetric charts were available from a comprehensive four-year study on extensive field observation and 30-year hindcast numerically simulation for the whole Caspian Sea, planned and funded by the Ports and Maritime Organization (PMO) [1]. The above-mentioned valuable data together with technical information on discharges and corresponding sediment contents of the rivers were employed to determine effective factors in sediment behavior and morphology changes. These findings, together with the necessary area for the marina basin and required natural depth, led to the potentially suitable locations for the marina. Figure 3 shows the final location of Chamkhaleh marina [2].

Three main concerns were key factors in the determination of the final layout for the marina: First,

results of the interaction between longshore current and LST and the structure passing through the surf zone. Second, the probability of the formation of a tombolo in the shadow of the marina (rubble mound breakwaters). Third, how the longshore current interacts with the river-mouth breakwater. In the following section the concerns are discussed.

3. Results and Discussion

In order to minimize the unfavorable results from having a solid and long obstacle in front of the longshore current and LST, a bridge was designed with suitable height and span (Figure 4). The bridge allows the current and companion sediment to move naturally. To avoid the formation of tombolo, empirical recommendations were applied for preliminary design and long period numerical simulations were carried out to investigate probable consequences of different conditions, such as the Caspian Sea level fluctuations. It has been shown that the formation of tombolo is very unlikely unless the Caspian Sea level drops dramatically. It should be added that from the start of the construction, tens of sticks were planted at nodes of a regular mesh, covering both sides of the access bridge (as can be seen in figure 4) to monitor the changes in topography and bathymetry of the study area. A report on the behavior of the neighboring coastal area in response to the presence of new marine structures is presented during likely oral presentation.

And for prediction of the results of the interaction of the longshore flow and the river mouth breakwaters, a series of 2D numerical simulations suggest that occasional contraction of longshore streamlines results in stronger currents in the vicinity of the river mouth, causing the deepening of the seabed.

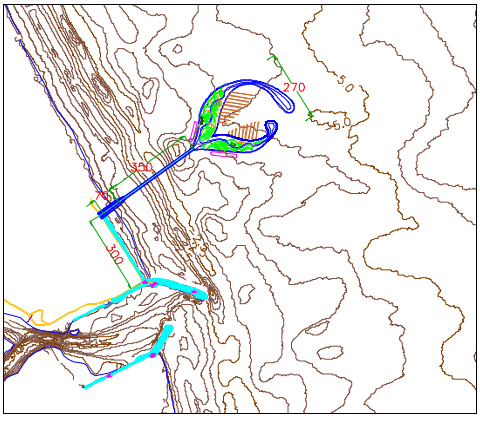

Figure 3. Final layout for Chamkhaleh marina

4. Conclusions

Chamkhaleh is a valuable coastal area with wonderful advantages for hosting various marine and coastal recreational activities. A modern marina will strongly support the role of Chamkhaleh to achieve the goals. Since a dominant longshore current and the resulting LST are present in Chamkhaleh coastal area and strong floods from the rivers do play important roles in the region, a creative engineering solution was required to reach a suitable layout for the marina as well as to avoid any unfavorable consequence by the LST and floods. A design consisting of an access bridge with optimized spans was proposed and constructed. Meanwhile, any changes in topography and bathymetry of neighboring areas were monitored. The results show the design has been successful and if the conditions remain without any dramatic changes, a safe and unique modern marina, using an innovative engineering solution will serve the public.

Figure 4. Accesses bridge to the Chamkhaleh marina

5. References

[1] Pouya Tarh Pars Consulting Engineers, 1394. "Reports on Monitoring and numerical simulations of the Caspian Sea" 12 volumes, PTP library, 950pp.
[2] Pouya Tarh Pars Consulting Engineers, 1397." Study for design and construction of Chamkhaleh marina for sea travel and tourism purposes". PTP library, CH-Mari-1-cs-re-006, 271pp.

14th International Conference on Coasts, Ports and Marine Structures
9 & 10 May 2023 , Tehran-IRAN
ICOPMAS 2022

READINESS AND RESILIENCE OF SEAPORTS TOWARDS THE INCREASING SIZE OF CONTAINER SHIPS

Rita Pombo[1], Carlos Coelho[2] and Hugo Lopes[3]

1) RISCO Research Centre, Dept. Civil Engineering, University of Aveiro, Aveiro, Portugal, ritanovo@ua.pt
2) RISCO Research Centre, Dept. Civil Engineering, University of Aveiro, Aveiro, Portugal, ccoelho@ua.pt
3) APDL, S.A., Leça da Palmeira, Portugal, hugo.lopes@apdl.pt

1. Introduction

The phenomena of ship upsizing and cascading of capacity have been fostered by the globalization of the world's economy and the pursuit of economies of scale. Additionally, regulatory changes related to decarbonization targets have also been impacting newbuilding orders [1]. Consequently, ports, which are the key nodes of the shipping network, have been pressured to cope with the increasing demand to accommodate mega-container ships and deal with a greater throughput at container terminals. This revolution in containerization has challenged seaports to evaluate and improve their readiness to provide service reliability to the shipping lines in order to attract and secure them, addressing demand trends in a profitable and sustainable way [2].

It is concluded that the majority of ports worldwide lack equipment, machinery and facilities to handle mega-container ships and the respective cargo, are still missing out on digitalization, have inadequate intermodal (and hinterland) connections, and do not have the financial capacity necessary to elevate their infrastructure at the fast pace that the industry requires [1-2]. In this context, with global trade increasingly dependent on containerized transportation and an uninterrupted trend of container ships becoming larger, this works aims to analyze how mega-container ships are impacting ports and how ports are reacting to this pressure in order to remain competitive.

2. Outlook and Forecast of Container Ships Size

The definition of a container ship class is a function of its draft and related capacity in TEU (Twenty-foot Equivalent Units). Since the beginning of containerization in the mid-1950s, container ships undertook six significant waves of changes, each representing new generations [3]. The size limit of the Panama Canal, which came to be known as the Panamax standard, was achieved in 1985 with a capacity of about 4,000 TEUs. In 1996, full-fledged Post Panamax containerships were introduced with capacities reaching 6,600 TEUs. By 2006, the third generation of Post Panamax containerships had a capacity in the range of 11,000 to 14,500 TEUs (the Emma Maersk, E Class). This new class started being particularly demanding for port infrastructures as their draught exceeded 15m and its width encompassed 22 containers across. A further extension of the design led to the introduction of the Ultra Large Container Ship (ULCS) class of 18,000 TEUs and above in 2013 (named 'Triple E' by Maersk). This class was further expanded, and by 2017, ships above 20,000 TEUs started to be delivered [3]. The Ever Alot container ship, delivered June 2022 with a carrying capacity of 24,004 TEUs, 400 m long, 62 m wide and a 17 m draft, is currently the world's largest.

There are already designs for bigger ships on the drawing boards, where some authors expect 30,000 TEUs vessels to appear in the year 2025 [4]. However, these are not anticipated to be constructed until sufficient volumes are demanded on the limited routes they could serve. Container ships in the range of 5,500 to 6,500 TEUs appear to persist as the most flexible in terms of the ports they can access and the market they can service.

3. Systemic Weaknesses of Seaports in Accommodating Mega-Containerships

It is verified that the emergence of mega-container ships is causing several problems in ports. It is reported a reduction in operational efficiency, congestion, limited capacity and infrastructure support, the existence of restrictions policies for seaport development, and constraints to additional spatial development [2]. Among these, unsuitable navigational access is the most common obstacle, namely due to insufficient channel width and water depth. Other major challenges comprise unsuitable crane capacity, limited berth size, less developed hinterland facilities, lack of intermodal connections, and the need for restructuring personnel training [5]. All these issues need strategic planning by port authorities and related operators, where a lot of investment is required to offer high-quality services, maximize the utilization rates and minimize the time in port, especially where diseconomies of scale happen [5].

4. Seaports' Successful Adaptation Practices

Nowadays, just a few seaports worldwide are able to accommodate ULCSs, with the majority of them located in Asia [2]. The Ports of Singapore, Tanjung Pelepas in Malaysia, and Hambantota and Colombo in Sri Lanka are examples that can be highlighted. In Europe, there is also a

list of ports able to be called by the newest generation of container ships, namely the Ports of Hamburg in Germany, Rotterdam in The Netherlands, Antwerp in Belgium, Algeciras in Spain, and Piraeus in Greece.

Every port has different constraints to overcome. For example, the Port of Santos in Brazil has only been approved in 2021 to receive vessels of 366 m in length, equating to 14,000 TEUs, the largest ships calling on the east coast of South America, after dredging the navigation channel to 15 m depth. A plan to dredge to 17 m is already being drafted. The Port of New York and New Jersey, which is the largest port on the United States east coast, needed to lift the Bayonne Bridge roadbed (which connects both states) to allow ships of more than 9,500 TEUs to pass through it for the first time. In Portugal, the Port of Sines has inaugurated this year (2022) an additional 204 m of quay length which allows the handling of three mega-vessels simultaneously. Finally, in the Port of Felixstowe, the largest container port in the United Kingdom, there are expansion plans involving 13 ha of new paved container yard and the reclamation of 3.2 ha of the seabed. Obviously, projects for new ports able to berth 30,000 TEUs vessels are already in force, which is the case of Jinhae New Port in South Korea [6].

From the literature review, major investments made by top container ports to enhance infrastructures' readiness to receive mother vessels relate to the development of deep-water terminals, channel deepening and land reclamation operations, acquisition of taller and more modern quay cranes, berths lengthening, acquisition of efficient port prime movers, and expansion of yard areas. Digitalization and automation of processes are also confirmed key enablers for higher efficiency and better performance. The incorporation of dry ports in the seaport framework to manage vessel size enlargement has been another measure ultimately considered to improve the efficiency of cargo handling and storage [2].

5. Discussion

Anticipation, preparation and adaption capacities are found the best weapons for ports to fight against disruptions and the best tools to build resilience. These are especially important in a time of climate emergency and energy transition, overburden with the management of the COVID-19 pandemic, the Ukraine invasion, and Europe's dependence on Russian energy. In addition to this, there are ongoing disturbances related to the swing of manufacturing production bases, restructuring of container carriers' strategic alliances, creation of new shipping routes (*e.g.*, resulting from the Arctic thaw) and disuse of others, and the continuous deepening and widening of water channels and transoceanic passages.

Nevertheless, rethinking and reengineering ports' infrastructures (including warehousing and logistics infrastructure) is the way forward to remain competitive and attractive, even though the question of whether container ships are close to reaching their peak capacity (as has occurred with bulk cargo vessels and, recently, aircraft) is still open to debate [7]. Furthermore, in this uncertain and complex environment, ports' redevelopment needs to be underpinned by the alignment of governments' strategic planning and policies, as well as local and global cohesive regulatory frameworks [1].

6. Conclusion

This work explored the implications of the emergence of mega-container ships on the sustainability of seaports, either in terms of their readiness to accommodate the vessel and the cargo, as well as in terms of resilience strategies adopted to ensure the continuation of competition and attractiveness.

It is clear that mega-container ships brought a wide list of significant hurdles and constraints to the planning and management of port facilities. It is reported a lack of preparedness in the majority of seaports, both in terms of physical and operational resources. Particularly, shallow depth has shown the most sizeable impact [2]. Therefore, anticipating future changes in maritime transport and making investments accordingly is vital to be ahead in the market and cope with the clients' needs. Especially, since it is verified that liner shipping operators will continue to deploy the most efficient size of vessels that their customers' cargo volumes require [8], as the historical trend and current studies demonstrate, despite the diseconomies of scales that seaports may face.

Future work comprises a categorized compilation of ports' development, innovation and expansion solutions envisaged to successfully accommodate mega-container ships, with regard to ports' container throughput, geographic and geostrategic position, landmass, hinterland, and proximity to main shipping routes.

7. References

[1] UNCTAD. "Review of Maritime Transport - 2021". No. UNCTAD/RMT/2021. 2021, ISBN: 978-92-1-113026-3.
[2] Salleh, N. H. M., Norliyana, Z., and Jagan, J., "The emergence of very large container vessel (VLCV) in maritime trade: implications on the Malaysian seaport operations", *WMU Journal of Maritime Affairs*, 20.1, January 2021, pp. 41-61.
[3] Rodrigue, J.-P., "The geography of transport systems" (5th ed.), *London: Routledge*, 480 p, May 2020.
[4] Park, N. K., and Sang, C. S., "Tendency toward mega containerships and the constraints of container terminals", *Journal of Marine Science and Engineering*, 7.5, May 2019, 131.
[5] Helmy, S., and A., Shrabia., "Mega container ships, pros, cons and its implication recession", *Journal of Shipping and Ocean Engineering*, 6, 2016, pp. 284-290.
[6] Son, W.-J., and Cho, I.-S., "Analysis of Trends in Mega-Sized Container Ships Using the K-Means Clustering Algorithm", *Applied Sciences*, 12.4, February 2022, 2115.
[7] Garrido, J., *et al*., "Predicting the future capacity and dimensions of container ships." *Transportation Research Record*, 2674.9, June 2020, pp. 177-190.
[8] World Shipping Council (2015) Some observations on port congestions, vessel size and vessel sharing agreements. World Shipping Council, Brussels.

14th International Conference on Coasts, Ports and Marine Structures
9 & 10 May 2023 , Tehran-IRAN
ICOPMAS 2022

SHORT-TERM FORECAST OF PORT THROUGHPUT USING ARIMA (CASE STUDTY: IMAM KHOMEINI PORT)

Saman Zare[1], Ali Fakher[2] and Seyede Masoome Sadaghi[3]

1) MSc Graduate, Faculty of Civil Engineering, University of Tehran, Tehran, Iran, saman.zare@ut.ac.ir
2) Professor, Faculty of Civil Engineering, University of Tehran, Tehran, Iran, afakher@ut.ac.ir
3) Assistant Professor, Road, Housing & Urban Development Research Center, Tehran, Iran, s.sadaghi@bhrc.ac.ir

1. Introduction

Forecasting the demand for cargo handling services is one of the key components of port planning studies. The main purpose of cargo forecasting is to determine amount, type and structure of the cargo passing through the port in a certain period. However, this matter has proven to be challenging due to different uncertainties regarding this subject and therefore different methods are implemented.

Generally, forecasting methods are divided into qualitative and quantitative methods. Quantitative methods are also divided into three subcategories: time series analysis, causal analysis, and combined method [1]. Qualitative methods are based on expert judgments and therefore are exposed to errors related to human knowledge. These methods are used when historical data is not available or difficult to obtain. Time series methods predict solely based on the past behavior of the desired variable. The main assumption of this method is that past events will maintain their trend. Different approaches can be adopted for this method with naïve forecasting being the most basic one in which the variable in question is assumed to behave similarly to the previous time period [2].

The most common time series forecasting methods are vector autoregressive models (VAR) and Autoregressive Integrated Moving Average (ARIMA) models. Causal analysis is another common forecasting method in which one or more explanatory variables are used to forecast the dependent variable [1]. With regard to seaports, the dependent variable is usually the throughput and a set of explanatory variables such as gross domestic product (GDP), hinterland population, GDP per capita or energy consumption.

Imam Khomeini port has been one of the main seaports of Iran in the past 80 years and currently acts as the main hub of bulk cargo in the country. The throughput of Imam Khomeini port can be divided into oil products and non-oil cargo which is mainly comprised of essential edible bulk commodities. This portion of the throughput is related to national domestic consumption and is less influenced by external factors such as economic sanctions. Hence, the non-oil throughput of Imam Khomeini port is selected as the case study in order to assess the precision of short-term trend-based forecasting methods for ports of Iran. In this research, the non-oil throughput of Imam Khomeini port is predicted until 2024 using ARIMA model.

2. Literature Review

Studies carried out on port cargo and traffic forecasting are mainly focused on presenting and evaluating various methods and finding relationships between various descriptive variables. Some of the related literature to this research are listed in Table 1.

Table 1. Literature review summary

Author	Year	Method
Schulze & Prinz [3]	2009	SARIMA
Ming et al. [4]	2013	ARIMA
Min & Ha [5]	2014	ARIMA & SARIMA
Rashed et al [2]	2016	ARIMA Intervention
Liu et al. [6]	2017	ARIMA & BP Network

3. Methodology

ARIMA models are statistical models based on autocorrelation of the recorded values in a time series [7]. Unlike regression methods, ARIMA models describe the behavior of a variable based on its past values. Implementing these models is a relatively simple and straightforward process and has proven to be very useful for forecasting time series especially in the absence of data for descriptive variables and has produced satisfactory results especially in the field of transportation.

This model is comprised of two main components, autocorrelation (AR) and moving average (MA) [8]. The written form of this model is ARIMA (p,d,q), where p is the order of autocorrelation, q is the order of the moving average, and d is the degree of differentiation needed to obtain stationarity in the time series which after the model can be formulated as below:

$$X_t = \theta_0 + \sum_{i=1}^{p} k_i X_{t-i} - \sum_{i=1}^{q} \lambda_i X_{t-i} + \varepsilon_t \qquad (1)$$

Where X_{t-i} is the recorded observation, p is the time lag, k_i is autoregressive parameter, θ_0 is constant component, q is the number of return periods, λ_i is moving average parameter and ε_t is disturbance term.

The four-step Box-Jenkins methodology was initially developed to estimate general ARIMA models in 1976. However, it is widely used for different univariate time series modeling methods [8]. This methodology was implemented in this study and detailed explanation of the process is presented in Figure 1.

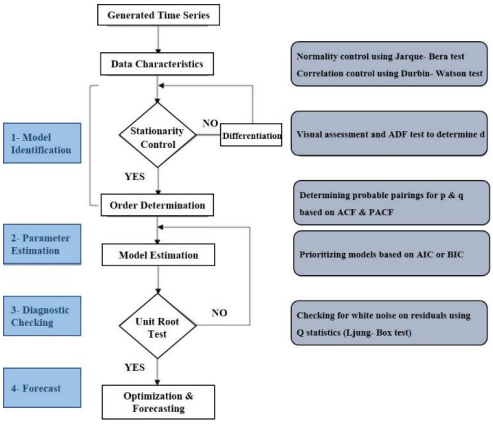

Figure 1. Implemented forecasting procedure

4. Results and Discussion

Monthly time-series on the throughput of Imam Khomeini port was generated from March 1999 to March 2019 using data provided by PMO. The time period was divided into a training sample (1999-2015) and an evaluation sample (2015-2019). The ARIMA model was developed based on the training sample and the accuracy of the model was evaluated calculating mean absolute percentage error (MAPE) values based on the evaluation sample. Since the MAPE value was within the acceptable range of less than 20%, the model proved to be sufficiently accurate and was subsequently used to forecast Imam Khomeini port throughput until March 2024. By using this model, the non-oil throughput of Imam Khomeini port in 2024 is expected to be around 33.2 million tons. The specifications of the model is presented in Table 2 and the actual and forecasted time-series are displayed in Figure 2.

Table 2. Model specifications

Model Parameters	ARIMA (1,1,1)
Jarque- Bera Test Value	9.32
Durbin-Watson Statistics	2.008
ADF Test after 1st differentiation	OK
Akaike Info Criterion	27.833
Ljung- Box Test	OK
MAPE	10.24%

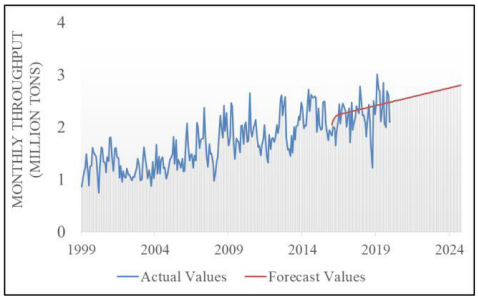

Figure 2. Imam Khomeini port throughput actual and forecast values

5. Conclusion

ARIMA model proved to be accurate enough for short-term forecast of non-oil throughput of the Imam Khomeini port. The developed model predicted an annual throughput of around 33.2 million tons by 2024. Since the non-oil throughput of Imam Khomeini port is mainly comprised of essential edible commodities which is related to national domestic consumption, it is less influenced by external factors such as international sanctions therefore using the past trend to predict the future proved to be sufficiently accurate.

6. References

[1] P. Kotcharat, “A forecasting model for container throughput-empirical research.pdf,” World Maritime University, 2016.
[2] Y. Rashed, “Container Throughput Modelling and Forecasting: An Empirical Dynamic Econometric Time Series Approach,” University of Antwerp, 2016.
[3] P. M. Schulzea and A. Prinz, “Forecasting container transshipment in Germany,” Appl. Econ., vol. 41, no. 22, pp. 2809–2815, 2009.
[4] M. Shu, Y. Huang, and T. Nguyen, “Forecasting Models for the Cargo Throughput at Hong Kong Port and Kaohsiung Port,” Recent Res. Appl. Econ. Manag., vol. I, pp. 189–193, 2014.
[5] K.-C. Min and H.-K. Ha, “Forecasting the Korea’s Port Container Volumes With SARIMA Model,” J. Korean Soc. Transp., vol. 32, no. 6, pp. 600–614, 2014.
[6] Q. Liu, L. Xiang, and X. Liu, “Forecast of Port Container Throughput Based on TEI @ I Methodology,” no. 88, pp. 451–461, 2019.
[7] T. Anh, T. Tran, and M. Takebayashi, “Time Series Analysis for Viet Nam Container Cargo Movements - Implications for Port Policy Management,” J. East. Asia Soc. Transp. Stud., vol. 11, pp. 2392–2411, 2015.
[8] S. P. Washington, M. G. Karlaftis, and F. L. Mannering, Statistical and econometric methods for transportation data analysis, Second edition. 2010.

14th International Conference on Coasts, Ports and Marine Structures
9 & 10 May 2023 , Tehran-IRAN
ICOPMAS 2022

MODELING AND OPTIMIZATION OF THE PROCESSES OF BERTHING AND UNBERTHING OF VESSELS

Seyed Sadra Razavi[1], Hassan Sayyaadi[2]

1) Bachelor's degree, Mechanical Engineering Department, Sharif University of Technology, Tehran, Iran, paarchins@gmail.com
2) Faculty of Mechanical Engineering Department, Sharif University of Technology, Tehran, Iran, sayyaadi@sharif.edu

1. Introduction

In maritime missions, one of the most important parts is the processes of berthing and unberthing ships because these two processes are the final and beginning stages of a sea voyage. On the other hand, these two processes have their sensitivities because the slightest mistake may cause irreparable damage to the vessel. For these reasons, marine companies always seek to perform these operations in the best possible way and with the highest efficiency [1].

Due to the high volume of exchanges, the maritime industry is trying to move towards increasing productivity. One of the sectors that can be investigated is the operations of berthing and unberthing vessels.

In this article, the processes of berthing and unberthing of vessels are modeled by using machine learning. With the help of machine learning, it is possible to model the phenomena without having a very deep knowledge of the sciences governing the phenomena, and it also takes less time and cost than simulating with software.

Because machine learning only uses mathematical models, it may not be very accurate in simulation, which accuracy can be measured with formulas, so it uses optimization algorithms to increase the accuracy of these modelings. Optimization algorithms do not only use mathematical models but also use a series of natural optimal patterns that have emerged as a result of evolution and have become computer codes. In this article, a genetic algorithm is used to optimize the model.

With this method, the most optimal mode can be found for these processes with the lowest cost.

2. Modeling

Modeling is a series of mathematical processes in which a phenomenon in the real world is transformed into a function in the computer with the help of its effective parameters. This process can be done with the help of a series of interface software or modeling codes.

3. Machine Learning

It is a relatively new branch of computer science, based on some branches of mathematics, which can be used to produce a logical function called "objective function" for various phenomena and examine those phenomena with this function. In this project, with the help of machine learning, a function has been produced for the berthing and unberthing of vessels, and with these functions, the time of these operations can be predicted [2]. For berthing, the following function was produced with 66% accuracy. This modeling has been done using the data collection of the hydrodynamic parameters of the vessels and the recorded duration of their mooring. Its accuracy was calculated by comparing the obtained formula with 20% of the data by using the root mean square (RMS):

$$y = (-8.97152895e - 2)\theta_1 + (2.34200694e)\theta_2 + (-6.05977043e - 1)\theta_3 + (4.6380793e - 5)\theta_4 + (-4.82403305e)\theta_5 \quad (1)$$

Θs are the parameters of the float, i.e. length, width, water inlet and submerged volume of the float, and the number of tugs.

$$y = (1.48213362e - 2)\theta_1 + (3.88313961e - 1)\theta_2 + (1.25566456e)\theta_3 + (4.30987512e - 5)\theta_4 \quad (2)$$

For unberthing, a formula similar to the above formula was obtained, with the difference that the coefficient of the number of tugs becomes zero, and this factor is removed from the formula, and the formula is as follows:

The accuracy of this function is 40%.

4. Optimization

Optimization is a type of modeling, but instead of using only mathematical concepts, it uses algorithms derived from the social behavior of living organisms [3]. These algorithms have converted some social behavior of living

organisms, such as finding food, which has improved during evolution and becomes the most optimal form, into codes and mathematical patterns. There are different optimization algorithms such as artificial neural networks or ant nests. This project uses the genetic algorithm derived from Darwin's theory [4].

After applying the genetic algorithm to the data by "GeneXproTools" software, the berthing function was obtained as follows, which has an accuracy of 70%:

$$\left(d[3]+\left(\frac{\left(\left(\left(\frac{d[5]+d[3]}{2}\right)+d[4]\right)+\left(\frac{G_1C_1+d[3]}{2}\right)\right)+d[3]}{2}\right)\right)+ep3Rt(d[3])+\left(\frac{d[1]+d[3]}{2}\right) \quad (3)$$

and:

$$G1C1 = -4/48469496749779$$

For its unberthing, a function with 96% accuracy is produced as follows:

$$\left(d[1]-\left(\left(\frac{\left(\frac{d[2]+G_1C_6}{2}\right)+(d[1]-G_1C_3)}{2}\right)+\left(\frac{gepMax2(G_1C_6,G_1C_6)+d[2]}{2}\right)\right)\right)+\left(\frac{(G_2C_6-G_2C_5)+d[1]}{2}\right)+((((gepMax2(d[1],G_2C_4)-d[1])+G_2C_2)+d[2])-G_2C_3) \quad (4)$$

and the registers are equal to:

$$G1C6 = -3/8706625568407$$
$$G1C3 = -1/6971343119602$$
$$G1C8 = 7/22281563768426$$
$$G1C9 = -6/38721884823145$$
$$G2C6 = -0/60396130252998$$
$$G2C5 = -6/00573747978149$$
$$G3C3 = 4/26581926938688$$
$$G3C2 = 3/20093417157506$$
$$G3C4 = 4/37604907376324$$

The figure below shows the convergence of the actual and optimization results, the yellow line is the actual results and the green line is the optimization results for the unberthing process:

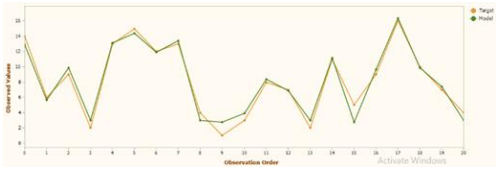

Figure 1. Convergence of real results and optimization for unberthing

5. References

[1] A master's Guide to: Berthing/2021/Standard Club
[2] IBM Developer Skills Network/Saeed Aghabozorgi/2020/IBM Corporation
[3] Ferreira, C. (2001), "Gene expression programming: A new adaptive algorithm for solving problems," Complex Systems, 13 (2): 87-129.
[4] A Simulation Model for Optimization of the Internal Handling Fleet Size at Shahid Rajaee Container Port Based on Performance Evaluation/Parham Azimi, Mohammad Reza Ghanbari/Journal of Optimization in Industrial Engineering 8 (2011) 19-3

DETERMINING OF MARINE TOURIST AND PASSENGER DOCKS LOCATIONS FOR GUILAN PROVINCE USING AN AHP APPROACH

Mehdi Kamyab Roodsari[1], Mohammad Ali Sotoudeh[2], Vahid Salmasi[2], Kazem Esmailpour[2]

1) Maritime Tourism Infrastructures Development, Port and Maritime Organization, Tehran, Iran, mkamyab@pmo.ir
2) Farasazan Handaseh Consulting Engineers, Tehran, Iran, fshandaseh@gmail.com

1. Introduction

Tourism in the third millennium is considered as one of the most important drivers for the development of territories. The World Tourism Organization has predicted more than 2 billion international tourists by 2035. Per each land-visiting tourist that enters a country, 12 jobs are created, while per each marine tourist, 15 jobs are created. In 2019, the Middle East has taken a larger share of world tourism than other regions of the globe with an 8% growth in the tourism sector. Iran is among the top 10 countries in the world in terms of natural resources. However, Iran has not taken advantage of the mentioned opportunities until now. In fact, Iran has been ranked 89th in terms of attracting tourists amongst 140 countries in the world. Despite the fact that the tourism sector is considered as one of the most important sources of income for many developing countries, this sector comprises less than 0.5% of the Iran's economy.

The main purpose of this study is the site selection of recreational and passenger harbors in the coasts and ports of Guilan province to take the advantage of tourism potentials of the area that have been of interest to tourists due to their special ecological, structural and spatial characteristics. With regard to tourism in marine and coastal environments, in the first decade of the 2000s, Hall [1] claimed that “marine and coastal tourism is one of the fastest growing areas among the world’s largest industries. Yet despite increased public awareness about the economic and environmental significance of marine tourism, it is only in recent years that a substantial body of research has emerged”. Coastal and offshore areas (as destinations of sailing tourism) have been rarely noticed compared to other forms of maritime tourism. In recent years, among relatively infrequent publications where studies on maritime sailing tourism have constituted the subject of interest, one can cite the following examples: Parrain’s analysis of sailing routes and stopovers across the Atlantic [2]; a study of critical factors in the maritime yachting tourism experience [3]; an estimation of the economic impacts of yachting in Greece by means of the tourism satellite account [4].

Guilan province, on the coasts of the Caspian Sea, from Chaboksar in the east to Astara in the west, has more than 270 km of coastline, and the tourist attractions of this province are well-known nationwide. Before the covid-19 pandemic, it hosted about 30 million tourists every year. Considering the importance of marine tourism and the potentials of Guilan, in this study, a comprehensive study on the coastline of this province has been done using AHP approach. The results of this study have been extracted in the form of GIS maps.

2. Methodology

In this study the multi-criteria decision-making method was applied to determine the priorities of site selection of recreational and passenger ports considering the key parameters. Table 1 shows the effective key parameters for planning of tourist and passenger ports and docks. As mentioned in table1 each of main parameters is divided to one or more detailed parameters.

Having introduced the key parameters, they are weighted by forming a group of experts. Then, according to the available statistical studies and field observations, points are assigned to each of coastal locations.

3. Result and Discussion

The results of this study are extracted in the form of GIS maps. Two scenarios of recreational docks and marine traveling terminals are considered. It should be mentioned that the key parameters in two scenarios have different impacts. The priorities of 1. Tourist and 2. Traveling docks and port locations are shown in figure 1 and 2.

As shown in these figures, by respect to zones with highest points, Astara, Anzali, and chamkhale can be introduced as the most potential coasts for planning and development of recreational and tourist docks and Astara, Anzali’s marina, Caspian free zone, and Chamkhale for passenger ports.

Table 1. Key Parameters

Indicators	Main criteria
Climatic comfort of tourists	Climate
Biocapacity (per capita)	Environment
Ecological footprint (per capita)	
Distance from environmentally sensitive areas	
Distance from sensitive infrastructure areas	
Earthquake	Natural hazards
Flood	
Landslide	
Storm	
Waves	
Storm surge	
Water level fluctuations	
Sedimentation	
Population density	Social
Distance from residential zones	
Safety	
Roads	Accessibility
Rails	
Airport	
International accessibility	
Coastline accessibility	
Port accessibility	
Province intake	
Intra-provincial trips	Trips
Extra-provincial trips	
Intra-provincial passengers	
Extra-provincial passengers	
Distance from attractive zones	Tourists
Distance from selected tourism zones	
Distance from selected tourism corridors	
Distance from Elite Tourist Village	
Tourism ranking	
The residential facilities	
Catering services	
Distance from coastal tourism centers	

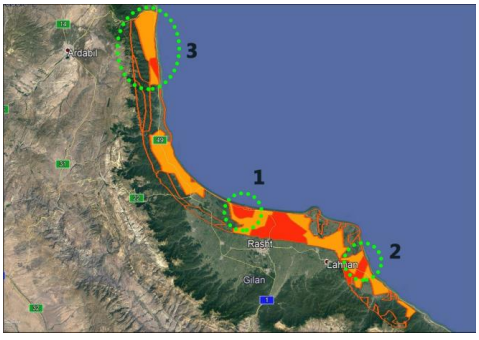

Figure 1. Priorities of recreational and tourist docks

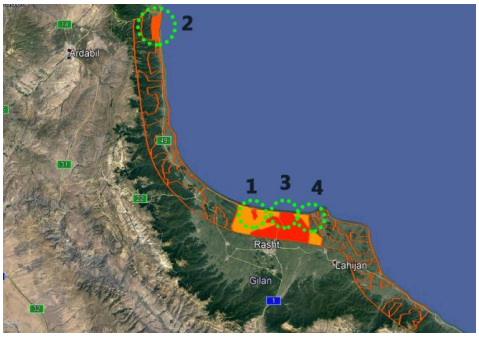

Figure 2. Priorities of passenger ports

4. Conclusion

In this study, the research purpose, i.e. the determination of priority of site selection for passenger-tourism ports and docks in the Guilan province, have been presented. The Analytic Hierarchy Process (AHP) approach was applied to investigate multiple criteria impact. Due to its unique assets in the country, Guilan province has always been considered as one of the most important tourist destinations. On the other hand, tourism is one of the topics that has not been properly emphasized in the field of planning and design focusing on the development of the coasts and ports of Guilan province. In this study, a comprehensive survey has been done on existing tourism and marine travel destinations of Guilan coasts; Then by defining the key parameters and assigning weight to them, a GIS map of the desired areas for planning and developing has been extracted. The results of this study show that Haviq, Anzali, Chamkhale and Caspian free zone, are the first priorities for establishing docks.

5. References

[1]. HALL, C. M. (2001): Trends in ocean and coastal tourism: the end of the last frontier? Ocean & Coastal Management, 44(9–10): 601–618.
[2] PARRAIN, C. (2011): Sailing Routes and Stopovers: Spatial Disparities Across the Atlantic. In: Micallef, A. Journal of Coastal Research (Special Issue), 61: 140–149.
[3] MIKULIĆ, J., KREŠIĆ, D., KOŽIĆ, I. (2015): Critical factors of the maritime yachting tourism experience: an impact-asymmetry analysis of principal components. Journal of Travel & Tourism Marketing, 32: 30–41.
[4] DIAKOMIHALIS, M. N., LAGOS, D. G. (2008): Estimation of the economic impacts of yachting in Greece via the tourism satellite account. Tourism Economics, 14(4): 871–887.

14th International Conference on Coasts, Ports and Marine Structures
9 & 10 May 2023 , Tehran-IRAN
ICOPMAS 2022

NECESSITY OF DEVELOPING SEA PASSENGER INFRASTRUCTURE OF TURKMEN PORT

Zahra Rashid[1], Fazilat Fakher[2], Reza Tayebi[3], Mahdi Kamyab Roudsari[4]

1) Faculty of Architecture, University of Tehran, Tehran, Iran, zahra.ra222@gmail.com
2) Department of Urban Design & Planning, University of Shahid Beheshti, Tehran, Iran, fazilat.ff@gmail.com
3) Pars Geometry Consultants, Tehran, Iran, r_tayebi@parsgc.com
4) Maritime Tourism Infrastructure Development, Ports & Maritime Organization, Tehran, Iran,mkamyab@pmo.ir

1. Introduction

Turkmen Port is located on Southeast of the Caspian Sea and on the east coast of Mian-Kale Bay in Iran. Gorgan Bay, due to the existence of Ashuradeh and Miankalah islands, there is the possibility of creating suitable marine tourism projects. Turkmen Port is one of the recreational and touristic ports of this region and provides tourism services for domestic and foreign travelers. The infrastructure of the port was the basis of port activities, the quality of which affects the better performance of the port, but the decrease in the water level of the Caspian Sea in the past years, the existing infrastructure for the marine tourism industry, including the existing docks, has faced many problems in operation.

Figure 1. The current activity status of the port

In this article, the future of Turkmen port and its development plans are discussed. Port infrastructure is the basis of port activities for serving ships, moving cargo and passengers. The development of port infrastructure requires long-term investment and planning. Continuous improvement of the quality of port infrastructure is critical for developing countries as it contributes to better port performance.

2. Discussion and Detect

The future performance and development of the port can be predicted according to the country's macro-economic and political situation as well as plans and documents that affect the legal functions and procedures related to the development of sea passenger infrastructure in Turkmen port. The following results have been obtained from the study of comprehensive plans of commercial ports, comprehensive plan of small ports, integrated management plan of coastal areas, comprehensive tourism plan and urban comprehensive plans:

1-Turkmen port is one of the small ports with multi-purpose use and function. 2-The high nature tourism attractions of the region have the potential of cultural, sports and nature tourism. 3-Gorgan Bay is appropriate for building resort islands and has recreational and championship level boating capabilities. 4-Turkmen port is considered as a recreational and economic tourism destination. 5-The problem of Gorgan Bay is the heavy sedimentation of the opening and the access channel, due to which the port has dried up and has no special function. 6-Tourism plans in the region lead to the reconstruction plan of Bandar Turkmen beach and Ashurade Island. 7-One of the environmental capabilities and limitations of Bandar Turkman city is its proximity to Gamishan wetland, which is one of the most important wetlands and valuable habitats for native and migratory birds. 8-Most spaces seen in the tourism plan of Ashuradeh Island have been moved to the coast of Bandar Turkmen due to the problems that may cause for island environment. 9-It is proposed to organize or hand over Turkmen port. 10-Turkmen port should be considered with the current local function or change of use. 11-touristification has been suggested for Turkmen port. 12-The landlord model is appropriate. 13-The port has a tourist pier suitable for boating.

Identifying the current state of the port, including its strengths and weaknesses, and examining the limitations and opportunities for progress are necessary for the development of Turkmen port infrastructure. One of the important features of this port is the extension of the railway line up to the pier and the connection of this line to the national rail network. On the other hand, due to the lowering of the water level and the receding of the sea level, the harbor basin is filled with mud and sediments, so the water depth at the bottom of the docks is not sufficient for safe boat traffic and mooring. The approximate length of the main breakwater arm of Turkmen port is 165 meters. This port is connected to the city water network, electricity and telephone facilities and it has a VHF device. This port has 500 square meters of office building and 3300 square meters of covered warehouse.

Since Turkmen port is considered as a passenger and tourism port, the needs of development according to this port's circumstances should be considered. In this article, it has been discussed that with attracting domestic and foreign tourists, sea travel with cruise ships, sea tours, recreational floating parking, water and sea sports and sightseeing and shopping on port hinterland, the following results have been obtained:

1-Due to the low water level and the problems of Turkmen port, the ferry terminal and the cruise terminal in Turkmen port are not operational. Therefor a marina can be built for the establishment of pleasure boats in order to activate marine tourism in Turkmen port, and it can be considered as a place for parking pleasure boats.

2- Due to the low depth and low turbulence of the sea, the beaches of Bandar Turkman are prone to water sports and the ability to sail at a recreational and championship level.

According to the latest statistics obtained from the Cultural Heritage and Tourism Organization, the Ports and Maritime Organization and field studies, the number of passengers has increased between 1988 and 1995 with an average slope of 13%. And in 1996, it decreased by 67%.

The decrease in passengers may be due to the problems that have occurred and the decrease in water depth, so it is expected that with the improvement of the existing situation, the increase in the number of passengers will take the same increasing trend as before, and considering the 13% slope of the increase in passengers, the number of passengers in the peak month in the next 15 years will reach The number will reach about 140 thousand people. According to calculations, on average, during the peak month, about 650 people visit the pier per hour. On the other hand, the depth of the water and its limitations, the port can accommodate a 6-meter-long and 2.3-meter-wide boat with a 0.6-meter intake.

The strategic direction for this port should be conservative. Ports that have inappropriate economic performance and continue to operate only due to the dependence of local communities, need minimal reforms to fulfill the governance duties of the ports organization and reach a stable state. According to the reviews, forecasts, feasibility, capabilities and opportunities of the region and Turkmen port infrastructure, the following uses can be considered in the port: 1-Tourism and tourist complex, 2-Craft market, 3-Beach camping, 4-Commercial, 5-Sports fields, 6-Restaurant and traditional tea house, 7-Temporary accommodation camping, 8-Lookout, and the development of sports such as: 1-Boating, 2-Horse riding, 3-Cycling.

Factors that are effective in the physical design of Turkmen port include: 1-Wharf location, 2-functional relationship desirability, 3-economic optimization, 4-Coordination by condition of the land and existing uses

3. Summary and Proposed Plan

The final plan of the required uses of the port is presented in ***Figure 2***.The water sports and passenger services of the port have been formed according to the location of the pier around it. The existing shed space is proposed for service and welfare uses, and administrative development has been seen in the same direction as the existing office buildings, and recreational-sports spaces have been placed next to the water sports pool. At 60 meters from the end of the pier, a shade is proposed for the comfort of passengers. In order to make maximum use of the available features of the site and organize the train buses that arrive at the port, a canopy has been planned for boarding and disembarking passengers.

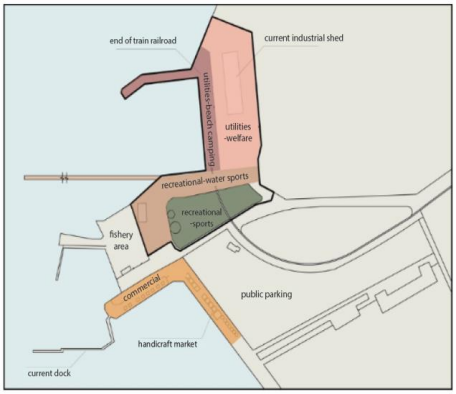

Figure 2. The proposed plan of Turkmen port

The studies and investigations on the necessity of developing Turkmen port infrastructures show:

1- Turkmen port is playing support role for Miankala port. This has become necessary for the development of Turkmen port in recent years, due to the environmental limitations of development in Miankala region.

2- The development of the infrastructure of Turkmen port, considering the nature tourism attractions, the cultural, sports and nature tourism potential of the region will increase the port's passengers, which is accompanied by commercial and economic prosperity. 3- The receding of the sea has caused the existing unsafe pier to lose its function, and it is necessary to build a suitable pier with a longer length for the operation of the port again.

4. References

[1]. NCE company. 2007. Tourism Village Master Plan (Sounds of Life in Eastern Caspian)
[2]. The Central Headquarters of the Coordination of Travel Services of the country-www.AmareSafar.ir
[3]. Vice President of Investments and Plans. Office of Sample Tourism Areas. Bandar Turkmen Coast. Code: 270203
[4]. Consulting Eng. of Pouya Tarh Pars. 2018. "Identifying and providing emergency solutions to save Gorgan Bay and Miankale Lagoon"
[5]. IR.Ports and Maritime Organization. MAAB Consulting Eng. ICZM integrated management plan studies of the country's coastal areas. Optimal land use plan of the country's coastal areas. Studies of cultural heritage and tourism.
[6]. IR.Ports and Maritime Organization. 2007. Comprehensive plan of commercial ports.

14th International Conference on Coasts, Ports and Marine Structures
9 & 10 May 2023 , Tehran-IRAN
ICOPMAS 2022

PORT PLANNING APPROACHES IN DECREASING WATER LEVEL CONDITIONS (CASE STUDY: LAKE URMIA)

Arman Aminzadeh Vahedi[1], Mahdi Kamyab Roudsari[2] and Saman Zare[3]

1) Adab Danan International Management & Investment Consultant Group, arman_aminzadeh@yahoo.com
2) Project Manager for Maritime Tourism Infrastructures Development, PMO, Tehran, Iran, mkamyab@pmo.ir
3) Adab Danan International Management & Investment Consultant Group, Tehran, Iran, saman_zare@ut.ac.ir

1. Introduction

Water level fluctuations in water bodies such as seas or lakes is mainly resulted from climate change, construction of dams, excessive exploitation of water resources and unprecedented droughts.

This phenomenon can affect the performance of the coastal systems in different ways such as inundation of coastal facilities, excessive flooding, erosion and also disrupting the ongoing port operations which can cause undesirable socio-economic impacts considering the vital role of ports in the coastal zone economy [1].

Although the potential impacts of water level changes have become a growing concern for communities around the world, few studies have been conducted to assess the effects of this matter on port inoperability and possible solutions for improving the performance of ports in these conditions [2].

Lake Urmia, located in northwest of Iran with a recorded area of about 5,500 square kilometers, has experienced severe water level decrease of around 7 meters in the past 25 years mainly due to excessive exploitation of groundwater resources and construction of dams for agricultural purposes [3,4]. Subsequently, Golman Khaneh and Sharaf Khaneh -the two recreational ports of the lake- have become almost inoperable. The study area and location of aforementioned ports is displayed in *Figure 1*.

The main objective of this research is to evaluate important factors regarding port development approaches in these circumstances using analytical hierarchy process (AHP) method for the ports of Lake Urmia

2. Methodology

This study was based on multi-criteria decision making procedures and was conducted by implementing Analytical Hierarchy Process (AHP) method [5]. First, evaluation criterions were determined using Delphi method. Then, importance factor for every criterion was estimated using pair-wise comparison matrix. The selected criterions were as follows:

- Development costs
- Ease of construction
- Simplicity of navigation operations
- Simplicity of port service operations
- Dependence to lake water level

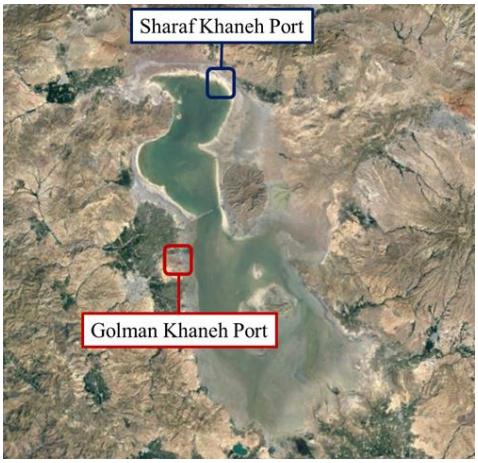

Figure 1. Study area

The considered approaches in development of Lake Urmia ports masterplan were as follows:

- Convergent onshore approach (constructing an artificial basin using breakwaters and directing water to the port location through dredged channels- AP1- Figure 2-a)
- Divergent onshore approach (constructing an offshore platform and accessing via fixed piers- AP2- Figure 2-b)
- Divergent offshore approach (constructing an offshore and accessing via specialized vessels e.g. air boats- AP3- Figure 2-c)
- Subsequently, each approach was evaluated based on each criterion and the most suitable approach was determined. Hierarchical structure of the study is presented in Figure 3.

3. Results and Discussion

The importance factor of criterions were calculated after analyzing the pair-wise comparison matrix results. As shown in *Table 1*, “dependence to lake water level” proved to be the most important criterion.

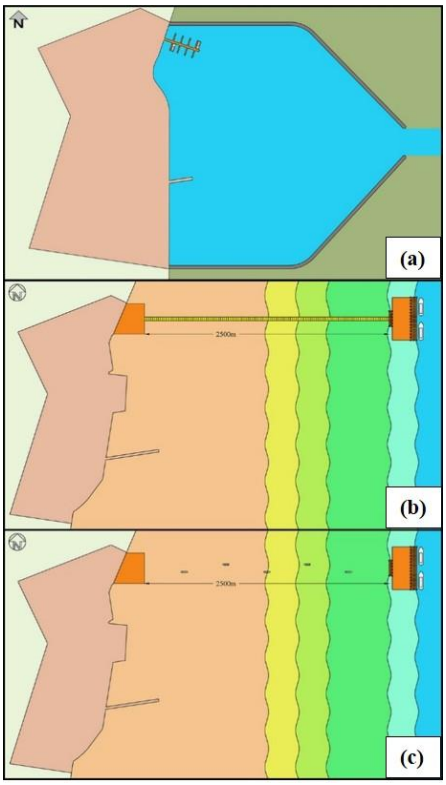

Figure 2. Conceptual development approaches for Lake Urmia ports

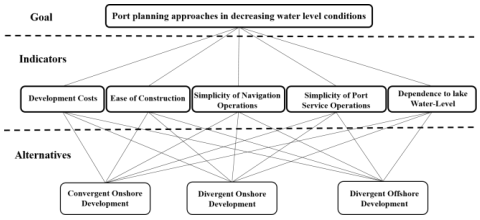

Figure 3. Hierarchical structure of the study

Table 1. Calculated importance factor for each criterion

Criteria	Importance Factor
Dependence to lake Water level	0.376
Simplicity of Navigation Operations	0.235
Simplicity of Port Service Operations	0.177
Development Costs	0.123
Ease of Construction	0.088

According to the results of pair-wise comparison of the approaches with regard to each criterion (*Table 2*) convergent onshore approach was selected as the most suitable approach.

Table 2. Evaluation values of each approach

Criteria	Evaluation Value of Approaches		
	AP 1	AP2	AP3
Dependence to lake Water level	0.778	0.111	0.111
Simplicity of Navigation Operations	0.294	0.157	0.594
Simplicity of Port Service Operations	0.626	0.243	0.132
Development Costs	0.613	0.251	0.136
Ease of Construction	0.540	0.297	0.163
Overall	0.565	0.186	0.249
Ranking	1	3	2

4. Conclusion

Due to the current situation of Lake Urmia, dependence to the water level proved to be the most important factor in development planning of ports. Reviving the two ports by constructing an artificial basin using breakwaters and directing water to the port location through dredged channels - convergent onshore approach- was selected as the most suitable approach for this matters mainly because direct access to water is provided with a higher level of certainty.

5. Acknowledgements

This study was conducted as a part of “Lake Urmia Maritime Tourism Masterplan” studies and was supported by the Department of Maritime Tourism Infrastructure Development of the Ports & Maritime Organization of Iran.

6. References

[1] Hardy, R. D., Hauer, M. E., "Social vulnerability projections improve sea-level rise risk assessments," Applied Geography, vol. 91, pp. 10-20, 2018.
[2] Gracia, V., Sierra, J. P., Gomez, M., Pedrol, M., Samp´e, S., García-Le´on, M., & Gironella, X., "Assessing the impact of sea level rise on operability using LIDAR-derived digital elevation models," Remote Sensing of Environment, vol. 232, 2019.
[3] Urmia Lake Restoration National Committee, Hydrological database, available at: www.ulrp.ir/en/hydrological-data/.
[4] Parsinejad, M., Rosenberg, D., E., Alizade Govarchin Ghale, Y., Khazaei, B., Null, S., E., Raja, O., Safaie, A., Sima, S., Sorooshian, A., Wurtsbaugh, W., A., "40-years of Lake Urmia restoration research: Review, synthesis and next steps, Science of The Total Environment," vol. 832, 2022,
[5] Saaty, T.L., "Decision making with the analytic hierarchy process", Int. J. Services Sciences, Vol. 1, No. 1, pp.83–98, 2008.

14th International Conference on Coasts, Ports and Marine Structures
9 & 10 May 2023 , Tehran-IRAN
ICOPMAS 2022

ANALYSIS OF HEAVY LIFTING ON AN ANCHORED TUBULAR PILE QUAY-WALL

Mehdi Shahmohamadi[1] and Amir Davazdah Emami[2]

1) Structural Engineer, Ph.D., Tehran, Iran, mshahm@ut.ac.ir
2) Marine Structures Engineer, Taghdis Tehran, Iran, a_demami@yahoo.com

1. Introduction

This paper represents the structural analysis of an anchored pile quay wall located in quay 3 of Khadamti Pars port in Asaluyeh, Iran.

The heavy lifting operation was mandatory for unloading two reactors with 915 tons gross weight from a general cargo ship; however, the quay was not designed or previously utilized for such operation, and thorough analysis for a safe and reliable operation by ensuring the sufficient strength of the system and avoiding any minor damage to the quay was of high importance.

After some site visits, the structural strength of the quay-wall system was assured by utilizing the as-built drawings and a rational analysis procedure.

A brief review of applied loads, structural model, and execution procedures is presented here.

This study directed to the extension of the capacity of the wharf and presented a reliable procedure for similar future operations.

2. Lifting Plan and Applied Loads

Two cranes of MANITOWOC M18000 with 750 tons and TEREX/DEMAG CC6800 with 1250 tons capacity were used for lifting. After lifting the loads from the ship, two bogies with 19 axes were used to transfer the reactors to the installation site. The execution plan is shown in the flowing figure:

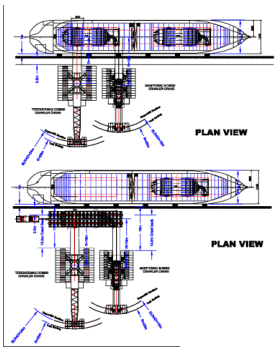

Figure 1. The execution plan for heavy lifting.

From the calculations in the execution plan, the applied loads beneath the crawler cranes were obtained. To reduce the applied pressure, two types of wooden and steel spreader mats were utilized beneath the undercarriage of cranes. The size of each mat varied from 6 to 8 meters, leading to the following applied pressures.

Table 1. Applied pressure beneath the undercarriage of cranes and under bogie tires.

Equipment	Applied Pressure (t/m^2)	Reduced Pressure (t/m^2)
TEREX/DEMAG CC6800	57.3	24.9
MANITOWOC M18000	60.2	23.6
Bogie	60	19.84

3. Structural Model

Based on as-built drawings of the quay, a simplified structural model for each case of applied loads was created.

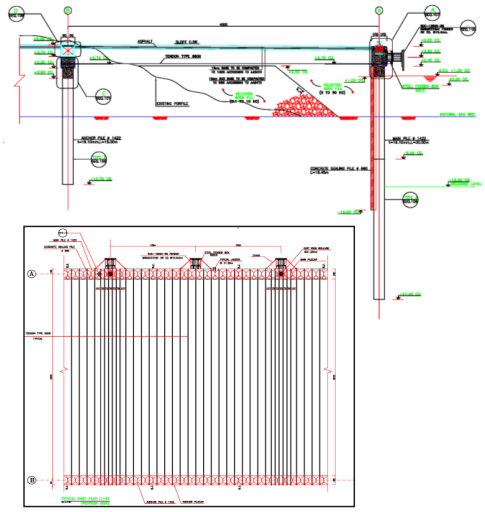

Figure 2. Section and tie rods plan of quay 3.

All steel piles were hollow tubular of grade X52 with a minimum yield strength of 355 MPa and diameter of 56 inches and 3/8 inches' thickness, and for corrosion allowance, the thickness of piles was reduced to 16.1mm. All tie rods were tendons with seven wires of grade 6809 from Dywidag Company and 1.5 meters spacing with increasing the numbers to three near the positions of bollards. Beside the wall, rockfill with different sizes and weights ranging from 5 to 50 kilograms was poured.

3.1. Applied Loads

From the previous calculations in the execution plan, the applied pressure on the surface of the wharf is given in below figures in three cases:

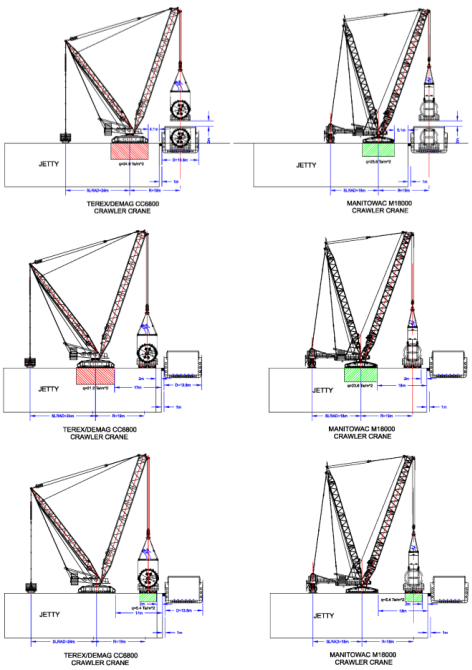

The applied active lateral earth pressure on the quay wall was calculated as in [1].

3.2. Structural Analysis of Quay Walls

For the calculation of structural demands of steel tubular piles and tie rods, SAP2000 and PLAXIS software was utilized. The force in tie rods is given below:

Table 2. Forces in tie rods

Case	F(kN)
1	1232
2	1059
3	1220

Considering the design codes, the capacity of cables was about 2500kN, which shows the adequate capacity of tie rods. Also, the maximum stress ratio of piles was below 0.95.

During the operation, two theodolite surveying were used to control settlement or any unusual deformations. It was seen that the maximum deflections were about 3 millimeters.

Figure 3. During operations pictures

4. Conclusion

Based on a simplified approach, an anchored sheet-pile quay-wall is analyzed for the heavy lifting operation of two 915 gross weight reactors.

The analysis has been verified through field operation, showing the accuracy of the analysis procedure.

This analysis represented the capacity of similar future operations leading to diversifying the operational capability of the port.

5. References

[1]- Advanced Soil Mechanics, Braja. M. Das., Third Edition, 2007.

14th International Conference on Coasts, Ports and Marine Structures
9 & 10 May 2023 , Tehran-IRAN
ICOPMAS 2022

APPLICATION OF THIN DAMPING PLATES IN A SEMI-SUBMERSIBLE PLATFORM TO REDUCE HEAVE MOTION RESPONSE

Arefeh Emami[1] and Ahmad Reza Mostafa Gharabaghi[2]

1) Department of Civil Engineering, Hormozgan University, Bandar abbas, Iran, emami@hormozgan.ac.ir
2) Faculty of Civil Engineering, Sahand University of Technology, Tabriz, Iran, mgharabaghi@sut.ac.ir

1. Introduction

A semi-submersible platform is one of the most favorable semi-floating units used for gas and oil exploration in deep waters due to its large deck area and payload capacities. However, conventional semi-submersibles are susceptible to the heave motion response which this can often limit the operability of drilling rigs or even lead to damage to the risers and mooring system. Therefore, it is important to improve the heave motion of this platform. Moreover, it is necessary to shift its natural heave frequency away from the frequency of daily waves because of resonance phenomena. In the literature, different concepts have been suggested for reducing the heave motion of semi-submersible such as modifying its geometry, adding its draft, installing heave plates or additional material [1-4].

In this study, the installation of thin damping plates (TDPs) at the top and bottom of the pontoons of a typical GVA 4000 drilling semi-submersible platform was proposed to reduce its heave motion response under the action of a monochromatic small amplitude wave train propagating. An analytical solution based on the Eigenfunction Matching Method (EMM) was applied to determine the heave motion. After ensuring the solving process, TDPs were added to the pontoons of the semi-submersible platform. The effects of TDPs with different sizes on heave motion behavior were investigated. The results of the heave motion response showed that the modification of the conventional semi-submersible using TDPs not only reduces the heave motion response but also displaces the resonant frequency to a lower frequency.

2. Mathematical Model

Consider a typical GVA4000 drilling semi-submersible in a constant water depth of h_1. As a schematic, two thin-damping plates are attached at the top and bottom of its pontoons. The Cartesian system is chosen on the free surface water that its origin is in the center of the semi-submersible platform with z axis vertically upward and x axis horizontally along the pontoons. It is assumed that the fluid is incompressible, inviscid and the flow is irrotational. Because of considering a monochromatic small amplitude wave train propagating in the x direction, the problem can be simplified as 3-D to 2-D [5]. Thus, the velocity potential is written as the following:

$$\varphi(x,z,t) = Re\{\phi(x,z)\}e^{-i\omega t} \quad (1)$$

Where 'Re' is the real part of complex expression, ϕ is the spatial part. In the wave-structure interaction issue, the wave field incident upon a floating structure can be divided into two parts: scattered wave field (ϕ_S) and radiated field (ϕ_R). The scattering potential is decomposed into the diffraction wave potential (ϕ_D) and the incident wave potential (ϕ_I). Thus, the velocity potential is decomposed as the following:

$$\phi = \phi_I + \phi_D + \sum_{L=2}^{4} \phi_R^L \quad (2)$$

where L =2, 3, and 4 are related modes of sway, heave, and roll oscillations, respectively. In this study, the wave train is assumed to be a small amplitude wave, so, induced motion of the structure can be assumed to be small, therefore, the interaction between different modes can be ignored. Thus, the heave mode is just considered. Moreover, the wave potential is obtained by assuming the linear wave of airy theory and the velocity potential satisfies the Laplace equation. According to what was said, the incident wave potential is extracted in the absence of the semi-submersible as Equation 3.

$$\phi_I = -i\frac{Ag}{\omega}\frac{cosh(k(z+h_1)}{cosh(kh_1)}exp(ikx) \quad (3)$$

The radiation potential is calculated by assuming the oscillation of the structure in the absence of waves. So, to calculate the radiation potential, a typical GVA4000 semi-sub with two TDPs is considered (Figure 1). Firstly, the radiation potential is expressed as Equation 4.

$$\phi_R^{(3)} = Re\{-i\omega A_R^{(3)}\phi_R^{(3)}(x,z)\} \quad (4)$$

where, $A_R^{(3)}$ is the heave oscillation displacement. Secondly, the fluid domain is divided into 12 different regions. The governing Laplace equation and the related boundary conditions for each region are considered. The equation of radiation potential in each region is extracted using the method of variables' separation. Then, the unknown coefficients appearing in each equation are estimated using EMM. Notability, the EMM is a common solution technique for wave radiation and scattering problems. After calculating the radiation and incident potential, the added mass and damping are extracted form real and imagine parts of the radiation potential. Also, the exciting forces is calculated using Haskind method. So, the heave motion displacement is determined by solving the one degree of freedom equation. Finally, response amplitude operator (RAO) is obtained. Note that the RAO provides the response amplitude of the platform per unit incident wave amplitude. By multiplying 2nd power of the RAO in wave spectrum, the heave motion response spectrum is calculated.

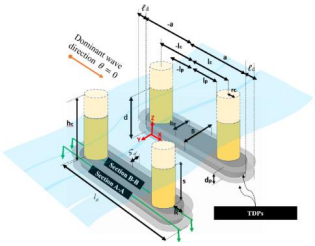

Figure 1. A GVA4000 with two TDPs as schematic

3. Verification of the Developed Solution

To ensure developed analytical solution for the heave motion response of the platform under study, the GVA4000 without TDPs was considered and compared with the experimental results of Clauss and Schmittner [6]. Except for the peak value, the developed method can predict the heave motion response with acceptable accuracy (Figure 2).

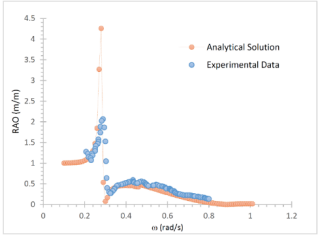

Figure 2. Comparison between the analytical solution and experimental data

4. The Results and Discussions

To determine the heave motion response of the modified GVA4000, it is assumed that this platform has been located at North Sea, and a JONSWAP spectrum with a significant wave height of 11.92 m and zero-up crossing period of 10.8 s is governed on it. The heave RAO and the response spectrum of modified GVA4000 with variable TDPs are illustrated in Figures 3 and 4, respectively. The values of frequency in RAO peaks, the heave motion response, and the percentage of improving the heave motion response rather than the original platform are presented in Table 1. The results illustrated that even using TDP with minimum width ratio of B/bp=1.1 reduces more than 20% the heave motion response, as well as the natural heave frequency of the modified GVA4000 is shifted away from the daily waves' frequency.

5. Conclusion

In this study, two TDPs were added to the pontoons of a typical GVA4000, and its heave motion response was investigated by an analytical method. The results showed that to apply TDPs significantly decreased the heave motion response. Moreover, it can shift away natural frequency from the daily wave frequency, so, the risk of creating a resonate phenomenon will be almost eliminated. It is concluded that to attach TDPs to the pontoons of a semi-submersible drilling platform can improve its performance, particularly in the heave motion.

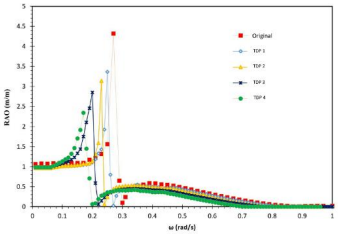

Figure 3. RAOs of modified GVA4000 with variable TDPs

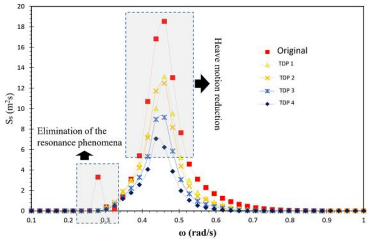

Figure 4. Heave response spectrum of modified GVA4000

Table 1. percentage decrease of heave motion response

TSDs with various sizes		Frequency in RAOs peak (rad/s)	Heave response (m)	Percentage decrease of heave motion response
TDPs	B/dp			
TDP 1	1.1	0.25	2.3764	21.04
TDP 2	1.2	0.23	2.3138	30.08
TDP 3	1.4	0.2	1.9786	52.25
TDP 4	1.6	0.17	1.6816	78.8
Original		0.28	3.01	-

6. References

[1] Wang, S., Cao, Y., Fu, Q., and Li, H. "Hydrodynamic performance of a novel semi- submersible platform with nonsymmetrical pontoons", *Ocean Engineering.* 110, 2015, pp. 106-115.

[2] Zhu, H., Ou, J., and Zhai, G., "Conceptual design of a deep draft semi-submersible platform with a moveable heave plate", *Journal of Ocean University of China.* 11 (1), 2012, pp. 7-12.

[3] Emami A, Gharabaghi AR. "REDUCING HEAVE RESPONSE AMPLITUDE OPERATOR OF A SEMI-SUBMERSIBLE PLATFORM USING PORO-ELASTIC PLATES". In The 13th Int Conf on Coasts, Ports & Marine Structures, 2018, pp. 229-230.

[4] Liapis, S., Li, Y., Lu, H., and Peng, T. ""Bigfoot" Direct Vertical Access Semisubmersible Model Tests and Comparison with Numerical Predictions". *Journal of Offshore Mechanics and Arctic Engineering,* 138(5), 2016, pp. 051301.

[5] Emami A, Gharabaghi AR. "Application of poroelastic layers in a semi-submersible platform: Devising an efficient heave motion response reduction method". Ocean engineering. 201 2020, pp. 107148.

[6] Clauss, G.F., Schmittner, C., and Stutz, K. "Time-domain investigation of a semisubmersible in rogue waves", In: *ASME 2002 21st International Conference on Offshore Mechanics and Arctic Engineering*: American Society of Mechanical Engineers, 2002, pp. 509-516

AN UNDERWATER GROUND IMPROVEMENT METHOD FOR CAISSON TYPE WHARFS

Mohammad Morsalnejad[1], Saeed Askarian[2] and Ali Fakher[3]

1) Pars Geometry Consultants, Tehran, Iran, m.morsalnejad@parsgc.com
2) Pars Geometry Consultants, Tehran, Iran, s.askarian@parsgc.com
3) Civil Engineering Faculty, Tehran University, Tehran, Iran, afakher@ut.ac.ir

1. Introduction

There is a possibility of encountering loose granular or soft fine-grained soil layers in many parts of the Iran southern coastline. These types of soils may be susceptible to liquefaction and settlement, therefore construction of marine structures such as breakwaters and wharfs on these types of soil is challenging and ground improvement is inevitable in such projects.

On the other hand, the majority of ground improvement methods that are used in nearshore areas cannot be implemented on the seabed due to reasons such as lack of specialized machinery, complexity of operations at sea, environmental problems, etc. In this paper, a practical method for the ground improvement of the seabed in a liquefiable area is introduced. The proposed method can be implemented using the equipment of marine contractors in Iran. The ground improvement method has been used under the caisson type wharfs of the newly constructed Tombak port (Figure 1) and the quality control tests performed on it indicated the acceptable quality of the implemented method.

Figure 1. Tombak port located in Pars Special Economic Zone

2. Ground Improvement Method of Replacing Self-Compacted Materials and Driving Vibration Piles

2.1. Construction Stages

Ground improvement methods should be selected according to technical, financial and time schedule conditions of the projects. In Tombak port project a 9 meters thick loose to medium dense sandy layer was encountered in the upper part of the seabed which was susceptible to liquefaction. Thus, ground improvement was necessary in order to mitigate liquefaction phenomena under caisson type wharfs. The ground improvement method included the following steps:

- Dredging to the final depth of loose and liquefiable soil
- Replacing selected granular materials
- Compacting the replaced material by driving vibration piles

Dredging and material replacement section is shown in Figure 2. Driving vibration piles into the replaced material and the plan of piles are presented in Figure 3 Figure 4.

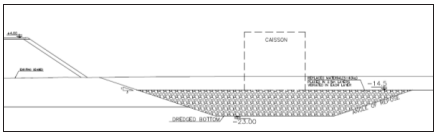

Figure 2. Dredging and replacing material section

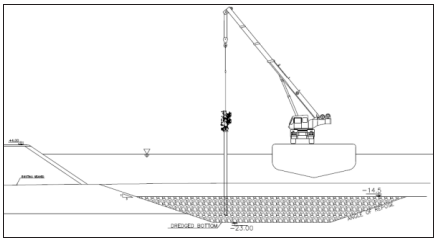

Figure 3. Driving vibration piles for the compaction of replaced material

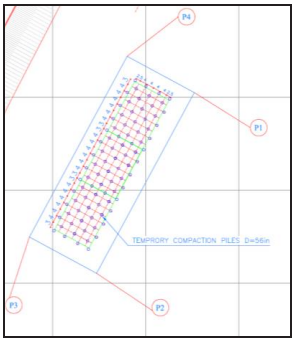

Figure 4. Vibration piles plan

2.2. The Use of Self-Compacted Materials

The materials used in the replacement method were designed to be self-compacted. Technical specifications of these materials are presented in Table 1. However, real field data and inspections revealed that due to material limitations, there is a low chance of gathering completely self-compacted materials. Hence compaction of the replaced material seems necessary. [1]

Table 1. Technical features of self-compacted materials

Specification	Range
Weight	10 ~ 40 kg
Aggregates passed through sieve No.4	<10 %
Aggregates L/D	<1.5

2.3. Vibration Piles

Although self-compacted granular materials were used to replace seabed soil but it needs some compaction because self-compacted material is an ideal theoretical material. In practice the prepared materials have some deviation to real self-compacted materials and therefore some compaction is necessary to compensate any deviation from theoretical self-compacted materials.

In order to compact the replaced materials, 56 inches' steel piles were driven into the bottom of the replaced layer using vibrator hammers. Figure 5 shows the operation of compacting materials using vibrator hammers placed on a barge [2, 3].

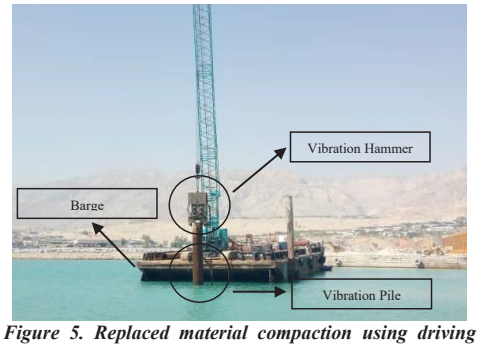

Figure 5. Replaced material compaction using driving steel piles into the bottom of the layer

3. Quality Control

In Tombak project, various methods of inspection were used to control the quality of the implemented ground improvement method which are described below.

3.1. Control of Settlement Occurred in Replaced Materials after Initial Driving of Vibration Piles

The settlement occurred during pile driving was measured by various methods. First, a diver was sent underwater to provide images of the subsided materials. Second, an index was placed from the water surface on the materials before and after pile driving and the amount of subsidence was measured. Third, the amount of settlement was measured by hydrographical survey. Results revealed a settlement equal to 5% of the replaced material height during pile driving operation. Comparison of settlement amounts with the theoretical calculations of fill material densification, revealed that the replaced materials were well compacted. [4]

3.2. Control of Vibration Time of the Piles

The time of vibration until the pile reaches the final depth of the replaced layer was considered as an indicator to measure the compaction of the replaced material. Therefore, vibration time was measured by performing secondary pile driving in the replaced materials after initial compaction. According to Figure 6, comparison of the measured values showed that the duration of the secondary vibration has increased compared to the initial vibration, which indicates desirable densification of materials during initial compaction.

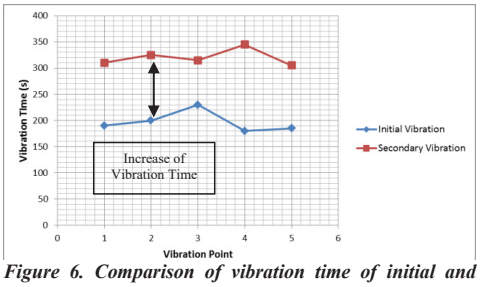

Figure 6. Comparison of vibration time of initial and secondary vibration

4. Conclusion

A new underwater ground improvement technique has been presented. It is based on (i) dredging of problematic seabed, (ii) replacement of self-compacted granular material and (iii) densification of granular material by vibration piles.

According to quality control data, the method has been successfully used in Tombak port for two caisson type wharfs. Useful data are presented in the paper as lesson learned. The presented method is applicable in similar marine projects.

5. References

[1] Pars Geometry Consultants, Geotechnical calculation report of LPG caisson wharfs, Tombak port, Assaluyeh, Iran; 2019.
[2] Jonker G., Vibratory pile drving hammers for pile installations and soil improvement projects. OTC 5422 - Offshore Technology Conference; 1987.
[3] Massarsch K.R., Fellenius B.H., Deep vibratory compaction of granular soils. Chapter 19 in Ground Improvement-Case Histories; 2005.
[4] Bement R.A.P., Ground compaction due to vibrodriving of piles. Phd Thesis, Durham University – United Kingdom; 1996.

14th International Conference on Coasts, Ports and Marine Structures
9 & 10 May 2023 , Tehran-IRAN
ICOPMAS 2022

THE INFLUENCE OF SACRIFICIAL ROCK LAYER IN TOE STABILITY OF RUBBLE MOUND BREAKWATER

Mohammadkazem Imani[1], Mehdi Shafiefar[2], Mohammadreza Kiani[3], Habib Namdari[4]

1) MSc of Marine Structures, Tarbiat Modares University, Tehran, Iran, mohammadkazem.imani@modares.ac.ir
2) Professor, Department of Marine Structures, Tarbiat Modares University, Tehran, Iran, shafiee@modares.ac.ir
3) MSc of Marine Structures, K.N. Toosi University, Tehran, Iran, kianymohammadreza@gmail.com
4) MSc of Marine Structures, Tarbiat Modares University, Tehran, Iran, h.namdari@modares.ac.ir

1. Introduction

The toe structure of a breakwater has different functions such as support for the main armor layer, preventing damage caused by scouring, shortening the downward extent of the armor layer and preventing the washout of the bed material under armor layer. This paper presents the case study concerning toe stability of Pasrsian port breakwater by experimental tests on physical model.

In Parsian breakwater, concrete units were selected as the main armor layer due to the fact that the yield of near quarries couldn't supply armor rocks with the required size. In concrete armored breakwaters, heterogeneous packing could increase the porosity in top rows and eventually result in instability. Therefore, the number of rows in which the concrete units can be placed would be limited. According to the SUGRA guidance for Accropode units, this the maximum number of rows shall be 20, which leads designers to consider toe berm for breakwaters in deep water.

Because of uncertainties in hydrodynamic processes and loads in the wave breaking zone and the limited valid studies for toe stability of breakwaters [1], a comprehensive experimental study was carried out in order to ensure the stability of toe layer of Parsian port breakwater.

2. Physical Model and Experiment

The experimental investigations were carried out on physical model in the wave flume of the Hydraulic Laboratory of Tarbiat Modares University. A schematic representation of the employed physical model is illustrated in *Figure 1*. The wave flume has 16 meters length and one meter width and depth. Four water level gauges were employed to record the fluctuation of water level. One sensor was placed in front of the wave paddle and three near the model. In order to separate incident and reflected wave, three gauges were placed at the distance of one wave length to the structure following Mansard method. To ensure the correctness of different aspects of breakwater design, armor tonnage, crest level and toe layer tonnage, in operational and design levels, three return periods were defined for the waves as shown in Table 1, where H_s is the significant wave height obtained from time-domain analysis and T_p is the peak wave period.

Table 1. Tests specifications

Return Period	H_s (cm)	T_p (s)
1	7.5	1.1
100	10.4	1.3
1.2 H_{s100}	12.2	1.4

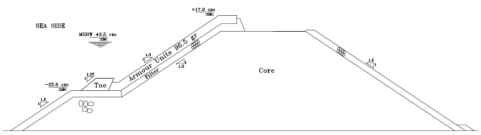

Figure 1. Physical model of Parsian breakwater

3. Discussion

During the experimental study on the toe stability of the Parsian breakwater, different cube units and placing patterns were tested to achieve a minimum level of damage. Different level of damage was set for the concrete and rock part of the toe which is shown in Table 2. N_{od} as a damage level was introduced by Van der Meer and is defined as the number of stones removed from the toe structure in a strip with a width of 1 D_{n50} [2]. In order to meet the stability criteria, the idea of using rock layer in front of the concrete units as the primary part of the toe was followed. The sacrificial rock layer was allowed to experience a higher level of damage. This placed in the way that to reduce both up and downward forces on concrete units.

Table 2. Considered acceptable damage level

	$N_{od}(H_s)$	$N_{od}(1.2H_s)$
Concrete units	0	0
Sacrificial rock	0.5	2

3.1. Accropode units with or without sacrificial rock layer

In the first prototype design, 10-14 ton rocks or Accropode units were used for toe layer which in the largest dimension would be as heavy as the main armor Accropode units. With respect to this design criteria, the physical model was scaled by the factor of 50.36 and was built in the wave flume. By implementing the test replicating a 100-year return period wave, N_{od} equal to

0.25 was recorded while the test of 1.2 times of design wave resulted in the complete collapse of the toe layer. Therefore, the idea of using sacrificial rock layer in front of concrete units was tested. By placing the rock in front, N_{od} in concrete units was reduced to 0 and 0.18 in different levels of return period respectively. Although the use of a sacrificial toe showed a considerable positive effect on toe stability, but the defined criteria weren't still met.

Figure 2. Toe layer consisting of three rows of Accropode units- after implementing the test of 1.2 times H_s

3.2. Concrete cubes with or without rock layer in front

In order to get the acceptable result, different placement patterns, a variety of cube units in tonnage (cube1 and cube2), and the presence of the rock layer in front of cube units were tested. Figure 3 shows the damage in the toe layer during the test with wave height corresponding to a return period of 100-year. Approximately 20 percent of cube1 units moved more than 1 D_n from their initial position (N_{od}=0.6). Hence, the toe layer consisting of cube1 units and the sacrificial rock layer were tested (Figure 4). Although the toe layer remained stable after running the test of design level, by performing the test of 1.2 times of design level about 10 percent of cube1 units dislodged. The result of these tests reveals that using cube1 units with or without sacrificial toe couldn't meet the stability criteria. So it was decided to use cube units with three times greater tonnage (cube2).

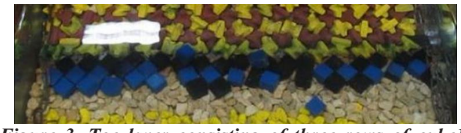

Figure 3. Toe layer consisting of three rows of cube1- after implementing the test of H_s

Figure 4. Toe layer consisting of three rows of cube2 with sacrificial rock- after the test of 1.2 times H_s

It was supposed that by increasing the tonnage of cube units by three times, toe layer would remain stable even without the rock layer in front. Different patterns of placing cube2 units, Parallel and perpendicular to the section, were tested. Both patterns experienced an unacceptable level of damage by conducting the test of H_s equal to 12.2 cm, as seen in Figure 5 and 6. It seems that due to the higher-pressure difference between the front and the rear side of units, the cubes in perpendicular to the section were demolished. Figure 7 shows that the toe layer enhances the stability of the structure by adding a rock layer in front of the cube units. It can be seen that only the rocking and moving of stones was observed.

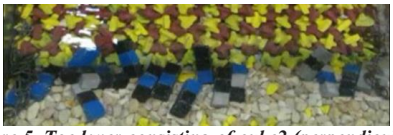

Figure 5. Toe layer consisting of cube2 (perpendicular) - after implementing the test of 1.2 times H_s

Figure 6. Toe layer consisting of cube2 (parallel) - after implementing the test of 1.2 times H_s

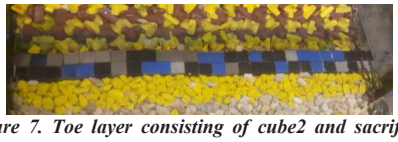

Figure 7. Toe layer consisting of cube2 and sacrificial rock - after implementing the test of 1.2 times H_s

4. Conclusion

This study investigates the stability of the toe layer on physical model of the Parsian breakwater. In this regard, different concrete units with different patterns of placement and influence of the rock layer in front of the structure were studied. The experimental results show that using sacrificial in front of concrete units reduces the moving of units significantly (Figure 8). In fact, sacrificial rock layer decreases destabilizing pressure while passing both the crest and trough of waves.

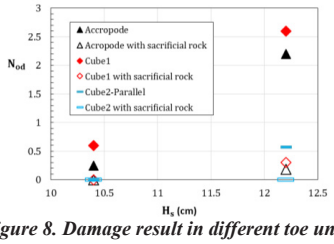

Figure 8. Damage result in different toe units

5. References

[1] Herrera MP, Molines J, Medina JR. Hydraulic stability of nominal and sacrificial toe berms for mound breakwaters on steep sea bottoms. Coastal Engineering. 2016 Aug 1; 114:361-8.

[2] Van der Meer JW, d'Angremond K, Gerding E. Toe structure stability of rubble mound breakwaters, proceedings of ICE 1995.

[3] Etemad-Shahidi A, Bali M, van Gent MR. On the toe stability of rubble mound structures. Coastal Engineering. 2021 Mar 1;164:103835.

14th International Conference on Coasts, Ports and Marine Structures
9 & 10 May 2023 , Tehran-IRAN
ICOPMAS 2022

NUMERICAL SIMULATION OF INTERACTION OF WAVE AND CASSION INTERSECTION

Ali Ghasemi[1], Mehdi Shafieefar[2] and Mohammadreza Khosravi[3]

1) Engineering Faculty, Qom University, Qom, Iran, Ghasemi.ali89@gmail.com
2) Civil Engineering Faculty, Tarbiat Modares University, Tehran, Iran, shafiee@modares.ac.ir
3) Pars Geometry Consultants, Tehran, Iran, mr.khosravi@srbiau.ac.ir

1. Introduction

Breakwaters are one of the most important coastal structures that are used to provide a calm area to enable the construction of other coastal structures and the berthing of vessels. A caisson breakwater is a type of breakwater which is used in ports. In these breakwaters, the intersection of caissons and the selection of the appropriate structure for that area are challenging[1][2][3]. Figure 1 shows some examples of a caisson breakwater's intersection.

Figure 1. Examples of caisson breakwater intersection[4]

Figure 2 shows examples of the demolition of the intersection of the caissons caused by incorrect design.

Figure 2. Examples of the demolition of the intersection of the caissons

Tombak service -export port is located near Tombak village on the northwest coast of the Persian Gulf, at the coordinates of E 52.203 and N 27.702. The port consists of two breakwater arms. The eastern arm is a rubble mound breakwater, and the western arm has rubble mound and caisson sections. The caissons used in the western breakwater are two types with a width of 21 and 14 meters. In this study, the interaction of waves and the intersection of two types of caissons are simulated. Also, the parameters affecting the performance of caissons at the intersection are investigated.

2. Model Setup

A numerical simulation of the intersection of caissons has been performed using FLOW 3D software. Figure 3 shows the geometry of the model that is scaled from 1:40 to the prototype.

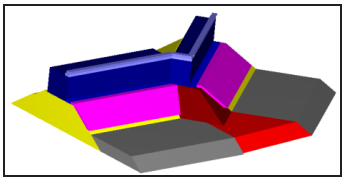

Figure 3. Geometry of model and other characteristics

One of the most important parameters of simulation is the dimension of the calculation mesh. In order to well simulate a caisson intersection, the dimension of the model is 19*1*1.3 and the number of mesh is 800,000. Also, the boundary condition is wave propagation at the first and the wall at the bottom and sides. The initial condition is water depth and the turbulence type is RNG[5]. The characteristics of the model and wave are presented in Table 1 and Table 2 [6].

Table 1. Structure information

	Structure Information	
	Site Condition	Prototype
Caisson Width (m)	21-14	0.523-0.35
Caisson Height (m)	17	0.425
Substructure Height (m)	21.3	0.533
Water Depth (m)	37	0.92

Table 2. Wave information.

	Wave Information	
	Site Condition	Prototype
Wave Height (m)	4.64	0.116
Wave period (s)	9.25	1.58

3. Results

One of the effective results at the caisson intersection is overtopping. The maximum and accumulative volume of overtopping are shown in Figure 4. The average of overtopping is 5.2 lit/s/m which is less than the allowable volume.Other parameter which evaluate is scouring between two caissons. Figure 5 shows current velocity components.

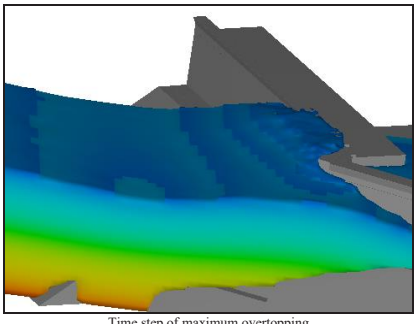
Time step of maximum overtopping

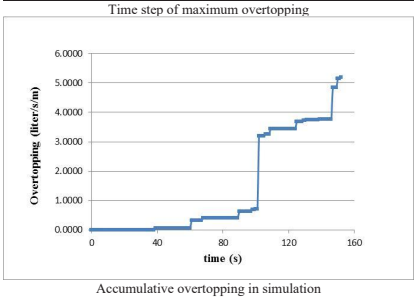

Accumulative overtopping in simulation

Figure 4. The maximum and accumulative volume of overtopping

According to simulation results and the scale of the model, the maximum current speed at the caissons is 2.8 m/s. due to using the scouring block and checking the results using the Pilarczyk formula, the scouring is not accrued at the caisson intersection.

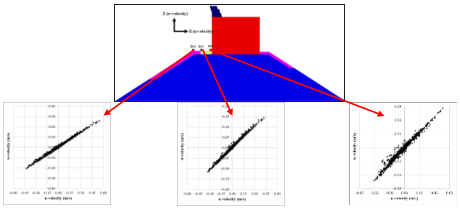

Figure 5. Current velocity components at the caisson intersection

The pressure on the caissons is the last parameter is evaluated. Figure 6 shows the pressure distribution on different parts of the caisson body.

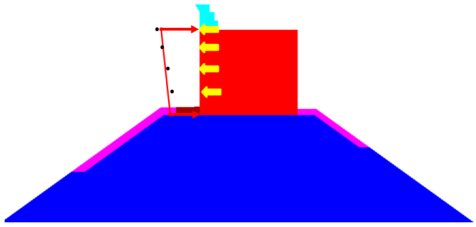

Figure 6. Pressure distribution on the caisson (red line: Goda formula, black point: present study)

Based on the results, the maximum pressure that occurs at the water surface is about 1.6 kPa. It means the pressure on the real structure is about 66 kPa. However, the calculated pressure using the Goda formula is about 55 kPa. So the error of the model is about 30%, which is acceptable.

4. References

[1] J. L. Lara, I. J. Losada, and R. Guanche, “Wave interaction with low-mound breakwaters using a RANS model,” Ocean Eng., vol. 35, no. 13, pp. 1388–1400, 2008.
[2] K. Suh, J. Kil, and W. Sun, “Wave Reflection from Partially-Perforated-Wall Caisson Breakwater,” pp. 1–35.
[3] C. Engineering and A. Sv, “EXPERIMENTAL INVESTIGATION ON CAISSON BREAKWATER SLIDING Piero Ruol 1, Paolo Martin 1, Thomas Lykke Andersen 2 and Luca Martinelli 1,” pp. 1–11, 2000.
[4] Earth.google.com
[5] Flow Science, “User Manual: FLOW-3D® Cast 3.2,” pp. 1–49, 2009.
[6] Amirabadi, R. and Ghasemi, A., 2018. Numerical modeling investigation of irregular wave interaction with perforated caisson breakwater. Journal of Marine Engineering, 14(27), pp.69-79.

14th International Conference on Coasts, Ports and Marine Structures
9 & 10 May 2023 , Tehran-IRAN
ICOPMAS 2022

COMBINATION OF STONE COLUMNS AND DYNAMIC REPLACEMENT AS SOIL IMPROVEMENT METHOD FOR RECLAIMED LANDS OF KANGAN PDH/PP PROJECT

Mohammad Mohammadnia[1], Saeed Askarian[2] and Ali Fakher[3]

1) Pars Geometry Consultants, Tehran, Iran, m.mohammadnia@parsgc.com
2) Pars Geometry Consultants, Tehran, Iran, s.askarian@parsgc.com
3) Civil Engineering Faculty, University of Tehran, Tehran, Iran, afakher@ut.ac.ir

1. Introduction

Kangan Polymer Development Company is going to construct the PDH / PP project in the southeast side of phases 22-24 of South Pars region. The lands intended for the construction of the project has been mainly reclaimed from the sea by using fine fill material containing marl. The location of the project in the aerial photo is shown in Figure 1. In the present paper, special ground improvement aspects of the mentioned case study are presented which may be useful for similar near shore reclaimed areas.

Figure 1. Location of PDH/PP project

2. Selection of Ground Improvement Method

In Kangan PDH/PP Project, 9 boreholes and 5 inspection wells were drilled during geotechnical study. Investigations revealed that most of the soil consists of clay (CL) and marl. Thickness of the clay layer ranges between 10 to 16 meters. Geological studies show that most of the surrounding mountains in the area contain clay and marl material, which reveals the nature of the fine soil of the reclaimed area.

Several ground improvement methods where investigated in the design process of the project. Some ground improvement methods such as jet grouting, deep mixing, rigid inclusion, micro pile, reinforced concrete and steel piles, etc. are based on creating a resistant column in the soil. These improvement methods are very expensive and are not feasible due to the large area of the project land (about 40 hectares). Some other ground improvement methods such as lime and cement-based stabilization methods or replacement of the soil with selected material, were also not selected in this project because performing these methods required deep underwater excavation of the existing fine material which was not applicable according to budget and project time limitations. Dynamic compaction was another method for ground improvement. However due to the high clay content of the soil and high water level, dynamic compaction was not a reliable method. Another ground improvement technique which could be performed for fine soils is preloading. The preloading method was not selected for Kangan PDH/PP project, because it required a huge amount of fill material as the surcharge load and also the method takes time to get effective in the deep clay layers.

Dynamic replacement is an improvement method which is applicable in lands containing high fine content. The method was designed for the reclaimed area of Kangan PDH/PP project. However, in some parts in the southern area of the project in which the thickness of the reclaimed soil increased, there was a concern that the dynamic replacement method may not be effective for deep layers. Therefore, the combination of stone columns and dynamic replacement was used for the mentioned area.

3. Combination of Stone Columns and Dynamic Replacement Method

In the first step of the combined method, stone columns are constructed in a certain pattern to the required depth of improvement. The columns shall consist of selected stone materials with low water absorption and high strength to ensure durability. In the next step, dynamic replacement is performed in the area between the columns. In this method the excess pore water pressure due to the tamper impacts is dissipated in a shorter time because of the presence of the stone columns which makes the dynamic replacement method more effective especially in deeper soil layers. Figure 2 shows a schematic pattern of the combined ground improvement method.

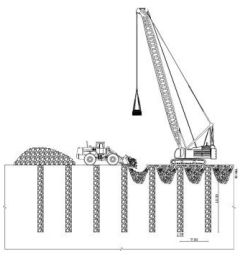

Figure 2. Schematic pattern of the combination of stone columns and dynamic replacement

Figure 3 shows the implementation of dynamic replacement and stone columns at the project site.

Figure 3. Implementation of dynamic replacement and stone column at the project site

The design of the combined ground improvement method was performed using Plaxis-V8.6 software. Stone columns are modelled as clusters with higher strength and permeability.

4. Lessons Learned from Trial Ground Improvement Patterns

After completing the preliminary design, a number of trial patterns with different distances between the stone columns and different dynamic replacement patterns were designed, executed and tested. In fact, different combination of stone columns spacing, dynamic replacement spacing, tamper weight and height of tamper drops were assigned as trial patterns. Also, different ratios of height to diameter of tampers were selected. The following results were obtained by testing the trial patterns:

- The presence of stone columns increases the effectiveness of the dynamic replacement method. As an example, N_{SPT} values after dynamic replacement are compared in the presence and absence of stone columns in Figure 4.
- A denser stone column pattern makes the dynamic replacement method more effective. Finally, stone columns where performed in a 7*7 grid in the project.
- The first design of heavy phases of the dynamic replacement method was equal to 800 ton-meter per impact. However, trial patterns revealed that the design could be optimized to 600 ton-meter per impact due to the presence of the stone columns. In fact, using stone columns results financial optimization in the project.
- The use of a higher height to diameter ratio for tampers resulted greater depth of stone penetration during dynamic replacement. Figure 5 shows the special tampers used in the project. By using the special tampers materials where replaced 1 meters deeper than using ordinary tampers during dynamic replacement.

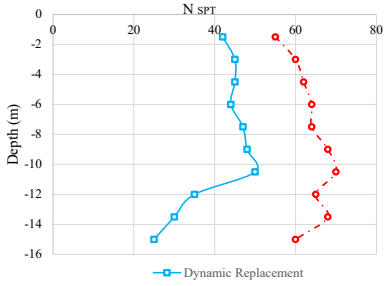

Figure 4. An example of a dynamic replacement pattern with a main phase distance of 5 m and a sub phase of 2.5

Figure 5. Special tampers used in project

5. Conclusion

Kangan PDH/PP plant is going to be constructed on reclaimed land. Most of the reclaimed area consists of fine clayey and marl materials. A novel combination of stone columns and dynamic replacement was selected as ground improvement method. The following conclusions may be presented:

- The novel proposed soil improvement method was proven to be applicable and feasible in reclaimed areas.
- According to quality control tests performed, the presence of the stone columns increased the effectiveness of the dynamic replacement method.
- Using tampers with higher height to depth ratio results an increase in stone penetration depth in dynamic replacement method.

6. References

[1]- Lukas, R. (1995). Geotechnical engineering circular No. 1-Dynamic compaction (No. FHWA-SA-95-037). United States. Federal Highway Administration. Office of Technology Applications.
[2]- Li, X., & Xi, P. (2021). Study of Numerical Simulation of Dynamic Replacement Soft Soil Foundation Pit. World Scientific Research Journal, 7(4), 1-8.
[3]- Fahmi, K. S., Fattah, M., & Shestakova, A. (2018). Behavior of foundation soil improved by stone column under cyclic load. In MATEC Web of Conferences (Vol. 239, p. 05015). EDP Sciences.

14th International Conference on Coasts, Ports and Marine Structures
9 & 10 May 2023 , Tehran-IRAN
ICOPMAS 2022

AN INVESTIGATION OF THE EFFECT OF A TRIANGULAR COGGED FLOOR ON THE WAVE TRANSMISSION COEFFICIENT IN FLOATING BREAKWATERS

Saeed Osouli[1], Habib Hakimzadeh[2] and Nazila Kardan[3]

1) Department of Civil Engineering, Sahand University of Technology, Tabriz, Iran, sa_osooly98@sut.ac.ir
2) Department of Civil Engineering, Sahand University of Technology, Tabriz, Iran, hakimzadeh@sut.ac.ir
3) Department of Civil Engineering, Azerbaijan Shahid Madani University, Tabriz, Iran, n.kardan@azaruniv.ac.ir

1. Materials and Methods

The equations governing a Cartesian coordinate system are discretized using the finite volume approach in this model. In modeling the fluid interfaces and free-surfaces problems the Volume of Fluid (VOF) approach was used [1]. The unknown Reynolds stresses were modeled using the eddy viscosity concept and k-ε (RNG) turbulence model [2]. In order to understand the behavior of the irregular waves that mainly cover the ocean surface, a wave spectrum model (Jonswap spectrum) may be applied. The incident and reflected coefficient were separated using Zelt et al (1993) method [3].

2. Mesh Independent Study

To validate the numerical results, seven different numbers of meshing were applied in the computational domain in conditions of significant wave height H (1/3) =10 cm, corresponding wave period Tm =0.63 s, and SWL[1] =60 cm. The coefficients of transmission (Ct), reflection (Cr), and energy dissipation (Cd) were correctly established in a post-analysis process using the relevant hydraulic data. Figure 1 shows the validation of mesh independent investigation. Overall, as the total cells increased, the numerical results of the coefficients converged to a specific value (at about 800,000 cells). So the total cells of 830592 were used for the further simulation processes.

Table *1* summarizes the breakwater draft, width and length, mooring line characteristics, and other parameters for test conditions. Figure 2 shows a sketch of the wave flume including the dimensions and location of the F.B. breakwater. It is approximately 18 m long, 0.81 m deep, and 0.9 m wide. In experimental conditions, the surface elevation was measured using five-wave gauges (WGs).

3. Parametric Study

The floating breakwaters' performances are somewhat different from conventional breakwaters, in which their attenuating mechanisms can reflect, dissipate, or transmit the waves to the lee side of the structure or a combination of these. Zelt et al. (1993) established a method for obtaining three parameters of separating reflected waves (Hr), incident waves (Hi), and as well as transmitted waves (Ht), for further hydraulic data analysis. Transmission (Ct), reflection (Cr), and energy dissipation (Cd) coefficients can be computed using dimensionless parameters:

$$Ct = Ht/Hi \quad (1)$$

$$Cr = Hr/Hi \quad (2)$$

$$Cd = Hd/Hi \quad (3)$$

$$Ct^2 + Cr^2 + Cd^2 = 1 \quad (4)$$

4. Validation

The defined F.B. models were based on experiments conducted by Forouzandeh et al. [4], in which the range of wave heights (2 ~ 12 cm), and waves mean periods (0.63 ~ 1.26 sec) were selected according to the experimental test. Also, the JONSWAP wave spectrum was used to generate the irregular waves as the incidental waves [5], and the water depth was set to 0.6 m. The numerical simulation results for the transmission coefficients of the floating breakwater are shown in Figure 3. The transmission coefficients are then plotted against dimensionless parameters kh (wave number multiplied by water depth) that were used.

5. Models

In Figure 4, the geometrical characteristics of models (all models with the same weight equal to 34.53 kg) were depicted. A number of triangular cogs were made at the bottom of the pontoon-type model so that the models have tentatively the same weight. Then, the numerical results of the transmission coefficients were compared with the rectangular base model.

Table 1. Characteristics of the floating breakwater.

breakwater	draft	0.08 m	mooring lines	weight	0.01 kg/m
	weight	16.32 kg		length	1.88 m
	length	0.85 m		diameter	0.0015 m
	height	0.16 m		Young's modulus	70 GPa
	width	0.24 m			

[1] Still Water level

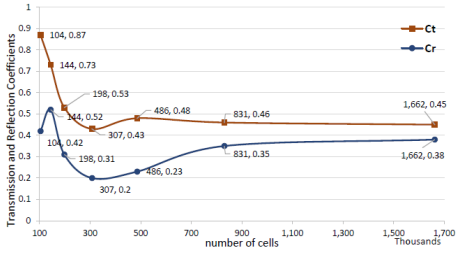

Figure 1. Predicted magnitudes of Ct and Cr for mesh independent study.

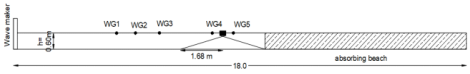

Figure 2. A sketch of the numerical setup

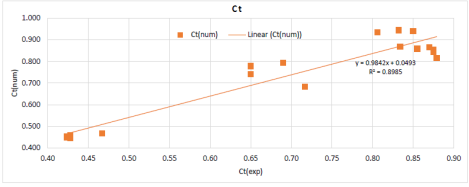

Figure 3. The transmission coefficients for the experimental and numerical study.

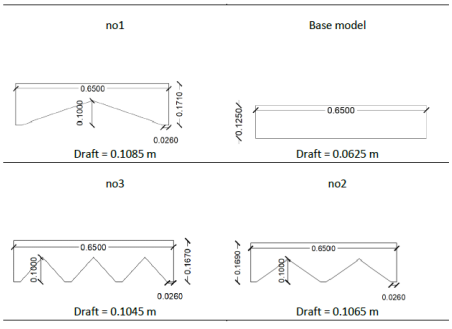

Figure 4. Geometries of the models with the same weight.

6. Results and Discussion

Figure 5 shows the graphical numerical results of the models. It is observed that the cogged F.B. models mainly enhance the performance of F.B., by decreasing the transmission coefficients. It is clear that, by increasing the wave periods (or reducing kh), the performance of F.B. models decreases.

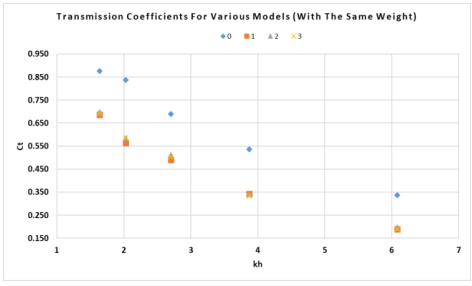

Figure 5. Impact of cogged floors on transmission coefficient

7. References

[1] I. Flow Science, "FLOW-3D, Version~12.0." Santa Fe, NM, 2019, [Online]. Available: https://www.flow3d.com/.

[2] S. F. Abdullah, A. Fitriadhy, M. Hairil, and A. Jusoh, "Hydrodynamic performance of cylindrical floating breakwater in waves," *Int. J. Automot. Mech. Eng.*, Vol. 14, No. 4, pp. 4715–4729, 2017, doi: 10.15282/ijame.14.4.2017.10.0371.

[3] J. A. Zelt, J. E. Skjelbreia, and Wave Technologies, "Estimating incident and reflected wave fields using an arbitrary number of wave gages," *Proc. Coast. Eng. Conf.*, Vol. 1, pp. 777–788, 1993, doi: 10.1061/9780872629332.058.

[4] N. Forozande, H. Hakimzade, and P. Aghtoman, "Experimental Investigation On Effect Of Draught, Mass And Sheet Height In Pontoon Floating Sheet Breakwaters On Transmission And Reflection Coefficients Subject To Irregular Waves," *Int. J. Marit. Technol.*, Vol. 7, No. 13, pp. 17–28, 2011.

[5] Y. Goda, "Random seas and design of maritime structures," *Advanced Series on Ocean Engineering*, Vol. 33. pp. 1–732, 2010.

14th International Conference on Coasts, Ports and Marine Structures
9 & 10 May 2023 , Tehran-IRAN
ICOPMAS 2022

A NUMERICAL STUDY ON DYNAMIC RESPONSE OF CAISSON QUAY WALLS WITH IMPROVED BACKFILL

Amir Reza Zarnousheh Farahani[1], Babak Ebrahimian[2]

1) Faculty of Civil, Water and Environmental Engineering, Shahid Beheshti University, Tehran, Iran, Email: a.zarnoosheh@mail.sbu.ac.ir
2) Faculty of Civil, Water and Environmental Engineering, Shahid Beheshti University, Tehran, Iran, Email: b_ebrahimian@sbu.ac.ir, ebrahimian.babak@gmail.com

1. Introduction

Gravity quay walls, which provide their stability through their weight, are among the most widely used options for the construction of port structures, especially in dense and high-quality seabed soil condition. Accordingly, caisson-type quay walls are one of the most suitable gravity systems used for the construction of wharf retaining structures due to their many advantages such as high durability, easy construction and the possibility of using in larger water depth. One of the most widely used methods to improve the seismic performance of gravity quay walls rested on a dense foundation soil layer is the replacement of backfill soil with proper granular materials. There are different patterns for replacing the backfill soil, each of which has advantages and disadvantages in terms of their performance and functionality. In the present study, a number of improvement patterns of the backfill soil are explored and their impacts on the seismic response of the caisson-type quay wall are compared by numerical simulation.

2. Numerical Simulation

According to Figure (1), the model analyzed in this work has a length of 110 *m* and includes a caisson wall with a height of 12 *m* which is rested on a rubble mound layer with a thickness of 1 *m* over dense sandy seabed with 4 *m* thick.

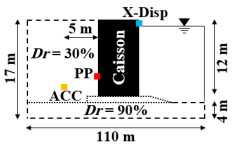

Figure 1. Geometry of the studied numerical model.

A two-dimensional (2D) finite-difference plane strain model has been developed to predict the seismic response of the caisson wall [1]. The Mohr–Coulomb and elastic constitutive models are employed to describe the mechanical behavior of the dense seabed sand materials with a relative density of 90% and the concrete wall, respectively. The UBCSAND model is used to describe the behavior of liquefiable sandy backfill with a relative density of 30%. Contact conditions between wall and adjacent soil are modeled via special interface elements allowing for slipping and gapping through the Coulomb frictional law. Element size is selected small enough to allow the seismic wave propagation throughout the numerical model. The sea water is simulated through the hydrostatic pressures applied to the front side of the wall. Correspondingly, the hydrodynamic effects are exerted by the Westergaard's added masses on the seaward face of the wall. In dynamic analyses, the free-field condition is applied to the lateral boundaries eliminating the wave reflection into the model [2]. To avoid spurious oscillations at very small deformations and high frequency components of motions, 5% of Rayleigh damping, centered at a frequency of around 2 *Hz* (close to the fundamental frequency of the system), is considered in the dynamic analyses. The values of constitutive constants for different parts of the studied numerical model are presented in Table (1).

Table 1. Constitutive constants.

Parameter	Seabed	Foundation	Improved Zone	Backfill
Constitutive model	Mohr	Mohr	Mohr	UBC
Dr (%)	90	-	-	30
γ_{sat} (kg/m^3)	1964	2000	2000	1850
ϕ (Degree)	34	35	40	-
K (MPa)	158.3	166.7	150	-
G (MPa)	73	76.9	69.2	-
C (kPa)	0	0	0	-
ψ (Degree)	1.0	1.2	5	-
k (cm/s)	0.0125	50	50	0.0125
$(N_1)_{60}$	-	-	-	5
ϕ_{cv} (Degree)	-	-	-	28

The input motion used in the dynamic analysis is a horizontal acceleration time history with a peak acceleration of 0.3g and a frequency of 5 *Hz*. Figure (2) shows the comparison between the horizontal acceleration, horizontal displacement, and pore water pressure time histories obtained from both the present numerical study and 1g shaking table tests [2]. Concerning Figures (2) overall agreements are observed between the numerical results and the experimental observations.

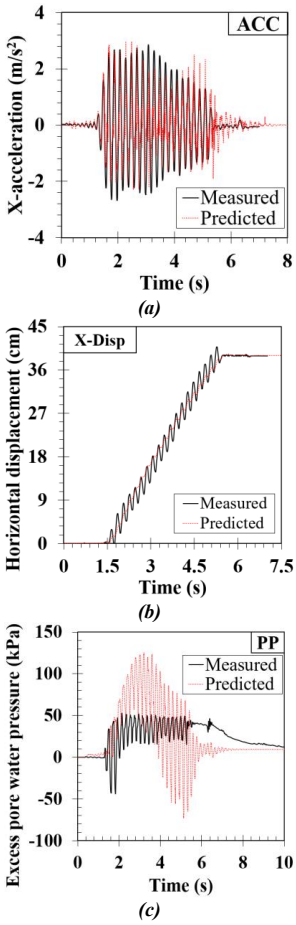

Figure 2. Comparison between the current numerical results and the corresponding experimental observations: (a) horizontal acceleration, (b) horizontal displacement, and (c) excess pore water pressure time histories.

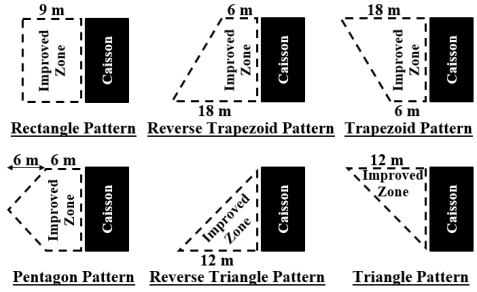

Figure 3. Studied backfill replacement patterns.

3. Effect of Backfill Replacement

In the present study, six improvement patterns of backfill soils are explored, as demonstrated in Figure (3). Horizontal displacement and rotation angle of caisson quay wall with different replacement patterns are shown in Figure (4). It is apparent that the backfill soil treatment behind the caisson-type quay wall has improved the seismic performance of the wall and reduces the horizontal displacement and rotation angle of caisson quay wall to less than half. Among the studied backfill replacement patterns, Reverse Trapezoid pattern has the most effect on improving the seismic performance of caisson quay wall.

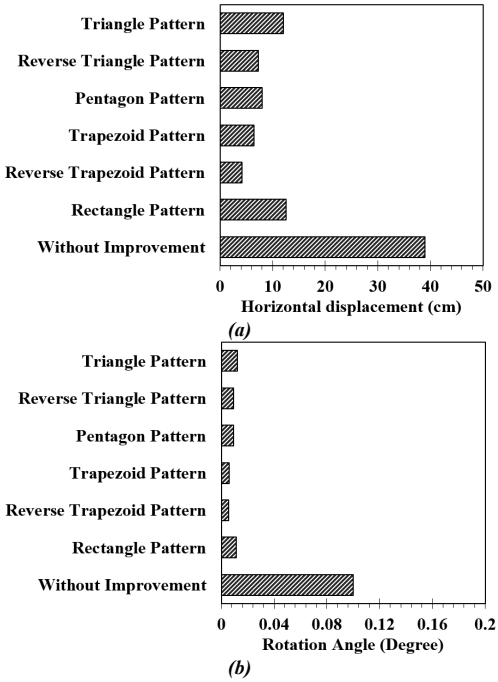

Figure 4. Deformations of the caisson-type quay walls with improved and unimproved backfills: (a) residual horizontal displacement at the top of the wall, and (b) residual rotation angle of the wall.

4. References

[1] Itasca Consulting Group, Inc. (2019). FLAC version 8.0: Fast Lagrangian Analysis of Continua. User's Guide. *Minneapolis: Itasca Consulting Group.*

[2] Ghalandarzadeh, A., Rahimi, S., & Kavand, A. (2020). Dynamic pore water pressure of submerged backfill on caisson quay walls: 1 g shake table tests. *Soil Dynamics and Earthquake Engineering*, *132*, 106091.

THE DAMAGE OF CASPIAN PORT RUBBLE MOUND BREAKWATER

Yasaman Ghafourian[1], Mohsen Soltanpour[2] and Babak Banijamali[3]

1) Formerly, Civil Engineering Dept., K. N. Toosi University of Technology, Tehran, Iran, yasamangh@email.kntu.ac.ir
2) Civil Engineering Dept., K. N. Toosi University of Technology, Tehran, Iran, soltanpour@kntu.ac.ir
3) Darya-Bandar Consulting Engineers, Tehran, Iran, babak.banijamali@daryabandar.com

1. Introduction

Based on the hydrodynamic and geotechnical conditions, different types of breakwaters are constructed to protect the harbors from the wave attacks and to provide a calm area for ships berthing. Two main categories of breakwaters are rubble mound, which are made out of large heaps of loose elements, and monolithic, which have a cross section acting as one block, e.g., caissons. Rubble-mound breakwaters are subjected to various damages such as overtopping, Armour units sliding, foundation subsidence, etc. Considering the importance and high cost of the breakwaters, their proper design and construction are essential to ensure the appropriate performance of the ports. Reviewing the details of the design and construction of the Caspian Port, the damage to the western breakwater of Caspian port is studied in this paper.

2. Study Area

Caspian Port is located in the south coast of the Caspian Sea, about 16 kilometers east of Anzali in Gilan Province of Iran (Figure 1). The lengths of the east and west arms of rubble mound breakwaters are about 2250 m and 2357 m, respectively. Also, 22 dock posts have been designed in the 200 ha harbor.

Figure 1. Caspian Sea and the under-construction Caspian port (2019).

On 17th January 2019, when the breakwater where still under the construction, a severe storm resulted to a considerable damage to the western breakwater and sliding of armour units down the breakwater slope (Figure 2).

Figure 2. Sliding of antifer armour units (photo: January 2021, 21st).

A site visit was conducted on 21st of January 2021 in order to examine the extent of damages and the details of the failures of breakwater. The damaged parts of the breakwater and the selected pattern of the Antifer units were visually investigated and interviews with local people and authorities were conducted during the visit to find the clues/evidences regarding the condition of the breakwater at the time of the storm. The existing evidences confirmed the absence of secondary armour layer in January 2019, which has been resulted in considerably reduced protection against the storm waves. Figure 2 shows the overtopping and scouring of the crest materials, as well as sliding of Antifer units of the crest.

3. Review of Design and Construction

3.1. Design Parameters

Table 1 presents the summary of the selected parameters for the design of Caspian Port breakwater by consultant. The significant wave height of 5.08 m is less than the 100-years wave height of 5.68 meters, calculated by Golshani and Rezaei (2020) [4], based on the 30-years hindcast data of "Monitoring and Modeling studies of the southern Caspian Sea".

3.2. Design Wave

41 years wave rose of ERA5 satellite (1979-2020) shows that the waves are mostly coming from the northeast direction. 11-years hindcast data (1992-2003) of "Iranian Seas Wave Modeling (ISWM)" and time series of 30-years hindcast wave data of "Monitoring and Modeling studies of the southern Caspian Sea" both reveal that the wave

height of the storm on 17th January 2019 has not been unprecedented. The latter estimates revealed that the wave height of the storm is Hs=3.6 m, which is much lower than the design wave height of the breakwater, i.e., 5.08 m.

Table 1. Design parameters of Caspian port breakwater.

Design parameter values			
Significant wave height (H_S) (m)	5.08	Density of water (kg/m^3)	1025
Density of concrete units (kg/m^3)	2300	Peak period (s)	10
Density of rock (kg/m^3)	2400	Breakwater slope	1.5
Permeability coefficient	0.4	Stability factor (trunk)	7.5
Damage level	2	Stability factor (head)	5

3.3. Design of Rubble-Mound Breakwater

14-ton double-layer Antifer armour units have been used in this rubble mound breakwater [1]. By using 100-years design wave height of 5.68 m, and the KD coefficients of 7.5 and 5 for trunk and head, respectively, the minimum tonnage of Antifer armour units in trunk and head will be 16 t and 24 t, respectively, following Hudson formula. This indicates the instability of used armour units in head and trunk against the 100-years design wave. Moreover, similar cross sections is not acceptable by the regulations of the design codes, considering the severe collision of waves and 3D diffraction at the head. The life performance of core structure is important to ensure the stability of the rubble-mound breakwater. Considering the required width for the passage of vehicles, Rock Manual suggests minimum top core widths of 7 m (two trucks) and 9 m (a truck and a crane) [1]. As built drawings show 10.50 m width of core at level +2 and 7.50 m at level +3, which is in the range of the minimum values of the Rock Manual. The weight of core materials is also within the recommended range of shore protection manual, i.e., W/200-W/4000, assuming 16 t Antifer blocks (W) [3]. Assuming KD=7.5 for Antifer blocks, the weight of filter materials do not agree with the regulations of CEM [2], SPM [3] and OCDI [5], i.e. W/10. The thickness filter layer in trunk and head is also less than the recommended values. The design and construction of toe is also of great importance. The tonnage of 3-5 t agrees with W/10, i.e. the regulation of SPM manual for the weight of toe materials [3]. However, the height and width of the toe do not meet the CEM regulation, i.e. 3 times of the nominal diameter of armour units (Dn50) [2].

3.4. Placement Method of Antifer Armour Units

Concrete armour units can generally be placed in both random and regular way [1]. Figure 3 shows the placement method of Antifer blocks in breakwater, which can not be found in the design codes. Unfortunately, no laboratory studies were done to confirm the proper performance of this method against the wave action. Moreover, the combination of stone and concrete blocks makes it almost impossible to estimate the porosity of the armour layer. Besides the absence of the second armour layer in January 2019, the placement method of armour units can also be blamed for the failure of the breakwater under the high waves of the storm.

Figure 3. Placement method of antifer armour units (photo: January 2021, 21st).

4. Summary and Conclusion

The rubble mound breakwater of the Caspian Port suffered multiple failures under the wave attacks of the storm on 17th January 2019. The study revealed that the attacking storm waves were less than the design wave height of the port. The significant damage to the breakwater could have been prevented if the armour layer was placed according to a credible design code of practice before the storm. Although the failure of breakwater can be mainly related to the incompletion of the second armour layer at the time of the storm, the improper placement pattern of the Antifer blocks, insufficiency of the used stones in armour layer, and the absence of proper materials in filter layer have also contributed to the instability of the armour units. Since the design wave height of the port is less than the 100-years extreme waves, future damages to the trunk and head of the port breakwater under the extreme storm waves are probable. As the breakwaters are likely to damage in the event of larger storms with different directions, further studies are necessary to ensure the life service of the port.

5. References

[1] CIRIA, CUR, & CETMEF, *the rock manual*, 2nd Ed, (C683), 2007.
[2] Coastal Engineering Manual (CEM), Part VI, US Army Corps of Engineers, 2011.
[3] Shore Protection Manual (SPM), Coastal Engineering Research Center, *department of the Army Waterways Experiment Station*, *Corps of Engineers*, 1984.
[4] Golshani, Aliasghar., Rezaei, Seyed Meysam, Modeling the waves induced by the January 2019 storm in the Caspian Sea in order to investigate the reasons of partial damage of western arm of Caspian Port breakwater, *Journal of Oceanography*, 11. 49-59. 10.52547/joc.11.42.49, 2020 (in Persian).
[5] OCDI, Technical standards and commentaries for port and harbor facilities in japan, *The Overseas Coastal Area Development Institute of Japan*, 2002.

14th International Conference on Coasts, Ports and Marine Structures
9 & 10 May 2023 , Tehran-IRAN
ICOPMAS 2022

THE STABILITY COEFFICIENT (K_D) OF ICELANDIC-TYPE BERM BREAKWATER WITH ACCROPODE UNIT IN THE CLASS I ARMOUR

Habibollah namdari[1], Mehdi Shafieefar[2]

1) Master student, Facaulty of civil engineering, Tarbiat Modarres University, Tehran, Iran, h.namdari@modares.ac.ir
2) Professor, Facaulty of civil engineering, Tarbiat Modarres University, Tehran, Iran, shafiee@modares.ac.ir

1. Introduction

Berm breakwaters have been introduced in the early 1980s as mass armoured reshaping structures, where the wave action causes that the structure reshapes into a more favorable S-shape. Later, the multilayered less reshaping structures known as the Icelandic type have become popular for locations with severe wave loading where large stones are available. Berm breakwaters are divided into different categories depending on the reshaping and on the construction method. Van der Meer and Sigurdarson [1] proposed a classification of berm breakwaters partly based on their structural behavior, such as hardly reshaping, partly reshaping, and fully reshaping (*Table 1*).

Table 1. Classification of berm breakwaters, given for the 100-years condition.

Breakwater type	Abbrevation	$H_{sD}/\Delta D_{n50}$	S_d	Rec/ D_{n50}
Hardly reshaping berm breakwater (Icelandic-type)	HR-IC	1.7-2.0	2-8	0.5-2
Partly reshaping Icelandic-type berm breakwater	PR-IC	2.0-2.5	10-20	1-5
Partly reshaping mass-armoured berm breakwater	PR- MA	2.0-2.5	10-20	1-5
Fully reshaping mass-armoured berm breakwater	FR-MA	2.5-3.0	--	3-10

In this study, the stability of icelandic type berm breakwater with accropode armour units has been investigated and compared with the case where stone is used as armour.

2. Experimental Setup and Procedures

Experimental research was carried out in the wave flume of the Coastal and Hydraulic Engineering laboratory of the Tarbiat Modares University. The flume has a length of 16 m, a width of 1 m and a height of 1 m. The cross-section is given in *Figure 1*. The nominal diameter of the accropode and armourstone at the lower slope and at the berm was 33 mm. the nominal diameter of the rocks in the Classes II and III were 26 and 19 mm respectively. The core consisted of stones with a nominal diameter of 10 mm. The width and position of the berm with respect to the water level were varied. The berm widths were $6D_n$, and $8D_n$. Two different water depths (d) of 0.40, and 0.45 m were studied to investigate the effect of the position of the berm with respect to the still water level. In other words, the still water levels (SWL) were at, and 0.05 m above the berm (d_b/d = 0 and 0.125 where db is vertical distance between berm and SWL; d_b/D_n = 0 and 1.51).

Per test, the incoming significant wave height in front of the toe was gradually increased to define the wave height leading to failure. The damage was repaired after each series of test runs, but not after each individual test run, similar to Van Gent [2]. Each test run was carried out with about 1000 waves. The recorded damage was cumulative for each test series.

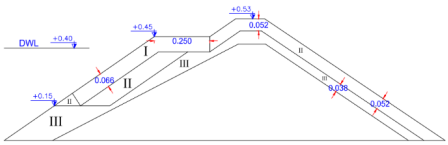

Figure 1. Cross-section of the model

3. Determine the Damage

In this study damage is defined in the following way:
No damage: No units are displaced.
Initial damage: A few units are displaced.
Failure: The underlayer is exposed to direct wave attack.

1- Damage level (only for Class I armourstone):

$$S_d = A_e/D_{n50}^2 \quad (1)$$

2- Relative damage number: (for concrete Armour layer)

Damage to concrete units can be described by the relative damage number N_{od} which is defined by the number of displaced units related to a width (along the longitudinal axis of the breakwater). The definition of N_{od} is comparable with the definition of S. Although S includes displacement and settlement, it does not take into account the porosity of the armour layer. In this study, the damage number was found by counting the displaced units out of the armour layer in the reference area from the camera records.

$$N_{od} = \frac{number\ units\ displaced\ out\ of\ the\ armour\ layer}{L/D_n}$$

where L is the width of the model structure excluded one nominal diameter from each side wall and D_n is the nominal diameter of the Accropode.

Table 2. Range of the parameters for the experimental data set.

Parameter	Symbol	Value
Upper and lower slope angle	cot α	1.5
Relative density for accropode and rocks	Δ	1.4
Rock size Class I (m)	D_{n50}	0.033
Accropode size Class I (m)	D_{n50}	0.033
Berm width (m)	B	0.2 and 0.25
Wave steepness (sp = $2\pi H_s/gT^2_p$,Hs=Hm0)	S_p	0.019-0.041
Wave height(m)	H_s	0.079-0.135
Stability number	$N_s = H_s/\Delta D_n$	1.6-3

4. Results and Discussion

Different stability coefficients are defined for different placements. The Hudson stability coefficient (K_{DH}) is based on the significant wave height were the first displacements appear within a damage ratio of 0–5%. If this first damage exceeds the damage ratio of 5%, the significant wave height from the preceding wave series is applied to calculate the K_{DH} value.

For Accropode armour, a different damage level is required because it results in a chain reaction. The significant wave height before the wave series at which the first displacement appears is applied for the calculation of the stability parameter, K_{D0}, for Accropode. Therefore, a damage ratio of 0% is required before the first displacement.

The stability coefficient K_D can be calculated as a function of N_s and the lower slope angle cot α as shown below.

$$K_d = \frac{N_s^3}{\cot \alpha} \qquad (2)$$

5. Conclusions

This result shows that the icelandic type berm breakwater with accropode armour in class I is more stable than the armourstone. These stability coefficients increase with increasing berm width similar to the armourstone.

Table 3. The stability coefficients on the lower layer for armourstone.

Berm Levels		B=6D_n	B=8D_n
Emerged berm	N_s	1.84	2.04
	K_{D0}	4.01	5.62
	N_s	2.04	2.25
	K_{DH}	5.62	7.39
Berm at SWL	N_s	1.71	1.84
	K_{D0}	3.21	3.21
	N_s	1.84	2.04
	K_{DH}	4.01	5.62

Table 4. The stability coefficients on the lower layer for accropode unit armour.

Berm Levels		B=6D_n	B=8D_n
Emerged berm	N_s	2.47	2.77
	K_{D0}	10.02	14.18
	N_s	2.66	2.94
	K_{DH}	12.58	17.01
Berm at SWL	N_s	2.21	2.47
	K_{D0}	7.17	10.02
	N_s	2.47	2.66
	K_{DH}	10.02	12.58

6. References

[1] Van der Meer, J.W., Sigurdarson, S., 2016. Design and Construction of Berm Type Breakwaters, first ed., vol. 40. World Scientific, Singapore.
[2] Van Gent, M.R.A., 2013. Rock stability of rubble mound breakwaters with a berm. Coast Eng. 78, 35–45.

14th International Conference on Coasts, Ports and Marine Structures
9 & 10 May 2023 , Tehran-IRAN
ICOPMAS 2022

INVESTIGATION OF ARMOUR STABILITY OF BERM BREAKWATER USING SPH-DCDEM METHODS

Mohammad Reza Torabbeigi[1], Hassan Akbari[2]

1) Department Of Civil and Environmental Engineering, Tarbiat Modares University, Tehran, Iran, m_torabbeigi@modares.ac.ir
2) Department Of Civil and Environmental Engineering, Tarbiat Modares University, Tehran, Iran, akbari.h@moderes.ac.ir

1. Introduction

Berm Breakwaters are rubble mound structures constructed with a large porous berm at or above still water level ate the seaward side. During wave attack, the seaward slope profile of berm breakwater is reshaped into the S-shaped profile, which is more stable than the initial profile. A typical Cross-section of a berm breakwater with initial and reshaped profiles is indicated in Figure1. Rescission (Rec) and Width (B) of the berm layer are the most critical parameters for stability control of berm breakwaters. Complete failure occurs typically when Rec > B [1].

Berm recession is the most critical parameter to evaluate the stability of berm breakwaters. Based this parameter, berm breakwaters are categorized on their stability condition into three types, hardly reshaping, partly reshaping, and fully reshaping berm breakwaters [2]. Since the recession of berm breakwater against waves is a complicated phenomenon, many experimental studies have proposed practical formulas for evaluating the expected berm recession. However, understanding this phenomenon needs an in-depth knowledge of Fluid-Structured Interaction (FSI). Numerical techniques, which can calculate the wave loads on the armour units and analyze the interaction, can investigate the armor units' stability during the wave attacks.

Wave and rubble mound structure interaction problems can be investigated by SPH-DEM techniques, for example simulating displacement of 2D cross-shaped block under wave action on an impermeable breakwater sloped at 1:1.75 [3], analyzing the armour units stability in high-crested breakwater [4], simulation of failure of a caisson type composite breakwater during a tsunami [5].

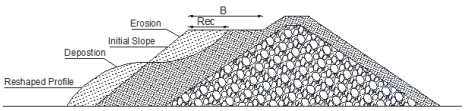

Figure 1. Definition of cross-sectional and deformation parameters of a berm breakwater[6]

This paper aims to numerically investigate the stability of spherical armour units placed on the top of the berm layer of berm breakwater under the wave design characteristic. In this regard, SPH is utilized to solve the fluid properties due to wave propagation and calculate the wave force applied to each armour unit. In addition, the DEM method is employed to investigate the stability of the armour units by considering the interaction forces between armour units and wave forces and moments.

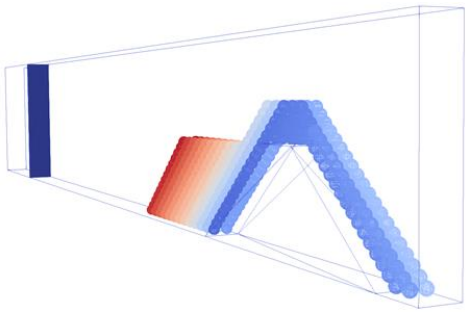

Figure 2. 3D Modeling of Core and Berm layers of berm breakwater

2. Governing Equations

In SPH method, the fluid domain is represented by a set of nodal points where physical quantities such as position, velocity, density and pressure are approximated. Therefore, each fluid particle having physical quantities such as mass, velocity, density, pressure and position. Each particle interacts with others according to some equations that have been derived from Navier-Stokes equations. In the solid phase, following the original idea of Koshizuka et al [7] a rigid body is represented by a set of particles whose relative position remain unchanged. In addition, for contact detection and shape representation of bodies Distributed Discrete Element Method (DCDEM) is utilized. The SPH-DCDEM in the DualSphysics is based on the multi-sphere approach with nonlinear viscoelastic contact for computation [8].

In this study, the open-source code DualSphysics [9] is utilized for the SPH-DCDEM simulation and more details are available in Violeau and Rogers [10].

3. Numerical Model

In this study, in order to the simulation of the reshaping berm breakwater, a 3D SPH-DEM model was utilized. The rubble mound breakwater is separated into two different layers (Core and Berm) layers (Figure 2). The core layer is simulated as a rigid boundary, and armour block units of the berm layer are simulated with the DEM bodies with 0.017 (m) diameter.

The specific weight of each armour unit is 2.65 (kg/m3).In addition, the water depth is equal to 0.24 (m), and the regular wave with 0.124 (m) height and 1.1 (s) period was simulated.

4. Result and Discussion

The displacement of armour units of the berm layer, and fluid particles velocity at t=7.5 (s), 7.75 (s) and t=8 (s) are represented in Figure 3.

As the wave runs down on the berm layer at the time t=7.5 (s), the velocity vectors of the fluid particles reach a speed of 1.5 (m/s), and the wave forces reduce the interlocking of units between the armour. Due to regular wave attacks, displacement of armour units will be removed and limited to sliding mode and low displacement in the following time steps.

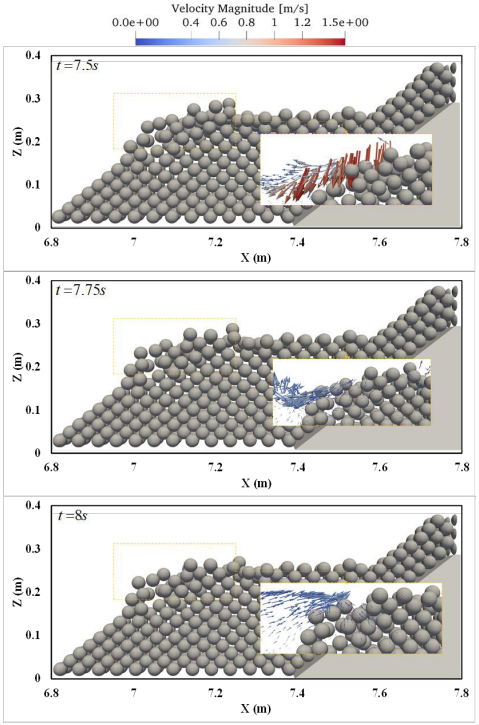

Figure 3. Reshaping the armour units of berm breakwater due to wave-structure interaction.

5. Conclusion

In this study, the armour stability of armour units of berm breakwater using SPH-DCDEM method was investigated. The SPH method was used to simulate fluid domain, and DEM method was used to investigate interlock phenomenon between armour units. By numerical scheme the interaction of wave and armour units was simulated. Furthermore, the displacement of hardly reshaping berm breakwater successfully simulated.

6. References

[1] H. F. Burcharth *et al.*, *State-of-the-art of Designing and Constructing Berm Breakwaters*. PIANC General Secretariat, 2003.

[2] J. der Meer and S. Sigurdarson, *Design and construction of berm breakwaters*, vol. 40. World scientific, 2016.

[3] B. Ren, Z. Jin, R. Gao, Y. Wang, and Z. Xu, "SPH-DEM Modeling of the Hydraulic Stability of 2D Blocks on a Slope," *J. Waterw. Port, Coastal, Ocean Eng.*, vol. 140, no. 6, p. 04014022, 2014, doi: 10.1061/(asce)ww.1943-5460.0000247.

[4] M. Sarfaraz and A. Pak, "An integrated SPH-polyhedral DEM algorithm to investigate hydraulic stability of rock and concrete blocks: Application to cubic armours in breakwaters," *Eng. Anal. Bound. Elem.*, vol. 84, no. April, pp. 1–18, 2017, doi: 10.1016/j.enganabound.2017.08.002.

[5] T. Iwamoto *et al.*, "Application of SPH-DEM coupled method to failure simulation of a caisson type composite breakwater during a tsunami," *Soil Dyn. Earthq. Eng.*, vol. 127, no. August, p. 105806, 2019, doi: 10.1016/j.soildyn.2019.105806.

[6] H. Akbari and M. Torabbeigi, "SPH modeling of wave interaction with reshaped and non-reshaped berm breakwaters with permeable layers," *Appl. Ocean Res.*, vol. 112, no. December 2020, p. 102714, 2021, doi: 10.1016/j.apor.2021.102714.

[7] S. Koshizuka, A. Nobe, and Y. Oka, "Numerical analysis of breaking waves using the moving particle semi-implicit method," *Int. J. Numer. methods fluids*, vol. 26, no. 7, pp. 751–769, 1998.

[8] R. B. Canelas, A. J. C. Crespo, J. M. Domínguez, R. M. L. Ferreira, and M. Gómez-Gesteira, "SPH-DCDEM model for arbitrary geometries in free surface solid-fluid flows," *Comput. Phys. Commun.*, vol. 202, pp. 131–140, 2016, doi: 10.1016/j.cpc.2016.01.006.

[9] A. J. C. Crespo *et al.*, "DualSPHysics: Open-source parallel CFD solver based on Smoothed Particle Hydrodynamics (SPH)," *Comput. Phys. Commun.*, vol. 187, pp. 204–216, 2015, doi: 10.1016/j.cpc.2014.10.004.

[10] D. Violeau and B. D. Rogers, "Smoothed particle hydrodynamics (SPH) for free-surface flows: past, present and future," *J. Hydraul. Res.*, vol. 54, no. 1, pp. 1–26, 2016.

14th International Conference on Coasts, Ports and Marine Structures
9 & 10 May 2023 , Tehran-IRAN
ICOPMAS 2022

EVALUATION OF DYNAMIC PERFORMANCE OF MONOPILE FOUNDATION OF OFFSHORE WIND TURBINES IN SANDY SOIL USING NUMERICAL MODELING

M. Ali Masoumi[1], S. Mohammad Sadegh Sahraeian[2], Mohammad Amir Najafgholipour[3] and Ali Shafiee[4]

1) Civil and Environmental Engineering, Shiraz University of Tech., Shiraz, Iran, m.masoumi@sutech.ac.ir
2) Civil and Environmental Engineering, Shiraz University of Tech., Shiraz, Iran, sahraeian@sutech.ac.ir
3) Civil and Environmental Engineering, Shiraz University of Tech., Shiraz, Iran, najafgholipour@sutech.ac.ir
4) Civil Engineering, California State Polytechnic University, Pomona, USA, ashafiee@cpp.edu

1. Introduction

Nowadays, the tendency to use energy renewable sources is increased due to the development of industry and the problems in the use of fossil fuels such as its instability in the future and environmental issues. Wind turbines are one of the most important and sustainable tools for renewable energy production.

The main purpose of the foundation in this infrastructure is to transfer structural and environmental loads to the ground. In general, 25% of the total cost of an offshore wind turbine project is spent on the design and implementation of the foundation [1]. Because of the development of wind farms in seismic areas, including East Asia, southern Europe, and the United States, as well as the importance of the foundation of the wind turbine in the design and implementation, it is necessary to study the seismic behavior of wind turbine foundations.

In this study, a parametric study on the seismic behavior of monopile foundation of offshore wind turbines (OWT) employing numerical modeling is performed.

2. Verification

In this study, to verify the numerical model, its results are compared with the results of dynamic centrifuge modeling reported by Wilson et al [2]. Wilson et al. conducted a series of centrifuge model tests on individual and group piles located in Nevada sand under a series of specific earthquakes.

The finite element method is employed using OpenSees for numerical modeling of monopile for OWTs. SANISAND constitutive model with calibrated parameters for Nevada sand proposed by Taiebat et al. [3] is used. In this study, the 1995 Kobe earthquake with PGA=0.22g is considered a reference earthquake record in all analyzes. The earthquake time history applied to the models is shown in Figure 1. Also, the verification results of the numerical model including the excess pore water pressure ratio (r_u), displacements, and accelerations are shown in Figure 2.

3. Model Descriptions and Methodology

The NREL offshore wind turbine with a capacity of 5 MW and a hub height of 90 m is considered in this study. This wind turbine is modeled by a hollow cylindrical section with an Elastic Beam-Column element. Also, the load of Rotor and Nacelle is modeled with a lumped mass at the top of the tower. The superstructure is supported by a monopile foundation and the dimensions of the model ground are 100×70 m² with a height of 35 m. The soil is modeled with 2784 to 4524 Brick UP 3D elements and the monopile is modeled with Elastic Beam-Column element. The soil-structure interaction is provided by linear elastic elements in OpenSees software and the earthquake time-history is applied in the longer direction of the model.

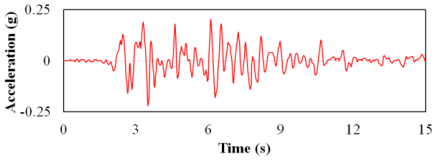

Figure 1. Record of earthquake applied to the models

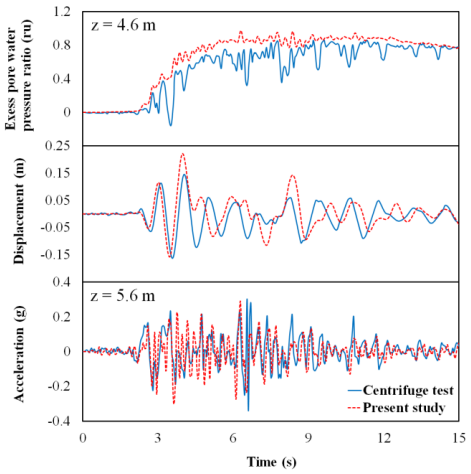

Figure 2. Comparison of the results of numerical and centrifuge modeling.

4. Cases of Parametric Study

In this study, the effects of various parameters such as dimensions of monopile (diameter and length), soil relative density, and the existence of wind load (cyclic and static) are evaluated. The considered cases are presented in Table 1.

Table 1. Cases of parametric study

h	Model No.	D	L	Dr (%)	Wind load
Monopile diameter effect	Model 1	4	25	70	-
	Model 2	6			
	Model 3	8			
Monopile length effect	Model 4	6	20	70	-
	Model 5		25		
	Model 6		30		
Sand relative density effect	Model 7	6	25	30	-
	Model 8			50	
	Model 9			70	
	Model 10			90	
Wind load effect	Model 11	6	25	70	Cyclic
	Model 12				Static

5. Results

The displacement of the tower head and foundation settlement for different cases are shown in Figure 3. Also, the rotation of monopile is presented in Table 2. As the diameter and length of monopile and sand relative density increase, the tower head displacement and monopile's settlement and rotation are decreased. The static wind load causes more displacement and rotation in comparison to the cyclic wind load which indicates a more critical case. Because the maximum allowable rotation after an earthquake is about 0.5 degrees [4], models 7, 11, and 12 are not acceptable.

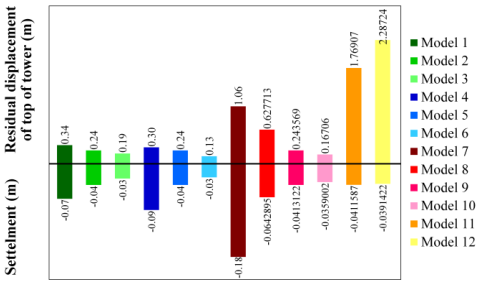

Figure 3. Residual displacement of tower head and settlement of monopile for each model.

Table 2. Residual rotation of monopile for each model.

Model No.	1	2	3	4	5	6
Rotation (°)	0.18	0.13	0.1	0.16	0.13	0.11
Model No.	7	8	9	10	11	12
Rotation (°)	0.55	0.33	0.13	0.09	0.91	1.18

The profiles of excess pore water pressure ratio at a 1 m distance from the monopile are shown in Figure 4. As the figure indicates, in most of the cases, especially in the shallower parts, the ground is almost liquefied which would enhance the settlement and rotation of the foundation and displacement of the tower.

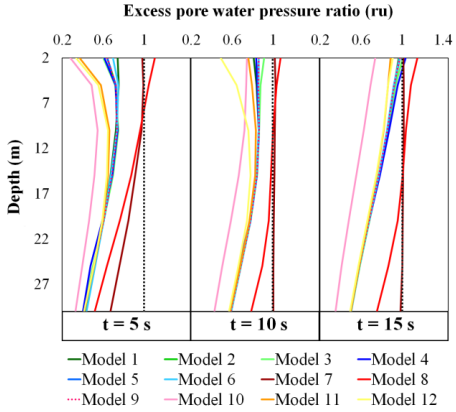

Figure 4. Profiles of excess pore water pressure ratio (r_u) at a different time for each case.

6. Conclusion

In this study, a parametric study on the seismic behavior of the monopile foundation of OWT is presented. The results indicate that increase in monopile length and diameter is reduced the monopile settlement and rotation and displacement of the tower. Because in this study, just an individual earthquake time history is applied to the model, the performance of the foundation in case of occurrence of other types of earthquake time histories should be investigated. Also, the improvement of monopile seismic performance by enhancing the sand density is verified. Finally, it is shown that the existence of wind load especially static wind load creates a worse performance.

7. References

[1] Wang, Xuefei, et al. "Feasibility study of offshore wind turbines with hybrid monopile foundation based on centrifuge modeling." Applied energy 209 (2018): 127-139.

[2] Wilson, Daniel W., Ross W. Boulanger, and Bruce L. Kutter. "Observed seismic lateral resistance of liquefying sand." Journal of Geotechnical and Geoenvironmental Engineering 126.10 (2000): 898-906.

[3] Taiebat, Mahdi, et al. "Propagation of seismic waves through liquefied soils." Soil Dynamics and Earthquake Engineering 30.4 (2010): 236-257.

[4] Kaynia, Amir M. "Seismic considerations in design of offshore wind turbines." Soil Dynamics and Earthquake Engineering 124 (2019): 399-407.

14th International Conference on Coasts, Ports and Marine Structures
9 & 10 May 2023 , Tehran-IRAN
ICOPMAS 2022

PHYSICAL MODELING OF KANGAN PORT BREAKWATER

Peyman Badiei[1], Soroush Aliasgary[2], Mohammad Hosein Golchin[3] and Mohammad Bagheri[4]

1) School of Civil Engineering, College of Engineering, University of Tehran, pbadiei@ut.ac.ir
2) School of Civil Engineering, College of Engineering, University of Tehran, Soroush.asgary@ut.ac.ir
3) School of Civil Engineering, College of Engineering, University of Tehran, m.hossein.golchin@ut.ac.ir
4) Ports and Maritime Organization (PMO), Tehran, Iran, mbagheri@pmo.ir

1. Introduction

In costly projects, it is essential to achieve a high degree of confidence in the technical and economic performance of the design and the application of physical models are the best choice in this course. Due to the complexities of coastal structures on one hand and the simplified assumptions used in their design, it either is quite possible for the design to be over or under estimated. Physical (scale) models are carried out to optimize the geometry of the proposed design and improve its performance [1]. In this paper, a description of the physical modeling process of Kangan Port static berm breakwater is presented. According to the contract between the Ports and Maritime Organization and the Vice Chancellor for Research of the University of Tehran, the experiments on the two-dimensional physical modeling of the Kangan's breakwater development were assigned to the Water Institute of the University of Tehran and were carried out at the Hydraulic Laboratory at the School of Civil Engineering.

2. Description and Design of Experiments

These experiments were carried out to ensure the armor layer and lee side stability of the berm breakwater and control the overtopping volume.

The layout of the Kangan Breakwater is shown in Figure 1. According to the wave climate and the numerical modeling results presented by the Consultant, the E5 section is exposed to the highest waves and at the greatest depth. Therefore, section E5 was suggested for modeling.

The Hudson Equation is used to select the scale of the physical model, taking into account laboratory equipment, breakwater characteristics, and wave generator characteristics. On this basis, the relationship used for scaling of armor and filter layer calculations is given as follows [2]:

$$\frac{\overline{W_m}}{\overline{W_p}} = \frac{1}{\lambda^3}\frac{\rho_{sm}}{\rho_{sp}}\frac{\left(\frac{\rho_{sp}}{\rho_{wp}}-1\right)^3}{\left(\frac{\rho_{sm}}{\rho_{wm}}-1\right)^3} \qquad (1)$$

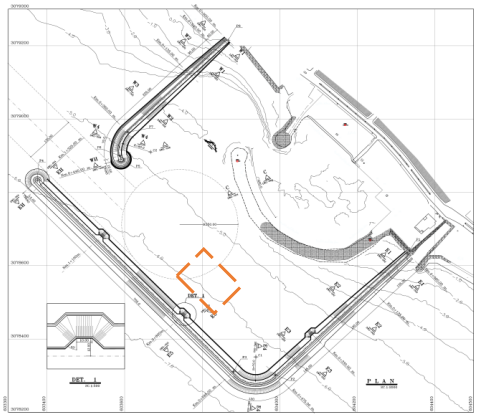

Figure 1. Location plan of Kangan port breakwater arms

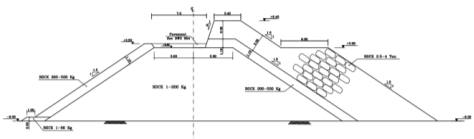

Figure 2. E5 section of the eastern breakwater with armor 2.5 to 4 tons

In the above relation, W_m is the weight of the model materials and W_p is the weight of the prototype materials. λ is the scale of the model, ρ_{sm} is the density of model materials, ρ_{sp} is the density of prototype materials, ρ_{wp} is the density of seawater and ρ_{wm} is the density of laboratory water. Details of scaling calculations and assumptions are provided in Table 1. It should be noted that the scales obtained in this table have been determined based on the densities of 2.3 t/m^3 for prototype and 2.5 t/m^3 for model, respectively. The density of seawater is assumed to be 1.03. Given the above values and considering the dimensions of the breakwater, the largest possible scale of 25 was applied. In Table 1, P is equivalent to Prototype, S is equivalent to Scale, and M is equivalent to Model.

Table 1. Determining the scale of the laboratory model

		Leaside Armour-Filter		Seaside Armour		Unit
P	W_p	200 kg	500 kg	2.5 ton	4 ton	
S	λ	25	25	25	25	-
M	V_m	0.0032	0.0079	0.0397	0.0635	lit
	W_m	8	20	99	159	gr
	ρ_{sm}	2.5	2.5	2.5	2.5	t/m^3
	ρ_{wm}	1	1	1	1	t/m^3
	Δm	1.5	1.5	1.5	1.5	-

3. Wave Generation Equipment

The wave flume at the Hydraulic Laboratory of the School of Civil Engineering has a length of 25.2 meters, a width of 1 meter, and a useful height of 1.2 meters. It is constructed on a concrete foundation with a thickness of 0.5 meters as shown in Figure 3.

Figure 3. Wave flume University of Tehran

The wave generator of this flume is of piston type that can generate regular and irregular waves. The range of motion of the wave generator paddle (stroke) is in the range of -12 to +12 cm. The period of regular waves that can be generated by the paddle is between 0.5 to 6 seconds. Figure 4 shows a schematic view of the dimensions of experiments in the wave flume. The distance of the sensors from the structure was determined according to Mansard method [3].

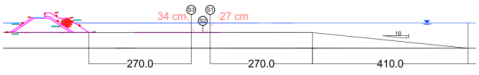

Figure 4. Implementation of model cross-section in flume (sizes are in centimeters)

4. Results

Table 2 shows the characteristics of the target waves and the features of the resulting waves. Also, as an example, the wave spectrum obtained from test 2 is shown in Figure 5.

Table 2. Comparison of target wave specifications with final test results

Test. No	d (cm)	Target	Results		
		Tp (s)	Hs (cm)	Tp (s)	Hs cm)
1	30.1	1.56	9.8	1.48	10.1
2	30.1	1.56	12.3	1.55	12
3	30.1	1.56	14.7	-	-
4	36.4	1.56	9.8	-	-
5	36.4	1.56	12.3	1.62	12.9
6	36.4	1.56	14.7	1.56	15
7	35.5	1.56	12.3	1.56	12.8

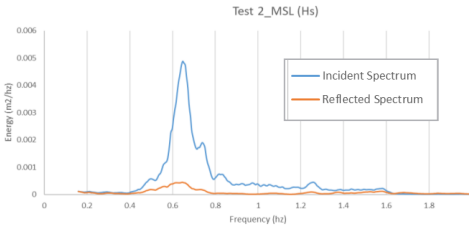

Figure 5. Incident and reflection spectrum of test 2

The experiments were designed to control the stability of armor layer and the volume of overtopping.

Overtopping was only observed in experiments 5 and 7, as shown in Table 3. Berm destruction was minimal and negligible in tests 1, 2, and 4, which are the design conditions for static berm breakwaters. As the test has been planned for residual stability, no repair has been done between the tests. In tests 5 and 6, despite the lack of repair between experiments, the damage was limited to the displacement of 10 pieces of armor.

Table 3. Overtopping tests results

Test. No.	Model overtopping (L)	Prototype overtopping results (L/m.s)
5	68.74	4.77
7	28.37	1.99

5. References

[1] Guidelines for physical model testing of rubble mound breakwaters." *Coasts, marine structures and breakwaters: Adapting to change: Proceedings of the 9th international conference organised by the Institution of Civil Engineers and held in Edinburgh on 16 to 18 September 2009*. Thomas Telford Ltd, 2010.

[2] Hughes, S. A. (1993). Physical models and laboratory techniques in coastal engineering (Vol. 7). World Scientific.

[3] Mansard, Etienne PD, and E. R. Funke. "The measurement of incident and reflected spectra using a least squares method." Coastal Engineering 1980. 1980. 154-172.

14th International Conference on Coasts, Ports and Marine Structures
9 & 10 May 2023 , Tehran-IRAN
ICOPMAS 2022

INVESTIGATING THE EFFECT OF THE TYPE OF SEABED SEDIMENTS ON THE SETTLEMENT OF BREAKWATER MATERIALS

Mohammad Hadi Moeini [1] Majid Jandaghi Alaee[2] and Habibollah Namdari[3]

1) PhD in Coastal Eng., Pouya Tarh Pars Cons. Eng. Company, Tehran, Iran, mhmoeini@gmail.com
2) PhD in Coastal Eng., Pouya Tarh Pars Cons. Eng. Company, m.j.alaee@ptpco.com
3) MSc in Coastal Eng., Pouya Tarh Pars Cons. Eng. Company, Tehran, Iran, h.namdari@modares.ac.ir

1. Introduction

Breakwaters are one of the main and most expensive components in the construction of ports. In our country, like many countries in the world, rock-fill materials are used to build most of the breakwaters. In some coastal areas of our country, the material of the seabed is such that during the construction of the breakwater, the settlement of the layers of the seabed or the subsidence of the materials in the lower layers may occur. This causes the construction costs to increase significantly. Therefore, it is appropriate to provide a realistic estimate of the amount of subsidence by knowing the condition of the seabed before constructing the breakwater. One of the easiest ways to know the seabed is to check the grading and morphological condition of the seabed. In this article, an attempt is made to investigate the impact of seabed grading on the settlement of the breakwater by providing seabed grading information from the construction area of two breakwaters where subsidence occurred.

2. Study Area and Breakwaters Settlement

In this study, the seabed condition and the breakwater settlement in the two projects of Nakhl Nakhda and Bandar Deylam are investigated. Nakhl Nakhda project is located on the eastern coast of Bandar Abbas city, about 8 kilometers east of Haqqani port. The current status of this project is shown in Figure 1. This breakwater was completed in 2015. By a distance from the coast, some settlements have been observed during the construction of the breakwater. For the settlement of the breakwater in this project, the maximum value of 5 meters has also been reported, which has been reduced to about 2 meters after adopting a series of special construction operations [1].

Deylam Port is also located on the northern coast of Bushehr province and in Deylam Bay (Handijan Bay). The current harbor includes two jetties (Figure 1) that were completed in 2002. During the construction of these jetties, a significant subsidence of the materials in the seabed has been observed. For the amount of subsidence in Deylam Port project, significant values even up to more than 15 meters have been reported. Based on this, the amount of subsidence increases with the distance from the coast, so that the highest amount of subsidence and settlement has been observed at the end of the constructed jetties.

Figure 1. Layouts of the Nakhl Nakhoda (up) and Deylam Project (down)

3. Seabed Sediment Data

In order to evaluate the type of sea bed material and its relationship with the amount of breakwater settlement, a series of sea bed sampling has been defined from both projects. In the Nakhl Nakhda project, seabed sampling was conducted at about 20 points around the breakwater, and Laser Scattering Particle Size Distribution tests were performed on the samples. Figure 2 shows the location of the samples and the average diameter of the sediment particles in micrometers.

As seen, the sea bed sediments in the initial sections of the breakwater are sandy and have an average particle size of about 100 micrometers. In the areas where the

settlement of the breakwater begins, the average diameter of the particles decreases and turns from sand to silt and clay, so that the average diameter of the particles reaches about 50 micrometers or less. Considering that by continuing to deeper waters, the diameter of the particles also decreases and reaches the range of 20 microns, it is expected that the amount of settlement and subsidence of the breakwater will increase in these areas.

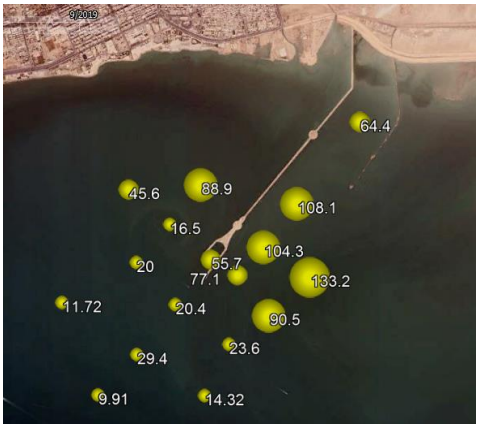

Figure 2. The location and average diameter (in micrometer) of the seabed samples in Nakhl Nakhoda

For Deylam port, sea bed materials have been sampled and Laser grading tests have been carried out at around 40 points around the constructed jetties. Figure 3 shows the sampling location and the average diameter of the sediment particles in micrometers in the Deylam project. As seen, near the shoreline, the sediments of the seabed are of sand type with a maximum average size of about 150 microns, while their diameter decreases by moving away from the coast and they become silt and clay. At the water depths below about -2 (CD), the sea bed sediments are very fine with the diameter of less than 10 microns (Figure 4). A sample of a laser grading test for a point with -4 m depth is shown in Figure 5. A point that should be considered in this regard is the possible impact of the construction of the jetties on the characteristics of the seabed sediments and the change in the type of sediments due to the sedimentation caused by the construction of the jetties.

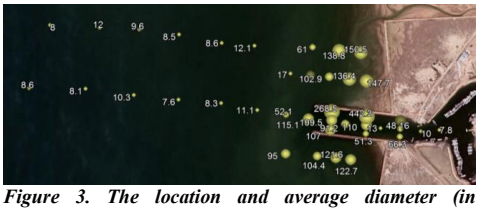

Figure 3. The location and average diameter (in micrometer) of the seabed samples in Deylam

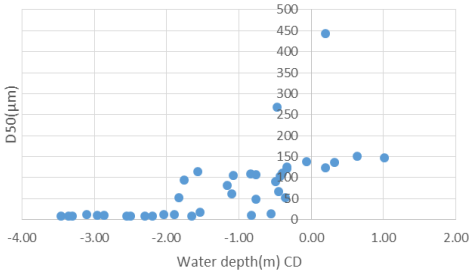

Figure 4. The average diameter (D50) of sea bed samples versus water depth in Deylam

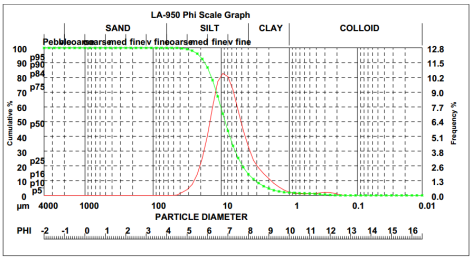

Figure 5. A sample of laser grading test for a point with -4 m depth in Deylam

4. Conclusion

In this research, the characteristics of the seabed sediments in two breakwater sites that faced subsidence and settlement during construction were investigated. In order to analyze the characteristics of sea bed sediments, several sediment samples were taken from each site and subjected to Laser Scattering Particle Size Distribution test. The obtained results indicate that in both situations, the type of sea bed sediment in the coastal area is sand and it turns into silt and clay by moving towards the sea. Also, in both locations, during the initial sections of the construction of breakwaters, significant subsidence and settlement are not observed, and the amount of subsidence and settlement increases with the movement towards greater depths and fine-grained sediments.

5. References

[1] Kazemi Aski, A., Bardideh, A., and Jandaghi Alaee, M., "A study on the settlement of Nakhl-E-Nakhoda breakwater and the applied solution", Proceeding of the 11th intentional conference on coasts, ports and marine structures (ICOPMAS) *2014,* pp. 572-575.

14th International Conference on Coasts, Ports and Marine Structures
9 & 10 May 2023 , Tehran-IRAN
ICOPMAS 2022

EXPERIMENTAL STUDY ON THE STABILITY OF SINGLE-LAYER ARMOUR UNITS FOR LOW-CRESTED/SUBMERGED BREAKWATERS

Ali Pak[1], Mohammad Mohammadnia[2] and Naser Saadat khah[3]

1) Sharif University of Technology, Department of Civil Engineering, Tehran, Iran, Email: pak@sharif.edu
2) Sharif University of Technology, Dept. of Civil Engineering, Tehran, Email: mo.mohammadnia@gmail.com
3) Darya Pajouh Sazehpardazi Company, Tehran, Iran, Email: Saadatkhah@sazehpardazi.com

1. Introduction

Low-crested/submerged breakwaters are rubble-mound structures that have become increasingly important in coastal protection projects in recent years. These structures are more environmentally-friendly comparing to high-crested breakwaters because they do not hinder the sea view from the shore, do not affect the water quality, require less geomaterials for construction while protecting the beach against erosion. Using single-layer concrete armour blocks for reinforcing the outer layer of low-crested/submerged breakwaters is an innovative idea that requires analytical and experimental investigations. In this study a large number of model tests have been carried out in a hydraulic flume to study the performance and stability of two types of concrete blocks for this purpose.

A number of researchers have studied the applicability of single-layer concrete armour units for protecting the "high-crested" breakwaters. Accropode, Xbloc and Core-loc have been the most used concrete blocks for single-layer armour so far. Few studies have been done on the stability and performance of single-layer concrete armour units for low-crested/submerged breakwaters. [1], [2], [3] describe the results of the investigations on the performance of single-layer armour units.

2. Test Plan and Procedures

The physical model tests were carried out in the hydraulic flume of the department of civil engineering of the University of Tehran. The flume has 25.2 m length, 1.0 m width, and 1.3 m depth. The wavemaker of this flume is capable of producing both regular and random waves. The maximum wave height that can be produced by wave maker is 250 mm. The wave height fluctuations at the breakwater toe are measured using voltage resistance wave sensors with the accuracy of 0.1 mm. These gauges recorded the wave height with the frequency of 50 times per second. The scale of the tests was 1:30. Froude similarity law was used for similitude purpose.

The tests were carried out for 3 different conditions: 1) the crest of the breakwater was considered slightly above the Mean Sea Level (MSL) i.e., positive freeboard, 2) equal to MSL i.e., zero freeboard, and 3) slightly below the MSL i.e., negative free board. In this study, the height of the breakwater was 370 mm. Negative freeboard (submerged breakwater) was tested with 410 mm water depth at the breakwater toe and positive freeboard was tested using 330 mm water depth. The crest width was 5D (five times the armour diameter) and the breakwater slope was 1V:1.5H in all the tests. Waves generated in the flume were both regular and random with three periods of 1.643 sec., 2.008 sec. and 2.373 sec (corresponding to 9, 11 and 13 seconds in reality). The wave periods were selected corresponding to the wave periods at the Persian Gulf and Oman Sea regions.

Two types of concrete armour blocks were used in this investigation: Xbloc and modified Xbloc (Dezhpod). A typical placement of the armour units on the breakwater in the flume is illustrated in Figure 1.

Figure 1. Placement of modified Xbloc

Since the aim of this study was evaluating the stability of single-layer armours under the impact of waves, accurate identification of the failure is of utmost importance. Among the existing criteria for distinguishing the instability or damage to the armour layer due to wave impact, Initiation of Damage [ID] was used in this study. Initiation of Damage, by definition, starts when at least one armour unit is moved from its initial position to an amount equal to armour diameter. The tests were carried out by gradual increasing the wave height until Initiation of Damage of the armour layer was observed. The range of the wave heights generated in the flume was between 120 - 200 mm which is correspondent to wave heights between 3.6 m to 6.0 m in reality.

3. Results and Discussion

18 set of tests were carried out in the laboratory to investigate the performance and stability of single-layer Xbloc armours placed on low-crested/submerged breakwater subjected to wave action at various conditions. The results are summarized in Table 1.

Table 1. Results of Experiments using Single-layer Xbloc at Different Conditions of Breakwater Freeboard and Wave (Xh: harmonic wave tests, Xr: random wave test)

Test No.	Wave Period (s)	Water Depth (mm)	Wave Height (m)	Test No.	Wave Period (s)	Water Depth (mm)	Wave Height (mm)
Xh1	1.643	330	170.9	Xr1	1.643	330	168.9
Xh2	2.008	330	156.8	Xr2	2.008	330	154.3
Xh3	2.373	330	152.1	Xr3	2.373	330	150.4
Xh4	1.643	370	173.5	Xr4	1.643	370	168.5
Xh5	2.008	370	164.2	Xr5	2.008	370	160.3
Xh6	2.373	370	155.3	Xr6	2.373	370	151.4
Xh7	1.643	410	191.6	Xr7	1.643	410	183.7
Xh8	2.008	410	180.8	Xr8	2.008	410	172.4
Xh9	2.373	410	174.5	Xr9	2.373	410	164.9

For better interpretation of the results and also for design purposes, non-dimensional parameters of N_S and R_C are used as shown in Figure 2. R_C and N_S as defined as follows:

$$R_C=L-h \qquad N_S=H/(\Delta D_{n50})$$

In these relations L is the total height of the breakwater (370 mm), h is the water depth at the breakwater toe, H is the wave height corresponding to Initiation of Damage, D is the average armour unit diameter, and Δ is the ratio between concrete density and water density.

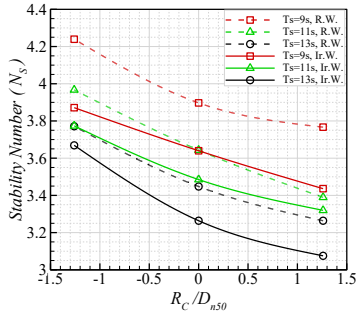

Figure 2. Experiments results performed on Xbloc units (R.W.: Regular wave, Ir.W.: Irregular wave)

Figure 2 reveals that the non-dimensional stability number (N_S) for irregular waves are less than that for the regular waves for all cases of wave periods, indicating that the irregular waves in reality create more critical conditions for the armour layers. Values of N_S generally show a decreasing trend with R_C. This decreasing trend means that submergence can provide more stability for the armours used as single-layer. Another interesting point is decreasing N_S with increasing the wave period which indicates longer wave periods can impose more damage to the armour layer.

One of the disadvantages of Xbloc units is its vulnerability to damage during transportation and placement. This is mainly because of its special geometric configuration and outward projections. In this study an improved version of Xbloc units called Dezhpod has also been examined. Dezhpod is similar to Xbloc, however, some changes are applied to its shape in order to enhance its structural integrity. The same tests were carried out on Dezhpod to compare its performance with Xbloc. The results of the tests on the newly developed blocks are shown in Table 2.

Table 2. Results of Experiments using Single-layer Dezhpod at Different Conditions of Breakwater Freeboard and Wave (Dh: harmonic wave tests, Dr: random wave test)

Test No.	Wave Period (s)	Water Depth (mm)	Wave Height (mm)	Test No.	Wave Period (s)	Water Depth (mm)	Wave Height (mm)
Dh1	1.643	330	171.4	Dr1	1.643	330	169.4
Dh2	2.008	330	157.6	Dr2	2.008	330	154.9
Dh3	2.373	330	153.1	Dr3	2.373	330	151.6
Dh4	1.643	370	172.4	Dr4	1.643	370	169.7
Dh5	2.008	370	165.3	Dr5	2.008	370	162.1
Dh6	2.373	370	154.9	Dr6	2.373	370	152.6
Dh7	1.643	410	190.9	Dr7	1.643	410	183.9
Dh8	2.008	410	182.4	Dr8	2.008	410	172.6
Dh9	2.373	410	173.8	Dr9	2.373	410	163.8

Comparison between the values of Table 1 and 2 demonstrate the fact that behavior of Dezhpod is very similar to Xbloc. Careful review of the values shows that the performance of Dezhpod is slightly better because it has higher stability numbers.

4. Conclusions

Using single-layer armours for protecting the low-crested/submerged breakwater in a new idea that has not been studied in-detail before. In this study two types of concrete armour blocks were used to protect low-crested and submerged breakwaters. Based on the obtained results the following conclusions can be drawn:

- Employing single-layer armour blocks is safe and economical.
- Submergence of the crest increases the stability of the blocks used as single-layer armour.
- The performance of the Xbloc units can be improved if some changes are applied to its shape.

5. Acknowledgement

The financial support provided by the deputy of research and technology of Sharif University of Technology for conducting the experimental studies is gratefully acknowledged.

6. References

[1] Salauddin, M., "A review on the development and applications of single-layer concrete armour units in the design of rubble mound breakwaters", *Jordan Journal of Civil Engineering*, 2018, Vol.12, No.1.
[2] Besley, P. & Denechere, M., "Single-layer armour systems – Toe, Crest, and roundhead details", *Coasts, Marine Structures, and Breakwaters Conference*, EICC, Scotland, 2009
[3] Denechere, M. & Thomson, I. "Experience with Single-layer Breakwaters armours", *COPEDEC*, 1999

14th International Conference on Coasts, Ports and Marine Structures
9 & 10 May 2023 , Tehran-IRAN
ICOPMAS 2022

NUMERICAL MODELING OF WAVE INTERACTION WITH A VERTICAL WALL BY LATTICE BOLTZMANN METHOD (LBM)

Farshid Mennati'Nezhad[1], Kourosh Hejazi[2], Nima Ghomri[3] and Hamid Reza Shirkavand[4]

1) Coastal and offshore engineering Department, K. N. Toosi university of technology, Tehran, Iran, f_mennatinejad@email.kntu.ac.ir
2) Coastal and offshore engineering Department, K. N. Toosi university of technology, Tehran, Iran, HejaziK@kntu.ac.ir
3) Water and Hydraulic Structures Department, K. N. Toosi university of technology, Tehran, Iran, hshirkavand@kntu.ac.ir
4) Coastal engineering Department, K. N. Toosi university of technology, Tehran, Iran, nima.ghomri@gmail.com

1. Introduction

Evaluation of the hydrodynamic forces on the solid structures is one of the most interesting aspects in modeling with the lattice Boltzmann method (LBM). In the present paper, the momentum exchange method (MEM) was used to calculate hydrodynamic forces, which was firstly proposed by Ladd and Anthony [1,2]. In this approach, hydrodynamic forces are obtained by distribution function differences in all directions of all lattice cells. Whereas the MEM is considered an explicit approach for updating the dynamics of the particles, Aidun et al. [3] proposed a relatively more accurate approach based on the MEM which involves the hydrodynamic analysis of particles suspended in fluid. This work aims to develop a numerical model based on the LBM and MEM to evaluate wave-structure interaction.

2. Lattice Boltzmann Method

The lattice Boltzmann method (LBM) was initially proposed to solve the problems in the mesoscopic scale. However, the particle distribution function parameter (f) describes particle behaviors on the microscopic scale. In this article, the D_2Q_9 scheme is applied, and macroscopic parameters such as density (ρ) and velocities ($\boldsymbol{V}$) are obtained directly from the distribution function, which are presently as follows:

$$\rho = \sum_{i=0}^{n} f_i \qquad \rho \boldsymbol{V} = \sum_{i=0}^{n} f_i \tag{1}$$

The equilibrium distribution function (f_i^{eq}) represents the movement of particles toward an equilibrium state. The following equation gives the equilibrium distribution function:

$$f_i^{eq} = \rho w_i (1 + 3(\boldsymbol{c}_i.\boldsymbol{V}) - 1.5(\boldsymbol{V}.\boldsymbol{V}) + 4.5(\boldsymbol{c}_i.\boldsymbol{V})^2) \tag{2}$$

where w and c represent weighting factors and discretized velocities, respectively. Collision and streaming are two primary operators to model the fluid dynamics. The collision operator simulates the interaction between particles with the relaxation time (τ) and the equilibrium distribution functions, and streaming describes the movement of particles within the domain. In each timestep, a particle moves from its cell to its neighbor cell according to its direction.

$$\tilde{f}_i(\boldsymbol{x}, t + \Delta t) = f_i(x, t) + \frac{\Delta t}{\tau}\left(f_i(x, t) - f_i^{eq}(x, t)\right)$$
$$f_i(\boldsymbol{x} + \Delta x, t + \Delta t) = \tilde{f}_i(\boldsymbol{x}, t + \Delta t). \tag{3}$$

3. Free Surface Modeling

In this paper, the free surface evolution was modeled based on the volume of fluid (VOF-like) method. In this approach, the physical domain is discretized into fluid, air and interface areas. The fluid domain is surrounded by interface cells, and the mass transfer between cells is calculated directly by using the flux of the distribution functions during the streaming step. The volume fraction (ε) parameter for each cell is the fraction of the mass (m) of the cell to its volume (v). The free surface is captured by the mass of each cell in each and every time step. The free surface is shaped by mass fluxes between cells.

$$m^{t+1} = m^t - \sum_i \phi_i \cdot \Delta t \qquad \phi_i = [f_i - f_i^n] A_i \tag{4}$$

In the above equation A_i defines as a wet area between two adjacent cells.

4. Momentum Exchange Method

Simplicity and computational efficiency are the MEM marked features. Hydrodynamic forces are obtained by calculating momentum exchange at each boundary cell in every lattice direction. Differences between outgoing and incoming momentums of distribution functions result in momentum exchange on the corresponding link$i$.

$$\delta F_i(x, t) = \tilde{f}_i(x, t) e_i - f_{\bar{i}}(x_{f,t}) e_{\bar{i}} \tag{5}$$

In each time step of the computations, the total force exerted from fluid to the obstacle is calculated from the summation of all momentum fluxes in each boundary link:

$$F = \sum_{i=0}^{8} \delta F_i(x_w, e_i) \tag{6}$$

5. Wave-Structure Interaction

In order to evaluate the ability of the model to simulate wave forces, experimental modeling of wave forces acting on a vertical wall by Didier results [4] was utilized, which

was basically conducted for the validation of numerical simulations

5.1. Free Surface Measurement

A wave gauge is located at 1.703 m apart from the right-hand side of the domain. The LBM simulation results and the experimental measurements show a good agreement (Figure 1). The test is performed in a tank of 0.3 m depth of water with a wave period of 1.3 s, a wavelength of 1.965 m, and a wave height of 0.1 m.

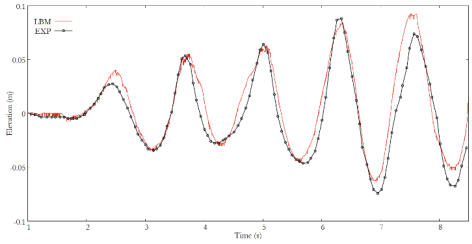

Figure 1. Comparison between the LBM simulated results and experimental measurements for the free surface

5.2. Wave Force

The LBM simulated results for wave forces on the vertical wall is shown in Figure 2, and are compared with the extracted measured values from pressure sensor B (PS-B), which is set 0.11 m above the berm. The same comparison is demonstrated in

Figure ***3*** for pressure sensor A (PS-A), which is set 0.055 m above the berm.

The results in both cases have the same trend as the experimental values of the Didier work. The initial validation for wave forces shows compliance with the reference data and implies the stability of the simulator.

The MEM is useful for general trend of the hydrodynamic forces, and is not capable of simulating shock waves which are formed in the third and fourth incident waves.

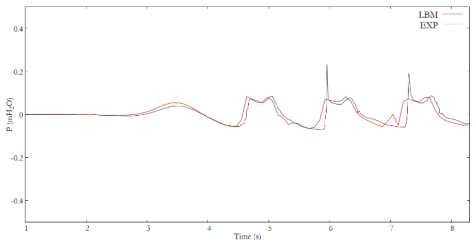

Figure 2. Comparison between the LBM simulated results and experimental measurements for wave forces in PS-B

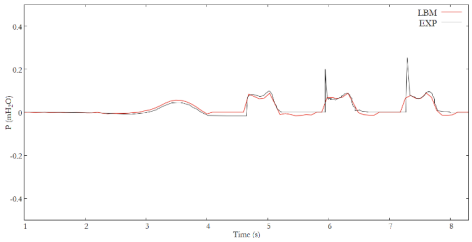

Figure 3. The simulated results of the LBM and experimental measurements for wave forces in PS-A

6. Conclusion

In this work, the application of the LBM for modeling wave-structure interaction was presented. The MEM was utilized for its relatively fewer computations and consequently less processing time. Despite the simplicity in implementation, the MEM may be used for wave-structure interaction problems leading to decent results. The simulation results for free surface capturing and wave forces show a favorable agreement and the same trend between the LBM framework and the experimental data, which demonstrate the ability of the present model to simulate the complicated wave-structure interaction. However, the performance comparison for modeling shock waves shows the shortcoming of the MEM in this particular aspect.

7. References

[1] Ladd, A. J. C., "Numerical simulations of particulate suspensions via a discretized Boltzmann equation. Part 1. Theoretical foundation", *Journal of Fluid Mechanics*, vol. 271, pp. 285–309, Jul. 1994, doi: 10.1017/S0022112094001771.

[2] Ladd, A. J. C., "Numerical simulations of particulate suspensions via a discretized Boltzmann equation. Part 2. Numerical results", *Journal of Fluid Mechanics*, vol. 271, pp. 311–339, Jul. 1994, doi: 10.1017/S0022112094001783.

[3] Aidun, C. K., Lu, Y., and Ding, E.-J., "Direct analysis of particulate suspensions with inertia using the discrete Boltzmann equation", *Journal of Fluid Mechanics*, vol. 373, pp. 287–311, Oct. 1998, doi: 10.1017/S0022112098002493.

[4] Didier, E., Neves, D., M. R., and Neves, M.. "Wave interaction with a vertical wall: SPH numerical and experimental modeling", *Ocean Engineering*, vol. 88, pp. 330–341, Sep. 2014, doi: 10.1016/j.oceaneng.2014.06.029.

14th International Conference on Coasts, Ports and Marine Structures
9 & 10 May 2023 , Tehran-IRAN
ICOPMAS 2022

NUMERICAL SIMULATION OF BASIN OF SEAWATER INTAKE SYSTEM

Ali Ghasemi[1], Mehdi Shafieefar[2] and Mohammadreza Khosravi[3]

1) Engineering Faculty, Qom University, Qom, Iran, Ghasemi.ali89@gmail.com
2) Faculty of Civil and Environmental Engineering, Tarbiat Modares University, Tehran, Iran, shafiee@modares.ac.ir
3) Pars Geometry Consultants, Tehran, Iran, mr.khosravi@srbiau.ac.ir

1. Introduction

Providing new sources of water is critical in face of decreased precipitation. Desalinated seawater is one of the most important new sources. A commonly used method of seawater intake is by using the systems that comprise pipelines and pump basins. In such a system, dimensions of the required basin and its components are determined based on hydraulic formulas first. These dimensions are then analyzed via numerical simulation. The prior researches are discussed in this study, and then the CFD modeling of the Lian desalination plant basin is presented.

The possibility of creating a vortex in the basin should be taken into account when designing the basin. Vortices may be formed due to three main categories: a) Eccentric orientation; b) Viscosity induced velocity gradients; c) Eddies formed by obstruction [1]. The required minimum submergence of pumps is another factor that should be to considered in basin design to avoid the formation of a vortex.

The situation of flow at the entrance of the suction bell depends on many components. Designing of the pump bay is in a way that the flow is uniform and the air cannot ingest into the pump [2].

To overcome the challenges produced by the decrease of water flow and the basin's minimum water level, Sami Abdel-Fattah and Abdel-Ghani El-Shaikh used ANSYS software to simulate the El-SHABAB basin and modify its design [2].

Zhaol et al have studied the mechanism of vortex formation. The flow parameters in the pumping bay, as well as the examination of pump performance in the presence of mixed flows, were investigated in this study. The effectiveness of anti-vortex structures, as well as their impact on current uniformity, has been demonstrated. The probability of cavitation in sharp areas, as well as the possibility of its expansion, was also looked into [3].

2. Model Setup

This project is planned to produce 50,000 m3/day fresh water. There are eight pumps in the pump basin, each with a capacity of 0.292 m3/s (six operational pumps and two spare pumps). The basin's geometry is depicted in Figure 1. The FLOW-3D software was used to simulate the Lian desalination basin. This software, which is compatible with complex flow conditions in two-dimensional and three-dimensional modeling, is one of the most powerful and user-friendly among the computational fluid dynamics tools.

There are several physical parameters for modeling different phenomena in FLOW-3D software. Gravity, viscosity-turbulence, and spring-well are three physical factors that were employed in this simulation. Results of studies have already showed that the best model of turbulence in this type of simulation is spinning.

Determining the computing grid and boundary conditions is one of the most critical aspects of numerical modeling. The nested mesh capability is used in this simulation and a smaller mesh is used as a patch in place of the pumps (Figure 1 and Figure 2). Symmetry is employed as a boundary requirement on all sides of the computing grid. Also, pumps are simulated as a sink that sucked the water with a rate -0.3 m^3/s.

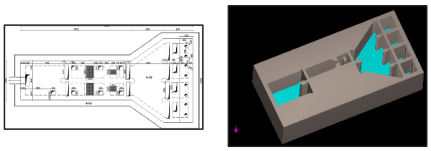

Figure 1. Geometry of Basin, left AutoCAD, and right FLOW-3D

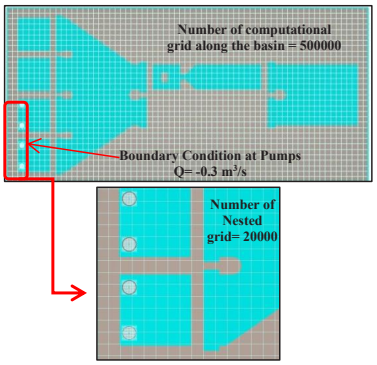

Figure 2. Number of computational gird

3. Results

A simulation of the basin with a comparable condition was undertaken to compare the RNG and LES turbulence models (Figure 3). According to the findings, the RNG model produces superior flow generation than the other. As a result, the RNG model is applied to simulate different scenarios.

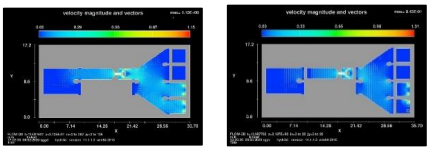

RNG LES

Figure 3. Flow speed in the basin in RNG and LES models

Because of the basin's geometry, two situations were chosen as critical scenarios, and the results were monitored in accordance with ANSI guidelines (Figure 4 and Figure 5). The flow speed at the position of the screens (band screen and bar screen) should be between 0.3 and 0.9 m/s, and at the location of the pumps should be less than 0.5 m/s, according to ANSI requirements. These criteria are met in the basin, according to the results of both scenarios. The flow speed in each part of basin is presented in Table 1.

Table 1. Comparison of flow speed between ANSI and scenarios

	Flow speed (m/s)		
	bar screen	band screen	pump
ANSI	0.3 ~ 0.9	0.3 ~ 0.9	0.5
Scenario 1	0.35	0.4	0.35
Scenario 2	0.45	0.6	0.45

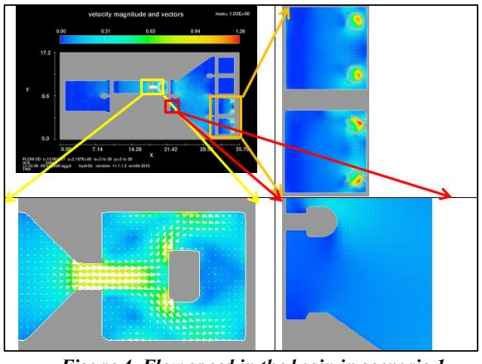

Figure 4. Flow speed in the basin in scenario 1

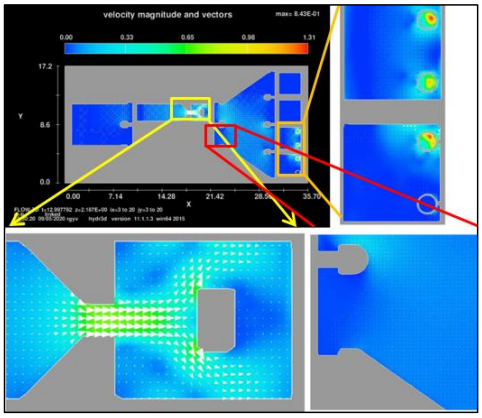

Figure 5. Flow speed in the basin in scenario 2

4. References

[1]. Ruçhan Müge Tataroğlu, Numerical Investigation of Vortex Formation at Intake Structures Using Flow 3d Software, 2014.
[2]. Sami Abdel-Fattah and Abdel-Ghani El-Shaikh, CFD Technique for Solving Low Water Level Problem of Axial Flow Pumps, American Journal of Water Science and Engineering, Vol. 3, No. 3, 2017, pp. 34-44
[3]. Y X Zhao1, C G Kim1 and Y H Lee, "CFD study on flow characteristics of pump sump and performance analysis of the mixed flow pump", 6th International Journal of Pumps and Fans with Compressors and Wind Turbines, 2013.

14th International Conference on Coasts, Ports and Marine Structures
9 & 10 May 2023 , Tehran-IRAN
ICOPMAS 2022

COMPARISON BETWEEN THE PERFORMANCE OF XBLOC AND CUBE ARMOURS FOR LOW-CRESTED AND SUBMERGED BREAKWATERS, AN EXPERIMENTAL STUDY

Mohammad Mohammadnia[1], Ali Pak[2]

1) Ph.D. Candidate, Dept. of Civil Engineering, Sharif University of Technology, Tehran, Iran, mo.mohammadnia@gmail.com
2) Professor, Department of Civil Engineering, Sharif University of Technology, Tehran, Iran, Pak@sharif.edu

1. Introduction

Low-crested breakwaters have various applications such as beach protection from erosion, creating a beach suitable for tourism, and reducing the design wave for the main breakwaters. A low-crested breakwater can be used if significant overtopping is acceptable. Due to changes in water level caused by the tide, the breakwater crest can be either submerged or visible.

. The armour layer, which protects the breakwater against the waves attack, can be made of stone or concrete blocks. The stability of the armour layer is due to the weight and interlocking between the blocks. Concrete blocks are usually used when it is hard or uneconomical to provide suitable stone for the armour layer. One of the advantages of concrete blocks over natural stone is the possibility of making it in various forms, which creates more interlocking between the armours. Concrete blocks can also be produced with any weight. In the present paper, the performance of two concrete blocks: Cube and Xbloc is investigated and compared. Cube and Xbloc are both bulky type armour. The stability of Cube blocks in the armour layer is mainly due to their weight, however, the stability of Xbloc in the armour layer is more due to interlocking between the blocks. Figure 1 shows two- and three-dimensional images of Cube and Xbloc armours.

Figure 2 shows examples of using Xbloc and Cube armours in real projects.

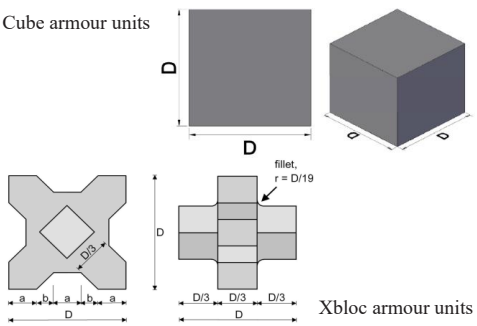

Figure 1. 2-D and 3-D image of Cube and Xbloc armors used in experiments

Used Xbloc armour units for the coastal road Reunion Island in France

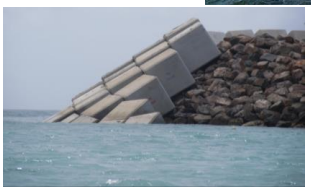

Used Cube armour units on Sal Rei Harbor breakwater, eastern Cape Verde

Figure 2. Xbloc and Cube armours in breakwater

2. Methodology and Laboratory Experiments

The aim of this experimental study is investigating the performance of two types of artificial concrete armour units for protecting low-crested / submerged breakwaters. Currently there is no formulae for designing armour layers for low-crested/submerged breakwaters [1,2,3]. The study was conducted in a large hydraulic flume at the civil engineering department of Tehran University. The flume is 25.2 meters long, 1-meter-wide and 1.3 meters high. This flume can produce waves with periods between 0.5 to 6 seconds and a maximum wave height of 25 cm. Three sensors of the resistance wave gauge type were installed just before the breakwater toe to measure the wave height. These sensors record the amount of water level by measuring changes in voltage. The measurement error of the mentioned sensors is 0.1 mm. These sensors record 50 data per second. Figure 3 shows the actual image of the flume, and Figure 4 shows the sensors used.

The method of implementing the Xbloc armour layer in the laboratory is shown in Figure 5. Since the performance of Xbloc armour is mainly due to interlocking, if the Xbloc units are assembled by hand in the laboratory, it may influence the interlocking between the units, so a thread is used to carefully place the blocks in the armour layer.

Figure 3. Hydraulic flume of the Faculty of Engineering, University of Tehran

Figure 4. Resistance wave gauge sensors used in the laboratory to measure the wave height

Figure 5. Proper placement of the armor layer in the laboratory

3. Conclusion

In all experiments on single-layer Xbloc and Cube armours, with increasing the water depth at the breakwater toe, the wave height required for the armour layer failure increased and consequently, the stability number N_S also increased. This means that increasing the depth of water at the breakwater toe for low-crested/submerged breakwater increases the armour layer stability.

In all experiments performed on Xbloc and Cube armours, with increasing the wave period, the wave height required for the armour layer failure decreased (lower Ns values obtained). In other words, increasing the wave period reduces the stability of the armour layer. This happens for two reasons. The first reason is that the force applied by the waves affects the armour layer over a longer time period and the second reason is that in the case of higher wave periods, the longer time interval between the waves causes the downward force of the previous wave (rundown) to be more effective to displace the armour units.

A comparison between Xbloc and Cube armours subjected to same geometric and hydraulic conditions showed that the performance of single-layer Xbloc armour was better than that of single-layer Cube armour with "irregular placement", however, the performance of a single-layer Cube armour with "regular placement" is better than the performance of a single layer Xbloc armour. This is because for "regular placement", Cube armours due to their flat surfaces, lean over each other on the breakwater slope, resulting in improving the stability of the armour layer. However, for Xbloc armour, firstly, due to their special geometric shape, the armour blocks engage with the filter layer more than that for the Cube armour, and therefore the weight of Xbloc armours is not fully applied to the lower row of the armours. As a result, one of the main factors in the stability of the armour layer becomes less effective when using Xbloc. Therefore, the performance of the single-layer Xbloc armour is not as well as that of the single-layer Cube armour with regular placement. For the case of "irregular placement" of Cube armours, the above advantages are lost because the armour layer stability decreases due to reducing the weight of the cubes of the upper layer on the lower layer and lack of suitable support for placing the armour on top of each other.

Structural examination of Xbloc and Cube armour while working in the laboratory showed that Xbloc armour has structural weaknesses in the corners that cause it to fail during transportation and placement on the breakwater. In contrast, for Cube armours due to their bulky and simple geometry, the possibility of breaking armour parts is very low. From this point of view, Cube armours are superior to Xbloc armours. In the prototype scale, using Xbloc armours requires obtaining the necessary permissions from the inventor. As a result, using Xbloc armour can be costlier than Cube armour.

Due to the simple geometric shape of the Cube armours, the required effort for form-working, construction, transportation, and placement of the cubes on the breakwater are less. On the other hand, Cube armours need more concrete volume comparing to Xbloc; in this regard, the cost of concrete required to produce Cube armours is higher than that for Xbloc. But overall, because of the lower cost of molding, warehousing, lower probability of breakage, and higher production speed, Cube armour units are more cost-effective comparing to Xbloc.

4. References

[1] Hudson, R.Y., 1959. Laboratory investigation of rubble-mound breakwaters. Reprint of the original paper as published in the Journal of the Waterways and Harbors Division of ASCE, proceedings paper 2171.

[2] Muttray, M., ten Oever, E. and Reedijk, B., 2012. Stability of low crested and submerged breakwaters with single layer armouring. Journal of Shipping and Ocean Engineering, 2(3).

[3] Vieira, Filipe, Francisco Taveira-Pinto, and Paulo Rosa-Santos. "Single-layer cube armoured breakwaters: Critical review and technical challenges." Ocean Engineering 216 (2020): 108042.

14th International Conference on Coasts, Ports and Marine Structures
9 & 10 May 2023 , Tehran-IRAN
ICOPMAS 2022

UNCERTAINTY ANALYSIS OF SOIL LIQUEFACTION POTENTIAL PREDICTION

Maedeh Mehrvarzan[1], Ali Derakhshani[2]

1) Department of Civil Engineering, Faculty of Engineering, Shahed University, Tehran, Iran, m.mehrvarzan9131@gmail.com
2) Department of Civil Engineering, Faculty of Engineering, Shahed University, Tehran, Iran, adera@shahed.ac.ir

1. Introduction

Various models for predicting soil liquefaction potential are available in the technical literature. The proposed models for predicting liquefaction potential do not take into account input uncertainties that affect the results.

In general, input uncertainties affect the reliability of system responses. To improve the reliability of designs, input uncertainties must be considered collectively. For this purpose, various approaches have been used to analyze engineering systems, from engineering judgments to complex statistical and intelligent methods. Fuzzy set theory can be considered as the most general method used to analyze uncertainty in engineering [1, 5].

2. Methodology

Uncertainties in inputs can affect the estimated liquefaction potential. For a reliable design, analysis of possible uncertainties is essential. In this paper, the uncertainty analysis of soil liquefaction resistance based on a fuzzy set theory using fuzzy numbers is performed.

In this paper, considering the uncertainty in the input parameters, the sensitivity of the model to predict the liquefaction potential against uncertainty is investigated by the fuzzy method. [5]

The input parameter uncertainties are introduced by triangular fuzzy numbers with at most ± 5% uncertainty i.e. ΔX = 0.05Xc. Following the analysis procedures, first, the input fuzzy numbers are discretized by several α-cuts to make the appropriate intervals. Then, the fuzzy capacity energy intervals are found by solving optimization problems with many objectives using a Genetic Algorithm (GA).

3. Data

The input fuzzy parameters are configured with six α-cuts where α equals 0, 0.2, 0.4, 0.6, 0.8, and 1. It is worth noting that α = 0 and 1 correspond to the support and crisp values of the fuzzy number (Figure (1)).

This method is applied to the Prediction model of Baziar et al. (2007). and all relevant fuzzy values are calculated. The database used in this study includes the experimental test results reported by, Baziar et al. (2007, 2011).

This database has been employed in the assessment of liquefaction triggering using the strain energy concept and ANN model. [1, 4]

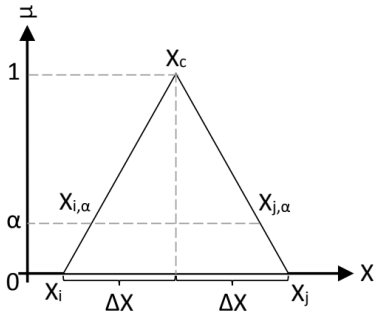

Figure 1. Triangular membership function [1].

4. Results and Discussion

Considering the results, the smaller the base of the triangles, the lower the sensitivity of the model to uncertainty. "Cut and paste it at the end of the sentence.", the effect of the greatest uncertainty on the results of the models is considered. To provide an overview of the impact of uncertainty on the predictive model, the membership functions of several statistical criteria are plotted in Figure (2).

The computed statistical indices are correlation coefficient (CC), root mean squared error (RMSE), and mean absolute error (MAE). Their formulas are as follows:

$$CC = \frac{\sum_{i=1}^{M}(Y-\bar{Y})(Y_{per}-\bar{Y}_{per})}{\sqrt{\sum(Y-\bar{Y})^2}\sqrt{\sum(Y_{per}-\bar{Y}_{per})^2}} \quad (1)$$

$$MAE = \frac{\sum_{i=1}^{M}|Y-Y_{per}|}{M} \quad (2)$$

$$RMSE = \sqrt{\frac{\sum_{i=1}^{M}(Y-Y_{per})^2}{M}} \quad (3)$$

Where,
(Y): measured energy values,
($\overline{Y}$): average measured energy values,
(Y_{per}): predicted energy values,
($\overline{Y}_{per}$): average predicted energy values and
(M): the total number of data.

Based on the presented results, it is observed that the fuzzy numbers calculated using this model have a short support length and are therefore less affected by uncertainty.

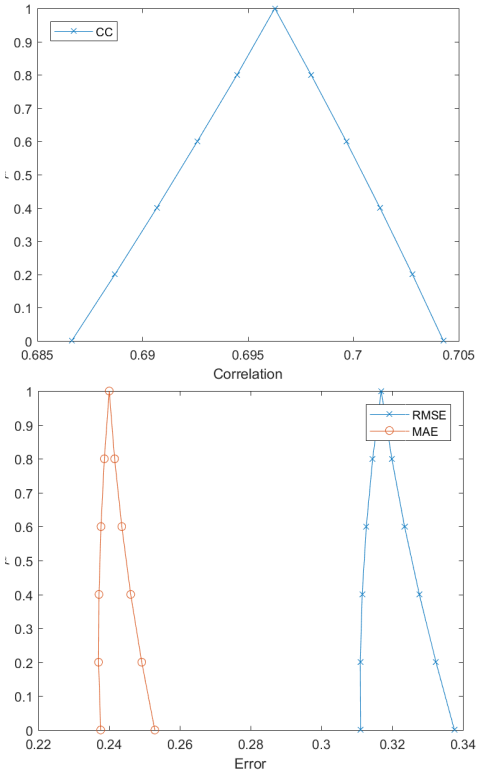

Figure 2. Membership functions of MLR models; CC (top), RMSE and MAE (bottom)

5. Conclusions

Among the various models available to predict soil liquefaction resistance (capacity energy), the model developed by Baziar et al. (2007) (using multiple linear regression) was investigated under the effects of input uncertainties.

The reliability of the predictions made by this method was evaluated and compared using fuzzy statistical indicators including correlation coefficient (CC), mean absolute error (MAE) and root mean squared error (RMSE). According to the output diagrams given in Figure (2), it is inferred that this model is accurate and has little vulnerability to prediction uncertainties.

6. References

[1] Derakhshani A. On the uncertainty analysis of uplift capacity of suction caissons in clay based on the fuzzy sets theory. Ocean Engineering. 2018 Dec 15; 170:416-25.
[2] Ghasemi Rozveh S, Derakhshani A. Uncertainty analysis of liquefaction-induced lateral spreading using fuzzy variables and genetic algorithm. Bulletin of Engineering Geology and the Environment. 2021 Dec; 80(12):9185-200.
[3] Avval YJ, Derakhshani A. New formulas for predicting liquefaction-induced lateral spreading: model tree approach. Bulletin of Engineering Geology and the Environment. 2019 Jul;78(5):3649-61.
[4] Baziar MH, Jafarian Y. Assessment of liquefaction triggering using strain energy concept and ANN model: capacity energy. Soil Dynamics and Earthquake Engineering. 2007 Dec 1;27(12):1056-72.
[5] Alavi AH, Gandomi AH. Energy-based numerical models for assessment of soil liquefaction. Geoscience Frontiers. 2012 Jul 1; 3(4):541-55.
[6] Chen Z, Li H, Goh AT, Wu C, Zhang W. Soil liquefaction assessment using soft computing approaches based on capacity energy concept. Geosciences. 2020 Sep; 10(9):330.

14th International Conference on Coasts, Ports and Marine Structures
9 & 10 May 2023 , Tehran-IRAN
ICOPMAS 2022

TURNING PORTS INTO ENERGY HUBS BY USING ON-SHORE POWER SUPPLY AND RENEWABLE SOURCES OF ENERGY BASED ON SMART MICRO-GRIDS (CASE STUDY: AMIRABAD PORT)

Majid Rohipour Asrami[1], Abdolreza Esmaeli[2]

1) Ports and Maritime Organization, Amirabad port's Senior Electrical Expert, Mazandaran, Iran, Rohipour.Asrami@gmail.com
2) Plasma and nuclear fusion research school, Nuclear science and technology research institute, Tehran, Iran Aesmaeli@aeoi.org.ir

1. Introduction

Undoubtedly, Applying On-shore power supply (OPS) is certainly one of the most secure and practical methods to build green ports to comply with international conventions. A case study was carried out in Amirabad port to examine the feasibility of the vessel's electrical supply and afterwards a confirmation letter was received from Iran's Ports and Maritime Organization to implement the plan in eight other ports in Iran. The study was aimed at turning the ports into a power hub in an attempt to reduce carbon footprint and increase the use of renewable energies and to remove the pollutants.

The generators in ships were shut down while mooring on the berth and instead, the ships were connected to the port's power grid supplied by renewable energy. Zones schematic and connecting cables of ships' power supply in Amirabad port berths were submitted and a general cost for the project was also estimated. The system is expected to operate on the basis of micro-grid and smart energy grids [1].

2. On-shore Power Supply in Amirabad Port

Regarding the types of ships commuting to the Amirabad port - general cargos - and the required power supply, there are 13 berths in three operational zones (Figure 1) to maximally use the existing infrastructure which is fed by four to-be-built substations, 1000 and 1250 transformers and fifteen 400amp power plugs.

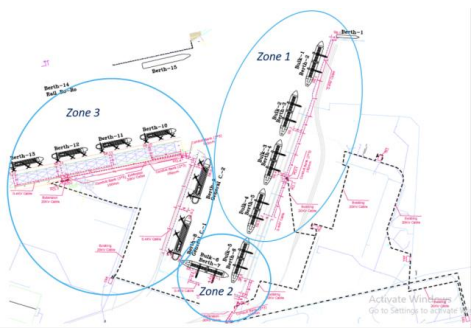

Figure 1. Zones and cable connection related to On-shore power supply in Amirabad port

Amount of average consumption current is:
V=400 v, f=50 Hz, P=200 Kw, Lmax= 490 m, P. F=0.8,
Therefore: I≈360 A

3. Estimating the Implementation Cost of On-Shore Power Supply System in Amirabad Port

According to the feasibility studies, Return of Capital certainly takes place in the second year [1]. Table 1 presents a summary of cost estimation based on price lists from the Iranian Planning and Budget Organization on the fields of construction, electricity and mechanics issued in 2020 [2,3].

Table 1. Summary of cost estimation for On-shore power supply implementation in Amirabad port

No.	Subjects	Total cost ($)	Percentage (%)
1	Construction	274,150	19.92
2	Electrical Installations	35,340	2.57
3	Mechanical Installations	42,398	3.08
4	Road	27,973	2.03
5	Electrical distribution	996,654	72.40
6	Total	1,376,514	100

4. Smart Energy Micro-Grids

Smart energy micro-grid is an integrated, automated network between the producer and the consumer and bilaterally provides the network manager with the required data. Such a technology will economize power consumption, reduce the costs and enhance reliability and power quality. To implement a smart energy grid, a smart energy micro-grid employs advanced digital technology and normal standards for transferring the know-how [4,5].

5. On-shore power supply system using renewable energies in an infrastructure of Smart energy micro-grid

The system provides electrical power with renewable and green energies such as solar and wind energy and stores the power in rechargeable batteries as a practical method. Rechargeable batteries perform a dual function as a source of storing power; first, they store the power when there are no ships in the berths and are used as the main source of supply when the required power exceeds the capacity of solar and farm resources. Second, they provide power for direct current (DC) loads. Studies indicate that the area is prone to wind and solar power generation. Required technology and the cost totally depend on the distance between the generating system and the port along with the climate situation of the area.

Thanks to advanced digital technology and power grid connection, smart micro-grid technology is practically applicable to provide power for ships and renewable resources, as presented in Figure 2 and Figure 3 [6,7].

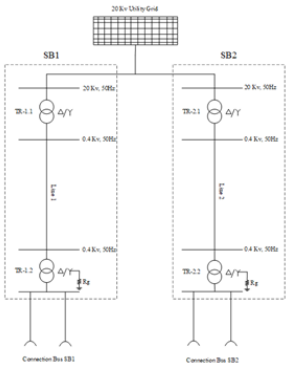

Figure 2. On-shore power supply system single-line

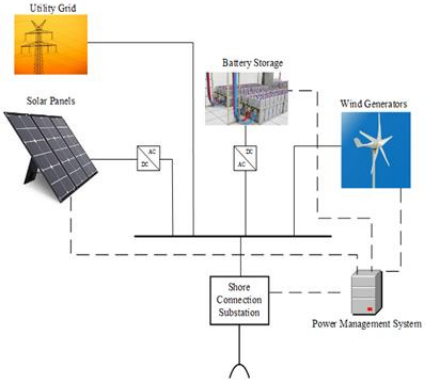

Figure 2. On-shore power supply system based on smart power micro-grid

6. Conclusion

Turning ports into energy and power hubs using a combination of on-shore power supply system and smart power micro grids, along with storing batteries and renewable energies are the best technical, economic and ecological strategy to exploit the potentials in ports and Amirabad port to present it in power market.

7. References

1.Esmaili A,Rohipour asrami M,Zanjani M ," Investigation and feasibility study of Onshore power supply in ports (case study : Amirabad Port), ICOPMAS 2016, Tehran, Iran
2. Designing and simulation of Onshore power supply system by using local grids in Amirabad port, study project, Saman Energy Consultancy Engineering company, 2018
3.Sergi Espinosa Sanes ,"Design of a shore power system for Barcelona's cruise piers: Cruise pollution study, rules analysis, design and Simulation", Thesis, Barcelona University, Bachelor's Degree in Naval Systems and Technology Engineering, Barcelona, 2 September 2015
4.Graheil.M, 2013, "The Concepts of Smart Grids".
5.Prousalidis. J, Lyridis. D. V,Dallas. S,Papaleonidas. S, Mitrou. P,Vergetis. E,Vaimaki. E, Aggelopoulos. S, Kourmpelis. T,Georgiou. V,Katsikas. P,Boutsika. T,Spathis. D, 12-16 May 2017, «The ports as smart micro-grids: development perspectives», Proceedings of HAEE.
6. Prousalidis j, Antonopoulos G, Greig A and Bucknall R, "Green shipping in emission controlled areas: combining smart grids and cold ironing", XXIth International Conference on ElectricalMachines-ICEM2014, pp.2299-2305.
7. Patrik Ericsson, Ismir Fazlagic, "Shore-side power supply. A feasibility study and a technical solution for an on-shore electrical infrastructure to supply vessels with electric power while in port", Master of Science Thesis, Chamlers University of Technology, ABB,Goteborg 2008.

14th International Conference on Coasts, Ports and Marine Structures
9 & 10 May 2023 , Tehran-IRAN
ICOPMAS 2022

DEVELOPMENT A MASS FLOW RATE MEASUREMENT SYSTEM FOR SHIP'S LOAD WEIGHING IN TERMINALS

Hossein Mousazadeh[1], Nazila Tarabi[2], Jalil Taghizadeh-Tameh[2], Farzad Mohammadi[3], Hossein Azimi[4]

1) Associate Prof., Mechanical Engineering of Biosystems, University of Tehran, Iran, Email: hmousazade@ut.ac.ir
2) Ph.D. Candidate, Mechanical Engineering of Biosystems, University of Tehran, Iran, tarabi99@ut.ac.ir, taghizadeh68@ut.ac.ir.
3) Ph.D. student, Mechanical Engineering of Biosystems, University of Tehran, Iran, Farzadmohammadi@ut.ac.ir
4) Deputy Directorate for Resources, Planning and Development in Port and Maritime Organization of Amirabad. Azimi.zmt@gmail.com

1. Introduction

Import/export of granular materials have a noticeable share of world trades in ports. Loading and unloading of cereals (wheat, barley, corn …), petrochemical materials, cement and other granular/bulk materials are usually daily duty in seaports. In-situ weighing of these loads would be advantages in the concept of 'smart ports'. Mass flow measurement systems would be essential parts in solid flow systems. Some common weighing technologies were based on; centripetal force, impact force, coriolis, microwave, force flow and capacity [1]. Considering some comparison parameters such as; simplicity, accuracy, flow capacity, maintenance, versatility, non-invasive, non-intrusive, cost and vibration-tight the capacitance based measurement (tomography) would be one of the considerable candidates. Hunt (2014) introduced a weighing system using electrical capacitance tomography (ECT) to mass flow rate measurements in a 12 cm pipe [2]. The ECT mainly is based on medical CT technology and develops together with computer and sensor technology. The idea of process tomography was evolved in mid-1980's [3].

This research focuses on development and application of in-situ 2D ECT for solid mass flow rate measurement in loading/unloading of ships in the terminal of ports and trucks loading. Comparison five well-known image reconstruction algorithms in order to apply for solid mass flow measurement are main scopes of this research.

2. Materials and Methods

In-situ weighing of trucks in terminals would enhance the accuracy, improve loading/unloading capacity and time, and would match to smart port concepts in the seaports. The ECT system designed in this research was combination of concepts introduced by Hab (2010) [4] and [5] and Styra et al., (2010) [4] with some modifications (Figure 1).

ECT problems usually solved based on Finite Element Method (FEM). The FE analysis of any problem involves basically four steps: (A) discretizing the solution region into a finite number of sub regions or elements ,(B) deriving governing equations for a typical element ,(C) assembling all the elements in the solution region, and (D) solving the system of equations obtained to calculate potential in any point inside the medium.

Once the nodal potential calculated, potential in any point of the medium would be interpolated and the sensitivity is derivable before imaging. Any ECT algorithm is mainly consist of two phases; forward problem and inverse problem. The solution to the forward problem in two-dimensions can be expressed as Equation 1:

$$C_{ij} = F(\epsilon(x,y)) \quad \begin{Bmatrix} i = 1, \dots N-1 \\ j = i+1, \dots N \end{Bmatrix} \tag{1}$$

where F is a nonlinear forward mapping from the permittivity space into the measurements space [6].

Figure 1. ECT system designed for solid mass flow measurement in ports.

2.1. Inverse Algorithms

The inverse problem, estimating the permittivity distribution from the measured capacitance as Equation 2 [6].

$$\epsilon(x,y) = F^{-1}(C_{ij}) \quad \begin{Bmatrix} i = 1, \dots N-1 \\ j = i+1, \dots N \end{Bmatrix} \tag{2}$$

where F^{-1} is the inverse nonlinear mapping from the measurements space to the permittivity space. Five well-known and fast algorithms that gives an acceptable results and are suitable for in-situ operations as well includes; LBP, Tikhonov, SVD, ART and SIRT algorithms [7, 8]. Each algorithm has its own pros and cons. The five given algorithms are compared by some assessment parameters.

2.2. Evaluated Parameters

Two common quantitative evaluation parameter that used to compare five given algorithms were MAPE and RMSE as Eq. (3-4).

$$MAPE = \frac{|A_{fill-desi} - A_{fill-tomo}|}{A_{fill-desi}} \quad (3)$$

$$RMSE = \sqrt{\left(\frac{A_{fill-desi}}{A} - \frac{A_{fill-tomo}}{A}\right)^2} \quad (4)$$

where A_{fill_desi} and A_{fill_tomo} illustrates the desired area filled and the estimated area filled by high permittivity material. All process in this project are performed by a specially developed program based on C# programming software.

3. Results and Discussions

To evaluate the developed system performance with different algorithms, number of 146 set of data is read for each algorithm. Typical data measurement and reconstructed images are shown in the Figure 2. Objects with different shapes and sizes are located inside medium and number of desired filled element are counted. After five reconstruction algorithms are performed, number of estimated filled elements counted once again. It is assumed that all elements area are equal for all 2048 elements inside the phantom.

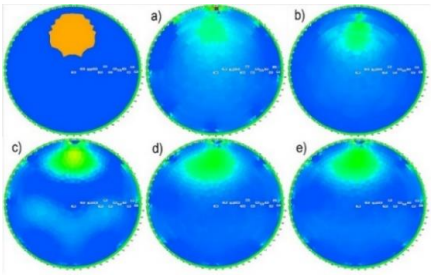

Figure 2. Typical reconstructed images by; a) LBP, b) Tikhonov, c) SVD, d) ART and e) SIRT algorithm for the object illustrated in the left corner of top row.

The RMSE and MAPE of data calculated based on Eq. (3-4) to obtain the most optimum reconstruction method. According to the Figure 3, the Tikhonov obtained least error in both RMSE and MAPE parameters. While the LBP has maximum error. The last three methods lies between these two bounds.

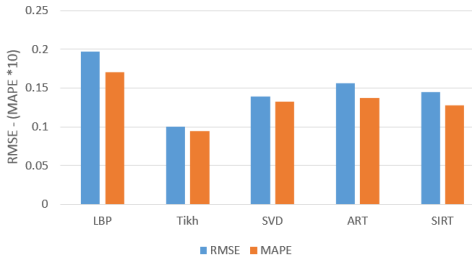

Figure 3. Evaluation parameters MAPE and RMSE

4. Conclusion

Five image reconstruction methods evaluated for an in-situ ECT system for solid mass flow rate measurement. This system would be installed on a hopper discharge funnel in terminal ports for loading/unloading of ships. According to evaluated results between five evaluated algorithms the Tikhonov algorithm was the best suited one to this measurement system. Finally it is concluded that ECT based measurement system by Tikhonov reconstruction algorithm would be capable for suitable weighing in online and in-situ manner.

5. Acknowledgments

The authors would like to acknowledge the Ports and Maritime Organization for funding the project by grant No. 6668/S20, 2020-2022.

6. References

[1] Basu, S. Plant Flow Measurement and Control Handbook (Book Chapter; SOLID FLOW MEASUREMENT). 2019.
[2] Hunt, A. Weighing without Touching Applying Electrical Capacitance Tomography to Mass Flowrate
Measurement in Multiphase Flows. Measurement and Control. 2014, Vol. 47(1) 19–25.
[3] Zhang, L. F., Wang, H. X. A new normalization method based on electrical field lines for electrical capacitance tomography. Meas. Sci. Technol. 2009. 7pp.
[4] Styra, D., Babout, L. Improvement of AC-based Electrical Capacitance Tomography Hardware. Electronics and electrical engineering. 2010. 7, 103.
[5] Anonyms. Process tomography Ltd. Electrical capacitance tomography system, Operating manual. (Fundamentals of ECT), 2009, Vol 1.
[6] Alhosani, E. Electrical capacitance tomography for real-time monitoring of process pipelines. A thesis submitted for the degree of Doctor of Philosophy. University of Bath. 2019.
[7] Marashdeh, Q. Advances in electrical capacitance tomography. A thesis submitted for the degree of Doctor of Philosophy. The Ohio State University. 2006.
[8] Li, Y. Key issues of 2D 3D image reconstruction in electrical tomography. A thesis submitted for the degree of Doctor of Philosophy. University of Manchester. 2008.

MECHANICAL AND DURABILITY PROPERTIES OF BASALT FIBER RIENFORCED CONCRETE

Hesammodin Nasaj Moghadam[1], Farshid Jandaghi Alaee[2], Pooriya Bakhshi Qalibaf Toosi[3]

1) PhD candidate, Shahrood University of Technology, Shahrood, Iran. Hesamnasaj1990@gmail.com
2) Department of Civil Engineering, Shahrood University of Technology, Shahrood, Iran. fjalaee@shahroodut.ac.ir
3) MSc, Shahrood University of Technology, Shahrood, Iran. Toosi.pooriya@gmail.com

1. Introduction

One of the most important issues for civil engineers is the durability of marine concrete structures [1]. The use of fibers in Reinforced Concrete (RC) members is a useful method to reduce the crack width and increase the durability of marine reinforced concrete structures subjected to corrosion [2]. Steel fiber is one of the most widely used fibers in the manufacture of fiber reinforced concrete. A considerable disadvantage of using steel fibers in marine environments is the corrosion of fibers buried in concrete matrix and the fibers located on both side of the crack face during the bridging action. Another important challenge of using steel fibers is the severe local corrosion at their contact with rebars in concrete. Basalt fibers have been recently used in marine structures as a green and high resistant to acidic environments. Compared to other fibers, basalt fibers have excellent environmental coordination, suitable physical and mechanical properties and stable chemical properties [3].

Figure 1. Corrosion problems in marine structure such as bridges and pontoon.

In this study, a finite element model for a single twisted fiber pull-out is presented. Then, the mechanical properties and several durability parameters such as electrical resistivity, depth of penetration of water under pressure and water absorption for Normal Concrete (NC) and Basalt Fiber Reinforced Concrete (BFRC) are investigated.

2. Finite Element Modeling

The single fiber pull-out test was modeled and verified using ABAQUS 6.11. In this model, three parts including: twisted fiber, Interfacial Transition Zone (ITZ) and concrete matrix were simulated (see Figure 2).

In order to validate the FE model, the force-slip diagram was compared with the test results [4]. The compressive strength of the matrix was 44 MPa and the twisted fiber had a triangular cross-section with 1mm side and 38.1 mm pitch length. Figure 3 compares the test results with the model results obtained from ABAQUS. It can be seen that there is a good agreement between the test and model results. The maximum pull-out force in the laboratory sample and the model were 91.8 and 89 N, respectively.

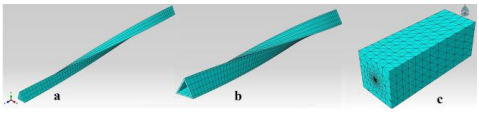

Figure 2. Finite element mesh of a) twisted steel fiber b) ITZ c) concrete mix.

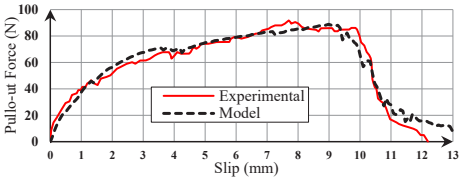

Figure 3. Comparison of the test and model results in pull-out of a single twisted fiber.

3. Experimental Program

For standard specimens, a conventional concrete and BFRC with $w/b = 0.45$ were used (see Table 1). The basalt fiber had a length of 43 mm and diameter of 0.65 mm and a density of 2100 kg/m^3 (see Figure 4). The modulus of elasticity and the tensile strength of the fibers were 44 GPa and 1000 MPa, respectively. For each case, three specimens were cast and tested. The presented values are the average of the measured parameters.

Table 1. Concrete mix design.

Mix Proportions	NC	BFRC (1%)	BFRC (1.8%)
Cement (kg/m^3)	424	424	424
Water (kg/m^3)	208	208	208
Sand (kg/m^3)	1066	1066	1066
Gravel (kg/m^3)	458	458	458
S200[1] (kg/m^3)	130	130	130
S400[2] (kg/m^3)	43.5	43.5	43.5
Microsilica (kg/m^3)	43	43	43
SMF[3]	8.7	10.55	13
SNF[4]	-	2.4	4.3
Fiber (kg/m^3)	-	21	38

1. Fine quartz sand
2. Quartz powder
3. Sulfonate Melamine Formaldehyde superplasticizer
4. Sulfonate Naphthalene Formaldehyde superplasticizer

Figure 4. Twisted basalt fiber.

4. Mechanical Properties

Compressive strength test was performed on 150 mm cubic specimens according to BS 1881-116:1983. The results are shown in Figure 5. The indirect tensile strength of the cylindrical samples was measured according to ASTM C 496/C 496M-04 and the results are given in Figure 6.

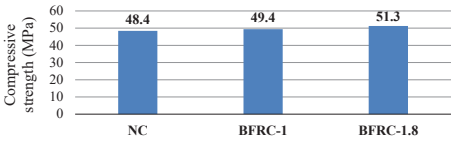

Figure 5. Compressive strength of NC and BFRC.

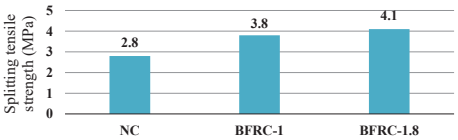

Figure 6. Splitting tensile strength of NC and BFRC.

5. Durability Testing

The results of water penetration test for NC and BFRC are shown in Figure 7. The penetration depth of all prisms was measured at the age of 28 by using the standard BS EN 12390-8:2009.

Figure 7. Depth of water penetration for NC and BFRC.

Figure 8 shows the results of the electrical resistivity of BFRC and NC at the age of 28 days. This non-destructive test was performed according to AASHTO T 358-19.

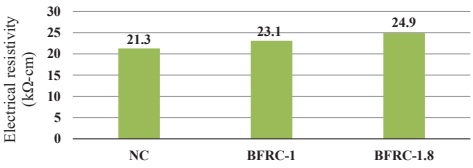

Figure 8. Electrical resistivity of NC and BFRC.

The results of the water absorption test are presented in Figure 9. The recorded results were performed according to BS 1881-122:2011.

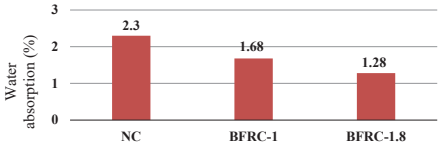

Figure 9. Water absorption of NC and BFRC.

6. Conclusion

The present study shows the effect of basalt fiber on the mechanical and durability properties of concrete mixes. According to the test results:

- Basalt fiber addition had no significant effect on the compressive strength of the composite. By adding 1 and 1.8% of twisted basalt to NC, the compressive strength was only increased by 2 and 6%, respectively.
- By addition of 1 and 1.8% basalt fibers to NC, the splitting tensile strength was improved by 36 and 46%, respectively. Moreover, the brittle fracture of NC was changed to a ductile.
- The depth of water penetration in the mixes was reduced with increase in the volume fraction of fibers. In fact, the well distributed basalt fibers improve the integrity of the composite.
- The electrical resistivity of BFRC-1 and BFRC-1.8 was improved by 9 and 17% compared with NC, respectively. The increase in electrical resistance of concrete is caused by the reduction of porosity and also the reduction of micro cracks and good adhesion between basalt fibers and cement matrix.
- The addition of basalt fiber to NC contributes to the reduction of the void content, so water absorption in BFRC-1 and BFRC-1.8 was decreased by 27 and 44%, respectively, in comparison with NC.

7. References

[1] Alexander, M. G., "Marine Concrete Structures: Design, Durability and Performance", 1st ed., Elsevier Science & Technology: Cambridge, UK, 2016, pp. 65–114.

[2] Banthia, N., Gupta, R., "Hybrid fiber reinforced concrete (HyFRC): Fiber synergy in high strength matrices", Mater. Struct., 2004, 37, pp. 707–716.

[3] Sheng'ai, C., Xuefeng, X., Xianjiao, Y., Zhao, C., ChengYan, H. ZuoLei, L., "Experimental study on the interfacial bond between short cut basalt fiber bundles and cement matrix", Construction and Building Materials, 256, September 2020.

[4] Sujivorakul C., Development of High-Performance Fiber Reinforced Cement Composites Using Twisted Polygonal Steel Fibers, University of Michigan, Ann Arbor, MI., Doctoral Thesis, 2002.

14th International Conference on Coasts, Ports and Marine Structures
9 & 10 May 2023 , Tehran-IRAN
ICOPMAS 2022

DESIGN, CONSTRUCTION AND EVALUATION OF CENTRIPETAL SOLID-PARTICLE MASS FLOW METER FOR PORT TERMINAL FUNNELS

Farzad Mohammadi[1], Hossein Mousazadeh[2] and Ail Jafari[3]

1) Department of Mechanical Engineering of Biosystems, University of Tehran, Tehran, Iran, FarzadMohammadi@ut.ac.ir
2) Department of Mechanical Engineering of Biosystems, University of Tehran, Tehran, Iran, hmousazade@ut.ac.ir
3) Department of Mechanical Engineering of Biosystems, University of Tehran, Tehran, Iran, Jafarya@ut.ac.ir

1. Introduction

Measuring and controlling the flow rate of high throughput bulk solids is a requirement frequently encountered in many different industries such as chemical, power, food, animal feed, grain, cement, coal, glass, aluminum, and polyolefin production operations. In this regard, one of the main problems when loading bulk materials in ports is the time-consuming process of loading and re-weighing (Figure 1). Therefore, real-time measurement of bulk solids during loading can be very efficient. Usually, high-capacity metering equipment is physically large, complex, expensive, and cumbersome, and delivers only marginally accurate performance with questionable long-term stability.

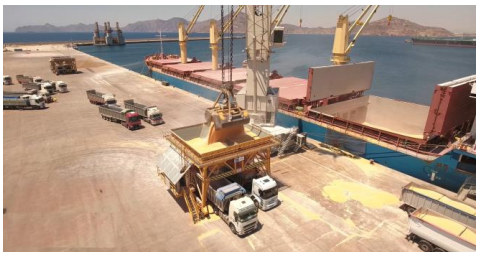

Figure 1. Loading bulk truck materials in ports

Variables, such as the volumetric flow rate, volumetric concentration, solids' velocity and the mass flow rate of the solids, are important characteristics that are often required to be measured (and controlled) to achieve efficient utilization of energy and raw materials [1, 2, 3, 4]. The methodologies of metering mass flow rate of solids in a pipeline can be divided into indirect (inferential) measurements and direct measurements [1].

As explained by Yan [1], both the instantaneous volumetric concentration of solids and the instantaneous velocity of solids over the pipe cross section need to be measured to infer the mass flow rate of solids in an indirect (inferential) measurement mass flow meter.

The direct approach of solids' mass flow measurement is a more straightforward way compared with indirect (inferential) measurement [5]. In the case of solid flow normally mass flow is measured, as volume flow cannot be considered accurate enough. On account of variations in bulk density, entrapped gas/air mass flow are normally measured for measurements of solid flow.

All weighing systems where the material being weighed is, or may be, in net motion relative to the weighing machine can be referred to as dynamic weighing systems. Therefore, dynamic weighing systems also include direct weighing methods like Coriolis, impact, and/or centripetal type measurements [6].

According to the above, measuring the mass flow rate of bulk materials is one of the basic needs of many industries, including loading and unloading of bulk materials in ports, and various researches have been done in this regard. Therefore, the main purpose of this research is to provide a method that can measure the rate of bulk materials on a large scale at the lowest cost and without the need for continuous maintenance or calibration. In this regard, and according to the request of the Ports and Maritime Organization of Amirabad Port Special Economic Zone, the purpose of the current research is to design, construct and evaluate an online mass flow meter for granular materials based on centripetal force during loading and unloading at the port.

2. Material and Method

2.1. Theory of Operation

In the designed meter, material is guided through a curved sensing plate [6]. When an object moves in a circular path, there will be acceleration towards the center of the circle along a radius. This radial acceleration, called centripetal acceleration, and is given by mv^2/R, where v represents linear or tangential velocity in a circular path of radius (R). So, for mass m, according to Newton's second law, there will be force mv^2/R. This force is referred to as outward centrifugal force. According to Newton's third law there will be an inward centripetal force as a reaction force.

2.2. Design and Construction of the Flow Meter

Based on the theory mentioned in the previous section, the modeling of the mass flow rate measuring device of bulk materials based on centrifugal force was performed according to Figure 2 in SolidWorks-2018 software. The device consists of two parts, electronic and mechanical. The mechanical part of the device includes: 1- main chassis, 2- intake flange, 3- tangential plate, 4- diverter plate, 5-

measurement pan, 6- pan arm, 7- rotating shaft, and 8- pillow block bearings. The electronic part includes: 1- S-shaped load cell, and 2- Arduino UNO-R3 and AD620 instrument amplifier. In addition, a slide gate valve was used to open and close the intake flange, which was controlled by a DC motor with a power screw mechanism. After designing, a prototype is constructed and installed under a funnel for assessment.

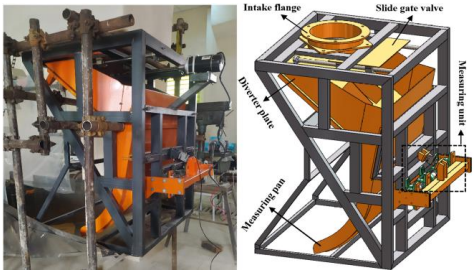

Figure 2. Real and 3D view of solid-particle mass flow meter based on centrifugal force in SolidWorks.

2.3. Tests and Evaluation

2.3.1. EDEM Testing.

In order to detect the pattern of material passing and also to investigate the velocity of grain material (Wheat) on the measuring pan in the occurrence of various passing rate, EDEM analysis was performed.

2.3.2. Load Cell Calibration.

Initially, for stationary calibration of load cell using standard weights from 100 to 1800 N with steps of 100 N and for validation from 0.5 to 50 N with steps of 0.5 N. The measurements were performed in 3 replications.

2.3.3. Actual Evaluation of the Flow Meter.

In order to evaluate the device, certain quantities of wheat were flowed in seven different amounts from 5 to 35 kg in steps of 5 kg with a random passage rate through the flow meter. Three records were used for calibration and three more records were used for device validation.

3. Results and Discussion

3.1. EDEM Analysis Results

The results of EDEM analysis, in addition to observing the material passage and use for redesign of the device, were used to determine the material flow rate in different positions of the slide gate valve, which for three states of 10, 15 and 30 cm are 15.62, 32.90 and 66.75 kg/s was obtained. Also, the velocity of the material on the measuring pan was obtained for three different rates of 2.55±0.18 m/s. Due to the fact that the velocity of the material on the measuring pan is equal at different rates, it shows that the error resulting from changing the velocity of the material will not occur in the measurement of the device.

3.2. Load Cell Calibration

The results showed that there was a strong correlation between the signals of the load cell and corresponding values standard weights. A linear model expressed the calibration identity for load cell. The load cell was able to accurately measure the force within their defined ranges with a prediction accuracy of more than 99% with RMSE= 3.88 N.

3.3. Flow Meter Evaluation Results

The results showed that there was a strong correlation (more than 0.99) between the data obtained from the area under the force-time diagram and the direct measurement of wheat weight. The best model found between the cumulative data and the corresponding values measured by the scales was the linear regression equation. The centripetal mass flow meter was able to accurately measure the weight within their defined ranges with a prediction accuracy of more than 99% with RMSE= 0.065 kg. The average standard deviation of the data was 0.145 kg, indicating the fact that different (random) rates have no effect on the measurement accuracy of the device.

4. Conclusions

In this paper, a flow meter based on measuring the centripetal force of the petal was designed, constructed and evaluated in order to measure the bulk solids rate. The results of EDEM simulation were used to analyze the pattern of material shedding when passing through the device. The results of the actual evaluation of the device showed the reliability of this method for real-time measurement of bulk material passing rate.

5. Acknowledgments

Authors would like to acknowledge the Ports and Maritime Organization for funding the project by grant No. 6668/S20, 2020-2022.

6. References

[1] Yan, Y., "Mass flow measurement of bulk solids in pneumatic pipelines", *Measurement Science and Technology*, 7, 12, 1996, pp. 1687–1706.

[2] Arakaki, C., Ghaderi, A., Datta, B.K., Lie, B., "Non-intrusive mass flow measurements in pneumatic transport", in: CHoPS-05, 2006 the 5th International Conference for Conveying and Handling of Particulate Solids, Sorrento, Italy, 27th–30th August, 2006.

[3] Ahmed, Wael H., Ismail, Basel I., "Innovative Techniques for Two-Phase Flow Measurements", *Recent Patents on Electrical Engineering,* Bentham Science Publishers Ltd., 2008.

[4] Coulthard, J., Byrne, B., Yan, Y., "Non-restrictive measurement of solids mass flow rate in pneumatic conveying systems", Measurement and Control, 24, 1991, 113–119.

[5] Zheng, Y., and Liu, Q., "Review of techniques for the mass flow rate measurement of pneumatically conveyed solids", *Measurement,* 44, 2011, pp. 589-604.

[6] Basu, S., *Plant Flow Measurement and Control Handbook: Fluid, Solid, Slurry and Multiphase Flow, Chapter VIII - Solid Flow Measurement,* Academic Press; 1st edition, 2018, pp. 677-801.

14th International Conference on Coasts, Ports and Marine Structures
9 & 10 May 2023 , Tehran-IRAN
ICOPMAS 2022

DURABILITY OF A SUSTAINABLE CONCRETE MADE WITH PERSIAN GULF'S WATER AND SEA DREDGED SAND (SWSSC) IN HARSH MARINE ENVIRONMENT

Mohammad Jahani[1], Shore Shahnoori[2] Saeed Moradi[1, 3], Moslem Zebardast[4] and Meysam Khalifeh[5]

1) Department of Civil Engineering, University of Hormozgan, Bandar Abbas, Iran. Jahani.m.edu@gmail.com
2) Department of the Built Environment, University of Technology, Eindhoven, Netherlands s.shahnoori@tue.nl
3) Road, Housing & Urban Development Research Center, Bandar Abbas, Iran. Saeed.moradi69@yahoo.com
4) Shipbuilding Industry Expert, Bandar Abbas, Iran. Moslem.zebardast@gmail.com
5) Department of Civil Engineering, University of Hormozgan, Bandar Abbas, Iran. Meysam.khalifeh@gmail.com

1. Introduction

Due to the finiteness of the natural resources on earth, in a sustainable and circular system, the byproducts of one industry are sources for others. Hence, according to SDGs, nations should seek integrated methods to control climate change, minimise natural resources' usage, neutralise CO_2 emissions and GHE, etc. Thus, construction materials as primary sources of emissions and natural resource depletion in the building industry need crucial considerations. On the other hand, the exploitation rate of natural mines has risen tremendously, and the freshwater (FW) shortage crisis is a serious matter of human life. Therefore, using abundant marine resources such as seawater (SW) and dredged marine sand (DMS), primarily due to limitations on mineral aggregates and FW in islands and marine constructions, is an environmental and economical solution. Structures subjected to climate variables, such as marine environments, even though they require scaled maintenance plans set for different periods, must have a determined technical service life and estimated durability to meet the economic and environmental needs of the project [1].

Concrete is the most widely used construction material globally, and its production requires almost 2 billion tons of FW annually, nearly 9% of the annual FW consumption worldwide [1, 2]. The main difference between SW and FW relates to the ratio of salt and ions contained in them. SW comprises a salinity of 3.5% (Persian Gulf), and its main components are K, Ca, S, Mg, Na, and Cl [1-3]. These values may vary depending on the climate and environmental conditions of the sea. Previous research showed that using SW and/or DMS in the concrete mixture changes hydration product formation, and porosity decreases the slump and workability while increasing brittleness [3-5]. The effects of SW usage in concrete depend on several factors: the ratio of minerals in SW, the water-to-cement rate (w/c), and the types and properties of the cement and pozzolans in the mix.

On the other hand, the density, strength, and shape of the coarse aggregate particles of the DMS are similar to the natural gravels. DMS usage reduces the costs of mine exploitation and adapts to the demand for the sustainable development of marine organisms [1, 4]. Other examples used pozzolans on Sea-Water Sea-Sand Concrete (SWSSC) are similar to [6, 7].

28 days *180 days*

Figure 1. Placing the samples in tidal conditions to investigate SF's effectiveness on the characteristics of SWSSC after curing

2. Experimental Program

The experimental procedure of this study is categorised into three main sets. First is the mix of design and programming, in addition to the required tests on the raw materials. The second category provides the specimens (mixing, casting, curing etc.). The final is the mechanical and permeability tests on the specimens. The samples were prepared with two w/c ratios: 0.35 and 0.4, using a certain percentage of supplementary cementitious materials (SCMs) replacing the cement (400 kg/m^3) and DMS replacing the fine quarry aggregates. The samples were cured for 7 and 28 days in laboratory conditions, then transferred to the tidal beach of the Persian Gulf for 180 days and afterwards subjected to several destructive and non-destructive tests concerning durability and mechanical properties.

3. Outcomes of the Laboratory Tests

Using SW as mixing water of SWSSC concrete increased its compressive strength and electrical resistivity at early ages (i.e., 7 days) compared to reference concrete, as stated in previous research [1-3]. However, FW concrete was more resistant to carbonation than SWSSC after 6 months, subjected to tidal conditions. On the other hand, the porosity and durability of concrete made of DMS in the optimal percentage also improved. Notwithstanding, the long-term performance and durability parameters of

reference concrete and SWSSC were still impaired by harsh tidal conditions but positively developed when using SCMs such as Silica fume (SF). Owing to its high source of SiO_2, SF in the concrete formed dense C-S-H, filled the capillary cavities existing in the SWSSC cementitious composite, and considerably stopped the carbonation processes.

Figure 4. Comparing SW and FW on the carbonation depth and investigating the effectiveness of adding SF on accelerated carbonation depth of SWSSC results. The Left: reference concrete, Middle: SWSSC, Right: modified SWSSC with SF.

SF's properties led to a faster reaction between the crystallised $Ca(OH)_2$ and SW. The reduced w/c ratio of SW-mix and the addition of the SF caused significant improvement in the durability tests of SWSSC in 180 days. In particular, the sustainability of SWSSC is highly improved by using 10% SF.

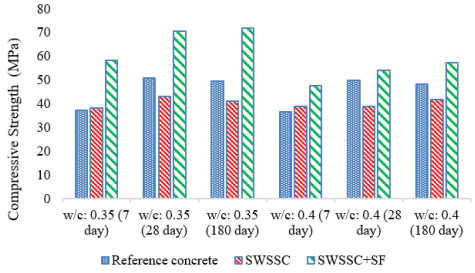

Figure 2. Effect of SW, FW and DMS combined with SF on concrete's compressive strength in two W/C ratios (i.e., 0.35 and 0.4) after 7, 28, and 180 days (i.e., 180 days old samples are being kept in the tidal condition).

4. Discussion and Conclusion

Using SW rather than FW and 25% DMS replacing fine mineral aggregates improves strength parameters in the short term. However, long-term mechanical properties and durability parameters of SWSSC, such as permeability, carbonation depth, CS and ER, dramatically deteriorated; but all significantly improved by adding a 10% SF.

Carbonation depth in SWSSC was more progressive than that in ordinary concrete, which can be attributed to the presence of SW as it was used in the cement paste from the beginning. As one of the essential outcomes, adding a 10% SF has significantly reduced the depth of carbonation after a period of 6 months in the tidal zones of the coast.

In this study, the SF has improved the sustainability parameters of SWSSC, such as strength, porosity, and permeability to carbonation, in one of the most challenging environments. So it is noteworthy that using SF, even in reinforced SWSSC according to ACI 222, reduces the reinforcing elements' corrosion risk. Due to the results, this research is convenient for eco-friendly breakwaters construction.

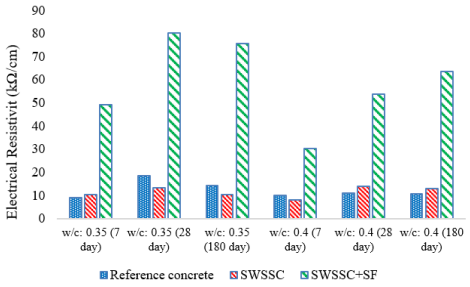

Figure 3. Effects of Sw, Fw, and DMS combined with SF on concrete's special electrical resistance in two W/C ratios (i.e., 0.35 and 0.4) after 7, 28, and 180 days (i.e., 180 days old samples have been kept in the tidal condition).

5. References

[1] Jahani, M., Shahnoori, S., Moradi, S., & Ershadi, C. (2022). Cleaner Production Towards a Green Concrete: Multi-scale Experimental Study on Long-term Performance of a Sustainable Modified-SWSSC. American Journal of Construction and Building Materials, 6(1), 43-59.

[2] Jahani, M., Shahnoori, S., & Moradi, S. (2022). Long Term observations in an Experimental study on durability of a Sustainable Concrete Made with Sea-water and Sea-sand in Tidal Conditions. The 2nd (hybrid) International Conference of Circular Systems for the Built Environment; Advanced Technological and Social Solutions for Transitions, ICSBE2, 09th December 2021, TU Eindhoven. Published by Technische Universiteit Eindhoven, 9th March 2022. ISBN 978-90-386-5486-7.

[3] Younis, A.; Ebead, U.; Suraneni, P.; and Nanni, A. (2018). "Fresh and hardened properties of seawater-mixed concrete," Constr. Build. Mater., vol. 190, pp. 276–286, 2018.

[4] Moradi, S. and Shahnoori, S. (2021). "Eco-friendly mix for Roller- Compacted Concrete: Effects of Persian-Gulf-Dredged marine sand on durability and resistance parameters of concrete," Construction and Building Materials, vol. 281, p. 122555, 2021.

[5] Sikora, P., Cendrowski, K., Abd Elrahman, M., Chung, S. Y., Mijowska, E., & Stephan, D. (2020). The effects of seawater on the hydration, microstructure and strength development of Portland cement pastes incorporating colloidal silica. Applied Nanoscience, 10(8), 2627-2638.

[6] Yi, Y., Zhu, D., Guo, S., Zhang, Z., & Shi, C. (2020). A review on the deterioration and approaches to enhance the durability of concrete in the marine environment. Cement and Concrete Composites, 113, 103695.

[7] Li, H., Farzadnia, N., & Shi, C. (2018). The role of seawater in the interaction of slag and silica fume with cement in low water-to-binder ratio pastes at the early age of hydration. Construction and Building Materials, 185, 508-518.

14th International Conference on Coasts, Ports and Marine Structures
9 & 10 May 2023 , Tehran-IRAN
ICOPMAS 2022

"MAH DREDGER" – DREDGING CONTROL SYSTEM UNDER ANDROID

Mohamad Sagheb[1], Shahriar Gharehdaghi[2] and Amir Ghazai[3]

1) Marine Science and Technology, Azad University, Tehran, Iran, Mahkashand@gmail.com
2) Marine Science and Technology, Azad University, Tehran, Iran, Sh.gharehdaghii@gmail.com
3) Mahkashand Co, Tehran, Iran, Mahkashand@gmail.com

1. Introduction

Ports always need maintenance for the safety of navigation, berthing, loading and unloading of goods and Dredging is one the most important operation. Dredgers can deepen port and channels for port traffic improve. Dredgers excavate from the seabed to the design depth. Dredging is a costly process, and Dredging more or less than the design depth is not economical.

Therefore, accurate dredging of the seabed will be very important in cost and time. So, many dredgers use a "Dredging control system".

Figure 1: cutter suction Dredger

2. Control of Dredging

There is some type of "Dredging control system" (D.C.S) in the world. These systems are equipped with several sensors like inclinometer and GPS. They are mounted on the arm (Ladder) and vessel's cabin (Bridge).

Usually all of the D.C.S s are general and they have many modules that are not used. Also they work under Windows operating system. So they need to personal computer (PC), monitor, UPS and 220v power. In addition to a lot of space, they also need an expert man.

3. Software for Control of Dredging

The "Hypack" Software is one of most famous Hydrographic and Dredging software in the word. It is widely used in Iran because it is cheaper than other software and also it is userfriendly. But I think it must be complete for better operation.

Hypack has "Dredging Pack" module that almost is used in all dredger in IRAN. We have been able to equip four dredgers with "Hypack Dredging Pack" in our country. Using these experiences, we have written an Android program for Dredging control system. This program is simple and user friendly.

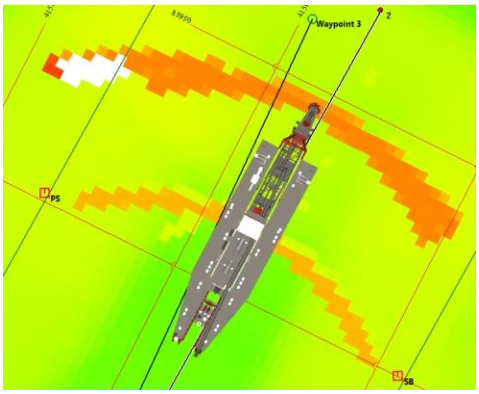

Figure 2: Hypack Dredging Monitoring

4. Mah Dredger Software

We in "MAHKASHAND" company have decided to have better software for Hydrography and Dredging control system. So we have provided a dredging control system software under "Android". Our article is about new dredging control system which named "Mah Dredger". This software will be an effective program for dredging, which will soon be installed on a suction cutter dredger in Anzali port and a floating excavator in Turkmen port.

Because the program is activated under Android, so this program can be used on a tablet or phone, and it occupies little space and does not need electricity.

"Mah Dredger" software has several advantage over "Hypack". For example, Operation, drawing and volume calculation is simpler than "Hypack" and doesn't need to special expertise. Actually it was designed for dredger's operator and they can use from "Mah-Dredger easily like an android app. They can be dredging Line, calculate volume and even choose them Dredger's shape. Also "Mah-Dredger" uses of tide algorithm which also has provided in our company. The dredger's captain can see vessel position, dredged volume, tide height, and even amount of over-dredging online.

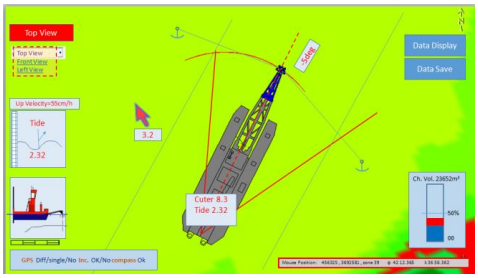

Figure 3: Mah Dredger Software

5. Advantage of Mah Dredger

- Available on Tablets.
- Fast and practical
- User friendly and easy to learn
- Remove inefficient menus
- Native and upgradeable by us
- No need for electricity

"Mah Dredger" has been developed using over than 15 years of experience in this field and experiences of dredger's operation.

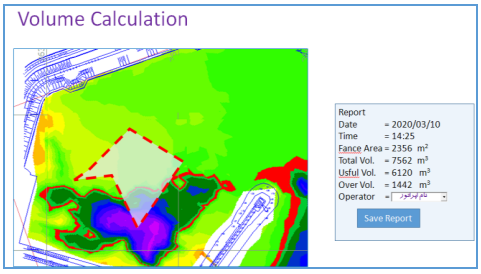

Figure 4: Volume Calculation

6. Reference

[1] Dredge track presentation system express
[2]https://www.royalihc.com/dredging/dredging-equipment/electrical-and-automation/dredge-track-presentation-system-express
[3] https://www.hypack.com/dredgepack
[4] Hypack software manual
[5] Sagheb M. (2011) 'Dredging operations control and produce online maps', M.Sc Thesis in Hydrography, North Tehran branch University, Iran.

9 & 10 May 2023 , Tehran-IRAN

ICOPMAS 2022

OFFSHORE AND PIPLINE

14th International Conference on Coasts, Ports and Marine Structures
9 & 10 May 2023 , Tehran-IRAN
ICOPMAS 2022

WCSPH SIMULATION OF MOTION RESPONSE AND POWER ABSORPTION OF A HEAVING POINT ABSORBER IN THE PERSIAN GULF

Kaveh Soleimani [1], Mohammad Javad Ketabdari [2] and Kambiz Soleimani[3]

1) Amirkabir University of Technology, Tehran, Iran, Kv.soleimani@aut.ac.ir
2) Amirkabir University of Technology, Tehran, Iran, Ketabdar@aut.ac.ir
3) Science and Research Branch, Islamic Azad University, Tehran, Iran, Kambiz_solaimani@yahoo.com

1. Introduction

Wave energy devices are normally tuned to work at resonance in highly energetic locations where a considerable wave power could be extracted. These two conditions necessitate using nonlinear CFD models such as the SPH to evaluate the response of wave power devices [1-2]. In this research, the SPH-based SPHysics model [3] was used to simulate the regular wave interaction with a heaving point absorber. This device has a small size relative to wave length [4]. The model was first verified using an analytical solution of the equation of motion where a good correspondence was found between the two sets of data. Then, as a case study, the device's performance under the wave condition of Faroor Island in the Persian Gulf was investigated.

2. Study Area

Faroor (54.30 E and 26.17 N) is a small island in the Persian Gulf. The weather in this region is hot. To study the climate of the region, the data recorded by the Faroor wave buoy were used. The water depth at the location of the buoy was 26.25 m. Based on the wind rose of the area that is shown in Figure 1, the majority of winds originate from east to northeast directions. As shown in Figure 2, the dominant wave direction is also east to northeast.

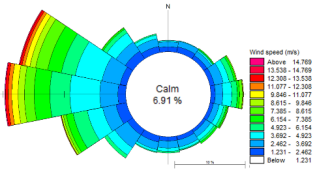

Figure 1. Annual wind rose of Faroor.

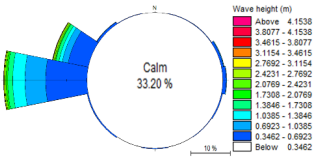

Figure 2. Annual wave rose of Faroor.

3. The Equation of Motion in SPH Model

The motion of the device is evaluated by summing the contributions exerted on the boundary particles for entire device. The force on each boundary particle is computed by summing up the contribution from all the surrounding water particles within the surrounding kernel. The boundary particle k experiences the following force per unit mass:

$$f_k = \sum_{a \in WPs} f_{ka} \tag{1}$$

where WPs denotes the water particles and f_{ka} the force per unit mass exerted by water particle a on boundary particle k. The equations of basic rigid body dynamics are used for the motion of the considered point absorber which in translational degrees of freedom is given as:

$$M\frac{dV}{dt} - b_{pz}V = \sum_{k \in BPs} m_k f_k \tag{2}$$

where M is the device mass, V is device velocity, b_{pz} is the PTO coefficient and BPs denotes the boundary particles. This equation is integrated in time to predict the values of V for the beginning of the next time-step.

The PTO force and the pneumatic power across the damper are given by the following equation

$$F_{pto} = b_{pz}V \tag{3}$$

$$P_{pto} = b_{pz}V.V \tag{4}$$

4. Validation

In this section for a simple model of heaving wave absorber, the SPH model results of the displacement and velocity were compared with the analytical data from the solution of Eq. 1. The length, width and draft of the floating body were 0.3 m, 0.3 m and 0.15 m, respectively. The wave height, period and water depth were set to 0.15 m, 1.5 s and 1.5 m, respectively. A PTO coefficient of 100 Nm/s was applied to the cylinder. The analytical model and numerical setup are shown in Figure 3. A comparison between the numerical and analytical data on the heaving displacement and velocity of the device are shown in Figures 4 and 5 where good correspondence is evident.

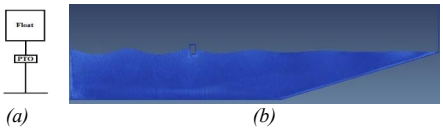

(a) (b)

Figure 3. Simulation of the floating body a) Analytical model b) SPH model.

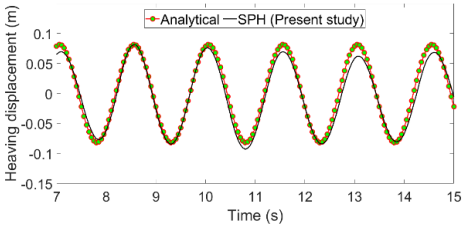

Figure 4. Validation of the device heaving displacement.

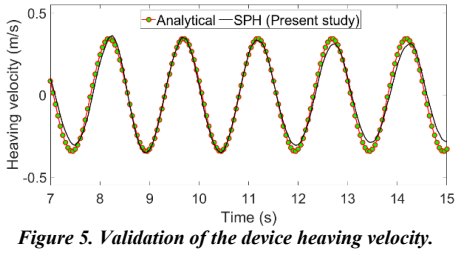

Figure 5. Validation of the device heaving velocity.

5. Case Study

In this section, the performance of a point absorber was evaluated on Faroor Island in the Persian Gulf. Previous investigations showed that the point absorber is a candidate for wave power absorption in this area [5]. Analysing the buoy data of the Faroor island indicated that the wave height and period are H=1.153 m and T=5.92 s, respectively. Using Froude similitude, these values for numerical modeling were downscaled to a water depth of 1.5m, resulting in T=1.41 s and H=0.066m. The device under consideration is the one that was numerically modelled by Agamloh et al [6] with a height, radius and draft of 1 m, 0.3 m and 0.5 m, respectively. The PTO coefficient was set to 300. The heaving displacement, velocity and absorbed power are shown in Figures 6-8, respectively. These are the results of the simulation in a wave tank of 1.5m depth. For predicting the performance of the device in real sea conditions, a reverse similarity operation should be performed.

6. Conclusion

In this research, an SPH simulation was performed to investigate the wave-point absorber interaction considering the wave data of Faroor Island in the model scale. The validation section demonstrated that the SPH model could predict the motion response of the device with acceptable accuracy. Using wave data of Faroor Island and the similarity laws, the device performance in the modeled wave condition of the area was predicted using the SPH method. This procedure showed how an SPH model could be used for the prediction of the device performance in real sea conditions.

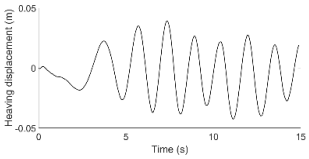

Figure 6. Heaving displacement of the device.

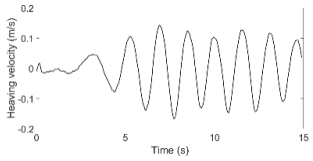

Figure 7. Heaving velocity of the device.

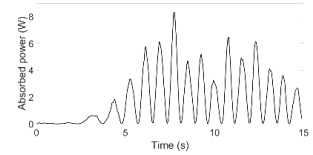

Figure 8. Absorbed power by the device.

7. References

[1] Ketabdari, M.J., Soleimani, K. and Khorasani, F., "Modeling of multipurpose fixed breakwater wave energy converter using SPH method," in *Complementary Resources for Tomorrow*, Springer, 2020, pp. 149-162.

[2] Soleimani, K., Ketabdari, M.J. and Bingham, H.B., "WCSPH simulation of the forced response of an attenuator oscillating water column wave energy converter," *European Journal of Mechanics-B/Fuids*, 95, 2022, pp. 38-51.

[3] Gomez-Gesteira, M., Rogers, B.D., Crespo, A.J.C., Dalrymple, R.A., Narayanaswamy, M. and Dominguez, J.M., "SPHysics – development of a free-surface fluid solver – Part 1: Theory and formulations," *Computers & Geosciences,* 48, 2012, pp. 289-299.

[4] Soleimani, K., and Ketabdari, M. J., "Performance analysis of a tuned point absorber using SPH calm water and wave tank simulations", *Journal of Ocean Engineering and Science*, 2022, pp. 3-28.

[5] Soleimani, K., Ketabdari, M.J. and Khorasani, F., "Feasibility study on tidal and wave energy conversion in Iranian seas," *Sustainable Energy Technologies and Assessments,* 11, 2015, pp. 77-86.

[6] Agamloh, E.B., Wallace, A.K. and von Jouanne, A., "Application of fluid–structure interaction simulation of an ocean wave energy extraction device," *Renewable Energy,* 33, 2008, pp. 748-757.

14th International Conference on Coasts, Ports and Marine Structures
9 & 10 May 2023 , Tehran-IRAN
ICOPMAS 2022

NUMERICAL ANALYSIS OF HULL FORM EFFECTS ON COUPLED DYNAMIC RESPONSES OF A SEMI-SUBMERSIBLE FLOATING OFFSHORE WIND TURBINE

Mohamad Javad Eslahi[1], Saeid Kazemi[2], Mojtaba Ezam[3], Majid Ghodsi Hassanabad[4]

1) Faculty of Engineering, Science and Research Branch, IAU, Tehran, Iran, mj.eslahi@srbiau.ac.ir
2) Faculty of Engineering, Science and Research Branch, IAU, Tehran, Iran, saeid.kazemi@srbiau.ac.ir
3) Faculty of Natural Res. and Environment, Science and Research Branch, IAU, Tehran, Iran, ezam@srbiau.ac.ir
4) Faculty of Engineering, Science and Research Branch, IAU, Tehran, Iran, m.ghodsi@srbiau.ac.ir

1. Introduction

Excessive use of fossil fuels has aggravated the energy crisis and the problem of environmental pollution. This trend of using one side and the pollution caused by the use of these fuels has faced humanity with problems in the meantime. Therefore, it is very necessary to find a clean and renewable energy source to replace fossil energy. As one of the most promising and non-polluting sources of renewable energy, wind energy has a high replacement capability and has attracted the attention of the world. Meanwhile, installation of wind turbines in offshore wind farms can cause less visual pollution and noise compared to turbines located on or near the coast. Also, as water depth increases rapidly with distance from shore, the cost base of downstream wind turbines increases. Therefore, floating offshore wind turbines (FOWT) are a more economical option for offshore wind farms with a water depth of more than 50 meters. The types of floating turbines include semi-submerged, spar, and tension leg models, as shown in Figure 1.

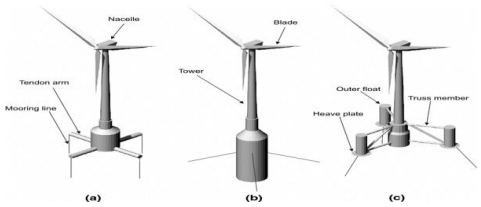

Figure 1. Types of floating wind turbines

In this paper, the coupled dynamic analysis of a semi-submersible offshore wind turbine in waves, wind and current will be performed considering the mutual effects between the wind turbine, the restraint system and the platform. The main purpose of this study is to investigate the hull form effect of sub-structure on the wind turbine responses.

2. Governing Equations

In this research, a powerful numerical analyze was used for aero-servo-hydro-elastic coupling simulation of a floating wind turbine. The goal is to identify a suitable configuration for the platform that is able to perform more effectively in the face of forces and influencing factors. We kept the dimensions of the platform as small as possible. The amplitude of the peaks of the response amplitude operator (RAO) and the integral area of the RAOs in a wide range of frequencies for certain degrees of freedom and are chosen as the objectives of this research, which should be minimized. Through an efficient frequency domain simulation approach, we show that the upscaling techniques proposed in this research lead to the design of platforms with better performance, and platforms with smaller dimensions can perform better. In this research, the design is done in a non-linear way.

2.1. Wind Force

The potential power in the wind is calculated by the time derivative of the kinetic energy equation.

$$P_{avail} = \frac{dE}{dt} = \frac{1}{2} \cdot m \cdot v_0 \quad ^2 \tag{1}$$

Wind profile power law

In order to estimate the vertical changes of wind speed u(z), we use the following equation to calculate it:

$$u(z) = u_r \cdot \left(\frac{z}{z_r}\right)^{\alpha} \tag{2}$$

2.2. Aerodynamic Model

The aerodynamic loads on the elements of the sections (such as the tower, monopile and floating platform) are calculated by considering the drag with the Morrison equation (Morrison et al. (1950)). The loads on the blades are calculated using the BEM algorithm. Hansen (2008c).

$$F_{\text{aero}} = \frac{1}{2}\rho V_P^2 C_D A \tag{3}$$

$$F_L = C_L \frac{1}{2}\rho |W|^2 C \cdot L$$
$$F_D = C_D \frac{1}{2}\rho |W|^2 C \cdot L \tag{4}$$

2.3. Hydrodynamic Model

Hydrodynamic loads are calculated using the classic Morrison equation. The Morrison equation for calculating hydrodynamic loads on wind turbine support structures does not take into account the fact that the platform structure deflects incoming waves. Therefore, when the wavelength λ

is less than five times the diameter. According to IEC-61400-3-1 (2019), in these cases the coefficient of the MacCamy-Fuchs equation is added to the Morrison equation.

$$F_{\text{hydro}}(z) = \rho C_D R|u-\dot{x}|(u-\dot{x}) + \pi\rho R^2 a + (C_M - 1)\,\pi\rho R^2(a-\ddot{x}) \quad (5)$$

$$C_M = \frac{4}{\pi(kr)^2\sqrt{A_1(kr)}} \quad (6)$$

$$A_1(kr) = J_1'^2(ka) + Y_1'^2$$

$$C_M = \frac{0.581(kr^2)+0.718kr+0.780}{(kr)^3-0.256(kr)^2+0.381kr+0.389} \quad (7)$$

2.4. Time Domain Simulation

A simulation is performed in the time domain by solving the dynamic equation of motion for each step. In time step n, the equation of motion is defined as follows:

$$M\ddot{d}_n + C d_n + f_n^{int} - f_n^{ext} = 0 \quad (8)$$

$$M\Delta\ddot{d}_n + C\Delta\dot{d}_n + \Delta f_n^{int} - \Delta f_n^{ext} = 0 \quad (9)$$

$$\Delta f_n^{int} = \frac{\partial f^{int}}{\partial d}\Delta d_n = K_n^{int}\Delta d_n \text{ and}$$
$$\Delta f_n^{ext} = \frac{\partial f^{ext}}{\partial d}\Delta d_n = K_n^{ext}\Delta d_n \quad (10)$$

2.5. Damping

During the time simulation, high-frequency responses may occur that have no physical meaning but are mostly artifacts of the numerical algorithm. We removed these by applying numerical damping to the equations. Here, we have implemented the Hilbert-Hughes-Taylor (HHT) method, which is a modified form of the Newmark-beta method.

2.6. Mooring Lines System

The semi-submersible platform of 10 MW turbine is selected in this research. Anchor points are placed in the same position as in NREL's 5 MW semi-submersible platform. Components such as cables, wires, and anchor lines suspended under their own weight assume the shape of a catenary. Calculate the shape assuming a linear length of l, height (between endpoints) h and vertical distance d, we can solve for the sags parameter by numerically solving Eq.

$$k = \mu\left[-2\left(1+\frac{2H_F}{\mu Z_F}\right)^{-\frac{1}{2}} + \cosh^{-1}\left(1+\frac{\mu Z_F}{H_F}\right)\right]^{-1}\Bigg|_{X_{F,EQ}} \quad (11)$$

$$K_{11} = \sum_{i=1}^{n} k_i \cos^2(\phi_i),$$

$$\frac{2}{x}\sinh\left(\frac{sd}{2}\right) - \sqrt{L^2-h^2} = 0$$
$$x_{\text{left}} = \frac{1}{2}\left(\ln\frac{l+d}{l-d} - d\right) \quad (12)$$

3. Simulation of 10 MW FOWT Model

NREL's 5 MW semi-submersible platform has been upgraded to support 10 MW DTU wind turbine.

$$sf = \sqrt{\frac{10MW}{5MW}} = \sqrt{2} \quad (13)$$

The main geometric dimensions of the new platform obtained by increasing the scale of each length by sf are reported in the table below.

Table 1. 10MW oc4 platform

10MW DTU Upscaled Platform	
Depth of platform base below SWL	28.30 m
Elevation of main column above SWL	14.14 m
Elevation of o_set columns above SWL	16.97 m
Length of upper columns	36.77 m
Length of heave plates	8.48 m
Depth to top base columns below SWL	19.80 m
Diameter of main columns	8.30 m
Diameter of o_set columns	16.97 m
Diameter of heave plates	33.94 m
Diameter of pontoon and cross-braces	1.6 m
Platform CM location below SWL	21.27 m
Water depth	200 m

10 MW model and several optimal models of this type were modeled. A 10 MW turbine was designed based on NREL's initial settings, and finally, some optimal semi-submersible platforms were made considering three key geometric variables, the diameter of the outer cylinders, their radial distance from the center of the platform, and the height of these cylinders. The results of these simulations based on 3 motion responses in roll, pitch, and yaw are given in Figure 2.

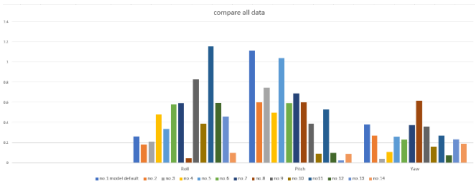

Figure 2. Data comparison

4. Results

In the present study, a research based on the frequency domain was conducted with the aim of finding the optimal configuration. Several 10 MW semi-submersible platforms have been simulated. An initial model is simulated by comparing with the benchmark results in other articles. Then, several frequency domain models for the upgraded platform designed to support 10 MW DTU. The results show that an optimal configuration for the semi-submerged platform is d = 17 meters, platform radius r = 35 meters, base height h = 15 meters.

MULTI-DYNAMICS ANALYSIS OF FPSO CYRUS TELECABIN

Ramin Kharazmi[1], Shahsavar Arghash[2], Mohammad Fouladvandi[3], Reza Kharazmi[4], Hamed Payamani[5]

1) Iran Ofogh Industrial Development Company, Bandarabbas, Iran, raminkharazmi@aut.ac.ir
2) Iranian Offshore Oil Company, Tehran, Iran, arghash@yahoo.com
3) Iranian Offshore Oil Company, Tehran, Iran, fouladvandi92@gmail.com
4) Iranian Offshore Oil Company, Tehran, Iran, rezakharazmi19@gmail.com
5) Iranian Offshore Oil Company, Tehran, Iran, payamani.h@gmail.com

1. Introduction

Passenger transferring in offshore fields is an extensive challenge. At South Pars Oil Layout (SPOL), we have found a solution for transferring passengers between SPOL-A2 Well Head Platform (WHP) and Floating Production Storage and Offloading (FPSO) Cyrus is to use a tele cabin [1]. This tele cabin had two bases, one on the SPOL-A2 wellhead platform and the other on FPSO Cyrus that the point is this base movable. This paper presents a multi-dynamics analysis of the cable system of FPSO Cyrus tele cabin. This analysis was evaluated to demonstrate the design load tension on the main cable of the FPSO Cyrus tele cabin system.

2. Method and Application

This analysis was simulated by MSC Adams software. The Adams Machinery Cable module provides for the modeling of cable systems within the Adams View environment [2, 3].

The cable's mass and inertia are neglected. Dummy parts with pure kinematic constraints are used to track the tangent lines between pulleys. Angles between dummy parts of the same pulley determine the cable length that's around each pulley. Differential equations are used to track cable span physical length by integrating the pulleys' angular velocities. Cable span tension forces are computed from the difference between the cable span's pure geometry and physical length. Appropriate action-only forces are applied on the pulleys to replicate the effect of cable contact with friction.

The simplified cable provides a very fast solution that generates accurate loads on the pulleys as long as cable mass and inertia effects are negligible for the transmission effect. Winching effects are accounted for in terms of the addition and removal of cable length from the system. Pulleys can be offset from a base plane and rotated in and out of the plane during design time and disengage from the cable during a simulation.

3. Simulation Setup

3.1. Input Parameters

Input parameters are shown in Figure 1 and Table 1:

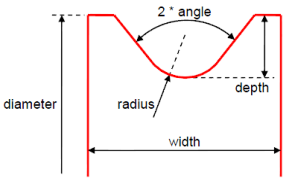

Figure 1. Example figure.

Table 1. Input parameters

	Parameter	Value	Dimension
Cable Parameters	Density	7850	Kg/m^3
	Young's Modulus, E	2.1*10 10	Kg/m^2
	Damping Ratio	0.01	-
	Diameter	16	mm
Pulley_1 Dimension	Width	0.0762	m
	Depth	0.025	m
	Radius	0.02	m
	Angle	20	deg
	Diameter	0.2032	m
Pulley_2 Dimension	Width	0.046725	m
	Depth	0.01585	m
	Radius	0.02	m
	Angle	10	deg
	Diameter	0.127	m
cabin dimension	Length	1.5	m
	Width	0.75	m
	Height	1.4	m
FPSO general particulars	LOA	245.5	m
	LBP	234	m
	Depth	21.5	m
	Maximum draft	15.291	m
	Minimum draft	9.5	m
Distance between FPSO and WHP		100	m

3.2. Modeling

Three cable systems are considered as follows:

i) Main Cable

Main Cable includes six spans. The Begin Anchor was Pneumatic Winch and wrapping order from respectively, STBD main structure pulley (Type of Pulley_1), next to Aft

cabin pulley (Type of Pulley_2), next to Fore cabin pulley (Type of Pulley_2), next to WHP pulley (Type of Pulley_1), next to Weight pulley (Type of Pulley_1), and the End Anchor was connected to a wight load by 2000 Kg.

ii) Aft-Drive Cable

Aft-Drive Cable includes two spans. The Begin Anchor was Port-Roller of FPSO FWD Winch and wrapping order from respectively, Port main structure pulley (Type of Pulley_1) and the End Anchor was connected to the aft of the cabin.

iii) Fore-Drive Cable

Fore-Drive Cable includes two spans. The Begin Anchor was STBD-Roller of FPSO FWD Winch and wrapping order from respectively, WHP-Drive pulley (Type of Pulley_1) and End Anchor was connected to Fore of the cabin.

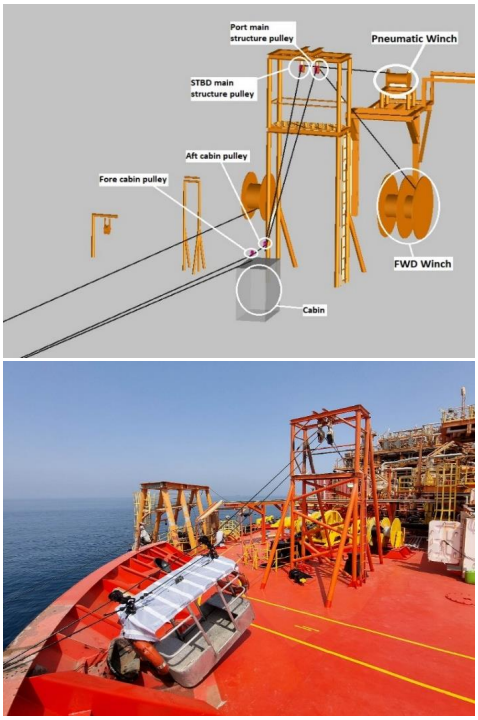

Figure 2. Modeling of cable system

3.3. Scenario

The scenario is transferring 300 kg load by cabin and began from FPSO to WHP, paused for a few seconds, and finally return to FPSO.

This action repeats in min, mid and max drafts and record live tension on the main wire rope.

4. Results

4.1. Load Case 1

In this case FPSO in the maximum draft: 15.291 m and cabin weight: 300 Kg.

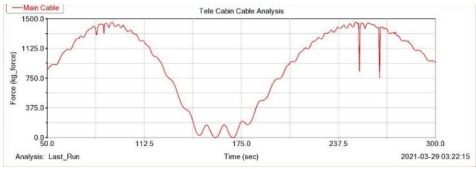

Figure 3. Main Cable Tension for Load Case 1.

4.2. Load Case 2

In this case, FPSO in the minimum draft is 9.5 m, and cabin weight is 300 Kg.

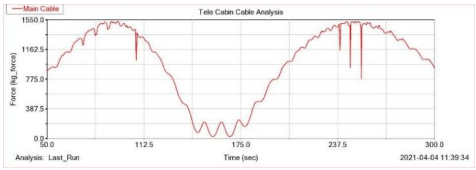

Figure 4. Main Cable Tension for Load Case 2.

4.3. Load Case 3

In this case, FPSO is about mid-draft: 13.5 m and cabin weight: 300 Kg.

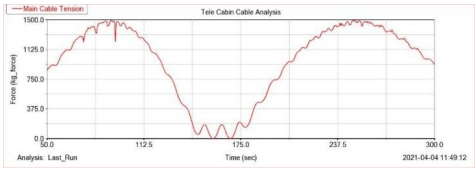

Figure 5. Main Cable Tension for Load Case 3.

5. Conclusion

As can be seen in Figures 2, 3, and 4, results for different load cases in different FPSO drafts, demonstrated that maximum tension on the main cable will be not more than 1550 Kg-Force.

The difference tension between maximum and minimum draft conditions is about 50 Kg-Force.

6. References

[1] Pataraya, D. I., "Calculation and design of cable systems on the example of suspension roads", *Metsniereba, Tbilisi,1991.*

[2] Huang S., "Dynamic analysis of three-dimensional marine cables", *Ocean Engineering*, 1994, pp. 587-605.

[3] Tanga, A., Lia, Y., Qua, H., Xiao J., "Dynamics modeling and simulating analysis of a wire driven parallel mechanism", *Procedia Engineering*, 2011, pp. 788-794.

14th International Conference on Coasts, Ports and Marine Structures
9 & 10 May 2023 , Tehran-IRAN
ICOPMAS 2022

REDUCING HEAVE RAO OF A SEMI-SUBMERSIBLE PLATFORM USING DOUBLE THIN DAMPING PLATES

Arefeh Emami[1], Ahmad Reza Mostafa Gharabaghi[2]

1) Department of Civil Engineering, Hormozgan University, Bandar abbas, Iran, emami@hormozgan.ac.ir
2) Faculty of Civil Engineering, Sahand University of Technology, Tabriz, Iran, mgharabaghi@sut.ac.ir

1. Introduction

A semi-submersible platform is one of the most common types of mobile offshore-drilling units, which can be used under intermediate to ultra-deep-water conditions. It has different applications that its most distinguishing one is oil and gas production. The large heave motion of a semi-submersible platform, due to the different environmental conditions, can create the limiting problems such as restrictions on the operability of drilling and damage to the risers or mooring systems. Controlling this motion, to address this shortcoming, is challenging [1]. So, the researchers have suggested different concepts for reducing the heave motion of semi-submersible such as altering its geometry form, installing heave plates or additional material [2]. In this study, double thin damping plates were attached to a conventional semi-submersible platform to reduce the heave motion of the response amplitude operator (RAO). First, a typical GVA4000 semi-submersible drilling platform was considered and its heave RAO under a monochromatic linear wave train in deep water was derived by semi-analytical solution based on the Eigenfunction Matching Method (EMM). The results were compared by available experimental data with a good agreement. Second, double thin damping plates were attached at the top and bottom of the pontoons. Added mass, damping, and wave force were extracted from semi-analytical solution. Finally, the one degree of freedom equation of heave motion was solved, and heave RAO was achieved. The results showed that the heave RAO of the proposed semi-submersible is decreased significantly compared to its original case. In the next sections, the steps of problem solving are explained.

2. Mathematical Model

A typical GVA4000 semi-submersible was considered in a constant water depth of h_1. Double thin damping plates were installed at the top and bottom of the pontoons. The Cartesian system was considered on the free surface water (z axis vertically upward and x axis horizontally along the pontoons). It was assumed that the fluid is incompressible, inviscid and the flow is irrotational. Because of considering a monochromatic small amplitude wave train propagating in the x direction, the problem can be simplified as 3-D to 2-D [2]. So, the velocity potential is written as the following:

$$\varphi(x, z, t) = \mathrm{Re}\{\phi(x, z)\}\, e^{-i\omega t} \quad (1)$$

Where 'R' is the real part of complex expression, ϕ is the spatial part. For a wave train approaching a floating structure, the wave-structure interaction can be divided into two parts: one as the diffraction of the incident wave train due to the fixed body which produces a scattered wave field, and the other as the radiation of the body forced to oscillate in the still water, so, the velocity potential can be expressed as [3]:

$$\varphi = \varphi_I + \varphi_D + \sum_{L=2}^{4} \varphi_R^L \quad (2)$$

where, φ_I is incident potential, φ_D is diffraction potential, and φ_R is radiation potential that L =2, 3, and 4 are related modes of sway, heave, and roll oscillations, respectively. in addition, the special part of two-dimensional velocity potential is satisfied by Laplace equation as following:

$$\nabla^2\Phi = 0 \Rightarrow \frac{\partial^2\Phi}{\partial x^2} + \frac{\partial^2\Phi}{\partial z^2} = 0 \quad (3)$$

According to Laplace equation and boundary conditions, incident wave potential is calculated as equation 4.

$$\phi_I = -i\frac{Ag}{\omega}\frac{\cosh(k(z+h_1))}{\cosh(kh_1)} exp(ikx) \quad (4)$$

The radiation potential is calculated by assuming the oscillation of the structure in the absence of waves. For harmonic small amplitude waves, the radiation potential can be written up as:

$$\varphi_R^{(3)} = \mathrm{Re}\{-i\,\omega\, A_R^{(3)}\, \phi_R^{(3)}(x,y)\} \quad (5)$$

Where, $A_R^{(3)}$ is the heave oscillation displacement. To calculate the radiation potential, a typical GVA4000 semi-sub attached by double thin damping plates is considered (Figure 1). The fluid domain is divided into 12 different regions. The governing Laplace equation and the related horizontal and vertical boundary conditions for each region were considered. The radiation potential in each region is obtained using the method of separation of variables. The unknown coefficients appearing in each equation are estimated using the EMM. Then, the added mass and damping are extracted form real and imagine parts of the radiation potential. Moreover, the exciting force is calculated using Haskind's method. By calculating those parameters, the equation of one degree of freedom of heave motion is easily written and RAO is obtained.

3. Verification of the Developed Solution

To verify the validity of the developed semi analytical solution, the heave RAO of a GVA4000 semi-sub was examined. Its heave RAO was extracted by EMM and verified by available experimental data. The results showed that the developed method can predict the heave RAO with acceptable accuracy (Figure 2).

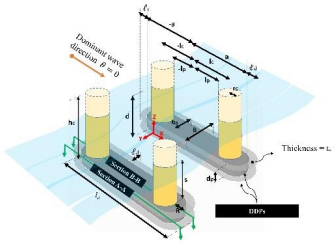

Figure 1. A semi-submersible with two TSDs as schematic

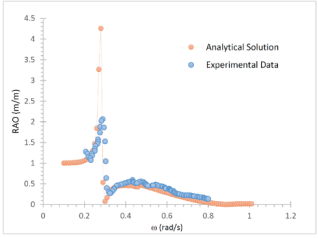

Figure 2. A comparison between semi-analytical solution and experimental data

4. The Results and Discussions

To determine the effect of attaching double thin damping plates on the semi-submersible, 4 double damping with different widths (DDP1 to DDP4) were considered. The B/bp for DDP1 to DDP4 was 1.1, 1.2, 1.4, and 1.6, respectively. The variation of the added mass, damping coefficient, exciting force, and heave RAOs with respect to the angular wave frequency were calculated using semi-analytical method. The results showed that the added mass becomes larger with increasing the plate's width due to the increased trapped water especially for the angular frequency more than about 0.18–0.24 rad/s (Figure 3). The damping coefficient becomes larger by increasing the plate width for frequencies more than about 0.3 rad/s and it is zero for any width at frequencies larger than 0.46 rad/s (Figure 4). The exciting force is larger by increasing the plate width for frequencies greater than about 0.2–0.3 rad/s, and there is a sudden rise for all widths at frequencies of about 0.46 rad/s (Figure 5). The RAO curve revealed that the peak value of RAO decreased with an increase in the width plates and the resonance frequency is also decreased related to the original GVA4000 (Figure 6). The percentage of RAO reduction relative to the original platform for double thin damping plates 1 to4 was 20.8, 26.20, 33.31, and 44.89%, respectively.

5. Conclusion

In this study, to improve heave RAO of a semi-submersible, double thin damping plates were installed on the pontoons of a typical GVA4000. The heave RAO was solved semi-analytically. The results revealed that using the plate reduces the peak value of the heave RAO and the resonant frequency is displaced to a lower frequency compared to its original one. Therefore, this method can be significant for improving the heave motion of the semi-submersible platform.

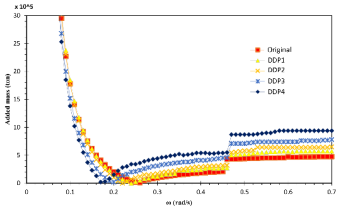

Figure 3. Added mass of Modified GVA4000 using DDPs

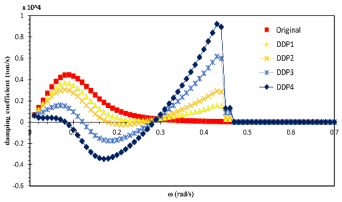

Figure 4. Damping Coefficient of Modified GVA4000

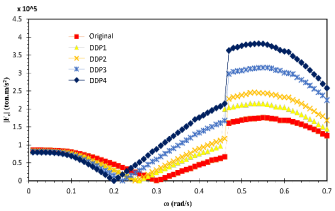

Figure 5. Exciting coefficient of Modified GVA4000

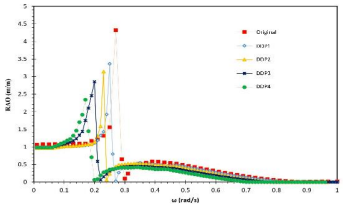

Figure 6. Heave RAO of Modified GVA4000

6. References

[1] Emami A, Gharabaghi AR. "REDUCING HEAVE RESPONSE AMPLITUDE OPERATOR OF A SEMI-SUBMERSIBLE PLATFORM USING PORO-ELASTIC PLATES". In The 13th Int Conf on Coasts, Ports & Marine Structures, 2018, pp. 229-230.

[2] Emami A, Gharabaghi AR. "Application of poroelastic layers in a semi-submersible platform: Devising an efficient heave motion response reduction method". Ocean engineering. 201 2020, pp. 107148.

[3] Linton, C. M, and Mciver, P. "Handbook of Mathematical techniques for wave/structure intractions CRC Press,". 2001

[4] Clauss, G.F., Schmittner, C., and Stutz, K. "Time-domain investigation of a semisubmersible in rogue waves", In: *ASME 2002 21st International Conference on Offshore Mechanics and Arctic Engineering*: American Society of Mechanical Engineers, 2002, pp. 509-516

14th International Conference on Coasts, Ports and Marine Structures
9 & 10 May 2023 , Tehran-IRAN
ICOPMAS 2022

INVESTIGATING THE EFFECT OF HEAVING POINT ABSORBER GEOMETRICAL PROPERTIES ON ITS HYDRODYNAMIC RESPONSE

Mohammad Javad Ketabdari[1], Kaveh Soleimani[2] and Ataollah Gharechae [3]

1) Amirkabir University of Technology, Tehran, Iran, Ketabdar@aut.ac.ir
2) Amirkabir University of Technology, Tehran, Iran, Kv.soleimani@aut.ac.ir
3) Chabahar Maritime University, Chabahar, Iran. a.gharechae@cmu.ac.ir

1. Introduction

Point absorber is a wave energy device with small sizes relative to wave length [1]. To maximize the absorber power, the point absorber is typically designed to behave as a resonant device. Conventional CFD methods might have some difficulties to predict the response of the device. However, SPH numerical method is a useful tool for this problem modeling and can provide more accurate results [2,3]. In this research, the SPHysics model [4] was used to study the effect of the geometrical properties of a heaving point absorber on its motion response and absorbed power. To validate the numerical data, an analytical model was used. The slight difference between the two data revealed the adequate accuracy of the model. Using three different radii, the effect of the device dimensions on its response was then evaluated.

2. Device equation of motion

One of the most important parts of a point absorber is its Power Take Off (PTO) mechanism by which the absorbed energy from waves is transformed into electricity. Since the considered buoy has a cylindrical shape, it is possible to obtain its motion responses by analytical models. The equation of motion for a heaving floating body is given as follows [5]:

$$(m+a_{wz})\frac{d^2z}{dt^2}+b_{rz}\frac{dz}{dt}+b_{vz}\left(\frac{dz}{dt}\right)\left|\frac{dz}{dt}\right|^n \quad (1)$$

$$+b_{pz}\frac{dz}{dt}+\rho g A_{wp} z = F_{z0}\cos(\omega t+\alpha_z)$$

where m, a_{wz}, b_{rz}, b_{vz}, b_{pz}, A_{wp}, F_{z0}, α_z and ω are the physical mass, the added mass, the radiation damping coefficient, the viscous damping coefficient, the PTO coefficient, the water plane area, the wave force amplitude, the phase angle between the wave and wave-induced heaving force, the angular frequency and the wave period, respectively. n is a number equal to 0 for laminar and 1 for turbulent flow. The natural frequency and the added mass are mathematically represented by the following equation

$$\omega_n = \sqrt{\frac{\rho g A_{wp}}{m+a_{wz}}} \quad (2)$$

$$a_{wz} = \rho\pi a^3\left\{\frac{a}{8(h-d)}-\frac{a}{2h}\left[\gamma+\ln\left(\frac{ka}{2}\right)\right]\right\} \quad (3)$$

where a, h, d, k and γ are the device radius, the water depth, the device draft, the wave number and the Euler's constant, respectively. The PTO force and the pneumatic power across the damper are given by the following equations where $\dot{U}$ is the device heaving velocity

$$F_{pto} = b_{pz}\dot{U} \quad (4)$$

$$P_{pto} = b_{pz}\dot{U}\dot{U} \quad (5)$$

3. The SPH method

The motion of the device is obtained by summing the contributions applied to the boundary particles for entire body. The force on each boundary particle is computed by summing up the contribution from all the neighboring water particles. The boundary particle k experiences the following force per unit mass:

$$f_k = \sum_{a\in WPs} f_{ka} \quad (6)$$

where WPs denotes water particles and f_{ka} the force per unit mass exerted by water particle a on boundary particle k. The equations of basic rigid body dynamics are used for the motion of the device:

$$M\frac{dV}{dt}-b_{pz}V = \sum_{k\in BPs} m_k f_k \quad (7)$$

where M is the device mass, V is the device velocity, b_{pz} is the PTO coefficient and BPs denotes the boundary particles. This equation is integrated in time to predict the values of V for the beginning of the next time-step.

4. Validation

In this section for a simple model of heaving wave absorber, the SPH model results for displacement and velocity were compared with the analytical data from the solution of Eq. 1. The length, width and draft of the floating body are 0.3 m, 0.3 m and 0.15 m, respectively. The wave height, period and water depth were set to 0.15 m, 1.5 s and 1.5 m, respectively. A PTO coefficient of 100 Nm/s was applied to the cylinder. The analytical model and numerical setup are shown in Fig. 1. Comparison between the numerical and analytical data demonstrates good correspondence as shown in Figs 2-3.

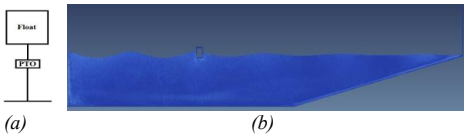

(a) (b)

Figure 1. Simulation of the floating body a) Analytical model b) SPH model

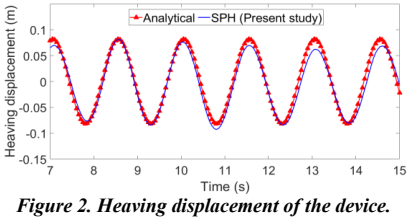

Figure 2. Heaving displacement of the device.

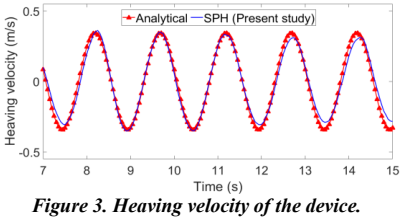

Figure 3. Heaving velocity of the device.

5. Case Study

In this section, considering the numerical results of tested point absorber by Agamloh et al. (2008) [6], the effect of the cylinder radius on its response was evaluated using three different radii of 0.3, 0.6 and 1.2 m that correspond to natural frequencies of 4.33, 4.14 and 3.71 rad/sec, respectively. In all simulations, water depth, wave height and wave period were 1.5 m, 0.15 m and 1.5 sec, respectively which results in a wave frequency of 4.19 rad/sec. As Figs 4-6 show, the cylinder with a natural frequency close to the wave frequency has the maximum motion response and power absorption. This is in fact a resonant floating body in this situation. This shows that the dimension of the heaving point absorber should be chosen so that its natural frequency placed close to the peak frequency of the spectrum of irregular real sea waves.

6. Conclusion

In this research, an SPH simulation was performed to investigate the effect of the device radius on its motion response as well as its power absorption capability. The model was first verified by comparing the analytical and numerical results of the motion response of a heaving floating body. Then a parametric study was performed to evaluate the effect of the device radius. The results showed that resonance phenomenon maximizes the device motions. So, the wave absorber should be designed to behave as a resonant device.

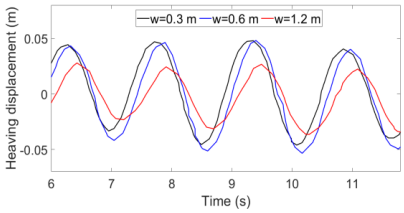

Figure 4. Radius effect on the device's heaving motion.

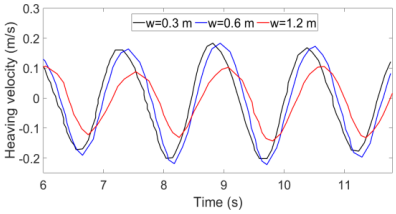

Figure 5. Radius effect on the device heaving velocity.

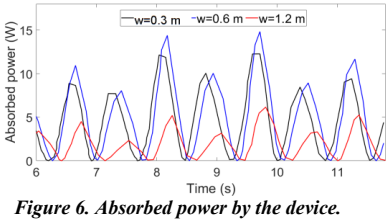

Figure 6. Absorbed power by the device.

7. References

[1] Soleimani, K., and Ketabdari, M. J., "Performance analysis of a tuned point absorber using SPH calm water and wave tank simulations", *Journal of Ocean Engineering and Science*, 2022, pp. 3-28.

[2] Ketabdari, M.J., Soleimani, K. and Khorasani, F., "Modeling of multipurpose fixed breakwater wave energy converter using SPH method," in *Complementary Resources for Tomorrow*, Springer, 2020, pp. 149-162.

[3] Soleimani, K., Ketabdari, M.J. and Bingham, H.B., "WCSPH simulation of the forced response of an attenuator oscillating water column wave energy converter," *European Journal of Mechanics-B/Fuids,* 95, 2022, pp. 38-51.

[4] Gomez-Gesteira, M., Rogers, B.D., Crespo, A.J.C., Dalrymple, R.A., Narayanaswamy, M. and Dominguez, J.M., "SPHysics – development of a free-surface fluid solver – Part 1: Theory and formulations," *Computers & Geosciences,* 48, 2012, pp. 289-299.

[5] Mc Cormick, M.E., *Ocean Engineering Mechanics*, New York: Cambridge University Press, 2010.

[6] Agamloh, E.B., Wallace, A.K. and von Jouanne, A., "Application of fluid–structure interaction simulation of an ocean wave energy extraction device," *Renewable Energy,* 33, 2008, pp. 748-757.

14th International Conference on Coasts, Ports and Marine Structures
9 & 10 May 2023 , Tehran-IRAN
ICOPMAS 2022

PRESENTING A NOVEL METHODOLOGY FOR ESTIMATING THE FAILURE FRAGILITY CURVES OF CORRODED OFFSHORE PIPELINES

Mohsen Abyani[1], Mohammad Reza Bahaari[2]

1) School of Civil Engineering, College of Engineering, University of Tehran, Tehran, Iran. mohsen.abyani@ut.ac.ir
2) School of Civil Engineering, College of Engineering, University of Tehran, Tehran, Iran. mbahari@ut.ac.ir

Abstract

This study presents a novel methodology to estimate the failure fragility curves for corroded offshore pipelines employing finite element simulation. In this algorithm, the random variables are selected by an efficient sensitivity analysis named Tornado Diagram Analysis. Thereafter, a combination of Latin Hypercube Sampling (LHS) method along with Simulated Annealing (SA) technique is used to generate the random simulations which represent the existent epistemic uncertainties. Each realization of this simulation matrix is keyed into the numerical model as the essential inputs to evaluate the probabilistic responses of the corroded pipeline from linear behavior to failure limit state as well as its failure fragility curves.

1. Introduction

In today's world, pipelines are one of the safest and the most economic utilities for transporting oil and gas materials from production sites to their markets and end users. Nevertheless, structural failure or degradation of such infrastructures can lead to irrecoverable environmental, financial and human losses. Thus, all the predominant threats to these structures from the commissioning to de-commissioning dates, such as corrosion should be comprehensively considered in the design state. In this regard, Cronin [1] studied the effects of corrosion defects on pipelines utilizing both experimental burst tests and numerical finite element analysis of the corroded pipelines. Huang et al. [2] presented a model to calculate the pressure of thick-walled vessels using finite element simulation verified by experimental tests. Al-Owaisi et al. [3] comprehensively investigated the effects of defect shape and location on closely spaced defects by conducting finite element analysis. They evaluated the results of their numerical models which were formed based on quadratic tetrahedron and quadratic hexahedron elements. Moreover, Abyani and Bahaari [4] developed a new finite element-based approach for reliability assessment of offshore pipelines subjected to internal corrosion.

From another perspective, Caleyo et al. [5] worked on the reliability evaluation of corroded pipelines to calculate their remaining life employing First Order Second Moment (FOSM) iterative method, Monte Carlo Simulation (MCS) technique and the first order Taylor series expansion of the limit state function. Leira et al. [6] inspected the system reliability of pipelines subjected to internal corrosion using enhanced MCS method to notably reduce the computational burden of such extensive assessments. Similarly, Abyani and Bahaari [7] compared the system reliability of corroded pipelines computed by MCS and LHS methods. The results of this work revealed that LHS method is capable of providing reliable results with considerably less time and computational costs.

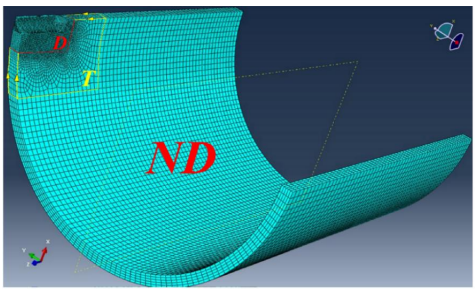

Figure 1. Presentation of the mesh network for the sample offshore pipeline

2. Finite element modeling

The 3D finite element model of a sample offshore pipeline subjected to internal corrosion defect is created in ABAQUS, using solid elements. Additionally, API 5L X65 material which is typically applied in most of the offshore pipeline projects, is considered in this investigation, as well. Also, eight node linear hexahedral reduced integration elements are utilized to construct the mesh network as they can lead to more accurate results in comparison with tetrahedral elements (see Figure 1) [3]. It is noted that all the numerical analyses are supposed to be performed by ABAQUS Python Scripting interface.

3. Methodology

A new probabilistic algorithm named Incremental Pressure Analysis (IPA) [7] is presented in Figure 2 which makes it possible to derive the failure fragility curves for corroded offshore pipelines. Its sequential steps are briefly described as follows:

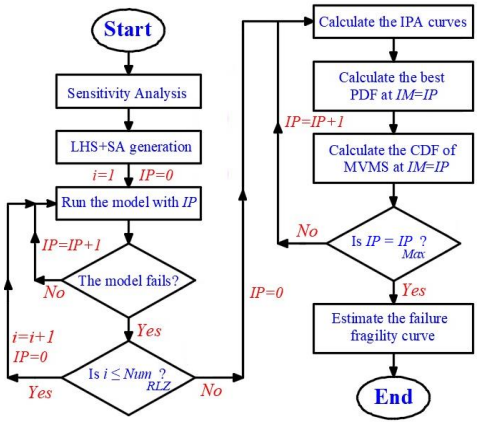

Figure 2. Presentation Flowchart of the IPA method

1) In the first step of this algorithm, a sensitivity analysis is conducted to select the random variables which are more important.

2) Thereafter, the random realizations are generated utilizing a combination of LHS and SA methods [4].

3) In the third step, the following loops are implemented to estimate the Maximum Von-Mises Stress (MVMS) of the pipeline at all the considered Internal Pressure (IP) levels:

```
    for i=1:1:number of realizations
  for j=1:1: failure IP
     MVMS(i,j)= MVMS
  end
end
```

In fact, MVMS of each step is determined through the finite element analysis which has been wisely programmed in ABAQUS Python Scripting interface.

4) Afterwards, the IPA curves can be achieved. In these curves, MVMS and IP (the horizontal and vertical axes) represent the structural response and the loading imposed on the pipeline, respectively. More specifically, these curves are computed for all the realizations which have been randomly generated in the second step of this flowchart.

5) After the calculation of the IPA curves, it is possible to find the appropriate analytical Probability Density Function (PDF) and Cumulative Distribution Function (CDF) of the MVMS at different IP levels, using reliable statistical measures (e.g. Kernel density function or strong goodness of fit tests). Additionally, the same process can be performed for another underlying random variable which is the failure IP (the IP level where the pipeline reaches its failure limit state). Thus, the failure fragility curve of the pipeline can be drawn using such statistical data. Finally, the failure probability of the pipeline at different IP levels is estimated by the mentioned fragility curve.

4. References

[1] Cronin, D. "Assessment of corrosion defects in pipelines, in mechanical engineering", The University of Waterloo: Waterloo, Ontario, Canada, 2000.

[2] Huang, X., Chen, Y., Lin, K., Mihsein, M., Kibble, K., and Hall, R. "Burst strength analysis of casing with geometrical imperfections", *Journal of Pressure Vessel Technology*, 129, 4, 2007, pp. 763–770.

[3] Al-Owaisi, S.S., Bechker, A.A., and Sun, W. "Analysis of shape and location effects of closely spaced metal loss defects in pressurized pipes", *Engineering Failure Analysis*, 68, 2016, pp. 172–86.

[4] Abyani, M., and Bahaari, M.R. "A new approach for finite element based reliability evaluation of corroded offshore pipelines", *International Journal of Pressure Vessels and Piping*, 193, 2021, 104449.

[5] Caleyo, F., Gonzales, J.L., and Hallen, J.M. "A study on the reliability assessment methodology for pipelines with active corrosion defects", *International Journal of Pressure Vessels and Piping*. 79, 2002, pp. 77-86.

[6] Leira, B.J., Naess, A., and Naess, O.E.B. "Reliability analysis of corroding pipelines by enhanced Monte Carlo simulation", *International Journal of Pressure Vessels and Piping*, 144, 2016, pp. 11-17.

[7] Abyani, M., and Bahaari, M.R. "A comparative reliability study of corroded pipelines based on Monte Carlo Simulation and Latin Hypercube Sampling methods", I*nternational Journal of Pressure Vessels and Piping*, 181, 2020, 104079.

14th International Conference on Coasts, Ports and Marine Structures
9 & 10 May 2023 , Tehran-IRAN
ICOPMAS 2022

THE EFFECT OF USING A TUNED MASS DAMPER (TMD) IN MITIGATION OF THE VIBRATION OF A TLP OFFSHORE WIND TURBINE

Mohammad Reza Tabeshpour[1], Erfan Bahaelou Horeh[2]

1) Associate professor, Mechanical Engineering Department, Sharif University of Technology, Tehran, Iran, Tabeshpour@sharif.edu
2) M.Sc. Student, Mechanical Engineering Department, Sharif University of Technology, Tehran, Iran, Erfan.bahaelouhoreh@mech.sharif.edu

1. Introduction

Today the air pollution which is caused by consuming fossil fuels makes us replace other clean sources of energy. One of the best choices is renewable energy. In this regard, seas and oceans have a large capacity of energy such as wind, wave and tidal energy. We can use them to provide a big amount of energy. Offshore wind turbines are one of the ways we can use to extract wind energy from oceans. The wealthy point about wind in oceans is that it is steadier than wind in onshore areas. Also, the wind in oceans blows faster than it does in onshore areas. However, using offshore wind turbines has some challenges. One of them which is so important is the vibration of offshore wind turbines. There are some solutions for controlling these vibrations. One of them is using a Tuned Mass Damper (TMD). In this research, we try to find out the effect of using TMD in a TLP offshore wind turbine numerically in surge motion.

2. Study

2.1. The Model

In this research, NREL 5MW MIT TLP is chosen because of its reputation in academic environment and also many researches that be done on this model. This model consists of a TLP platform and a 5MW turbine on this platform. [1] [2]
In this research, the mass ratio of the TMD is about 5% and the frequency ratio is considered about 1.

2.2. Wave Load

In this research, due to the platform's size and waves height, the Morison method is the best way to calculate the wave load. In this method, the wave load on each element consists of two parts, the drag part and the inertia part. [3]

$$f = f_D + f_I \quad (1)$$

After adding these two parts together, by integrating over the entire structure we can reach the wave load.

$$F = \int f.dy \quad (2)$$

For calculating each part of the wave load we can use equations (3) and (4).

$$f_D = \frac{1}{2}\rho C_D D V|V| \quad (3)$$

$$f_I = \rho C_I \frac{\pi D^2}{4} a \quad (4)$$

2.3. Wind Load

There are several theories for calculating wind load. In this research, however, the wave load is dominant. Therefore, we consider a simple theory for calculating wind load, and the wind load is considered constant. For reaching out the wind load on each part of the structure we have to use equation (11). [1]

$$F_{wind} = \frac{1}{2}\rho C A V^2 cos(\alpha) \quad (5)$$

2.4. The Governing Equations of the System without TMD

The TLP has movements in 6 degrees of freedom, however, in this research we focus on the surge behavior. For surge direction, we can write: [1]

$$(M + M_a)\ddot{x} + C\dot{x} + Kx = F_x \sin(\omega t) + F_{wind} \quad (6)$$

The surge stiffness of the mooring system would be [3]:

$$K = \frac{nT_0}{l} + \frac{nAE}{2l^3}x^2 \quad (7)$$

If we name the first part of K, k and the second part k´, finally, the driven equation of the system could be written as follow:

$$(M + M_a)\ddot{x} + C\dot{x} + kx + k' x^3 = F_x \sin(\omega t) + F_{wind} \quad (8)$$

This kind of non-linear differential equation is called Duffing equation.

2.5. The Governing Equations of the System with TMD

Since in this case and this situation, the system has two degrees of freedom, we have two dynamic equations.

First, for the main system we have: [4]

$$(M + M_a + M_d)\ddot{x} + C\dot{x} + Kx = F_x sin(\omega t) + F_{wind} + C_d\dot{x}_d + K_d x_d \quad (9)$$

Also, for TMD we can write:

$$M_d\ddot{x}_d + C_d\dot{x}_d + K_d x = -M_d\ddot{x} \quad (10)$$

It should be noted that in these equations x and x_d illustrate the displacement of the TLP and TMD from the reference point, respectively.

2.6. Load Cases

In this research, one wind load case and three wave load cases are considered and the response of the system against these load cases is studied to find out the efficiency of using TMD on offshore wind turbines in waves with different

heights and periods. Also, it should be noted that all waves are considered regular waves.

Table 1 - Wind case load

Case load	Speed (m/s)	Type
1	23	constant

Table 2 - Wave load cases

Case load	Wave height (m)	Wave period (s)
1	3.3	6
2	6.6	9.5
3	10	10

2.7. Numerical Study

For modelling this case in MATLAB, the Euler method is used. In this method by using the derivation concept, we attempt to reach the results of the differential equations.

$$f(t_0+h)=\sum_{i=0}^{\infty}\frac{f^{(i)}h^i}{i!}$$

$$=f(t_0)+f'(t_0)h+\frac{f''(t_0)h^2}{2!}+\cdots$$

$$\cong f(t)+f'(t_0)h \qquad (11)$$

3. Results

After solving governing equations numerically by MATLAB, in load case 1, we found out that using TMD in a TLP offshore wind turbine can reduce the displacement amplitude in surge motion by about 3.18%. Also, this reduction in velocity and acceleration was about 7.84% and 9.09%, respectively.

In load case 2, the efficiency of using TMD in surge displacement increased in comparison with load case 1 and it was about 3.62%. However, the efficiency of using TMD in surge velocity and acceleration decreased to 2.7% and 3.03%.

In load case 3, using TMD can reduce the amplitude of surge displacement by about 5.78% which was more than in other load cases. Also, the mitigation in the amplitude of velocity and acceleration in this load case was about 6.22% and 3.51%.

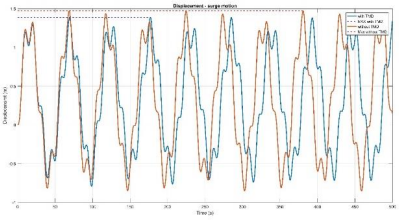

Figure 1- Displacement of TLP offshore wind turbine in load case 3 with and without TMD

4. Conclusion

In this research, we try to find out the efficiency of using TMD in a TLP offshore wind turbine in order to mitigate the amplitude of the vibrations.

Due to the obtained results, we figure out that by increasing the wave height and wave period the efficiency of using TMD in mitigation of the amplitude of surge displacement increased. In the other word, using TMD in severe waves is more effective than using it in waves with lower height and period. However, there is not any pattern or relation between wave height and wave period and efficiency of using TMD in velocity and acceleration of the surge motion.

Since the load cases in this research were limited, we suggest in future researches more load cases will be considered to obtain more accurate results. Also, investigating the efficiency of using TMD in other motions is another offer for future researches.

5. References

[1] A. Ebrahimi, M. Abbaspour and R. Mohammadi Nasiri, "Dynamic behavior of a tension leg platform offshore wind turbine under environmental loads," *Scientia Iranica,* vol. 21, no. 3, pp. 480-491, 2014.

[2] S.-P. Breton and G. Moe, "Status, plans and technologies for offshore wind turbines in Europe and North America," *Renewable Energy,* vol. 34, no. 3, pp. 646-654, 2009.

[3] M. Tabeshpour, Offshore Structures, Tehran: Scientific Publishing Institute of Sharif University of Technology, 2014.

[4] M. R. Tabeshpour and L. Nikmehr, "Numerical and Experimental Study on Dynamic Response Mitigation of Tension Leg Platform Using Tuned Mass Damper," *Journal of Ship Research,* vol. 00, no. 00, pp. 1-12, 2021.

[5] G. Malliotakis, P. Alevras and C. Baniotopoulos, "Recent Advances in Vibration Control Methods for Wind Turbine Towers," *Energies,* vol. 14, no. 7536, 2021.

[6] M. Vardaroglu, Z. Gao, A. M. Avossa and F. Ricciardelli, "Validation of a TLP wind turbine numerical model against model-scale tests under regular and irregular waves," *Ocean Engineering,* vol. 256, 2022.

[7] M. R. Tabeshpour and E. Malayjerdi, "Surge Motion Passive Control of TLP with Double Horizontal Tuned Mass Dampers," *International Journal of Acoustics & Vibration,* vol. 26, no. 1, pp. 4-8, 2021.

[8] W. Wang, X. Li, H. Zhao, B. Wang and Y. Li, "Vibration control of a pentapod offshore wind turbine under combined seismic wind and wave loads using multiple tuned mass damper," *Applied Ocean Research,* vol. 103, 2020.

14th International Conference on Coasts, Ports and Marine Structures
9 & 10 May 2023 , Tehran-IRAN
ICOPMAS 2022

RELIABILITY ANALYSIS OF ANCHORED SHEET PILE WALL BASED ON FUZZY LOGIC

Negin Sarshar[1], Ali Derakhshani[1]

1) Department of Civil Engineering, Faculty of Engineering, Shahed University, Tehran, Iran, adera@shahed.ac.ir

1. Introduction

Sheet pile wall is a type of retaining wall that is built to retain earth or water. The sheet pile wall is widely used due to its fast and quite simple construction. There are two main types of sheet pile walls; Anchored sheet pile walls and Cantilever sheet pile walls. When the height of backfill material behind a sheet pile wall is more than about 6 m, the anchored sheet pile wall becomes more economical [1].

Uncertainties in geotechnical engineering affect the reliability of the design, so it is necessary to consider these uncertainties in the analysis and design of geotechnical structures. The traditional way of dealing with uncertainties is to use conservative values for the design variables and (or) safety factors [2].

In this research, we investigated the reliability of anchored sheet pile wall penetrating into sandy soil by layering the soil and applying the uncertainty to each layer of soil using fuzzy the logic concept. Figure 1 shows the properties of soil layers and sheet pile.

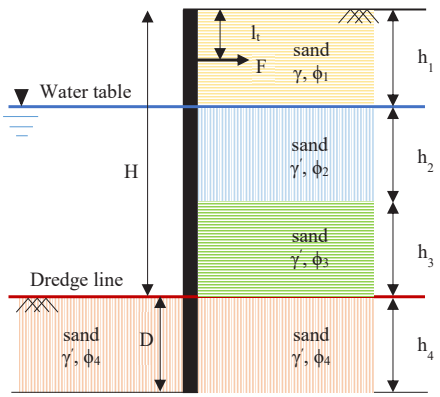

Figure 1. Properties of soil layers and anchored sheet pile.

2. Uncertainty Analysis

Fuzzy logic is used to apply the uncertainty to the soil and structure input parameters. A fuzzy number of an input parameter, for example, X, has a crisp value of X_c and the uncertainty of at most $\pm\Delta X$. The upper bound is $X_c + \Delta X$ and the lower bound is $X_c - \Delta X$ [3].

Some of the input parameters and their crisp and uncertainty values are presented in table 1.

Table 1. Input parameters and their uncertainties.

Parameter	Uncertainty	Lower bound	Crisp value	Upper bound
Friction angle of soil layers (φ_i)	5%	26.1	29°	31.9
Unit weight of soil (γ)	7%	13.76	16 KN/m^3	18.24
Submerged unit weight of soil (γ')	7%	7.9034	9.19 KN/m^3	10.4766
Depth of dredge line (H)	0.5%	8.91	9 m	9.09
Height of soil layers (h_i)	0.5%	2.97	3 m	3.03
Penetration depth of sheet pile (D)	0.5%	2.97	3 m	3.03
Depth of anchor rod (l_t)	0.5%	1.287	1.3 m	1.313
Anchor pull (F)	5%	108	120 KN/m	132
Section modulus of sheet pile (S)	5%	0.0011	0.0012 m^3/m	0.0013

3. Failure Probability

Failure modes of the sheet pile wall system are overturning, sliding, and flexural modes [2].

To evaluate the failure probability (FP) of the sheet pile wall system the fuzzy safety factor and normal cumulative distribution function were used [4].

$$FP = \Phi\left[\frac{1 - E(SF)}{\sigma(SF)}\right] \quad (1)$$

Where SF is the safety factor, E(SF) is the mean of SF, σ(SF) is the standard deviation of SF and Φ is the normal cumulative distribution function.

4. Results

Membership functions of overturning, sliding, and flexural safety factors considering layered soil with uncertain characteristics are shown in Figure 2.

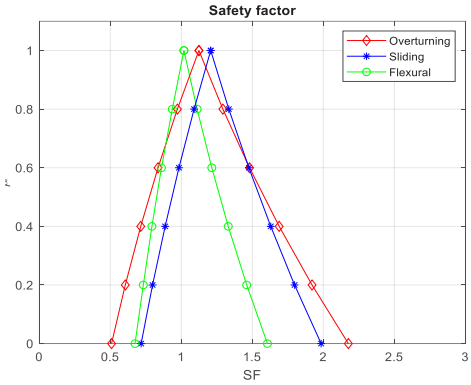

Figure 2. Membership functions of safety factors.

The failure probabilities of overturning, sliding, and flexural modes are displayed in Figure 3.

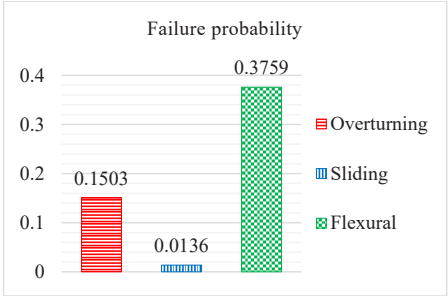

Figure 3. Failure probability.

Safety factors for the case where the uncertainty was not taken into account, were also calculated and presented in Table 2.

Table 2. Safety factors without consideration of uncertainty.

Overturning	Sliding	Flexural
1.1240	1.2069	1.0185

5. Conclusions

Sheet pile walls are one of the important waterfront geotechnical structures and it is necessary to maintain their stability. The penetrating sheet pile wall in the soil is subject to various uncertainties, including uncertainties in soil and structure properties. To design safely, it is essential to consider the uncertainties in the sheet pile wall analysis.

In this study, by layering the soil, the behavior of the sheet pile wall under uncertainty in the input parameters of each soil layer and also structure was investigated.

The uncertainties were applied based on fuzzy logic by fuzzification using triangular membership functions.

Fuzzy triangles of safety factors against overturning, sliding, and flexural were obtained; and accordingly, the failure probability was calculated for all three failure modes.

The results achieved by accounting for uncertainties in the input parameters were compared with those of the condition without uncertain parameters. It is observed that the sheet pile wall is safe and stable with crisp values of input parameters, while by considering the uncertainties, it may fail. Therefore, it is necessary to consider the uncertainties in the analysis and design of the sheet pile walls.

6. References

[1] Das, B.M., "Principles of Foundation Engineering", 8thedn. *CENGAGE learning,* United States, 2016.

[2] Basha, B.M., and Babu, G.S., "Target reliability based design optimization of anchored cantilever sheet pile walls", in *Canadian Geotechnical Journal*, 45, 4, 2008, pp. 535-548.

[3] Derakhshani, A., "On the uncertainty analysis of uplift capacity of suction caissons in clay based on the fuzzy sets theory", *Ocean Engineering*, 170, 2018, pp.416-425.

[4] Gong, W., Wang, L., Khoshnevisan, S., Juang, C.H., Huang, H. and Zhang, J., "Robust geotechnical design of earth slopes using fuzzy sets", *Journal of Geotechnical and Geoenvironmental Engineering*, 141, 1, 2015, p.04014084.

14th International Conference on Coasts, Ports and Marine Structures
9 & 10 May 2023 , Tehran-IRAN
ICOPMAS 2022

NUMERICAL INVESTIGATION OF BEARING CAPACITY OF A BUCKET FOUNDATION IN SANDY SOIL

Hamoun Alimoradi[1], Ali Noorzad[2] and Babak Ebrahimian[3]

1) Faculty of Civil, Water and Environmental Engineering, Shahid Beheshti University, Tehran, Iran, h_alimoradi@sbu.ac.ir
2) Faculty of Civil, Water and Environmental Engineering, Shahid Beheshti University, Tehran, Iran, a_noorzad@sbu.ac.ir
3) Faculty of Civil, Water and Environmental Engineering, Shahid Beheshti University, Tehran, Iran, b_ebrahimian@sbu.ac.ir

1. Introduction

One of the sources of clean and renewable energy is offshore wind, which has generated a lot of interest. It offers new ways to address the ongoing energy and environmental crises. A part of this renewable energy is produced by offshore wind turbines (OWTs). They are reaching new heights and larger capacities, while wind farms are moving deeper into the sea and ocean to harness the increased energy potential. Early in 2021, OWTs have produced 35 GW of electricity, a 14-fold increase from 10 years before. As a result, the foundation design and implementation of OWTs have become significant areas of research. The OWT foundation is a considerable portion of the overall cost of the OWT. Several studies have focused on the design of OWT's foundation. Both monopile and gravity-based foundations have been used for OWTs [1]. The suction caisson or skirted foundation is another name for the bucket foundation, which is a new and revolutionary kind of foundation already employed for OWTs, Figure 1. Bucket foundations are less expensive than deep foundations. In addition, no massive equipment is required for the installation of bucket foundations. In this work, the vertical (V), horizontal (H), moment (M), and tension (T) bearing capacities of a bucket foundation in loose sandy soil are analyzed numerically. The effects of geometrical parameters including bucket embedding depth (L), the bucket diameter (D), and the embedment ratio (L/D) have been studied through a series of 3D implicit finite element (FE) simulations.

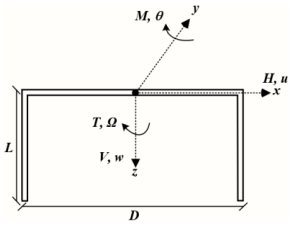

Figure 1: Schematic view of a bucket foundation and conventions of load and displacement directions.

2. Loading Approach

The bucket foundations supporting OWTs are vulnerable to self-weight, wind, wave, current, and other external forces that cause vertical and horizontal loads, overturning and tension moments. As a result, the vertical, horizontal, moment, and tension-bearing capacities must be investigated. These capacities can be calculated using the straightforward tangential intersection method, as shown in Figure 2, where two tangential lines along the initial and later portions of the load-displacement curve are plotted, and the bearing capacity is the point at which these two lines coincide.

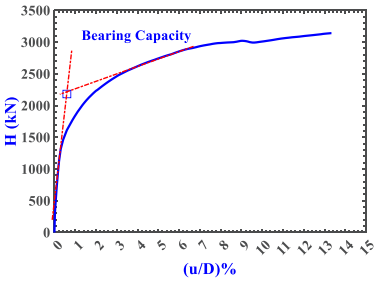

Figure 2: Tangential intersection method for determining bearing capacity.

3. Numerical Simulation

A three-dimensional model of the soil and bucket is developed to compute the bearing capacities. In this regard, a semicylindrical model is created considering the symmetry of the problem. It is worth noting that a non-associated flow rule and the ideal elastic perfectly plastic Mohr-Coulomb (M-C) constitutive model are utilized to describe the non-linear behavior of soil. The FE mesh is seen in Figure 3, which consists of about 11500 linear eight-node brick with reduced integration elements (C3D8R). The bucket has an outside diameter and length of 5 m, and a skirt thickness of 0.125 m. A sensitivity analysis is carried out to obtain the optimum finite element mesh size. In this regard,

a mesh size of less than 0.01D is employed to have an accurate distribution of local stresses and strains in the soil beside the caisson foundation and beneath its foot. However, larger meshes are applied in other areas of the numerical model to save the computation time and to properly capture the loads and the failure mechanism. To obtain the uniaxial bearing capacities for various embedment depth ratios, the model is subjected to incremental one-directional displacement using the displacement probe test approach.

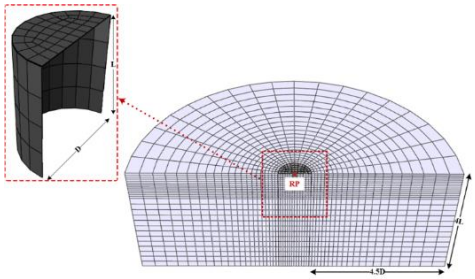

Figure 3: A typical FE mesh and bucket foundation shape.

4. Numerical Results of Uniaxial Bearing Capacity

The load-displacement curve is followed using the tangential intersection method until it achieves an approximately flat surface. The uniaxial capacities of a caisson foundation with D = 5 m and L/D = 0.5 are chosen as a typical result and shown in Figure 4. The ultimate bearing capacity of V is calculated to be between (5–8%)D. It is demonstrated in Figure 4 that the tensile load capacity grows noticeably in smaller strains compared to other load capacities owing to the more rapid soil densification. The moment bearing capacity significantly increases with increasing the embedment ratio (L/D).

5. Conclusions

In this research, the bearing capacities of a bucket foundations for offshore wind turbine has been examined by the FE method. The bucket foundation has been located in a saturated sand. The FE model takes into account the non-linearities of the soil material as well as the geometry. This research shows that the tensile load bearing capacity has significant amount compared to the horizontal load and moment bearing capacities. Thus, it should be taken into account in future works to have more optimum design of bucket foundations.

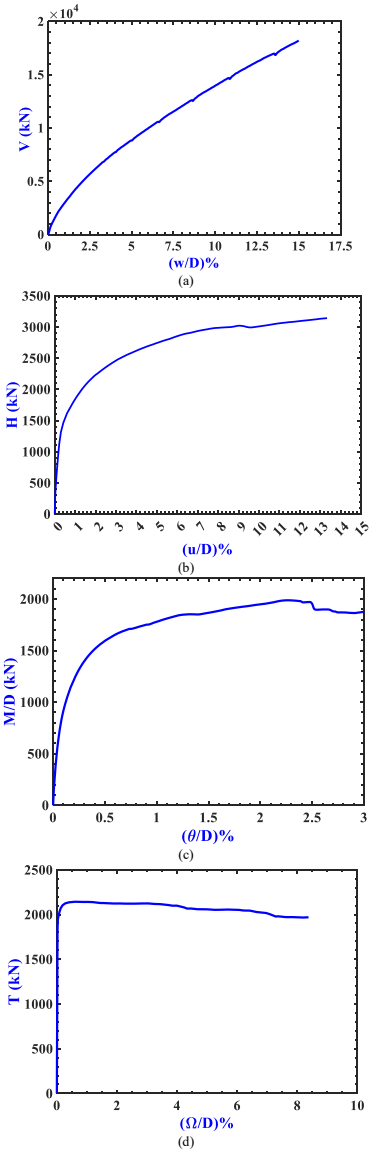

Figure 4. Uniaxial (a) vertical, (b) horizontal, (c) moment, and (d) torsional capacities.

6. References

[1] Randolph, M. F., Gaudin, C., Gourvenec, S. M., White, D. J., Boylan, N., and Cassidy, M. J., "Recent advances in offshore geotechnics for deep water oil and gas developments". *Ocean Engineering*, 38(7), 2011, pp. 818-834.

14th International Conference on Coasts, Ports and Marine Structures
9 & 10 May 2023 , Tehran-IRAN
ICOPMAS 2022

FUZZY RELIABILITY ANALYSIS OF CANTILEVER SHEET PILE WALL PENETRATED INTO THE CLAY

Maryam Sadat Seyedpour[1], Ali Derakhshani[2]

1) Department of Civil Engineering, Faculty of Engineering, Shahed University, Tehran, Iran, maryam.seyedpour@shahed.ac.ir
2) Department of Civil Engineering, Faculty of engineering, Shahed University, Tehran, Iran, adera@shahed.ac.ir

1. Introduction

The easy and quick installation of the sheet pile wall are among the features that make it one of the most frequently used retaining structures in marine environments. In common design methods based on deterministic approach, the wall penetration depth is determined in such a way that safety is evaluated by calculating the safety factors of the structure. However, in the presence of uncertainties during the laboratory and in-situ tests and also during the construction process, the accuracy of the obtained safety factors is not perfectly certain. This study investigates the effects of uncertainties on the stability of a cantilever sheet pile wall penetrated into the clay using the fuzzy set theory.

2. Deterministic Approach

Figure 1 indicates a cantilever sheet pile wall penetrated into the clay. The geotechnical and geometric properties as well as the earth lateral pressure diagram are also displayed in Figure 1. The wall with a depth of D is penetrated into the clay. The depth of dredged line is showed with H in front of the wall. The water level in front of the wall is up to the depth of h from the ground level. The soil at the back of the wall consists of two layers above and under the dredge line. The top layer is the sand with a unit weight of γ and a saturated unit weight of γ_{sat} and the bottom layer of the soil is the clay with a cohesion of c.

In order to obtain the pressure distribution diagram shown in the Figure 1, it is necessary to calculate the values of p_1 to p_4 as follows [1]:

$$P_1 = \gamma h k_a \quad (1)$$

$$P_2 = (\gamma h + \gamma' H) k_a \quad (2)$$

$$P_3 = 4c - [\gamma h + \gamma'(H - h)] \quad (3)$$

$$P_4 = 4c + [\gamma h + \gamma'(H - h)] \quad (4)$$

Where γ' is the submerged unit weight of the soil and k_a represents coulomb active pressure coefficient. By taking the moment about the point B, the value of d_2 can be obtained by solving the following equation.

$$d_2^2 \left(\frac{p_3 + p_4}{6}\right) - \frac{p_3 D^2}{2} + P(D + z) = 0 \quad (5)$$

Where P is the area of the pressure diagram $ACDE$ and z is the distance of the center of this area from the dredge line. Overturning safety factor (FS_o) is obtained by dividing the resisting moment by the overturning moment about the foot of the wall [2]:

$$FS_o = \frac{M_r}{M_o} \quad (6)$$

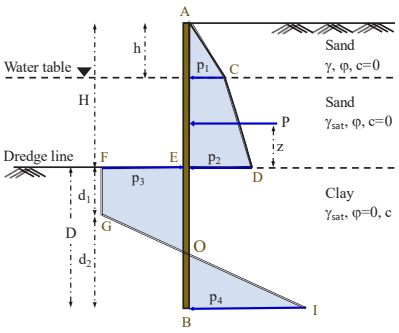

Figure 1. Sheet pile geometric and geotechnical parameters

Flexural stability (FS_f) is measured by dividing the section modulus of sheet pile profile S by the minimum required section modulus (S_{min}).

$$FS_f = \frac{S}{S_{min}} \quad (7)$$

$$S_{min} = \frac{M_{max}}{\sigma_{all}} \quad (8)$$

Note that the maximum moment per length of the wall, M_{max}, occurs at the point of zero shear. Also, allowable flexural stress of the sheet pile is denoted by σ_{all}.

3. Uncertainty Analysis

In fuzzy set theory [3], the membership of a in the set A is shown as $(a, \mu(a))$, in which μ is the membership function that assigns a real number in the interval [0,1] to a. The value of $\mu(a)$ is called the membership degree of a in A. Figure 2 displays a fuzzy triangular membership function which applies the uncertainty of Δx to the input parameter x. When $\mu(x)=1$, the parameter x equals the crisp value of x_c. The value of x may be any value in the interval $[x_a, x_b]$ when $\mu(x)=\alpha$. The most possible uncertainty is believed to occur

at $\mu(x)= 0$, in which the lowest and the highest conceivable values for the parameter are x_c-Δ and x_c+Δx, respectively. In order to find the safety factors fuzzy membership functions, for each α-*cut*, a nonlinear function is formed which should be once maximized and once minimized. This study employed the Genetic Algorithm (GA) to solve this optimization problem.

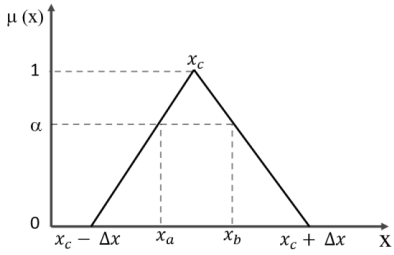

Figure 2. Fuzzy triangular membership function.

Table 1 presents the design variables and their uncertainty values. The upper bound and lower bound for each variable is considered to be equal to the crisp value plus and minus twice its standard deviation, respectively.

Table 1. Design variables and their crisp and uncertainty values.

Variable	COV (%)	Lower bound	Crisp value	Upper bound
γ (kN/m³)	7	13.76	16	18.24
γ_{sat} (kN/m³)	7	15.91	18.5	21.09
φ (degree)	5	27	30	33
H (m)	0.5	4.9	5	5.05
h (m)	0.5	0.99	1	1.01
D (m)	0.5	3.46	3.5	3.53
S (m³/m)	5	0.0005	0.0006	0.0007

4. Results

Figure 3 shows the membership functions for overturning and flexural safety factors. As the crisp values imply, while the design parameters are assumed accurate, the wall is considered safe since the safety factors are greater than 1. Under this assumption, overturning and flexural safety factors equal 1.6 and 1.2, respectively. Increasing the possible uncertainty, i.e., reaching to α=*0*, rises the uncertainty in the safety factors. The minimum possible value for overturning safety factor under the defined uncertainty values is 0.09. This means that in the highest possible uncertainty, the structure is in critical situation regarding this failure mode. However, the FS_o may peak at 4.3, which defines the overdesigned structure. At the same time, FS_f with a reduction of 37% reaches to 0.75 and peaks at 2 that is a 66% escalation.

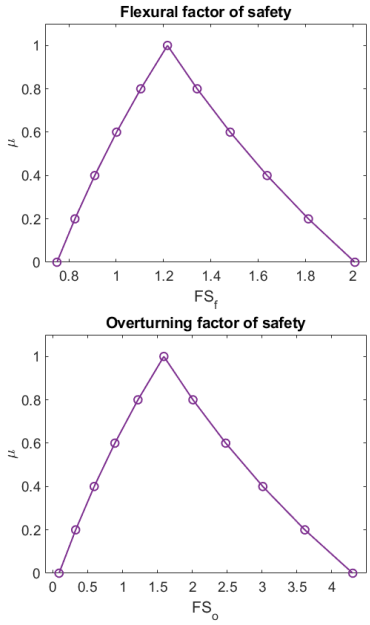

Figure 3. Fuzzy triangular membership function of the safety factors.

5. Conclusion

The presence of uncertainty in the design and construction process of sheet pile walls causes uncertainty in the safety factors of this widely used retaining structure. Therefore, it is necessary to investigate the effects of uncertainty on the stability of the structure. This study, using the fuzzy set theory, investigates the effects of uncertainty on the overturning and flexural safety factors of the sheet pile wall penetrated into the clay. Results indicate that a small variability in the input parameters causes large uncertainty in the safety factors. It can be concluded that ignoring uncertainty may result in an unsafe situation or overdesigned structure.

6. References

[1] Das, B.M., *Principles of foundation engineering*. 2015: Cengage learning.
[2] USACE, *Engineering and Design: DESIGN OF SHEET PILE WALLS*. 1994, U.S. Army Corps of Engineers, Washington, DC.
[3] Zadeh, L.A., *Zadeh, Fuzzy sets.* Inform Control, 1965. 8: p. 338-353.

14th International Conference on Coasts, Ports and Marine Structures
9 & 10 May 2023 , Tehran-IRAN
ICOPMAS 2022

CORROSION DEFECTS INTERACTION IMPACT ON FAILURE PRESSURE OF OFFSHORE PIPELINES

Soheyl Hosseinzadeh[1], Mohammad Reza Bahaari[2,] and Mohsen Abyani[3]

1) School of Civil Engineering, University of Tehran, Tehran, Iran, s_hosseinzadeh@ut.ac.ir
2) School of Civil Engineering, University of Tehran, Tehran, Iran, mbahari@ut.ac.ir
3) School of Civil Engineering, University of Tehran, Tehran, Iran, mohsen.abyani@ut.ac.ir

1. Introduction

An average of 10 percent of the total metal output in the world is estimated to be lost in corrosion. This issue affects the economy of a nation and its assets; In this regard, corrosion is considered one of the most repetitive causes of failure in offshore pipelines.

It is more than clear that failure caused by the impact of multiple defects is more probable to occur than a single defect. In this regard, some interaction rules have been developed for multiple defects, although the interaction of even two or more defects is still not well understood.

This paper aims to investigate the effect of interaction between corrosion defects using numerical modeling. Finite element models of corroded pipelines are defined and validated against existing results, considering different shapes of defects and spacing between them. ABAQUS software has been used to perform numerical models of corroded pipelines and to determine the impact of the interaction between defects aligned in the longitudinal directions.

1. Numerical Modeling

Finite element analysis will investigate the assessment of corroded pipeline failure pressure and the interaction effect amongst corrosion defects. The finite element model is performed by ABAQUS software.

1.1. Failure Criterion

There are various types of failure criteria presented in the literature. However, in the present study, the failure criterion has been chosen in a stress-based manner where the maximum von-mises stress generated in the whole elements of a ligament in pipeline thickness exceeds the material ultimate tensile strength (718.2 Mpa)[1].

1.2. Parameters and Characteristics

A parametric study was performed to study the parameters affecting the pipeline strength. The survey investigated the failure pressure of pipelines for different defects geometry and distances. All pipeline models were created in API 5l X80 steel with an inner radius of 386.4 mm and a 20 mm thickness. The most influential parameters were defined to study the effect of interaction between defects aligned longitudinally on pipeline burst pressure, as shown in Table 1.

Table 1. analyzed parameters

Defect Length	$\frac{d}{t}$	**0.2, 0.4, 0.5, 0.6, 0.8**
Defect Width	$\frac{w}{t}$	**1, 1.5, 2**
Defect Depth	$\frac{l}{t}$	**2, 6, 10, 14, 18**
Longitudinal Spacing	$\frac{S_l}{\sqrt{Dt}}$	**0, 0.5, 1, 2, 3, 3.5, 4**

1.3. Model Characteristics

The finite element model has been created in ABAQUS version 2019. A 3d model was performed to estimate the failure pressure of a pipe damaged by two longitudinally aligned corrosion defects. The characteristics of the model are as below.

1.3.1. Defect Model Geometry

As shown in

Figure *1*, Defects have been modeled in a rectangular shape. However, the corners of the considered rectangular shape are rounded to avoid stress concentration.

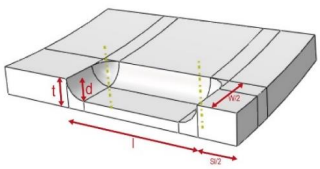

Figure 1. Defect shape

1.3.2. Material Properties

The material used in FEM models is API 5L X80 which has been used in previous studies [2,3]. The material properties are illustrated in

Table 2. The σ_y and σ_u refer to yield and true ultimate stress.

Table 2.material properties

Material	E(GPa)	v	σ_y(MPa)	σ_u(MPa)
API 5L X80	200	0.3	534.1	718.2

1.3.3. Boundary Conditions and Loads

The model represents a quarter model of a pipeline with a half circle section on X-Y surface which has been extruded in the Z direction and is damaged by two longitudinally aligned defects. The edges in length are considered to be avoided to move in the X direction, and the freedom of the faces in pipe start and end point are only available on X-Y surface. The farthest point from the defects has been considered rigid.

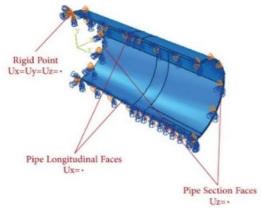

Figure 2. Boundary conditions

The pipeline tolerates internal pressure loads. The internal load starts at 0 MPa and increases until the failure criterion is reached, and the failure pressure will be found there.

1.3.4. Mesh Element

Models are meshed by C3D8R elements in ABAQUS software. A mesh sensitivity analysis has been performed to find the best element size and dimension ratio range. The defect and non-defect zone have been meshed by structure technic, and the transient zone is meshed by sweep technic, which has been illustrated in ***Figure 3*** by the yellow color

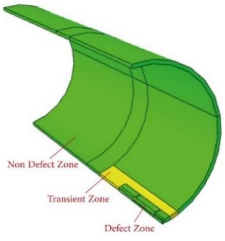

Figure 3. Mesh system

1.4. Verification

to verify the validity of the models, the results have been compared with an experimental test. A burst pressure experimental test for a corroded pipeline with two longitudinal defects has been performed by Benjamin et al. [4], and the present finite element model result has been compared. As illustrated in Table 3, the FEM results satisfy conformity with the experimental test results, and a 4% error is negligible.

Table 3-Results verification

P_f based on an experimental test [4]	P_f based on the current FEM model	Error
20.3 MPa	19.6 MPa	4%

2. FEM model results

According to *Table 1*, 91 FEM models were performed to study the effect of corrosion defects interaction on the burst pressure in various defects geometries. The results are illustrated in Figure 4.

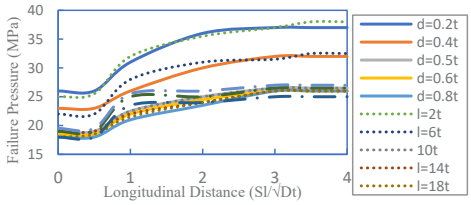

Figure 4. Effect of longitudinal distance on failure pressure

Obviously, the distance between the defects can significantly affect pipeline strength and decrease the burst pressure by up to 30%. Significantly in distances lower than $\sqrt{Dt}$ and it can be concluded from the results that in distances more than$3\sqrt{Dt}$, the interaction of defects can be neglected.

3. Conclusion

In this research, a finite element analysis was performed to study the effect of interaction between corrosion defects that are longitudinally aligned on the pipeline's overall strength against bursting. Therefore, 91 FEM models with various defects geometries were analyzed to find the burst pressure by increasing the internal pressure until the failure. The results illustrate that interaction between defects can decrease the strength of the pipeline up to 30% in the longitudinal distances lower than$\sqrt{DT}$.

4. Reference

[1] N. N. Idris, Z. Mustaffa, and N. N. A. Ismil, "Burst capacity due to corrosion acting at radial orientation of pipeline," *J. Phys. Conf. Ser.*, vol. 1529, no. 3, 2020, doi: 10.1088/1742-6596/1529/3/032086.

[2] E. Q. De Andrade *et al.*, "Finite element modeling of the failure behavior of pipelines containing interacting corrosion defects," *Proc. Int. Conf. Offshore Mech. Arct. Eng. - OMAE*, vol. 2006, 2006, doi: 10.1115/OMAE2006-92600.

[3] W. Z. Xu, C. B. Li, J. Choung, and J. M. Lee, "Corroded pipeline failure analysis using artificial neural network scheme," *Adv. Eng. Softw.*, vol. 112, pp. 255–266, 2017, doi: 10.1016/j.advengsoft.2017.05.006.

[4] A. C. Benjamin, J. L. F. Freire, R. D. Vieira, J. L. C. Diniz, and E. Q. de Andrade, "BURST TESTS ON PIPELINE CONTAINING INTERACTING CORROSION DEFECTS," *24th Int. Conf. Offshore Mech. Arct. Eng. (OMAE 2005)*, vol. 5, no. 1, pp. 781–783, 2005.

14th International Conference on Coasts, Ports and Marine Structures
9 & 10 May 2023 , Tehran-IRAN
ICOPMAS 2022

TWO DEGREES OF FREEDOM VORTEX-INDUCED VIBRATION RESPONSES OF TWO PIGGYBACK PIPELINES AT LOW MASS-DAMPING RATIOS

Adib Amini[1], Ahmadreza Mostafa Gharabaghi[2]

1) Civil Engineering Department, Sahand University of Technology, Tabriz, Iran, ad_amini@sut.ac.ir
2) Civil Engineering Department, Sahand University of Technology, Tabriz, Iran, mgharabaghi@sut.ac.ir

1. Introduction

From offshore to onshore, the pipeline is always the principal method to transport oil, gas, or even freshwater. Secondary pipelines are sometimes located near another one for economic or technical reasons. Two pipelines are either next to each other or stacked one on top of the other in a piggyback arrangement. By situating another body by a cylinder (in this case, a pipeline), the flow around it becomes more complicated than the single cylinder. Vortex-Induced Vibrations (VIVs) might be suppressed when distinctive configurations of the pipelines are arranged in piggyback. VIVs are the motions induced on bodies due to their interaction with external fluid flow leading to the generation of vortices which vibrates the pipeline with the frequency of the vortex shedding and causes fatigue and subsequently damage through the pipeline. There are many studies that have been conducted on a single-cylinder, but there are only a few that investigate the behavior of piggyback pipelines [1-3] or even the vibration in both In-Line (IL) and Cross-Flow (CF) directions [4] due to current.

2. Dimensional Analysis and Experimental Setup

2.1. Dimensional Analysis

There are three types of dimensionless parameters that can be applied in this study; 1) Flow parameters as Reynolds Number (Re=UD/ν), 2) structural parameters as the mass ratio (m^*), which reads as:

$$m^* = \frac{4m}{\pi \rho l (D^2 + d^2)} \quad (1)$$

damping ratio (ξ), which is obtained from the free vibration tests on the cylinders, and the mass-damping ratio (α) as follows:

$$\alpha = (m^* + 1)\xi \quad (2)$$

and 3) the fluid-structure interaction parameter as Reduced Velocity (V_r), which is defined as follows:

$$V_r = \frac{U}{D f_n} \quad (3)$$

where U is the flow velocity, f_n is the natural frequency of the cylinder, m is the mass of the cylinder, ρ and ν are the density, and kinetic viscosity of water, and l is the effective length of the cylinder with diameters of D and d.

2.2. Experimental Setup

In this research, in order to arrange the VIV setup and to study its response to a pair of cylinders in piggyback formation, the water flume at the Hydraulic Laboratory of the Sahand University of Technology is used. It is 10-meter long, 30 centimeters wide, and 50 centimeters in depth which can generate waves and currents up to 0.4 m/s with a maximum water depth of 30 centimeters without any turbulence. The supporting frame and cylinders are made of Plexiglas, which is highly suitable for such investigations. Figure 1 shows the experimental setup arranged for this research inside the flume, which includes the springs that provide 2-DoF for the cylinders. The diameters of the piggyback cylinders (d) are 10, 20 and 30 millimeters respectively, and the diameter of the main cylinder (D) is 30 millimeters.

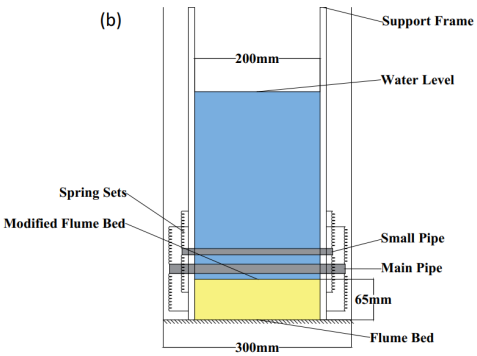

Figure 1. Details of the experimental setup for VIV

The experiments are performed for 6 different reduced velocities in Weak Torsion Regime (WTR). The spacing parameter for the two cylinders is defined as G/D = 0.5, the gap ratio e/D = 0.5 (i.e. the gap between the bottom of the flume and the main cylinder) and also the diameter ratio d/D = 1/3, 2/3 and 1 and the values of the mass-damping ratio is defined in Table 1 in both directions.

Table 1. The values of the Mass-Damping ratio

Mass-Damping parameter	Piggyback pipeline system (the main pipe with D = 0.03 m and the piggyback pipe)			Single-Pipe System
	$d_1 = 0.01$ **m**	$d_2 = 0.02$ **m**	$d_3 = 0.03$ **m**	$D = 0.03$**m**
α_x	**0.188**	**0.181**	**0.172**	**0.183**
α_y	**0.21**	**0.20**	**0.192**	**0.205**

3. Results

Several experiments were performed in the flume in order to evaluate the effect of different parameters on the behavior of the piggyback pipeline system. Figure 2 illustrates the relative IL and CF amplitude of vibration of the main cylinder for different reduced velocities and mass-damping ratios. It seems that as the diameter of the piggyback cylinder reduces, the relative amplitude of IL vibration decreases compared to the single cylinder. This is not the same for CF direction due to the interaction of two cylinders, particularly for the studied amount of gap and spacing ratios. When the A/D (dimensionless amplitude of vibration) reaches 0.15, it is denoted as the onset of the reduced velocity, which means it defines a point where vital vibrations of the pipes start here and can cause damage to the pipelines.

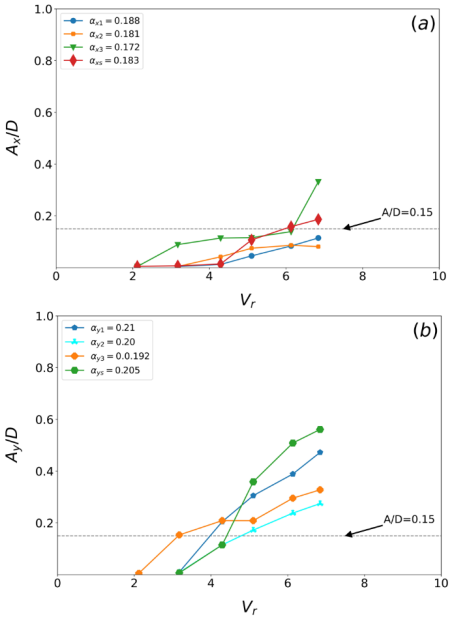

Figure 2. The relative vibration amplitudes for the main pipe in (a) IL direction, (b) CF direction

Figure 3 shows the relative CF vibration frequency of the main cylinder for different relative velocities and mass-damping ratios. The value of IL and CF frequencies of vibration is the same.

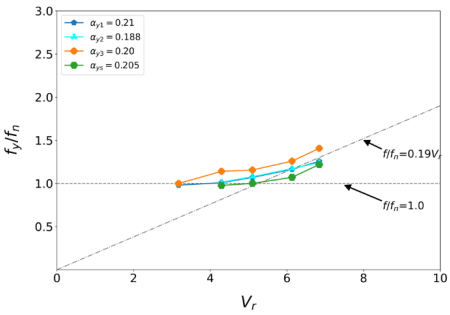

Figure 3. The relative vibration frequency for the main pipe in the CF direction

It is observed that the synchronization or lock-in phenomenon has been influenced by the presence of a piggyback cylinder, especially as its diameter increases to the diameter of the main cylinder. This can also be due to the interaction of two cylinders, particularly for the studied amount of gap and spacing ratios. For higher reduced velocities, the cylinder tends to vibrate in a more regular manner close to the line of Strouhal (i.e. f/f_n=0.19V_r). Both Figure 2 and 3 indicates that as the value of reduced velocity increases up to the initial stage of excitation, the amplitudes and the frequencies of the main pipe increase. The amplitude of vibration in the CF direction is dominant, as it is evident from Figure 2.

4. Conclusions

In this paper, the VIV behavior of two cylinders in a piggyback arrangement is studied, and it is shown that for low mass-damping ratios in the initial excitation regime, the suppression effect of the piggyback cylinder increases as the relative diameter decreases, particularly for IL relative amplitude of vibration comparative to the single cylinder.

5. References

[1] Vedeld, K. and A. Nestegård, Vortex induced vibrations of short side by side cylinders. Marine Structures, 2021. 79: p. 102996.

[2] Zang, Z., F. Gao, and J. Cui. Vortex shedding and vortex-induced vibration of piggyback pipelines in steady currents. in The Twenty-second International Offshore and Polar Engineering Conference. 2012. International Society of Offshore and Polar Engineers.

[3] Zang, Z.-P. and F.-P. Gao, Steady current induced vibration of near-bed piggyback pipelines: Configuration effects on VIV suppression. Applied Ocean Research, 2014. 46(1): p. 62-69.

[4] Jauvtis, N.a. and C. Williamson, The effect of two degrees of freedom on vortex-induced vibration at low mass and damping. Journal of Fluid Mechanics, 2004. 509: p. 23-62.

14th International Conference on Coasts, Ports and Marine Structures
9 & 10 May 2023 , Tehran-IRAN
ICOPMAS 2022

RECENT DEVELOPMENTS IN SURFACE CRACK EXTENSION IN OFFSHORE PIPES

A. Ghannadiasl[1], S. Ghaemifard[2]

1) Department of Civil Engineering, University of Mohaghegh Ardabili, Ardabil, Iran, aghannadiasl@uma.ac.ir
2) Department of Civil Engineering, University of Mohaghegh Ardabili, Ardabil, Iran, s.ghaemifard@uma.ac.ir

1. Introduction

In the offshore industry, metal pipelines are one of the initial systems for transportation and natural gas and oil production because of naivety, cost-effectiveness, and facility of installation that is used widely. Due to various functional and environmental dynamic loads, offshore metal pipelines tend to have fatigue problems [1]. Therefore, cracks happen in these systems due to the loads. Generally, in most cases, surface cracks are semi-elliptical shapes [2, 3]. Also, they may begin from corrosion holes or surface faults at weld toes or, based on material [4], become visible on either the interior or the exterior surface. So, surface crack is a vast hazard and a menace to the structural totality of metal pipes. This paper overviewed the numerical, experimental, and analytical viewpoints due to the surface crack.

2. Review of the Investigation on the Surface Crack Increase in Metal Pipes

In this part, the investigation advance of these scenarios is reviewed from a numerical, analytical, and experimental landscape. Figure 1 shows surface crack growth in various structures.

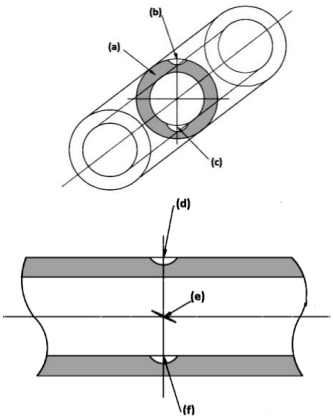

Figure 1. Surface crack growth in various structures: (a) Cross-Section, (b) peripheral external surface cracks, (c) peripheral internal surface cracks, (d) longitudinal external surface cracks, (e) inclined surface cracks, and (f) longitudinal internal surface cracks.

2.1. Experimental Investigation

A dependable and significant method for understanding calibrating, mechanisms, and verifying related analytical and numerical techniques, is experimental research. In Table 1, some experimental research on surface cracked metal pipes under cyclic loads is listed.

2.2. Estimating Surface Crack Growth in Metal Pipes by Analytical Techniques

Although numerical analysis is a cost-effective assessment and precise technique, its usage has been limited. The analytical technique is an effective option. Table 2 lists some analytical methods for surface cracked pipes.

Table 1. The accessible experimental research on a surface crack in metal pipes.

Authors	Scenarios	Detection Method	Material
Zhu et al. [5]	Longitudinal internal and external surface cracks	I	AISI4340H II steel
Yoo and Ando [6]	Peripheral internal surface crack	I	STS370 carbon steel
Singh et al. [7]	Peripheral external surface crack	II	SA333 seamless steel

(I=Beach Mark, II=Alternating Current Potential Difference)

2.3. Estimating surface Crack development in Metal Pipes by numerical Simulation methods

Because of the significant cost of the experimental research, numerical methods have been extensively used to measure the fracture mechanics parameters of surface cracks. Table 3 shows some numerical studies on surface cracked metal pipes under cyclic loads.

Table 2. Analytical techniques to appraise the Stress Intensity Factor of surface cracks in metal pipes.

Method	Authors	Standard
Numerical analysis method	Newman and Raju [8]	BS 7910, DNVGL-RP-F108
	Mechab et al. [9]	---
Weight function method	Anderson [10]	API 579-1/ASME FFS-1
	Fardaghaie et al. [11]	---

3. Conclusion

In this paper, the research on surface crack growth was reviewed from the numerical simulations, experimental research, and analytical assessment viewpoints. It is noticed that some extant challenges could be brief as:

1- Investigation of crack growth near girth welds in metal pipes is a certain subject.

2- Investigation of the effective parameters like the temperature, hydrogen enrichment, and their coupling on the surface crack increase in offshore metal pipes.

3- Research and studied about blended-mode surface crack development in metal pipes from the analytical and experimental points of perspective.

Table 3. The numerical simulations on surface crack growth in metal pipes.

Scenarios	Authors	Simulation Method
Longitudinal internal surface crack	Sharma et al. [12]	XFEM
peripheral external surface crack	Hwang et al. [13]	FEM
peripheral internal surface crack	Sonkar et al. [14]	XFEM

4. References

[1] Li, Z., Jiang, X., and Hopman, H.,"*Numerical analysis on the SIF of internal surface cracks in steel pipes reinforced with CRS subjected to bending.*"Ships and offshore structures. **15**(10): p. 1070-1083.2020

[2] Richard, H.A. and Sander, M., *Fatigue crack growth*. 2016: Springer.

[3] Li, Z., et al.,"*Experimental investigation on FRP-reinforced surface cracked steel plates subjected to cyclic tension.*"Mechanics of Advanced Materials and Structures. **28**(24): p. 2551-2565.2021

[4] Pisarski, H."*Assessment of flaws in pipe girth welds*".in *Welding of high strength Pipeline Steels International Seminar*."2011.

[5] Zhu, L., Tao, X., and Cengdian, L.,"*Fatigue strength and crack propagation life of in-service high pressure tubular reactor under residual stress.*"International journal of pressure vessels and piping. **75**(12): p. 871-877.1998

[6] Yoo, Y. and Ando, K.,"*Circumferential inner fatigue crack growth and penetration behaviour in pipe subjected to a bending moment.*"Fatigue & fracture of engineering materials & structures. **23**(1): p. 1-8.2000

[7] Singh, P., et al.,"*Crack initiation and growth behaviour of circumferentially cracked pipes under cyclic and monotonic loading.*"International journal of pressure vessels and piping. **80**(9): p. 629-640.2003

[8] Newman Jr, J. and Raju, I.,"*An empirical stress-intensity factor equation for the surface crack.*"Engineering fracture mechanics. **15**(1-2): p. 185-192.1981

[9] Mechab, B., et al.,"*Linear and non-linear analyses for semi-elliptical surface cracks in pipes under bending.*"International Journal of Pressure Vessels and Piping. **88**(1): p. 57-63.2011

[10] Anderson, T.L.,"*Developmenr of Stress Intensity Factor Solutions for Surface and Embedded Cracks in API579.*"Welding Research Council Bulletin.2002

[11] Fardaghaie, A., Shahrooi, S., and Shishehsaz, M.,"*A novel correlation to calculate stress intensity factors of the semi-elliptical crack in high-strength carbon steel pipe based on extended isogeometric analysis.*"Journal of the Brazilian Society of Mechanical Sciences and Engineering. **44**(1): p. 50.2022

[12] Sharma, K., et al.,"*Numerical simulation of semi-elliptical axial crack in pipe bend using XFEM.*"2014

[13] Hwang, J.-H., Kim, Y.-J., and Kim, J.-W.,"*Load interaction effect on fatigue crack growth in through-wall cracked pipes under large scale yielding: Experimental and numerical investigation.*"International Journal of Mechanical Sciences. **211**: p. 106761.2021

[14] Sonkar, V., Bhattacharya, S., and Sharma, K.,"*Numerical Simulation of Three Dimensional Fracture Mechanics Problems of Functionally Graded Pipe and Pipe Bend Using XFEM.*"Iranian Journal of Science and Technology, Transactions of Mechanical Engineering.2022

Upheaval Buckling Analysis of Subsea Pipelines Using Analytical Method

Younes Eskandari galeh,[1], Behrouz Asgarian[2]

1) Imam Khomeini Port Authority, Ahwaz, Iran, younes4mb@gmail.com
2) Faculty of Civil Engineering, K.N.Toosi University of Technology ,Tehran, Iran, asgarian@kntu.ac.ir

1. Introduction

Marine pipelines have become a critical means for transporting oil and gas, and their usage has increased over the years due to the growth of offshore industries and operational depths. However, high temperature and pressure levels can lead to buckling in these pipelines. This study addresses the problem of upheaval buckling of marine pipelines by considering the interaction between the pipeline and the soil. An analytical solution for the differential equation of the equilibrium is obtained, and the buckling load of the pipeline is calculated by minimizing the potential energy of the model. The analysis takes into account various factors such as corrosion, temperature gradients along the pipeline, and the separation of the pipe from the soil. The study investigates the effects of seabed softness on upheaval buckling by utilizing different soil properties in the analytical models. Overall, the results provide insight into the behavior of marine pipelines under different conditions and can assist in the design and operation of these critical structures.

2. Upheaval buckling analysis of pipeline using analytical method

In previous studies, the pipeline model on a rigid bed has been widely used as the simplest model for analyzing the upheaval buckling of pipelines. However, the seabed is not rigid and can deform under the weight of the pipeline, leading to a more complex problem. To accurately model the seabed flexibility, the deformed configuration and vertical forces acting on the pipeline are shown in Figure 1.

To simplify the problem, the symmetry of the solution is exploited, and only half of the model is considered for analytical solution. The deformed part of the pipeline is divided into two parts, with one part raised from the seabed and the other part sunk into the seabed. The equilibrium equation for each part is then written separately, taking into account the compatibility of deformations of the two parts. This approach allows for a more accurate analysis of the upheaval buckling problem and takes into account the interaction between the pipeline and the seabed.

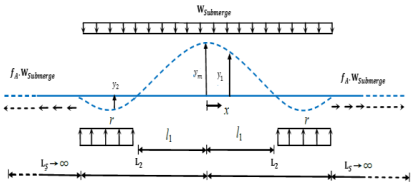

Figure 1. Upheaval buckling of pipeline on soft seabed. **[2]**

The differential equilibrium equations for parts 1 and 2 of the model are based on as follws:

$$0 < x < l_1 \qquad EI\frac{d^4 y_2}{dx^4} + P\frac{d^2 y_2}{dx^2} = -w \qquad (1)$$

$$l_1 < x < l_2 \qquad EI\frac{d^4 y_2}{dx^4} + P\frac{d^2 y_2}{dx^2} = r - w \qquad (2)$$

To analyze the deformation and buckling of the marine pipeline, the differential equilibrium equations for parts 1 and 2 of the model were derived. These equations were based on the principle of virtual work and the assumption of small deformations. The equations take into account the bending, tension, and compression of the pipeline, as well as the resistance from the seabed soil.

The resulting equations are complex and involve multiple variables, including the axial force, bending moment, shear force, and deflection of the pipeline. However, they are necessary for accurately describing the behavior of the pipeline under different loading and soil conditions. Through careful analysis and numerical methods, the equations can be solved to obtain a closed-form solution for the buckling load and deformation of the pipeline.

Overall, the derivation of the differential equilibrium equations is a crucial step in accurately modeling and analyzing the behavior of marine pipelines.

$$0 < x < l_1$$

$$y_1(x) = a_1\cos(mx) + a_2\sin(mx) + a_3 x + a_4 - \frac{r_0 x^2}{2m^2} \qquad (3)$$

$$l_1 < x < l_2$$

$$y_2(x) = a_5\cos(mx) + a_6\sin(mx) + a_7 x + a_8 + k\frac{r_0 x^2}{2m^2} \qquad (4)$$

The matrix coefficients are extracted by using MATLAB program as follows:

$$\begin{bmatrix} a_1 \\ a_4 \\ a_5 \\ a_6 \\ a_7 \\ a_8 \end{bmatrix} \begin{bmatrix} 0 & 0 & -m\sin(ml_2) & -m\cos(ml_2) & 1 & 0 \\ 0 & 0 & \cos(ml_2) & \sin(ml_2) & l_2 & 1 \\ \sin(ml_1) & 0 & -\sin(ml_1) & -\cos(ml_1) & 0 & 0 \\ -m^2\cos(ml_1) & 0 & m^2\cos(ml_1) & -m^2\sin(ml_1) & 0 & 0 \\ -m\sin(ml_1) & 0 & m\sin(ml_1) & -m\cos(ml_1) & 1 & 0 \\ \cos(ml_1) & 1 & -\cos(ml_1) & -\sin(ml_1) & -l_1 & -1 \end{bmatrix} =$$

$$\begin{bmatrix} -k\frac{r_0 l_2}{m^2} \\ -k\frac{r_0 l_2^2}{2m^2} \\ 0 \\ \frac{r_0}{m^2}+k\frac{r_0}{m^2} \\ \frac{r_0 l_1}{m^2}+k\frac{r_0 l_1}{m^2} \\ \frac{r_0 l_1^2}{2m^2}+k\frac{r_0 l_1^2}{2m^2} \end{bmatrix} \quad (5)$$

3. Total potential energy

To determine the buckling load of the system, it is assumed that the displacement shape obtained in the previous section is equivalent to the buckling shape of the subsea pipeline on the seabed [2]. This assumption allows us to use the displacement shape of the pipeline instead of the buckling shape. The potential energy equation of the beam is used to determine the buckling load. The total potential energy is given by:

$$V=\int_0^{l_0}0.5EI[(\frac{d^2y_1}{dx^2})^2+(\frac{d^2y_0}{dx^2})^2-2\frac{d^2y_1}{dx^2}\frac{d^2y_0}{dx^2}]dx+\int_{l_0}^{l_1}0.5EI(\frac{d^2y_1}{dx^2})^2dx+\int_{l_1}^{l_2}0.5EI(\frac{d^2y_1}{dx^2})^2dx$$
$$\int_0^{l_1}wy_1dx-\int_0^{l_0}wy_0dx+\int_{l_1}^{l_2}kwy_2dx-\int_0^{l_1}0.5P(\frac{dy_1}{dx})^2dx+\int_0^{l_0}0.5P(\frac{dy_0}{dx})^2dx-\int_{l_1}^{l_2}0.5P(\frac{dy_2}{dx})^2dx \quad (6)$$

4. verification

The validity of the analytical solution presented in this study has been verified through a comparison with previously published works [2]. The proposed model has been evaluated using various parameters, including the flexibility parameter (k) of the seabed soil, geometrical initial imperfection, a hypothetical force exerted on a section of the pipeline, and the thickness of the coating concrete. Figures 2 and 3 show selected examples of the results obtained from the verification process. The comparison demonstrates that the proposed analytical model provides reliable and accurate predictions for the buckling behavior of the subsea pipeline under a range of conditions. The verification of the model underscores its suitability for use in practical engineering applications.

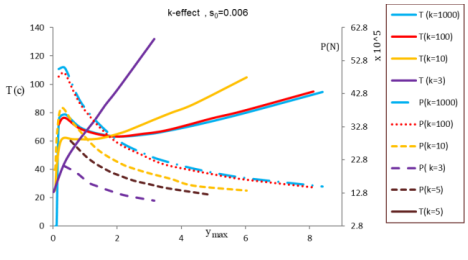

Figure 2. Temperature (T) –Axial Load (P)- Buckle amplitude (y_{max}) for different soil flexibility

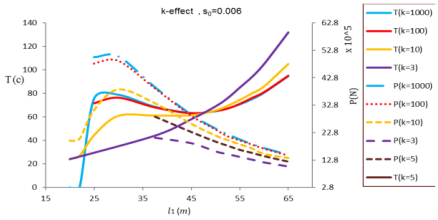

Figure 3. Temperature (T) –Axial Load (P) – Buckling length (l_1) for different soil flexibility

5. Conclusions

This study focuses on the analytical solution of upheaval buckling of marine pipelines on different seabed flexibilities, and the establishment of relationships between buckling force, buckling length, and temperature. The behavior of several different pipe samples with varying specifications was analyzed using MATLAB, and graphs of deformation-temperature, deformation-buckle force, deformation-maximum bending moment, deformation-compressive stress, and deformation-total potential energy were generated.

The analytical equations governing the behavior of the pipelines were extracted for different scenarios, including the effect of imperfect geometry, from which the relationship between temperature, buckling force, and buckling length were determined. The analysis was conducted for both rigid and soft seabeds. It was found that the concrete coating was an effective factor in preventing upheaval buckling of the pipeline, and that it increased the pipeline's resistance to buckling under high initial imperfection values.

The results showed that as the imperfection value increases, the temperature rise and buckling force significantly decrease, while the maximum bending moment increases. It was also noted that the deviation of the analytical solution depended on the imperfection value for the given soil conditions.

Overall, the study presents a comprehensive analysis of upheaval buckling of marine pipelines, considering various factors that affect the behavior of the pipeline. The results provide valuable insights for the design and operation of subsea pipelines, particularly in deep-water environments where the effects of high temperature and pressure can be significant.

6. References

[1] Ruowei. Ruowei Shi, Kuanjun. Wang, Fan.Long, "Upheaval Buckling of Offshore Pipelines with Geometrical Imperfection on Soft Sea bed,", Zhejiang University, Applied EJGE, 2013.

[2] Neil. Taylor and Aik. BenGan, "Submarine pipeline buckling imperfection studies," Applied Thin wall structures vol.295-323, 1986.

14th International Conference on Coasts, Ports and Marine Structures
9 & 10 May 2023 , Tehran-IRAN
ICOPMAS 2022

DETERMINING THE PERFORMANCE POINT OF THE JACKET PLATFORM UNDER HYDRODYNAMIC LOADS

Mehrdad Bakhtiar[1] and Naser Shabakhty[2]

1) Marine Engineer, Iran University of Science & Technology; mehrdadbakhtiar@gmail.com
2) Assistant Professor, Iran University of Science & Technology; shabakhty@iust.ac.ir

1. Introduction

Standards for the design and evaluation of offshore structures consider the ultimate capacity of platforms as a design criterion. This method cannot meet all the needs of designers and operators of offshore platforms. For example, a quarter of the platforms in the path of Hurricane Ivan were severely damaged [1]. Designers of building structures introduced the design method based on performance in order to increase the reliability of the structure and control the amount of building damage due to earthquakes. This method allows designers to change the performance levels defined for the structure according to the type, conditions and degree of risk based on the uses of the building and consider the nonlinear behavior of the structure elements. In this research, using the performance-based design method introduced in building structures, this method has been introduced in offshore structures and how to determine their performance point under the influence of waves.

2. Identification Method

There are three common ways to calculate a performance point:

- Experimental coefficients: This method has been introduced in FEMA356 which predefines coefficients used, the values of which are presented based on experience for different conditions [2].
- Capacity Spectrum: in the displacement spectrum-acceleration spectrum coordinates, the spectral displacement of the performance point of the structure is determined by the ATC40 code [3].
- Method N2: It was proposed in 1980. The initial idea of this method is based on the Q model developed by Saeedi and Sezan [4]. In 1999, this method was formulated based on the acceleration-displacement format by Fajfar this Method [5]. This method is very similar to the capacity spectrum method however; it has higher accuracy. The main difference between these methods is that, in the ATC40 method, the linear demand spectrum is used, but in the N2 method, the nonlinear spectrum. In addition to the nonlinear analysis data of Structural elements is required for nonlinear force-displacement curves.

3. Case Study

Figure 1 shows the SPD19A jacket structure in Phase 19 of South Pars has been studied as a case study because the concepts used are from the studies conducted in normal buildings, where the connection of the structural members is considered rigid and the foundation is placed on a rigid foundation.

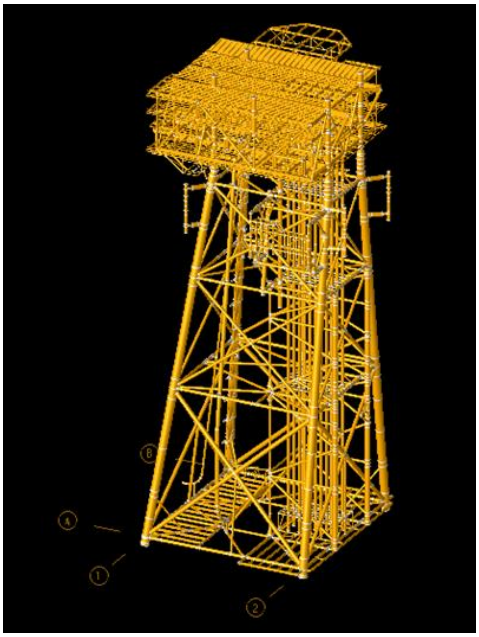

Figure 1. Pushover curve in the southeast direction

The wave height of the project is based on 100-year storm limit conditions. Information about the wave height and its periodicity is provided for the directions studied in Table 1.

Table 1. Wave Height and Period

Direction	Wave height (meters)	Wave period (seconds)
South	11.6	10.8
Southeast	10.8	10.4
Southwest	8.8	9.5

The spectrum used in this study is a JANSWAP spectrum by the wave height and period of the return period of 100 years. The spectrum is divided into 1/8 and used the obtained spectrum; the irregular wave is determined by the indefinite spectral amplitude method. An irregularly generated wave is a combination of 1,200 regular waves.

4. Result

The lateral load pattern is intended for static incremental load analysis depending on the displacement pattern [6]. To convert elastic demand curves to inelastic curves, relations (1) and (2) are used.

$$S_a = \frac{S_{ae}}{R_\mu} \quad (1)$$

$$S_d = \frac{\mu}{R_\mu} S_a = \frac{\mu}{R_\mu} \frac{T^2}{4*\pi^2} S_{ae} = \mu \frac{T^2}{4*\pi^2} S_a \quad (2)$$

The two parameters used in this formula are the reduction coefficient due to ductility Rμ and the ductility coefficient μ, S_{ae} is the spectral elastic acceleration, S_d is the displacement of the target of one degree of freedom structure.

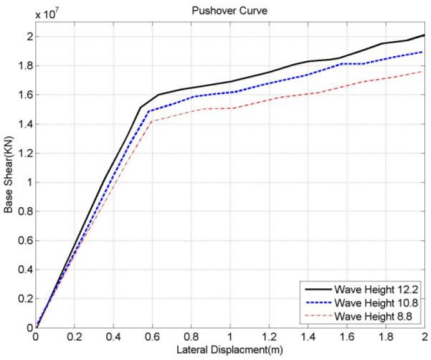

Figure 2. Pushover curve in the south direction.

The capacity curves in the elastic part had the same slope and all three curves yielded at the same displacement limit, while figure 2 shows the base shear at the yield point was slightly different for each wave height. At this point, the structure's capacity curve has changed its slope and the load capacity decreases, but it still has the load capacity. The capacity curves have fluctuations in the plastic region, which can be due to member yielding or hardening due to the redistribution of the input force between the elements due to the formation of plastic joints in the elements. The results showed that the first point of yielding occurred in the vertical braces that were under the effect of compressive force. The reason for the difference in the curves was due to the difference in the loading pattern applied to the structure.

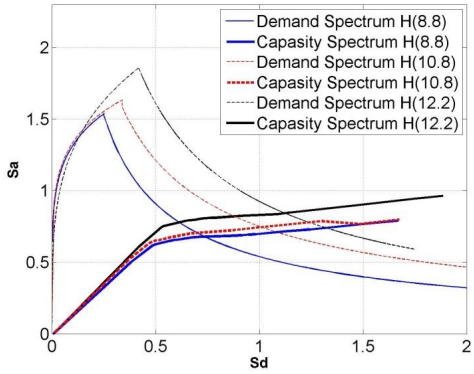

Figure 3. Demand spectrum and capacity spectrum in the south direction

5. Conclusion

The results show that with increasing wave height, the performance points of the structure increase, the intersection of the demand spectrums and the capacity spectrums in figure 3. The value of the demand spectrum for more critical conditions has a higher value, which increases the value of the operating point in the structure. The difference in the values obtained was due to changes in the amount of demand spectrum, and the value of the capacity spectrum for waves with different heights had the same patterns and a relatively equal value.

6. References

[1] API R. 2A-LRFD: API Recommended Practices for Planning, Designing and Constructing Fixed Offshore Platforms–Load and Resistance Factor Design

[2] FEMA P. Commentary for the Seismic Rehabilitation of Buildings, FEMA 356, Federal Emergency Management Agency. Washington, DC. 2000.

[3] Comartin C, Niewiarowski R, Rojahn C. ATC-40 Seismic evaluation and retrofit of concrete buildings. SSC 96. 1996;1.

[4] Saiidi M, Sozen MA. Simple and complex models for nonlinear seismic response of reinforced concrete structures. University of Illinois Engineering Experiment Station. College of Engineering. University of Illinois at Urbana-Champaign.; 1979.

[5] Fajfar P, Krawinkler H, editors. Nonlinear Seismic Analysis and Design of Reinforced Concrete Buildings: Workshop on Nonlinear Seismic Analysis of Reinforced Concrete Buildings Bled, Slovenia, Yugoslavia, 13-16 July 1992. CRC Press; 1992 Mar 20

[6] Asgarian B, Raziei A. Comparison of Incremental Dynamic and Pushover analysis of Jacket Type Offshore Platforms. InInternational Conference on Offshore Mechanics and Arctic Engineering 2007 Jan 1 (Vol. 42673, pp. 575-582).

9 & 10 May 2023 , Tehran-IRAN

MARINE ENVIROMENT

14th International Conference on Coasts, Ports and Marine Structures
9 & 10 May 2023 , Tehran-IRAN
ICOPMAS 2022

SAFETY RISK ASSESSMENT OF WATERWAY USING "WILLIAM FINE" TECHNIQUE AND "SHEL MODEL" (CASE STUDY SHAHID RAJAEE APPROACH CHANNEL)

Sanaz Moradi[1], Ali Moradi[2]

1) Ph.D. student on Sea Structures, University of Azad Research Branch, Tehran, Iran, moradisanaz70@yahoo.com
2) Ph.D., Researcher, Marine Safety Officer, PMO, Tehran, Iran, Ali8ir@yahoo.com

1. Introduction

A ship can face many dangers during navigation in restricted waters e.g., approach channels. These dangers increase as the ship approaches the open sea to the port. While ravaging in limited waters, increasing traffic density, narrowing of the maneuver area, and existing shallow water as the ship approaches the port, are the most important factors in increasing the risk. These factors cause restrictions on ship maneuvers [1]. The fact that ships usually navigate in the port areas causes them to face these dangers frequently. If necessary, precautions are not taken, and marine accidents such as collision, contact, and grounding may occur. These accidents lead to human injuries and loss of life, economic losses, and environmental damages. The difficulties faced by a ship navigating in the port area vary depending on the ship's characteristics, the port's structure, environmental conditions, and the human factor [PIANC][1]. The study, it was aimed to assess the waterway risks using the "William Fine" technique and the "SHEL" model to analyze navigational risks encountered by ships while navigating in the "Shahid Rajaee" (SR) Port Approach Channel.

2. Research Model

The analysis concerns maritime traffic in the S.R Approach channel and will be used following the formula which is the "William Fine" technique.

$$R = P \times E \times C \quad (1)$$

Where: R: is Risk Score, P, is Probability of Occurrence (Ranges; 1-10), E, is the extent of exposure (Ranges: 1-7), C, is Intensity of Consequence (Ranges; 1-10) [2]. In addition, the "SHEL" model will be used to identify waterway risks which consist of 4 components namely; Software, Hardware, Environment, and Liveware. These components are identified and listed in Table 1 for SR Approach Channel [3].

3. Determining Hazards by Experts Review

The designated experts must have maritime experience in terms of maritime safety and the application of risk analysis. Experts that continue their careers in different fields in the maritime industry contribute to making the correct evaluations. Six people possessing the license have joined the studies. These experts have previously worked as oceangoing masters on different types of ships. Two of the experts that took part in the scenarios are pilots in the area, two of them are academicians at the maritime faculty, one of them is a simulator center coordinator at the maritime faculty and one of them is a training coordinator at a maritime firm.

4. The Nature of Risks in Maritime Area

The IMO[2] defines the word risk as "the combination of the frequency and the severity of the consequence." The ISO[3], on the other hand, defines risk as the "combination of the probability of occurrence of harm and the severity of that harm". When we look at the definitions of risk, it is understood that risk has two components. These components are stated as the "probability of occurrence of harm" and the "severity of harm". The word "harm" mentioned in the definitions is used to mean human injury, harm to health, or damage to the environment (ISO, 2018) [4].

5. Identifying SR Approach Channel Risks

To identify the risks in the SR Approach channel literature study as well as experts' reviews carried out. Following risks identified according to the "SHEL Model" mainly Software, Hardware, Environment, and Liveware, Risks are categorized in Table 1.

6. Discussions

Tables 2-1 and 2-2 show the expert reviews in four distinguished aspects according to the "SHEL" model (Actually Table 1 is divided into two Tables to ease the calculations). The Software and Hardware components are included in the Table 2-1, representing S_1 to S_8 for the Software component and H_1 to H_8 for the Hardware component. (see Table 2-1)

[1] . Permanent International Association of Navigation Congress (2014).,

[2]. International Maritime Organization -2013

[3] . International Organization for Standardization -2018

Table 1. Classified Risks in SR - "SHEL" model theory

No	Software (S)	Hardware (H)	Environment (E)	Liveware (L)
1	Port State Control (S_1)	Ship Conditions (H_1)	Navigational Condition (E_1)	Seafarer Training (L_1)
2	Flag State Control (S_2)	Ship Quality (H_2)	Visibility (E_2)	Seafarer Skill (L_2)
3	Pilotage (S_3)	Traffic Condition (H_3)	Wind and Wave (E_3)	Fatigue (L_3)
4	Management (S_3)	Ships draft (H_4)	Pollution (E_4)	Rest Hours (L_4)
5	Safety Policy (S_5)	Configuration (H_5)	Obstructions (E_5)	Psychology (L_5)
6	Effective Information (S_6)	Topography (H_6)	Dust and Fog (E_6)	Physical Fitness (L_6)
7	Hydrography (S_7)	Cargo (H_7)	Shallow Water (E_7)	Ergonomy (L_7)
8	Marine Charts (S_8)	Machinery (H_8)	Tide and Current (E_8)	Competency (L_8)

Table 2-1. Applying the "William Fine" Technique and "SHEL" Model

S	P	E	C	R	ALL	H	P	E	C	R	ALL
S_1	7	2	7	98	A	H_1	9	2	8	144	A
S_2	7	3	6	126	A	H_2	8	2	8	128	A
S_3	9	5	8	360	H	H_3	7	1	7	49	N
S_4	9	2	9	162	A	H_4	8	1	7	56	N
S_5	8	3	8	192	A	H_5	7	2	4	56	N
S_6	9	2	8	216	H	H_6	6	1	7	42	N
S_7	8	1	8	64	N	H_7	6	2	5	60	N
S_8	7	1	9	63	N	H_8	9	1	7	63	N

The Environment and liveware components are included in the Table 2-2, representing E_1 to E_8 for the Environment component and L_1 to L_8 for the Liveware component (see Table 2-2).

Table 2-2. Applying the "William Fine" Technique and "SHEL" Model

E	P	E	C	R	ALL	L	P	E	C	R	ALL
E_1	8	2	7	112	A	L_1	10	3	9	270	H
E_2	6	2	5	60	N	L_2	9	3	9	243	H
E_3	8	2	7	112	A	L_3	8	2	6	96	A
E_4	6	1	6	36	N	L_4	8	2	7	112	A
E_5	8	2	5	80	N	L_5	7	4	7	196	A
E_6	7	2	6	84	N	L_6	8	3	6	144	A
E_7	8	3	6	144	A	L_7	7	1	6	42	N
E_8	7	1	7	49	N	L_8	9	1	8	72	N

In Tables 2-1 and 2-2, P= Probability, E= Extent of explore, C= Intensity of Consequences, R= Risk Score and RL= Risk Level. The acceptable range of risk levels according to the "William Fine" technique is shown in Table 3.

Table 3. "William Fine" estimated risk score

Rank	Measures	Risk Level
200>	Urgent reform is needed to control risk and it needs to stop the under-consideration activity	High
90-199	Emergency conditions or necessary measures must be undertaken as soon as possible	Abnormal
89<	The potential risk factor is under control and consideration	Normal

7. Classified Risks

We identified 32 hazards (in 4 groups) associated with Software (n= 8), Hardware (n= 8), Environment (n= 8) and Liveware (n= 8). The highest rate of risks identified in Software and Liveware components (S_3=360 and S_6=216) To score each item equation (1) is used.

8. Conclusions

According to the results (see Tables 2-1 and 2-2), the most and greatest important risks are existing in the Software component of the "SHEL" model in the SR approach channel. The major risk of the channel is related to pilotage (S_3). Consequently, corrective actions according to Table 3 are required to mitigate the high risks, [5].

9. Result

Risk score for sub-components e.g., S_3 (Pilotage) is 360, S_6 (Provision of Effective Information) is 216, L_1 (Seafarer Training) is 270, and L_2 (Seafarer Skill) is 243 (see Table 3). However, Urgent reform is needed to control risks. Effective and continuous pilot training as well as seafarer training should be maintained by marine administrators and port authorities.

Sub-components e.g., S_1, S_2, S_4 (Software), H_1, H_2 (Hardware), E_1, E_3, E_7 (Environment's) L_3, L_4, L_5, and L_6 (Liveware) are considered abnormal risks. Hence necessary measures must be undertaken as soon as possible to mitigate the risks (see Table 3).

Sub-components e.g., S7, S8 (Software's), H_3, H_4, H_5, H_6, H_7, H_8 (Hardware's), E_2, E_4, E_5, E_6, E_8 (Environment's) L_7 and L_8 (Liveware's) are considered normal. Accordingly, Potential risk factor is under control and consideration (see Table 3).

10. References

[1] Tam, CheeKuang, Richard Bucknall, and Alistair Greig. "Review of collision avoidance and path planning methods for ships in close range encounters." The Journal of Navigation 62.3 (2009): 455-476.

[2] Galvani G, Ehrampoush M H, Ghanaian M T, Dehghani A, Hesami Arani M. Applying Job Hazard Analysis and William Fine Methods on risks Identification and assessment of Jobs in Hot Rolling Steel, Iran. J. Mazandaran. Univ. Med. Sci. 2017; 26 (145): 293-303[in Persian].

[3] Younes S, et al 2015, Conducting Risk assessment by William-Fine method in one of Kermanshah tile factory in 2014, CODEN (USA): JCRSDJ Available at www.jcrs010.com

[4] E Çınar et al. (2021). Evaluation of Ship Manoeuvres in Port by Using Fuzzy Fine Kinney Method. *International Journal of Environment and Geoinformatics (IJEGEO)*,8(4): 537-548, doi. 10.30897/ijegeo.938973

[5] J Montewka et al, (2010), Marine traffic risk modeling – an innovative approach, Proc. IMechE Vol. 225 Part O: J. Risk and Reliability, pp. 307-322, Poland DOI: 10.1177/1748006X11399988

[6] Li, Suyi, Meng, Qiang, Qu, Xiaobo (2012) An Overview of Maritime Waterway Quantitative Risk Assessment Models. published in the National University of Singapore

14th International Conference on Coasts, Ports and Marine Structures
9 & 10 May 2023 , Tehran-IRAN
ICOPMAS 2022

EVALUATION AND RANKING OF FACTORS AFFECTING THE IMPLEMENTATION OF METAVERSE IN THE PORT STATE CONTROL DEPARTMENT OF HORMOZGAN PROVINCE

Vahid Shah Moradi[1]

1) Ship control and Port state expert, Ports and Maritime Organization, Iran, vahid.shahmoradi.pmo@gmail.com

1. Introduction

Computer science innovations play an important role in everyday life because they change and enrich human interactions, communication, and social transactions. From the perspective of end users, three main waves of technological innovation have been recorded around the introduction of personal computers, the Internet, and mobile devices, respectively. Currently, the fourth wave of computational innovation is expanding around spatial and immersive technologies such as virtual reality (VR) and augmented reality (AR) [1]. This wave is expected to form the next pervasive computing paradigm that has the potential to transform (online) education, business, remote work, and entertainment. This is the new paradigm of the metaverse. In other words, the metaverse is a post-reality world, a permanent and stable multi-user environment that merges physical reality with digital virtuality. Regarding online distance education, Metaverse has the potential to overcome the basic limitations of two-dimensional webbased e-learning tools [2]. Metaverse, as a new media, can enable the presence of people in the 3D virtual world through interface tools. Because this technology will provide unique communication possibilities that were not possible for humans before, it can be imagined that the emergence of this media will create tremendous changes in all human relations in societies [3]. Regular breakdown of structure and machinery in ship operations may cause dangerous accidents. These losses can endanger the crew, and passengers inside the ship, pose a threat to the environment and damage the ship itself or the property of a third party. Any of these events may cause business performance instability, reputation, and loss of revenue. In addition, with the introduction and construction of a large number of new ships, it has become more difficult to monitor and inspect them by regulatory bodies and classification institutions to achieve optimal inspection results and eliminate risks due to high risk and classification. Metaverse is looking to rebuild the world, so the shipping industry is also affected by this rebuilding. The maritime transport industry is one of the most important fields of society's economy. Therefore, it requires strict technical and safety control and inspection; Also, due to the vast scope of Metaverse, we lack a clear understanding of how they work, why they are needed, the possibility of implementation in a specic organization, and their capabilities due to their new component. To deal deeply with these problems, we are looking to evaluate and rank the factors affecting the implementation of Metaverse in the port state control department of Hormozgan province.

2. Method

The current research is applied in terms of its purpose and is classified as descriptive-survey research that is based on determining the relationship between variables. Since the present research seeks to evaluate and rank the factors affecting the success of Metaverse implementation, it is descriptive. In this research, a survey method was used to collect data, and because the results of the research can be a guide for the successful implementation of Metaverse in the control department of the port state, especially in Hormozgan province, therefore, based on the purpose, it is classified as applied research. The statistical population of this research is all employees of the technical control and inspection department of ships in Hormozgan province. Using the stratified random sampling method, 30 people were selected as the available sample for the research. After collecting the questionnaires, the data were coded and then entered into Spss25 software. Descriptive and inferential statistics were used to analyze the data.

3. Findings

Figures 1, 2, 3 present the demographic characteristics of the sample. According to the results, 63.3% of people are over 40 years old and 83.3% of people have a master's degree, also 66.7% of them have more than 10 years of service experience.

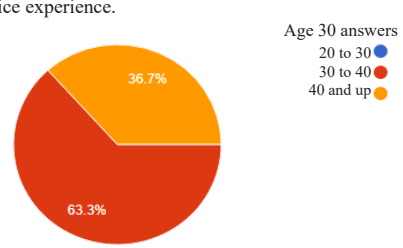

Figure 1. Demographic characteristics based on age

Table 1. The minimum, maximum, average and standard deviation values of factors affecting the implementation of Metaverse in the port state control department of Hormozgan province.

Statistics Variable	standard deviation	Average	Maximum	Minimum
Feasibility of implementation	1.24	3.1	5	1
Social influence	0.83	3.3	5	2
Participation and profit	1.18	2.63	5	1
Maintain security	1.19	3.13	5	1
Impact on the performance of inspectors	1.36	3.16	5	1
Remote vision	1.31	3.3	5	1
Activity at any time and place	1.43	3.23	5	1
Hardware and software limitations	1.32	3.36	5	1
feelings	1.25	3.46	5	1
Various unexpected situations	1.21	2.9	5	1

As in the table above, it can be seen that the average factors affecting the implementation of Metaverse in the port state control department of Hormozgan province are emotions 3.46, hardware and software limitations 3.36, social influence, and remote viewing 3.30. have been. In addition, the impact on inspectors' performance is 3.16, maintaining security is 3.13, and the feasibility of implementation is 3.10. It should be kept in mind that the most important factor from the point of view of the inspectors is the factor of emotions. They stated that emotions can be seen as a factor in the metaverse's entry into the inspection of ships.

As seen in table (4-6), the value of KMO is 0.88, which is above 0.7, and the value of Chi-square (X2) is 222.519. Considering that the significance level of Bartlett's test is less than 0.05 ($P \leq 0.05$), it can be said that the sample size of the present study is sufficient.

Table (3) is related to the ranking of factors affecting the implementation of Metaverse in the port state control department of Hormozgan province based on Friedman's test. Considering that the chi-square value (27.640) with the degree of freedom (9) is significant at the 0.05 level, it can be said that there is a significant difference between the factors affecting the implementation of Metaverse in the port state control department in terms of ranking. Based on the results obtained, according to the inspectors, among the effective factors are hardware and software limitations, feelings, activity at any time and place, remote viewing, social in+uence, impact on inspectors' performance, implementation feasibility, maintaining security, various unexpected situations, and participation and profit have the greatest impact on the success of Metaverse implementation.

4. Discussion and conclusion

The purpose of the current research was to evaluate and rank the factors affecting the implementation of Metaverse in the port state control department of Hormozgan province. The results indicated that there is a significant difference in the ranking of factors affecting the implementation of Metavari in the control and inspection department of ships in Hormozgan province. According to the inspectors, the biggest impact was related to software and hardware limitations. Because so far no research has investigated the factors affecting the implementation of Metaverse in the port state control department, therefore the current research has no background and is presented as new research. Ship safety inspection has many challenges, among them, fatigue and lack of energy, lack of skilled manpower, and waste of time and money can be mentioned. However, the arrival of the Metaverse can diminish these challenges to some extent. However, the entry of Metaverse in the inspection of ships has hardware and software limitations and its entry can only be considered as an emotional factor by the inspectors. Also, Metaverse creates activity at any time and place and remote safety review, but despite the existence of effects on the performance of inspectors, it can be pointed out that there is a lack of work. Of course, Metaverse causes errors in the inspection. It is possible to implement Metaverse in the ship inspection department, however, it requires maintaining safety and software and hardware infrastructure. According to the inspectors, the performance of Metaverse in unexpected situations is weak, and in this way, it is not possible to guarantee the security of the technical inspection and safety. The entry of Metaverse will lead to the creation of participation and profitability in the inspection department. According to what was said, the inspection and safety department of ships must upgrade its technical and technological infrastructure before the arrival of Metaverse. He has also trained special forces to work in Metaverse. They should take necessary measures to maintain security in Metaverse. They should keep in mind that the sudden entry of Metaverse in this sector has challenges that need attention. Among the main limitations of the current research was the lack of sufficient information regarding Metaverse in the shipping industry and other organizations.

5. References

[1] Kamenov, K. Immersive Experience—The 4th Wave in Tech: Learning the Ropes. Available online: https://www.accenture.com/gb-en/blogs/blogs-immersive-experience-wave-learning-ropes (accessed on 21 May 2021).
[2] Mystakidis, S. (2022). Metaverse. *Encyclopedia*, *2*(1), 486-497.
[3] Hemmati, M. (2020). Metaverse, an urban revolution, the impact of Metaverse on Ed Rock, audience from the city, https://civilica.com/doc/1387496

14th International Conference on Coasts, Ports and Marine Structures
9 & 10 May 2023 , Tehran-IRAN
ICOPMAS 2022

REVIEW OF EFFECTS OF AUGMENTED REALITY APPLICATION ON SHIPS TO PREVENT SEA POLLUTION BY SHIPS COLLISIONS

Mohammad Mahdi Rafiee[1]

1) National Iranian Tanker Company (NITC), Tehran, Iran, mehdirafieefff@gmail.com

1. Introduction

Examine a plan to prevent collision between the ships and reduce sea pollution and cost. According to the research conducted and statistics, most collision the ships occurs by fatigue, lacking of knowledge, or the use of the psychotropic substance by the officer of the watch (OOW).

By checking the information 22.1% of maritime accidents are collisions and 6% of its related to tanker ships, 65% of these collisions occur by fatigue 20% lack of knowledge, and 15% by use of psychotropic substances [1]. On January 6, 2018, SANCHI oil tanker accident to a vessel, that ship carried 135,000 tons of oil, about 1 million barrels. This accident caused 20 kilometers from the sea to be sullied.

In 2021 Xinxiang gan researched the development and integration of key technologies of ship radar [2]. This research only uses 2 aspects of the ship's hull, and by connecting the Automatic identification system (AIS) and Electronic chart display and information systems (ECDIS) it brought a two-dimensional view, which is not enough to prevent the collision and inform the OOW. In this system by connecting the Global positioning system (GPS) and RADAR also ECDIS and AIS and one screen take a three-dimensional view. This system can work as an OOW and make Automatic watchkeeping. By use of 4 cameras, this system gives us a 360° view and the AIS information of other ship take and show the accurate position of another vessel.

This system helps the OOW when watchkeeping at night or in foggy weather and reduces collision caused by fatigue or lack of knowledge, preserve the health of the seas, and doesn't let shipping companies have to pay financial damages.

2. Study Area

The Strait of Hormuz is one of the busiest shipping routes, which in recent decades, with the development of ports in neighboring countries, especially oil-rich countries, has caused heavy traffic of ships and oil and gas vessels. The sea of the Persian Gulf is full of various species of fish that provide food for the people of this region and is 93 meters deep.

3. Method

This method is done for the first time. As Shown in Figure 1, 4 watchkeepers who have enough skills are placed in 4 parts of the command bridge of the ship, and the OOW is located in the command bridge with a Walkie-talkie. The watchkeeper informs the officer of the position of the ships in the vicinity by using binoculars, and at night they inform the officer of their position by seeing the navigation lights of other ships. Now the officer knows about all the ships in the vicinity. Then, instead of the watchkeeper, 4 cameras that are able to see at night are also installed, which are connected to the device through the software. AIS all information that includes position, course and the speed of the ship sent through the antenna is installed on two ships that have the ability to send and receive signals, an antenna is connected to the AIS system The electronic signals are sent from and returned from the other ship, and the signal information that includes the ship's position is combined with GPS information, through the software that is similar to head-up in aircraft. As shown in Figure 2, The ship's close point to approach is checked by RADAR, and then if the ship is safe, a green box is placed next to it, and if it is unsafe, the box turns red, and the officer can take the necessary measures to prevent collisions and all maritime regulations will be updated soon and This system is located as a guide to help the officer.

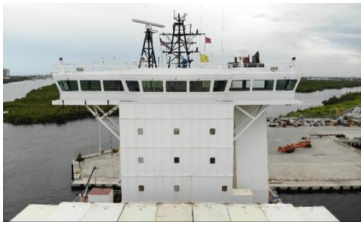

Figure 1. Ship bridge

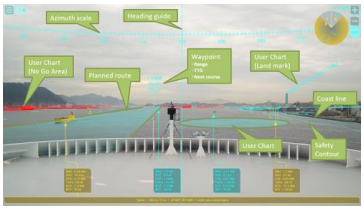

Figure 2. Use of the augmented reality

This device consists of a radio transmitter and receiver system that sends analog information over radio waves and a receiver that receives analog data and displays it digitally. Which sends the waves through the air, however, the information sent is noisy, which may result in loss of information. The system generally says that the network also uses a signal amplifier to keep the signal at distant distances and to send a channel. To send the signal they have been modulated or so-called on the waves of the carrier, respectively, by the sender of this device A flattener is used to separate the frequency, which is made up of two filters that separate the sending and receiving frequencies, or it can be made with a Transmitter The witch combines the communication between the sending and receiving frequencies. The area is then used after a filter remover. Image filtering can be used without direct image correction. The next step is to have an envious amplifier send the signal. The amplifier pushed the waveform to a lower frequency. After filtering out, it was an I / O amplifier and an emulator that gave me a signal that I received signal that I wanted to receive. On the opposite side of my signal, I entered the modulator, which then is a filter and an induction machine emulator and a mixer, and then a filter because a series of frequencies that have been erroneously erased are deleted. Next, the driver boosters the and the other. The other capacitors are used to set the frequency. The transistor that is used to amplify the signal is the resistance of 100 Kilograms and a mega. The next is a diod circuit that transforms the signal we make to digital zero and one and is transmitted by our sender, and on the other, there is the same transmitter and receiver system. The receiver receives the signal and breaks the code and identifies the zero-wake code, which contains all the information about the ship, and the scale It shows us on the monitor screen what side of the code it was sent to us. In fact, this code, like a session, indicates that it has a precise position signal due to its fast download speed. In the vicinity of the ship, the camera. These cameras display the space around the ship and when it receives a one-way signal from the float to the right of the ship, our camera is connected to the transmitter and displays on the monitor three-dimensionally accurate floating point. Through the program Digitally coded computer that separates the signal from the signal code to the code, for example, every code received if the space was close to the floating red, and if it was far away, it would be green if the angle was safe for us, with green and if not red.

4. Result

The conclusions show that during the research, by using this system, we can reduce about 70% to 80% of the collisions between ships that are caused by fatigue or drugs and lack of knowledge in the field of navigation. The research showed that if this system is used on ships, the watch officer has a lot of information about the ships around him, and the AIS system has worked better because it gives the watch officer a 360-degree view, and as a result, he can act quickly to prevent collisions. Research can also reduce collisions by developing this system on gas and oil ships, which greatly reduces pollution in or by this type of ship. At the time the guard was on the bridge of the ship, the ship was in one position. We collided with another ship that was far away and caused the warning system to operate on time with all the maritime laws that were given to it in the form of software and to notify the officer. By testing this method in stormy and foggy weather that he saw. There is a shortage of watchkeeper officers. This system worked well and determined the position of the vessels. By installing this system, the work efficiency of the watchkeeper officer increased and the result showed that pollution of the seas shown in Figure [3] can be prevented to a great extent The AR system helps the watch officer to see all the information needed to steer the ship at once, so there is no need to check multiple devices at the same time. For example, if a ship is going down at an angle of 180 degrees. And if we are moving upwards with a 360 angle and are in the position of collision from the front, the guard officer is informed by the augmented reality program and prevents the collision. so we wish can reduce pollution.

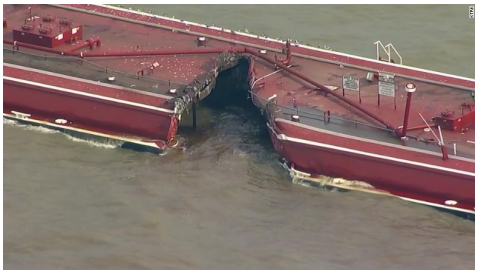

Figure 3. Ship pollution

5. References

[1] CHAI, Tian; WENG, Jinxian; DE-QI, Xiong. Development of a quantitative risk assessment model for ship collisions in fairways. *Safety science*, 2017, 91: 71-83.

[2] Gan, X., Liu, Q., Jin, Y., & Gan, Y. (2022, February). Research on the development and integration of key technologies of ship radar. In *4th International Conference on Informatics Engineering & Information Science (ICIEIS2021)* (Vol. 12161, pp. 260-263). SPIE.

14th International Conference on Coasts, Ports and Marine Structures
9 & 10 May 2023 , Tehran-IRAN
ICOPMAS 2022

AN OVERVIEW OF THE CONCEPT OF E-NAVIGATION: THE KEY TO SAFER MARITIME NAVIGATION

Mohammad Mahdi Gholami[1], Nader Pasandeh[2], Alireza Khoddam[3], Mehdi Rezaei[4]

1) Kanda Maritime Lab, Kanda Idea Co., Tehran, Iran, m.gholami@kandaidea.com
2) GA of Maritime Safety and Marine Environment Protection, PMO, Tehran, Iran, pasandeh@pmo.ir
3) Kanda Maritime Lab, Kanda Idea Co., Tehran, Iran, a.khoddam@kandaidea.com
4) Kanda Maritime Lab, Kanda Idea Co., Tehran, Iran, m.rezaei@kandaidea.com

1. Background

Despite the development and advancement of a variety of technology to facilitate spatial awareness and decision-making in the marine sector, maritime accidents continue to happen [1]. There is an inherent complexity associated with advancement and new technologies, exacerbating a new and unjustified burden on navigators. This burden is one of the factors contributing to increased navigational risk. Furthermore, there is a widespread consensus in the shipping industry that close to 80% of accidents are caused by human error [2]. Due to navigational errors caused by human error, it is likely that the overarching system that ships and land users acquire to navigate and control themselves could fail.

A compelling need has been expressed by the International Maritime Organization in 2006 at the 81st session of the Maritime Safety Committee, as a response to these concerns. Providing modern, proven tools that are optimized for good decision making for shipboard users and those ashore responsible for shipping safety is a key component of maritime navigation and communication. As a result, the overall goal is to improve navigation safety and reduce errors [3]. The future development of marine navigation systems may be hindered if current technological advancements are not coordinated properly, leading to incompatibility between vessels, lack of standardization on board and ashore, as well as an excessive level of complexity on board and ashore [3].

IMO's Secretary General advised that the mariner's role should not be reduced to that of a mere "monitor" and encouraged the Committee to incorporate the Human Element and all its shortcomings into the development of e-navigation [4]. Consequently, e-navigation is designed as a user-driven concept rather than a technology-based solution to ensure safe navigation.

2. E-Navigation Concept

Above-mentioned activities resulted in the development of the e-navigation concept by IMO, which is currently the controller, owner, and governor of the concept. Even so, this organization encouraged all interested parties to participate in the development process of e-navigation taking into account all international stakeholders.

2.1. Definition

E-navigation is defined as follows to meet the needs of present and future users [3]. The definition is clearly stated in [1].

"E-navigation is the harmonized collection, integration, exchange, presentation and analysis of marine information on board and ashore by electronic means to enhance berth to berth navigation and related services for safety and security at sea and protection of the marine environment."

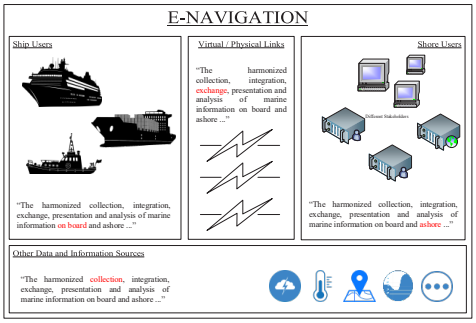

Figure 1. Important Elements in E-navigation

As shown in Figure 1, the definition of e-navigation specifies that it consists of three important elements. The first is the ship system and users, second is shore-based users and systems, and third is a link to facilitate the transfer of data and information between all users.

2.2. Implementation Plan

Implementation of e-navigation requires several important steps. First, the maritime sector's users must be identified. Their needs must be addressed. Secondly, the existing situation must be analyzed to ensure that rapid and realistic implementation occurs. Following the design of the system architecture, a gap analysis is conducted in order to determine which action is required at the moment in order to minimize costs and maximize efficiency. The implementation process follows. In order to summarize each round of implementation circle, the lessons learned

must be studied to make plans for the next round and to ensure maximum productivity. As technology and user needs evolve, e-navigation will evolve as well. As a result, the implementation process is a series of repeated operations, rather than a single-time deployment. Additionally, the issue of expandability must be considered when designing systems and related services.

3. Implementation Impact of E-Navigation

As it is clear from the definition, e-navigation is determined to bring integration and standardization to the navigation in the sea at each level of navigating. This includes the collection, exchange, presentation and analysis of marine information.

To achieve its core objectives, e-navigation utilizes a variety of services. A variety of data sources are utilized to collect data, including AIS, LRIT, weather forecasts, and others. Exchange of data falls under the scope of data transfer services. It is the goal of data transfer services to make sure that communication is seamless with the existing infrastructure as well as to suggest a new one based on emerging technology and user specific needs [5]. The presentation of information falls under the responsibility of gateway services that regulate users' access to information. The analysis of marine information falls under the responsibility of services referred to as added value services. A number of programming and data science capabilities are utilized in order to provide users with insight derived from the application of complex mathematical techniques. All services in e-navigation concept should be harmonized and coordinated in order to enhance navigation from birth to birth, which will ultimately result in an increase in safety and security as well as a better preservation of the marine environment as a whole.

4. Architecture

In order to achieve its promised goal, any technical system must have an explicit or implicit architecture [6]. To the maximum extent possible, the architecture should include all the core elements of marine navigation as well as services designed to facilitate their interaction. The overarching architecture of the e-navigation concept is shown in Figure 2. There is no doubt that communication between the ship and shore navigation teams is at the heart of e-navigation, that a wide range of inputs can be applied to such a system, but that there are two very clear results; safer navigation and improved operational efficiency [7].

As a result of the IMO's encouragement that coordinating bodies build on the aforementioned architecture, IALA developed a shore-based architecture in order to demonstrate the ideal structure of shore-side systems. In [6] all the core elements and set of services previously discussed in chapter 3 are carefully addressed in this detailed architecture, thereby enabling system engineers to develop the architecture locally to address the needs of their users. The presence of e-navigation services at the shore, as indicated in the red portion of Figure 2, makes maintenance and development considerably cheaper and simpler.

5. Conclusion and Future Trends

E-navigation refers to a broad concept that seeks to improve navigation safety, security, and environmental protection through the harmonized collection, integration, exchange, presentation, and analysis of maritime information onboard and ashore.

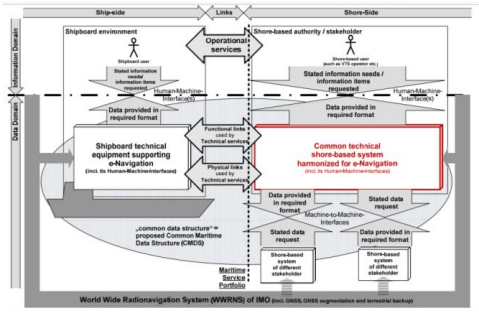

Figure 2. E-navigation overarching architecture [6]

In order to support this objective, it is anticipated that e-navigation will evolve and adapt over a long period of time as information, technologies, political and commercial objectives, and tasks change. In spite of these changes, the need for safe and efficient seaborne transport continues to increase as the maritime industry develops. E-navigation will thus be able to attract even more attention in the coming years.

6. References

[1] A. Weintrit, "e-Nav, Is It Enough?," *TransNav,* vol. 4, no. 10, 2016.

[2] The Nautical Institute , "HE Alert Article," [Online]

[3] IMO, "MSC 85/26/Add.1," [Online].

[4] D. Patraiko, P. Wake, A. Weintrit, "e-Navigation and the Human Element," *TransNav,* vol. 4, no. 1, 2010.

[5] N. K. Sari, "The Maritime Commons: A study on the e-navigation modus operandi," 2017. [Online].

[6] IALA-G1114, "A Technical Specification for the Common Shore-Based System Architecture (CSSA)," 2015. [Online].

[7] International Federation of Shipmasters' Associations (IFSMA), "Introducing the e-navigation Revolution," 2013. [Online].

14th International Conference on Coasts, Ports and Marine Structures
9 & 10 May 2023 , Tehran-IRAN
ICOPMAS 2022

ASSESSING THE SHIPS SEWAGE TREATMENT PLANT EFFLUENT COMPLIANCE WITH MARPOL73/78 CONVENTION

Fardad Fakhr Rahimian[1], Hossein Qahari[2]

1) Port and maritime organization, Bandar imam khomeini, Iran, rahimian.x@gmail.com
2) Port and maritime organization, Nowshahr, Iran, hq.hossein@yahoo.com

1. Introduction

One of the aims of the MARPOL Convention is preventing marine pollution caused by treated or untreated sewage of the ships. To attaining this aim, IMO set several standards in relation to annex IV of MARPOL convention [1] to control and monitor the quality of effluent that are discharging from the ships sewage treatment plants. Indeed, these standards determine some allowance limitations for harmful substances factors of effluents which must be controlled by the ships flag states. In this paper we examined the effluent of 50 different ships in BIK port and compliance of them by convention standard requirements.

2. Standards for Effluent of Ships Sewage Treatment Plant

The MARPOL Annex IV which aims to control pollution caused by discharge of sewage and effluent into the sea from ships, has set standards through the Marine Environment Protection Committee (MEPC) of the International Maritime Organization to standardize the effluent of the sewage treatment plant and has also improved these standards by changing the allowance limitation of these pollution factors, which are mentioned in the table below.

Table 1. Effluent contaminants standards

	Coliform	TSS	BOD	COD
MEPC.2(VI) [2]	200	100	50	-
MEPC.159 (55)[3]	100	35	25	125
MEPC.227 (64)	100	35 Qi/Qe	25 Qi/Qe	125 Qi/Qe

3. Effluent Analysis

This experimental study was conducted to explore effectiveness of the sewage treatment plants installed on board ships by sampling from effluent of the sewage treatment plant of fifty different ships and sending the samples to the laboratory for evaluating the harmful factors. In the following paragraphs, laboratory results and related diagrams are mentioned separately, also, compared to the standards of relative MEPC.

4. Total Coliforms

According to resolution MEPC.2 (VI) the acceptable quantity of thermotolerant coliforms is 250 mpn/100 ml, and this factor was decreased to 100 mpn/100 ml in resolution MEPC.159 (55). By measuring the quantity of thermotolerant coliforms in 50 samples, it was realized that 14 samples were out of allowance range in comparison to MEPC.2 (VI).

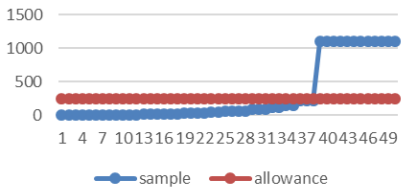

Figure 1. Samples coliform rate

5. Total Suspended Solids

The second crucial factor of effluents that was evaluated by the laboratory was TSS. According to MEPC.2 (VI) the acceptable quantity of this factor is 100 but, as per laboratory results which is shown in figure 2 only 4 samples complied with standard requirement.

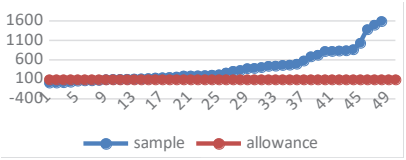

Figure 2. Samples TSS rate

6. Biochemical Oxygen Demand (BOD)

The third important examined factor was BOD that as shown in figure 3. Only 2 of the 50 samples complied with allowance limitation that is 25 and other 48 samples were out of the standard range, which points ineffectiveness of sewage treatment plants for reducing the BOD of effluents.

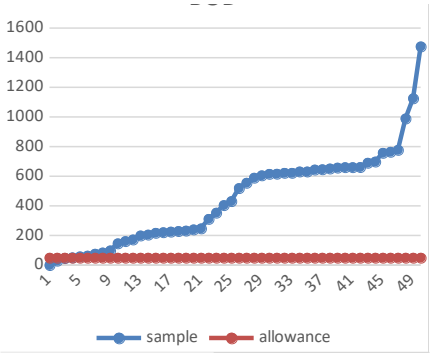

Figure 3. Samples BOD rates

7. Chemical Oxygen Demand (COD)

And finally the last important measured factor was COD that as per MEPC.159 (55) must be less than 125 but as shown in figure 4 by measuring the quantity of COD of all samples, it was determined that only three samples complied with resolution requirements, and others were far out of range.

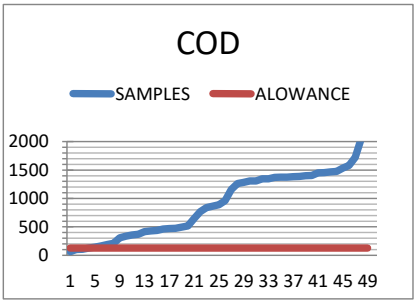

Figure 4. Samples COD rates

8. Results and suggestions

Based on this investigation on the performance of sewage treatment plants, the following items were identified as major causes of system malfunctioning:

1. Insufficient performance of periodical maintenance of system by the crew, because it is an unpleasant job;
2. Lack of familiarity of crew with the system;
3. Ineffectiveness of approval procedure requirements in the long run, because classification societies are merely required to test the system before its installation on board ships;
4. Absence of measuring equipment on effluent discharging pipe.

In order to address above elaborated issues, the following solutions can be taken into consideration:

.1 Since classification societies, renew the certificate every 5 years without testing the effluent, it is recommended that analysis of the effluent sample becomes compulsory on every annual survey.

.2 because of vitality of aeration system of the sewage treatment plant, it is recommended to set visual and audible alarms for malfunctioning of the aeration system to instigate awareness of engine crew.

.3 Whereas turbidity of effluent is an important factor for discovering system malfunction, it is recommended that a transparent tube be provided at the discharging pipe of the system, enabling the crew to monitor the performance of the treatment plant.

4 since disinfection materials, such as tablets and solutions, are used in sewage treatment plants for disinfecting the effluent, it is recommended to provide visual and audible alarms for these materials containers when they are empty and need to be recharged for awareness of the crew.

.5 It is further recommended to provide a sewage treatment logbook for the engine crew to fill out the routine maintenances, charging of disinfection materials, and their observation about turbidity of effluent, discharging quantity and position and other important issues.

9. References

[1] MARPOL consolidated edition 2020 – First published 1991 by the INTERNATIONAL MARITIME ORGANIZATION – 4Albert Embankment, London SE1 7SR.

[2] MEPC. 2(VI) Recommendation on international effluent standards and guidelines for performance tests for sewage treatment plants. Resolution adopted on 3 December 1976

[3] MEPC 159(55) Revised guidelines on implementation of effluent standards and performance tests for sewage treatment plants, Adopted on 13 October 2006 - entry into force 01.01.2010

14th International Conference on Coasts, Ports and Marine Structures
9 & 10 May 2023 , Tehran-IRAN
ICOPMAS 2022

SELF-PURIFICATION CAPACITY OF CHABAHAR BAY SUBJECT TO DESALINATION PLANTS DISCHARGE

Meisam Ebrahimi[1], Ahmad Shanehsazzadeh[2] and Reza Parsa[3]

1) Department of Civil Engineering, University of Isfahan, Isfahan, Iran, meisamebrahimi_88@yahoo.com
2) Corresponding author, Department of Civil Engineering, University of Isfahan, Isfahan, Iran, a.shanehsazzadeh@eng.ui.ac.ir
3) Sazeh Pardazi Consulting Engineers, reparsa@gmail.com

1. Introduction

In arid area, due to the scarcity of fresh water resources, human beings have turned to use other available water sources, including desalination of seawater [1]. Iran with long coastline in the north and south has a great capacity for the construction of desalination plants to produce fresh water for industrial, agricultural and drinking purposes. The sewage of desalination process is toxic brine and/or high temperature effluents which can destroy coastal and marine ecosystems. Therefore, it is important to understand and monitor the impact of the rapidly growing number of desalination plants on the environment. The study of effluent dispersion and accurate determination of salinity concentration in the ambient water is of particular importance [2].

Chabahar Bay located at the North West of Gulf of Oman (Fig. 1) with high coastline population concentration has a strategic contribution in the regional economy development. Some desalination plants are operating now and construction of many are under study. Study on the self-purification capacity of Chabahar bay to eliminate desalination brine discharge effects on the marine environment is essential for site selection and capacity identification of new desalination plants.

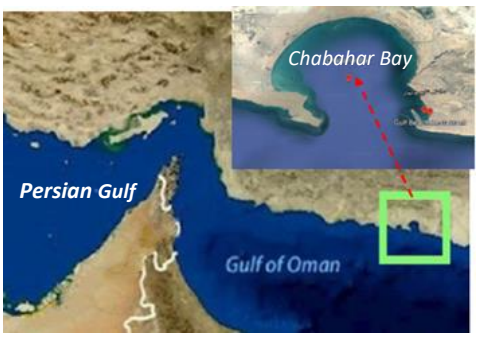

Figure 1. Chabahar bay at Gulf of Oman

In this study, by coupling CORMIX and MIKE3D software, the near and far fields dispersion of the brine plume in the marine environment of Chabahar bay is simulated in numerical manner. Near-field dilutions are simulated using a buoyant jet model incorporated in CORMIX, whereas far-field dilutions are estimated using a three-dimensional numerical model of MIKE3D. The models proved that realistically predict the distribution of the effluent plume in marine environment [3]. The outlet flow velocity which intensified by diffusers and tidal current are two agents for the saline plume diffusion and dispersion. The outfall of Konarak desalination plant is firstly assessed from the perspective of compliance with the environmental regulations. The method of improving the existing conditions by transferring the discharge to deeper water far from the coast is introduced. Then, by increasing the effluent discharge in the deep parts of the bay and adding more outlets, the amount of self-purification capacity of Chabahar bay in term of brine discharge of the desalination plants is investigated.

2. Dispersion of Konarak Desalination Plant Outfall

The numerical simulation of the current situation of Konarak desalination plant outfall discharge, which is directly released at the coastline, indicates that the environmental standards of Iran, in which the salinity at the radius of 200 meters from the source is limited to maximum 10% increase more than the ambient water, is not met. The plum is accumulated in the coast with the potential of serious damage to the coastal ecosystem. The results show that by draining the discharge by pipe 300 m far from the coastline at the depth of 1.3 meters (according to MSL), the environmental standards are met.

3. Self-purification Capacity of Chabahar Bay

The Chabahar Gulf self-purification capacity under the effect of a point source has also been investigated to evaluate total possible saline effluent volume discharge in the bay. The simulation results in different conditions of outlet flow and discharge depth indicate that the maximum tolerable point source discharge in the bay is 3 cubic meters per second, which is environmentally safe at a

distance of 1300 meters from the coastline corresponding to 4.2 meters depth of water (Fig. 2). Increasing the flow or decreasing the depth will increase the salinity more than the standard criterion.

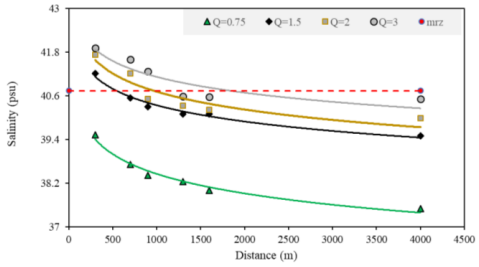

Figure 2. The salinity (in psu) at 200m distance from the outfall point for a number of discharges (Q) and for different outlet distance from the coastline. The standard limit is shown in the figure (red dashed line)

To determine the bay self-purification capacity, the number of outlets was increased so that the effects of the effluents on each other do not cause an unauthorized increase in salinity. The results show that 11 outlets with a distance of 800 meters along with an output discharge of 3 cubic meters per second and a total of 33 cubic meters per second is the maximum capacity of Chabahar bay. The examples of the brine flume dispersion for 11 outfalls with 3 cubic meters per second discharge is presented in Fig. 3, where the densities at two tidal times are compared. As evident in the figure, the plume distributes in the central bay area and does not touch the coastline which is acceptable.

4. Conclusion

Site selection for release of industrial effluents is of prime concern for maintaining the quality of the marine environment. In this study, the suitable location for brine discharge is suggested and the self-purification capacity of the Chabahar bay at Gulf of Oman subject to fast development of desalination plants is assessed. Near-field dilutions are simulated by CORMIX software, whereas far-field dilutions are estimated using MIKE3D software.

The simulation of the current situation of the Konark desalination plant saline water discharge indicates that the Iranian environmental criteria are not met. By moving the outfall 300 meters offshore at a depth of 1.3 meters, the criteria are met.

By carrying out different scenarios, it is determined that the distance of 1300 meters at the depth of 4.2 meters is the most optimal place for discharging the maximum flow rate of 3 cubic meters per second.

11 outlets with a discharge of 3 cubic meters per second with a total discharge of 33 cubic meters per second is feasible maximum capacity of Chabahar bay to ensure the quality of the marine environment.

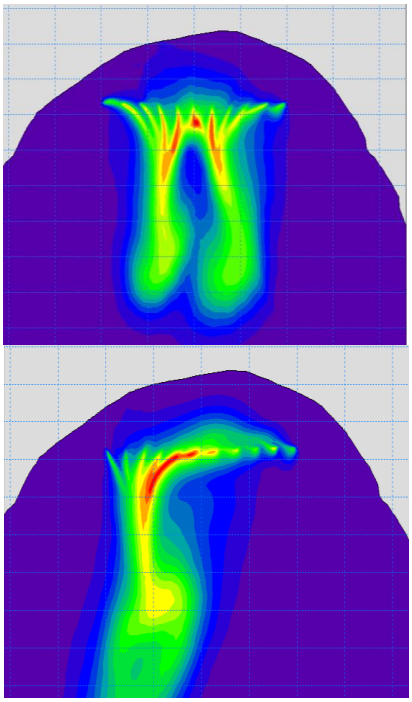

Figure 3. The saline plume distribution at two tidal times subject to 11 outfall discharges.

5. References

[1] Shiklomanov, I.A., World freshwater resources. Water in crisis: a guide to the world's fresh water resources. Clim. Change, 1993. 45: p. 379-382.
[2] Roberts, D.A., E.L. Johnston, and N.A. Knott, Impacts of desalination plant discharges on the marine environment: A critical review of published studies. Water research, 2010. 44(18): p. 5117-5128.
[3] Mohammadian, A., H. Kheirkhah Gildeh, and I. Nistor, CFD modeling of effluent discharges: a review of past numerical studies. Water, 2020. 12(3): p. 856.

14th International Conference on Coasts, Ports and Marine Structures
9 & 10 May 2023 , Tehran-IRAN
ICOPMAS 2022

POLYCYCLIC AROMATIC HYDROCARBONS POLLUTION AND SOURCE IDENTIFICATION IN SURFACE SEDIMENTS OF ANZALI PORT

Ali Azimi[1], Alireza Riahi Bakhtiari[2], Roma Tauler[3]

1) Ports and Maritime Organization, Tehran, Iran, aazimi@pmo.ir
2) Tarbiat Modares University, Noor, Iran, riahi@modares.ac.ir
3) Institute of Environmental Assessment and Water Research, Spanish Council for Scientific Research (CSIC), Barcelona, Spain, roma.tauler@idaea.csic.es

1. Introduction

The entry of petroleum compounds into marine ecosystems in various ways has endangered these ecosystems. Polycyclic Aromatic Hydrocarbons (PAHs) are among the most toxic compounds in the oil, which are of considerable importance in terms of threat to human health and the environment due to their carcinogenic and mutagenic properties [1].

2. Result and Discution

In this study, the concentration of PAHs in surface sediments of rivers and Anzali ports was measured in 24 stations. The highest concentrations of total PAHs were obtained in the surface sediments of R24 with the amount of 22230.49 ± 7987.75 ng.g^{-1} and R23 with the amount of 21442.45 ± 6279.32 ng.g^{-1} and the lowest concentrations were obtained in the station R4 with 5473.14 ± 1930.54 ng.g^{-1} and R3 with 7877.35 ± 3255.21 ng.g^{-1}. Due to the enclosure of the port by the breakwater and the approximate stillness of the water, which leads to severe deposition of contaminants in the bed sediments, and on the other hand, due to the entry of petroleum products through fuel and oil seepage of vessels and ships in the port area, higher concentrations of PAH compounds in these stations can be expected. Also, stations that receive high amounts of PAHs from central areas of the city that receive street dust and urban runoff, such as stations R11, R12, R15, R16, R17, R18, and R19 showed higher concentrations of PAH compounds compared to the stations located in the suburbs city and far from the port such as stations R4, R3, and R2 (Figure 1 & 2).

The total concentration range of PAHs in the sediments of China's Thai-Majia River was reported 311.69 to 3736.32 ng.g^{-1} by Liu et al. (2012) [2]. In the surface sediments of Zhoushan Archipelago and Xiangshan Port in the East China Sea, which is an important port in terms of trade, tourism, fishing and marine breeding the total concentration of 16 PAHs measured as 3.67 – 31.30 ng.g^{-1} with mean 15.01 ± 1.21 ng.g^{-1} in Zhoushan surface sediments and 11.58 - 481.441 ng.g^{-1} with mean 62.52 ± 32.85 ng.g^{-1} in Xiangshan Port [3]. They reported the origin of PAH compounds in the port and common sources from vehicle emissions and petroleum resources. The total concentrations of PAH compounds in the sediments of the Brahmaputra River in Guwahati, India during the two separate pre-Manson and post-Manson seasons, reported between 609 - 8620 ng.g^{-1} and 338 – 23.100 ng.g^{-1}, respectively [4]. The concentration range of polycyclic aromatic hydrocarbons in the surface sediments of the port of Olbia (northern Sardinia, Italy), was reported as 160 – 770 ng.g^{-1} [5]. The range of total concentration of PAHs in the sediments of the main water bodies of Curitiba urban area of Brazil was 131 – 1713 ng.g^{-1} [6]. PAH concentration in the surface sediments of Brazil's São Sebastião Canal (SSC), Brazil's largest offshore oil terminal, was reported in the range below than detection limit of 370 ng.g^{-1} [7].

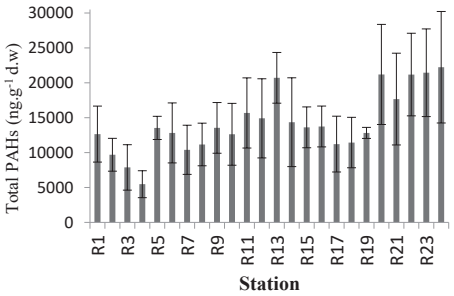

Figure1. Comparison of total concentrations of PAH compounds in surface sediments of Anzali rivers

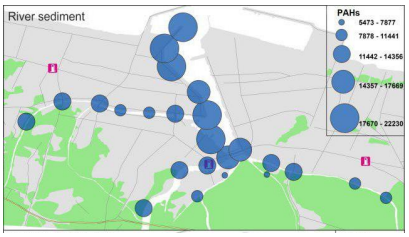

Figure2. Spatial distribution of the total concentration of PAH compounds in surface sediments (larger circles indicate higher concentrations of PAH compounds)

3. The pattern of PAH Compounds in Surface Sediments of Rivers and Anzali Port

In all studied stations, PAH compounds with lower molecular weight were predominant. So that the compounds with 2 and 3 rings in the surface sediments of the studied stations accounted for 83% and heavier compounds were 15% of the total PAH compounds (Figure 3). Compounds with simple structure or low molecular weight, including Phe, Flu, Pyr, Nap, and some of their methyl derivatives, are the main constituents of municipal and industrial wastewater [6]. Therefore, the entry of various wastewater into Anzali rivers along their route is one of the reasons for the predominance of these compounds in the sediments of riverbeds. Fuel and oil leaks from vessels, including numerous ships and launches in the port of Anzali, as well as boats that sail in rivers, are another important source of petrogenic compounds in the sediments of this region. 4-ring compounds with 7% and also 5-ring and 6-ring compounds with 8% had the lowest contribution of PAH compounds in the samples of river sediments (Figure 3).

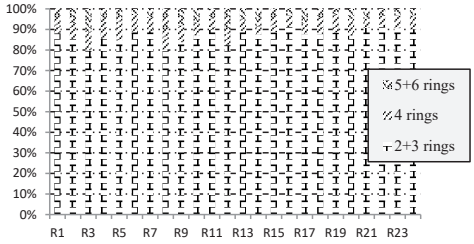

Figure3. Comparison of pattern of PAH compounds based on the number of aromatic rings in surface sediments of rivers and Anzali port

In the study on PAH compounds in the surface sediments of the Haihe River in Tianjin, China was observed that PAH compounds were predominant in 2 to 4 rings [8]. The contribution of 2-ring, 3-ring, 4-ring, 5-ring, and 6-ring PAH compounds in the sediments of the Thai-Majia River bed of China was 30.19%, 28.48%, 20.22%, 14.73%, and 6.38% of the total PAH compounds, respectively [9].

4. References

[1] Cocchieri, R.A., Arnese, A., Minicucci, A.M., 1990. Polycyclic Aromatic Hydrocarbons in Marine Organisms from Italian Central Mediterranean Coasts. Marine Pollution Bulletin, 21: 15-26.

[2] Liu, Y., Yu, N., Li, Z., Wei, Y., Ma, L., Zhao, J.F., 2012. Sedimentary record of PAHs in the Liangtan River and its relation to socio-economic development of Chongqing, Southwest China. *Chemosphere*, 89: 893-899.

[3] Wang, X., Xu, H., Zhou, Y., Wu, Ch., Kanchanopas-Barnette, P., 2015. Distribution and source apportionment of polycyclic aromatic hydrocarbons in surface sediments from Zhoushan Archipelago and Xiangshan Harbor, East China Sea. *Marine Pollution Bulletin*, 22: 243-254.

[4] Hussain, K., Balachandran, S., Hoque, R.R., 2015. Sources of polycyclic aromatic hydrocarbons in sediments of the Bharalu River, a tributary of the River Brahmaputra in Guwahati, India. *Ecotoxicology and Environmental Safety*, 122: 61-67.

[5] De Luca, G., Furesi, A., Micera, G., Panzanelli, A., Piu, P. C., Pilo, M. I., Spano, N., Sanna, G., and Sanna, G., 2005. Nature, distribution and origin of polycyclic aromatic hydrocarbons (PAHs) in the sediments of Olbia harbor (Northern Sardinia, Italy). *Marine pollution bulletin*, 50: 1223-1232.

[6] Leite, N.F., Peralta Zamora, P., Grassi, M.T., 2011. Distribution and origin of polycyclic aromatic hydrocarbons in surface sediments from an urban river basin at the Metropolitan Region of Curitiba, Brazil. *Journal of Environmental Sciences*, 23: 904-911.

[7] Silva, A.M.D., Bicego, M.C., 2010. Polycyclic aromatic hydrocarbons and petroleum biomarkers in So Sebastio Channel, Brazil: Assessment of petroleum contamination. *Marine Environmental Research*, 69: 277–286.

[8] Bin, J., Hai-long, Z., Guo-qiang, H., Hui D., Xin-gang, L., Hong-tu, S., Rui., L., 2007. Characterization and distribution of polycyclic aromatic hydrocarbon in sediments of Haihe River, Tianjin, China. *Journal of Environmental Sciences,* 19: 306–311.

[9] Liu, Y., Yu, N., Li, Z., Wei, Y., Ma, L., Zhao, J.F., 2012. Sedimentary record of PAHs in the Liangtan River and its relation to socio-economic development of Chongqing, Southwest China. *Chemosphere*, 89: 893-899.

MODELING IN 8 MODES FOR THE SALINITY DISTRIBUTION OF CHESHMEH KILEH RIVER AT THE ENTRANCE TO THE CASPIAN SEA

Mohsen Mohammadagha[1], Nasser Hadjizadeh Zaker[2],

1) University of Tehran, Tehran, Iran, mohammadagha@ut.ac.ir
2) University of Tehran, Tehran, Iran, nhzaker@ut.ac.ir

1. Introduction

Rivers create critical conditions on shores by enclosing all materials and pollutants and transporting them to the sea or ocean. For their fact, rivers rely on constant input as well as continuous output. [1] River-borne materials are carried by rivers plume from the land to the ocean. Its dispersal largely determines the fate of these materials and greatly influences. The coastal ecosystem and ocean circulation determine by scattering the fate of those elements and have great impacts. River discharge, waves, earth's rotation, winds, and including internal processes, are several factors that influence river plume dispersion, such as frontal dynamics, geostrophic conduct, and stratified-shear mixing. [2] In the same context, the Cheshmeh Kileh River is composed of two main tributaries called Do-Hezar and Se-Hezar, which originate from the high heights of Takht-e-Soliman, Alamut, and Khoshchal. Se-Hezar river is one of the large rivers with water, which after crossing with the Do-Hezar and Velmroud rivers, creates the Cheshmeh Kileh river, after passing Tonekabon city, it enters the Caspian Sea.

2. Material and Methods

In this research, numerical modeling has been used to show the salinity dispersion distance in the river column. This research has been applied the MIKE 3 Flow Model FM. This model was produced by the Danish Hydraulic Institute [3] for water modeling at three-dimension. The Mike 3 Flow Model software is widely used by researchers, being generally and scientifically had been confirmed in the world [4].

Figure 1. Location of Cheshmeh-Kileh River, coordinates of 36.822N and longitude 50.885E

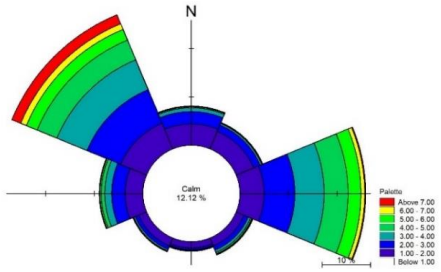

Figure 2. The wind rose plot, drawn by Mike software according to the data received from the Ports and Maritime Organization in transverse coordinates of 36.9N and longitude 50.9E (01/01/1983 to 01/10/2014)

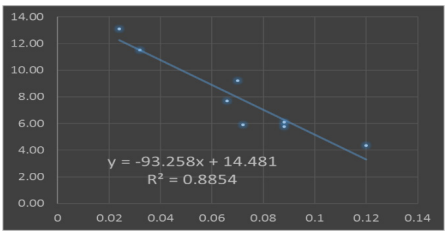

Figure 3. The total length of the KM Salinity expansion relative to the M / S flow velocity

3. Model Calibration

First, the data on water level, which was measured by the Ports and Maritime Organization, and compared with the results of modeling in the same period.

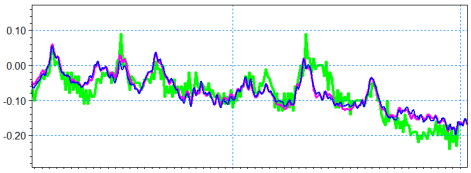

Figure 4. Water level verification chart; green color: field measurement, blue color: modeling with Mike software

4. Simulations Setup

In the early stages of mesh designing, depthometry data from the Iran National Cartographic Center in 2018, and the Global Site GEPCO with a precision of 30 seconds (GEPCO, 2018) were obtained. Then, the accuracy of the optimal mesh results was reviewed. The length of the sides of the mesh network on the coast of Tonekabon is 100 meters. The modeling time was performed from 12:00 AM on 01/01/2019 at 21060-time steps of 60-second. The range of that was between 36 and 47.5 degrees' north latitude and 46 to 55 degrees' east longitude.

5. Results

The results are described in order to investigate the amount of distribution of the salinity changes were obtained from the results of the hydrodynamic model. The salinity of the Caspian Sea is 12.3 PSU and the salinity of the Cheshmeh Kileh's river Tonekabon is 0.1 PSU [5]. The wind is one of the most important factors influencing marine currents, which is effective in the distribution of plumes. the results showed that the maximum salinity distribution length was 13.1 km, at a speed of 0.5 meters per second and at an angle of 45 degrees which has occurred in scenario number 1.

Table 1. Salinity plume distribution (Scenario 1~4)

Salinity plume distribution	Coordinate range			
	0° to 90°		90° to 180°	
Scenario number	1	2	3	4
Wind diagram orientation °	45°		135°	
Wind speed M / S (Minimum & average 30years)	0.5	2.5	0.5	2.5
Water flow average 50 years M^3 / S	14			
Water flow rate M / S	0.024	0.032	0.088	0.12
Total length of Salinity extension (Km)	13.10	11.50	6.10	4.35
The total area of Salinity extension (Km^2)	13.40	10.35	6.53	2.09

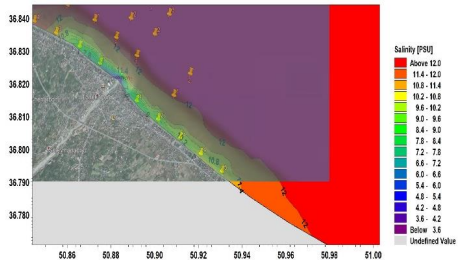

Figure 5. Maximum salinity distribution of 13.1 km, according to Scenario 1, at 36.822 degrees north and 50.885 east

Table 2- Salinity plume distribution (Scenario 5~8)

Salinity plume distribution	Coordinate range			
	180° to 270°		270° to 360°	
Scenario number	5	6	7	8
Wind diagram orientation °	225°		315°	
Wind speed M / S (Minimum and average 30years)	0.5	2.5	0.5	2.5
Water flow average 50 years M^3 / S	14			
Water flow rate M / S	0.072	0.088	0.066	0.07
Total length of Salinity extension (Km)	5.90	5.77	7.70	9.20
The total area of Salinity extension (Km^2)	4.44	3.52	5.56	4.97

6. References

[1] H. Sioli, "Tropical Rivers as Expressions of their Terrestrial Environmens," *Tropical Ecological Systems/ Trends in Terrestrial and Aquatic Research,* pp. 275-288, 1975.

[2] A. R. Horner-Devine, R. D. Hetland and D. G. MacDonald, "Mixing and Transport in Coastal River Plumes," *Annual Review of Fluid Mechanics,* vol. 47, pp. 569-594, 2015.

[3] DHI, MIKE 21 & MIKE 3 FLOW MODEL FM, user guide and scientific documentation of Hydrodynamic and Transport Module, Danish Hydraulic Institute, 2012, pp. 1-52.

[4] A. Payandeh, N. H. Zaker and M. H. Niksokhan, "Numerical modeling of pollutant load accumulation in the Musa estuary, Persian Gulf," vol. 73, p. 185–196, 2015.

[5] A. R. Karbassi, S. S. Bassam and M. Ardestani, "Flocculation of Cu, Mn, Ni, Pb, and Zn during Estuarine Mixing (Caspian Sea)," *International Journal of Environmental Research,* vol. 7, no. 4, pp. 917-924, Autumn 2013.

14th International Conference on Coasts, Ports and Marine Structures
9 & 10 May 2023 , Tehran-IRAN
ICOPMAS 2022

AN OVERVIEW OF CARBON FOOTPRINT IN MARITIME PORTS, CHARACTERISTICS, EFFECTS, AND WAYS OF ESTIMATION, A LITERATURE REVIEW

Seyed Behbood Issa Zadeh[1], Jose Santos López Gutiérrez[2], Maria Dolores Esteban Perez[3] and Gonzalo Fernandez-Sanchez[4]

1) Universidad politecnica de madrid, escuela tecnica superior de ingenerios de caminos, canales y puertos, Madrid, Spain(behbood.issazadeh@alumnos.upm.es),
2) Universidad politecnica de madrid, escuela tecnica superior de ingenerios de caminos, canales y puertos, Madrid, Spain (josesantos.lopez@upm.es),
3) Universidad politecnica de madrid, escuela tecnica superior de ingenerios de caminos, canales y puertos, Madrid, Spain (mariadolores.esteban@upm.es).
4) Universidad Europea, civil engineering department, Madrid, Spain, (g.fernandez.sanchez@facultyue.es)

1. Introduction

According to Objective 13 of sustainable development goals about climate change [1], addressing and identifying world climate change reduction actions are essential issues. One of the most important causes of this phenomenon is GHG emission; therefore, more than 90% of GHG is carbon emission[2]. In this study, the carbon footprint in maritime ports, its effect, and ways of its estimation are to be reviewed. In other words, it's an approach to evaluate some articles about carbon footprint in the literature review to give better ideas for more efficient further management and, therefore, to issue better policies to mitigate climate change.

A recent health board study shows that emissions from seaports and ships lead to about 19,000 annual lung cancer cases, while approximately 60,000 die every year from conditions caused by pollutants[3]. Carbon emissions from ships have increased gradually over time. They are estimated at circa 2.7% of total CO2 emissions globally, and marine activities in seaports account for circa 3% of total carbon emissions worldwide [4].

Based on the United Nations annual review of maritime transport, the annual CO2 emissions from maritime transport are estimated to be about 1000 (961) million tonnes of CO2eq [4]. Then paying attention to the amount of seaports' carbon footprint as critical maritime infrastructure is an essential issue because the intensive use of energy from primary sources has increased carbon emissions. Consequently, an all-out effort is needed to move towards clean, affordable, and resilient energy systems to help mitigate carbon emissions and limit global warming and climate change effects.

2. Methods

This cross-sectional study reviewed articles about carbon footprint in maritime ports as an infrastructure in marine transport. The critical literature review was conducted in 5 main steps: (i) online database search based on keywords (Scopus and Web of Science), (ii) first refinement based on selection criteria including title, abstract, and keywords of that paper, (iii) further refinement based on unique characteristics such as publishing year, language, type of document, type of access, region and country, etc., (iv) third refinement on abstract screening to consider focusing on the main topic and being related with the main subject, and (v) the last step is full-text review.

3. Results

Many types of industrial and un-industrial activities are done in seaports areas due to the role of ports as the intersection point of different transportation models; thus, for studying carbon footprint in seaports, the physical and environmental activities performed in ports are divided into some categories including direct and indirect activities, and then, some smaller sub-categories for each of them, for more accurate, better managing and systematic calculation of carbon footprint evaluation process. for instance, Various studies show that indirect factors like port service vessels and port commuters like employees, agencies, etc. have a more significant impact on carbon emissions in ports that are neglected and cannot be estimated well due to lack of sufficient inventories. [5].

On the other hand, this study states that previous researches concerning estimating carbon footprint in ports mostly are not in the life cycle approach (LCA), and the only amount of C.F in a period of operations evaluated; thus, findings can deviate resultant from reality. [6].

In studying the carbon footprint evaluation methods of different ports, the port activities are divided into two general categories according to the location: onshore part and offshore part. [7], [8].

As shown in Figure 1, land part activities (onshore activities) can classify into other various smaller subbranches like port heating systems, internal port transportation (including electric vehicles, combustion fuel vehicles, trains), cargo handlings equipment like shore cranes, and load/unload suction systems and waste management systems, etc. and maritime activities

(offshore activities) can divide in ships arriving, ships departing, ships hoteling in ports, service vessels like tugboats and various types of boats, etc.

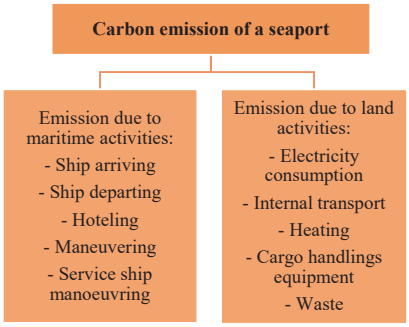

Figure 1. Carbon emission in a seaport

4. Conclusion

Three main factors contribute directly and indirectly to the carbon footprint in seaports: A) the consumption of fossil fuels, B) the high energy consumption of power systems, and C) the lack of professional management of resources.

Port-related activities such as employee transport, commuters, clients, and service vessel operations like tugboats and service boats can play an essential role in CO2 emission that in the new methods of activities estimation must be addressed.

Creating a suitable platform to minimize indirect factors such as transportation of personnel and people, building appropriate infrastructure for cheap electricity supply lanes for ships, as well as the use of renewable energy to generate electricity, heating, etc. can be an excellent way to reduce the emission of carbon in ports and, then mentioned activities and platforms can be operated efficiently just by intelligent management [8].

5. References

[1] "SDG Indicators — SDG Indicators." https://unstats.un.org/sdgs/metadata/?Text=&Goal=13&Target= (accessed May 17, 2022).

[2] T. Wiedmann and J. Minx, "A Definition of 'Carbon Footprint' ISA UK Research Report 07-01," 2007. [Online]. Available: www.censa.org.uk

[3] Y. Durmusoglu, S. Aksoy, C. Deniz,andY.Durmuşoğlu, "A Study of Renewable Energy in A Port Facility by Using Solar Organic Rankine Cycle Systems Dynamic Modelling, Simulation-Based Analysis and Optimization of Hybrid Ship Propulsion System View Project A study on the usage of alternative energy in a ship port terminal View project a study for renewable energy in a port facility by using solar organic Rankine cycle system," 2016.[Online].Available:https://www.researchgate.net/publication/308748179

[4] A. Alzahrani, I. Petri, Y. Rezgui, and A. Ghoroghi, "Decarbonisation of seaports: A review and directions for future research," Energy Strategy Reviews, vol. 38. Elsevier Ltd, Nov. 01, 2021. DOI: 10.1016/j.esr.2021.100727.

[5] V. C. Ballester, V. G. Lo-Iacono-Ferreira, M. Á. Artacho-Ramírez, and S. F. Capuz-Rizo, "The carbon footprint of valencia port: A case study of the port authority of Valencia (Spain)," International Journal of Environmental Research and Public Health, vol. 17, no. 21, pp. 1–16, Nov. 2020, DOI: 10.3390/ijerph17218157.

[6] O. Merk, "Shipping Emissions in Ports." [Online]. Available: www.internationaltransportforum.org/jtrc/DiscussionPapers/jtrcpapers.html

[7] G. Villalba and E. D. Gemechu, "Estimating GHG emissions of the marine ports-the case of Barcelona," Energy Policy, vol. 39, no. 3, pp. 1363–1368, 2011, DOI: 10.1016/j.enpol.2010.12.008.

[8] A. Carballo-Penela, I. Mateo-Mantecón, J. L. Doménech, and P. Coto-Millán, "From the motorways of the sea to the green corridors' carbon footprint: The case of a port in Spain," Journal of Environmental Planning and Management, vol. 55, no. 6, pp. 765–782, Jul. 2012, DOI: 10.1080/09640568.2011.627422.

INVESTIGATION OF MICROBIAL WATER QUALITY IN SOUTHERN OF THE CASPIAN SEA - STUDIES OF THE INTEGRATED COASTAL ZONE MANAGEMENT (ICZM) IN THE NORTHERN PROVINCES OF IRAN

Ali Azimi[1], Zohreh Faraji[2], Ehsan Rastgoftar[3] and Rasoul Ghanbari Maman[4]

1) Ports and Maritime Organization, Tehran, Iran, aazimi@pmo.ir
2) KhazarAb engineering advisory company, Sari, Mazandaran, Iran, zohrfaraji@gmail.com
3) Iranian National Institute for Oceanography and Atmospheric Sciences, Tehran, Iran, e.rastgoftar@inio.ac.ir
4) Ports and Maritime Organization, Tehran, Iran, rghanbari@pmo.ir

1. Introduction

Environmental pollution is one of the main causes of extinction and threat to the population of living organisms, which is especially important in the case of marine pollution due to its much easier spread. Pollution of marine resources not only destroys aquatic life but also endangers and threatens human life.

A variety of microorganisms, opportunistic and pathogenic can enter directly from urban sewage, or indirectly from swimmers' bodies because of diseases or not regarding principles of health before swimming causes contamination of these natural resources and so skin, gastrointestinal and respiratory diseases in humans [1]. Therefore, despite the medical importance of swimming, in case of contamination of swimming pool water with pathogens, can cause the transmission of bacterial infections. The most common disease caused by swimming is diarrheal disease [1]. In addition, because swimming pools are used by a wide range of people with different medical conditions, it is common for swimmers to develop opportunistic infections caused by bacteria. A study on the assessment of public health hazards to swimming pools in Lake Michigan by detecting fecal index viruses and bacteria showed fecal contamination in more than 15% of water samples [2].

Among opportunistic pathogens, bacteria are one of the most important microbial contaminants. The most important bacteria in the water of swimming pools and seas can be found in total coliforms (Escherichia, Klebsiella, Citrobacter) and Enterobacteriaceae (fecal coliforms, Pseudomonas, Aerogenesis, Streptococcus, Ficorrhagia, Ficorrhagia) [1]

According to the guidelines of the World Health Organization (WHO) and the European Economic Commission, the microbial quality of seawater for swimming is presented in the following table;

Table 1- Water quality requirements for swimming pools (European Economic Association and World Health Organization [1]

Microbiological agents	Optimum level	Threshold level
Total coliform count per 100 ml	500	10000
Counting fecal coliforms in 100 ml	100	2000
Fecal streptococci in 100 ml	100	400

Due to the dangers of microbial contamination of coastal waters for the health of tourists and environmental protection, in this study, microbial contamination on the southern shores of the Caspian Sea was investigated.

2. Method

A microbial sampling of seawater and measurements were performed throughout the coastal area of the South Caspian Sea during the summer of 2020 in the General Department of Environment of the studied provinces.

Figure1: Location of the studied stations on the southern shores of the Caspian Sea

According to the standard method of sampling, seawater is harvested from a depth of 21 to 31 cm below the surface of the water and is collected in open-pit bottles at room temperature. Determining of mean bacteria of total coliform was performed in the General Department of Environment of the studied provinces.

3. Results and Discussion

Based on sampling in 75 swimming pools on the Caspian Sea coast in the three northern provinces of the country, it was determined that on the coasts of Guilan province, Swan Beach swimming pool with 1430 MPN/100ml has the highest amount of coliform fecal microbes and Anbarsar swimming pool with 16 MPN/100ml has the lowest amount of coliform feces. A comparison of the levels of these bacteria in swimming pools of Guilan province with WHO, EEC, and national standards of Iran showed that among of 23 stations studied, 15 stations are higher than the standard limit in terms of microbial characteristics.

Surveys in Mazandaran province showed that among 49 studied swimming pools, 6 stations are above the standard limits in terms of the mentioned microbial indicators. Based on these results, microbial contamination in Ramsar, Noor, Chalous, and Mahmoudabad swimming pools was higher than the standards.

Based on the sampling and surveys of three swimming pools in Golestan province, all of the stations are higher than the standard limits in terms of coliform fecal index, and therefore due to the high load of microbial contamination, these areas need special management.

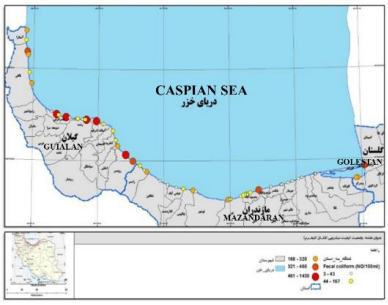

Figure2: Pollution map of swimming areas in the southern Caspian Sea (based on coliform fecal concentration)

4. Conclusion

Based upon this research findings and comparing the values of fecal coliform with the international standards, it can be concluded that the water of the southern Caspian Sea in the northern provinces of Iran is almost above the allowable level in many stations, which can threaten the health of swimmers. According to studies and observations, the reason for this pollution can be the discharge of municipal and agricultural wastewater and the lack of health facilities. Also, evacuation of petroleum products and oil wastes, along with human waste, increases turbidity and prevents the penetration of sun rays in the water, because the sun's rays play an essential role in killing bacteria and pathogens and so can have a great effect on reducing pollution [3]. Also, complete equipping of sanitary facilities and equipment in coastal projects along with continuous sanitary inspections and water quality assessment in the study area is essential.

5. References

[1] World Health Organization. Guidelines for Safe Recreational Water Environments: Volume 2. Geneva: WHO; 2006.
[2] Brinks MV, Dwight RH, Osgood ND, Sharavanakumar G, Turbow DJ, El-Gohary M, et al. Health risk of bathing in Southern California coastal waters. Arch Environ Occup Health. 2008; 63(3): 123-35.
[3] Mehrdadi.N. Evaluation of E.coli and fecal Streptococcus in coastal waters Mazandaran province in 2001 and compared with Standards. Sixth National Congress on Environmental Health. Mazandaran, IRAN; 2003. [In Persian].

14th International Conference on Coasts, Ports and Marine Structures
9 & 10 May 2023 , Tehran-IRAN
ICOPMAS 2022

ECOLOGICAL RISK ASSESSMENT OF LEAD IN SURFACE SEDIMENTS OF THE PERSIAN GULF, STRAIT OF HORMOZ AND GULF OF OMAN

Homira Agah[1], Afshin Aali[2], Samira Ghiasi[2], Kobra Heidari[3]

1) Iranian National Institute for Oceanography and Atmospheric science, Marine science faculty, Marine living department Tehran, Iran, aaagah_hom@yahoo.com
2) Islamic Azad University, Damavand Branch, Environmental department, Tehran, Iran, Afshinaali@yahoo.com; samiraghiyasi@yahoo.com
3) Khorramshahr university of Marine Science and Technology, Marine environment department, cobrahidari@gmail.com

1. Introduction

Sediments have a special importance in the term of bioavailability of heavy metals for benthic and other aquatic organisms. Several studies have been conducted regarding the concentration of heavy metals in the sediments of Persian Gulf and the Oman Sea, as important water and economic areas in the southern part of Iran. In this study, the concentration of lead (Pb) in the sediments of the Persian Gulf, the Strait of Hormuz and Oman Sea, based on the data of Heydari et al. (2017); Yousefi et al. (2019) (sediments of Chabahar and its surrounding areas) and Irandoust et al. (2021) (Bushehr and Strait of Hormuz) were compared and the ecological risk of this metal was calculated. The results of these studies showed that sediments of some stations had considerable lead concentration.

2. Results

Figures 1, 2 and 3 show the locations of the sampling sites and table 1 shows the geographic locations, depths, organic matters and concentrations of lead in the three study areas.

Heydari et al. (2017) [1], Irandoust et al. (2021) [2] and Yousefi et al. (2019) [3] performed their sampling in 2015, 216 and 2017, respectively. The concentrations of lead (average±SD) was 10.4±4.0; 29.5±16 and 22±7.6 mg. Kg^{-1} dry weight for Yousefi et al. (2017); Heydari et al. (2017) and Irandoust et al. (2021), respectively. The results showed that maximum lead concentrations were belonged to the sediments of Emam Port (41 mg. Kg^{-1}) and Sadaf at Bushehr, which were higher than threshold effect level (TEL: 30 mg. Kg^{-1}). Concentrations of lead in the other stations were lower than TEL.

Enrichment factor (EF) and Contamination Factors (CF) were used for determining sedimentary metal sources (Anthropogenic / natural) [4] and [5].

$EF= ((C_m/C_s)_x) / ((C_m/C_s)_c)$ $CF= C_{sample}/C_{background}$

While $(C_m/C_s)_x$ and $(C_m/C_s)c$ are the ratios of lead level on Fe concentrations in the sediments of study areas and in shale, respectively. Samples having enrichment factor >1.5 was considered indicative of human influence. When 0.5≤ EF≤1.5, it suggests that the heavy metals may be entirely originate from crustal materials or natural weathering processes [6].

CF is calculated as the ratio between the average lead level in sediment and the relevant background value [7]. It was classified into four groups, when CF<1, there is low metal enrichment by natural or anthropogenic inputs; 1≤CF<3, 3≤CF<6 and CF>6 shows that the sediment is moderately, considerably and heavily contaminated by an element, respectively (Table 2).

Potential of ecological risk (E^i_j) was calculated based on concentration factor and toxicity index (Tij), which is 5 for lead; E^i_j ≤40 indicates low ecological risk, 40< E^i_j ≤80 indicates moderate ecological risk, 80<E^i_j≤160 indicates considerable ecological risk, 160<E^i_j≤320 indicates high ecological risk, E^i_j >320 indicates very high ecological risk [8].

$E^i_r=T^i_r * CF_i$

The results of enrichment factors showed that lead in the study area was originated from natural sources; however anthropogenic sources has relatively affected on its concentrations in Tiss and coastal parts of Ramin. The results of concentration factors demonstrated low accumulation level of lead in the sediment of the three sampling areas, except Emam port, Sadaf and Naftkesh in Bushehr with moderate concentrations level. However, the lead concentrations were more than threshold effect level (TEL: 30 mg. Kg^{-1}), but its potential risk was in the low-risk range (*Eij* <30).

Table 1: The geographical locations, depths, lead concentrations, range and its average in the study areas.

Ref	Stations	Depth (m)	Longitude / Latitude	Pb
Yousefi et al. (2019)	Posm 1	12.1	25o19'58'' N 60o15'44'' E	12.7±0.7
	Posm 2	6	25o22'54'' N 60o15'21'' E	7.1±0.6
	Konarak 1	5	25o19'58'' N 60o15'44'' E	13.8±0.6
	Konarak 2	10.5	25o22'23'' N 60o28'30'' E	9.8±0.8
	Desalination plant	5.8	25o26'03'' N 60o30'14'' E	4.7±0.2
	Tiss 1	3.8	25o21'46'' N 60o35'40'' E	9.8±0.3
	Tiss 2	9	25o22'50'' N 60o33'59'' E	9.9±0.6
	Entrance of Gulf	13.6	25o17'44'' N 60o32'12'' E	10.2±0.2
	Ramin 1	4.5	25o15'42'' N 60o46'18'' E	20.0±0.6
	Ramin 2	13.2	25o15'33'' N 60o46'14'' E	7.6±0.4
	Reference	22.2	25o27'05'' N 60o60'29'' E	9.2±0.1
Heydari et al. (2017)	Arvand Kenar	Intertidal zone	28o21'29''N 48o31'03'' E	ND
	Bahregan		30o06'37''N 49o46'17'' E	ND
	Emam port		30o28'75''N 49o04'23'' E	41±3
	Abadan port		30o19'34''N 48o17'09'' E	18±1.6
Irandoust et al. (2021)	Sadaf - Bushehr	Intertidal zone	28o57'52''N 50o48'54'' E	32±3
	Parvaz-Bushehr		28o57'11''N 50o48'42'' E	16±1.5
	Naftkesh-Bushehr		28o55'56''N 50o48'25'' E	24±2
	Bandar Abbas		27o10'09''N 67o18'82'' E	16±2
Ref: Reference; ND: under detection limit. ; ERM: Effects Range Medium (NOAA); PEL: probable effect level ERL: Effects Range Low (NOAA); TEL: Threshold Effect Level.			TEL	30
			ERL	46.7
			PEL	112
			ERM	218
Average of earth crust				20*

Table 2: The enrichment and contamination factors and potential risk of the study areas.

Reference	Stations	EF	CF	Er
Yousefi et al. (2019)	Posm 1	1.1	0.64	3.2
	Posm 2	0.7	0.36	1.8
	Konarak 1	1.5	0.69	3.5
	Konarak 2	0.7	0.49	2.5
	Desalination plant	0.6	0.24	1.2
	Tiss 1	2.5	0.49	2.5
	Tiss 2	2.8	0.50	2.5
	Entrance of Gulf	1.0	0.51	2.6
	Ramin 1	3.8	1.0	5.0
	Ramin 2	0.9	0.38	1.9
	Reference	1.5	0.46	2.3
Heydari et al. (2017)	Arvand Kenar	0.0	0.0	0.0
	Bahregan	0.0	0.0	0.0
	Emam port	0.8	2.1	10.3
	Abadan port	0.35	0.9	4.5
Irandoust et al. (2021)	Sadaf - Bushehr	0.8	1.6	8
	Parvaz- Bushehr	0.6	0.8	4
	Naftkesh-Bushehr	0.7	1.2	6
	Bandar Abbas	0.7	0.8	4

CF: Contamination Factor, EF: Enrichment Factor, * Turekian and wedepohl 1961.

3. References

[1] Heydari Kobari; Khalili Purouliaqli; Aware of Hamira; Zulqarnain Hossein; Hosseini Seyyed Mahdi. 2019. Investigating the bioaccumulation of heavy metals in the sediments and muscle tissue of the mandible (Boleophthalmus dussumieri) in the coast of Khuzestan, Persian Gulf. *Natural environment,* Volume 74, Number 4, March 1400, pp. 694-707.

[2] Irandoust F. Agah H, Rossi L. Calizza F, Careddu G, Costantini M.L.Stable isotope ratios (δ 13 C and δ 15 N) and heavy metal levels in macroalgae, sediment, and benthos from the northern parts of Persian Gulf and the Gulf of Oman. 2021. *Marine Pollution* Bull. 3:111909. doi: 10.1016/j.marpolbul.2020.111909.

[3] Yousefi Majid, Aghaz Hamira, Taqvi Laebat. 2019. Investigating the concentration of heavy metals in sediments, Chabahar region, between Pezam and Ramin. *Darya Fanon Quarterly,* 7th year, No. 2 (series 20, pp. 87-98.

[4] Selvaraj, K., Ram Mohan, V., Szefer, P., 2004. Evaluation of metal contamination in coastal sediments of the Bay of Bengal, India: geochemical and statistical approaches. *Mar. Pollut. Bullet.* 49, 174–185.

[5] Vald'es, J., Vargas, G., Sifeddine, A., Ortlieb, L., Guinez, M., 2005. Distribution and enrichment evaluation of heavy metals in Mejillones Bay (23S), Northern Chile: Geochemical and statistical approach. *Mar. Pollut. Bullet.* 50, 1558–1568.

[6] Birch GF, Olmos MA. 2008. Sediment-bound heavy metals as indicators of human influence and biological risk in coastal water bodies. ICES *J. Marin. Sci.* 65: 1407–1413.

[7] Woitke, P., Wellmitz, J., Helm, D., Kube, P., Lepom, P., Litheraty, P., 2003. Analysis and assessment of heavy metal pollution in suspended solids and sediments of the river Danube. *Chemosphere* 51, 633–642.

[8] Håkanson, L., 1980. An ecological risk index for aquatic pollution control; a sedimentological approach. Water Res. 14, 975–1001.

EFFECTS OF NOISE POLLUTION ON MARINE LIFE

Reza Toliyan[1]

1) Bushehr Port and Maritime Administration, Employee of the Maritime Safety and Protection Department, Bushehr, Iran, Gh.toliyan@yahoo.com

1. Introduction

Humans receive most of the information they need from ambient through the energy of electromagnetic waves. However, in the sea, the opposite is true and they used sound waves to detect objects on it [1]. The marine environment of the oceans, which make up about 65% of the planet's life, hosts a wide range of sound waves (caused by waves, winds, biological activity, etc.) that can interfere with communication and other performance of marine animals [2]. Also one-third of the world's people rely on fish and other aquatic products for at least one-fifth of their annual protein intake [3]. Research has shown that compared to 50 years ago, the level of noise pollution in the seas has increased by at least 15 dB [4]. This is while in 2004 an increase of 10 dB between 1950 and 1975 was predicted [2]. Increased use of the seas for commercial transportation, geophysical exploration, wars and overfishing activities over the past few decades has led to high levels of noise pollution in the seas [5]. Unlike electromagnetic waves, which are strongly attenuated in the aquatic environment, sound waves can travel thousands of kilometers in water [3, 5].

2. Sources of Noise Pollution in the Sea

The most important sources of sound in the seas can be divided into the following two main categories:

2.1. Natural and Environmental Sources

Many sound sources in the seas come from natural origin. For example, wind, waves, sea state, thunder, lightning, seismic energy generated by earthquakes and swell patterns [2]. According to Knudsen et al. (1948), noise levels vary with sea state in the same way over the entire frequency band from 1 kHz to 100 kHz [6].

2.2. Anthropogenic Noise Sources

These sources include are: 1- Ships because of the sound of their propellers and engines. 2- Submarine equipment such as depth sounders 3- exploration and exploitation for hydrocarbon and natural resources 4- Military activity such as military sonar 5- Offshore oil and gas production rigs 6- Seismic activities [7]. Most ships produce sounds in a frequency range between 80 Hz and 300 Hz [3]. Frequency amplitudes lower than 300 Hz are important because the sound at low frequencies is not reduced in the water, and also the communication frequencies of the whales are in this range, which interfere with communication of these organisms with each other. The most important factors of sound production in the ship can be mentioned as follows: 1- Machinery on the ship's board and engine room 2- Improper repair and maintenance of the ship hull 3- Ship propeller 4- Cavitation [8]. Most of the ship's sound is related to cavitation. The frequency band of ships may interfere with the sound frequencies of whales, seals, sea lions and fish, as shown in Figure 1 [4, 8].

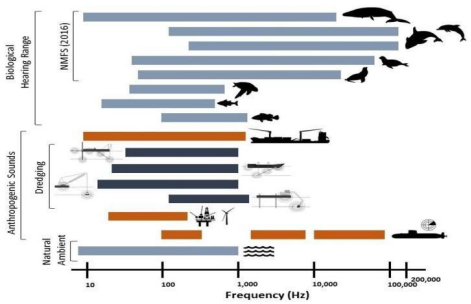

Figure 1: Hearing frequency ranges of selected fish and mammal species and main energy frequencies reported for anthropogenic and ambient sources.

3. The Effect of Noise Pollution on Marine Animals

Sound plays an essential role in critical activities for marine species, like attract mates, foraging, maintaining social structure, and avoiding predators [4-6]. For instance, cetaceans (whales, dolphins and porpoises) send and receive complex sounds to communicate with each other, navigate the water, find food, and obtain environmental information such as water depth [9]. The potential impact of noise pollution on marine life has shown in figure 2. [5]. Assessing the noise effects in the marine environment is difficult and expensive [5]. First, very little academic research has been done on how marine mammals response physically and behaviorally to intense sounds and to long-term increases in ambient noise levels. Second, interfering frequency may not only affect the auditory systems of these organisms, but may also have acute and chronic effects on other organs of aquatic biota (cumulative impacts) and have cause systemic disorders that eventually cause his death [10]. Summarily, the harmful effects of noise pollution on marine mammals can be described as follows: [6-9]

- Interfere with attract mates and social interaction and unable to communication
- Changes in hormone levels (Chornic and acute effects)
- Interfere with navigation and historical migration routes
- Interfere with feeding, identify the location of prey and Stay away from predators
- Interfere with feeding, identify the location of prey and Stay away from predators
- Interfere with find suitable habitat, announce location and territory and identify high risk areas.
- Permanent or temporary loss of hearing
- Psychological and physical injuries, such as internal bleeding and so on.
- Increasing in abundance and distribution

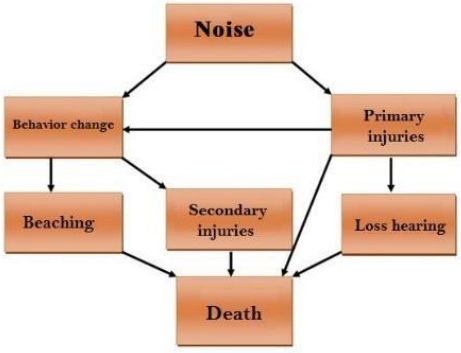

Figure 2. The potential impact of noise pollution on marine life

4. Recommendations

1. Adopting appropriate technologies to reduce noise and maintaining the noise level within conservative noise standards as set by regulatory bodies.
2. Replacing new navigation technologies with sonar techniques and minimizing the use of sound energy to identify and estimate the position, speed and nature of objects in the water. Preparing an EIA (Environmental Impact Assessment) to develop appropriate strategies and initiatives in each applicable sector.
3. Complete and accurate assessment of utilized equipment by all maritime organizations, including actual impacts and appropriate preventive efforts.
4. Determining the new transit shipping routes, especially in sensitive and protected sea areas.
5. Designing transmission and exhaust systems to reduce noise and vibration.
6. Modifying the construction of propellers to reduce cavitation and using flexible mounts to isolate the vibrating machinery from the hull and surrounding the noise-producing machinery in a tight, insulated enclosure.
7. Establishing rules and regulations for aquatic habitats and ensuring that they receive the least impact.
8. Strengthening and financially supporting supervisory authority for accurate and comprehensive monitoring.
9. Conducting studies to determine the sound threshold of marine life, especially animals that are endangered and are sensitive to noise pollution.
10. Promoting the culture and environmental knowledge of individuals.
11. This article has been done with the scientific and material support of PMO.

5. References:

[1] Weilgart, L. S. The impacts of anthropogenic ocean noise on cetaceans and implications for management. *Canadian journal of zoology*, 85(11), 2007, pp.1091-1116.
[2] Weilgart, L. I. N. D. Y., The impact of ocean noise pollution on fish and invertebrates. Report for OceanCare, Switzerland, 2018.
[3] Kar, A. and Datta, P. R., Logistics Cost Dynamics in International Business: A Causal Approach. Foreign Trade Review, 55(4), 2020, pp.478-495.
[4] McDonald M. A, Hildebrand J. A, Wiggins S. M. Increases in deep ocean ambient noise in the Northeast Pacific west of San Nicolas Island, California. The Journal of the Acoustical Society of America. 120(2), 2006, pp. 711-718.
[5] Borelli, D., Maritime Airborne Noise: Ships and Harbours. International Journal of Acoustics and Vibration, 24(4), 2019, pp.631-632.
[6] [6] Chahouri, A., Elouahmani, N. and Ouchene, H., Recent progress in marine noise pollution:

14th International Conference on Coasts, Ports and Marine Structures
9 & 10 May 2023 , Tehran-IRAN
ICOPMAS 2022

MONITORING OF HEAVY METALS IN SEDIMENTS OF MAHSHAHR CREEKS-NORTHWEST OF THE PERSIAN GULF

Ali Azimi [1]

1) Ports and Maritime Organization, Tehran, Iran, aazimi@pmo.ir

1. Introduction

Today pollution of aquatic ecosystems is one of the main problems of human life. Metals from anthropogenic pollution sources are continually released into aquatic ecosystems. Heavy metals are a serious threat due to their toxicity, long persistence, bio-accumulation, and bio-magnification in the food chain [1]. This study aimed to determine the concentration of the metals (Ni, Cd, Pb, Cu, and Co) in the sediments of Mahshahr Creeks. Since in this area fish is an important component of the human diet so the result of this study is important for indicating diet health.

The results obtained from this study would provide information on background levels of metals in the sediment of the Mahshahr Creeks, contributing to the effective monitoring of both environmental quality and the health of the organisms inhabiting this ecosystem.

2. Material and Methods

Sediment was sampled at selected sites (Ghanam, Ahmadi, and Jafari) from Mahshahr Creeks (Figure 1) in the winter (January 2011).

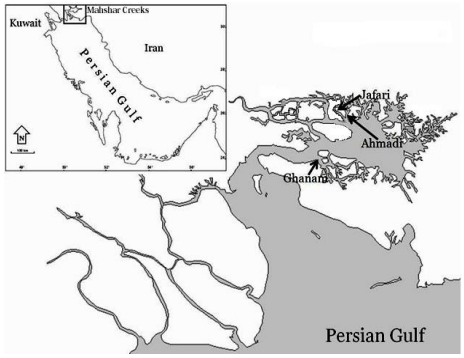

Figure 1. Map of the study area showing locations of sampling stations on the Mahshahr Creeks (Ghanam, Ahmadi, and Jafari).

Sediment samples were collected using a Van Veen grab to a depth of 5 cm. Metals concentrations were measured using an ICP-AES (Inductivity Coupled Plasma Atomic Emission Spectrometer).

3. Results

Metals concentrations in the sediment of three studied sites (Ghanam, Ahmadi, and Jafari) have shown in (Table 1). Among all metals, Nickel (Ni) has the highest concentration in sediment samples of sites and the lowest concentration belong to Cadmium (Cd). Based on the results of statistical analysis, only concentration of Co showed significant differences ($p<0.05$) in sediment samples. For Ni, Significant differences only have been seen between sediment of (Ghanam & Ahmadi), Cd (Ahmadi & Jafari), Pb (Ghanam & Jafari), Cu (Ghanam & Ahmadi, and also Ahmadi & Jafari).

Table 1. Recovery values of metals in the sediment-certified reference materials (IAEA-407 Estuarine sediment-Australia).

Metals	Muscle	Gill	Sediment
Ni	105%	98%	104%
Cd	96%	95%	94%
Pb	97%	106%	105%
Cu	104%	95%	95%
Co	95%	94%	94%

Table 2. Heavy metal concentration ($\mu g.gDW^{-1}$) in sediment taken from sampling sites of Mahshahr Creeks and compared to guidelines.

Stations	Ni	Cd	Pb	Cu	Co
Ghanam	18.3±3	0.2±0.08	4±1.5	9.17±0.9	16.5±1.2
Ahmadi	21.6±1.5	0.12±0.02	5.04±0.8	7±0.3	19.4±0.5
Jafari	24.6±2.3	0.33±0.14	6.5±0.46	9.2±1	22±1.2
ROPME	15-30	1.2-2	–	70-80	–
PEC (NOAA)	128	5	–	–	149
PEL (NOAA)	112.2	4.21	–	42.8	108.2
ERL (NOAA)	47	1.2	46/7	21	34
ERM (NOAA)	218	9.6	218	52	270
ISQG	30.2	0.7	–	15.9	18.7

4. Discussion

In this study concentration of metals in sediment from three sites of Mahshahr Creeks northwest of the Persian Gulf was determined. The result of this study supplied important information on heavy metals contamination in sediments of Mahshahr Creeks, Northwest of the Persian Gulf. As shown in (Table 2), the highest concentration of metals between studied sites was found in Jafari and the lowest in Ghanam. Jafari originates from Mahshahr Creeks and is stretched along PETZONE (Petrochemical Special Economic Zone) up to Mashahr and Sarbandar cities. This Creek is used as a municipal waste receptor [2]. Moreover, it receives a copious amount of petrochemical wastewater along its courses. Thus, the higher level of accumulated metals in sediments from Jafari could be related to anthropogenic activities and effluent discharges into the mentioned site. One of the other sites in this region is Ghazale, not investigated in this study. The proximity of Ghazale to the oil terminal turns this area into a waterway for oil tankers. Therefore, the enrichment of metals in this creek might reflect oil pollution in the area. Ahmadi is located between Jafari and Ghazale and consequently, a great amount of metal may displace in this Creek by movements produced by waves and tidal currents [3, 4]. Ghanam is located near the estuary of Mahshahr Creeks and therefore highly affected by currents coming from the Persian Gulf. Strong tidal currents cause the highest movement of water and sediment at this site. Among the investigated metals, Ni has the highest level in the sediment of all sites. Naturally, nickel has a high concentration in marine sediment and also, oil pollution. Ni is one of the main metals in oil components [5]. The lowest concentration among metals belongs to Cd.

5. References

[1] Eisler, R. 1988. Hazards to fish. Wildlife and invertebrates: A synoptic review. United States Fish and Wildlife Service. Biological Report, 85(1.12): 82-92.

[2] Abdolahpur Monikh, F., Hosseini, M., Peery, S., A., Ghanem, K., AbdiBastami, A and Karami, O. 2011. Heavy Metals Levels in Sediment and Ray Fish (Dasyatis bennettii) from Musa Estuary and Selech Estuary, Persian Gulf. American-Eurasian Journal of Toxicological Sciences .3 (4): 224-227.

[3] Feng, H., Cochran, J.K and Hirschberg, D.J. 2002.Transport and Sources of Metal Contaminants over the Course of Tidal Cycle in the Turbidity Maximum Zone of the Hud-son River Estuary.Water Research. 36(3): 733-743.

[4] Mubiana, V.K., Vercauteren, K and Blust, R. 2006. The Influence of Body Size, Condition Index and Tidal Exposure on the Variability in Metal Bioaccumulation in Mytilus edulis. Environmental Pollution. 144 (1): 171-179.

[5] Clarck, R.B. 1992. Marine Pollution.Third Edition. Clarendon Press. Oxford. 172p.

14th International Conference on Coasts, Ports and Marine Structures
9 & 10 May 2023 , Tehran-IRAN
ICOPMAS 2022

SITE SELECTION OF ARTIFICIAL CORAL REEFS USING HYDRODYNAMIC PROPERTIES OF THE WATER BODY

Michael J. Risk[1], Shadan Nasseri Doust[2], Mehrnoosh Abbasian[3], S. Abbas Haghshenas[4]

1) Department of Earth Sciences, McMaster University, Riskmj@mcmaster.ca
2) Institute of Geophysics, University of Tehran, Tehran, Iran, Shadan.nasseri.d@ut.ac.ir
3) Institute of Geophysics, University of Tehran, Tehran, Iran, Mehrnoosh.abasian@ut.ac.ir
4) Institute of Geophysics, University of Tehran, Tehran, Iran, SAHaghshenas@ut.ac.ir

1. Introduction

Coral reef ecosystems are declining worldwide. Chemical contaminants reach the marine environment from both land-based and water-based anthropogenic sources. These chemicals, created by various human activities, are one of the leading causes of coastal ecosystem degradation. The Persian Gulf, the world's warmest sea, is seeing an increase in the frequency and intensity of mass bleaching events.

Previous research in the Persian Gulf has found that bleaching episodes reduce species richness and variety of reef fish, with mean coral cover reducing by 85 percent after the 2007 bleaching event and 95 percent after the 2017 bleaching event. Building artificial reefs in marine protected areas may be one answer since they will give extra habitat for biodiversity and so may offer an innovative management solution for managing coral reef recovery and resilience [1]. Some studies comparing the potential of artificial reefs to natural reefs have been undertaken and demonstrate the feasibility of the process. These studies compared the biological communities of different types of reefs and assessed the conservation of natural reefs using artificial reefs [2, 3, 4].

The present study investigates the suitability of the Northern Persian Gulf coastal areas for establishing artificial reefs using three highly effective Hydrodynamic factors, Current magnitude, Distance from Pollutant Sources and pollution residence time. These factors are the outcomes of a reef-scale hydrodynamic model used to make policy decisions in various sections of the Persian Gulf (The Kish island in the Northern area) [5]. As the Gulf is the warmest sea supporting extensive corals, there may be resistant species that could be preserved and used in reef reclamation projects elsewhere. In addition, our model can also be used to identify areas where a natural larval settlement could be enhanced.

2. Hydrodynamic Modelling

Understanding surface and near-surface currents pave the way to various applications, such as pollution transport or biological and chemical investigations focusing on the movement and dispersion of floating material, regardless of their origin or nature. Moreover, Patterns in pollution transport along and across the shore have important implications for the conservation of coastal ecosystems, especially in the vicinity of strengthening currents entering a semi-closed domain (e.g. estuaries and bays) with complex topography [6].

In order to understand the hydrodynamics of pollutants and their plausible threats to coral reefs in the Northern parts of the Persian Gulf, due to their accumulation and phototoxic effects in the euphotic zone, the particle-tracking model was used to study the transport and flushing processes of potential pollutants. This may allow us to identify spots that would not be suitable for artificial reef deployment. At the same time, natural coral damages are highly likely. The current speed is also essential as the artificial corals should tolerate and adapt to the local condition.

There are many different pollutant behaviours; each pollutant must have its specific algorithm (calculation procedure) to represent its simulated behaviour. Each pollutant variable's algorithm must be derived from a thorough understanding of how that pollutant interacts in coastal waters. This might be in the form of a particle-tracking program or a time-stepping concentration equation. The concentration equations are adequate for widely dispersed chemicals; however, the numerical advection scheme must be used cautiously. The parameters that characterize how the contaminant behaves differently from a passive tracer are added to the advection-diffusion equation. These must be reflected in a particle-tracking model, maybe through a change in each particle's properties. The finite element method allows the discretization mesh of the domain investigated to be refined in the coastline where we have release points of the pollutants. We used a method that allows the user to specify the resolution along the coastline, permitting meshes of various resolutions to include the exact boundary curve specification.

3. Residence Time Estimation

We assume the constituent used to trace the water parcel behaves dynamically and passively. That is, both the water parcel and the constituent follow the same pathways. The residence time can then be determined experimentally.

We may consider an instantaneous release of the Oxybenzone into the water body at position x_0 and time t_0. The resulting total mass of tracer within the domain at time t is:

$$C_{x0}(t) = \iiint c_{x0}(x.t).dV \quad (1)$$

Where $c_{x0}(x, t)$ is the mass distribution of pollution in the volume V(t) of the water body.

Next consider the function $M_{x0}(t)$ as the amount of chemical pollutant per unit time that leaves the system:

$$M_{X0}(t) = C_{X0}(t_0) - C_{X0}(t) \quad (2)$$

Each particle leaving the system can be characterized by the time τ that has elapsed since its release time. Once these elements are arranged cumulatively, $M_{x0}(\tau)$ represents a probability distribution function of the water parcel containing the chemical component, leaving the domain which has spent less than or equal to τ in the domain or a specific point. $M_{x0}(\tau)$ may be called the residence time function. The probability density function $\phi_{x0}(\tau)$ for the residence time is equal to:

$$\phi_{x0}(\tau) = \frac{1}{M_0} \cdot \frac{dM_{X0}(\tau)}{d\tau} \quad (3)$$

Where M_0 is the total mass of chemical pollutant in the selected area.

The average residence time $<\tau_{x0}>$ would be equation

$$< \tau_{x0} > = \int_0^\infty \tau \phi_{x0}(\tau) \cdot dt \quad (4)$$

The average residence time, as it is stated in the equation (4), represents the expected lifetime for newly incorporated water parcels in the domain at position x_0.

Residence time calculations will be especially valuable in the case of identifying areas selected for enhanced larval survival.

4. References

[1]. Kirkbride-Smith et al., Artificial reefs and marine protected areas: a study in willingness to pay to access Folkestone Marine Reserve, Barbados, West Indies. 2016, PeerJ 4: e2175; DOI 10.7717/peerj.2175

[2]. Champion, C., Suthers, I.M., Smith, J.A., Zooplanktivory is a key process for fish production on a coastal artificial reef. Mar. Ecol. 2015, Prog. Ser. 541, 1–14. https://doi.org/10.3354/meps11529.

[3]. Keller, K., Steffe, A.S., Lowry, M.B., Murphy, J.J., Smith, J.A., Suthers, I.M., Estimating the recreational harvest of fish from a nearshore designed artificial reef using a pragmatic approach. Fish. 2017, Res. 187, 158–167. https://doi.org/10.1016/j. fishres.2016.11.022.

[4]. Smith, J.A., Cornwell, W.K., Lowry, M.B., Suthers, I.M. Modelling the distribution of fish around an artificial reef. Mar. Freshw.2017, Res. 68, 1955–1964. https://doi.org/10.1071/MF16019.

[5]. Nasseri Doust, Shadan and Abbasian, Mehrnoosh and Haghshenas, S. Abbas and Downs, C.A. and Risk, Michael J., , Occurrence, Distribution, and Fate of UV Filters around endangered coral species in the Persian Gulf,Fifth International Conference on Persian Gulf, 2022 Oceanography,Tehran,https://civilica.com/doc/1461114

[6]. Downs, Bishop, Diaz-Cruz, Haghshenas, Stien, Rodrigues, Woodley, Sunyer-Caldú, Nasseri Doust, Espero, Ward, Farhangmehr, S. Tabatabaee Samimi, Risk, Lebaron, DiNardo, Oxybenzone contamination from sunscreen pollution and its ecological threat to Hanauma Bay, Oahu, Hawaii, U.S.A., Chemosphere, (2021), 132880, ISSN 0045-6535

[7]. E. Gomez-Reyes, A.F. Blumberg. Flushing time in coastal lagoons, Transactions on Ecology and the Environment vol 7, 1995, WIT Press, www.witpress.com, ISSN 1743-3541

14th International Conference on Coasts, Ports and Marine Structures
9 & 10 May 2023 , Tehran-IRAN
ICOPMAS 2022

NUMERICAL AND FIELD STUDY OF NITRITE AND NITRATE DIFFUSION AND DISTRIBUTION WITH URBAN SOURCE IN THE COASTAL WATERS OF THE BANDAR ABBAS IN THE NORTH OF THE PERSIAN GULF

Akbar Rashidi Ebrahim Hesari[1], Seyed Shakib Asiaee Sahneh[2]
1) Assistant Professor, Department of Marine Physics, Tarbiat Modares University, Iran
2) Ph.D. in Physical Oceanography, Department of Marin Science and Technology, Hormozgan University, Iran

1. Introduction

It was thought that the vast expanse of the sea and ocean would accept any kind of pollutant and there was no need to worry about the pollution. However, with the increase of industries and population growth, as well as knowledge advances in the seas and oceans investigations, the consequences of the entry of pollutants were gradually observed, and concerns about the extinction of marine animal species and changes in physical and chemical processes in the sea increased. The potential dangers to species of animals and humans, and the impact of atmospheric processes from the sea, have led many countries to periodically monitor their coastal areas for the entry of pollutants [3].

2. Study Area, Model Parameters and Measurements

A numerical three-dimensional hydrodynamic model capable of predicting the diffusion of chemical pollutants dissolved in seawater was designed to study the diffusion of environmental pollutants including urban and treatment plant wastewater from Bandar Abbas due to the Gorsozan estuary into the coastal water of Bandar Abbas located in the northeast of Persian Gulf.

Governing equations of this model including momentum equations, continuity, temperature, salinity, bottom pressure tendency, representative of the vertical velocity, state equation for seawater, and an advection-diffusion equation for simulation of the diffusion of chemical pollutants dissolved in seawater were rewritten in the earth spherical coordinate system with the Sigma as normalized vertical array based on pressure[1], and solved using finite difference method on the structured modified Arakawa C grid. The two-step Lax-Wendroff scheme was used for the advection terms and the Dufort-Frankel scheme was used for the discretization of diffusion terms and second order derivatives.

The model calculates the rate of water level change at each time step during execution and considers two separate cases according to this rate. If this rate is positive, it is called wetting and otherwise it is called drying. Now, by determining the minimum depth for the two modes, the network expands the computational nodes to reach the desired depth and does not enter depths less than that in the calculations [4]. Applying this strategy will be helpful, except in cases where there are many changes, and ups and downs in the region [6]. Also, for the minimum depth of the model, after running the program with several different depths and comparing it with reality, the depths of one meter were determined for the regional model and 20 cm for the local model. The algorithm used to compute and dry computational cells is derived from Dietrich research [5].

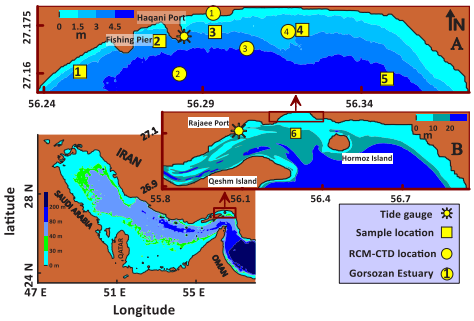

Figure 1. Study area (A), area of local model (small), and (B), regional model (medium), Gorsozan estuary, Location of measuring and sampling stations

In this model, the input parameters included bathymetry data, wind, temperature, and salinity data, and measurements related to the concentrations of nitrate and nitrite. The nitrate and nitrite concentrations were measured by spectrophotometry method at six stations of Bandar Abbas coastlines every season for the duration of one year

.

3. Results

To calibrate the model, several implementations were performed by changing the experimental parameters. Sometimes the discrepancy between the model results and the field data is due to the assumptions and methods used in modeling [9], which were also identified and eliminated as much as possible. To apply floor friction, Nihoul (1977) considers bed stress as a function of horizontal mean flow by introducing experimental drag coefficients and defines a linear relationship for stress in the bed boundary layer [10]. In this study, Nihoul method was used and the model was calibrated with its drag coefficients.

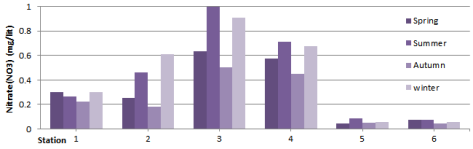

Figure 2. Nitrate measurement results from autumn 2019 to autumn 2020, with a maximum of 24.8 (mg /lit) is standardized.

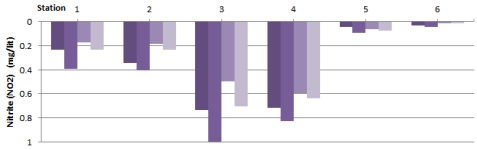

Figure 3. The results of nitrate measurements from autumn 2019 to autumn 2020, with a maximum of (6.4 mg/lit) is standardized.

The simulations showed that these pollutants were more distributed around Shilat Pier and in areas between Haghani and Sayadi Piers. The concentrations of nitrate and nitrite were determined more than 60% from the crossing point of Gorsozan estuary to the Persian Gulf until 6 km in the east and 5 km in the west.

These results were approved by measuring these two pollutants in the mentioned locations. The average concentration of nitrate in four seasons was measured 18.9 mg/L in Gorsozan estuary, 14.95 Mg/L in Shilat pier, and 9.32 mg/L in Haghani pier. Furthermore, the average annual concentration of nitrite was measured 4.7 mg/L in Gorsozan estuary, 4.45 Mg/L in Shilat pier, and 1.87 mg/L in Haghani pier (Figure 2, 3).

4. References

[1] Apel, J.R., 1999. Principles of ocean physics. London Academic press, pp. 13-245

[2] Boudreau, B.P., 1997. Diagenetic models and their implementation (Vol. 410). Springer, Berlin.

[3] Clark, E.B., Branch, A., Chien, S., Mirza, F., Farrara, J.D., Chao, Y., Fratantoni, D., Aragon, D., Schofield, O., Flexas, M.M. and Thompson, A., 2019. Station-Keeping Underwater Gliders Using a Predictive Ocean Circulation Model and Applications to SWOT Calibration and Validation. IEEE Journal of Oceanic Engineering.

[4] D'alpaos, L. and Defina, A., 2007. Mathematical modeling of tidal hydrodynamics in shallow lagoons: A review of open issues and applications to the Venice lagoon. Computers & Geosciences, 33(4), pp.476-496.

[5] Dietrich, J.C., Kolar, R.L. and Westerink, J.J., 2006. Refinements in continuous Galerkin wetting and drying algorithms. In Estuarine and Coastal Modeling (2005) (pp. 637-656.(

[6] Falconer, R.A. and Chen, Y., 1991. Improved representation of flooding and drying and wind stress effects in a two-dimensional tidal numerical model. PROC INST CIV ENG PART 2 RES THEORY., 91, pp.659-678.

[7] Haltiner, G.J.W. and Williams, R., (1980), Numerical prediction and dynamic meteorology, 2nd Edition, Wiley, New York, 496 p.

[8] Lin, H.C.J., Cheng, H.P.P., Edris, E.V. and Yeh, G.T.G., 2004. Modeling surface and subsurface hydrologic interactions in a south Florida watershed near the Biscayne Bay. In Developments in Water Science (Vol. 55, pp. 1607-1618). Elsevier

[9] Jahandideh-Tehrani, M., Helfer, F., Zhang, H., Jenkins, G. and Yu, Y., 2020. Hydrodynamic modelling of a flood-prone tidal river using the 1D model MIKE HYDRO River: calibration and sensitivity analysis. Environmental Monitoring and Assessment, 192(2), p.97.

[10] Nihoul, J.C., (1977), Three-dimensional model of tides and storm surges in a shallow well-mixed continental sea, Dynamics of Atmospheres and Oceans, vol. 2, p.29-47. [DOI: 10.1016/0377-0265(77)90014-8]

14th International Conference on Coasts, Ports and Marine Structures
9 & 10 May 2023 , Tehran-IRAN
ICOPMAS 2022

AN ARTIFICIAL CHANNEL, A SOLUTION TO KEEP GORGAN BAY ALIVE

Majid Jandaghi Alaee[1], Meysam Bali[2] and Hossein Nemati[3], M.H. Moeini[4]

1) Head of Technical Department, Pouya Tarh Pars Consultant Engineers (PTP), Tehran, Iran, mja@ptpco.coml
2) Project Manager Pouya Tarh Pars Consultant Engineers (PTP), Tehran, Iran, meysam_baali@yahoo.com
3) Ports and Maritime Organization, Tehran, Iran, mhn1982@gmail.com

1. Introduction

Covering an area of about 400 square kilometers, the Gulf of Gorgan also known as Gorgan Bay is the largest gulf in the southeast of the Caspian Sea. It is separated from the main water body by the Miankaleh peninsula extending to the Ashuradeh peninsula. The bay is currently connected to the sea through two narrow channels called Chapaghli and Ashuradeh (Figure 1). It is extended about 60 km along the bay axis with the maximum width and depth of approximately 12 km and 4 m and -26.5 m, respectively (when the Caspian Sea Level (CSL) is -26.5). The geometric characteristics of the Gorgan Bay are strongly dependent on/affected by the CSL, insomuch as the length, width and depth of the Gorgan Bay are decreased as a result of the CSL reduction within the last decade. As a result of decreasing the water level of the Caspian Sea, Khozeini channel has been closed. Moreover, the closure of the Ashuradeh and Chepgholi channels is anticipated in case the CSL reaches -27.6 and -27.9 m, respectively.

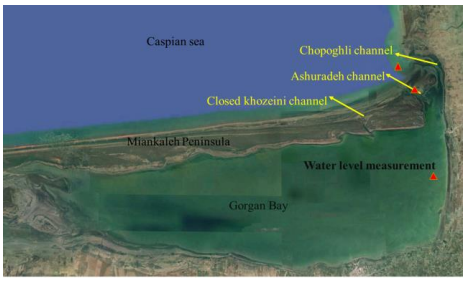

Figure 1. Gorgan Bay

The bay receives freshwater inflow from 10 small rivers and total discharge of all rivers into the bay is about 1.3 m^3 /s (about 12 cm/year). Based on the available data the annual precipitation is around 50 cm/year for the bay region. More importantly, the rate of evaporation is around 120 cm per annum [1,2] resulting in an annual unbalance of -60 cm for Gorgan Bay.

It is a fact that by further decrement of the CSL, the Chapaghli and Ashuradeh channels are expected to be blocked while the unbalance in the water budget causes the Gorgan Bay to be dried up. To avoid the dryness, it is a must to keep the natural channels open and maintain the water exchange between the Caspian Sea and Gorgan Bay. On this basis, PTP Consultants proposed that dredging of the channels is a vital solution to prevent drying up of the Gorgan Bay. According to the conducted technical and economic evaluations, the dredging of Ashuradeh channel is more economically viable and with lower risk in terms of environmental impacts, compared to the Chapaghli channel. Accordingly, the dredging of Ashuradeh channel is recommended in order to establish water exchange between the sea and Gorgan Bay.

The bathymetry of the Ashuradeh channel and how it connects to the sea is presented in Figure 2. As it is expected, as the water depth increases, the distance between Ashuradeh channel and the sea increases. For example, the distance between the mouth of Ashuradeh channel and the depth of -29 meters (relative to open seas water level) from the sea is approximately 2700 meters.

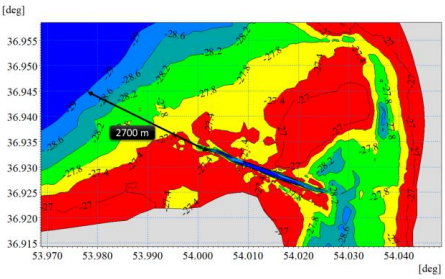

Figure 2. Bathymetry around the channels

Study on various water depths leads to -29.0 as the target water depth for the proposed artificial channel. Therefore, the distance between the seaward mouth of Ashuradeh channel and the target contour at the sea is about 2700 meters. The shape and layout of the proposed artificial channel is determined by comparison among the maximum influx of the seawater to the bay during different storms. During a storm, the wind-induced storm surge results in a difference in water levels between the sea and the bay, causing pump of the seawater into the bay. Under non-stormy conditions, only the connection between the sea and the bay remains with no water exchange (negligible density current is present) from the neither sides. Therefore, with adequate channel, it is expected that the greatest exchange of water between the sea and the bay will occur during and immediately after storms.

The shape of the artificial channel can be a rectangle with a fixed width of 150 m, length of 2700 m and 1.6m, corresponding depth to the contour of -29 meters, as presented in Figure 3 (alternative A). Also, the channel shape can be in the form of a trapezoid, with a variable width of 150 m to 450 m and a length of 2700 m with the depth down to the -29 meter (alternative B). To investigate the maximum exchange, alternative A with dredging down to -30 m is also examined (alternative C).

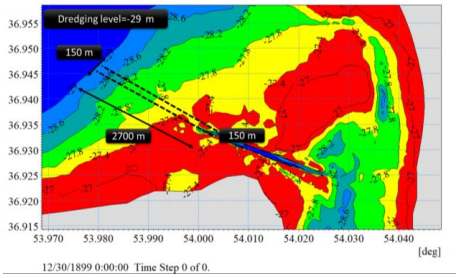

Figure 3: Rectangular channel with constant width of 150 m and length of 2700 m and depth, down to -29 m (alternative A)

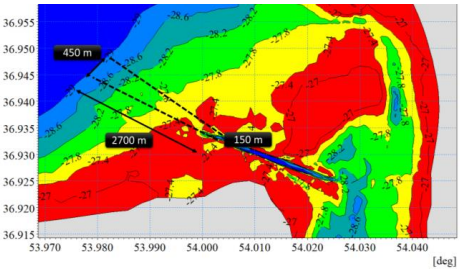

Figure 4: Trapezoidal channel with a variable width of 150 m to 450, length of 2700 m and depth, down to -29 m (alternative B)

2. Numerical Simulations

This study investigates the effects of the shape and depth of the proposed various channels i.e., the extensions of Ashuradeh channel to the sea and to the bay, on the water exchange between the Caspian Sea and the Gorgan Bay. In order to do this, the SW and HD modules of the Mike 21 model were simultaneously employed for simulation of the current induced by waves and wind. The incorporated computational domain of interest, together with the considered triangular grid are shown in Figure 5. This area consists of two open boundaries, the boundary condition information of which is provided by the large-scale current and wave model (well calibrated and verified during the Monitoring and Simulation of the Caspian Sea).

The calibrated and verified also show very good agreement with the water level measurements at three locations of the study area (Figure 1). As an example, the time series of the measured water level variations are compared with the results of the numerical model in Figure 6. Aslo agreement between the numerical results and limited flow data within Ashuradeh channel support the validity of the model for examining the various alternatives under different natural conditions.

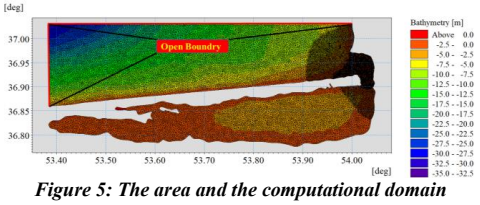

Figure 5: The area and the computational domain

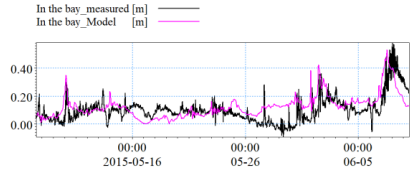

Figure 6: Comparison between observed and numerically simulated water elevation at the sea station.

3. Results

Important results corresponding to each of the proposed channel alternatives are investigated using various one-year numerical simulations: the amount of water exchange between the sea and the bay under different stormy conditions, flow velocity within Ashuradeh extended channel, and the distribution form of the seawater intrusion to the Gorgan Bay. The obtained numerical results revealed that the amount of water exchange between the sea and the bay in the trapezoidal channel (dredged to -29 meters) is about 20% more than the rectangular channel with the same depth. Moreover, the amount of water exchange between the sea and the bay in the rectangular channel (dredged to -30 meters) is just 7% more than the rectangular channel (dredged to -29 meters). From the considerable number of the numerical simulation, it can be clearly concluded that the channel in a trapezoidal form, not only keeps the connection between the sea and the bay open (against sedimentation, not mentioned in this manuscript) till the Caspian Sea level drops to -28.5, but also guarantees a great amount of water exchanged between the sea and the bay under stormy conditions.

4. References

[1] Ranjbar, M.H., Hadjizadeh Zaker, N., 2016. Estimation of environmental capacity of phosphorus in Gorgan Bay, Iran, via a 3D ecological-hydrodynamic model. Environ. Monit. Assess. 188 (11), 649.

[2] Ranjbar, M.H., Hadjizadeh Zaker, N., 2018. Numerical modeling of general circulation, thermohaline structure, and residence time in Gorgan Bay, Iran. Ocean Dyn. 68 (1), 35–46. https://doi.org/10.1007/s10236-017-1116-6.

14th International Conference on Coasts, Ports and Marine Structures
9 & 10 May 2023 , Tehran-IRAN
ICOPMAS 2022

THE INTEGRATED HYDRO-MEM HYDRODYNAMIC-ECOLOGICAL MODEL: A WETLANDS ASSESSMENT TOOLBOX FOR SCIENTISTS AND STAKEHOLDERS

Karim Alizad[1], James T. Morris[2] and Scott C. Hagen[3]

1) University of South Carolina, Baruch Institute for Marine and Coastal Sciences, Columbia, SC 29208, USA, Alizad@sc.edu
2) University of South Carolina, Baruch Institute for Marine and Coastal Sciences, Columbia, SC 29208, USA, Morris@inlet.geol.sc.edu
3) Deceased, Louisiana State University, Department of Civil Engineering, Baton Rouge, LA 70803, USA

1. Introduction

Climate change and sea-level rise threaten coastal systems such as wetlands and barrier islands around the world. Coastal wetlands are valuable ecological systems that provide habitats for many species, protect shorelines by dissipating waves, and purify coastal water [1, 2]. Scientific coastal wetlands assessment tools could help stakeholders and coastal managers to make informed decisions and guide their activities. Integrated wetland models that include hydrodynamic complexities and biological feedback processes can accurately assess wetland responses to different changes. Hydro-MEM is a coupled two-dimensional model that interconnects biological and hydrodynamic models and projects marsh response in the form of productivity, vegetation change, and migration to higher lands [3, 4]. This model has been applied to several marsh systems across the Gulf of Mexico and U.S. East coasts. Hydro-MEM projections were published by the United States National Oceanic and Atmospheric Association (NOAA) and the United States Northeast Conservation Planning Atlas [4-6]. This extended abstract aims to show the major findings of this model around different estuaries and demonstrate how different characteristics of estuaries including tide range, topography, geometry, and sediment availability can affect marsh system response to different sea-level rise (SLR) scenarios.

2. Methodology

Hydro-MEM was developed to include feedback between hydrodynamic and biology in the marsh system by coupling a hydrodynamic model (e.g., Advanced Circulation model [7]) and Marsh Equilibrium Model (MEM) [8] using time-step framework [3]. The main inputs of the hydrodynamic model include topography [9] and bathymetry, river inflow, tidal forcings, and geometry. At each time-step, the MEM part of the model generates marsh productivity and accretion (elevation change at marsh surface due to its response to SLR) using tidal datums (mean high water, mean low water, and mean sea level) from the hydrodynamic. Hydro-MEM uses the MEM outputs to update the hydrodynamic model inputs, namely surface roughness, topography, and SLR for the next time-step. This process will continue until the model reaches its targeted time. The model was validated and explained in detail in the previous Hydro-MEM publications [3-6]

3. Results and Discussion

In this presentation, the outputs from previous Hydro-MEM publications are compared to assess effective factors on marsh response to SLR. Figure. 1a and b show the regions where Hydro-MEM model were incorporated to investigate the response of the marsh systems to SLR. Two of those systems, the Apalachicola microtidal system in the northern Gulf of Mexico and Plum Island Estuary (PIE) in a mesotidal system in the northeast of the U.S., were selected by red circles to demonstrate the changes. Apalachicola microtidal estuary in Panhandle Florida (Figure. 1a) is a fluvial estuarine system, which receives fresh water and sediment from the largest river in discharge in the state of Florida. PIE with a higher tide range (2.9 m) receives a small amount of discharge and the tidal flow is the dominant flow in the creeks and rivers in the marsh system.

Hydro-MEM outputs were validated in both systems [5, 6], and marsh productivity results categorized in low, medium, and high productivity, drowned forest, and mudflat shows healthy marsh in the year 2020. The projections in Figure 1 are based on the intermediate NOAA SLR scenario (1 meter by the year 2100) [10].

Hydro-MEM projects inundation of marsh system in the microtidal estuary with the creation of some mudflat islands in addition to marsh migration to higher lands Figure 1c and e). However, the mesotidal system under the same SLR scenario is less vulnerable and most of the marsh system in the northern part of the estuary is shown to be more productive than the current condition with the creation of some mudflat islands in the center of the estuary (Figure 1 d and f). Further assessments show that the vegetation change in this mesotidal estuary from high marsh (*Spartina patens*) to low marsh (*Spartina alterniflora*) is the major effect of SLR. This is because of the water depth increase and time of inundation in the

marsh system characterized as hydroperiod, which is more favorable to low marsh than high marsh. Also, marsh migration is limited due to sharp elevation profile.

The most important effective parameters in vulnerability of a marsh system to SLR are topography, tide range, sediment transport, and consequently estuarine type. The difference in responses of these two estuaries to SLR indicates the vulnerability of microtidal marsh systems around the world and the need for scientific tools such as Hydro-MEM to plan accordingly.

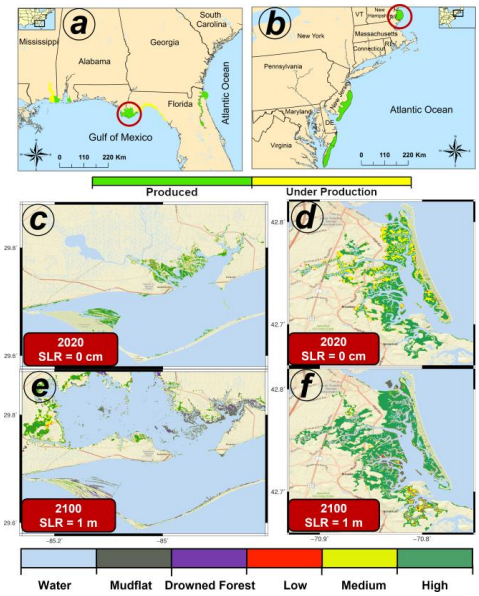

Figure 1. Hydro-MEM application in different estuaries around the United States coasts (a and b) with marsh productivity results for the year 2020 in Apalachicola, FL (c) and Plum Island Estuary, MA (d) and their projections for the year 2100 (e, f) categorized in water (blue), mudflat (gray), drowned forest (purple), and low (red), medium (medium), and high (green) productivity.

4. References

[1] E. B. Barbier, I. Y. Georgiou, B. Enchelmeyer, and D. J. Reed, "The Value of Wetlands in Protecting Southeast Louisiana from Hurricane Storm Surges," *PLOS ONE,* vol. 8, p. e58715, 2013.

[2] R. H. Kadlec, "Chemical, Physical and Biological Cycles in Treatment Wetlands," *Water Science and Technology,* vol. 40, p. 37, 1999.

[3] K. Alizad, S. C. Hagen, J. T. Morris, P. Bacopoulos, M. V. Bilskie, J. Weishampel, *et al.*, "A coupled, two-dimensional hydrodynamic-marsh model with biological feedback," *Ecological Modeling,* vol. 327, pp. 29-43, 2016.

[4] K. Alizad, S. C. Hagen, S. C. Medeiros, M. V. Bilskie, J. T. Morris, L. Balthis, *et al.*, "Dynamic responses and implications to coastal wetlands and the surrounding regions under sea level rise," *PLOS ONE,* vol. 13, p. e0205176, 2018.

[5] K. Alizad, S. C. Hagen, J. T. Morris, S. C. Medeiros, M. V. Bilskie, and J. F. Weishampel, "Coastal wetland response to sea-level rise in a fluvial estuarine system," *Earth's Future,* vol. 4, pp. 483-497, 2016.

[6] K. Alizad, J. T. Morris, M. V. Bilskie, D. L. Passeri, and S. C. Hagen, "Integrated modeling of dynamic marsh feedbacks and evolution under sea-level rise in a mesotidal estuary (Plum Island, MA, USA)," *Water Resources Research,* vol. Under Review, 2022.

[7] R. A. Luettich and J. J. Westerink, *Formulation and numerical implementation of the 2D/3D ADCIRC finite element model version 44. XX*: R. Luettich, 2004.

[8] J. T. Morris, P. V. Sundareshwar, C. T. Nietch, B. Kjerfve, and D. R. Cahoon, "Responses of coastal wetlands to rising sea level," *Ecology,* vol. 83, pp. 2869-2877, 2002/10/01 2002.

[9] K. Alizad, S. C. Medeiros, M. R. Foster-Martinez, and S. C. Hagen, "Model Sensitivity to Topographic Uncertainty in Meso- and Microtidal Marshes," *IEEE Journal of Selected Topics in Applied Earth Observations and Remote Sensing,* vol. 13, pp. 807-814, 2020.

[10] W. Sweet, R. Kopp, C. Weaver, J. Obeysekera, R. M. Horton, E. R. Thieler, *et al.*, "Global and regional sea level rise scenarios for the United States," NOAA CO-OPS 083, 2017.

14th International Conference on Coasts, Ports and Marine Structures
9 & 10 May 2023 , Tehran-IRAN
ICOPMAS 2022

THE CHALLENGES OF CASPIAN SEA WATER LEVEL CHANGE IN TERMS OF ZONING

Ali Azimi[1], Reza Ahmadian[2], Ehsan Rastgoftar[3], Mohamad Reza Allahyar[4], Hamid Khalili[5] and Rasoul Ghanbari Maman[6]

1) Ports and Maritime Organization, Tehran, Iran, aazimi@pmo.ir
2) Manager of Integrated Coastal Zone Management of Caspian Sea, Tehran, Iran, rahmadian2001@gmail.com
3) Iranian National Institute for Oceanography and Atmospheric Sciences, Tehran, Iran, e.rastgoftar@inio.ac.ir
4) Ports and Maritime Organization, Tehran, Iran, mallahyar@pmo.ir
5) Ports and Maritime Organization, Tehran, Iran, hkhalili@pmo.ir
6) Ports and Maritime Organization, Tehran, Iran, rghanbari@pmo.ir

1. Introduction

In this study, the challenges arising due to the retreat of the Caspian Sea in the defined zones and boundaries are presented and the shoreline changes due to changes in water level that lead to the retreat and advance of the shoreline are investigated.

2. Coastline Changes

One of the most important coastal phenomena, especially on the coast of the Caspian Sea, is the retreat and advance of the seawater, which will have many positive and negative effects on the coast. Fluctuations in the water level of the Caspian Sea are the most important and main factor in the progress and regression of the sea. Sea retreat increases the level of coastal land in proportion to the amount of slope in different parts of the coast [1].

In this study, coastline line changes in the northern provinces of the country have been studied. The basis for comparing shoreline changes is the compliance of the approved shoreline in the ICZM National Plan maps in 2006 and the shoreline drawn by the consultant based on the last water level line in 1398.

3. Sea Water Retreat

A comparison of the coastline of the National ICZM project and the current situation in 2019 shows that during this period due to changes in the water level line or sedimentation of river mouths or the direction of marine sediments to the coast by sea currents or some human activities such as construction wharves or water diversion facilities, etc., about 316,888 hectares have been added to the coastal area from the sea. However, this rate is not the same in all parts of the coast, and with the increase or decrease of the slope or in the mouths of rivers or in areas where human activities have taken place, the extent and length of sea retreat vary [2].

The amount of land added to the coast due to seawater retreat in the time interval between the preparation of the ICZM National Plan and the last water level line in 2019 in the three northern provinces of the country is presented in Table 1. Also, in Table 2, these statistics are presented separately for the cities of Iranian northern provinces. As can be seen from the tables, Golestan province and Gomishan city in the Miankaleh region had the highest rate of seawater decline. This is due to the drying of parts of the Miankaleh and Gomishan wetlands. Since these wetlands are coastal and supply most of their water from the sea, seawater fluctuations in recent years have hurt these wetlands and the decrease in water resources in recent years has increased the level of land in the proportionality plan. It is according to the previous plan (National ICZM) [3].

Examination of the coastline retreat values on the coasts of the northern provinces shows that the retreat rates in the cities of Talesh, Sangachin, Noor, and Gomish Tappeh are about 127 meters, 107 meters, 170 meters, and from 5.3 to 6 kilometers. Since there are no marine structures such as breakwaters along these shores, it seems that the shoreline changes are mostly due to changes in water level and the impact of coastal sediment transfer in these changes is very small. Using the slope data of the coasts extracted from the surveys of the Caspian Sea monitoring and simulation project, the average slope of the Sangachin region is equal to 1.3%. Assuming a difference in water level of about 1.18 meters between 1387 (-26.15 meters) and 1398 (-27.33 meters), the amount of horizontal change of the shoreline is equal to 90 meters. Comparing this number with 107 meters, it is concluded that the assumption of the shoreline slope due to the low water level is reasonable. For other images, the values calculated in the range of values are the difference between the two coastlines in Google Earth. Therefore, the low water level of the Caspian Sea plays an important role in shoreline changes.

Table 1. The amount of land added to the coast due to seawater retreat in the time interval between the preparation of the ICZM National Plan and the last water level line in 2019

State	Ratio of total area (Percentage)	Area (Hectares)
Golestan	63/7	20191/6
Mazandaran	29/5	9347/7
Guilan	6/8	2149/3
Sum of the total backward area of the northern provinces	100	31688/6

Table 2. The amount of land added to the coast due to seawater retreat in the time interval between the preparation of the national ICZM plan and the last water level line in 2019 by province and city

Province	City	Area (Hectares)	Proportion of total area (Percentage)
Golestan	Gomishan	17712/6	55/9
	Torkaman	1959/1	6/2
	Gaz port	519/6	1/6
	KordKuy	0/3	0/0
The total of Golestan province		20191/6	63/7
Mazandaran	Behshahr	5380/8	17
	Galougah	2442/4	7/7
	Nowshahr	190	0/6
	Noor	160/6	0/5
	Babolsar	159/7	0/5
	Mahmoud Abad	143/8	0/5
	Jouybar	133/4	0/4
	Abas Abad	107/3	0/3
	Fereisoun Kenar	102/3	0/3
	Ramsar	98/8	0/3
	Miandoroud	98/4	0/3
	Neka	94/3	0/3
	Sari	90/5	0/3
	Tonekabon	89/7	0/3
	Chalous	5/55	0/2
The total of Mazandaran province		9347/7	29/5
Guilan	Anzali Port	456/8	1/4
	Astaneh Ashrafieh	390/8	1/2
	Roudsar	356	1/1
	Talesh	252/9	0/8
	Langeroud	230/5	0/7
	Rasht	200/4	0/6
	Astara	124/1	0/4
	Rezvanshar	104/1	0/3
	Lahijan	33/6	0/1
The total of Guilan province		2149/3	6/8

4. Conclusion

Low water levels affect commercial transportation, recreational boating, hydroelectric power plants, and drinking water treatment plants. A low water level means that less than one cargo ship is loaded to prevent the ship from sinking, which can lead to an increase in the cost of goods. Yacht propellers break at the bottom of shallow lakes and may not be able to enter anchorages which can affect marine revenue. Water facilities depend on rainfall and level changes. Therefore, the low water level is an important issue in shoreline management and should be considered in hazard zoning.

References

[1] Frolov, A. V. "Modelling of the long-term fluctuations of the Caspian Sea level: theory and applications." GEOS, Moscow 171 (2003).

[2] Elguindi, N. and Giorgi, F., 2006. Projected changes in the Caspian Sea level for the 21st century based on the latest AOGCM simulations. Geophysical research letters, 33(8).

[3] A study and review of periodic and long-term changes in the water level of the Caspian Sea, studies of the Shoreline Management Plan (SMP), Integrated Coastal Zones Management plan (ICZM), Jihad Water and Energy Research Company, Winter 2018.

9 & 10 May 2023 , Tehran-IRAN

ICOPMAS 2022

INDEX

G

H

I

J

K

Iranian Coastal & Marine Structural Engineering Association (ICOMSEA)

The World Association for Waterborne Transport Infrastructure (PIANC)

International Hydrographic Organization (IHO)

International Harbour Masters Association (IHMA)

International Association of Marine Aids to Navigation and Lighthouse Authorities (IALA -AISM)

International Association for Hydro-Environment Engineering and Research (IAHR)

Iranian Association of Naval Architecture and Marine Engineering

Iranian Society of Marine Science and Technology

International Association of Ports and Harbors (IAPH)

Intergovernmental Oceanographic commission (UNESCO)

Coordinating Committee on Hydrometeorology & Pollution Monitoring of the Caspian Sea (CASPCOM)

Iranian National Commission (UNESCO)

Iranian Association of Geomorphology

Shipping Association of Iran

Iranian Hydraulic Association

Iranian National Institute for Oceanography and Atmospheric Science

Iranian Hydrographic Association

Islamic World Science Citation Center

Water Research Institute

Presidential Center for Progress and Development

Association of Sea Oriented Development

Iranian Shipowners Association

icopmas.pmo.ir

3rd Floor, Building No.2 of Ports & Maritime Organization,
Shahidi St., Shahid Haghani highway., Vanak Sq., Tehran-IRAN

Tel: +9821 84932346 | Fax: +9821 84932756 | Email: icopmas@pmo.ir